AN ULTRASONOGRAPHIC STUDY OF MUSCULOSKELETAL INJURIES AND MAMMARY GLAND TUMOUR IN SMALL ANIMALS

A thesis submitted to the Faculty of Veterinary Medicine,
University of Glasgow.
For the Degree of Doctor of Philosophy

by

MD ZUKI ABU BAKAR@ZAKARIA.
D.V.M. (Putra University of Malaysia)

Division of Veterinary Anatomy,
Department of Veterinary Preclinical Studies,
School of Veterinary Medicine,
University of Glasgow,
March, 1999

VOLUME 1

CONTENTS - VOLUME 1

Page

ACKNOWLEDGEMENTS

In the name of Allah, the Beneficent, the Merciful.

I wish to express my profound and sincere gratitude to my supervisor Professor John S. Boyd for his excellent supervision, constructive criticism and constant encouragement in the preparation of this thesis.

I am most grateful for the help and full co-operation given by the ultrasonographer supervisor, Mr. Calum Paterson and the ultrasonographer, Ms. Alison Dickie from the Division of Anatomy, Department of Veterinary Preclinical Studies, throughout the period of my study.

I wish to express my thanks to: Professor Stuart Carmichael, Director of the Glasgow University Veterinary Hospital; the other orthopaedic surgeons, Professor David Bennett, Mr. Alex Li and Mr. Neil Gibson; the soft tissue surgeons, Dr. Martin Sullivan and Mr Leigh Griffitths; the radiologist, Mr Tobias Schwarz; Head of nursing staff, Mrs Pamela McComb and members of the animal nursing staff, and to all members of the clinical staff and students who have given me full co-operation and provided a friendly environment during the work in the Small Animal Clinics.

My sincere thanks to Mr Alan May, the Photographer, for his help and full co-operation in producing the photographs for my thesis.

My thanks also to Mr. Alan Reid, Chief Technician Supervisor in the Division of Veterinary Anatomy for his help and full co-operation during preparation of the thesis, and also to the staff in the Division of Veterinary Anatomy: Mr. David Newham, Ms Sheena McMath, Miss Patricia Wilson, Mrs Frances Watterson and Mr Alan Purvis for their help and providing a friendly environment throughout my study.

My gratitude to members of staff in the histology lab: Mrs. Sheila Cranstoun and Mrs. Karen Gall for their help during the histology preparation, and to the Secretary of the Division of Veterinary Anatomy, Mrs Vi Winnie.

I wish to thank Ms. Sue Henderson and the staff at the PDSA, Shamrock Street, Glasgow for their helpful co-operation and allowing me to use their facilities.

I would also like to thank Mr Tom Mathieson, Clerk to the Veterinary School; the staff in the Veterinary Faculty Computer Centre, Vicky Dale, Susan Cain, Rena Cameron and Colin Naismith; the librarians in the James Heriot Library, Mary Findlay and Maureen McGovern; the janitors of the Veterinary School, Mr Kenneth Boswell and Mr James Caldwell for their helpful assistance.

I wish to acknowledge the financial support provided by the Putra University of Malaysia on behalf of the Government of Malaysia throughout the period of my study in Glasgow University Veterinary School, and my period of living in the United Kingdom.

Finally, thanks to my family especially my mother, Siti Zawiyah binti Abdul Wahab and my father, Abu Bakar @ Zakaria bin Daud, my family in law for their continuous encouragement and support, and to my wife Noor Subhi Abu Bakar for her patience, forebearance and her continuous encouragement and support. Thanks also to my lovely children, Muhammad Afiq and Nur Afiqah for their understanding, constant love and patience.

Praise be to Allah, who has given me the strength in completing this thesis.

DECLARATION

I declare that the work presented in this thesis was carried out by me personally.

4th Mei 1999

MD ZUKI ABU BAKAR@ZAKARIA

SUMMARY

With advances in ultrasound technology and the development of high resolution transducers, imaging of the musculoskeletal system and its pathology has become possible. The present study was carried out to assess the value of diagnostic ultrasonography using a high frequency transducer (7.5 MHz) in musculoskeletal injuries of small animals. In addition, an attempt was made to document the value of high resolution ultrasonographic imaging on canine mammary gland tumours and their ultrasonographic characteristics. Live animals used in this study were gathered from two main places in the Glasgow area: the clinical cases referred to the Glasgow University Small Animal Clinics (GUSAC) for fracture repair and wound healing studies and the cases referred to the People's Dispensary for Sick Animals (PDSA) for canine mammary tumour study. Canine cadavers collected from the Glasgow area were used for normal muscle imaging and a preliminary study of abdominal wounds. A B-mode real-time ultrasound scanner (Capasee, TOSHIBA) with a 7.5 MHz linear array transducer was used through out the study. The images were recorded during each examination for review at a later date.

Skeletal muscles of normal greyhound cadavers imaged ultrasonographically appeared as a homogenously hypoechoic structure with fine echoes scattered throughout the muscle parenchyma. Each muscle group could be identified, separated by a thin hyperechoic structure which was actually the connective tissue fascia. Bone appeared as a strong hyperechoic image with complete acoustic shadowing distally when the transducer was correctly inclined.

Normal ventral abdominal musculature (VAM) imaged ultrasonographically appeared isoechoic relative to the muscle tissue. The VAM with the presence of new incision site revealed a disorganised area with ill defined margins which was hypoechoic relative to the surrounding tissues. The VAM with the presence of an old incision site varied from hypoechoic to hyperechoic. The majority of the cadavers examined (17) fell into this group. Most of the VAM with an old incision

site appeared as an ill-defined disorganised hyperechoic area relative to the surrounding tissues.

Fluid accumulation within the subcutaneous tissue could be detected within 24 hours post-operation appearing anechoic to hypoechoic with acoustic shadowing artefact depending on the content of the fluid. The formation of fibrous tissue at the surgical site could be seen ultrasonographically and appeared as an hypoechoic structure with acoustic shadowing artefact in the early stages, and later with time it appeared as an ill-defined hypoechoic area with an echogenic centre and casting an acoustic shadowing artefact. When the fibrous tissue matured the surgical site appeared as a disorganised hyperechoic area with acoustic shadowing artefact.

A fracture site imaged longitudinally with ultrasound appeared as a discontinuity of the smooth bone surface. Soft callus formation could be detected and appeared as a disorganised hyperechoic structure with no artefact produced. However, it was not apparent radiographically. The repair process of bone fractures could be successfully monitored with ultrasound without any risk of exposure to radiation of the animal. Furthermore, complications of fracture repair could be detected at an early stage with ultrasound and the result was immediate. Haematoma formation at the fracture site could be demonstrated within 24 hours after operation and its resolution could be successfully monitored.

The ultrasonographic appearance of canine mammary tumour tissue was divided into three groups: group one was represented by small areas of tumour tissue which appeared anechoic to hypoechoic; group two was represented by areas of tumour tissue appearing as areas of mixed echotexture; group three was represented by large areas of tumour tissue which were large and appeared hyperechoic, sometimes with the presence of cystic structures. Acoustic enhancement artefact was the most prominent feature for all groups of tumour masses.

The normal axillary and superficial inguinal lymph nodes appeared as round hypoechoic to isoechoic structures relative to surrounding soft tissues. The enlarged abnormal regional lymph nodes varied in echogenicity from homogeneous hypoechoic structures through a mixed echotexture to a more echogenic echotexture relative to surrounding soft tissues. Ultrasonography would appear to offer potential to become a routine procedure in mammary tumour tissue detection in small animals in the future.

LIST OF TABLES

LIST OF FIGURES

LIST OF ABBREVIATIONS

MHz	Megahertz
PDS	Polydioxanone (suture material)
PDSA	People's Dispensary for Sick Animals

CHAPTER 1

INTRODUCTION AND REVIEW OF THE LITERATURE

1.1 General Introduction

Real-time ultrasound has become, in recent time, an important and widely accepted method for non-invasive imaging of the animal body, especially for abdominal, cardiac and reproductive organs application, and appears to offer great potential for further development in veterinary diagnosis. Results in various clinical studies have shown diagnostic ultrasound to be an accurate, versatile, and inexpensive technique producing cross-sectional images with negligible risk and with reasonable resolution.

Injuries of the musculoskeletal system in small animals have been well documented (Alcantara and Stead, 1975; Vaughan, 1979; Power, 1981; Richardson and Thacher, 1993; Johnson *et al.*, 1994). Numerous diagnostic tools are available at present to diagnose such abnormalities. However, most of the diagnostic techniques available require the animal to be sacrificed or to be put under general anaesthesia. With advances in ultrasound technology and the development of high resolution transducers, imaging of the musculoskeletal system and its pathology has become possible. Previous studies show that the advantages of diagnostic ultrasound clearly outweigh any potential risk that might arise during or after examination (Laine *et al*, 1985; Harcke *et al*, 1988; Kramer *et al.*, 1997). Most of the scientific reports on the value of ultrasonography for imaging musculoskeletal abnormalities have been written regarding the distal extremities of large animals (Genovese *et al.*, 1986; Henry *et al.*, 1986; Genovese *et al.*, 1987; Dik, 1990; Marr *et al.*, 1993; Dik *et al.*, 1994; Pugh *et al.*, 1994; Kofler and Edinger, 1995), and less attention has been paid to small animals (Gerwing and Kramer, 1995; Kramer *et al*, 1997). Ultrasonography has proved to be a useful diagnostic tool in evaluating the musculoskeletal injuries that cannot be seen with conventional radiography (Wilson, 1988; Kramer *et al.*, 1997). Thus, the present study was carried out to assess the value of diagnostic ultrasonography using an high frequency transducer (7.5 MHz) in musculoskeletal injuries of small animals.

In addition, an attempt was made to document the value of high resolution ultrasonographic imaging on canine mammary gland tumours and their ultrasonographic characteristics.

1.2 Ultrasonographic imaging

1.2.1 Development and historical review

The development of ultrasound began as early as 1880, when the Curie brothers discovered a means to produce and detect these high-frequency sound waves. Forty years later, during the first world war in 1912 the combined effects of the Titanic disaster and the threat to the allied powers by submarines made it essential to find a means for detecting unseen underwater obstructions. A former student of Pierre Curie, Langevin, applied the ultrasonic techniques developed by the Curies in the laboratory to submarine detection. It was the Second World War that lent impetus to the development of faster electronic technology. Langevin's crude system, which allowed for detection, but not ranging, of submarines, evolved into the sophisticated Sound Navigation and Ranging (SONAR) system which was so important in the Second World War at sea. This was based on pulse-echo principles.

In 1937, the Dussik brothers were the first to describe the use of ultrasound for imaging. However, the technique was too crude to be of clinical value, and was later abandoned. The experience in pulse-echo techniques gained by United State military during the war was applied. In 1949, gallstones and foreign bodies were detected in tissues by Ludwig and Struthers. In 1952, Howry, with an engineer, W. Bliss developed a machine to display the echoes from tissue boundaries, and published two-dimensional ultrasonic tomograms. Howry also develop the technique of obtaining and displaying the large echoes from organ boundaries with his Compound Water-bath Scanner in 1954. This required almost total immersion of the subject in water and the submerged transducer moved in a circle around the patient. Later, the first two-dimensional contact scanner was developed in 1958 by Ian Donald, Regius Professor of Midwifery at Glasgow University and an engineer, Tom Brown. By the late 1950s, diagnostic ultrasound was of proven clinical value in the investigation of the eye, the brain, the heart, the abdomen and pelvis of human beings. In the 1960s, the older scanners used a system in which the wide range of echo amplitudes was compressed into two levels and the images produced were either black or white. However, this approach was limited because it defined only major differences in tissue densities.

In early 1970s, the grey-scale imaging was developed and since then many amplitudes of echoes were represented by levels of grey-scale. The signals were stored in a scan converter and then displayed on a monitor. With advance in ultrasound, the original analogue converters were largely replaced by digital scan converters which store the echo information (location, amplitude) in a memory similar to that used in personal computers. In the late 1970s, real-time or dynamic imaging was becoming available, where the operator is allowed to observe movements of the scanned organs leading to the immediate establishment of the viability of an embryo. Because of the innocuous nature of the examination, which provides highly informative data, these diagnostic methods have flourished in human medicine. Until recently, almost no part of the human body has escaped ultrasonographic examination.

Diagnostic ultrasound has become widely used as a veterinary diagnostic aid in veterinary practice throughout the world since the report by Lindahl in 1966 (Detection of pregnancy in sheep by means of ultrasound, *Nature* 1966). With advances in ultrasonography technology, it is fast becoming an important part in diagnostic veterinary medicine. In the past, ultrasonography was used mainly in veterinary obstetrics (e.g Boyd and Omran, 1991). However, it has been utilised more recently to image other soft tissue structures and their abnormalities, for examples in tendons, muscle, heart, kidney, etc. With the latest technology, ultrasound machines for veterinary use have become compact, portable, easy to use and provide more information.

1.2.2 Physical principles of ultrasound

Ultrasonography is based on the pulse echo principle. A man stands on one side of a canyon and shouts "Hello" toward the other side producing a "pulse" that travels through the air at the sound speed of approximately 741 miles an hour (figure 1.1). Once it hits the opposite wall of the canyon, the reflected pulse called "echo" travels back to the man at the same speed of sound, and after a short times, he hears the echo. The pulse and echo can be used to calculate how far it is to the other side of the canyon providing that the speed of sound is known. This can be done by simply measuring the time it took for the pulse to be echoed back, times speed of sound and then dividing by two as this represent two trips across the canyon (Shirly *et al*, 1978; Bartrum and Craw, 1983).

Basically ultrasound imaging uses this same pulse-echo principle. A short pulse of ultrasound is discharged into the body and travels through the tissues at a constant speed until it encounters a reflecting surface. The reflected beam is received by the ultrasound scanner, which has been keeping tract of the time and converting it to a distance in the same manner as the man and his calibrated stopwatch (Bartrum and Craw, 1983).

Audible sound has a range in frequency from 16 to 20,000 cycles per second (hertz), while ultrasound is defined as sound frequency above the normal hearing range, approximately 20,000 hertz (Rantanen and Ewing, 1981). The sound, is actually a series of repeating pressure waves as shown in figure 1.2. The **period** is the time it takes to complete a single cycle. The **amplitude** is the peak pressure or height of the wave which measure the strength or "loudness"

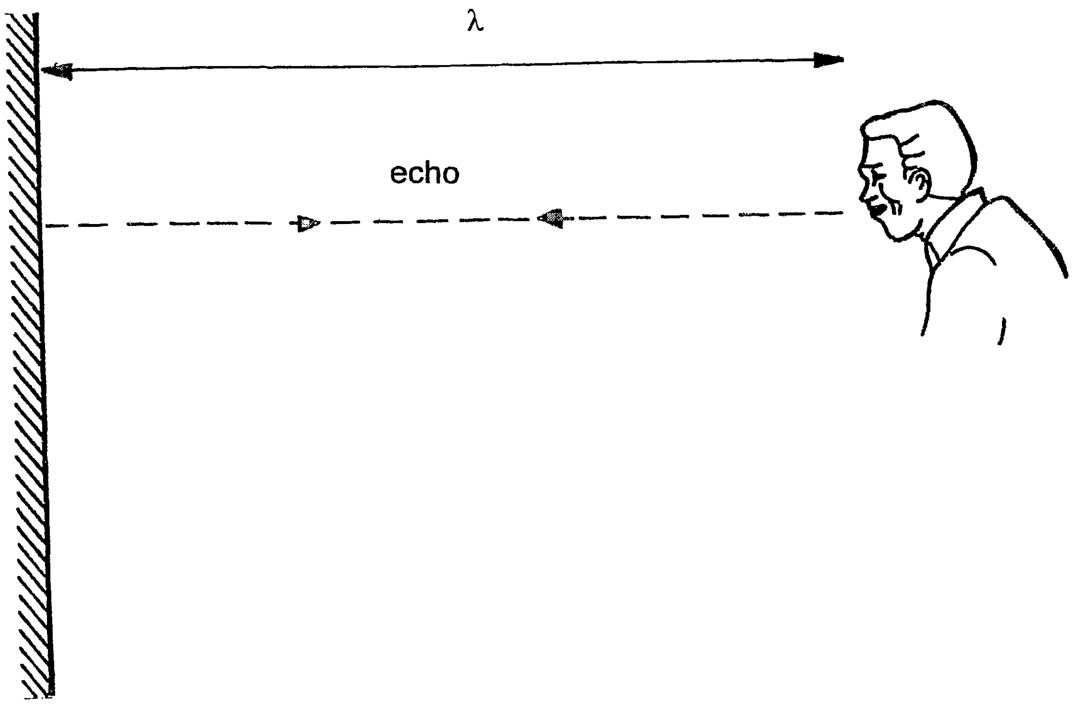

$$\lambda = \frac{v \times t}{2}$$

v = speed of sound in air

t = time between shout and echo being heard

Figure 1.1 A man shouts 'hello' towards canyon. The pulse-echo technique is based on the principle that the distance of a reflector (canyon) from a sound source (man) can be calculated by timing the return of an echo, provided that the speed of sound is known.

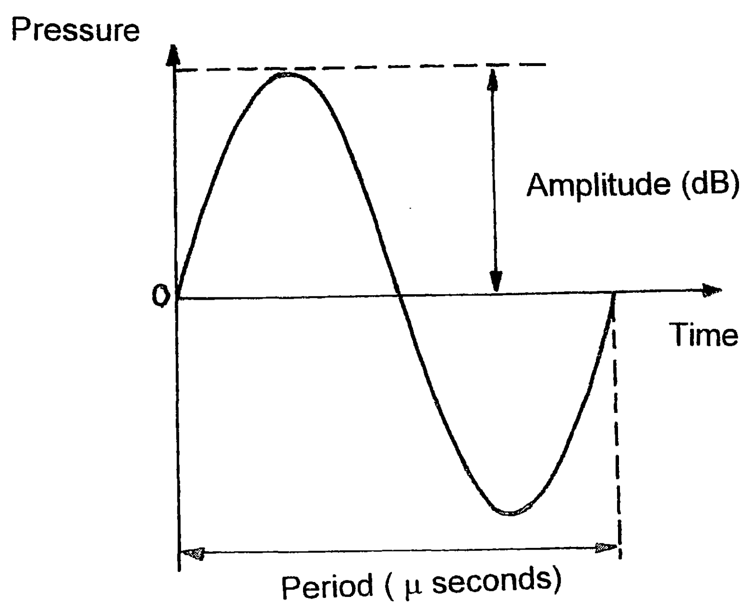

Velocity (metre per second) = speed of the sound

Frequency (MHz) = $\frac{1}{\text{period}}$

Wavelength (metres) = $\frac{\text{velocity}}{\text{frequency}}$

Figure 1.2 Common parameters of sound beam and the unit in which they are commonly expressed.

of the sound wave. The **velocity** is the speed of wave; it is dependent on the type and temperature of the material in which the wave is travelling (Bartrum and Craw, 1983). The denser the material, the greater the speed. The sound velocity in human soft tissue is constant (approximately 1540 meters per second), and the wavelengths used in ultrasound range from 1.0 to 1.5 mm (Bartrum and Craw, 1983).

Frequency is defined as the number of times a wave is repeated per second, and **wavelength** is the distance that the wave travels during one cycle. These two are inversely related if the sound velocity within the medium remains constant (Nyland, *et al.*, 1995). Frequency, wavelength and velocity have a constant relationship:

$$\mathbf{V = f}\,\lambda$$

Where **V** is the velocity (meter per second), **f** is the frequency in hertz (cycles per second), and λ is the wavelength (in meter). Thus, an higher frequency transducer results in decreased wavelength of the emitted sound, providing better resolution (see section 1.2.3). A higher frequency transducer also causes more rapid attenuation of the sound beam (see section 1.2.3). Thus, the sound penetration is limited. This means higher frequency is for fine detail in superficial structures and lower frequency is for deeper structures of the body.

Sound frequencies in the range of 1 to 10 MHz are commonly employed in diagnostic examinations (Rantanen and Ewing, 1981). A pulse echo system comprising around 5-6 wave cycles lasting less than one microsecond is used in B-mode diagnostic ultrasound (Goddard, 1995). The frequency of pulse emission is dependent on the speed of sound in tissue, and the total time needed for the sound pulse to cover its outward and return journeys (Nyland *et al.*, 1995).

Ultrasound waves are produced by the piezoelectric (pressure-electric) crystals mounted within the transducer's head. The term piezo is derived from the Greek word meaning pressure. When an electric current is applied, the crystals are deformed and generate ultrasound. These ultrasound waves are transmitted and propagated through the body tissues and in the mean time transfer energy to the adjacent tissue molecules. When reflected sound returns to the transducer, they meet and deform the crystals which generate an electric current. This electric current is then digitised and displayed on screen as an image of tissue interfaces (Nyland *et al.*, 1995).

1.2.3 Ultrasound and tissue interaction

When an ultrasound pulse travels through the soft tissues, it undergoes continuous modification of which the most significant is attenuation (Bartrum and Craw, 1983). The attenuation occurs through three process: absorption, reflection, and scattering. The attenuation rate in soft tissue and skeletal muscle is approximately 1 dB/cm/MHz and 3.0 dB/cm/MHz respectively (Rantanen and Ewing, 1981).

Absorption is the most predominant cause of attenuation where the ultrasound is converted into heat. The amount of absorption increases with the frequency of the sound beam. Thus, attenuation is directly proportional to the sound frequency and therefore, lower frequency ultrasound will penetrate more into soft tissue than higher frequency, but conversely, the poorer the resolution in the ultrasound image (Rantanen and Ewing, 1981).

Scattering of the sound beam occurs when the beam encounters an interface that is irregular and smaller than sound beam. The beam that interacts with this interface is scattered in all directions and results in energy loss. The intensity of the scattered sound increases with increasing frequency and is directly proportional to the frequency (Rantanen and Ewing, 1981).

Reflection is the redirection of a portion of the ultrasound beam back toward its source. It happens whenever the ultrasound beam passes from a tissue of one acoustic impedance to a tissue of different acoustic impedance. The acoustic impedance of a tissue (**Z**) is the product of the density of the tissue (**p**) and the speed of sound in the tissue (**c**). It is defined as:

$$\mathbf{Z = p \times c}$$

Since the speed of sound in soft tissues is assumed to be a constant (1540 meters per second), the only thing that affects the acoustic impedance is the density of the tissue. The amount of sound reflected at an interface is depend on how great the difference is between the two acoustic impedances that make up the interface. If the difference is very small such as in soft tissue to soft tissue interface, only a small percentage of the sound will be reflected and allows the majority of the sound beam to travel through the body. If the difference is very large such as between soft tissue and gas or bone, most of the beam is reflected and none is left to continue deeper. The beam is completely blocked and acoustic shadowing is produced (Bartrum and Craw, 1983).

Tissues of similar acoustic density are not themselves easily differentiated. However, serosal surfaces often provided strong lines of demarcation. These acoustically reflective surfaces which reflect the sound beam at the same angle to the ultrasound beam incidence are termed specular reflectors. The character of the reflected signal is dependent upon the ratio of reflector size and wavelength of the beam. Specular reflections occurs when the interface is larger than the sound width (Rantanen and Ewing, 1981). One of their properties is that the angle of reflection is equal to the angle of incidence. The echo has an "angle dependence" which means that the strength of the echo depends not only on the difference in acoustic impedance at the interface but also on the angle at which the beam strikes the interface (Bartrum and Craw, 1983).

Non-specular reflections (scattering) occurs when the sound beam meets an interface which is smaller than the sound beam width or irregular interfaces (Goddard, 1995). Some of the scattered ultrasound beam will return to the transducer and produce an echo. Many small parenchyma tissue echoes fall into this category. In contrast to specular echoes, the amplitude of a non-specular echo is not dependent on the beam angle.

The weaker echoes from deeper structures can be compensated by increasing the gain control. This will suppress electronically the amplitude of echoes from tissue interfaces near the crystal, and the amplitude of echoes from more distant tissue interface are progressively increased to compensate the sound wave attenuation (Nyland *et al.*, 1995). This is important for the uniformity of the image brightness throughout the depth of the display.

1.2.4 Resolution

The resolution can be defined as the system's ability to distinguish closely related structures (Nyland *et al.*, 1995). In general, there are two types of resolution involved in ultrasound imaging: *axial resolution* and *lateral resolution.*

Axial resolution refers to the ability to distinguish two objects placed close together along the path of the sound beam (Rantanen and Ewing, 1981; Herring and Bjornton, 1985; Nyland *et al.*, 1995). Axial resolution is determined by the length of the ultrasound pulse generated by the transducer, and improvement can be achieved by choosing a high ultrasound frequency. A higher frequency transducer emits a shorter wavelength, and therefore a shorter pulse. This means the axial resolution is shorter, thus the image produced is better (Rantanen and Ewing, 1981; Herring and Bjornton, 1985). However, the effective penetration depth is decreased due to high attenuation. Pulse length actually determines axial resolution but is directly dependent on the wavelength of the sound beam. Axial resolution cannot be better than one-half on the pulse length (Nyland *et al.*, 1995). For example, a 0.5 mm cyst could theoretically be resolved with a 7.5 MHz, but not a 3.0 MHz transducer, because of the superior axial resolution of the higher frequency.

Lateral resolution is refers to the ability to distinguish between two echoforming surfaces lying side by side in relationship to the sound beam axis (Herring and Bjornton, 1985; Nyland *et al.*, 1995). It is determined by the width of sound beam, which varies with the transducer frequency (Nyland *et al.*, 1995). Higher frequency transducers produce narrower beams, and the beam is narrowest at the focal point in focused ultrasound beam (Nyland *et al.*, 1995). Sound beams have the best resolution in the focal zone and the poorest close to the transducer where the beam is diverging (Rantanen, 1995). Lateral resolution decreases as one moves away from the focal point, but acceptable lateral resolution is found for several centimetres along the beam axis on either side of the focal zone (Rantanen and Ewing, 1981). Lateral resolution is a major contributor to image quality. A higher frequency transducer provides the best lateral resolution, however, due to the increase in attenuation rate per centimetre of tissue, the sound penetration is limited, and therefore, it is limited to use for tissues that are closer to the skin surface (Rantanen, 1995).

1.2.5 The transducers

The ultrasound transducer provides the link between patient and machine, and it is responsible for transmitting sound waves into the patient and receiving echoes (Drost, 1992). Piezoelectric crystals mounted in the head of the transducer generate ultrasound pulses when electric current is applied and send the beam of ultrasound into a receptive tissue (Goddard, 1995).

Each transducer is manufactured to emit primarily one ultrasonic frequency (Rantanen and Ewing, 1981). The frequency emitted by a transducer is dependent on the characteristics of the special piezoelectric crystals and it cannot be changed by the scanner's controls. Thus, changing the transducer is required to select the different frequencies because the crystals within the transducer produce sound at a specific frequency. Some transducers are capable of multifrequency operation in which they have multiple crystals, but each emits a different frequency. However, only one crystal is selectable at a particular time. Advances in transducer technology allow simultaneous imaging of the near and the far fields with sound waves of different frequencies (Nyland *et al.*, 1995). This allows the maximum resolution possible for a given depth without having to switch transducers.

Linear array transducer

This type of transducer usually has small groups of crystals (between 60 and 256 arranged in a line) and they are operated in turn, giving a rectangular field of view (Barr, 1990a). The main advantage of this type of transducer is that it allows a large field of view, even close to the scanning surface, which facilitates recognition of structures and the anatomical relationship between them. The major disadvantage is that it requires a relatively large contact area with the body surface. The most recent linear array transducers designed for veterinary used are much smaller and the problem is minimised. Some linear array transducers are designed with a convex scanning surface. This gives a mildly diverging field of view and a larger area of view during scanning (Barr, 1990a).

Sector transducer

This transducer produces a fan-shaped field of view and requires only a small skin contact area. It consists of a small number of crystals which are driven mechanically to produce a fan-shaped beam. This is achieved by mounting a small number of crystals on a rotating wheel, or by using a single crystal which oscillates to and fro (Barr, 1990a). A wide angle fan allows more structures to be seen but gives poorer resolution than a smaller angled fan. Generally, it has the advantage of being small and easy to use, and it requires only a small skin contact area. It is preferable to a linear array transducer for use in small animals because of their size and manoeuvrability (Barr, 1990a).

1.2.6 Ultrasound display modes

There are three modes of echo display, two of which are used more frequently in clinical applications in veterinary medicine.

Amplitude mode (A-mode)

A-mode ultrasonographic imaging is the simplest form of image display. It is a one-dimensional display of returning echo amplitude and distance. A single fixed beam of ultrasound is used, and the returning echoes are shown as peaks along a horizontal line (Barr, 1990a). The height of each peak denotes the strength of the echo, while the horizontal axis represents the depth of the reflecting structure (Barr, 1990a). This mode of imaging is least frequently used, but still has special use for ophthalmic examinations and other applications requiring precise length or depth measurements (Rantanen and Ewing, 1981).

Brightness mode (B-mode)

B-mode ultrasonographic imaging displays a two-dimensional image like a slice of tissue (Barr, 1990a). It displays the returning echoes as dots whose brightness or grey scale is proportional to the amplitude of the returned echoes and whose position corresponds to the depth at which the echo originated along a single line from the transducer (Feeney *et al.*, 1991). Thus, when a transducer is moved across the body, a two dimensional image of cross sectional anatomy is built up and displayed on the screen (Barr, 1990a). The position of the dots on the screen is determined by the time it takes for an echo to return to the transducer (Rantanen and Ewing, 1981). In B-mode echo, a bright echo may be very white on a black background or very black on a white background.

Real-time B-mode imaging displays movement of structures on an ultrasound image. Echoes are recorded continuously on a nonstorage cathode ray display screen. The cross-sectional image is assembled and displayed very rapidly, and is then updated continuously, allowing movement of structures within the section to be seen (Barr, 1990a).

Motion mode (M-mode)

M-mode is a one dimensional format displaying dots. A single ultrasound beam is used, and the returning echoes are displayed as a series of dots along a vertical line (Barr, 1990a). In this mode, time is displayed on the horizontal axis and distance is displayed on the vertical axis (Feeney *et al.*, 1991). The position of the dot along that line represents the depth of the reflecting structure, and the brightness of the dot denotes the strength of the echo (Barr, 1990a). The transducer is held in place over moving structure organs and the display is printed on a video monitor or recorded on a strip chart recorder. The motion of the dots (change in distance of reflecting interfaces from the transducer) is recorded with respect to time. M-mode is used primarily in echocardiographic studies to measure cardiac wall motion and valve excursions (Rantanen and Ewing, 1981).

1.2.7 Artefacts in muscular skeletal imaging

An artefact is defined as any record or image obtained in the course of applying a medial diagnostic technique which is not representative of the structures under study but is adventitious (Becker and Landau, 1986). Articles addressing these issues have been well published in the veterinary literature (Park *et al.*, 1981; Colby, 1985; Herring and Bjornton, 1985; Kirberger, 1995).

The artefacts encountered during routine ultrasonographic examination can affect the quality of image and contribute to image misinterpretation (Kremkau and Taylor, 1986). They result in added (not real), missing or improperly located echoes resulting in alteration of brightness, shape or size alteration. However, under proper technical conditions, useful artefacts are produced and can enhance accurate interpretation (Penninck, 1995).

Acoustic shadowing

Acoustic shadowing occurs as a result of nearly complete reflection or absorption of the sound beam (Sommer *et al*, 1979; Robinson *et al.*, 1981). This artefact can be produced by hyperechoic reflector such as gas or bone. Bone and other mineralised structures reflect only 20 - 30% of the sound beam and absorb most of the remaining (Kirberger, 1995). This results in a well defined clean shadow i.e. totally anechoic beyond them. A soft tissue-gas interface reflects 99% of the sound beam and usually results in an acoustic shadow (Penninck, 1995). Shadowing, may be more pronounced if the offending object is located in the focal zone when the beam is completely blocked (Ginther, 1986).

Reverberation artefact

This artefact occurs when a high intensity returning sound beam hits the transducer and is reflected back into the body for a second time. After being reflected back into the body and returning again to the transducer, the signal processor assumes that the signal has travelled once, and for a longer time through the body tissues and it is misinterpreted as originating from a point twice as deep as the original soft tissue-air interface. This reflection back into the body may occur several times resulting in multiple, evenly spaced reverberation echoes (Taylor *et al.*, 1980; Laing, 1983). The number of reverberating images depend on the penetrating power of the beam and the sensitivity of the probe (Curry *et al.*,1990). The distance between each reverberation is the same as that between the transducer and the original reflector. Reverberation differs depending on the size, location, nature, and number of reflectors encountered. This artefact is easily recognised by its regular arrangement of bright continuous echoes.

Acoustic enhancement

Acoustic enhancement or "through transmission" represents a localised increase of echo amplitude occurring distal to a structure of low attenuation (Kremkau and Taylor, 1986). These artefacts result when the ultrasound beam passes through a reflector-free structure (i.e., fluid-field). On an ultrasound scan, acoustic enhancement appears as an area of increased brightness.

This artefact is often helpful because it provides a diagnostic criterion of fluid accumulation within muscle. It is also helpful in differentiating cystic structures from solid, hyperechoic masses. In evaluating small cystic structures optimal enhancement is obtained if the structure lies within the focal zone and higher frequency transducers are used (Jaffe *et al.*, 1980).

Comet-tail artefact

This artefact contains a solid echogenic streak behind small gas collection or a metallic foreign body. Comet-tail artefact typically occurs with metallic objects and arises when there is a large acoustic impedance mismatch between the reflector and the surrounding tissues (Wendell and Athey, 1981; Ziskin *et al.*, 1982; Thickman *et al.*, 1983; Shah *et al.*, 1992). The greater the acoustic impedance mismatch, and the broader and more perpendicular the interface between the object and surrounding tissues, the more intense the comet-tail (Ziskin *et al.*, 1982).

Edge shadowing

This artefact is regularly seen at the edges of a rounded structure such as the bladder, gallbladder, kidney, and even the medulla-diverticulum junction of the kidney (Penninck, 1995). An acoustic shadow may occasionally occur distal to the lateral margins of these structures. The shadow results from the interaction of the sound beam with the curved periphery of rounded structures (Laing, 1983).

Ring down artefact

Ring-down artefact contains a series of closely spaced echoes or a solid echogenic streak behind an abdominal gas collection (Kirberger, 1995). Although ring down artefact appears ultrasonographically similar to comet tail artefact, it is produced by a completely different mechanism (Avruch and Cooperberg, 1985). Ring down artefact originates from a small collection of fluid trapped between at least two layers of gas bubbles. When the fluid is struck by an ultrasound pulse, it emits a continuous sound wave back to the transducer which may be seen as a solid echogenic streak or a number of closely spaced echogenic lines (Avruch and Cooperberg, 1985). Ring-down artefacts are most likely to occur with gastrointestinal gas but is also seen in biliary tree gas or abscess formation (Kirberger, 1995).

1.3 **Applications of diagnostic ultrasonography**

1.3.1 Introduction

Diagnostic ultrasonography has been used since the last decade. Until recently it was well developed in human medicine, but now has greatly expanded in veterinary practice in recent times. It is now being applied widely in various soft tissue disorders in humans including muscle injuries (Fornage *et al.*, 1983; Laine *et al.*, 1985; Takebayashi *et al.*, 1995). Its use in the assessment of primary diseases of skeletal muscle in human has been well documented (Heckmatt *et al.*, 1980; Heckmatt *et al.*, 1982; Cady *et al.*, 1983). However, in companion animals the use of ultrasonography in the assessment of the musculoskeletal system is relatively limited (Kramer *et al.*, 1997)

1.3.2 Ultrasonography of skeletal muscle

1.3.2.1 Anatomy

In mammals, skeletal muscle comprises approximately one-third to one-half of the total body weight (Hermanson and Evans, 1993). Fibres of muscle are the cellular units of the skeletal muscle. Skeletal muscle fibres are cylindrical multinucleated giant cells which are vary in length from a few millimetres to several centimetres (Craigmyle, 1986). Each muscle fibre has a well-developed thin sarcolemma, within which lie the many nuclei. The nuclei are oval in longitudinal section and appear circular in transverse section (Craigmyle 1986). Within the muscle fibre there are numerous longitudinal cylindrical myofibrils which are composed of numerous myofilaments of actin and myosin (Williams *et* *al.*, 1989). The myofibrils exhibit cross striation when viewed under electron microscope. Any given skeletal muscle has a connective tissue investment which has three components. The epimysium is the connective tissue containing many fat cells that covers the surface of the muscle (muscle sheath) and dips in to continue with the perimysial septa. Many muscle fibres are grouped into bundles (fasciculi) of varying size and pattern and an individual muscle may consist of many fasciculi. Each fasciculus is surrounded by an endomysium of highly vascular areolar connective tissue (Craigmyle, 1986).

The size of an individual muscle fibre depends on the species as well as on the physical condition of the animal, since individual muscle fibres are capable of hypertrophy as well as atrophy (Hermanson and Evans, 1993).

Blood vessels, lymphatic, and nerves enter and leave the muscle from the epimysium by way of perimysium (Cormack, 1987). The muscle fibres have several different types. The population and ratio of these fibre types are altered by physical activity and various endocrine, neurologic, vascular, and muscle diseases (Milton and Henderson, 1983). However, this area is not dealt with in this study.

Most skeletal muscles are attached by connective tissue to a bone or cartilage. This connective tissue attachment may be in the form of a cord like tendon or a flat, sheet-like aponeurosis. Some muscles have no demonstrable tendons or aponeurosis but attach directly to the periosteum of bones through fleshy attachments (Hermanson and Evans, 1993). The proximal fixed point of muscle attachment is the origin and the movable distal point of attachment is the insertion or termination. In the limb, the insertion is always distal to its origin, although functionally it may be the most fixed point at some phase of the stride. Certain muscles have equally fixed or mobile attachments, and the naming of an origin and an insertion is rather arbitrary. The expanded fleshy portion of a muscle is its belly, the origin is the head, and the termination is a tail. Minor divisions of origin or termination are called slips. A muscle may have more than one belly (digastric) or more than one head (triceps) and several slips (Hermanson and Evans, 1993).

1.3.2.2 Ultrasonography of normal skeletal muscle

Muscle structure on ultrasonography is shown to depend on the angle of inclination of the transducer (Cady *et al.*, 1983). If the transducer is perpendicular to the fascicular axis, the parenchyma echoes are dense, and ultrasonography in a plane parallel to the fasciculi reveals several linear echoes. The two fascias, epimysium and perimysium that surround the group of muscles and bundles (fasciculi) respectively, can be detected by ultrasound and appear as hyperechoic structures (Laine *et al.*, 1985; Smith *et al.*, 1996).

A study by Lamminen *et al.* (1988) shows that normal ultrasonographic appearances of muscles tissue were similar in healthy children. A similar ultrasonographic pattern has also been shown in adult man (Gunreben and Bogdahn, 1991). In general, skeletal muscle consists of relatively hypoechogenic muscle fibres separated by hyperechogenic fibroadipose septa. The ultrasonographic image of the normal skeletal muscle fibres scanned transversely appears as homogenous poorly organised fine echoes corresponding to the fibroadipose septa scattered throughout the hypoechoic muscle parenchyma (Fornage *et al.*, 1983; Vincent, 1988; Fornage, 1989; Kaplan *et al.*, 1990; Craychee, 1995). Occasionally, large intramuscular echogenic septa can be visualised on a transverse scan, revealing a thin reticular pattern. Longitudinal scanning of muscle results in an image of homogenous multiple fine parallel echoes, the fine echoes again originating from fibroadipose septa and perimysium which surround the muscle bundles (Fornage *et al.*, 1983; Vincent, 1988; Fornage, 1989; Kaplan *et al.*, 1990; Craychee, 1995).

The outer margins of muscle are highly echogenic because of the surrounding connective tissue fascia. In both transverse and longitudinal scans, muscle is normally hypoechoic relative to subcutaneous fat or tendons (Vincent, 1988; Kaplan *et al.*,1990; Craychee, 1995). However, it may be poorly echogenic in some instances, especially in obese patients (Vincent, 1988). Fibrous connective tissue between fat lobules appears as short linear or curvilinear echoes (Yeh and Rabinowitz, 1982).

The feathery appearance of normal skeletal muscle imaged ultrasonographically has been demonstrated in the human gastrocnemius muscle which is due to the multiple muscle bundles (fasciculi) surrounded by the fibroadipose septa (perimysium) (Fornage, 1989; Kaplan *et al.*, 1990). This gives a characteristic of 'herringbone pattern'. Anderson *et al.*, (1984) demonstrated that the normal human psoas muscle on ultrasonography appeared as striated homogenous bundles lying posterior and medial to the kidney on sagittal sections. In normal horses, the triceps muscle appeared ultrasonographically as echoic striation separated by anechoic areas (Smith *et al.*, 1996). The thickness of the muscular body increases during muscular contraction. Thus, alterations of the internal texture during contraction causes a more hypoechoic background (Fornage, 1989; Kaplan *et al.*, 1990).

1.3.2.3 Ultrasonography of skeletal muscle injury

The use of ultrasound to evaluate muscular disorders has been reported in the literature (Yousefzadeh *et al.*, 1982; Fornage *et al.*, 1983; Anderson *et al.*, 1984; Beckmann *et al.*, 1985; van Holsbeeck and Introcaso, 1992). The structural changes can be detected by ultrasound before there are significant changes in other parameters, such as all over tissue density (Cady *et al.*, 1983).

Muscle rupture

Rupture of the muscle belly with tearing and separation of its segments is rarely observed in small animals (Milton and Henderson, 1983). Muscle rupture normally occurs secondary to dislocation and displacement of a fracture fragment, such as distal femoral fracture with rupture of the quadriceps femoris muscle (Milton and Henderson, 1983). Rupture of muscle may be partial or complete and is often difficult to differentiate (Bloomberg, 1985). It occurs mostly in young animals. The cause of muscle rupture is a powerful active contraction of a flexor at the same time that forced passive extension occurs (Peacock and van Winkle, 1976). Rupture of the gracilis (dropped thigh), triceps (dropped shoulder), and gastrocnemius (dropped hock) muscles have been encountered in racing greyhound (Vaughan, 1969; Hickman, 1975; Vaughan, 1979).

Muscle rupture is clearly demonstrated by the discontinuity in the muscle with disruption of the fibroadipose septa ultrasonographically (van Holsbeck and Introcaso, 1990). Fragments of torn muscle originating from the walls of the cavity can be identified within the haematoma which fills the gap. The torn muscle fragments are demonstrated as free floating when gently pressure is applied, and is referred to as "bell clapper" sign (Fornage *et al.*, 1983; Harcke *et al.*, 1988).

Ultrasonographic findings of acute muscle rupture were variable according to the site of rupture and its severity (Laine *et al.*, 1985). The typical characteristics of muscle fibres disappear at the site of the rupture. The muscle appears hypoechoic with hyperechoic lines and anechoic areas. Anechoic areas at the rupture site or around mean haematoma or bleeding. Rupture of muscle fascia produces anechoic areas that can be seen between neighbouring muscle sheaths, and the rupture site can also be identified. Echogenicity is dependent on the severity of the muscle injured or ruptured, the spasm, the amount of intramuscular and extrafascial bleeding, and the age of the injury. A cavity full of fluid with thickened, hyperechoic walls may be present at an old muscle rupture site. The fluid is normally seen as an anechoic area (Laine *et al.*, 1985).

Haematoma

Haematoma formation is a hallmark of muscle rupture and occurs due to disruption of the blood vessels (van Holsbeck and Introcaso, 1990). Haematomas have variable ultrasonographic appearances depending on the age, stage of development, location, and the frequency of the transducer (Wicks *et al*, 1978; Wisner *et al.*, 1995). It may sometimes resemble an abscess or solid mass depending on the stage of the haematoma (Wicks *et al.*, 1978), and may have a well defined or irregular margin with or without internal septa (Braunstein *et al.*, 1981; Craychee, 1995). With a high frequency transducer (5 to 10 MHz), fresh clots appear highly echogenic, but appear anechoic with lower frequency transducers (Craychee, 1995). Anderson *et al.* (1984) have shown that the ultrasonographic appearance of a psoas haematoma varied from hypoechoic in a non-organised haematoma to a more echogenic, complex appearance in an organised haematoma. Acutely, a haematoma may appear as a cystic lesion with an hypoechoic centre, and as it matures and organises, it may develop discrete septations and echogenicity may increase centrally (Wisner *et al.*, 1995).

Muscle spasm

Muscle spasm is normally present with an injured tissue (Laine *et al.*, 1985). In cross section the quantity of muscle fibre per square centimetre is increased, which means that the interspace between the muscle fibres is diminished (Laine *et al.*, 1985).

Muscle spasm appears hyperechoic when scanning an area of cramping muscle, but the echoes are still well arranged as in normal muscle mass. The hyperechoic area disappears gradually when the transducer is moved away from the "cramp centre" (Laine *et al.*, 1985).

Muscle abscess

The most common cause of abscesses in muscle is due to infection by pyogenic bacteria (Hulland, 1993) The early stages consist of local, ill-defined cellulitis. Healing may take place with a minimal scarring or it may proceed to the formation of a typical abscess with a liquefied centre, a pyogenic membrane, and an outer fibrous sheath. The lesion may then slowly organise if it is effectively sterilised, and heals (Hulland, 1993).

The ultrasonographic appearance of an abscess depends upon the stage of its formation (Cartee and Rumph, 1984; Hager, 1986; Craychee,1995). An abscess may be hypoechoic with variable amount of internal echoes or anechoic with acoustic enhancement deep to it, depending upon its internal composition (Braunstein *et al.*, 1981; Smith and Webbon, 1994). The amount of internal echoes will depend on the consistency of the pus, with thick pus being more echogenic (Smith and Webbon, 1994). A mature abscess may appear as a cavitary hypoechoic mass with a thickened wall and could have internal septations, while immature abscesses with no clear walls, may appear as a uniformly hypoechoic-to-hyperechoic soft tissue mass (Craychee, 1995). In general, the less viscous materials are hypoechoic and may contain fine-to-coarse internal echoes. Inspissated materials can appear moderately to brightly echogenic, while mixed materials yield mixed patterns. The presence of gas will contribute variable amounts of bright, specular echoes with associated air artefacts (Craychee, 1995). A chronic abscess will often have a hyperechogenic capsule (Smith and Webbon, 1994).

Muscle atrophy

Atrophy of muscle is broadly defined as reduction in muscle fibre diameter or cross sectional area (Hulland, 1993). It may be due to disuse or denervation. Interference with venous drainage, arterial blood supply, or nerve supply results in degenerative changes in muscles (Bloomberg, 1985). In one study in humans using ultrasonography, muscle thickness was generally reduced in spinal muscular atrophy with an associated increased in subcutaneous tissue thickness that was not related to obesity (Heckmatt *et al.*, 1988a). Although reduced in volume, the affected muscle is otherwise indistinguishable ultrasonographically from a normal one (Farrow, 1996). Therefore, muscle atrophy could be proved by evaluating the muscle's cross-sectional area (Gunreben and Bogdahn, 1991).

Muscle hypertrophy

Hypertrophy of muscle fibres is often physiologic and desirable (Hulland, 1993). Highly trained animals such as horses and greyhounds have many more fibres in strategic places and have slightly larger fibres. The process of hypertrophy of fibres is accomplished by adding sarcomeres, myofilaments to the periphery of myofibrils, and by adding new myofibrils to existing ones by a process of longitudinal splitting (Hulland, 1993).

Myositis

Myositis is a general term used to denote inflammation of muscle (van Holsbeeck and Introcaso, 1990). It can occur as a result of trauma, infection, or systemic disease. Ultrasound is particularly valuable in the early diagnosis of bacterial myositis, when the clinical picture is still nonspecific. Muscle fibres become relatively hyperechoic, the fibroadipose septa are distended with inflammatory exudate and appear relatively hypoechoic. Involved muscles are increased in diameter (van Holsbeck and Introcaso, 1990).

Cellulitis

Cellulitis is an ill-defined process generally involving the subcutaneous fat, which appears swollen and hypoechoic with widely scattered echoes (Craychee, 1995). Ultrasonographic findings in inflammatory processes involving muscle will obviously depend on the type of process and on the stage at which the examination is performed (Adams, 1975). Subcutaneous cellulitis is characterised by a thickened subcutaneous space in a diffuse infiltration of hypoechoic areas and an increase in the size of the veins (Fornage and Rifkin, 1988). Cellulitis without abscess formation appears as a diffuse increase in echogenicity associated with a decrease in the definition of normal anatomic structures (Wisner *et al.*, 1995).

1.3.2.4 Healing of muscle injury

Regeneration is a unique adaptation of skeletal muscle that occurs in response to injury. A review on the regeneration of the skeletal muscle fibres has been written by Carlson and Faulkner (1983). One of the long unrecognised adaptive responses of skeletal muscle is its ability to regenerate after injury. It was commonly believed, until recently, that skeletal muscle fibres were unable to repair themselves after damage caused by injury or disease.

Muscle cells which compose of myofibrils have the capability of regenerating if they are not strangulated by extensive fibrous tissue (Peacock and Van Winkle, 1970). Individual muscle fibres do not undergo cell division and do not contribute to the healing process. If the basic unit of muscle fibre is destroyed, regeneration does not take place. A small population of morphologically undifferentiated (satellite) cells that lie adjacent to the muscle fibres may form myoblasts and may contribute to muscle regeneration. The myofibrils of muscle fibres are capable of regeneration if the muscle is anatomically apposed, so that scar tissue development is minimal and the muscle fibre is not strangulated by fibrous tissue. The ability of the muscle to regenerate is greater when its continuity is not completely disrupted, then when the muscle is completely injured (Peacock and Van Winkle, 1970).

Repair of transected muscle occurs predominately by invasion of the wound and haematoma with capillaries and fibroblasts from the muscle or surrounding tissue. Fibrous protein is deposited and results in scar tissue and adhesion formation. Careful apposition of the muscle segments enhances healing by maximum muscle regeneration, minimum scar tissue, and minimum adhesions. Stress or movement during the early stages of repair may increase the amount of fibrous tissue deposition, scar tissue, and adhesions (Peacock and Van Winkle, 1970).

The role of ultrasound in the evaluation of healing muscle injury lies in three areas. First is the assessment of the extent of injury, second is the stage of healing, and the final role is the assessment of the magnitude of the scar formation (van Holsbeck and Introcaso, 1990). The earliest detectable change toward healing is increased echogenicity of the margins of the wound. These hyperechoic bands will progressively increase in thickness as healing proceeds, and eventually the entire cavity will be filled in. Over a period of weeks the region will demonstrate further organisation, and more normal muscle architecture can be identified (van Holsbeck and Introcaso, 1990). The scar tissue is primarily collagenous in composition and appears more echogenic than the surrounding muscle tissue, to varying degrees, depending on the severity of the fibrosis (Craychee, 1995). Ossification of the scar tissue can occur, and appears brightly echogenic with acoustic shadowing (Craychee, 1995).

In a study of healing of a partially ruptured gastrocnemius muscle in a rat (Lehto and Alanen, 1987), the injured area and development of an haematoma were visualised during the first 5 days after trauma with ultrasonographical and histological observations. Later, disorganisation of regenerating muscle fibres appeared ultrasonographically more clearly than the scar tissue area demonstrated histologically.

1.3.2.5 Ultrasonography of wound healing

Ultrasonography has been shown to be highly effective for the early recognition of post-operative haematoma formation after hip and femoral shaft surgery (Glacer *et al.*, 1988). Ultrasonographic evaluation of the early post-operative incisional sites in dogs has been reported (Trout *et al.*, 1994). The most common clinical sign in wounds that developed early post-operative incision-site complications was swelling of the surgical site. Ultrasonography of the dogs that developed early post-operative complications at the incision-site revealed fluid accumulation, distal enhancement associated with fluid accumulation, disruption of muscle fibres and gas accumulation. Fluid accumulations were anechoic and poorly demarcated. Fluid of mixed echogenicity that contained hyperechoic, floating material was suggestive of an abscess. Using ultrasonography, muscle fibre disruption was difficult to assess in dogs with incision-site complications (Trout *et al.*, 1994).

The use of ultrasonography to monitor the healing of ventral midline incisions after exploratory laparatomy in 21 ponies has been reported (Wilson *et al.*, 1989). The complications observed included drainage, para-incisional oedema, suture sinus formation, suture abscess, superficial dehiscence and incisional hernias. The incision lines could be detected initially but after two to three weeks the exact location of the line was not usually ultrasonographically discernible.

1.3.3 Ultrasonography of foreign bodies in muscle

Foreign body detection in skeletal muscle by means of ultrasonography has been reported in animals and humans (Cartee and Rumph, 1984; Little *et al.*, 1986; Fornage and Schernberg, 1986; Fornage *et al.*, 1987; Gooding *et al.*, 1987; Dik, 1990; Shah *et al.*, 1992). In humans, foreign bodies occur most often in the hands and feet, and in decreasing order of frequency, include fragments of wood, glass, and metal (Anderson *et al.*, 1982, Harcke *et al.*, 1988).

Ultrasonography can demonstrate foreign bodies that are invisible on radiographs such as wood (Little *et al.*, 1986; Gooding *et al.*, 1987; Shah *et al.*, 1992). A foreign body normally shows as an hyperechoic foci with shadow or reverberation artefacts on ultrasonography (Fornage and Schernberg, 1986; Shah, *et al.*, 1992), or comet tail artefact which is often associated with a metallic object (Ziskin *et al.*, 1982). The best example is the Kirschner wire which is identified as a bright echogenic object with comet tail artefact on ultrasound (Fornage and Rifkin, 1988). Reverberation artefact is produced with all different types of metallic foreign bodies, while wood and pencil graphite produce acoustic shadowing (Shah *et al.*, 1992). Foreign bodies are best identified when located in a homogeneous or slightly hypoechoic area such as in fat or muscle (Fornage and Schernberg, 1986). Frequently, the configuration and size of the foreign bodies cannot be determined because only the proximal surface of the foreign body is evident (Kaplan *et al.*, 1990); the distal wall being obscured by the artefacts. Ultrasonography is considered superior to radiographs not only for the demonstration of nonopaque foreign bodies but also because of the ability to localise a foreign body in three dimensions (Fornage and Schernberg, 1986).

1.3.4 Ultrasonography of bone

1.3.4.1 Anatomy

Bone is primarily formed by intramembraneous ossification by which the flat bones of the skull are developed, or by endochondral formation such as the formation of long bone (Alexander, 1985). Bone consists of cells in a specialised intercellular matrix called osteoid. It comprises about one-third of organic and two-third of inorganic material (Evans, 1993). Their main functions are for support and protection while providing levers for muscular action. They also serve as a storehouse for minerals and as a site for fat storage and blood cells formation (Evans, 1993).

There are two types of bone structure. The compact or dense, forms the outer shell of all skeletal parts, while spongy or cancellous, occupies the interior of the extremities of all long bones. The periosteum is an outermost and investing layer of connective tissue that covers the nonarticular surfaces of all bones. The endosteum is similar in structure to periosteum but is thinner. It lines the large medullary cavities, being the condensed peripheral layer of the bone marrow. Both periosteum and endosteum provide cells (osteoblasts) that aid in repair of injury (Evans, 1993). Osteoblasts do not divide and their primary function is to synthesise and secrete the organic matrix of bone. Osteocytes are actually osteoblasts that have become engulfed in the matrix that is being synthesised (Alexander, 1985).

1.3.4.2 Fracture of bone

Bone fracture can be defined as a complete or incomplete discontinuity or break in a bone (Burk and Ackerman, 1996). Fracture is categorised as simple or closed when there is no communicating wound to the outside, or as open, sometimes called compound, when the fracture is exposed (Alexander, 1985). It is called complete or incomplete when classified according to the extent of bone damage or patterns of fracture (Alexander, 1985). A complete fracture has total disruption of the continuity of bone. When only single fracture lines present, it is called transverse, oblique, spiral or longitudinal according to the direction in relation to the bone. When there are several fracture lines, they are called comminuted or multiple in which several fracture lines are in communication at a common point in comminuted fracture, while in multiple fractures the bone is fractured into three or more pieces that do not meet (Alexander, 1985).

Fracture of long bones due to accidental injury are quite common in small animals (Denny, 1978; Philips, 1979; Lang, 1980). Denny (1978) and Philips (1979) agree that the majority of bone fractures in small animals involve animals of less than 3 years of age. A number of papers have been published on the incidence of the bone fracture in specific regions in dogs such as the fore limb (Ormrod, 1966), the hind limb (Singleton, 1966), the pelvis (Bennett, 1975; Denny, 1978) and the femur (Alcantara and Stead, 1975; Lee, 1976).

Pelvis

Structurally, the pelvis is formed by the ossa coxae, the sacrum, and the first coccygeal vertebra. The os coxae is composed of four distinct bones namely, ilium, ischium, pubis, and acetabular bone. These bones fused during the twelfth postnatal week, forming the socket called acetabulum, which receives the head of the femur in creation of the hip joint (Evans, 1993).

The term “pelvis fracture” usually refers to fractures of any of the three pelvic bones, as well as to those involving the acetabulum. Pelvic fractures are relatively common, accounting for approximately 20 to 25% of all fractures, with the ilium as the most common bone involved (Alexander, 1985). Most pelvic fractures are the result of direct trauma with the road traffic accident as the major cause (Denny 1978; Philips 1979). Fractures of the pelvis are often multiple but are seldom compound. Displacement is variable, and seems to depend somewhat on the violence of the original force (Alexander, 1985).

Fractures of the pelvis can occur at different positions and more than one fracture site (Denny 1978), and are frequently comminuted (Singleton 1966; Philips 1979). Although certain combinations of the fracture sites were observed such as fracture of the ipsilateral ilium, pubis and ischium, no specific combination could be predicted (Denny 1978).

Femur

The femur (*os femoris*) is the heaviest bone in the skeleton. Proximally it articulates with the os coxae forming a flexor angle of 110 degree cranially, and distally with the tibia forming a flexor angle of 110 degree caudally. The femur head (*caput femoris*) is smooth and nearly hemispherical, supported by a neck and trochanters The shaft or body is nearly cylindrical, and is straight proximally and arched distally (Evans, 1993).

The femur is one of the most frequently fractured bones in the dog, accounting for approximately 25% of all fractures reported in a series of 4146 cases seen at the Small Animal Clinics of the New York State College of Veterinary Medicine (Alexander, 1985). As in pelvic fracture, the major cause of femur fracture is due to road accidents (Philips 1979). Alcantara and Stead (1975) found that most fractures occurring in animals were with open epiphyses. However incidence is more common n the cat than in the dog. In young animals, fracture of the distal femur is more common. Beyond two years of age, distal diaphyseal fractures occurred almost exclusively.

Humerus

Proximally it articulates with the scapula in forming the shoulder joint and distally it articulates with the radius and ulna in forming the elbow joint (Evans, 1993). The body of the humerus varies greatly in shape and size, depending on the breed (Evans, 1993). Fracture of the humerus represent 6.9% of the total fractures seen in dogs (Alexander, 1985).

1.3.4.3 Healing process

Some researchers noted that the repair process starts some distance away from the end of the fracture fragments at a point where the circulation is intact (Buttler, 1975; Harris, 1990). Fracture healing needs an adequate blood supply, and if the blood supply has been compromised as a result of injury, or the fracture involves a bone with a poor blood supply, fracture healing will be delayed (Ackerman and Silverman, 1978).

The healing of a traumatic fracture is a complex process which comprises a progressive sequence of changes. There are several overlapping processes of bone healing, namely, inflammation, soft callus formation, hard callus formation and remodelling. The term 'soft callus' appears to be contradictory in that 'callus' implies hardness (Latin *callum* or *callus* = hard integument); it can be defined as *the soft, collagenous, revascularizing, osteogenic blastoma which unites the bone fragment and from which the bone regenerates* (Williams *et al.*, 1989).

When a fracture occurs the periosteum is torn and may be stripped for a variable distance from the bone ends (Vaughan, 1966). An inflammatory oedematous response to the soft tissues as well as to the bone begins immediately after fracture, and within a very short time mobilisation and proliferation of fibroblasts occurs in the outer layer of the periosteum (Buttler, 1975). Periosteal proliferation usually becomes evident within 10 to 14 days after injury. However, in growing animals, periosteal proliferation may be evident as early as 3 to 5 days (Burk and Ackerman, 1996).

Rupture of the blood vessels in the periosteum, the bone marrow and frequently those in the adjacent soft tissue cause the environment of fracture to become hypoxic and acidic, resulting in osteocytic disruption and the release of lysosomal enzymes, followed by tissue necrosis at and close to the site of injury (Williams *et al.*, 1989). The resultant haemorrhage coagulates after 6-8 hours and produces a large haematoma which contains fragments of bone, periosteum, muscle fascia and bone marrow. Most of these fragments degenerate and are removed by phagocytes. During this phase, osteoclasts and macrophages erode necrotic bone and remove tissue debris from the fracture site. Mast cells, polymorphonuclear release mediators stimulate the proliferation of reparative cells, i.e. osteoblasts, endothelial cells and in some circumstances chondroblasts. As inflammation is overlapped by soft callus formation, cells near the fracture site are induced to develop into osteoblasts which produce new bone (Williams *et al.*, 1989).

The haematoma then undergoes organisation and is gradually replaced by granulation tissue. The granulation tissue develops into loose connective tissue. The fibroblasts at this time produce numerous collagenous fibres mostly parallel to the long axis of the bone and in this manner the *fibrous* (temporary) *callus* is formed (Vaughan, 1966). The time taken for the haematoma to become organised and replaced by granulation tissue varies, depending mostly on its size. Vaughan (1966) reported that it could be completed in 7 days or take as long as 30-60 days while Williams *et al.*,(1989) reported that it occupies approximately three or four weeks. A soft tissue blastoma of soft callus develops around and between the fragments of bone, reducing their mobility. The soft callus contains proliferating osteoblasts, fibroblasts and osteochondroblasts, embedded in a matrix, rich in glycoproteins and collagen, into which new blood vessels grow (Williams *et al.*, 1989). The external soft callus is derived from the proliferation of osteoblasts in the osteogenic layer of periosteum, while the internal soft callus from endosteal cells. The enhanced proliferative activity of the osteogenic layer of the periosteum extends beyond the immediate fracture site, elevating the overlying fibrous component of the periosteum and producing a collar-like soft external callus which unites the bone fragments from the fracture site (Williams, *et al.*, 1989). The blood is supplied to the fracture site initially by the periosteum, but later in the regenerative process the normal centrifugal blood flow from endosteal circulation is re-established. The external and internal surface of the soft callus are electonegative throughout this process (Williams *et al.*, 1989).

Hard callus formation is started when the external and internal soft callus are gradually converted into woven bone mainly by endochondral ossification, unless the fracture is immobilised with a compression plate, when intramembraneous ossification predominates (Williams *et al.*, 1989). There is no specific cell responsible for the deposition of bone (Vaughan, 1966). Any connective tissue cells of the periosteum, endosteum or marrow reticulum may differentiate into osteoblasts and produce spongy bone. The trabeculae of the spongy bone are formed in an irregular interwoven pattern and consequently this tissue is referred to as "woven bone" (Vaughan, 1966). The trabeculae of the immature bone of the primary bony callus are next removed by osteoclastic resorption and are replaced by adult, lamellar bone in which the lamellar are formed in a closed parallel arrangement (Vaughan, 1966). Both cellularity and vascularity continue to increases as the oxygen gradient is maintained. The pH of the matrix of the callus gradually increases to the neutral level during this phase. This stage commences at about three or four weeks after injury and continues until attainment of firm bony union, about two or three months later for most adult human long bones (Williams *et al.*, 1989).

In the final phase of the reparative process the bone is remodelled by the resorption of excess callus until the original contour of the bone is re-established and the medullary cavity is re-canalised. This reconstruction is slow and may take many months (Vaughan, 1966). This phase overlaps with the formation of hard callus. As a result of changes in vascularity, the oxygen supply of the fracture site returns to normal. Remodelling can be considered to be complete when the fracture site can no longer be identified either structurally or functionally (Williams *et al.*, 1989).

1.3.4.4 The rate of healing

The healing rate of bone fracture has been well discussed (Vaughan, 1966). The average clinical evidence of union in uncomplicated diaphyseal fracture in dogs is 3-4 weeks. No movement can be detected between the bone ends at this time and the soft tissue swelling has subsided. Deep palpation at the fracture area may cause pain and there may be no more than a 50 per cent return of limb function. Secondary bony callus is slowly formed and the process of consolidation may not be completed for 12-16 weeks. A useful indication of the time needed for fractured bones to regain normal strength may be obtained from an experimental study on rabbits in which Falkenberg (1961) found that the absolute tensile strength of a fractured radius was 50 per cent of normal on the 80th day. From these observation, it is imperative that most diaphyseal fractures should be fully supported beyond the stage of primary bony callus and preferably for a period of 6-8 weeks (Vaughan 1966).

The rate at which a fracture heals depends upon the animal's age, general health and nutrition, the blood supply to the bone, and the stability of the fragments (Burk and Ackerman, 1996). As a result, fractures in young, growing animals, in areas with a rich blood supply, and those that are rigidly immobilised heal more rapidly (Burk and Ackerman, 1996). In aged animals healing is slower and clinical union may take 8-16 weeks (Vaughan, 1966). Fractures in cancellous bone , as at the proximal and distal extremities of long bones, usually heal more rapidly than those in the cortical bone of the diaphyses. Similarly, union is quicker in oblique and spiral fractures because there is a large vascular area to promote tissue growth. When fragments are impacted, union is more rapid than when there is a gap between them. It appears that the healing rate is also subject to individual variation since fractures identical in position and type do not necessarily heal in the same time. In pathological fractures the healing time may be greatly disturbed depending on the cause of the change in bone structure. Conditions included in this category are neoplasm, osteoporosis, hyperparathyroidism, rickets and osteomyelitis (Vaughan, 1966).

1.3.4.5 Primary bone healing

Primary bone healing occurs when a fracture is accurately reduced and rigidly fixed (Buttler, 1975). Thus, healing occurs without any significant external callus formation and the fracture site becomes difficult to recognise. A prerequisite for primary bone healing is that the fragments remain stable in the fracture site, at least during the initial stages of bone healing to eliminate any micro movement (Buttler, 1975). Some motion and interfragmentary strain will occur when a small gap is present, even if a heavy plate is used, which results in resorption of the contact surface (Buttler, 1975).

1.3.4.6 Complications of fractures

The complications of fractures has been divided into general and local (Hickman, 1966). General complications comprise the conditions such as shock, fat embolism and hypostatic pneumonia. Local complications are divided into those that occur early i.e. at the time of the accident and those that develop later. Early complications comprise local soft tissue injuries, the severance of major arteries, veins and nerves, the involvement of joints and if the fracture is compound, infection. Late complications develop consequently upon treatment and during the process of healing. This is the most important group and is subdivided into mal-union, delayed-union, non-union and other miscellaneous groups.

Infection interferes greatly with the healing process because of damage to the tissues at the fracture site, and the hyperaemia associated with infection may persist for a long time (Vaughan, 1966). Re-ossification cannot begin until the infection is removed, and the hyperaemia has subsided. Most infected fractures will unite once the infection has been cleared, but in some instances result in non-union (Vaughan, 1966).

Mal-union

The term mal-union implies that a deformity is present although the fracture has healed satisfactorily. This is due to such factors as poor reduction and alignment, inadequate immobilisation and artificial fusion of the epiphyses (Hickman, 1966).

Delayed-union / non-union

Delayed union can be defined as the condition that exists in a fracture that is not healing in the time normally required for that particular bone and that type of fracture (Aron, 1983). In the majority of cases healing progresses normally but at slower rate than is usual (Hickman, 1966) whereas non-union can be defined as the condition that exists in a fracture in which signs of repair have ceased (Aron, 1983), and will not occur without surgical intervention (Hickman, 1966). It is generally attributed to such factors as infection, hyperaemia which is precipitated by movement, foreign body reaction, avascular necrosis, interpositioning of soft tissues and distraction (Hickman, 1966). Some of the factors such as the actual site of the fracture, soft tissue damage, displacement fragments, loss of bone substance, open wounds and infection are the direct result of the accident and beyond our control (Hickman, 1966). Multiple forces such as bending, shearing and rotation, destruction and overriding, inadequate blood supply, a gap between fracture fragments, damage to the blood supply that involves a nutrient artery, and infection caused by contamination from the original trauma or at the time of fracture repair, are the major causes. The less common causes are osteoporotic bones of old age, poor nutrition and resulting negative nitrogen balance, metabolic effects, usage of corticosteroids or anticoagulants, and radiation (Aron, 1983). Non-union was observed in the radius and ulna, femur, tibia and humerus (Philips, 1979).

Osteomyelitis

Osteomyelitis is defined as an inflammation of the bone marrow and adjacent bone (Caywood, 1983). It occurs as a result of infection and sometimes following local radiation therapy, implant corrosion, or trauma (Caywood, 1983). Post traumatic osteomyelitis is an infection of bone after trauma or surgery to the bone, tends to remain localized to the bone and is not a systemic condition (Braden, 1991). Infection during surgical repair of a fracture is commonest cause of osteomyelitis in dogs (Vaughan, 1975). Long bones such as the femur and humerus are frequently affected. Loosening of implants, with consequent loss of fracture immobilisation, is a common feature. Screws become less securely embedded and the plate may lift off the bone. Bone lysis is sometimes evident immediately adjacent to the implant (Vaughan, 1975). The pathological changes of infected bone vary in degree and extent. A slight change is first suspected when a fracture site becomes increasingly painful 7-10 days after operation (Vaughan, 1975). Acute inflammatory response results in the production of exudate containing bacteria. In severe cases, sinuses appear and discharging pus or a straw-coloured fluid. Within 2 or 3 weeks of surgery complete disruption of the fracture commonly occurs. Screws and plates become detached and lie free in the adjacent soft tissues (Vaughan, 1975). On radiography, the presence of a small amount of periosteal reaction and increased radio-density of adjacent soft tissue can be detected within the first 2 weeks. By the third and fourth week excessive periosteal reaction near the bone ends is seen extending some distance away from the fracture site (Vaughan, 1975). The fracture line appears wide because of rarefaction of the bone ends (Vaughan, 1975).

1.3.4.7 Ultrasonography of bone, bone fracture and its healing

The ultrasonographic appearance of bone is an intensely hyperechoic line with acoustic shadowing deep to the interface due to the reflection and absorption of sound waves (Kramer *et al.*, 1997). Bone fractures can be evaluated ultrasonographically. However, the exact relation of the fracture ends is difficult or impossible to assess, because there are no points of orientation (Kramer, *et al.*, 1997).

The use of ultrasound to detect and confirm a pelvic fracture in horses with severe hind limb lameness has been reported (Reef, 1992). The fracture site can be identified as shown by bony discontinuity. The area of muscle disruption and haemorrhage with multiple fragments around the fracture site were also demonstrated. Ultrasonography can build up a three-dimensional image of the injured area by manipulating the probe (Smith and Webbon, 1994). Thus, nondisplaced or incomplete fractures can be identified ultrasonographically, although with difficulty. Ricciardy *et al.* (1993) reported that the ultrasound image is directly correlated with consolidation of the fracture site and in relationship to callus remodelling. The intensity of reflected echoes and the visualisation of the longitudinal artefact structure are significantly related to the calcification process of the periosteum (Ricciardy *et al.* 1993). The variations of reflected echo demonstrate a correlation between the ultrasound image and mechanical status of external callus (Ricciardy *et al.* 1993).

Ultrasound gives important information about the soft tissues surrounding the fracture site, and indicates callus formation at an early stage (Maffuli *et al.*, 1992; Eyres *et al.*, 1993; Maffuli and Thornton, 1995). Ultrasound is also more sensitive than conventional radiography at showing the early phases of organisation of the callus, and its disorganised echo pattern at the fracture site of patients with non-union (Maffuli and Thornton, 1995).

The progress of fracture healing can be assessed ultrasonographically. Initially, the unmineralised callus can be identified between two ends of bone. As healing progresses, mineralised callus is identified casting an acoustic shadow (Smith and Webbon, 1994). Immature callus can be seen ultrasonographically before it is visible radiographically (Young *et al.*, 1990; Derbyshire and Simpson, 1992). The ultrasonographic appearance of the new bone consist of echogenic foci within the distraction site, which become aligned in the longitudinal plane and increase in number and size until they coalesce as echodense bone (Young *et al.*, 1990; Maffuli *et al.*, 1992). Periosteal callus is seen in the vicinity of the acute fracture as an irregular contour. Ricciardi *et al.* (1992) found that there was a direct correlation between ultrasonographic changes and the calcification of the periosteal callus. There was also a correlation between the morphologic development visible on ultrasound and the stage of the callus formation (Ricciardi *et al.* 1992).

1.3.5 Ultrasonography of the canine mammary glands

1.3.5.1 Anatomy

The mammary gland (*Glandular mammaria*) is a modified cutaneous glands and is an accessory gland of the skin (Evans and Christensen, 1993). It consists of epithelial glandular tissue (*lobuli glandulae mammariae*), connective tissue, and the covering skin (Evans and Christensen, 1993). Embryologically, mammary glands are first seen in the form of bilateral linear thickenings of the epithelium extending from the axilla to the inguinal region. This continuous ridge breaks up into a number of discrete parts, each of which in time gives rise to a single gland (Silver, 1966). The great majority of the mammary region is occupied not by glandular tissue but by relatively dense stroma and fat (Silver, 1966). The lactating organ in the female is a compound tubulo-alveolar system supported by connective tissue stroma and covered by slightly modified skin (Silver, 1966).

Mammary glands are typically arranged in two bilaterally symmetrical rows extending from the axillary to the inguinal regions (Evans and Christensen, 1993). The formation of mammary glands is not always symmetric, and uneven numbers of functional mammae are common (Evans and Christensen, 1993). The number of glands varies from 8 to 12, with 10 being the most commonly encountered (Evans and Christensen, 1993), although there may be four mammae on one side and five on the other (Adams, 1986). Thoracic glands are adherent to the underlying pectoral muscles with relatively little intervening areolar connective tissue, abdominal glands are attached loosely to the underlying fascia by loose areolar and adipose tissue while inguinal glands are suspended from the body wall by an extension of the cutaneous trunci muscle and surrounded by abundant adipose tissue (Evans and Christensen, 1993).

1.3.5.2 Lymphatic drainage

Lymphatic connections between all mammary glands have been described previously (Habel, 1978; Miller *et al.*, 1979). Details of the lymph drainage of the mammary glands in the bitch have been given by various anatomists (Silver, 1966; Sautet *et al.*, 1992; Patsikas and Dessiris, 1996a, 1996b).

Earlier studies reported that there are two drainage areas for mammary glands generally, i.e. a cranial drainage area, formed by cranial and caudal thoracic glands and cranial abdominal gland which drain into the axillary lymph node, and a caudal drainage area where caudal abdominal, inguinal, and occasionally, cranial abdominal glands drain into the superficial inguinal lymph node (Silver, 1966; Fidler and Brodey, 1967). There is sometimes a connection between the lymphatic drainage of the cranial and caudal pairs of abdominal glands and, if this is present, it allows the possibility of retrograde lymphatic spread of tumour tissue from thoracic to inguinal regions and vice versa (Silver, 1966). Recently, a study conducted by Sautet *et al.* (1992) found that the cranial thoracic gland always drained to the axillary lymph node, caudal thoracic, cranial and caudal abdominal glands drained to both the axillary and superficial inguinal lymph nodes, while the inguinal gland drained to the superficial inguinal lymph node only. Glands draining to contralateral lymph nodes were not found and there was also no evidence of lymph vessels connecting the two rows of mammary glands.

Patsikas and Dessiris (1996a) reported that lymph from the caudal abdominal and inguinal mammary glands usually drains into the superficial inguinal lymph node and this observation supports the previous finding. Direct lymphatic connection between the caudal abdominal and inguinal mammary glands was not demonstrated. However, they have found indirect lymphatic connection between the caudal abdominal and inguinal mammary glands through the superficial inguinal lymph node. They concluded that lymph can pass from one gland to another, through their common regional lymph node, by retrograde flow. Furthermore, they have found a lymphatic connection of superficial inguinal lymph nodes between both sides. However, lymphatics of the mammary glands that cross the midline were not demonstrated.

1.3.5.3 Tumours of the canine mammary gland

The reports on the mammary gland tumours in dogs have been well documented in the literature (Anderson and Jarret, 1966; Fowler *et al.*, 1974; Misdorp and Hart, 1979a, 1979b). It is well accepted that the age of the animal plays an important role in the occurrence and development of tumour (Owen, 1966;

Priester, 1979; Zaninovic and Simcic, 1994). The peaks of age that have occurred are at 9 - 10 years (Priester, 1979).

Most mammary gland tumours occur in the posterior (caudal) glands (Anderson and Jarrett, 1966; Bostock, 1986). The exact cause of tumours in this site is unknown, but a good deal of circumstantial evidence indicates that the development of the neoplastic process is influenced by the female sex hormones. This has been supported by fact that hormone imbalance in some dogs of advanced age is the factor responsible for the development and growth of mammary tumours (Evans, 1993). The size of tumour is important in dogs because it is correlated with the histologic pattern. Invasive tumours over 5 cm in diameter are uniformly fatal within a year, while tumours over 5 cm that are not invasive are almost all behaviourally benign (Yager and Scott, 1993). Tumours that have been present long enough to be that large, and yet still have exhibited no clinically obvious spread, are almost certain to be benign mixed mammary tumours (Yager and Scott, 1993).

Early studies has shown that regional lymph nodes (axillary and superficial inguinal) are the most common seat of secondary tumours (Cotchin, 1954). Malignant spread of tumour of the anterior glands (cranial and caudal thoracic glands) always have axillary lymph node metastasis, however there was evidence that the superficial inguinal lymph node also could be involved (Fidler and Brodey, 1967). Owen (1966) reported that clinically detectable lesions of the regional lymph nodes (superficial inguinal and axillary) occur in relatively few bitches with mammary gland tumours and may indicate metastatic tumour spread or simply lymphadenitis or lymphoid hyperplasia consequent upon tumour breakdown. In addition, absence of palpable enlargement of lymph nodes does not necessarily indicate freedom from metastatic spread of the tumour. In one study, Fidler and Brodey (1967) showed that 62% of the bitches with mammary tumour had regional (axillary and superficial inguinal) lymph nodes involvement. However, this result was based only on examination of 1 or

2 sections of each node. Undoubtedly, if the lymph node were serially sectioned,
the percentage of the bitches which had positive nodes would be increased.

Malignant mammary tumours

Malignant tumours often metastasize, invade basement membranes, and are composed of anaplastic cells with a high mitotic rate (Hargis, 1995). Anaplastic cells are pleomorphic, have large vesicular nuclei with an increase in size and number of nucleoli, and have less organelles (Hargis, 1995). Malignant cells develop surface alterations that allow invasion, implantation, and metastasis via blood or lymph vessels (Hargis, 1995).

The speed of growth is the most useful factor in the clinical assessment of malignant tumours (Else and Hannant, 1979). Some carcinomas may appear to be encapsulated on palpation (Anderson and Jarrett, 1966). This is because the tumour compresses the adjacent mammary tissue, forming an interface which feels like a capsule and gives the impression that the tumour is well encapsulated (Anderson and Jarrett, 1966). Another sign of malignancy is direct attachment of the tumour to the overlying skin, so that it cannot be moved under the skin. Infiltration of the skin may be a marked feature, causing thickening and ulceration (Anderson and Jarrett, 1966). Another important indication of malignancy is the spread of tumour to the regional lymph nodes. The spreading may follow the lymphatic drainage of the affected glands (Anderson and Jarrett, 1966) as has been reviewed under section 1.3.5.2. Several researchers found that malignant mammary neoplasm is more common than benign mammary neoplasm (Priester, 1979; Zaninovic and Simcic, 1994). However, Bostock (1986) found that the incidence of benign tumour (51%) was more than malignant (49%).

Benign mammary tumours

Most of the benign mammary tumours have a slow growth rate and are normally sharply demarcated from the surrounding tissue. They are freely movable without infiltration and occasionally are distinctly pedunculated. The covering skin can be moved over the tumour (Owen, 1966). Benign neoplasms do not metastasize, do not invade the basement membrane, grow by expansion so are circumscribed, and are composed of well differentiated cells that closely resemble the cells of tissue in origin (Hargis, 1995). Mammary epithelial neoplasms in bitches are behaviourally benign in at least 80% of cases (Yager and Scott, 1993).

1.3.5.4 Ultrasonography of soft tissue tumours

A large number of tumours and tumour-like lesions can be identified ultrasonographically within the soft tissues (Harcke *et al.*, 1988). These include benign soft tissue tumours as well as malignant lesions. However, the difference in the nature of these lesions does not appear to be significant ultrasonographically (Harcke *et al.*, 1988). This has been supported by Wisner *et al.* (1994) who reported that the ultrasonographic characteristics of benign and malignant lesions may be similar and they suggested that definitive diagnosis by ultrasound examination alone is unlikely. The tumours usually present as well-defined, complex masses or as solid masses consisting of medium -level echoes (Harcke *et al.*, 1988). Most soft tissue tumours are hypoechoic relative to surrounding tissue, except fat containing tumours which are occasionally hyperechoic (Vincent, 1988). Solid tumours appear as more or less hypoechoic and homogenous masses with more or less regular contours. However, this does not provide a clue to the histological type (Fornage *et al.*, 1985). Ultrasonography can readily determine the liquid or solid content of a soft tissue tumour (Fornage and Rifkin 1988; Kramer *et al.*, 1997). Additionally, its deep extension, its accurate size, and its relationship with the adjacent structures can be ascertained (Fornage *et al.*, 1985).

The mass lesions can be differentiated by differences in their echo patterns (Tamura, 1992). Malignant tumours showed irregular margins and are less homogenous, usually with a focal hypoechoic area (Tamura, 1992). Additionally, muscle fibre disruption, and infiltration of adjacent tissues, can be identified (Craychee, 1995). Benign tumours often have a homogenous echopattern, regular margins, and displacement or spreading, rather than rupture of adjacent muscle fibres (Craychee, 1995).

There are no ultrasonographic criteria using B-mode imaging alone which give any information regarding the aggressiveness or type of a tumour. The only exception is the lipoma, which has a characteristic ultrasonographic appearance; background pattern is nearly anechoic, with diffuse hyperechoic foci and widespread lines (Kramer *et al.*, 1997).

1.3.6 Ultrasonography of the lymph nodes

1.3.6.1 Anatomy

Lymph nodes are intercalated in the course of the lymph vessels and consist of an accumulation of lymphatic tissue enclosed by elastic fibres and smooth muscle fibres (Bezuidenhout, 1993). In the human, lymph nodes are small, oval or reniform bodies, 0.1 - 2.5 cm long (Williams *et al.*, 1989). In animals, they are vary widely in size, some being microscopic, others many centimetres in length, depending on size of animals and their location (Bezuidenhout, 1993). Each usually has a slight indentation on one side, the hilus, which is usually not prominent and, through which blood vessels enter and leave, and an efferent lymphatic vessel emerges (Bezuidenhout, 1993). Several afferent lymphatic vessels enter peripherally. Near the centre of the lymph node the trabeculae become finer and form a meshwork of connective tissue. Beneath the fibrous capsule and around the trabeculae and septi extends a very complex system of lymph sinuses which separates the connective tissue from the lymphoreticular parenchyma. The lymphatic tissue fills the space between the septi and trabeculae. Lymph nodes are traditionally divided into three regions namely, superficial cortex, the deep cortex or paracortex, and the medulla (Evans, 1993). Lymph node parenchyma appears to be lighter at the centre and darker at the periphery when stained with haematoxylin and eosin. The darker sections are due to densely the packed nuclei of the lymphocytes (Evans, 1993). In the human, lymph nodes are particularly numerous in the neck, mediastinum, caudal abdominal wall, abdominal mesenteries, pelvis and proximal regions of the limbs (Williams *et al.*, 1989).

1.3.6.2 Axillary lymph node

The axillary lymph node (*Lymphonodus axillaris*) is usually in the form of a disc with the diameter range from 0.3 to 0.5 cm (Bezuidenhout, 1993). It lies 2 to 5 cm caudal to the shoulder joint in the angle formed by the diverging brachial and subscapular blood vessels. It is bounded laterally by the teres major, medially by the transversus thoracis, and ventrally by the dorsal border of the deep pectoral muscle (Bezuidenhout, 1993). The accessory axillary lymph node (*lymphonodus axillaris accesssorious*), when present lies caudal to the principal node in the fascia between the adjacent borders of the deep pectoral and latissimus dorsi muscles, caudal to the muscles of the brachium. It varies in size from less than 1 mm to 1.5 cm (Bezuidenhout, 1993). The afferent vessels of the axillary lymph node come mainly from the thoracic wall and the deep structures of the thoracic limb. Both the thoracic and cranial abdominal mammary glands of each side have lymphatics which drain into the axillary nodes (Bezuidenhout, 1993). The number of axillary lymph nodes varies in each dog. According to Evans and Christensen (1993), there is usually one axillary lymph node on either side, while Patsikas and Dessiris (1996a,1996b), and Chretien *et al.* (1967) found two axillary lymph nodes on either side.

1.3.6.3 Superficial inguinal lymph node

The superficial inguinal lymph nodes (*lymphonodi inguinales superficialis*) usually two in number, begin a few millimetre cranial to the vaginal process and lie in the fat which fills the furrow between the abdominal wall and the medial surface of the thigh. In the male, right and left nodes lie along the dorsolateral borders of the penis (Bezuidenhout, 1993). When a single node is present, the external pudendal vessels lie lateral to it, but when two nodes are present these vessels usually run between the cranial and caudal poles of the nodes, or the cranial node lies medial to the vessels in a deeper location than the caudal node. Their shape and size vary between wide extremes, but the nodes are usually oval and about 2 cm long (Bezuidenhout, 1993).

The afferent vessels to the superficial inguinal lymph node come from the ventral half of the abdominal wall, including the caudal abdominal and inguinal mammary glands. In the male, the afferent vessels come from the penis and skin of the prepuce and scrotum. Other afferent vessels come from the ventral part of the pelvis, the tail, and the medial side of the thigh, stifle joint and crus. The superficial inguinal lymph nodes receive the efferent vessels from the popliteal node and thus serve as one of the nodal stations for the whole pelvic limb (Bezuidenhout, 1993). The number of superficial inguinal lymph nodes varies in each dog from 1-2 (Schummer *et al.*, 1981), or two and rarely 3-4 (Saar and Getty, 1975), or 3-5 (Chretien *et al.*, 1967).

1.3.6.4 Ultrasonography of normal lymph nodes

Normal lymph nodes are seldom visualised with ultrasound because their echogenicity is similar to that of subcutaneous tissue (Solbiati *et al.*, 1992). Many superficial lymph nodes can be imaged with a high-frequency transducer and a stand-off pad. Most of these lymph nodes are flat and oval, homogenous, and hypoechoic to the surrounding fat and fibrous tissue (Homco, 1996). In one report on the canine regional cervical lymph nodes by Wisner *et al.* (1991), the lymph nodes were characterised as round to oval hypoechoic structures. It is important to bear in mind that they are often indistinct during routine ultrasonographic examination as they tend to be similar in echogenicity to adjacent mesenteric or muscular tissues (Pugh, 1994). Normal lymph nodes have an axial diameter between 2 and 5 mm. (Solbiati *et al.* 1992). Peripheral lymph nodes such as the axillary, superficial cervical, and popliteal appear as mostly hypoechoic oval structures (Cartee and Mahaffey, 1995).

Ultrasonographic examination of normal lymph nodes in the human reveals a central or slightly eccentric echogenic line which is thought to represent fat in the hilum and is called the hilar fat sign (Marchal *et al.*, 1985; Smeets *et al.*, 1990; Mittelstaedt, 1992). This hyperechoic line has been reported in the normal canine medial iliac lymph node and histologically appears to represent fat, fascia, and vessels that are probably near the hilus (Spaulding and Richey, 1993). However, this hilar fat sign has not been demonstrated by Homco (1996), probably because of the extremely small size compared with the human counterparts.

1.3.6.5 Ultrasonography of diseased lymph nodes

Most diseases of the lymph nodes, whether inflammatory or neoplastic, result in some degree of node enlargement, and any change in shape toward a rounded appearance should suggest disease (Smeets *et al.*, 1990). Abnormal lymph nodes generally become hypoechoic as a result of inflammation or infiltration (Saunders *et al*, 1992; Pugh, 1994). Tiny micronodules of disease tissue within the parenchyma may create a grainy appearance (Rubaltelli *et al.,* 1990). Loss of the hilar fat sign has been described in human as an indicator of malignancy (Smeets, *et al.*, 1990), and the presence of central echogenic line (hilum) in enlarged lymph node is a valid criterion of benignity (Rubaltelli *et al.*, 1990). However, in a recent study, Tsunoda-Shimizu and Saida (1997) found that the presence of an echogenic hilum and the longitudinal to transverse diameter ratio were not considered adequate criteria for differentiating malignancy from benignity. Absence of the echogenic hilum can be due to factors other than neoplastic disease, such as fatty replacement (Rubaltelli *et al.*, 1990).

Metastasize to lymph nodes in gastrointestinal cancer in human has been demonstrated to have an hypoechoic structure with well defined demarcation (Akahoshi *et al.*, 1992). Although ultrasound evaluation of lymph nodes cannot definitely discriminate between malignant and benign neoplasm, there are suggestive patterns. Lymph nodes associated with malignant disease are generally larger and more numerous than in benign diseases (Smeets *et al.*, 1990; Mittelstaedt, 1992). Lymph nodes associated with malignant disease are more hypoechoic than those associated with benign disease (Smeets *et al.*, 1990). Most lymph nodes involved in malignant disease tend to develop a round shape, but in benign disease, they tend to retain their original oval or spindle shape despite an increase in size (Smeets *et al.*, 1990).

In a study of metastatic breast tumour in axillary nodes, Feu *et al.* (1997) reported that the hilus usually was hyperechoic in benign nodes, although it could be hypoechoic when there was adipose infiltration. When there was increased vascularization, however, the hilus was hyperechoic. The hypoechoic hilus in those nodes with adipose infiltration was usually distinguished from the cortex by means of a continuous hyperechoic transition line that histopathologically corresponded to fibrovascular tissue that delineated the fat from the lymphatic tissue. When the central zone of the lymph nodes was composed of sinuses and variable amounts of lymphoid tissue but no adipose tissue, it was also seen as a hypoechoic zone if the number of blood vessels was high. The echogenicity seemed to depend more on the number of vessels than on the size of the vessels. Hyperechoic findings at ultrasound were related to a higher number of vascular walls (Feu *et al.*, 1997).

Rubaltelli *et al.* (1990) in a general study of the lymph nodes showed that a linear internal echo pattern was associated with benign lesions. The axial diameter of the lymph nodes was the most accurate dimension in predicting tumour invasion (Solbiati *et al.*, 1992). In normal cervical lymph nodes the diameter range was between 2 and 5 mm. Reactive lymph nodes tended to have an oval shape, whereas metastatic nodes were rounded. There was no specific echopattern indicating the nature of enlarged lymph nodes. Reactive lymph node also tended to be less echogenic than the thyroid gland, with smooth margin and without necrosis or calcifications. Lymph nodes involved with inflammatory or granulomatous disease were usually hypoechoic, anechoic and frequently showed coarse calcifications (Solbiati *et al.*, 1992).

Differentiation of the metastatic lymph nodes from reactive lymph nodes and lymphadenitis can be difficult since their ultrasonographic appearance may be similar (Wisner *et al.*, 1994). Lymph nodes associated with inflammatory processes may be enlarged and appear homogenously hypoechoic. The distinctness of the margins of the nodes will vary depending on whether a significant inflammatory response occurs locally. Oedema fluid and cellulitis may decrease the definition of lymph node borders (Wisner *et al.*, 1995).

CHAPTER 2

GENERAL MATERIALS AND METHODS

2.1 **The animals**

2.1.1 Normal muscle imaging

The animals used in the study of normal muscle imaging were adult, normal greyhound cadavers which had been euthanased for other reasons and collected from the Glasgow area. The greyhound cadavers had been euthanased within 24 hours upon arriving at the Division of Anatomy, Glasgow University Veterinary School. The greyhound cadavers were prepared for ultrasound scanning immediately after arrival. The scanning was carried out within 24 hours of arrival of the cadavers.

2.1.2 Muscle skeletal injury imaging

Twenty three animals (nineteen canine and four feline) with fractures of the long bones (involving either femur, humerus or tibia) or fracture of the pelvic bones were included in this study. The animals used were gathered from orthopaedic cases referred to the Glasgow University Small Animal Clinics (GUSAC) within the period of June 1996 to February 1998. All of these animals had undergone orthopaedic surgery which was carried out by a group of experienced surgeons in the Small Animal Clinic. The methods of fixation included both internal and external fixation techniques. Animals with fractures which were treated with additional external bandaging were not included in this study.

2.1.3 Mammary tumour imaging

Twenty-eight bitches of different breeds with clinical evidence of mammary gland tumour were used in this study. Of the 28 cases, 26 were obtained from the clinical cases referred to the People's Dispensary for Sick Animals (PDSA), Glasgow, and two cases were obtained from the Glasgow University Small

Animal Clinics (GUSAC). The details of breed, age and previous history of each bitch were obtained during consultation and from hospital records. The bitches participating in this study were first examined by a veterinarian before being referred for ultrasonographic examination.

2.1.4 Wound healing imaging

The animals used in this study were collected from the clinical cases referred to the Glasgow University Small Animal Clinics (GUSAC). The animals of different breeds and age which had received abdominal surgery for various reasons were included in this study.

For the preliminary study of the ventral abdominal musculature imaging of female cadavers, thirty one adult female cadavers of different breeds and age which had been euthanased for other reasons were used. The cadavers were collected from the Glasgow area and the dogs had been euthanased within 24 hours upon arrival at the Division of Anatomy, Glasgow University Veterinary School. The cadavers were examined within 24 hours of arrival.

2.2 **Ultrasound equipment**

2.2.1 The scanner

A B-mode real-time ultrasound scanner (Capasee, TOSHIBA) was used in this study. It was portable, being mounted on an adjustable pedestal and fitted with castors which make it easy to be transferred. The scanner possessed a freeze mode, a magnification or zoom mode, and gain setting control to obtain the optimum image. Additionally, the scanner was provided with a press control key board with annotation facilities permitting images to be permanently identified on videotapes and photographs. The same scanner was used throughout the study to obtain the optimum consistency of the images. The scanner was connected to a video recorder (Panasonic). The images were recorded using super VHS video tape during each scanning for revision at a later date.

2.2.2 The transducers

A 7.5 MHz linear array transducer (figure 2.1) was used throughout this study. For the ultrasonographic imaging of the muscles of normal greyhound cadavers both the 7.5 MHz linear array and 3.5 MHz linear-convex transducers were used. The 3.5 MHz linear-convex transducer was used as a comparison. The 7.5 MHz frequency transducer was then selected on the basis of the size and depth of object under examination. The 7.5 MHz transducer produced better resolution on muscle imaging in greyhound cadavers as compared to the 3.5 MHz frequency linear-convex transducer. The axial and lateral resolution were 0.5 and 1 mm respectively for the 7.5 MHz transducer.

2.3 **Prescanning preparation including scanner calibration**

For ultrasonographic examination, the dogs were put on a table. The position of the dog was dependant on which area was to be scanned. For example, the dog was put in dorsal recumbency when scanning the ventral abdominal mid-line and when scanning the mammary glands and its regional lymph nodes; lateral recumbency was selected when scanning the pelvic and pectoral limbs. The hair was clipped prior to scanning. Ultrasound gel was applied to avoid air entrapment and to give a better contact between the transducer and the skin. In the study of the progress of bone healing in chapter 5, the technique of scanning without clipping the hair was applied. This technique required a large volume of gel and the site of scanning was soaked with water prior to applying the ultrasound gel.

Scanning was performed in a semi-dark room in order to maximise the clarity of the images on the screen. The ultrasound scanner and video recorder were connected and relevant identification was annotated on the screen. The machinery was located on the side most convenient for the operator. Prior to every ultrasound examination, the scanner was calibrated; the gain settings for near field, mid field and overall were adjusted to produce the optimum image. The time gain setting was adjusted prior to each scanning and remained constant throughout the scanning. Contrast and brightness were adjusted on the monitor to give best result.

2.4 **Principle of image interpretation and terminology**

Echogenicity is a term used to describe the tissue appearance that results from the composite of the returning echoes detected by the transducer (Ginther, 1986). Echogenic structures created "bright" echoes in black background image. The echogenicity comparison is relative and subjective (Feeney, *et al.*, 1991). Terms used to describe the appearance of ultrasound images should relate to a tissue's echo intensity, attenuation and image texture. A recent publication correlating normal sectional anatomy of the dog with ultrasonographic and computed tomographic (CT) imaging provides an excellent reference for image interpretation (Feeney, *et al.*, 1991). A number of terms used to describe the image in this study are summarised in the following list.

Term	Description
Hyperechoic	Bright echoes, appearing white on conventional scans. Represent highly reflective interfaces. e.g. bone
Anechoic	Absence of echoes, appearing black on conventional scans. Represent complete transmission of sound. e.g. fluid. In fluid-filled anechoic areas, no echoes are detected in the cavity and there is increase sound intensity (far or distant enhancement) beyond the anechoic area. In solid anechoic areas, there is no distant enhancement beyond the anechoic area.
Hypoechoic	Sparse echoes, appearing dark grey on conventional scans. Represent intermediate reflection/ transmission. e.g. soft tissue. There is no distant enhancement beyond the hypoechoic area.
Isoechoic	The echoes that are detected in the mass have essentially the same intensity as those in the area surrounding it, and there is no distant enhancement or shadowing beyond the isoechoic area.

2.5 Recording and photographic system

The scanned images were recorded on high quality super VHS videotapes using a VCR video recorder (Panasonic) with playback facilities. Taped ultrasound scanned images were reviewed later using the Apogee system ultrasound machine which had a high quality viewing monitor. The system had slow motion and freeze frame facilities, so that a significant frame could be selected for further study or photographic purposes.

For documentation, a thermal printer (Sony UP 811) was connected to the viewer using the video outlet and selected frames were recorded onto sensitised paper (Sony UPP 1105) and the frame number was recorded from the viewer counter.

2.6 Technique of ultrasonographic imaging

An assistant was needed during scanning to restrain the dog. Generally, the scanning was done longitudinal and transverse to the muscle fibre direction. The transducer was generally held perpendicular to the skin surface. Details of the technique of ultrasonographic imaging for each experiment is elaborated on in chapters 3, 4, 5 and 6.

2.7 Electronic measurement

Measurements was done by freezing an image on the screen and then measuring using electronic callipers. Measurement was obtained either during scanning or during tape review.

Figure 2.1 A 7.5 MHz linear array transducer used in this study.

CHAPTER 3

ULTRASONOGRAPHIC IMAGING OF SKELETAL MUSCLE IN NORMAL GREYHOUND CADAVERS

3.1 Introduction and aim of the study

Improvement in ultrasound technology and the development of high resolution transducers in recent times have made imaging of the musculoskeletal system in the small animal veterinary field possible. Until now, ultrasonographic imaging of the musculoskeletal system in humans has been well documented (Heckmatt *et al.*, 1988b; Wilson, 1988; Harcke *et al.*, 1988; Fornage, 1989; Kaplan *et al.*, 1990; van Holsbeeck and Introcaso, 1992). In small animal veterinary practice a few articles have been found in the literature (Smith and Webbon, 1994; Craychee, 1995: Kramer *et al.*, 1997). The ultrasonographic appearance of normal skeletal muscle imaged longitudinally is that of an homogenous hypoechoic background with multiple, fine parallel echoes (Kaplan *et al.*, 1990; Kramer *et al.*, 1997). The homogenous hypoechoic background is representing the muscle fibres or muscle bundles, and the multiple, fine parallel echoes represent the fibroadipose septa (perimysium) surrounding the muscle bundles (fasciculi) (Kaplan, *et al.*, 1990). In transverse images the muscles have a moderately circular appearance, with spotted areas of increased echogenicity representing the perimysium scattered throughout a homogenous hypoechoic background (Fornage *et al.*, 1983; Fornage *et al.*, 1987; Gooding *et al.*, 1987). The connective tissue fascia enveloping the muscle appears hyperechoic, separating the muscle groups (Kaplan *et al.*, 1990). Muscle generally appears less echogenic relative to subcutaneous tissue or tendons, and the echogenicity of contracted muscle is often less than that of relaxed muscle (Kaplan *et al.*, 1990).

By using the advance B-mode real time ultrasound scanner (Capasee, TOSHIBA) equipped with an high resolution 7.5 MHz linear array transducer and 3.5 MHz linear array transducer, the present study was carried out with the aim of observing and defining the normal ultrasonographic characteristic of skeletal muscle of the thigh, ventral abdominal, brachial and scapula regions of normal greyhound cadavers. In addition, the images produced by the different frequency transducers were compared.

3.2 Materials and methods

Animals and preparation technique

Adult greyhound cadavers which had been euthanased for other reasons within 24 hours of arriving at the Division of Anatomy, Glasgow University Veterinary School were used in this study. Upon arrival, the greyhound cadavers were examined physically prior to ultrasound scanning. Skin preparation was performed on the thigh, brachial, scapular and ventral abdominal regions immediately after the arrival of the cadavers. The thigh region was prepared from the level of the hip joint to the level of the stifle joint. The brachial region was prepared from the level of the shoulder joint to the level of the elbow joint. The scapular region was prepared from the dorsal border of the scapula to the level of shoulder joint, and the ventral abdominal region was prepared from the level of the xyphoid cartilage to the pubic brim. The hair of these regions was removed using clippers.

For the thigh muscle scanning, the right and left thighs were marked transversely and longitudinally respectively with a permanent marker pen on both lateral and medial aspects of the thigh at two centimetre interval as illustrated in figure 3.1. The marked lines were then identified by numbers. For the brachial and scapula regions, the areas for scanning were marked transversely perpendicular to the body of the humerus and the spine of scapula respectively at two centimetre intervals and identified by numbers (as illustrated in figure 3.2). Similarly, the ventral abdominal region was marked transversely across the mid-line at two centimetre intervals from the pubic brim to the level of the xiphoid cartilage and identified by numbers.

Ultrasonographic imaging

Ultrasonographic imaging was conducted in a semi-dark room. The cadaver was laid on the table in lateral recumbency for scanning of the thigh, brachial and scapular regions, and in dorsal recumbency with all four legs tied to the table legs for scanning of the ventral abdominal region. Ultrasound gel was applied to the skin prior to scanning. The transducer was then applied directly in contact with the skin surface. The scanning was done on both lateral and medial aspects of the thigh and brachial regions, on the lateral aspect of the scapula region, and on the ventral abdominal region according to the marked lines.

To scan the thigh muscles, the transducer was moved slowly but firmly from caudal to cranial aspect in transverse scans, and from proximal towards distal in longitudinal scans according to the marked lines on both lateral and medial aspects. The sagittal scans were performed sagittally from proximal to distal on the caudal aspect. The scanning technique for thigh region (transverse, longitudinal and sagittal scan) is illustrated in figure 3.3. The hind limb was slightly extended during scanning by traction of the pes. The scanned images of each level were identified by number according to the number of the marked lines.

For the brachial and scapular regions, the scanning was performed transversely perpendicular to the humerus and spine of scapula respectively according to the marked lines, and longitudinally along the muscle fibres on the lateral aspect of the brachium. Longitudinal scans were also done on the scapular region parallel to the spine of the scapula on both caudal and cranial sides of the spine of scapula. The humerus was used as a reference point in sagittal and para-sagittal scans of the brachium. Scanning of the ventral abdominal region was performed transversely across the mid line (linea alba). Similarly, all the scan images were identified by numbers according to the numbers of the marked lines.

A real time B-mode portable scanner (Capasee, TOSHIBA) connected with 7.5 MHz transducer was used in the study. For comparison, a 3.5 MHz transducer was used in the muscle scanning. All scanned images were recorded on super VHS tape using a Panasonic video recorder connected to the scanner. The recorded images were later reviewed using an Interspec (Apogee-cx) ultrasound machine. The thermal copies of the best images were produced during review and labelled accordingly.

Gross section preparations

For the thigh muscle, after scanning was done, the cadaver was frozen in a standing position at -20 °C for at least three days. This was done by suspending the cadaver in a metal frame. The cadaver was suspended from the sacral region and the thoracic region. The cadaver was suspended with the hind paws just touching the ground. After three days, the hind limbs were then sectioned from the body at the fourth lumbar vertebra. The two hind limbs (left and right) were then separated. The right and left hind limbs were serially sectioned transversely and longitudinally respectively according to the marked levels. The ventral abdominal region was also sectioned transversely according to the marked levels. The sections were placed in sequence on the tray and identified by numbers according to the number of the marked lines. The sections were cleaned to remove the excess fat and dirt by passing under running tap water for a few seconds and gentle rubbing of the surface with wet paper tissue. The sections were partially thawed prior to examination to correlate with the scanned images produced earlier on. The sections were then wrapped with cling film prior to putting back into the freezer. For photography the sections were arranged on a tray and left to partially thaw. Photographs of the sections were performed by a photographer.

For the brachial and scapular sections, after the scan was done the left and right fore limbs were removed from the body prior to freezing. The fore limbs were then placed on the tray and frozen to simulate a standing position. The limbs were serially sectioned according to the marked lines, cleaned, partially thawed and examined as above. Photographs were taken as above.

Figure 3.1 Schematic diagram of the lateral aspect of thigh region of right and left hind limbs. The area of thigh region is marked and identified by numbers on both lateral and medial aspects. The scanning was done following to the marked lines. **A**, Transverse scan of the lateral aspect of the right thigh. **B**, Longitudinal scan of the lateral aspect of the left thigh.

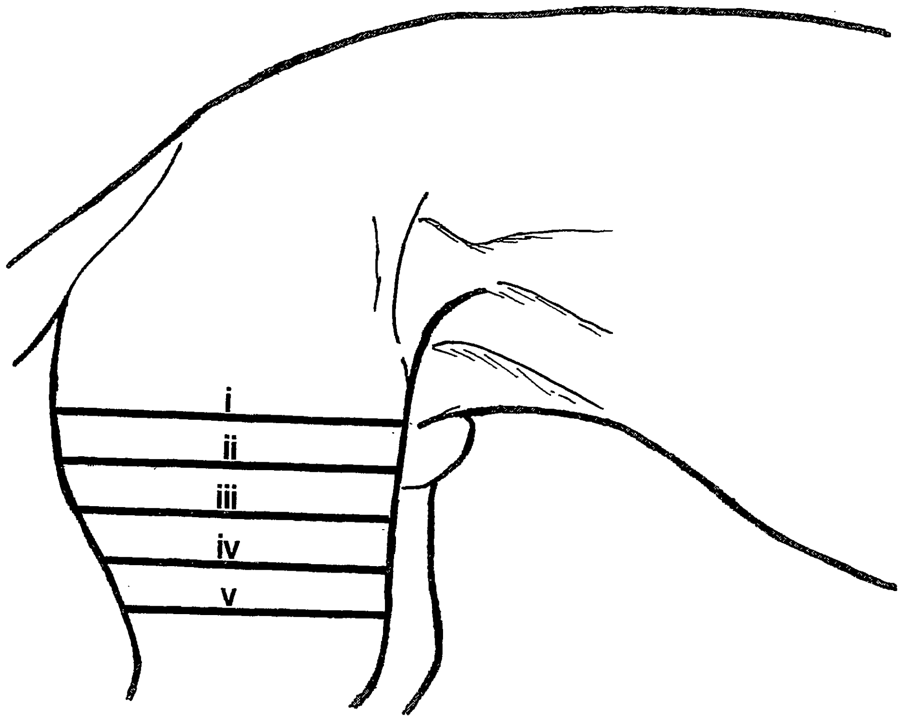

A

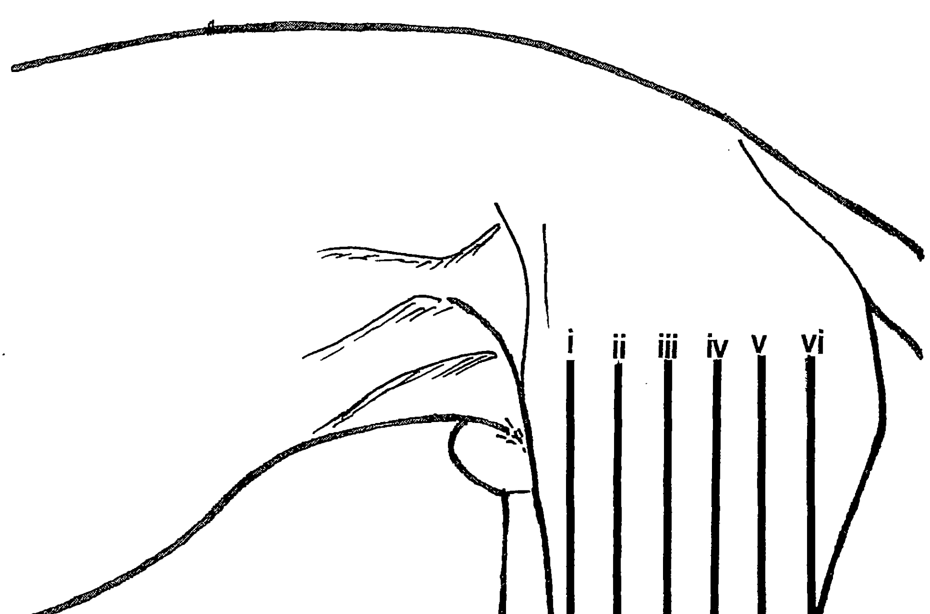

B

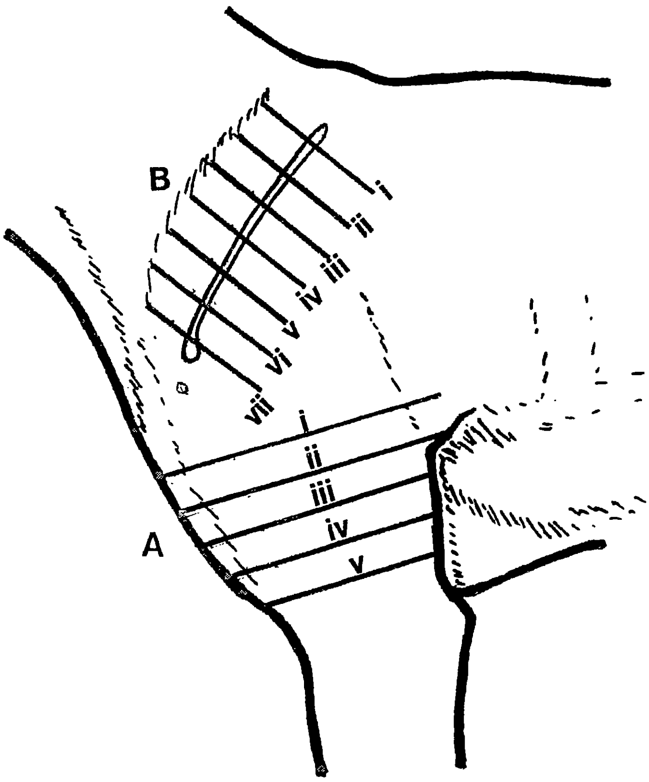

Figure 3.2 Schematic diagram of the lateral aspect of the brachium and scapular regions. The scanning levels are marked by numbers on both the scapular and brachial regions. **A**, levels of ultrasonographic scans of the brachial region. **B**, levels of ultrasonographic scans of the scapular region.

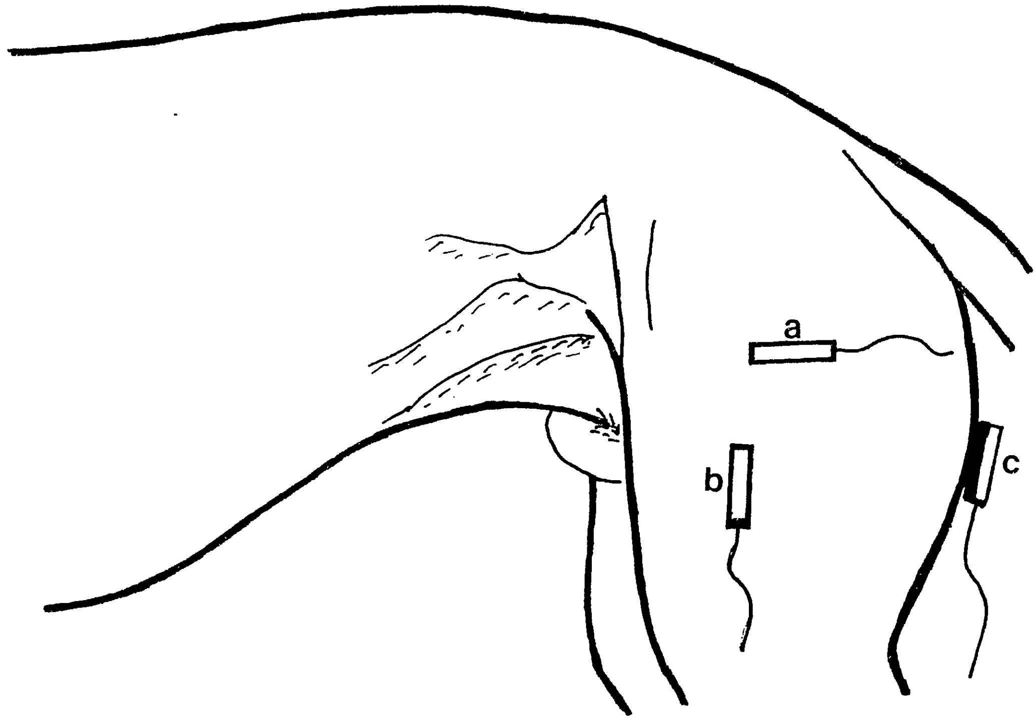

Figure 3.3 Illustrated diagram of scanning technique used in this study. **a**. Transverse scan, **b**. Longitudinal scan, **c**. Sagittal scan.

3.3 Results

Skeletal muscles of the normal greyhound cadavers imaged ultrasonographically in general showed the same characteristics. Serial ultrasonographic images of the thigh muscle scanned transversely from the lateral and medial aspects correlated well with the thigh gross anatomy sections (figure 3.4). The ultrasonographic images of brachial muscles scanned transversely on the lateral aspect and their correlation with the cross sections are shown in figure 3.5, and the scapular muscles scanned transversely across the spine of the scapula and longitudinally parallel to the spine of scapula are shown in figure 3.6 and 3.7 respectively. Sagittal scans of the brachial muscles are shown in figure 3.8. Normal skeletal muscle imaged ultrasonographically appeared as an homogenously hypoechoic structure with fine echoes scattered throughout the muscle parenchyma. Each muscle group could be identified, separated by a thin hyperechoic structure which was actually the connective tissue fascia. The normal skeletal muscle imaged transversely perpendicular to the muscle fibres appeared homogenously hypoechoic with poorly organised fine echoes corresponding to the fibroadipose septa scattered throughout the muscle parenchyma (figures 3.4, 3.5 and 3.6). In longitudinal image along the muscle fibres, skeletal muscle appeared as homogenous fine parallel echoes scattered throughout the hypoechoic muscle parenchyma (figures 3.9 and 3.10). As in the transverse scan, the muscle groups were separated by the thin hyperechoic layers of connective tissue fascia. The bone appeared as a strong hyperechoic image with complete acoustic shadowing distally when the transducer was correctly inclined (figure 3.11).

Sagittal scanning of the thigh muscle caudally demonstrated a typical ultrasonographic appearance of the skeletal muscle imaged along the muscle fibres (figure 3.10). In contrast, the sagittal scan of the brachial muscle caudally appeared as in a transverse scan (figure 3.8). The connective tissue fascia (perimysium and epimysium) appeared as hyperechoic fine parallel echoes in sagittal scan along the muscle fibre axis. Ultrasonographic imaging of the thigh muscle longitudinally on the latero-caudal aspect demonstrated two different groups of muscle with different muscle fibre orientation. The semitendinosus and semimembranosus muscles appeared hypoechoic with fine parallel echoes while the gracilis muscle appeared as homogenous and hypoechoic with fine echoes (figure 3.12). These groups of muscle were separated by hyperechoic connective tissue fascia.

The comparison of longitudinal and transverse images of the thigh muscles using 7.5 MHz and 3.75 MHz are demonstrated in figure 3.13. The 7.5 MHz linear array transducer was found to have better resolution with finer detail than the 3.75 MHz transducer in imaging of the thigh muscle. The ultrasonographic image of the ventral abdominal mid-line scanned transversely is shown in figure 3.14. The linea alba appeared isoechoic relative to the surrounding muscle tissue. The connective tissue fascia enveloping the rectus abdominis muscle appeared hyperechoic.

The caput longus of the triceps muscle gaves a characteristic of “feathery appearance” on a longitudinal scan (figure 3.15). This appearance was produced by sheaths of connective tissue (perimysium) surrounding the muscle bundles.

Figure 3.4 Serial transverse scans of the normal thigh muscle on (**A**) caudo-lateral aspect and (**B**) cranio-medial aspect using a 7.5 MHz transducer and their correlation with the gross anatomy sections. The ultrasonographic appearance of normal skeletal muscle imaged transversely is of poorly organised fine echoes scattered throughout the hypoechoic muscle parenchyma. The fine echoes are corresponding to the fibroadipose septa. The muscle groups are well separated by the connective tissue fascia (perimysium) surrounding them. The overall increase in echogenicity of the muscle echotexture in **B** is due to the high gain setting. The images correlate well with the gross anatomy sections. **sm**, m. semimembranosus, **st**, m. semitendinosus, **bf**, m. biceps femoris, **a**, m. adductor, **g**, m. gracilis, **sr**, m. sartorius, **rf**, m. rectus femoris, **vm**, m. vastus medialis, **vi**, m. vastus intermedius, **vl**, m. vastus lateralis, **f**, femur.

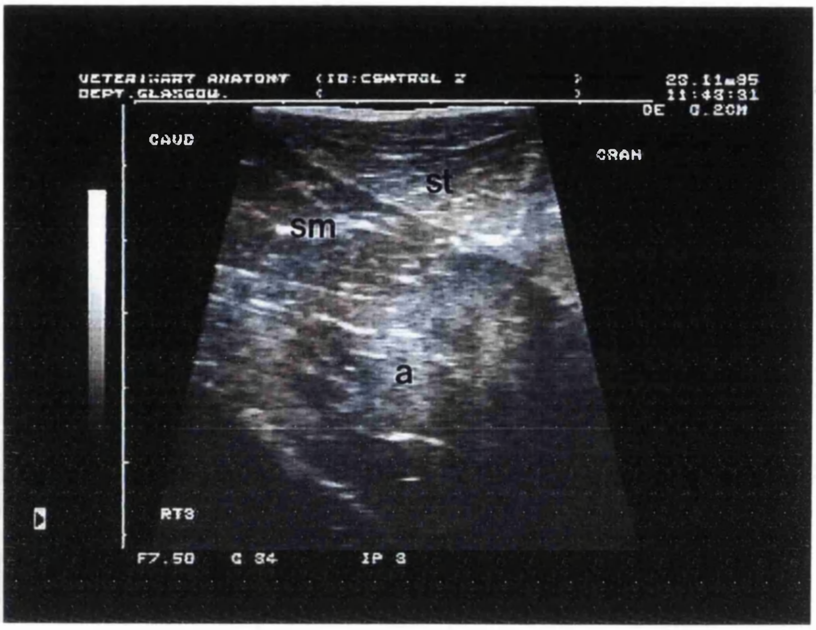
VETERINARY ANATOMY
DEPT.GLASGOW.
11:43:31
DE 0.2CM
CAUD
CRAN
st
sm
a
RT3
F7.50
G 34
IP 3

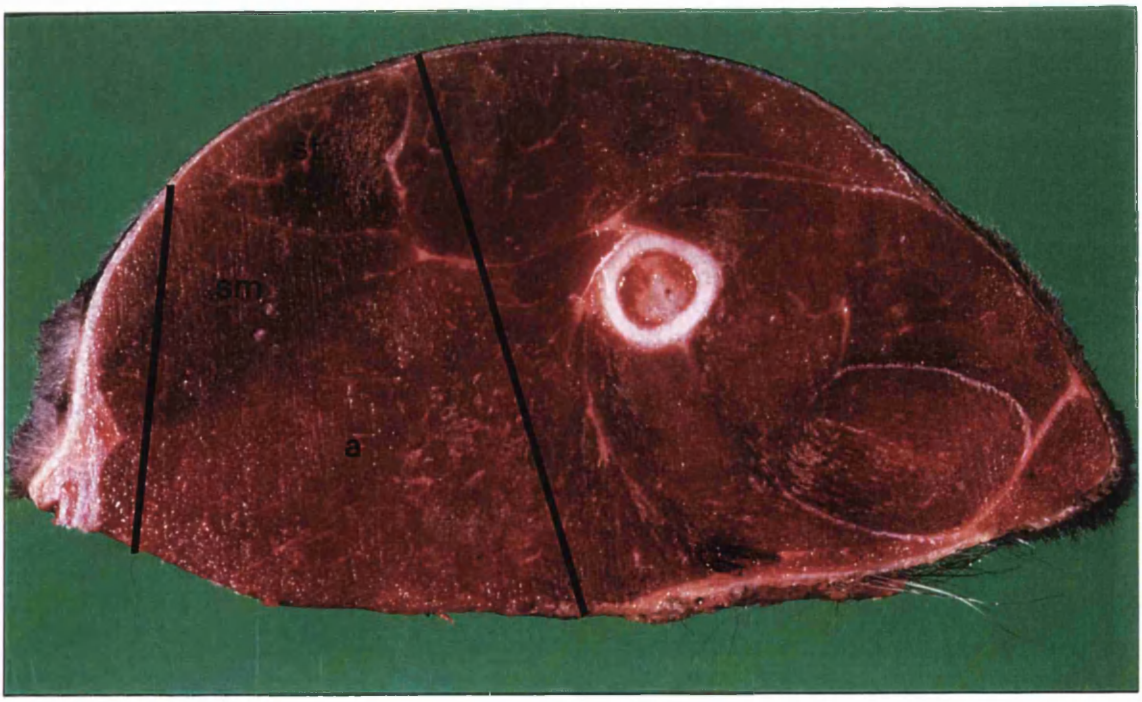
st
sm
a

Figure 3.4 A (i)

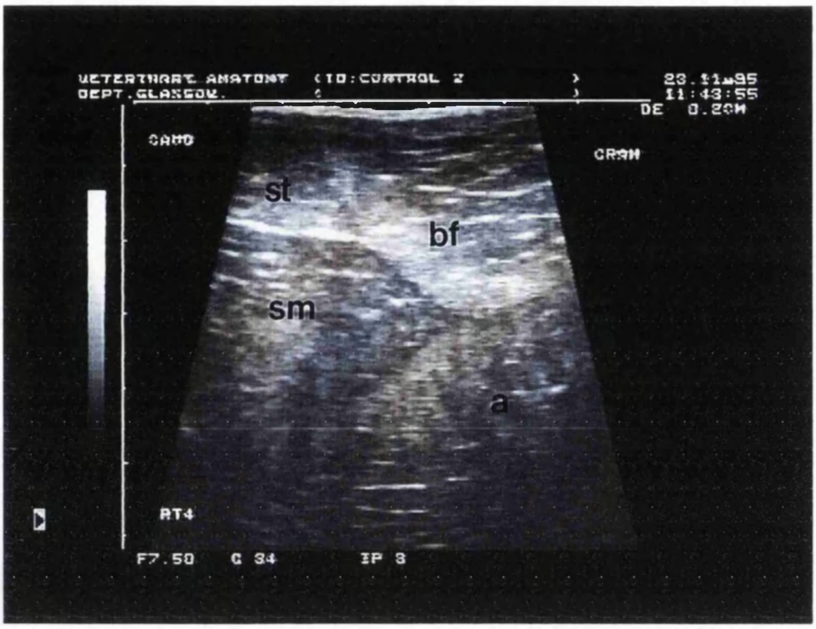

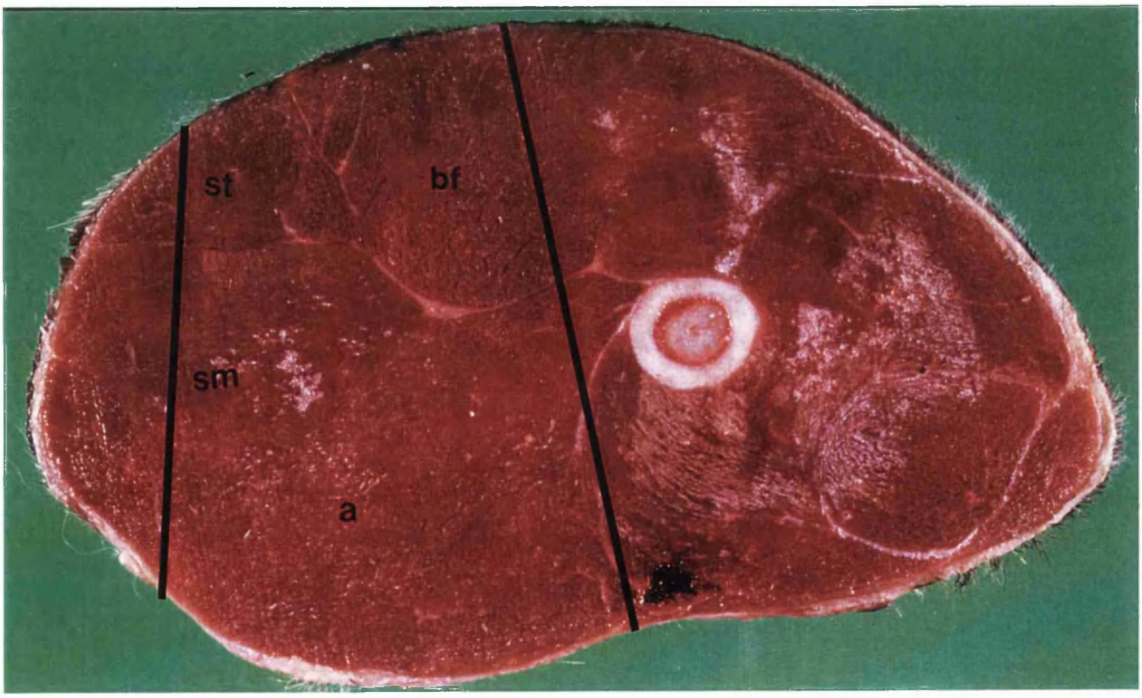

Figure 3.4 A (ii)

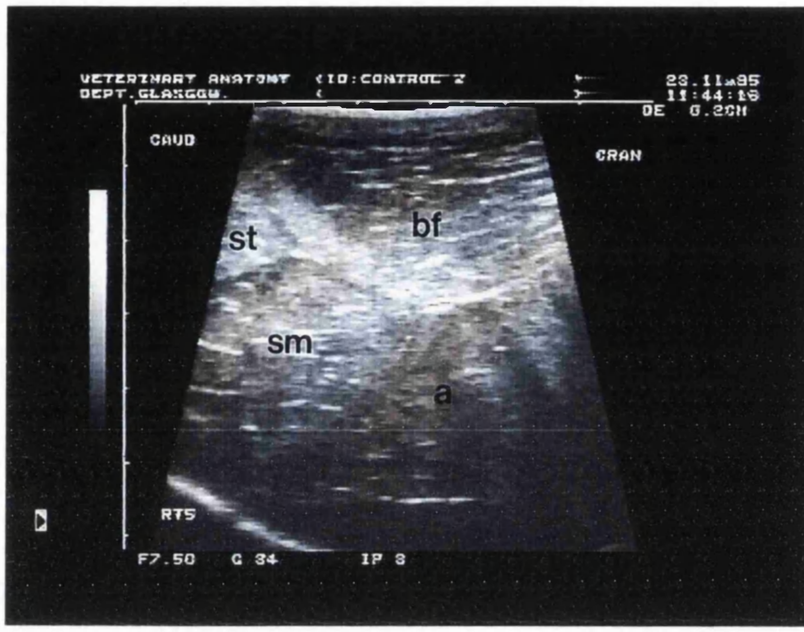

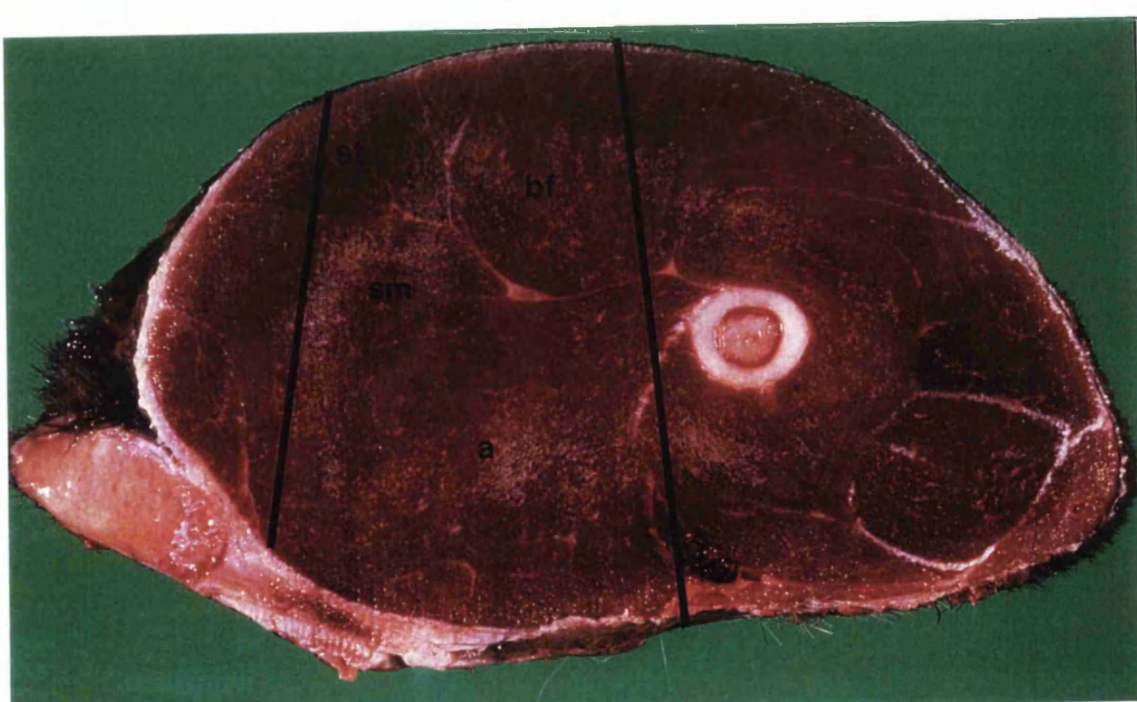

Figure 3.4 A (iii)

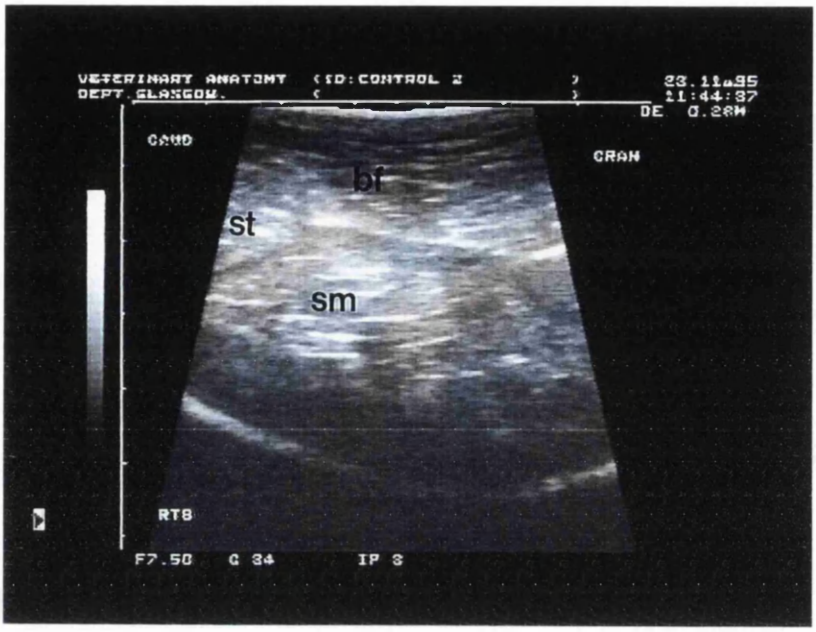

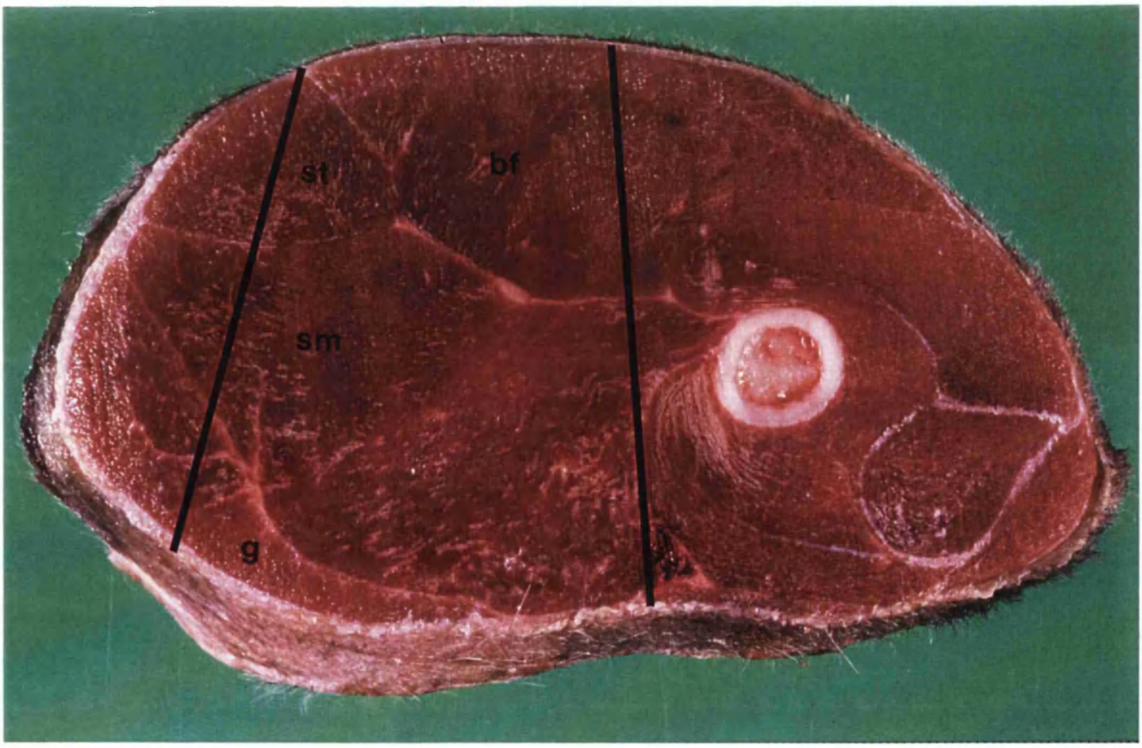

Figure 3.4 A (iv)

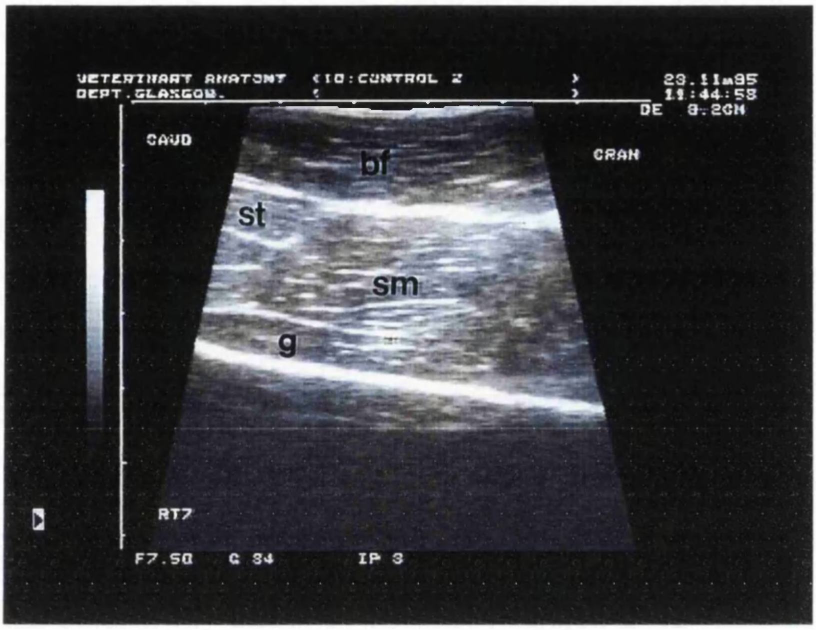
VETERINARY ANATOMY
DEPT.GLASGOW.
CAUD
CRAN
bf
st
sm
g
RT7
F7.50
G 34
IP 3
DE 8.2CM

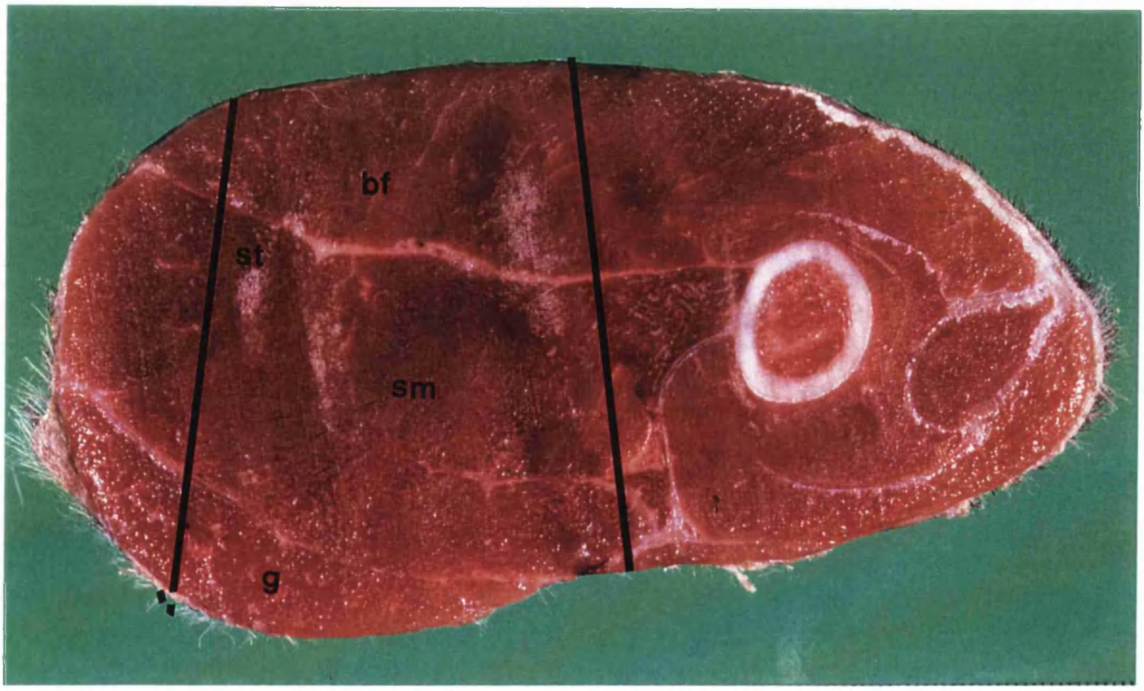
bf
st
sm
g

Figure 3.4 A (v)

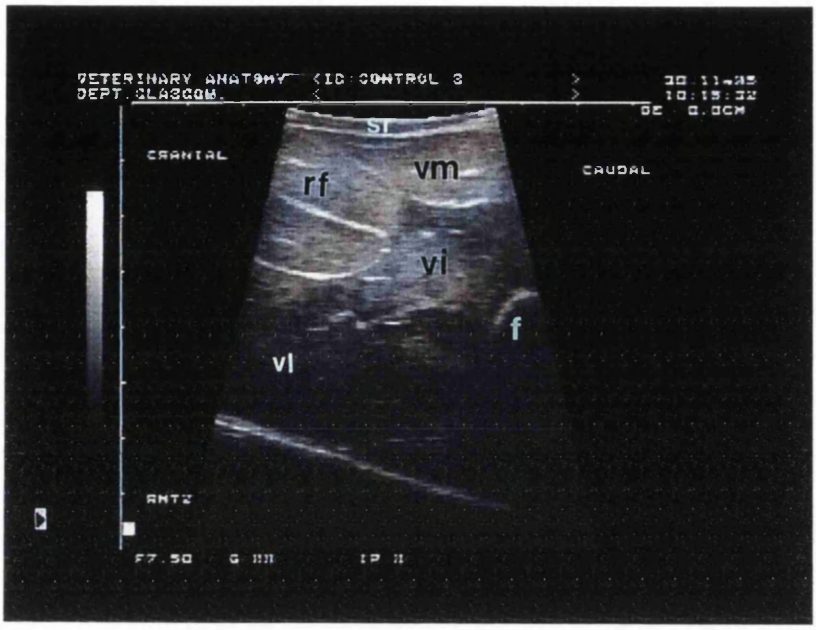
VETERINARY ANATOMY
DEPT. GLASGOW.
CRANIAL
CAUDAL
sr
rf
vm
vi
f
vl

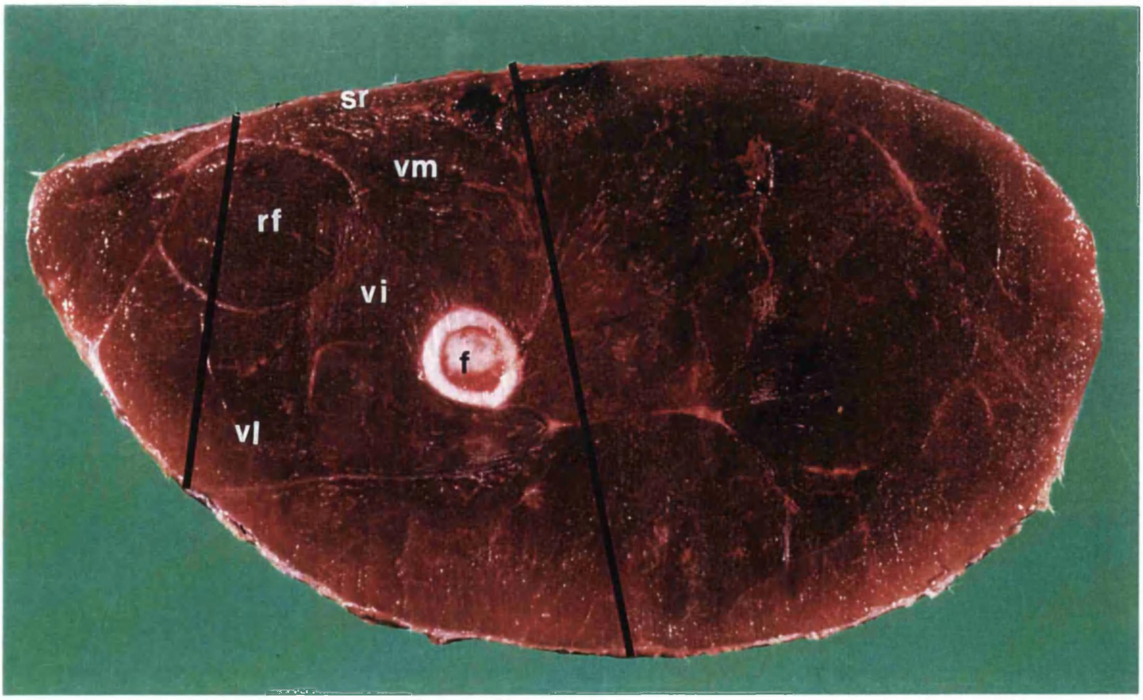
sr
vm
rf
vi
f
vl

Figure 3.4 B (i)

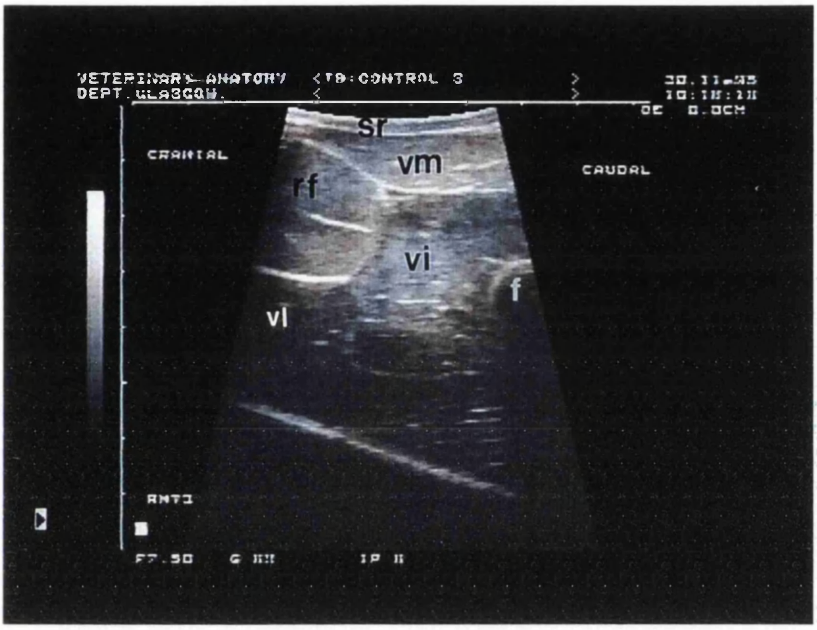

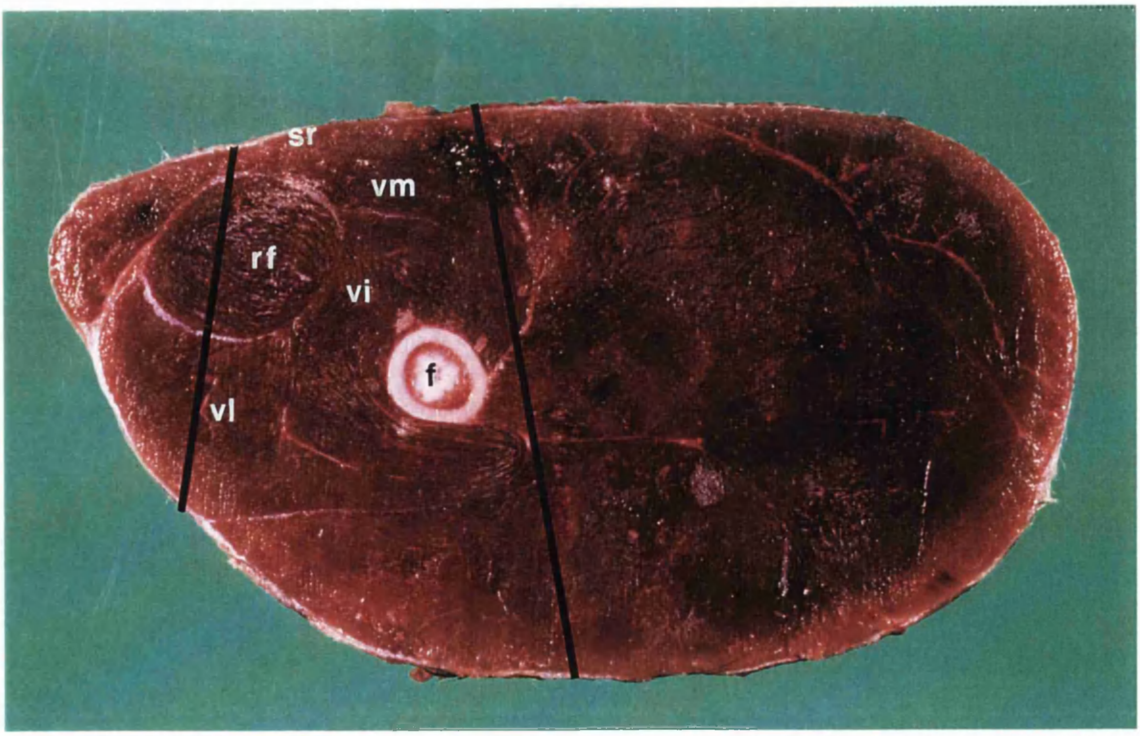

Figure 3.4 B (ii)

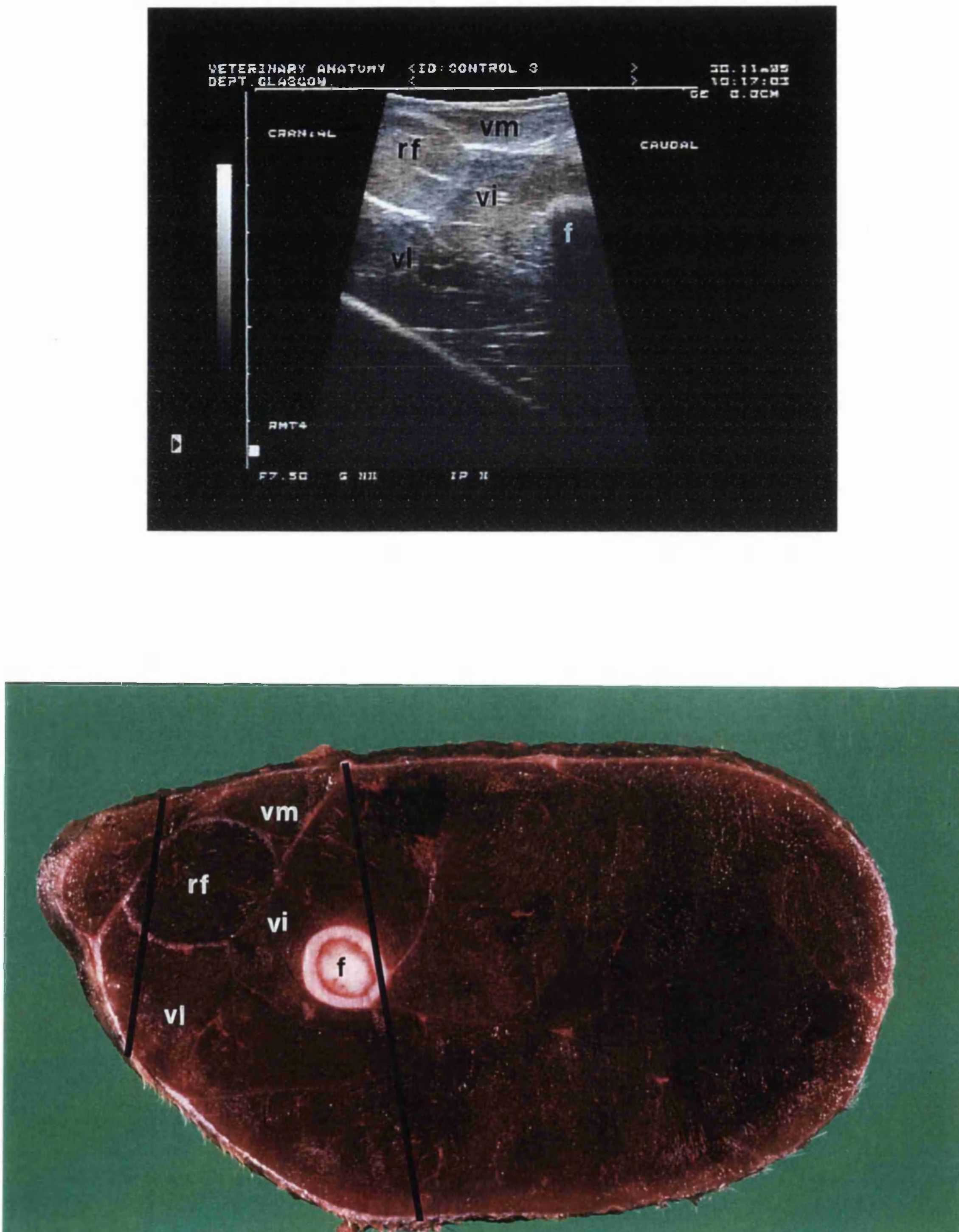

Figure 3.4 B (iii)

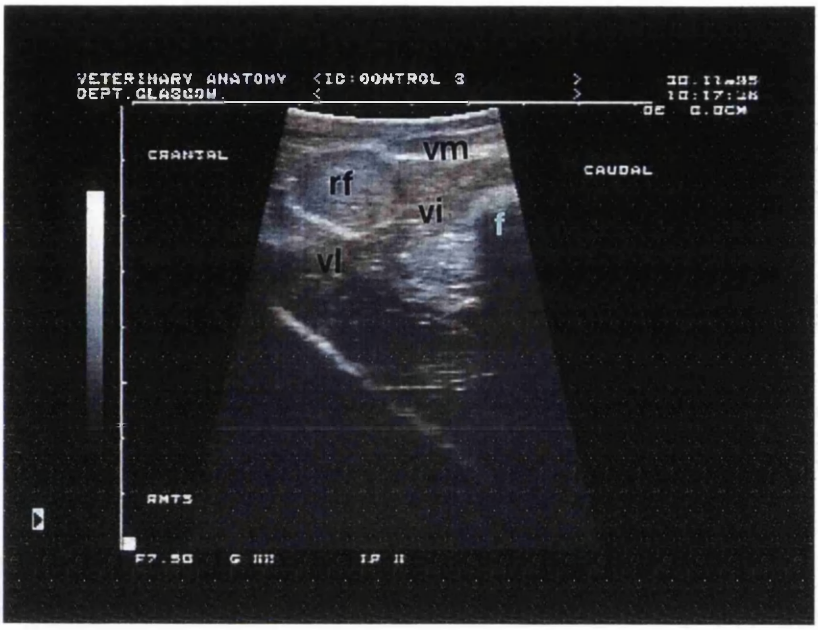

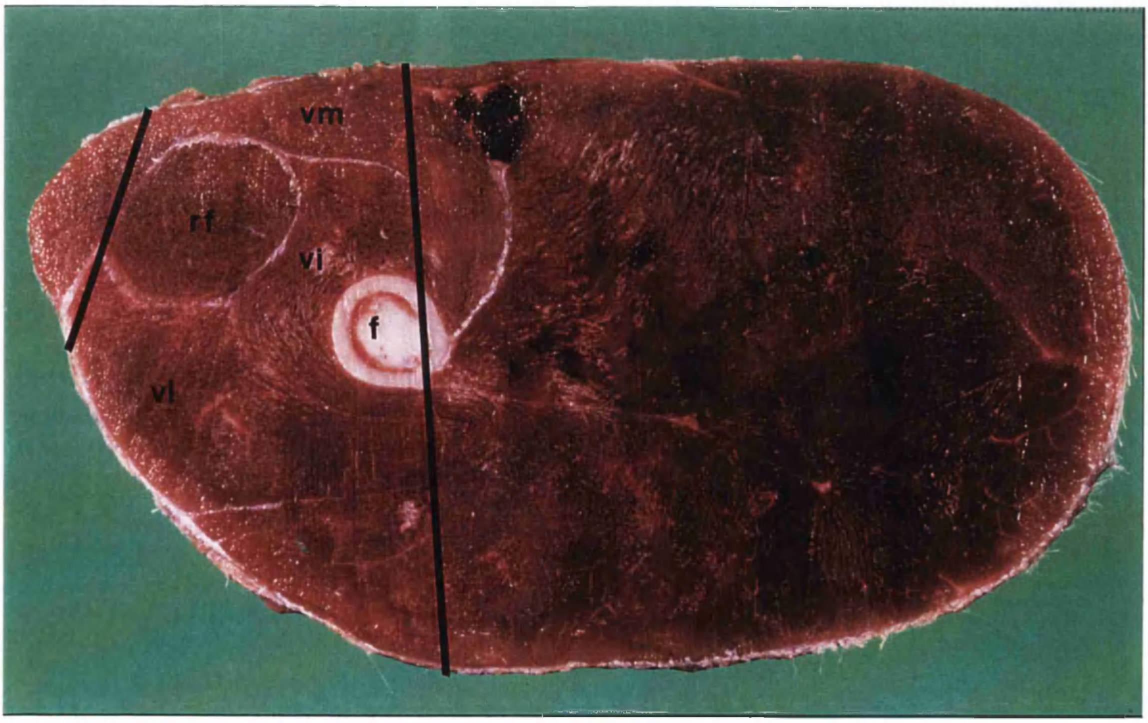

Figure 3.4 B (iv)

Figure 3.5 Transverse scans of the normal brachial musculature on the lateral aspect of the left fore limb. Note that the muscle structure appears hypoechoic with disorganised fine echoes scattered throughout the muscle parenchyma. The images correlate well with the gross anatomy sections. m. triceps brachii; **CL**, caput lateralis, **CP**, caput longus, **CM**, caput medialis, **CA**, caput accessorius, **H**, humerus, **B**, m. brachialis.

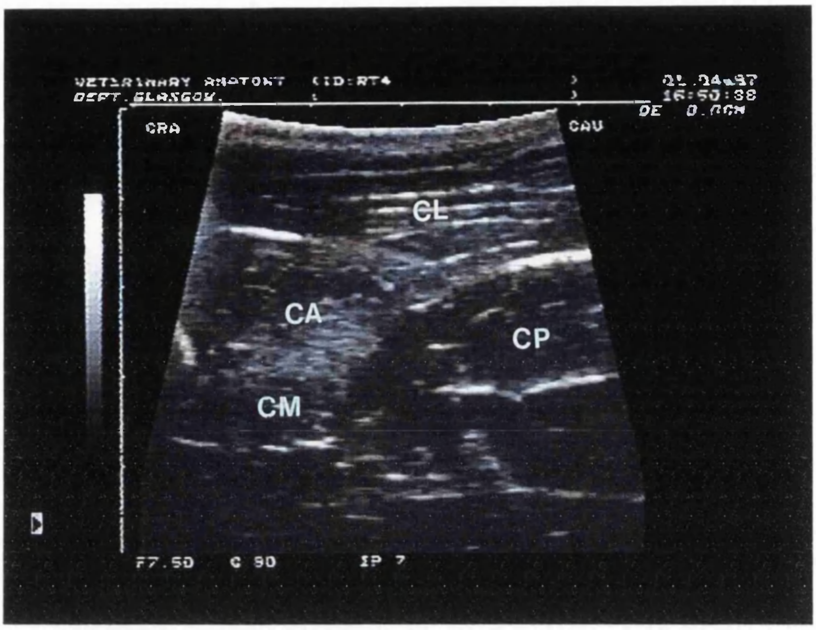

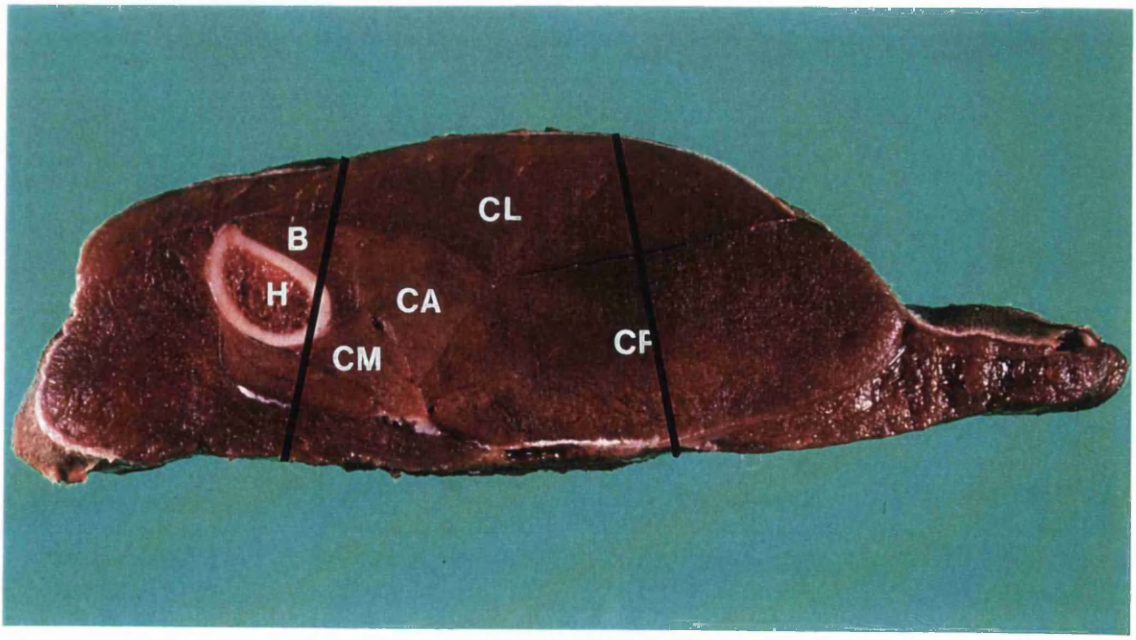

Figure 3.5 (i)

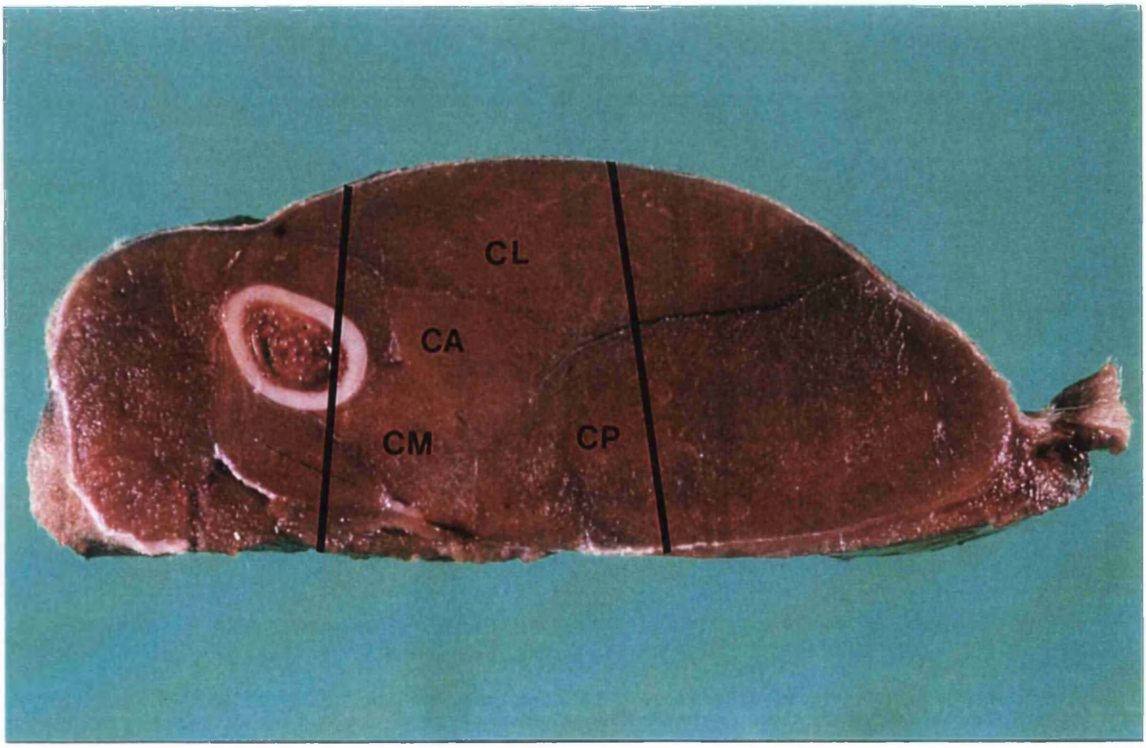

Figure 3.5 (ii)

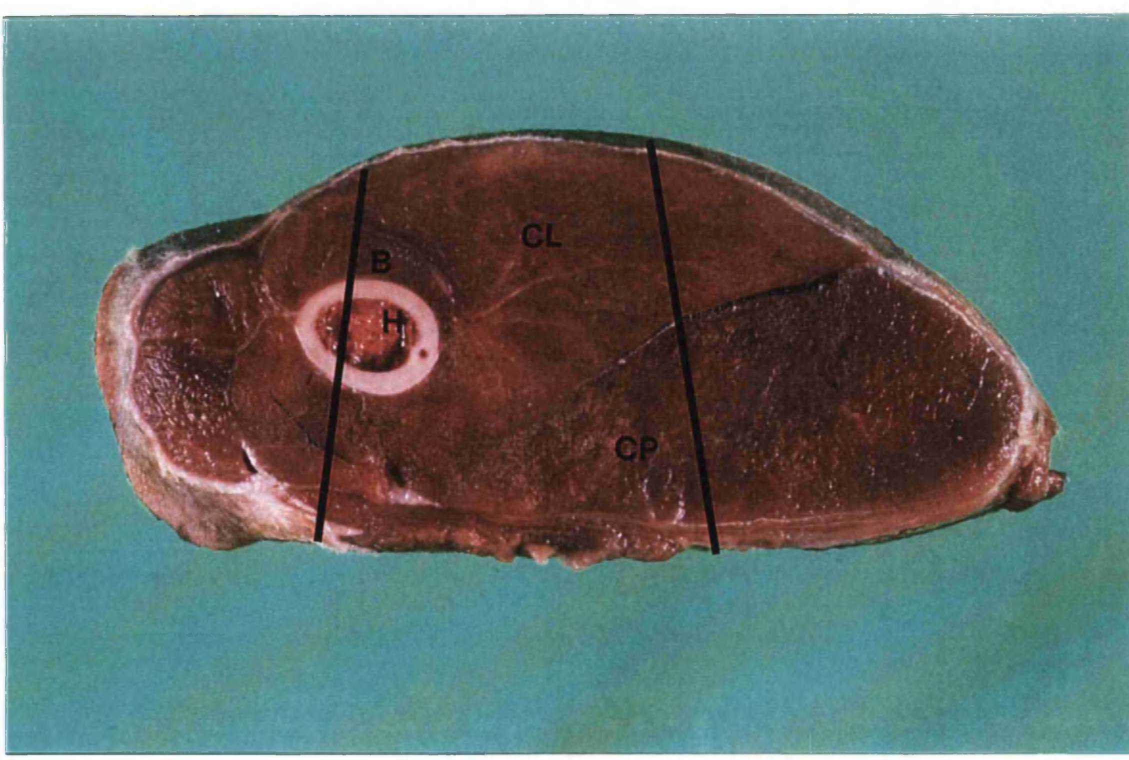

Figure 3.5 (iii)

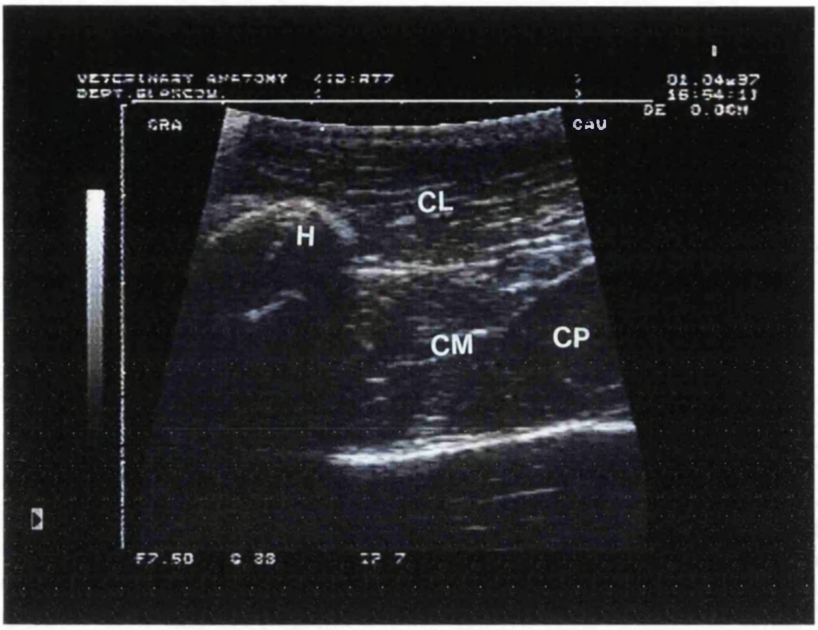

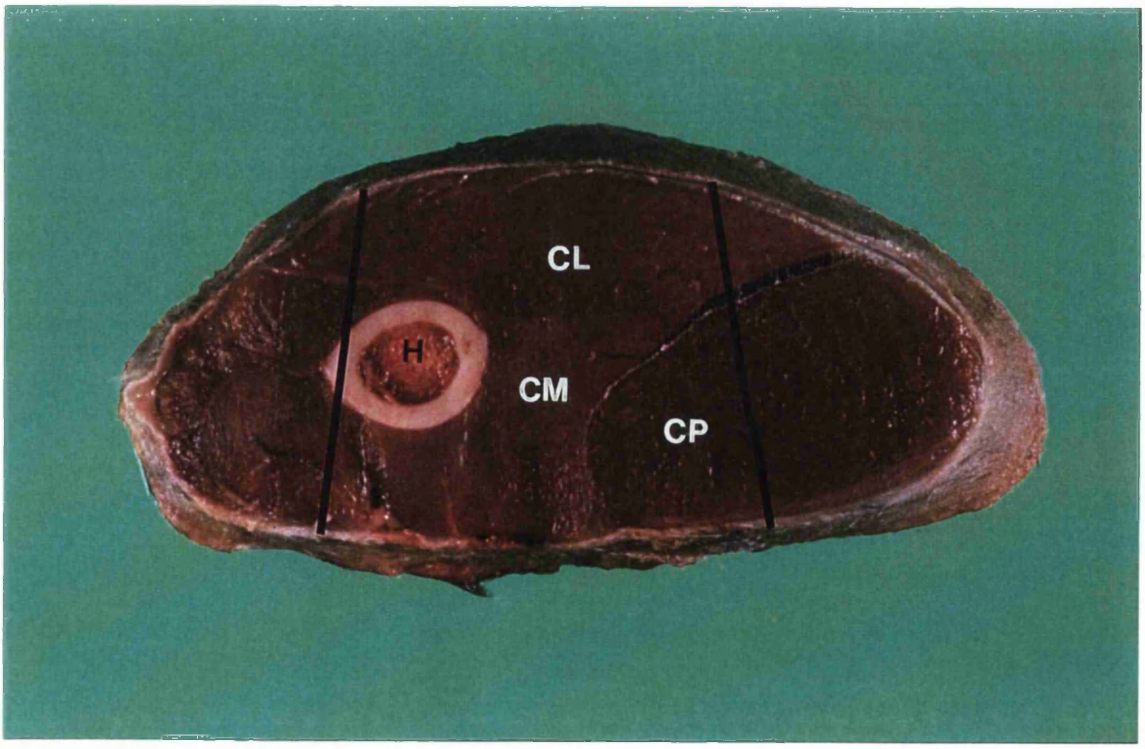

Figure 3.5 (iv)

Figure 3.6 Transverse scans of the normal muscle of the scapular region (**a,b,c,d**) and their correlation with gross anatomy sections (**e**). Note that the skeletal muscle imaged transversely appears hypoechoic with fine echoes scattered throughout the muscle parenchyma. **SC**, spine of scapula, **S**, body of scapula, **SP**, m. supraspinatus, **IP**, m. infraspinatus, **D**, m. deltoideus, **CP**, m. caput longus, **T**, m. trapezius.

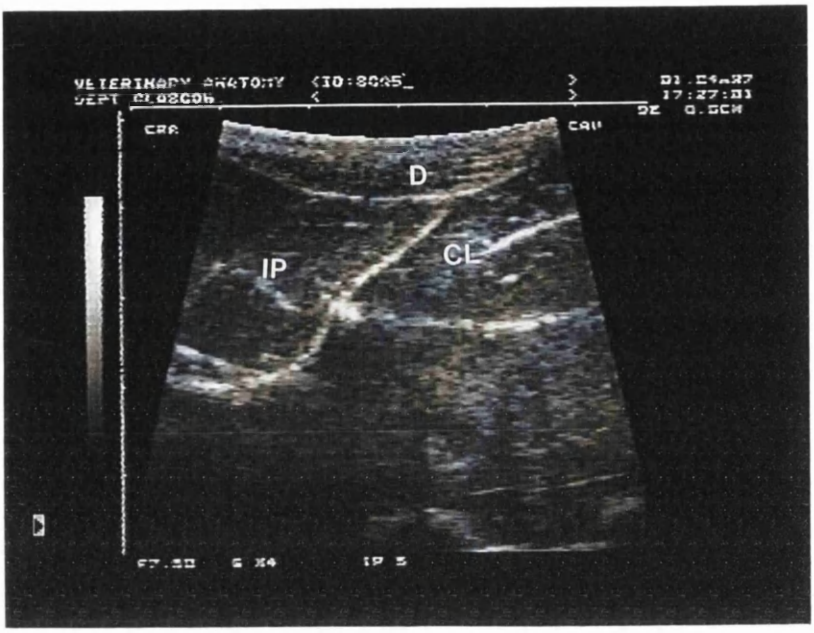

Figure 3.6a

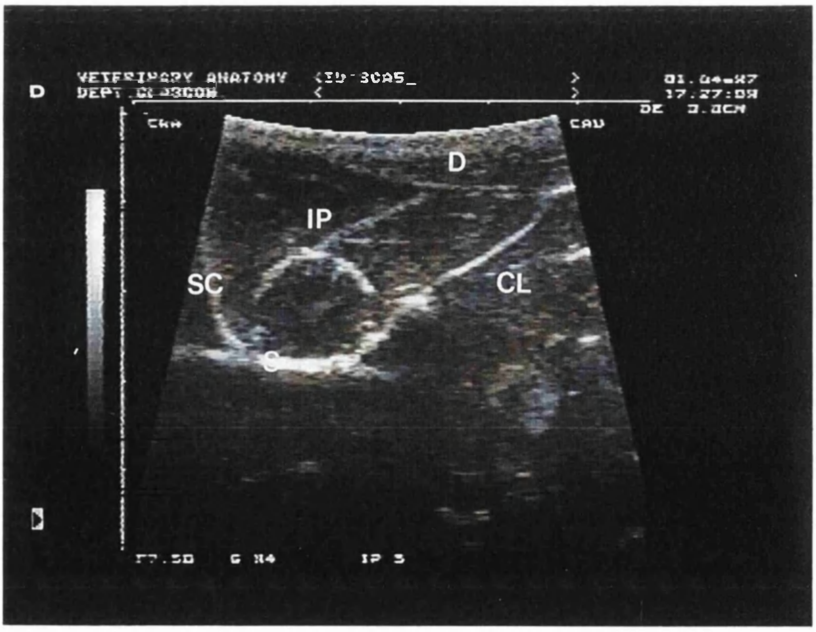

Figure 3.6b

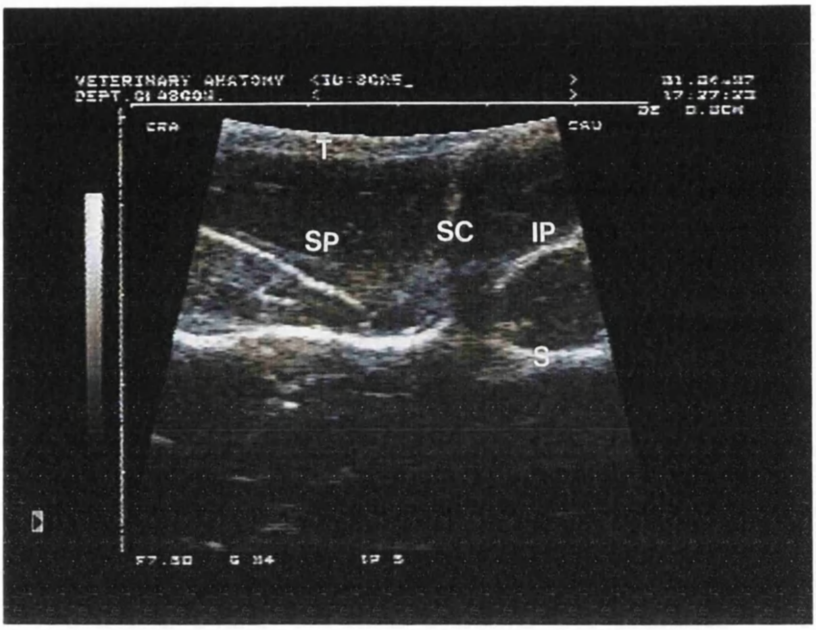

Figure 3.6c

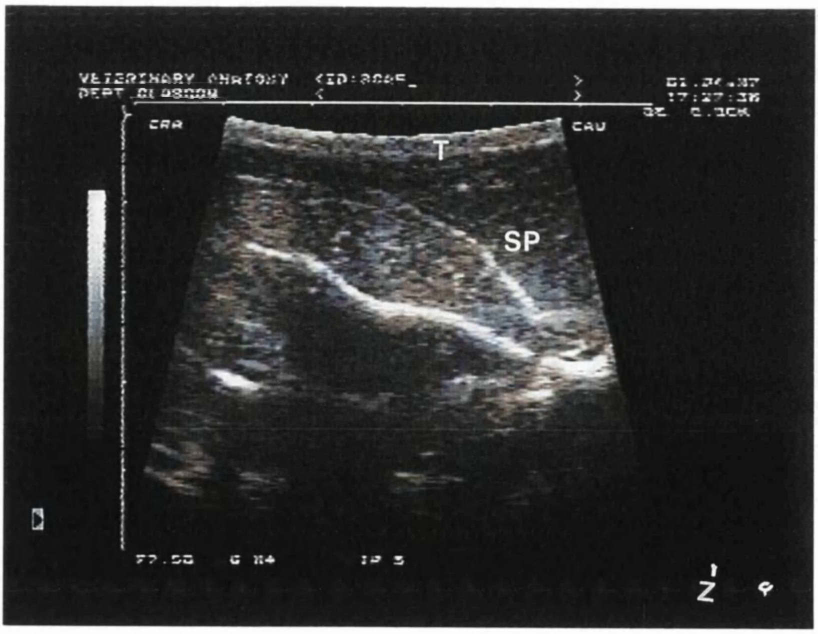

Figure 3.6d

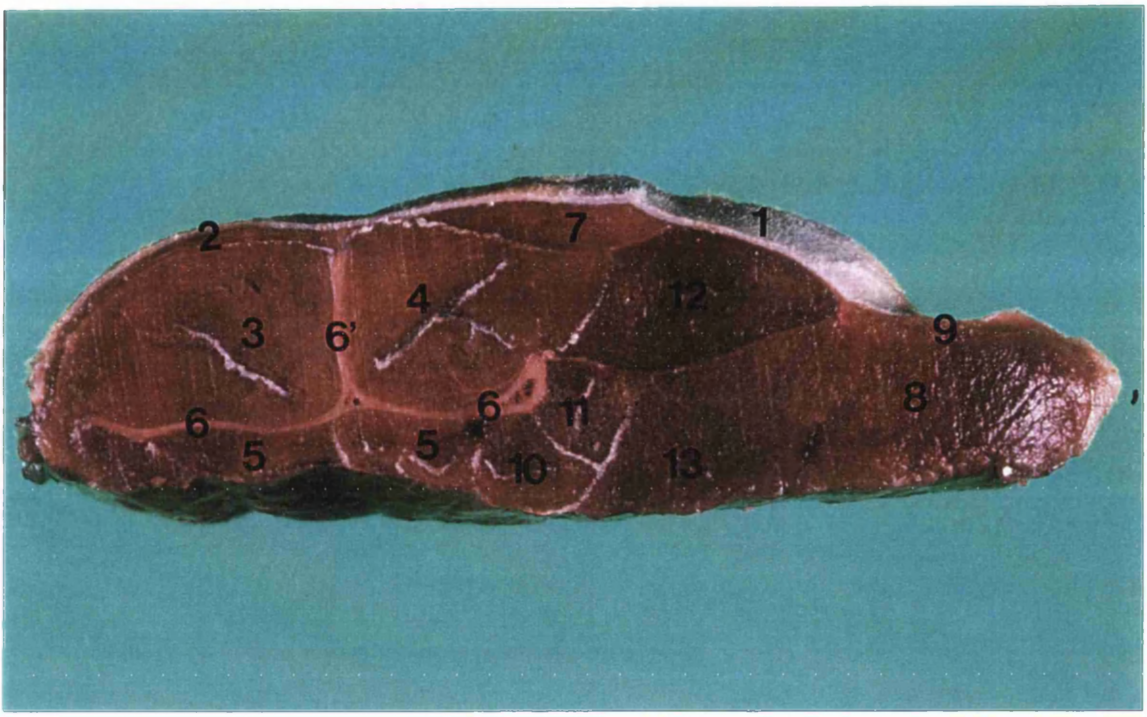

1	skin	7	m. deltoideus
2	m. trapezius	8	m. latissimus dorsi
3	m. supraspinatus	9	m. cutaneous trunci
4	m. infraspinatus	10	m. teres major
5	m. subscapularis	11	m. teres minor
6	body of scapula	12	m. triceps brachii (caput longus)
6'	spine of scapula	13	m. tensor fascia antebrachi

Figure 3.6e

Figure 3.7 Ultrasonographic images of normal muscles of the scapular region scanned longitudinally, parallel to the spine of the scapula. **a**, m. supraspinatus, **b**, m. infraspinatus. Note the thick line of hyperechoic material in **b** is actually the connective tissue fascia as demonstrated in the gross anatomy section in figure 3.6e. **S**, body of scapula, **SP**, m. supraspinatus, **IP**, m. infraspinatus.

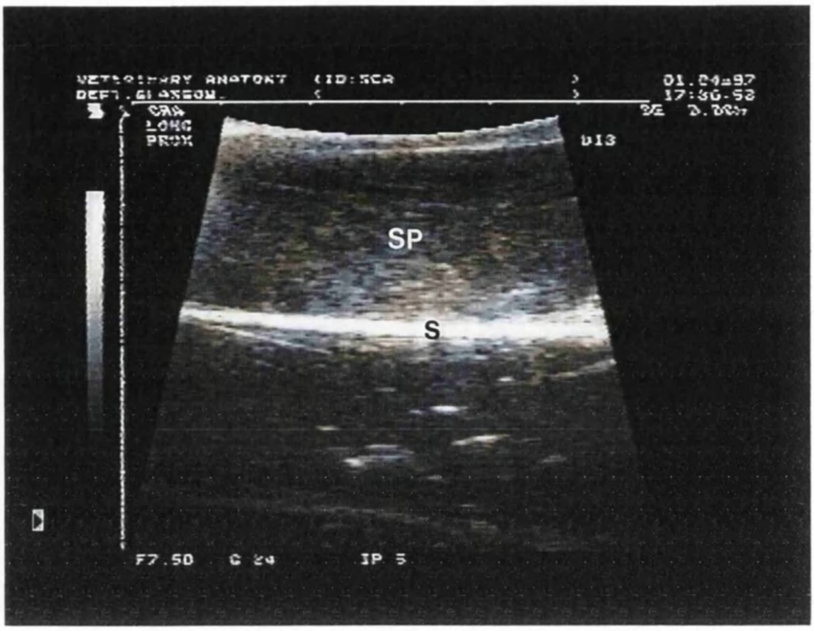

Figure 3.7a

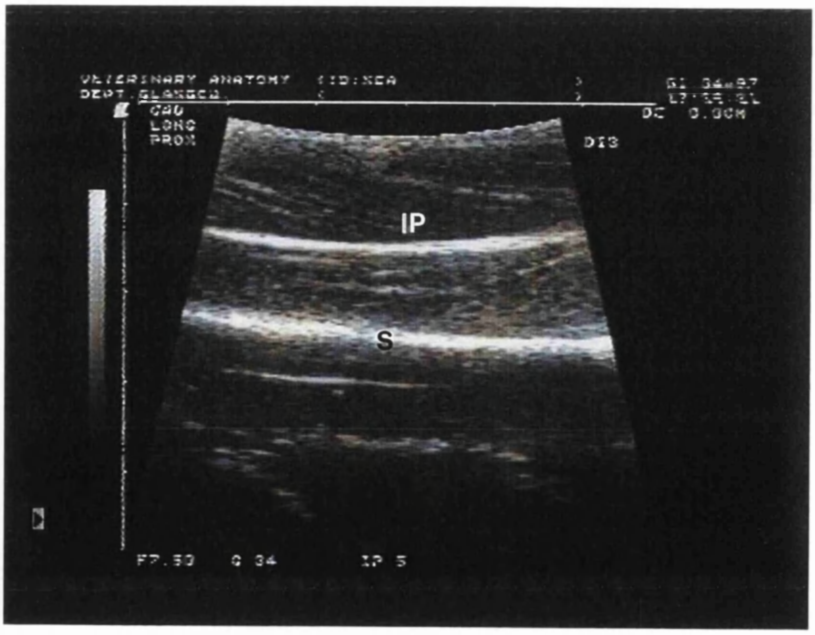

Figure 3.7b

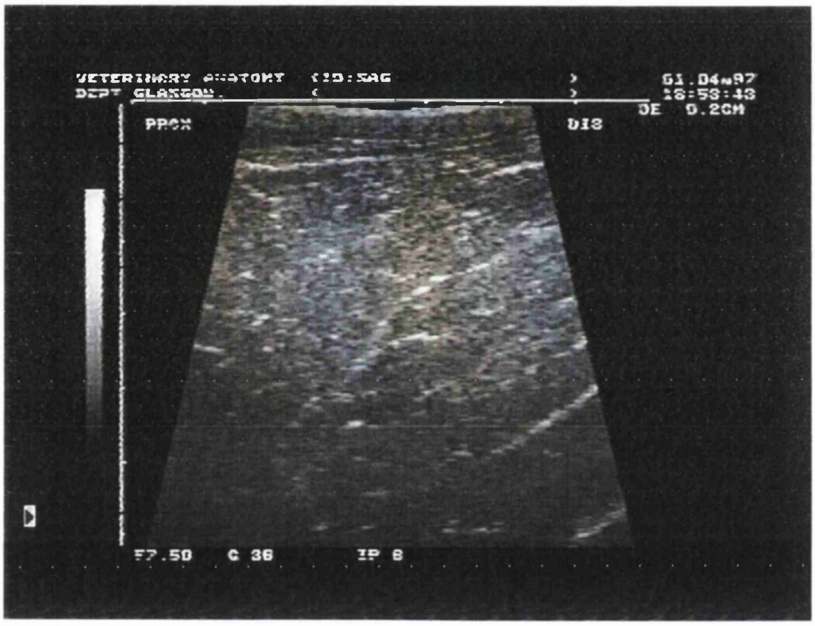

Figure 3.8 Sagittal scan of the normal brachial muscles of the left fore limb from the caudal aspect. Note that muscle tissue appears hypoechoic with disorganised fine echoes scattered throughout the muscle parenchyma.

Figure 3.9 Longitudinal scan of the normal thigh muscles from the lateral aspect caudal to the femur and its correlation with the gross anatomy section. Note that the muscle structure appears homogenously hypoechoic with fine parallel echoes scattered throughout the muscle parenchyma. The two muscles, biceps femoris and adductor are clearly separated by a connective tissue fascia, the epimysium, which appears as an hyperechoic straight line. **BF**, m. biceps femoris, **A**, m. adductor.

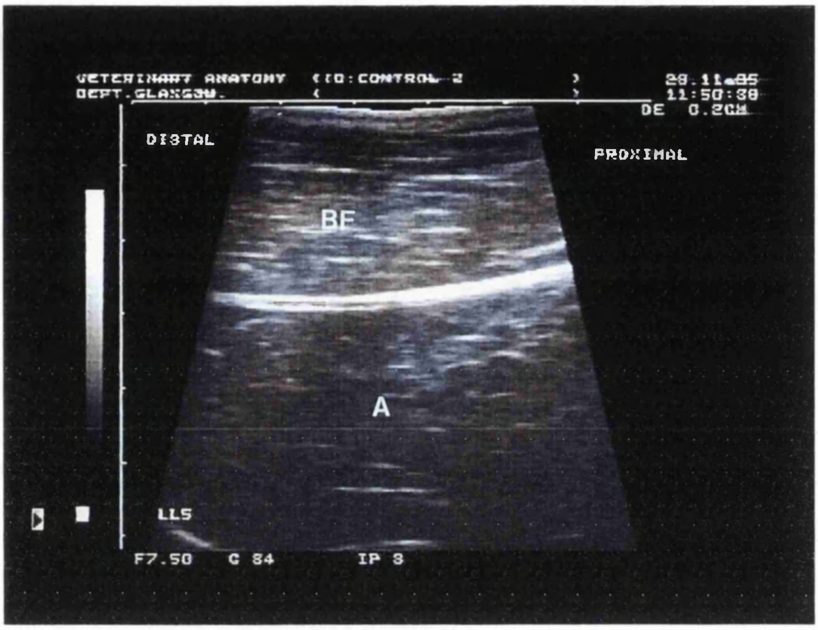
VETERINARY ANATOMY
11:50:38
DE 0.2CM
DISTAL
PROXIMAL
BF
A
LLS
F7.50
C 84
IP 3

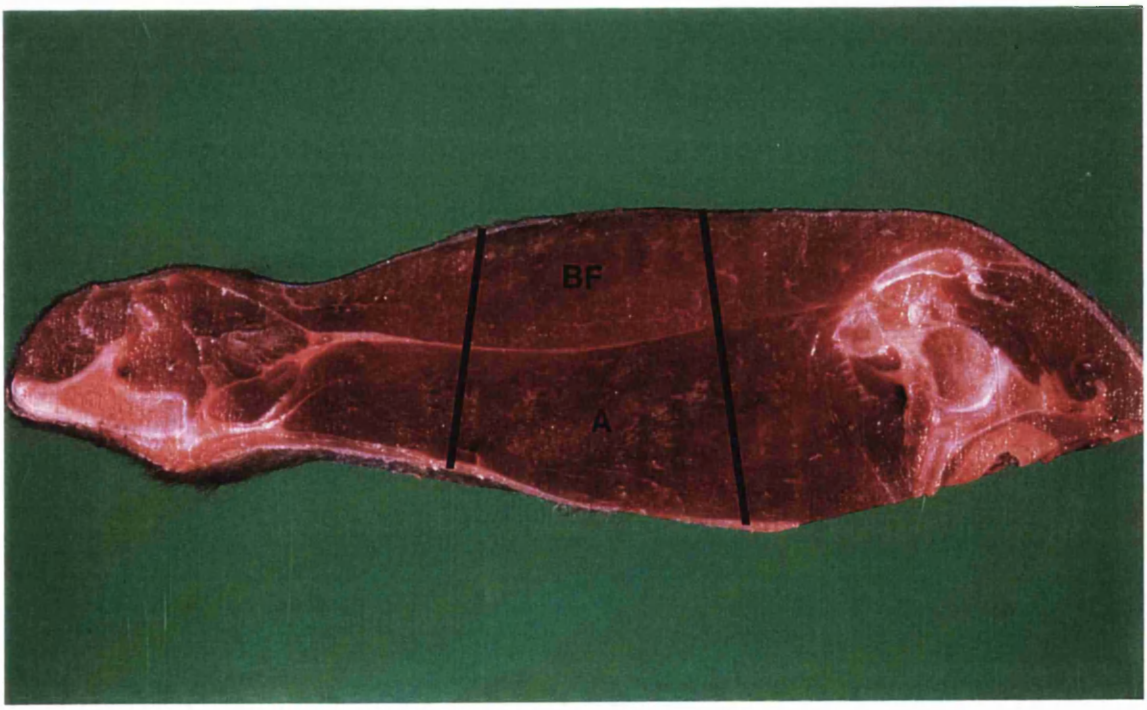
BF
A

Figure 3.9

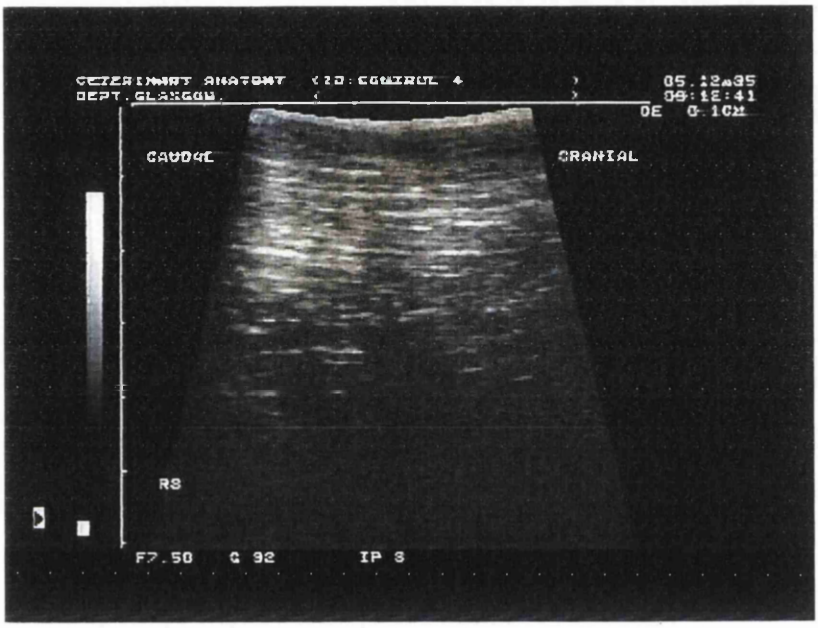

Figure 3.10 Sagittal scan of the normal thigh muscle from the caudal aspect using a 7.5 MHz transducer. Note that the muscle appears hypoechoic with fine parallel echoes corresponding to the fibroadipose septa surrounding the muscle fibres.

Figure 3.11 The longitudinal scan of the normal thigh muscles of the left hind limb on the lateral aspect demonstrates the femur which appears as an intense hyperechoic image. **BF**, m. biceps femoris, **VL**, m. vastus lateralis, **F**, femur.

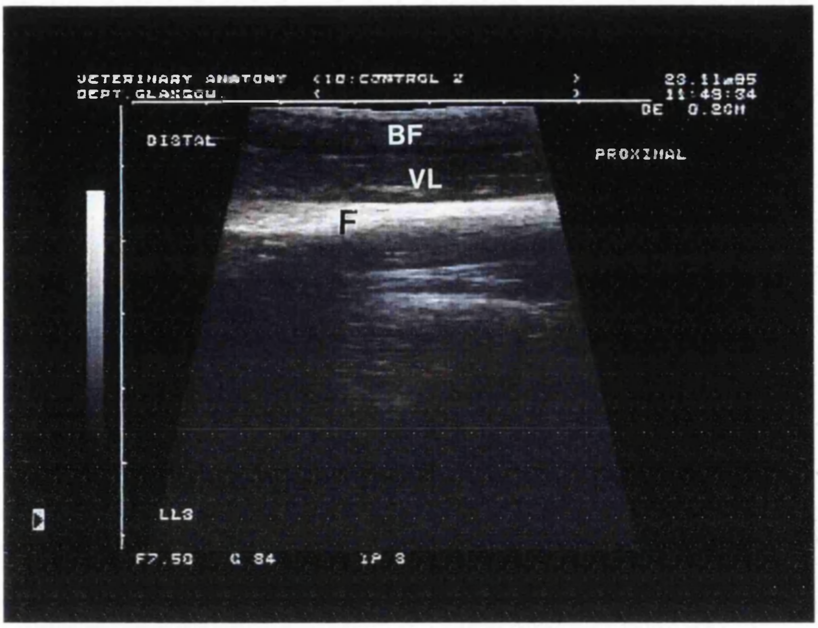
VETERINARY ANATOMY
11:49:34
DE 0.2CM
DISTAL
BF
VL
F
PROXIMAL
LL3
F7.50
G 84
IP 3

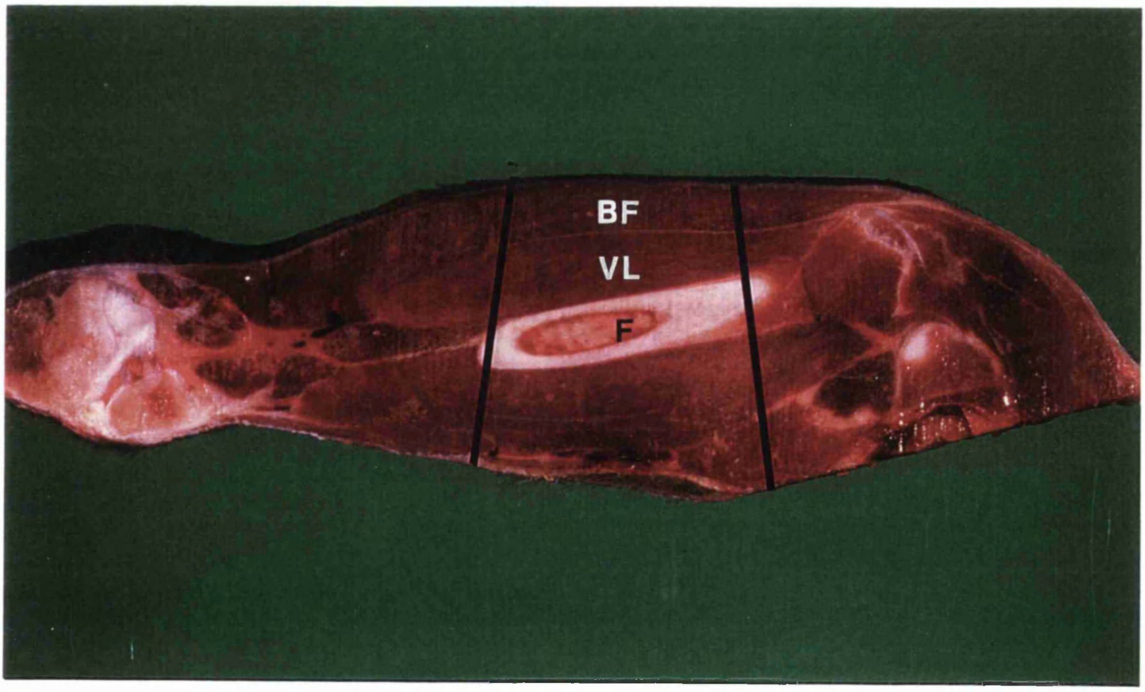
BF
VL
F

Figure 3.11

Figure 3.12 The longitudinal scan of the normal thigh muscle from the caudo-lateral aspect demonstrates the muscle fibres of different individual muscle groups which run slightly oblique to each other. This is shown by fine parallel echoes within the hypoechoic background demonstrated by the semitendinosus (**st**) and semimembranosus (**sm**) muscles and the homogenous fine echoes demonstrated by the gracilis muscle (**g**). Anatomically, the fibres of the gracilis muscle run slightly oblique to those of the semimembranosus and semitendinosus muscle fibres.

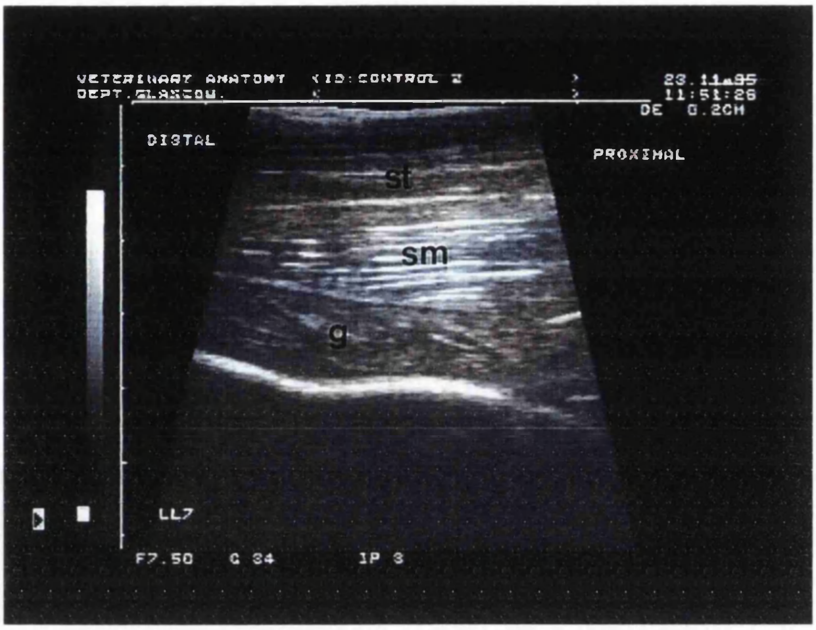

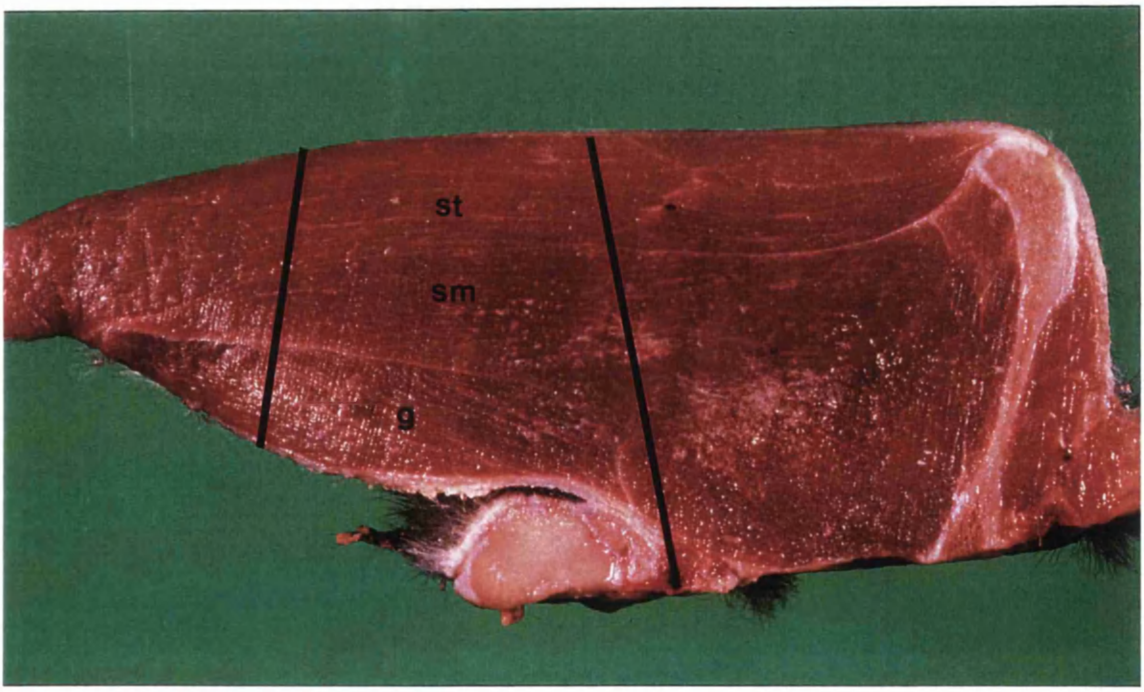

Figure 3.12

Figure 3.13 Transverse scan of the normal thigh muscle from the cranio-lateral aspect (**a**) using 3.75 MHz transducer and (**b**) using 7.5 MHz transducer. Note that the muscle echotexture is more clear in **b** with fine detail as compared to the image in **a**. However, the penetration is reduced in **b** as the sound beam is attenuated more quickly with the 7.5 MHz frequency transducer. The femur appears hyperechoic with acoustic shadowing artefact in **a**. **BF**, m. biceps femoris, **SM**, m. semimembranosus, **ST**, m. semitendinosus, **F**, femur, **A**, m. adductor.

Figure 3.13a

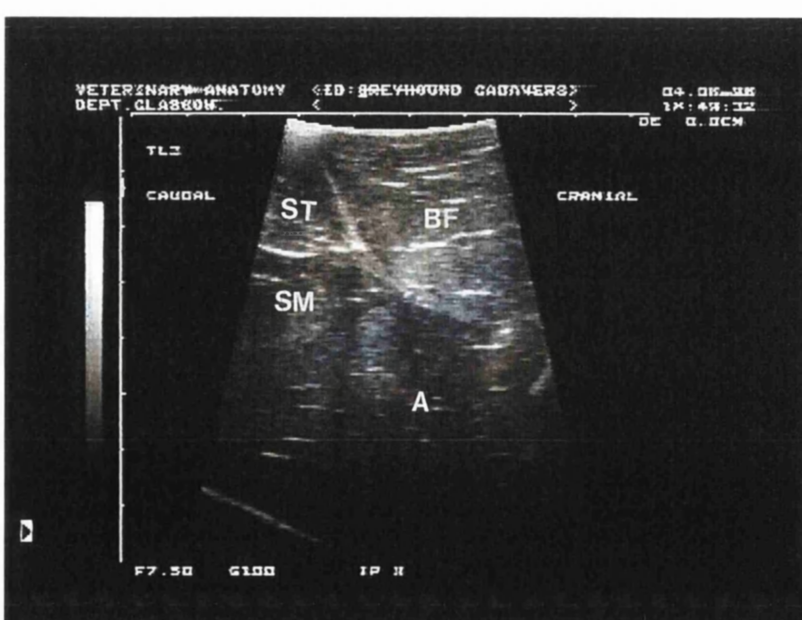

Figure 3.13b

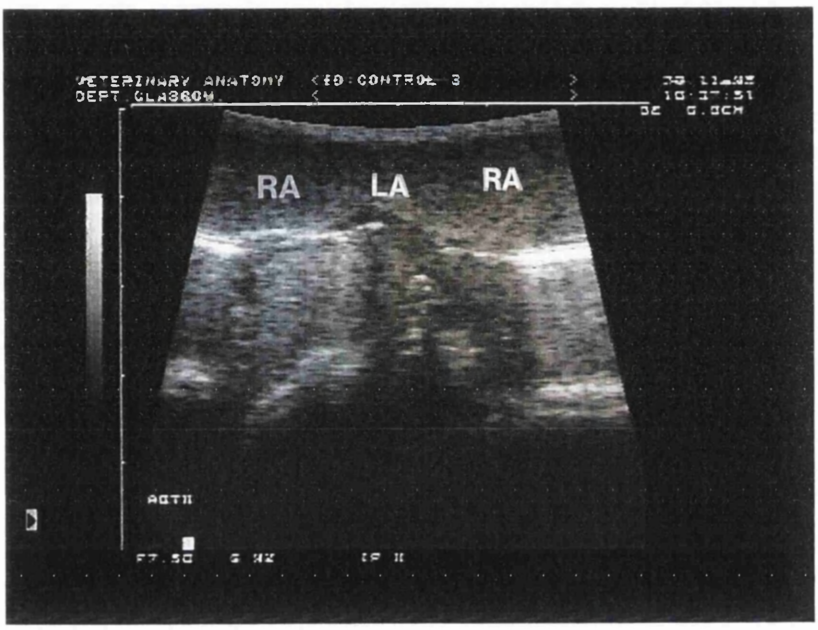

Figure 3.14 Transverse scan of the normal ventral abdominal mid-line caudal to the umbilicus. Note that the ventral abdominal mid-line (linea alba) appears isoechoic relative to the muscle echotexture. **LA**, linea alba, **RA**, m. rectus abdominis.

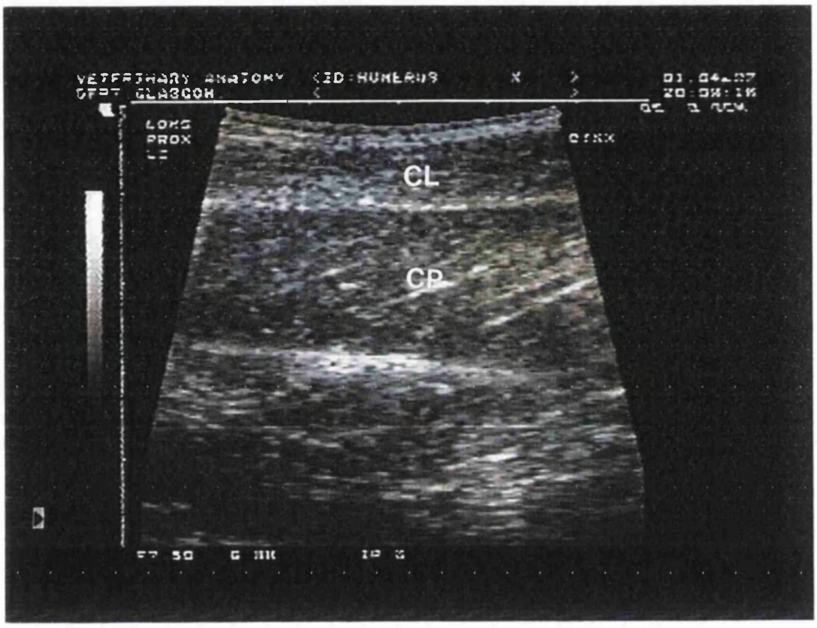

Figure 3.15 Longitudinal scan of the normal brachial muscle on latero-caudal aspect of the left fore limb. Note that the normal muscle appears hypoechoic with a characteristic of "feathery appearance" produced by the triceps muscle (caput longus). The connective tissue fascia, the perimysium, surrounding the muscle fibres is responsible for this appearance. **CL**, caput lateralis, **CP**, caput longus of m. triceps brachii.

3.4 **Discussion**

The normal ultrasonographic appearance of the skeletal muscles has been published in both human and animals (Fornage *et al.*, 1983; Vincent, 1988; Harcke *et al.*,1988; Fornage, 1989; Kaplan *et al.*, 1990; Craychee, 1995; Smith *et al.*, 1996; Kramer *et al.*, 1997). The typical muscle has a bright outer margin caused by the connective tissue fascia, with a medium level central echo pattern representing the muscle fibres or muscle bundles (Harcke *et al.*,1988). Muscle fibres are surrounded by a thin loose connective tissue, called endomysium. A mass of muscle fibres blocks together and forms a bundle of muscle fibres. This bundle is surrounded by a dense connective tissue membrane or fascia called perimysium. The bundles form a muscle which is surrounded by a thick fascia called epimysium (Craigmyle, 1986). These two fasciae, perimysium and epimysium which are highly echogenic substances can be detected by ultrasound. The perimysium, in particular gives rise to a typical characteristic ultrasonographic imaging of the muscle. Thus, a longitudinal scan parallel to the muscle long axis revealed an image of homogenous fine parallel echoes, the fine echoes originating from fibroadipose septae, perimysium which surround the muscle bundles. The muscle groups can be differentiated from each other by an hyperechoic white line which is actually the fasciae surrounding them (epimysium).

Although most muscles are arranged along the long axis of the extremity in a parallel fashion, there are usually slight obliquities in the individual muscles, with each having a slightly different orientation (Harcke *et al.*, 1988). This could suggest why the ultrasonographic appearance of the thigh musculature imaged longitudinally from latero-caudal aspect has two different appearances as demonstrated in figure 3.12. The bundles of the semimembranosus and gracilis muscles are actually not running parallel with each other. The semimembranosus muscle bundles are running from the ischiatic tuberosity to the medial side of the distal end of the femur and the proximal end of the tibia while the bundles of gracilis muscle are running from the pelvic symphysis to the cranial border of the tibia (Evans and Christensen, 1993). Thus, this is why the semimembranosus and gracilis muscles appeared as two different characteristics when the thigh musculature was scanned longitudinally from a latero-caudal aspect. Similarly, in the sagittal images of the thigh and brachial muscles, the thigh muscle appeared hypoechoic with fine parallel echoes on a sagittal scan, while the brachial muscle appeared hypoechoic with homogenous fine echoes scattered throughout the muscle parenchyma on sagittal scans as demonstrated in figure 3.10 and 3.8 respectively. Muscle structure with ultrasonography has also been shown to depend on the angle of inclination of the transducer (Cady *et al*, 1983). If the probe is roughly perpendicular to the fascicular axis, the parenchymal echoes are dense and ultrasonography in a plane parallel to the fasciculi reveals several linear echoes at right angles to the transducer.

Results from this study also demonstrated that the transducer of 7.5 MHz frequency produced better images of skeletal muscle with high resolution and more information could be obtained from the ultrasound image as compared to the image produced by the transducer of 3.5 MHz frequency. Previous researchers have suggested that the higher frequency transducer should be used when examining the superficial structures and the extremities (Wilson, 1988; Fornage, 1989). However, the choice of the transducer is highly dependent on the size of the animal and the objective of the examination. In the present study, the greyhound cadavers were of medium size, therefore the frequency of 7.5 MHz produced the best image. Although the 7.5 MHz frequency transducer has been shown to produce better resolution, the sound beam penetration is limited. Thus, as the thigh musculature in a large dog is thick, the use of a lower frequency transducer (3-5 MHz) may be indicated to allow deeper penetration into the muscle, but it is often less precise. The previous studies demonstrated that 3.5 MHz transducer has an advantage in large muscular area such as thigh, where the increased penetration and large field of view was necessary to see deep structures (Kaplan *et al.*, 1990; Christensen *et al.*, 1988).

A feathery appearance of the skeletal muscle was demonstrated by the *caput longus* of the triceps muscle in this study when imaged longitudinally from the latero-caudal aspect. Such appearance was not demonstrated by other muscles of the thigh region. A thin layer of fat and connective tissue fascia (perimysium) surrounding the muscle bundles is responsible for the feathery appearance of the individual muscle seen ultrasonographically (Kaplan *et al.* 1989, 1990; van Holsbeeck and Introcaso, 1990). Kaplan *et al.*, (1990) showed the feathery appearance of normal skeletal muscle on a longitudinal scan of part of lateral head of gastrocnemius muscle. The results suggested that not all individual muscle groups in the animal body produce the characteristic of 'feathery appearance' on a longitudinal scan along the muscle fibres. Only certain individual muscles produce this characteristic such as *caput longus* muscle in this study.

The echogenicity of the skeletal muscle structures in this study was found to be varied between cadavers. The variability in echogenicity of skeletal muscle imaged ultrasonographically has been reported and it could be due to the gain setting and the inclination of the transducer (Cady *et al.*, 1983) or it might be due to muscle hypertrophy (van Holsbeeck and Introcaso, 1990).. When the gain setting is set higher for the near and far field, more sound is reflected back to the transducer, and therefore the overall image is more bright and echogenic. In contrast, when the gain setting is set lower, less sound is reflected back, and the overall image is less bright and hypoechoic. In this study, the overall increase of echogenicity for the near field in the ultrasonographic image of skeletal muscle shown in figure3.4B was due to the gain setting for the near field being set a bit higher, therefore the overall echogenicity of the near field was increased as compared to the far field. In hypertrophied muscle, the muscle cells and therefore the bundles have became larger while the connective tissue within muscle remains constant. Thus, the image will appear hypoechoic compared to the normal muscle. Hypertrophied muscle imaged ultrasonographically in humans has been demonstrated to have an hypoechoic appearance (van Holsbeeck and Introcaso, 1990).

CHAPTER 4

ULTRASONOGRAPHIC IMAGING OF ABDOMINAL WOUND HEALING AFTER ABDOMINAL SURGERY IN DOGS

4.1 Introduction and aims of the study

Ultrasonography can be used to detect subtle differences in acoustic impedance of soft tissues and, therefore, is a sensitive technique for locating and characterizing fluid collections and masses (Christensen *et al.*, 1988). The development of a haematoma and of fibrous scars can be followed up by ultrasonography, but it is not possible to determine the point of time after injury very accurately. Nevertheless, ultrasonography is a method of great value in the diagnosis of muscle injuries and, given certain limits, in the follow up of the healing process (Kullmer *et al.*, 1997). In a study of post-operative incision site complications using ultrasound, Trout *et al.* (1994) reported that ultrasonography is a sensitive technique that could be used to detect and localise fluid accumulations at a surgical site. However, many ultrasonographic features of surgical sites were not specific for dogs with early post-operative incision site complications. In human beings, ultrasonography has been used successfully for the diagnosis of haematomas, seromas, and inflammatory processes such as abscesses (Vincent, 1988; Jain *et al.*, 1992; Berstein and Hansen, 1991; Howard and Einhorum 1991). Ultrasonography has also been shown to be highly effective in the early recognition of post-operative haematoma formation after hip or femoral shaft surgery, including total hip replacement (Glaser *et al.*, 1988; Parrini *et al.*, 1988). Ultrasonography has also been used to monitor healing of ventral abdominal mid-line incisions after exploratory laparotomy in 21 ponies (Wilson, *et al.* 1989). In an experimental study on the healing of a ruptured gastrocnemius muscle in rats, Lehto and Alanen, (1987) have pointed out the accuracy of ultrasonography in the examination of muscle trauma, especially during the early phase of healing. Ultrasonography has also been shown to be useful in defining mass location, lesion margins tissue of origin, lesion tissue characteristics, invasion into nearby blood vessels and oesophagus, and the optimal location for directing needle aspiration or tissue biopsy (Fornage *et al.*, 1983).

The present study has been carried out with the main aim of evaluating the use of B-mode ultrasonography to monitor the progress of abdominal wound healing after abdominal surgery, e.g. ovariohysterectomy and any changes that might occur during the reparative phase. In addition a preliminary cadaver study of the ventral abdominal mid-line was also carried out ultrasonographically to observe the images created from old incision sites.

4.2 A PRELIMINARY ULTRASONOGRAPHIC IMAGING OF THE VENTRAL ABDOMINAL MIDLINE (VAM) OF FEMALE CADAVERS

4.2.1 Materials and methods

The animals and preparation technique

Thirty one adult, female canine cadavers of different breeds which had been euthanased for other reasons were collected from the Glasgow region and were used in this study All of these cadavers had been euthanased within 24 hours upon arriving at the Division of Veterinary Anatomy, Glasgow University Veterinary School. Upon arrival, the cadavers were selected and examined physically prior to ventral abdominal mid-line scanning. The cadavers were then put on a table in dorsal recumbency to expose the ventral abdominal mid-line. This was accomplished by tying up all the four limbs to the four table legs. The hair on the ventral abdominal area from the level of the xyphoid cartilage to the level of pubic brim was removed using clippers. The ventral abdominal muscles including the linea alba were examined physically by means of palpation prior to the ultrasound scan. Ultrasound gel was then applied prior to scanning to give the best contact between transducer and the skin.

Ultrasonographic examination

Ultrasonographic examination for each cadaver was done in a semi-dark room. Prior to the ultrasound examination, the scanner was calibrated, the gain settings for near field, mid field and overall were adjusted for each examination to give the optimum image quality. The scanning was done transversely across the ventral abdominal mid-line with the transducer head held perpendicular to the ventral abdominal mid-line as illustrated in figure 4.1. This allowed the ventral abdominal mid-line to appear at the centre top of the image on the screen just under the skin and subcutaneous tissue. The transducer was then moved slowly and firmly along the ventral abdominal mid-line from the level of the xyphoid cartilage to the pubic brim to detect of any changes in the ultrasonographic image. In some cases, a sonolucent stand-off pad was used.

Ultrasonographic examination was performed using a real time B-mode ultrasound scanner, (Capasee TOSHIBA) equipped with a high resolution 7.5 MHz linear array transducer. The ultrasound machine was connected to a video recorder (Panasonic) during each scanning session. A high quality (super VHS) video tape was used to record the images during each session. The recorded images were reviewed at a later date using an Interspec (Apogee-cx) ultrasound machine. Thermal copies of the best images were printed during the review and labelled.

Histological preparation

After each examination, a block of muscle sample approximately two centimetres square was taken from each cadaver from the area approximately 3-5 cm caudal to the umbilicus depending on the size of the animal. The muscle samples were then put in 10% formalin for histologic examination. The tissue samples were sectioned and processed for haematoxylin and eosin as previously described by Lendrum *et al.*, (1962) and Culling, (1974).

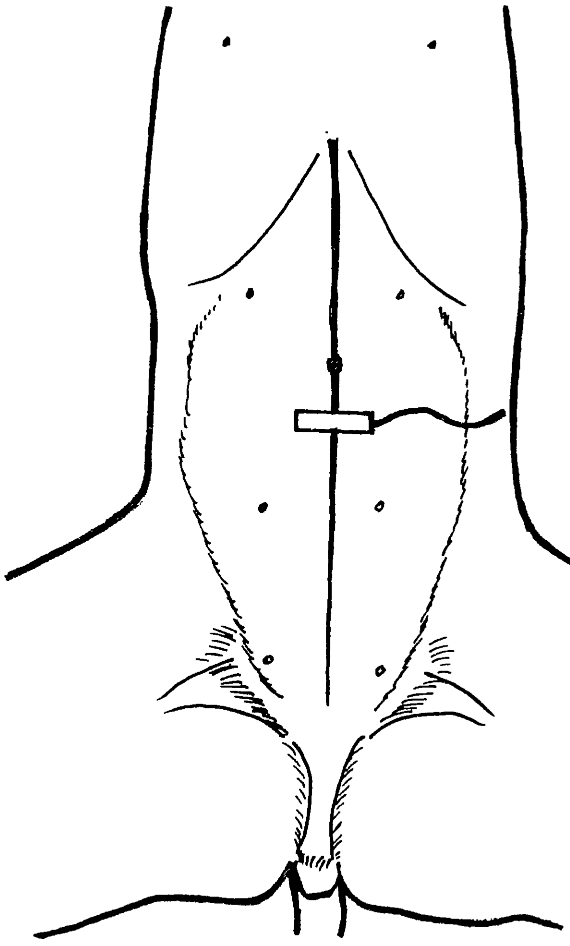

Figure 4.1 Illustrated diagram demonstrating the technique of ventral abdominal mid-line (VAM) scanning. The cadaver is lying on the table in dorsal recumbency. The scanning is done transversely across the ventral abdominal mid-line. The transducer head moves slowly and firmly from the level of the xyphoid cartilage to the pubic brim with VAM placed directly under the transducer head.

4.2.2 **Results**

The summary of the ultrasonographic and histological examination of the ventral abdominal mid-line in 31 cadavers is shown in table 4.1. For the purpose of this study, the ultrasonographic appearance of the ventral abdominal mid-line (VAM) has been divided into three groups: group one represent the ventral abdominal mid-line with the presence of a new incision site, group two represent the ventral abdominal mid-line with the presence of an old incision site, and group three represent the normal intact ventral abdominal mid-line (without any sign of incision site. Of the 31 cadavers examined ultrasonographically, 9 (29%) cadavers were found to have normal VAM, 5 (16%) cadavers were found to have a new incision site, and 17 (51.6%) cadavers were found to have an old incision site

Normal ventral abdominal mid-line

A normal ventral abdominal mid-line was found in nine cadavers. Ultrasonographic appearance of the normal ventral abdominal mid-line was constant (figure 4.2). Normal VAM imaged ultrasonographically appeared isoechoic relative to the muscle tissue. No area of altered echogenicity was found along the VAM or in the adjacent rectus abdominis muscle. The rectus abdominis muscle imaged ultrasonographically appeared as an homogenous hypoechoic structure and was well enveloped by the hyperechoic connective tissue fascia, the perimysium. Histologically, no evidence of scar tissue formation was found in the muscle adjacent to the VAM.

VAM with a new incision site

Ultrasonographic examination of the VAM with the presence of new incision site revealed a disorganised area with ill defined margins which was hypoechoic relative to the surrounding tissues (figure 4.3). The ventral abdominal mid-line has lost its normal isoechoic appearance. Histologically, there was an accumulation of high number of inflammatory cells at the VAM which corresponded to the hypoechoic area imaged ultrasonographically. In cadaver 18, ultrasonographic examination revealed an hypoechoic area in the subcutaneous tissue superficial to the rectus abdominis muscle, and there was also an hyperechoic area adjacent to the ventral abdominal mid-line (figure 4.4). Histologically, there was an area of inflammatory cells accumulating in the subcutaneous tissue which corresponded to the hypoechoic area on ultrasound, and area of scar tissue formation in the rectus abdominis muscle adjacent to the mid-line on both sides which correspond to the hyperechoic structure on ultrasound. In cadaver 21, some blood was still present during ultrasonographic examination and the suture material was still intact. The dog was believed to have died during surgery. Ultrasonographic examination revealed an ill-defined disorganised hypoechoic area, casting acoustic shadowing artefact (figure 4.5). In this animal subcutaneous tissue appeared hypoechoic relative to muscle structure. There was also fluid collection present in the subcutaneous tissue as shown by the anechoic area. Histological examination was not carried out in this case because the block of muscle proved difficult to process.

In four cadavers (1, 4, 12 and 18) the suture materials still remained at the incision site. In these cadavers, the ultrasonographic findings were constant as shown in figure 4.3. The ultrasonographic images revealed an ill-defined hypoechoic area which corresponded to the area of the high number of inflammatory cells found with histological examination.

VAM with old incision site

The majority of the cadavers examined (17) fell into this group. Ultrasonographic appearance of the VAM with the presence of an old incision site varied from hypoechoic to hyperechoic. Most of the VAM with an old incision site appeared as an ill-defined disorganised hyperechoic area relative to its surroundings (figure 4.6). These hyperechoic areas which were imaged ultrasonographically corresponded to the areas of scar tissue formation on histological examination. In four cadavers (7, 11, 28 and 29), the VAM with an old incision site appeared as a poorly disorganised hypoechoic structure relative to the surrounding tissue (figure 4.7). Histological examination revealed a high level fat lobules around the scar tissue which was believed to be responsible for the hypoechoic appearance on the ultrasound image in these cadavers. In three cases (14, 22 and 31), the incision site imaged ultrasonographically appeared almost isoechoic to the surrounding muscle (figure 4.8). Histological examination revealed a small number of fat lobules around the scar tissue.

The subcutaneous tissue superficial to the rectus abdominis muscle and just under the skin imaged ultrasonographically had a variable appearance. It appeared from hypoechoic to hyperechoic relative to the muscle tissue. Of the 30 cadavers scanned in this study, 19 cadavers demonstrated subcutaneous tissues with hyperechoic appearance, seven cadavers demonstrated subcutaneous tissues with isoechoic appearance and the remaining four cadavers demonstrated subcutaneous tissue with hypoechoic appearance. Skin imaged ultrasonographically appeared as a hyperechoic layer. The fascia consisting of dense connective tissue enveloping the rectus femoris muscle appeared hyperechoic on ultrasound.

Table 4.1 Summary of ultrasonographic and miroscopic findings on VAM caudal to the umbilicus.

Cadaver no.	Ultrasonographic finding	Histological finding
1	An ill-defined hypoechoic area at VAM. S/c tissue appeared more echogenic relative to muscle.	Area of high number of inflammatory cells. Suture materials still present.
2	Area of increased echogenicity within muscle. S/c tissue appeared more echogenic than muscle.	Area of scar tissue formation within muscle.
3	Area of increased echogenicity within muscle. S/c tissue appeared more echogenic than muscle.	Area of scar tissue formation within muscle.
4	An ill-defined hypoechoic area. S/c tissue appeared more echogenic than muscle.	Area of high number of inflammatory cells with the presence of suture materials.
5	Area of increased echogenicity within muscle. S/c tissue appeared more echogenic than muscle.	Area of scar tissue formation.
6	Normal muscle characteristics. S/c tissue appeared more echogenic than muscle.	Normal
7	Disorganised hypoechoic area within muscle. S/c tissue appeared less echogenic than muscle.	High level of fat lobules around scar tissue.
8	Area of increased echogenicity within muscle. S/c tissue appeared more echogenic than muscle.	Area of scar tissue formation.

S/c = subcutaneous tissue

Table 4.1 continued

Cadaver no.	Ultrasonographic finding	Histological finding
9	Normal muscle characteristics. S/c tissue appeared more echogenic than muscle.	Normal.
10	Area of increased echogenicity lateral to the VAM. S/c tissue appeared more echogenic than muscle.	Area of scar tissue found lateral to the VAM.
11	Ill-defined hypoechoic area. S/c tissue appeared less echogenic than muscle.	Area of scar tissue formation with a high level of fat lobules around area.
12	Ill-defined hypoechoic area. S/c tissue appeared more echogenic than muscle.	Muscle block was difficult to process.
13	Normal muscle characteristic. S/c tissue appeared more echogenic than muscle.	Normal.
14	Area of slightly increased echogenicity (almost isoechoic) just lateral to the VAM. S/c tissue appeared more echogenic than muscle.	Area of scar tissue adjacent to the VAM with few fat lobules around.
15	Area of increased echogenicity within muscle. S/c tissue appeared more echogenic than muscle.	Area of scar tissue formation.
16	Area of increased echogenicity lateral to the VAM. S/c tissue appeared isoechoic relative to muscle.	Area of scar tissue formation lateral to the VAM with fat lobules around.

S/c = subcutaneous tissue

Table 4.1 continued

Cadaver no.	Ultrasonographic finding.	Histological finding
17	Normal muscle characteristics. S/c tissue appeared isoechoic relative to muscle.	Normal.
18	An ill-defined hypoechoic area within s/c tissue just above the VAM. Area of increased echogenicity at VAM. S/c tissue appeared more echogenic than muscle.	An area of high number of inflammatory cells just above RA muscle, and area of scar tissue formation on both side of VAM.
19	Normal muscle characteristics. S/c tissue appeared less echogenic than muscle.	Normal.
20	Area of increased echogenicity within muscle. S/c tissue appeared isoechoic relative to muscle.	Area of scar tissue formation with increased level of fat lobules around.
21	Disorganised hypoechoic area with acoustic shadowing artefact. S/c tissue appeared less echogenic than muscle.	Block of muscle difficult to process.
22	Area of slightly increased echogenicity (almost isoechoic) lateral to the VAM. S/c tissue appeared more echogenic than muscle.	Area of scar tissue formation lateral to the VAM with few fat lobules around.
24	Area of increased echogenicity at VAM and lateral to VAM. S/c tissue appeared more echogenic than muscle.	Area of scar tissue at VAM and lateral to the VAM with fat lobules around.

S/c - subcutaneous tissue   RA - m. rectus abdominis

Table 4.1 continued

Cadaver no.	Ultrasonographic finding	Histological finding
25	Normal muscle characteristics. S/c tissue appeared isoechoic relative to muscle.	Normal, high level of fat lobules at VAM.
26	Normal muscle characteristic. S/c tissue appear more echogenic than muscle.	Normal.
27	Normal muscle characteristics. S/c tissue appeared more echogenic than muscle.	Normal.
28	An ill-defined hypoechoic area at VAM. S/c tissue appeared isoechoic relative to muscle.	Area of scar tissue formation at VAM and slightly lateral to it with high level of fat lobules at the middle of VAM and around scar tissue in muscle.
29	An ill-defined disorganised hypoechoic area within muscle. S/c tissue appeared isoechoic relative to muscle.	Area of scar tissue formation with high level of fat lobules around.
30	Area of increased echogenicity at VAM. S/c tissue appeared more echogenic than muscle.	Area of scar tissue formation just lateral to the VAM.
31	Area of slightly increased echogenicity (almost isoechoic).s/c tissue appeared more echogenic than muscle.	Area of scar tissue formation at VAM and just lateral to it with fat lobules around.

S/c - subcutaneous tissue

Figure 4.2 Transverse scan of the normal VAM caudal to the umbilicus in cadaver 6. The VAM appears isoechoic relative to the muscle tissue (arrow). The subcutaneous tissue in this animal appears hyperechoic relative to the muscle tissue. Note also that the rectus abdominis muscle is surrounded by the hyperechoic connective tissue fascia, the perimysium. Histologically, there is no scar tissue formation found. **sc,** subcutaneous tissue, **ra,** m. rectus abdominis.

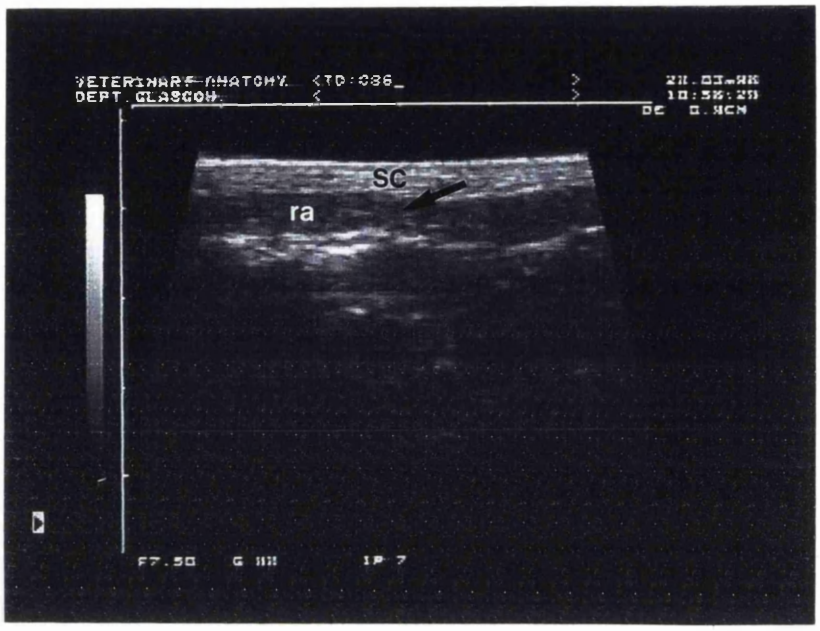

Figure 4.2

Figure 4.3 Transverse scan of the VAM caudal to the umbilicus with the presence of new incision site in cadaver 4 demonstrates a disorganised hypoechoic area with an ill-defined margin at the VAM (arrow heads). Histologically, there is an area of inflammatory cell accumulation at the VAM which corresponds to the hypoechoic appearance on ultrasound. The subcutaneous tissue appears isoechoic relative to the muscle tissue. **sc**, subcutaneous tissue, **ra**, m. rectus abdominis muscle.

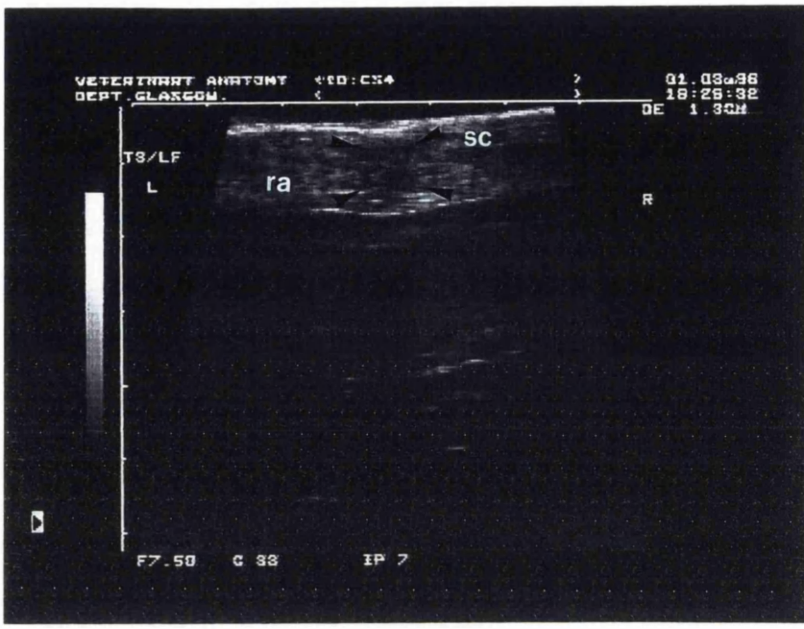

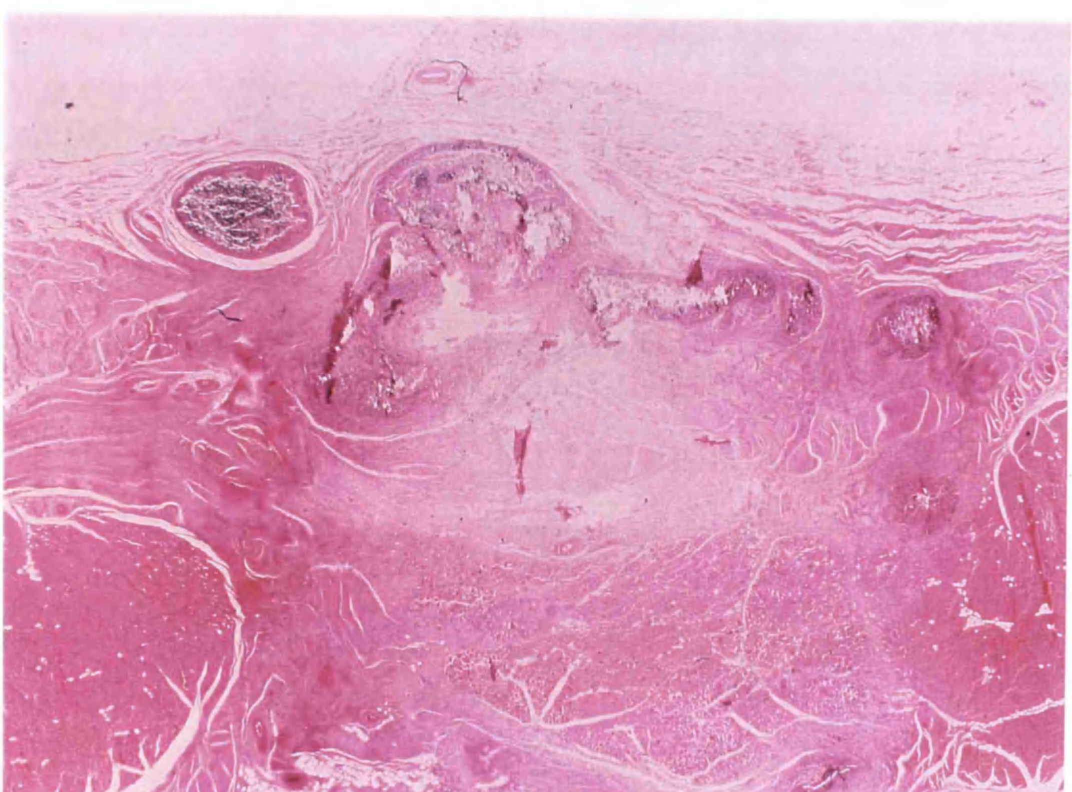

Figure 4.3

Figure 4.4 Transverse scan of the VAM in cadaver 18 with the presence of new incision site demonstrates an hypoechoic area within the subcutaneous tissue (arrow) just above the VAM. Histologically, there is area of inflammatory cell accumulation in the subcutaneous tissue which is responsible for the hypoechoic appearance on ultrasound. **sc**, subcutaneous tissue, **ra**, m. rectus abdominis.

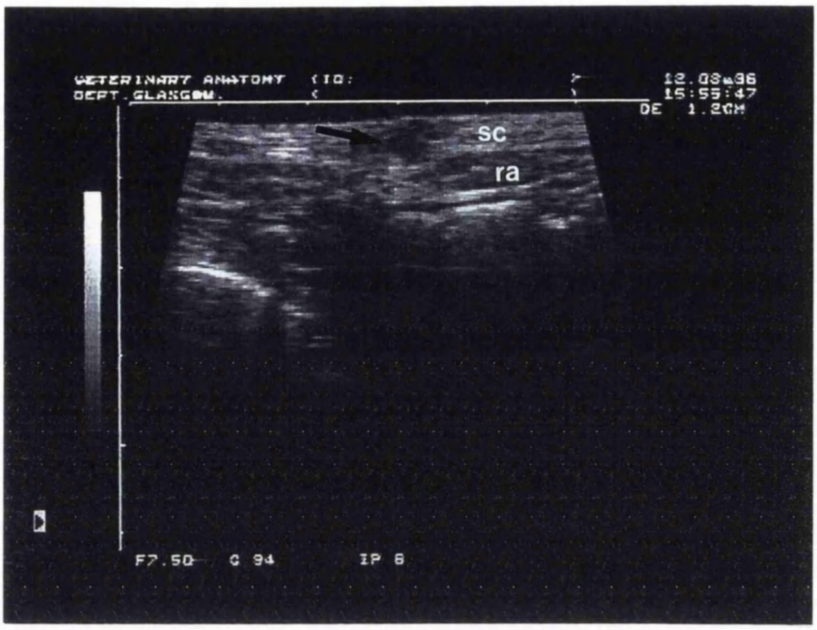
VETERINARY ANATOMY (ID:
DEPT. GLASGOW.
15:55:47
DE 1.2CM
sc
ra
F7.5G C 94 IP 8

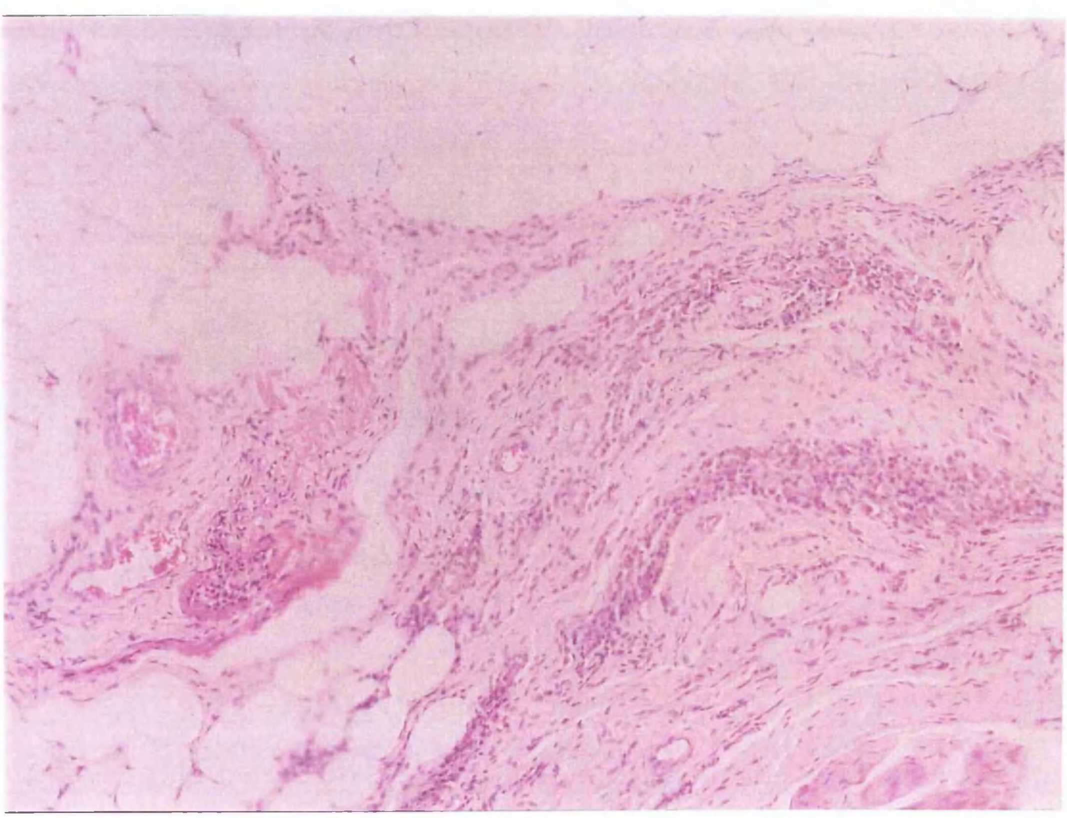

Figure 4.4

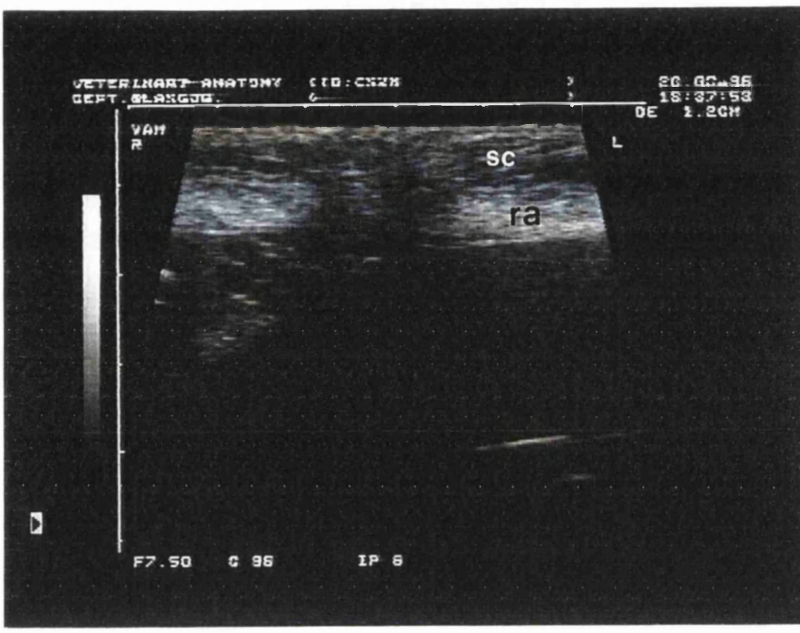

Figure 4.5 Transverse scan of the VAM with fresh incision site in cadaver 21 demonstrates a disorganised homogeneous hypoechoic area with acoustic shadowing artefact at the incision site. Note also that the subcutaneous tissue appears hypoechoic relative to the muscle tissue in this animal. **sc**, subcutaneous tissue, **ra**, m. rectus abdominis.

Figure 4.6 Transverse scan of the VAM caudal to the umbilicus in cadaver 3 with the presence of an old incision site demonstrates an hyperechoic area relative to the surroundings (arrow heads). Histologically, there is scar tissue formation on both sides of the rectus abdominis muscle adjacent to the VAM. Note also that the subcutaneous tissue appears hyperechoic relative to the muscle tissue in this animal. **sc**, subcutaneous tissue, **ra**, m. rectus abdominis.

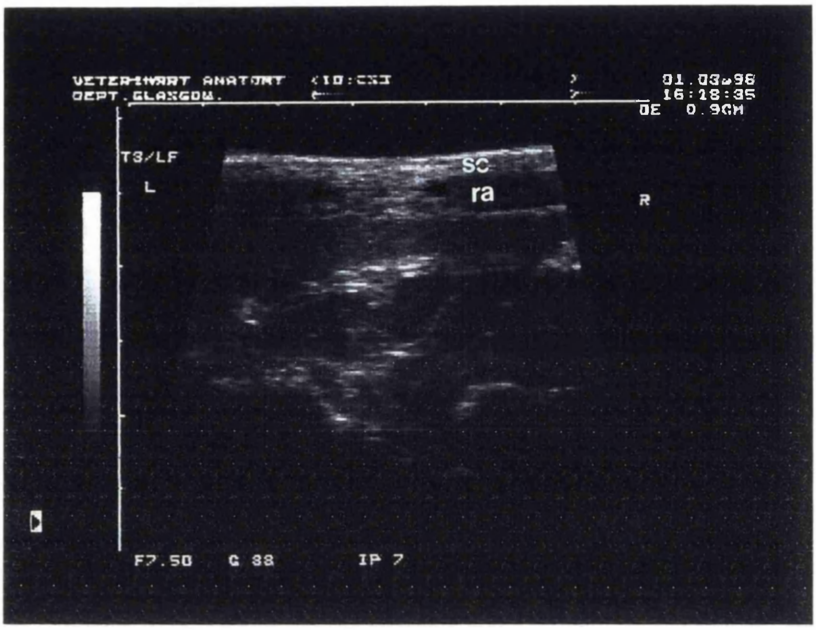

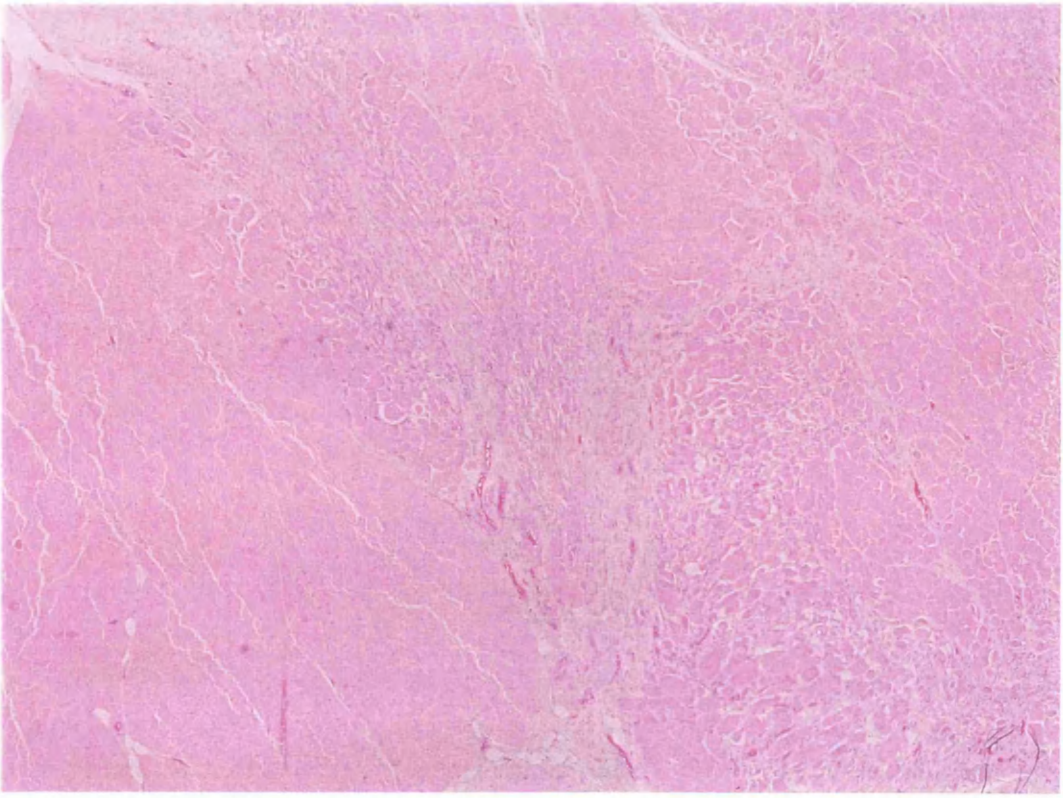

Figure 4.6

Figure 4.7 Transverse scan of the VAM caudal to the umbilicus in cadaver 11 with the presence of an old incision site demonstrates a disorganised hypoechoic area (arrow). Histologically, there is scar tissue formation found in the muscle with a high level of fat lobules around. Note also that the subcutaneous tissue appears hypoechoic relative to the muscle tissue in this animal. **sc**, subcutaneous tissue, **ra**, m. rectus abdominis.

Figure 4.7

Figure 4.8 Transverse scan of the VAM caudal to the umbilicus in cadaver 22 with the presence of an old scar tissue demonstrates slightly hyperechoic area (almost isoechoic) relative to the surroundings (arrow heads). Histologically, there is a presence of scar tissue formation in the muscle with little fat lobules. Note also the subcutaneous tissue appears hyperechoic relative to the muscle tissue. **sc**, subcutaneous tissue, **ra**, m. rectus abdominis.

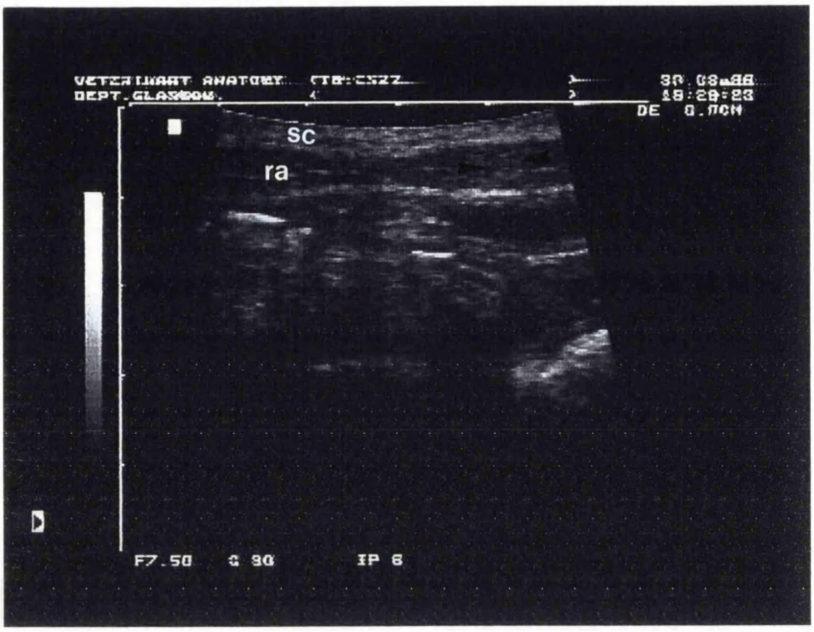

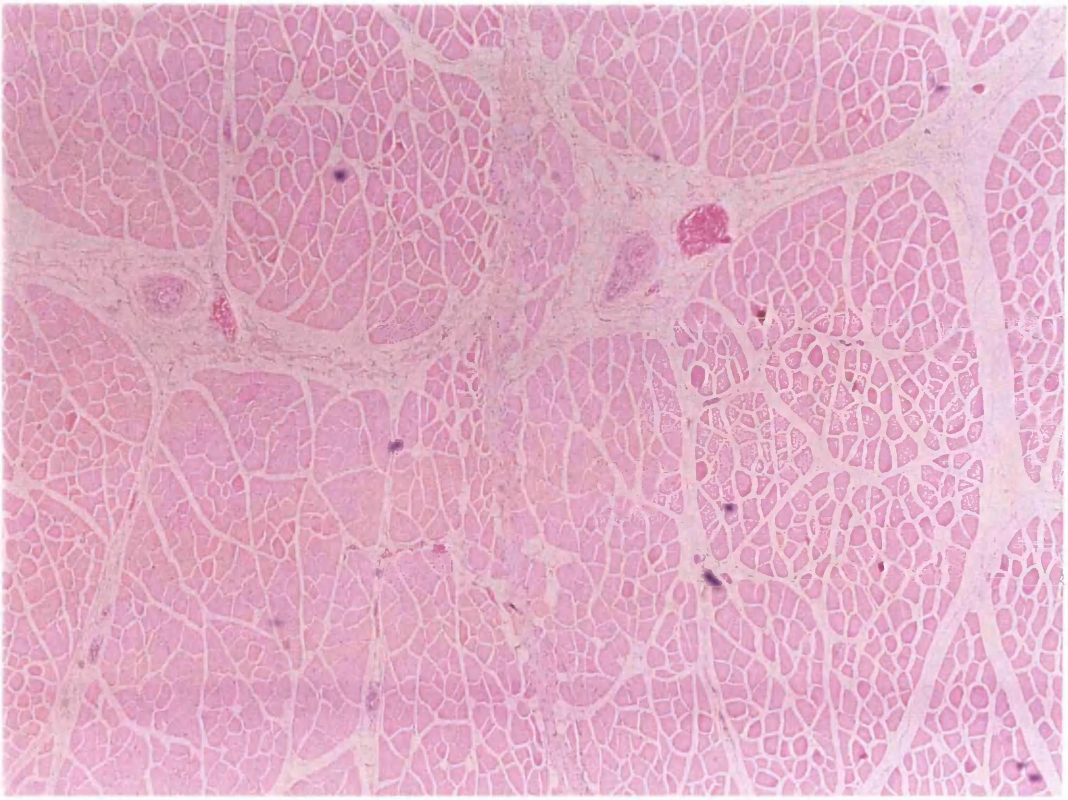

Figure 4.8

4.3 ULTRASONOGRAPHIC IMAGING OF THE PROGRESS OF WOUND HEALING AFTER ABDOMINAL SURGERY

4.3.1 Materials and methods

Animals and preparation technique

Five dogs of different breeds, sex and age referred to the Glasgow University Small Animal Clinics (GUSAC) were used in this study. The dogs had undergone ventral abdominal surgery for various reasons. The surgery was carried out on the ventral abdominal midline (VAM). The ventral abdominal area had been prepared earlier for abdominal surgery. The hair had already been removed. Thus, it was only necessary to apply ultrasound gel prior to ultrasonographic examination.

Ultrasonographic examination

A real-time B-mode ultrasound machine (Capasee TOSHIBA) connected with a 7.5 MHz linear array transducer was used in this study. A video recorder (Panasonic) was connected to the scanner to record the scanned images. The animal was laid on the table on lateral recumbency during scanning. In certain circumstances scanning was carried out in a standing or sitting position. The ultrasonographic examination was done transversely across the ventral abdominal midline (wound) from cranial to caudal as shown in figure 4.1. This was to allow the wound to appear at the centre of the ultrasonographic image. A further longitudinal scan was done along the wound (incision site) from cranial to caudal. Initial scanning was carried out on day one (approximately 24 hours) post-operation. Subsequent scans were carried out on the basis of one day apart while the animal was still in the hospital. An ultrasonographic examination was then carried out when the animals returned for wound assessment and removal of suture material. The scanned images for each of the cases were recorded during scanning on a super VHS video tape for revision at a later date. The best images were printed during review and labelled accordingly.

4.3.2 **Results**

Of the five cases involved in this study, four of them exhibited successful closure of the abdominal wound and one demonstrated complications in the healing process. A successful case (case 1) and the problem case (case 2) are discussed in detail to illustrate the healing process.

Case 1

An eight months old, male Labrador Retriever, weighing 31 kg was referred to the Glasgow University Veterinary School with the complaint of vomiting and diarrhoea for almost one month. Radiographic examination suggested the possibility of a foreign body in the small intestine. Enterotomy was carried out on the day following admission. A straight incision was made on ventral abdominal midline (linea alba). Intussusseption of the ileocaecocolic junction was found and reduced, and the whole portion of affected intestine was resected. End-to-end anastomosis of the intestine was then carried out. Abdominal muscle was closed with PDS, the ileocaecocolic junction with vicryl and the skin was closed with monofilament nylon.

Day one post-operation

Ultrasonographic examination of the ventral abdominal wound scanned transversely on day one (approximately 24 hours) post-operation demonstrated a wound which appeared as an ill-defined hypoechoic area with acoustic shadowing artefact (figure 4.9). The rectus abdominis muscle on both sides of the wound appeared well defined and almost isoechoic relative to the subcutaneous tissue. The edges of the wound (surgical site) appeared to have been well apposed. The wound on the skin and subcutaneous tissue appeared hypoechoic with acoustic shadowing artefact and was found not to be parallel with the wound in the muscle. A small fluid accumulation within the subcutaneous tissue at the surgical site of the skin appeared anechoic with ill-defined margins. The wound was found to be exactly on the linea alba i.e. in between the two rectus abdominis muscle, but at a certain point it was found on the muscle just lateral to the linea alba. The suture material within the subcutaneous tissue appeared hyperechoic with acoustic shadowing artefact (figure 4.10).

Longitudinal examination along the wound demonstrated a disorganised pattern of muscle with intermittent acoustic shadowing originating from the skin surface which was due to suture material in the skin (figure 4.11). Areas of haemorrhage and small fluid accumulations within the subcutaneous tissue appeared anechoic to hypoechoic with acoustic shadowing artefacts.

Day two post-operation

Ultrasonographic examination of the ventral abdominal wound on transverse scanning demonstrated an ill-defined hypoechoic area with acoustic shadowing artefact (figure 4.12). The supposed haemorrhagic area within the subcutaneous tissue superficial to the rectus abdominis muscle was still visible and appeared as an ill-defined hypoechoic area with acoustic shadowing artefact (figure 4.13). The area of muscle damage appeared disorganised and hypoechoic. Areas of supposed haemorrhage and small fluid accumulation within the subcutaneous tissue were still present and appeared anechoic to hypoechoic with acoustic shadowing artefact on the longitudinal scan (figure

4.14). The ultrasonographic images were almost similar to those of the day one examination.

On day 10 post-operation the dog returned for suture removal. Scanning of the wound site revealed satisfactory union of the recti muscles and the fluid accumulation had been resolved.

Case 2

A six year old female Samoyed, weighing 17 kg was referred to the Glasgow University Veterinary Small Animal Clinic having been diagnosed as having diabetes mellitus. Ovariohysterectomy had been carried out on this animal by a ventral abdominal midline surgical approach.

Day one post-operation

Ultrasonographic examination of the ventral abdominal wound on day one post-operation demonstrated the wound (surgical site) which appeared as an ill-defined hypoechoic area casting acoustic shadowing artefact (figure 4.15). The incision site was found to have good apposition between the rectus abdominis muscles of each side. The subcutaneous tissue appeared slightly hypoechoic relative to the rectus abdominis muscle. At a certain point the wound (incision site) on the skin was found to be non parallel with the wound in the linea alba (figure 4.16). The area of supposed haemorrhage within the subcutaneous tissue at the wound in the skin appeared as an ill-defined hypoechoic structure with acoustic shadowing artefact. A longitudinal scan of the ventral abdominal wound demonstrated a disorganised muscle structure, indicating the area of muscle damage (figure 4.17). A hypoechoic layer within the subcutaneous tissue suggested an area of haemorrhage or pooling of serous fluid. The intermittent acoustic shadowing artefacts originating from the skin were due to suture material in the skin.

Day 11 post-operation

Ultrasonographic examination was carried out a day after removal of suture material. Ultrasonographic examination of the ventral abdominal wound on a transverse scan demonstrated the wound which appeared as a disorganised hypoechoic area with an echogenic centre, casting an acoustic shadowing artefact (figure 4.18). The echogenic area of the wound was suggestive of the presence of fibrous tissue formation which was essential for the wound healing process. The area surrounding the surgical site appeared disorganised and hypoechoic suggestive of soft tissue damage. The subcutaneous tissue appeared isoechoic relative to the rectus abdominis muscle. A large fluid accumulation had developed at the surgical site between the subcutaneous tissue and the rectus abdominis muscle and appeared anechoic on ultrasound with acoustic enhancement artefact (figure 4.19).

Ultrasonographic examination of the ventral abdominal wound on a longitudinal scan demonstrated that the wound appeared as a disorganised area of mixed echogenicity indicating an area of muscle damage with intermittent acoustic shadowing artefacts emanating from the ill-defined hypoechoic areas within the muscle (figure 4.20). These ill-defined hypoechoic areas were actually the original sites of the suture material which has been infiltrated by serum and cellular debris.

Day 13 post-operation

Ultrasonographic examination of the ventral abdominal wound on day 13 post-operation demonstrated that the wound now appeared as a disorganised echogenic area, casting acoustic shadowing artefact (figure 4.21). The area surrounding the surgical site appeared more organised than on the previous scan. The large fluid accumulation with acoustic enhancement artefact separating the subcutaneous tissue and rectus abdominis muscle was still present. A small portion of fibrous tissue formation was seen protruding into the fluid space at the surgical site.

Longitudinal scan of the wound demonstrated that the surgical site appeared as a disorganised echogenic structure representing the area of muscle damage with the presence of fibrous tissue formation (figure 4.22). The small hypoechoic areas which were casting intermittent acoustic shadowing artefact were still visible but appeared smaller than on the day 11 examination. These hypoechoic areas represented the original sites of the reabsorbing suture material. The small portion of fibrous tissue protruding into the fluid space could also be seen on longitudinal scan. There was some echogenic material present within the fluid area suggesting that this was consolidating.

Day 15 post-operation

Ultrasonographic examination of the ventral abdominal wound on day 15 after surgery on a transverse scan demonstrated that the wound appeared as a disorganised hyperechoic structure with acoustic shadowing artefact (figure 4.23). The fibrous tissue appeared to have an hyperechoic appearance compared to the image on the day 13 post-operation. The large fluid accumulation between the subcutaneous tissue and the rectus abdominis muscle was still present. The small portion of fibrous tissue protruding into the fluid space seen on day 13 post-operation has increased in size and appeared hyperechoic (figure 4.24). The presence of echogenic material indicated that there was consolidation taking place.

Ultrasonographic examination of the wound on a longitudinal scan demonstrated a disorganised hyperechoic structure with the presence of some hypoechoic areas producing acoustic shadowing artefact (figure 4.25). These small hypoechoic areas within the muscle represented the original sites of suture material and were still visible on ultrasound. The disorganised hyperechoic structure was due to the presence of fibrous tissue formation.

Day 17 post-operation

Ultrasonographic examination of the ventral abdominal wound on day 17 post-operation on a transverse scan demonstrated that the wound appeared as a disorganised hyperechoic area with acoustic shadowing artefact (figure 4.26). The overall dimensions of the wound appeared to be smaller than on the day 15 examination. The large fluid accumulation was still present and appeared as in the previous scan. The fibrous tissue protruding into the fluid space area had increased in size and appeared hyperechoic (figure 4.27). This protruding fibrous tissue was moving during scanning. Aspiration was performed on the swelling and clear straw coloured serosanguinous fluid was removed. A longitudinal scan of the surgical site (wound) demonstrated a disorganised hyperechoic area representing the area of muscle damage and the presence of fibrous tissue formation (figure 4.28). The small hypoechoic areas with acoustic shadowing artefacts could still be seen. The animal was discharged from the clinic on the following day and the owner reported that the wound continued to heal satisfactorily and the swelling remained reduced in size.

Figure 4.9 Transverse scans of the ventral abdominal wound approximately 24 hours post-operation demonstrate an ill-defined hypoechoic area with acoustic shadowing artefact (arrow). The rectus abdominis muscle on both sides of the wound appears well defined and almost isoechoic relative to the subcutaneous tissue. The edges of the wound (surgical site) appears to have well apposed. The wound on the skin and subcutaneous tissue appears hypoechoic with acoustic shadowing artefact (arrow head) and is not parallel with the wound in the muscle. A small fluid accumulation within the subcutaneous tissue (small arrow) appears anechoic (**b**). Note also that the wound is exactly on the linea alba i.e. in between the two rectus abdominis muscles in **a**, but the wound is on the muscle just lateral to the linea alba (small arrow) in **b**.

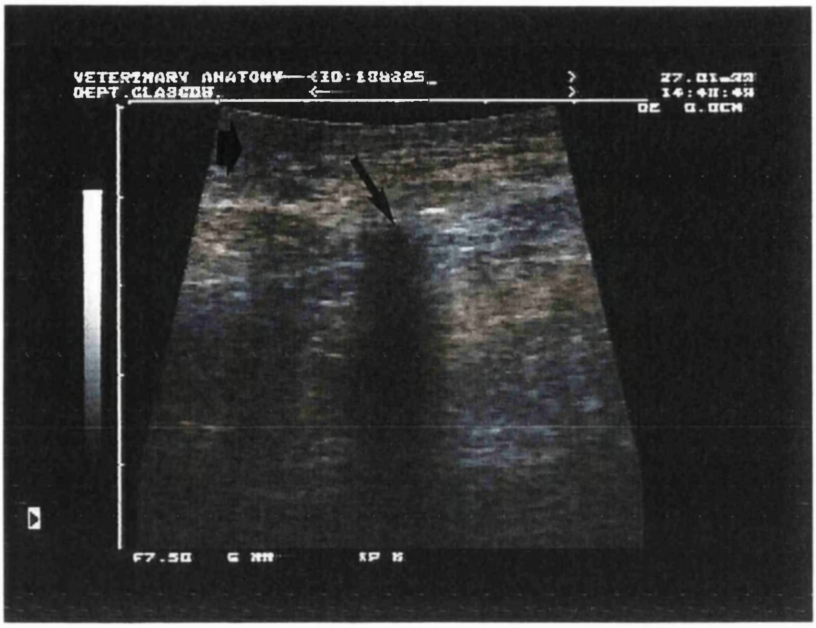

Figure 4.9a

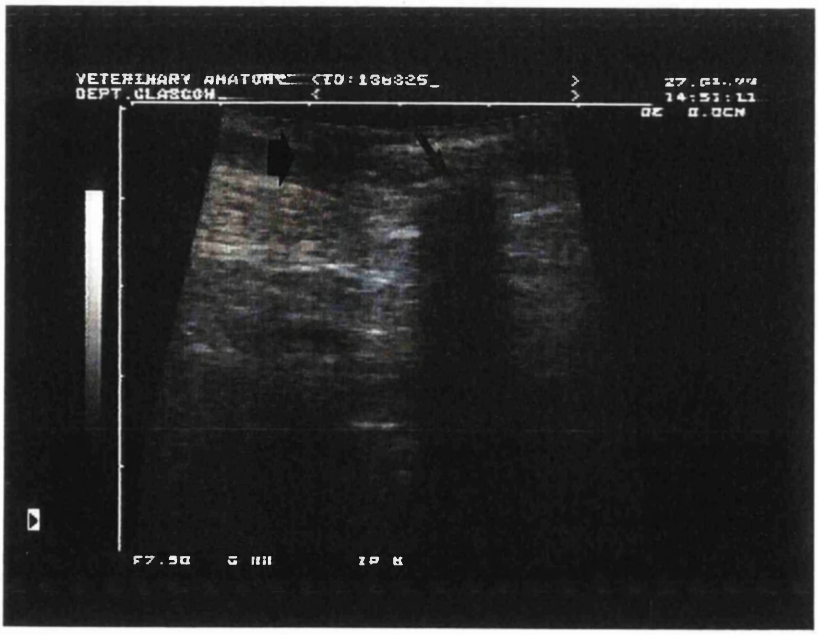

Figure 4.9b

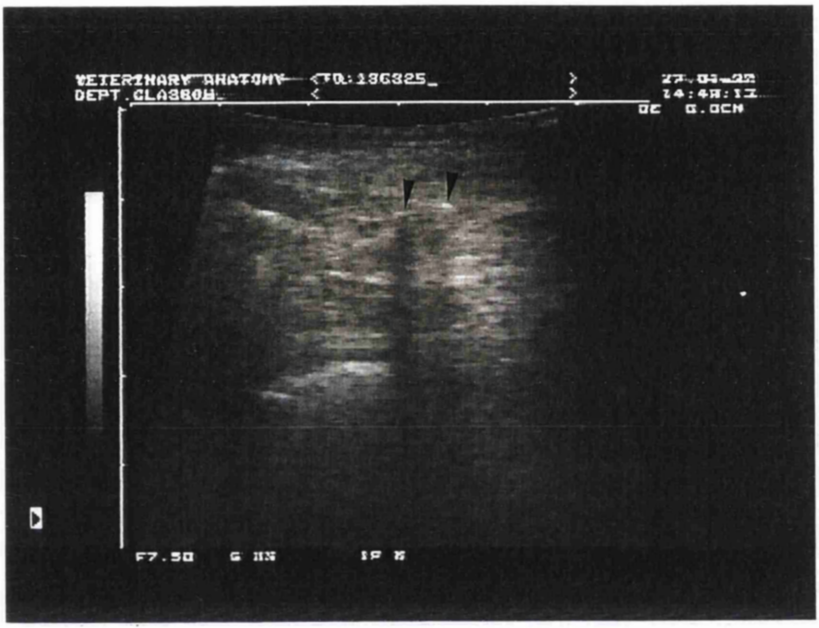

Figure 4.10 Transverse scan of the ventral abdominal wound approximately 24 hours post-operation demonstrates that the suture material used to close the linea alba appears hyperechoic with acoustic shadowing artefact (arrow heads).

Figure 4.11 Longitudinal scan along the ventral abdominal wound approximately 24 hours post-operation demonstrates a disorganised pattern of muscle with intermittent acoustic shadowing originating from the skin which is due to suture material in the skin (**a**). Areas of supposed haemorrhage and small fluid accumulations within the subcutaneous tissue appear anechoic to hypoechoic structures with acoustic shadowing artefacts (**b**).

Figure 4.11a

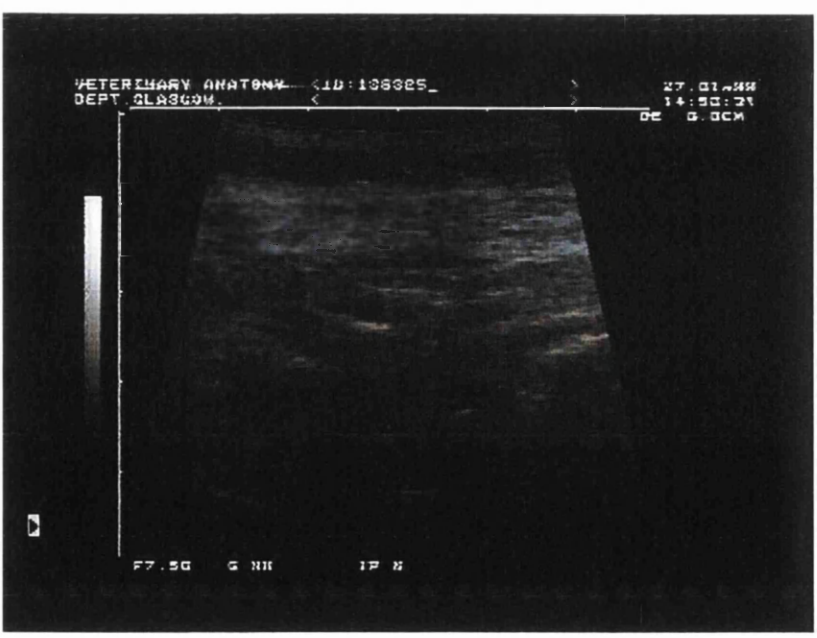

Figure 4.11b

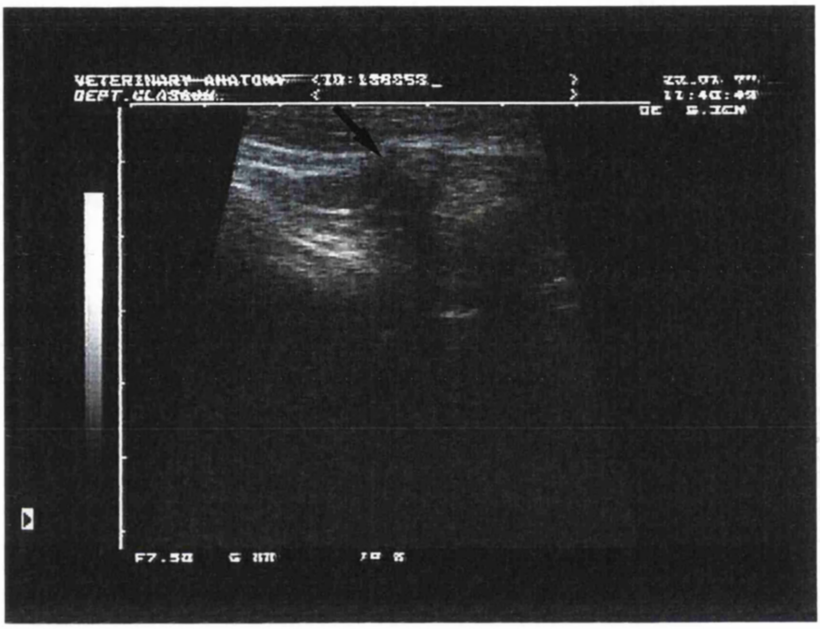

Figure 4.12 Transverse scan of the ventral abdominal wound on day two post-operation demonstrates an ill-defined hypoechoic area (arrow) with acoustic shadowing artefact.

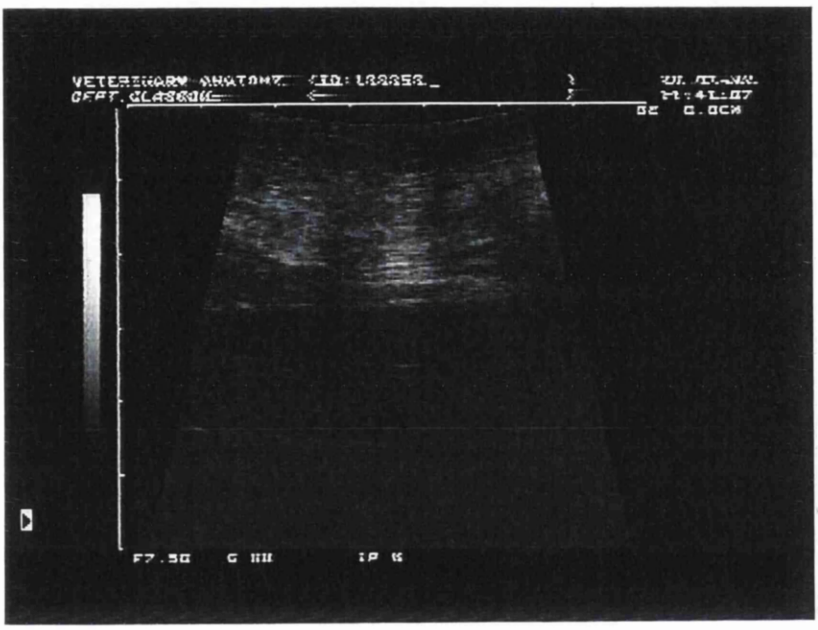

Figure 4.13 Area of supposed haemorrhage within the subcutaneous tissue superficial to the rectus abdominis muscle imaged longitudinally on day two post-operation appears as an ill-defined hypoechoic area with acoustic shadowing artefact. Note also that the area of muscle damage appears disorganised and hypoechoic.

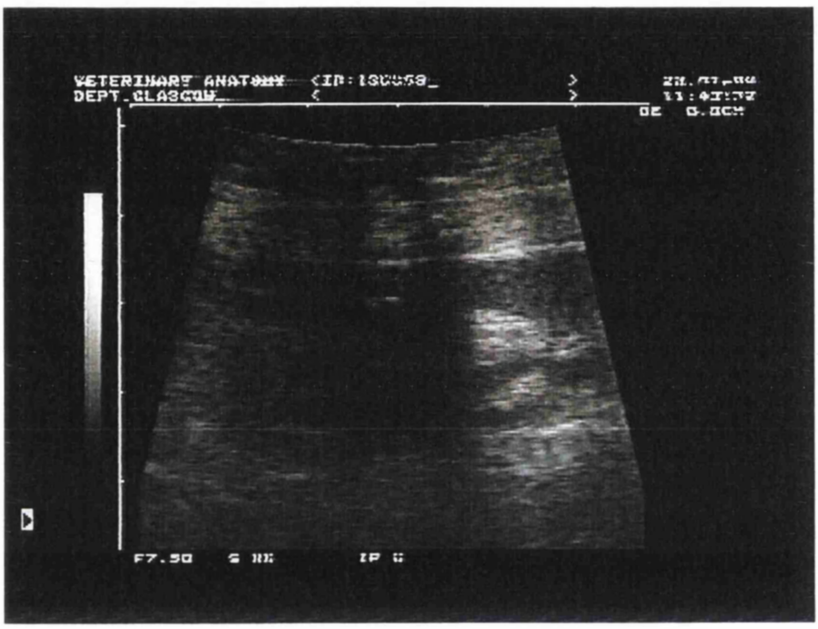

Figure 4.14 Longitudinal scan of ventral abdominal wound on day two post-operation demonstrates areas of supposed haemorrhage and small fluid accumulations within the subcutaneous tissue, appearing anechoic to hypoechoic with acoustic shadowing artefact.

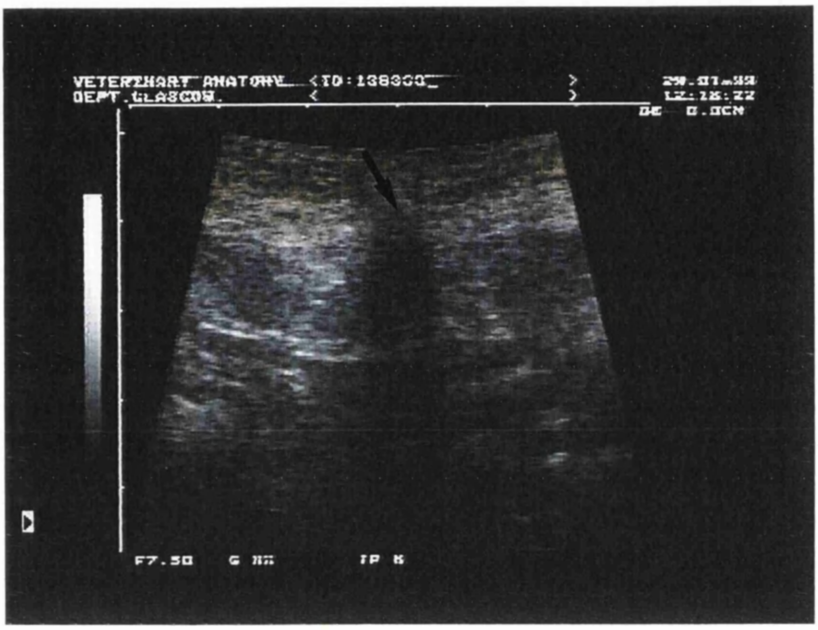

Figure 4.15 Case 2. Transverse scan of the ventral abdominal wound on day one post-operation demonstrates an ill-defined hypoechoic area (arrow) with acoustic shadowing artefact. The incision site is well appose between the two rectus abdominis muscles. Note also that the subcutaneous tissue appears slightly hypoechoic relative to the rectus abdominis muscle.

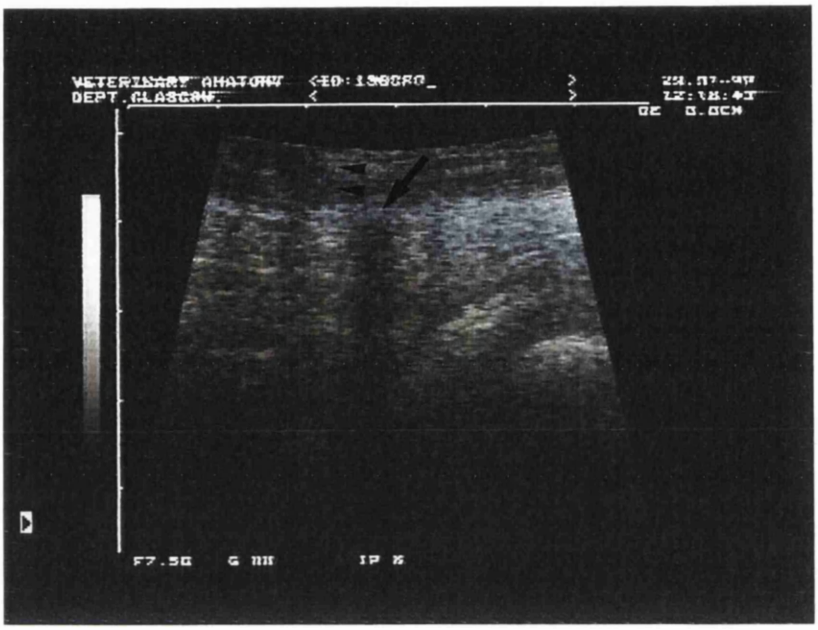

Figure 4.16 Case 2. Transverse scan of the ventral abdominal wound approximately 24 hours post-operation demonstrates the wound on the skin (arrow heads) which is not parallel with the wound on the linea alba (arrow). The supposed haemorrhagic area at the skin wound appears ill-defined and hypoechoic with acoustic shadowing artefact.

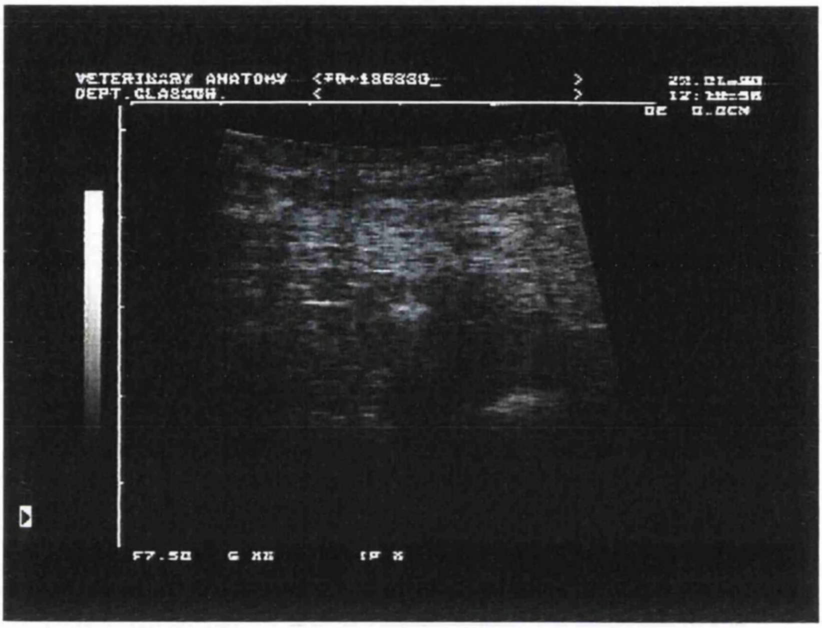

Figure 4.17 Case 2. Longitudinal scan of the wound approximately 24 hours post-operation demonstrates a disorganised muscle structure suggestive of muscle damage. A hypoechoic layer within the subcutaneous tissue represents the area of supposed haemorrhage or pooling of serous fluid. Note also the intermittent acoustic shadowing artefacts originating from the skin, due to the suture material.

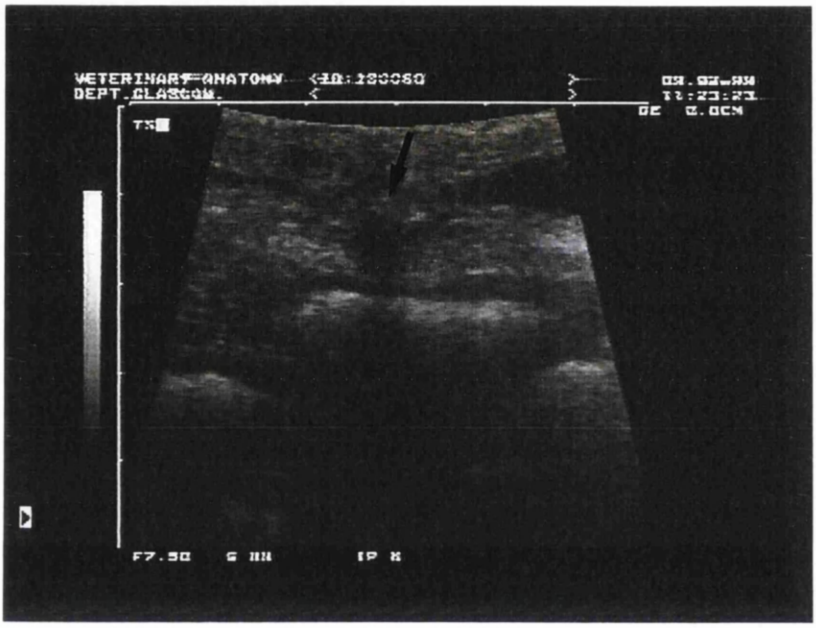

Figure 4.18 Case 2. Transverse scan of the wound on day 11 post-operation demonstrates a disorganised hypoechoic area (arrow) with an echogenic centre and casting acoustic shadowing artefact. The echogenic area of the wound is suggestive of the presence of fibrous tissue formation which is essential for the wound healing process. Note also that the area surrounding the surgical site appears disorganised suggestive of soft tissue damage.

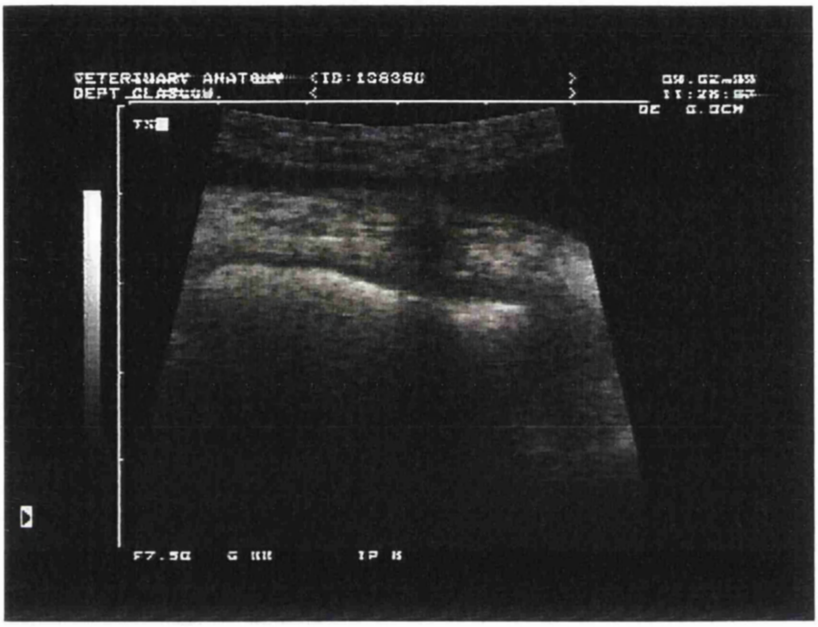

Figure 4.19 A large fluid accumulation has developed at the surgical site in between the subcutaneous tissue and rectus abdominis muscle scanned on day 11 post-operation appearing anechoic on ultrasound with acoustic enhancement artefact.

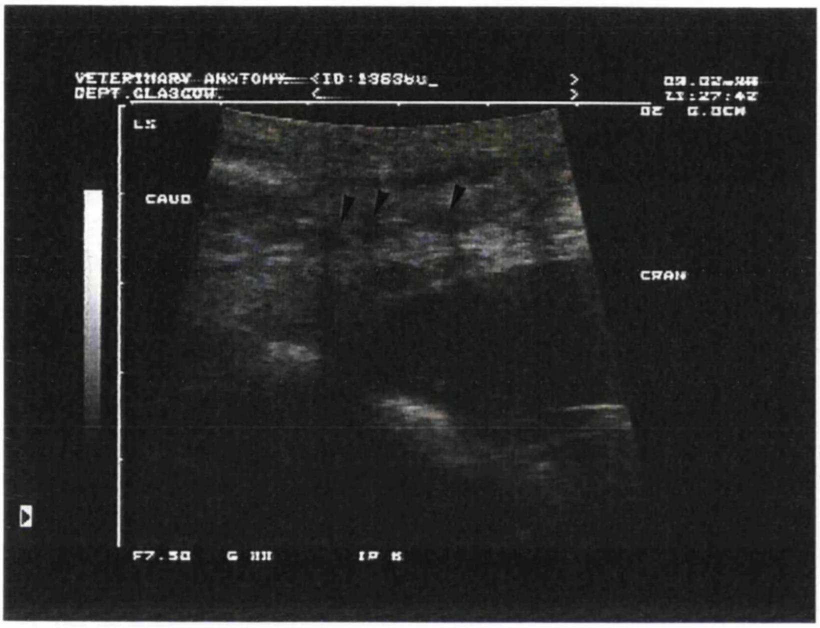

Figure 4.20 Longitudinal scan of the ventral abdominal wound on day 11 post-operation demonstrates a disorganised hypoechoic to echogenic structure representing the area of muscle damage with intermittent acoustic shadowing artefacts emanating from the ill-define hypoechoic areas (arrow heads). These hypoechoic areas are actually the original sites of the suture material and have been filled by serum and cellular debris.

Figure 4.21 Transverse scan of the ventral abdominal wound on day 13 post-operation demonstrates a disorganised echogenic area (arrow) casting an acoustic shadowing artefact (**a**). The area surrounding the surgical site appears more organised than on the previous scan. Note also the fluid filled area is still present appearing anechoic with acoustic enhancement artefact. A small portion of fibrous tissue formation (small arrow) can be seen protruding into the haematoma (**b**).

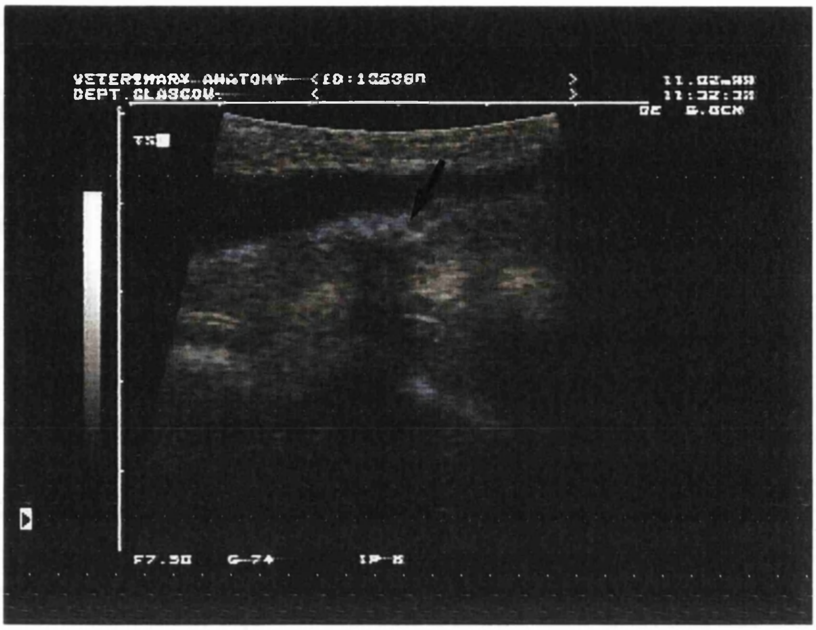

Figure 4.21a

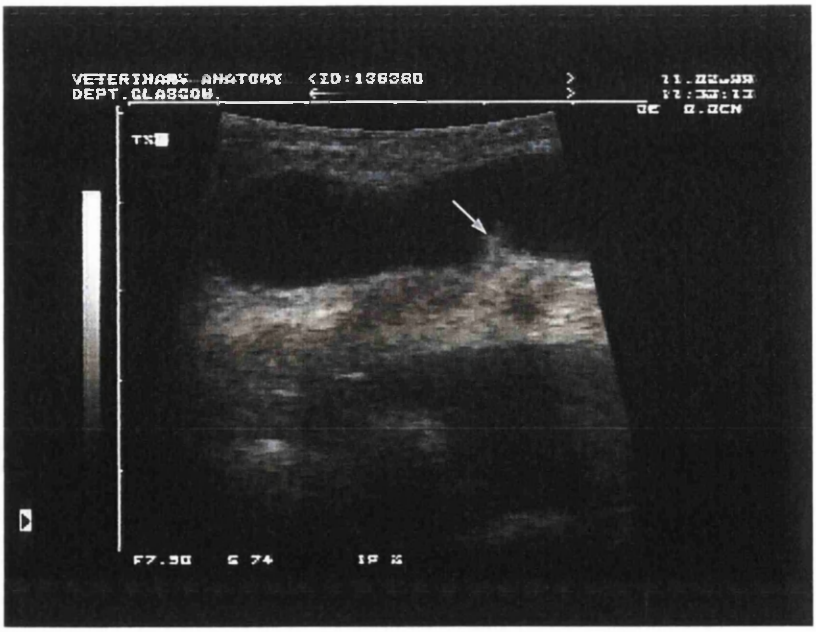

Figure 4.21b

Figure 4.22 Longitudinal scans of the ventral abdominal wound on day 13 post-operation demonstrate a disorganised echogenic area representing the muscle damage with the presence of fibrous tissue formation. Small hypoechoic areas (arrow heads) which are casting intermittent acoustic shadowing artefact are still visible but appear smaller than on the day 11 examination. These hypoechoic areas represent the sites of suture material undergoing reabsorption. A small portion of fibrous tissue protruding into the fluid space can also be seen. Some echogenic material within this area in **b** is suggestive that the fluid space is consolidating. The overall increase in echogenicity in **a** is due to acoustic enhancement artefact caused by the fluid accumulation.

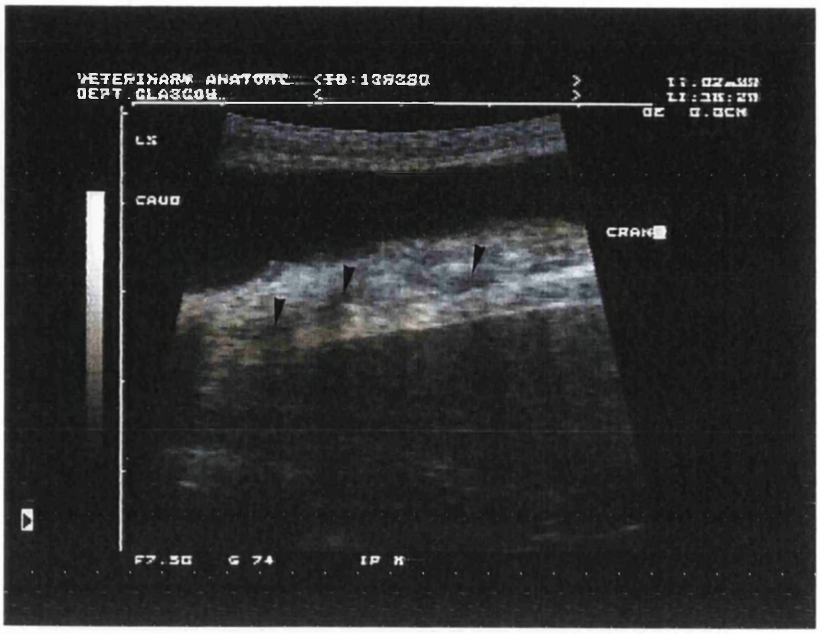

Figure 4.22a

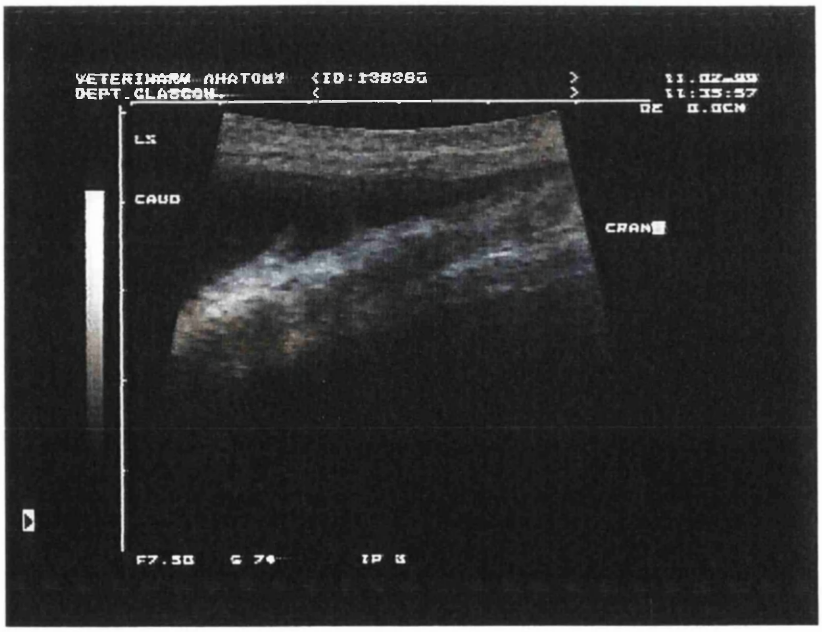

Figure 4.22b

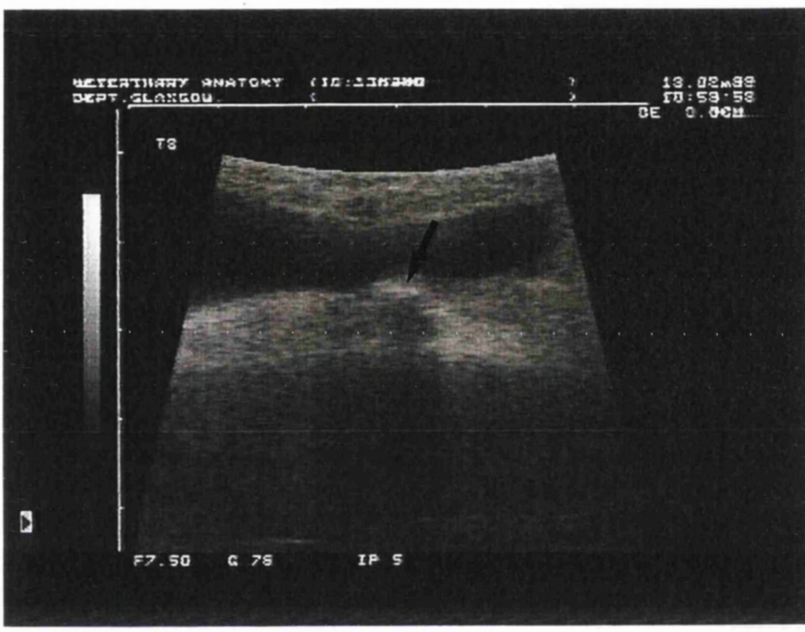

Figure 4.23 Transverse scan of the ventral abdominal wound on day 15 post-operation demonstrates a disorganised hyperechoic area (arrow) with acoustic shadowing artefact. Fibrous tissue appears to have an hyperechoic appearance compared to the image on the day 13 post-operation. The large fluid accumulation between the subcutaneous tissue and the rectus abdominis muscle is still present.

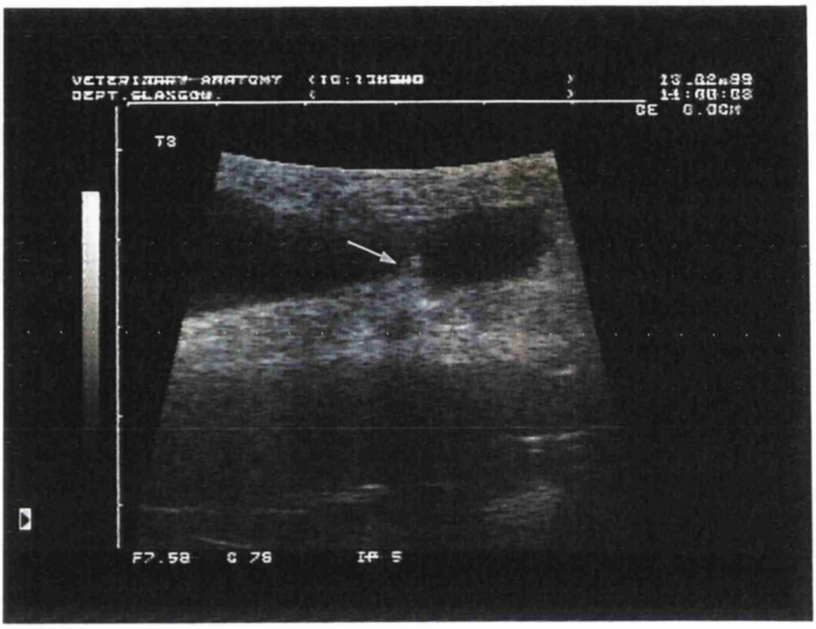

Figure 4.24 Transverse scan of the ventral abdominal wound on day 15 post-operation demonstrates a small portion of fibrous tissue (arrow) protruding into the fluid space. It appears hyperechoic and is increasing in size. Note that the presence of echogenic material within the fluid indicates that there is consolidation taking place.

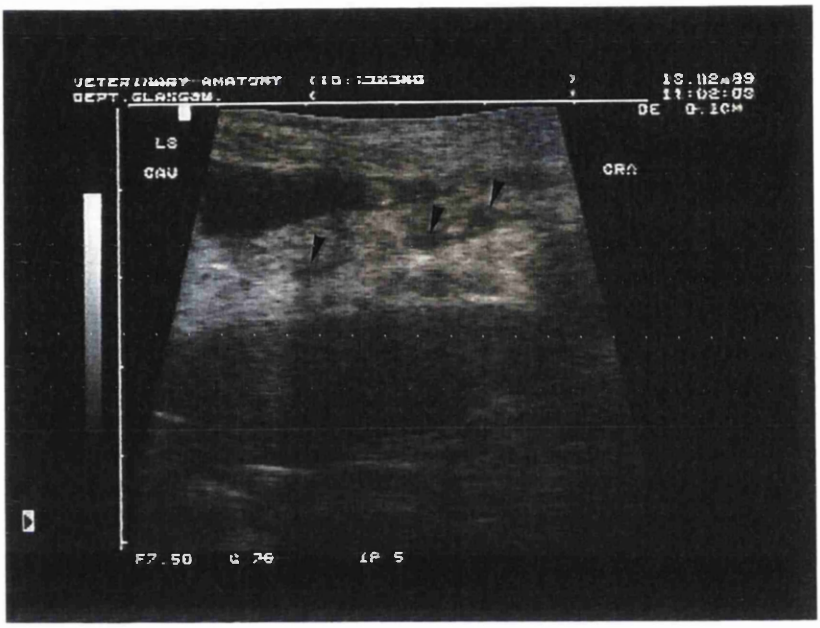

Figure 4.25 Longitudinal scan of the ventral abdominal wound on day 15 post-operation demonstrates a disorganised hyperechoic structure with the presence of some hypoechoic areas producing acoustic shadowing artefacts (arrow heads). These small hypoechoic areas within the muscle were actually the site of suture material being reabsorbed and are visible on ultrasound. The disorganised hyperechoic structure is due to the presence of fibrous tissue formation.

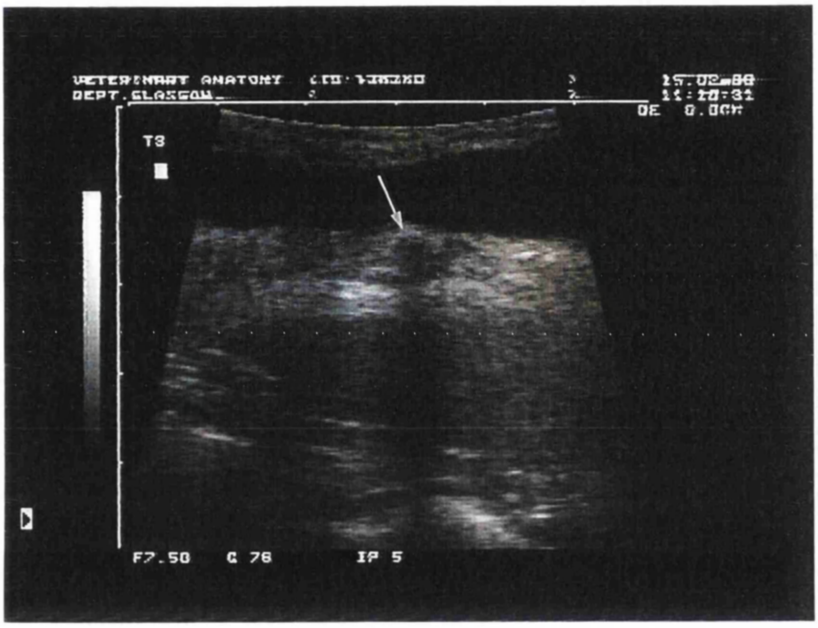

Figure 4.26 Transverse scan of the ventral abdominal wound on day 17 post-operation demonstrates a disorganised hyperechoic area (arrow) with acoustic shadowing artefact. The wound appears somewhat smaller than on the day 15 examination. The large fluid accumation is still present and appears as in the previous scan.

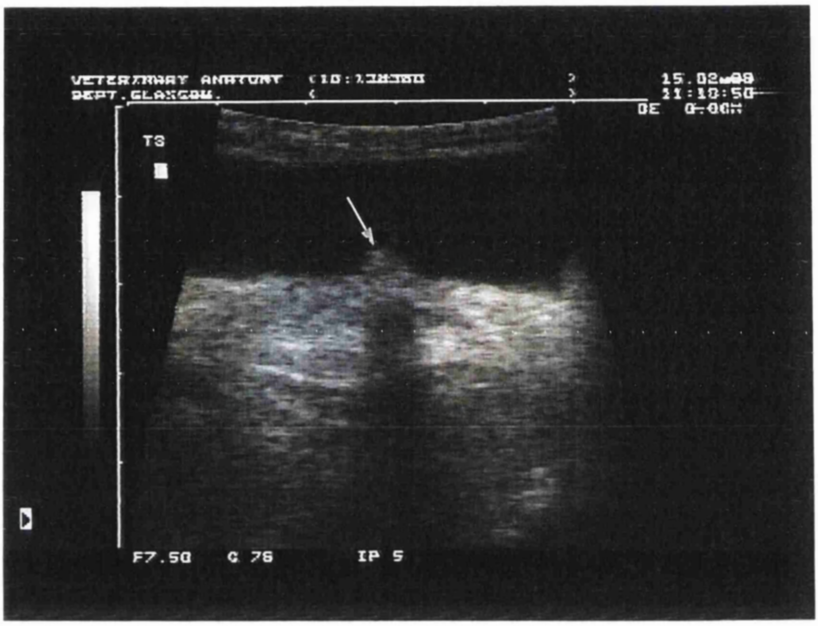

Figure 4.27 Longitudinal scan of the ventral abdominal wound on day 17 post-operation demonstrates the fibrous tissue (arrow) protruding into the fluid filled area and is increasing in size compare to the previous scan. It appears hyperechoic.

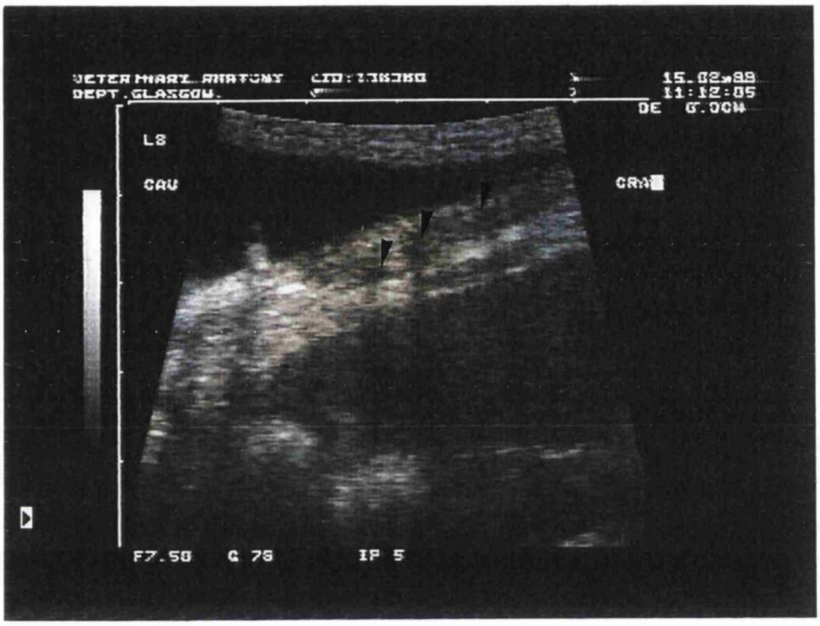

Figure 4.28 Longitudinal scan of the ventral abdominal wound on day 17 post-operation demonstrates a disorganised hyperechoic area representing the area of muscle damage and the presence of fibrous tissue formation. Note also that the small hypoechoic areas (arrow heads) with acoustic shadowing artefacts are still visible.

4.4 **Discussion**

An old injury with scar tissue formation can be differentiated by high resolution ultrasonography (Gerwing and Kramer, 1995). Careful comparison of both sides of an animal may reveal an echogenic area in a tendon that represents a scar or incomplete tear (Wilson, 1988). Results of this study show that the ultrasonographic appearance of scar tissue within the muscle varied from hypoechoic to hyperechoic. Therefore, to differentiate between the scar tissue and normal muscle texture, the scanned image must be observed carefully. Ultrasonographic appearance of the scar tissue is however, thought to depend on the stages of the scar tissue formation (Wilson, 1988).

The ultrasonographic image of new scar tissue formation with the presence of a high number of inflammatory cells on histological examination appeared as an disorganised hypoechoic area with an ill-defined margin relative to its surroundings. This is an accord with Laine *et al.* (1985) who demonstrated an hypoechoic area in a human hamstring muscle after partial rupture which had healed within 8 to 9 weeks. This hypoechoic area was suggested to be due to formation of new collagen fibres. In this study, the hypoechoic area of the new incision site imaged ultrasonographically corresponded to the area of the high number of inflammatory cells on histological examination. Thus, the result suggests that an inflammatory area within muscle or subcutaneous tissue gives an hypoechoic appearance on ultrasonographic image. Old scar tissue formation has been reported to have an hyperechoic appearance (Laine *et al.*, 1985). Similarly, in this study scar tissue formation within muscle without the presence of high fat lobules appeared hyperechoic relative to the surrounding tissues.

Most of the old incision sites with the presence of scar tissue imaged ultrasonographically appeared as disorganised hyperechoic areas relative to the surrounding muscle. However, in some animals the old incision site appeared as hypoechoic or isoechoic structure relative to the surroundings. This discrepancy seemed to depend on the amount of fat lobules present around the scar tissue. The higher the level of fat lobules around the scar tissue the less echogenic it became. The results are in accord with Laine, *et al.* (1985) who reported that the image of scar tissue (fibrosis) in muscle gives a variable appearance in ultrasonography, but, the most common one is a disorganised hyperechoic structure. There is a direct relationship between the echoic intensity and the amount of collagen (Henry *et al.*, 1986). In this study, the scar tissue with a higher proportion of fat lobules around the scar on histological examination corresponded to the area of disorganised hypoechoic or isoechoic structures on ultrasound. Thus, the ultrasonographic appearance of the VAM with an old incision site in this study depended on the amount of fat lobules around the scar tissue as demonstrated histologically. This was probably due to the sound beam being largely absorbed by the fat lobules, and therefore the sound reflection was less. The amount of scar tissue decreasing as healing progresses together with improving orientation of regenerating muscle fibres made the ultrasonographic differentiation between normal and healing muscular tissue become more difficult (Lehto and Alanen, 1987).

The presence of suture materials within the muscle in three cases (4, 12 and 18) except in case 21, suggested that the surgery was done within a few weeks of euthanasia. In normal circumstances, the common absorbable suture material used to close the muscle layer is surgical gut (catgut) and this is absorbed by the body within seven days (Vasseur, 1985). In these animals, ultrasonographic findings were constant. The images revealed an ill-defined hypoechoic area which corresponded to the area of increased inflammatory cells on histological examination.

Studies in the human demonstrated that subcutaneous tissue is generally more echogenic than muscle (Yeh, 1985; Kaplan *et al.*, 1990). In some circumstances the subcutaneous tissue appeared poorly echogenic especially in obese patients

(Vincent, 1988; Kaplan *et al.*, 1989). In this study, the subcutaneous tissue was found to have variable appearances. However, the majority of cases appeared more echogenic than muscle. Thus, the result suggested that the subcutaneous tissue in dogs imaged ultrasonographically had a variable appearance.

Findings in this study also show that the majority of the ventral abdominal surgical incisions made in the animals within this study were not exactly on the VAM. Most of the incisions were made in the rectus abdominis muscle adjacent to the VAM as shown by both ultrasonographic and histological examination. This study also found that the reason for having ventral abdominal surgery done on animals in this study was not necessarily only for ovariohysterectomy purposes. This is because in some cadavers with the presence of an hyperechoic area when imaged along the ventral abdominal mid-line caudal to the umbilicus and the presence of scar tissue formation histologically, the uterus and ovary were still intact. Thus, this suggested that the surgery had been done for some other reason.

Thus searching for a surgical site with ultrasound could be a useful tool to decide whether a bitch has undergone an ovariohysterectomy but it could not preclude that the animal had undergone surgery for some other reason.

The ultrasonographic appearance of the wound (surgical site) at the early stage (approximately 24 hours post-operation) was ill-defined hypoechoic with acoustic shadowing artefact. With time the wound appeared hypoechoic with some degree of an echogenic centre and casting acoustic shadowing artefact. This is consistent with the finding by Wilson, *et al.*, (1989). By day 11 post-operation the wound (surgical site) was found to have a disorganised echogenic structure with acoustic shadowing artefact. By day 13 post-operation the wound appeared as disorganised hyperechoic with acoustic shadowing artefact due to the presence of fibrous tissue formation. It has been reported that the most common finding of fibrosis in muscle was as a disorganised hyperechoic structure (Laine *et al.*, 1985; Fornage *et al.*, 1983). Thus, it is an accord with the finding in this study. The disorganised hyperechoic structure was suggestive of fibrous formation which is essential for the healing process in soft tissue injury. In a recent study, Kramer *et al.* (1997) reported that muscle healing can be ultrasonographically evaluated. The fibrous tissue formation (scar tissue) in the muscle is visible ultrasonographically and characterised as a hyperechoic area with or without acoustic shadowing artefact between normal muscle. In addition, development of the scar tissue depends on the extent of ruptured muscle fibres.

Ultrasonographic appearance of the suture material in the linea alba has been reported to have a focal hyperechoic appearance with acoustic shadowing artefact (Wilson *et al.*, 1989). Similarly, in the live animal study the suture material used to closed the linea alba appeared hyperechoic with acoustic shadowing artefact. In addition, the suture material in the skin produced intermittent acoustic shadowing artefact on ultrasound as seen in this study. The suture material used to closed the linea alba and the skin in this study were PDS and nylon respectively. The hypoechoic to anechoic areas surrounding the suture material have been observed and described as a suture sinus (Wilson *et al.*, 1989). However, in this study the small areas of hypoechoic to anechoic appearance with acoustic shadowing artefacts in the muscle were observed on day 11 post-operation. They were actually the original sites of suture materials in the muscle. These hypoechoic to anechoic areas which produced acoustic shadowing artefacts were believed due to serum and blood which contained cellular debris. These areas decreased in size with time.

Fluid accumulation at the surgical sites not only results from sequestration of inflammatory by-products, but also may be caused by the surgical procedure itself. Dissection performed during the surgical approach, soft tissue damage associated with iatrogenic injury, and incomplete haemostasis during surgery may contribute to the accumulation of small amounts of blood or serous fluid during the early post-operative period. The ultrasonographic appearance of fluid collection within the body is well known. Fluid accumulation or oedema may appear relatively anechoic and become echogenic as they are organised

(Fornage *et al.*, 1983). Small or thin fluid collections may not show acoustic enhancement artefact (Fornage *et al.*, 1983). In the present study, a large fluid accumulation developed in between the subcutaneous tissue and the rectus abdominis muscle at the surgical site area and appeared anechoic with acoustic enhancement artefact. The presence of a large fluid accumulation at the surgical site in case two increased the overall echogenicity of the ventral abdominal muscle due to acoustic enhancement artefact. With time echogenic material was present within the fluid filled area suggesting that the consolidation was taking place. The small accumulation of fluid within the subcutaneous tissue at the surgical site in case one was detected and appeared anechoic. The areas of supposed haemorrhage and small fluid accumulations within the subcutaneous tissue appeared hypoechoic with acoustic shadowing artefact.

The incision site on the ventral abdominal midline in this study was not consistently found to be on the linea alba; at certain points it was found on the rectus abdominal muscle just lateral to the linea alba as shown in figure 4.9b. This is consistent with the earlier findings in the preliminary study of the old ventral abdominal wound where the hyperechoic area of scar tissue was found in the rectus abdominal muscle lateral to the linea alba. This has also been shown in the histology sections. The wound (incision site) on the skin and subcutaneous tissue were also found not to be consistently parallel with the wound on the muscle in a number of cases. Thus, this means that the incision site on the skin does not always indicate the exact site of the wound in the muscle or linea alba underneath the skin.

Results from this study also demonstrated that the wound (surgical site) can be evaluated in both transverse and longitudinal scans. However, the transverse scan seems to be easier than the longitudinal scan in evaluation of the surgical wound. The wound is easily evaluated by comparing with the normal adjacent tissues in transverse scan. In longitudinal scan, the wound required to be scanned more carefully because the wound was mobile when applying pressure.

Furthermore, the wound area was thin and at certain points the wound on the skin was not parallel with the wound on the muscle or linea alba.

CHAPTER 5

ULTRASONOGRAPHIC IMAGING OF NEOPLASIA OF THE CANINE MAMMARY GLAND

5.1 Introduction and aims of the study

Tumour formation in the mammary gland in dogs has been well documented in the literature (Anderson and Jarrett, 1966; Owen, 1966; Fidler and Brodey, 1967; Misdorp *et al.*, 1972; Fowler *et al.*, 1974; Misdorp and Hart, 1979a, 1979b; Moulton *et al.*, 1986). They are by far the most common tumours in the bitch (Moulton, 1990). Tumours of the mammary glands occur more frequently than in any other organ and represent about 25 per cent of all forms of neoplasm in bitches (Anderson and Jarrett, 1966). Incidence tends to increase with age with bitches between 9 - 10 years old being the highest affected group (Priester, 1979). However, mammary tumours are less common in ovariectomized bitches (Anderson and Jarrett, 1966).

Diagnosis of canine mammary gland tumours has commonly been accomplished through physical examination by means of palpation and by radiography. The use of ultrasonography in the evaluation of breast tumours in human patients has been well accepted (Hayashi *et al.*, 1985; Bassett *et al.*, 1991; Yang *et al.*, 1996; Kolb *et al.*, 1998). Ultrasonography can be used to detect the local changes, lesion and tumours of the breast. In small animal practice, ultrasonography has been proved to be a useful diagnostic tool in detecting soft tissue tumour masses (Fornage *et al.*, 1985; Harcke *et al.*, 1988; Vincent, 1988; Fornage and Rifkin, 1988; Craychee, 1995). The tumours usually present as well defined, complex masses or as solid masses consisting of medium level echoes (Harcke *et al.*, 1988). Most soft tissue tumours are hypoechoic relative to surrounding tissue, except fat containing tumours which are occasionally hyperechoic (Vincent, 1988). Solid tumours appear as more or less hypoechoic and homogenous masses with more or less regular contours (Fornage *et al.*, 1985). Ultrasonography can readily determine the liquid or solid content of a soft tissue tumour (Fornage and Rifkin 1988). Additionally, its depth of extension, its accurate size, and its relationship with the adjacent structures can be ascertained (Fornage *et al.*, 1985).

Early studies of the canine mammary gland tumour show that the regional lymph nodes (axillary and superficial inguinal) are the most common seat of secondary tumours (Cotchin, 1954). Malignant spread of tumours of the cranial mammary glands was always through the axillary lymph node, while tumours of the caudal mammary glands when they metastasised normally had superficial inguinal lymph node involvement (Fidler and Brodey, 1967). The tumour tissue metastasised through the lymphatic system that connected between the glands and the lymph nodes and played an important role in the metastases of tumour tissue (Silver, 1966, Sautet *et al.*, 1992; Patsikas and Dessiris, 1996a, 1996b).

The ultrasonographic appearance of the normal and abnormal lymph nodes in human and small animals has been described (Marchal *et al.*, 1985; Rubaltelli *et al.*, 1990; Saunders *et al.*, 1992; Pugh, 1994). Normal lymph nodes are often indistinct due to their small size and echogenicity similar to the surrounding soft tissues (Pugh, 1994). Lymph nodes altered by infiltrative or inflammatory processes may become visible due to enlargement or altered echogenicity (Pugh, 1994). In human patients, ultrasonographic evaluation in the abdominal region for lymph node enlargement, change in shape and echo pattern was shown to be useful in detecting colorectal cancer, (Rafailson *et al.*, 1992) and gastric cancer, (Akahoshi *et al.*, 1992).

The use of ultrasonography to study tumours of canine mammary glands and to detect regional lymph node metastases has not been previously documented. Using the advantages of high resolution ultrasound, the present study was carried out with the aim of determining whether ultrasound could be a reliable diagnostic tool in the evaluation of canine mammary gland tumours and their spread as well as to detect regional lymph node metastases.

5.2 Materials and Methods

Animals

Twenty-eight bitches of different breeds with clinical evidence of mammary gland tumours were used in this study. Of the 28 cases, 26 were obtained from the clinical cases referred to the People's Dispensary for Sick Animals (PDSA), Glasgow, and two cases were obtained from the Glasgow University Small Animal Clinic (GUSAC). The breed, age and previous history of each bitch were obtained during consultation and from hospital records. The bitches participating in this study were first examined by a veterinarian before being referred for ultrasonographic examination.

Ultrasonographic imaging

All the mammary glands and the regional lymph nodes (axillary and superficial inguinal) on both sides were identified as shown in figure 5.1. The scanning was carried out in a semi-dark room. Each dog was placed on the table in dorsal recumbency during examination. Excessive hair around the teats and at the axillary and inguinal areas was removed using hair clippers. The mammary glands and the regional lymph nodes were examined physically by means of palpation prior to scanning. They were gently palpated using the tips of fingers and thumb. An acoustic coupling gel was then applied prior to scanning. Ultrasonographic imaging was performed using an ultrasound scanning unit (TOSHIBA Capasee) equipped with 7.5 MHz curvilinear array transducer. The same machine and transducer were used throughout the study.

The mammary glands and the regional lymph nodes were scanned systematically from left axillary lymph node (LAN), then the glands cranial to caudal, and onto the left superficial inguinal lymph node (LIN). This was repeated from the right axillary lymph node (RAN) to right superficial inguinal lymph node (RIN) as shown in figure 5.1. For each mammary gland, the scanning was done transversely both cranial and caudal to the teat and sagittally on both lateral and medial sides of the teat with the transducer's crystal face held perpendicular to and in contact with the skin. The transducer was moved gently for about 3-5 cm away from the teat in both transverse and sagittal planes depending on the size of the dog. To image the superficial inguinal lymph node, the transducer was placed in the inguinal region just caudal and lateral to the inguinal mammary gland with the hind limb elevated. The femoral artery and vein were used as a marker to locate the superficial inguinal lymph node. Similarly, to image the axillary lymph node, the transducer was placed in the axillary region with the fore limb elevated. The axillary artery and vein were used as a marker to locate the axillary lymph node. The transducer was adjusted caudally and cranially until the lymph node was identified. The lymph nodes were assessed ultrasonographically for their size and echogenicity. Echogenicity of the lymph nodes was compared with that of the surrounding fatty tissue and described as being hypoechoic or isoechoic. Measurements where appropriate were obtained by freezing the images on the scanner monitor and then measured using the electronic calliper. Time taken to complete each examination was recorded. The result and comments on each dog were referred to the consulting surgeon for further action. After three to five months the animals were re-called for re-scanning to see whether there was evidence of tumour tissue remaining after surgery. All the scanned images were recorded on super VHS tape during examinations using a Panasonic VHS video recorder. The recorded images were later reviewed. The best images were labelled and thermal copies were printed during the review.

Figure 5.1 Identification of the mammary glands and the regional lymph nodes (axillary and superficial inguinal).

LAN	-	left axillary lymph node
LT1	-	left cranial thoracic mammary gland
LT2	-	left caudal thoracic mammary gland
LA1	-	left cranial abdominal mammary gland
LA2	-	left caudal abdominal mammary gland
LI	-	left inguinal mammary gland
LIN	-	left superficial inguinal lymph node
RAN	-	right axillary lymph node
RT1	-	right cranial thoracic mammary gland
RT2	-	right caudal thoracic mammary gland
RA1	-	right cranial abdominal mammary gland
RA2	-	right caudal abdominal mammary gland
RI	-	right inguinal mammary gland
RIN	-	right superficial inguinal mammary gland

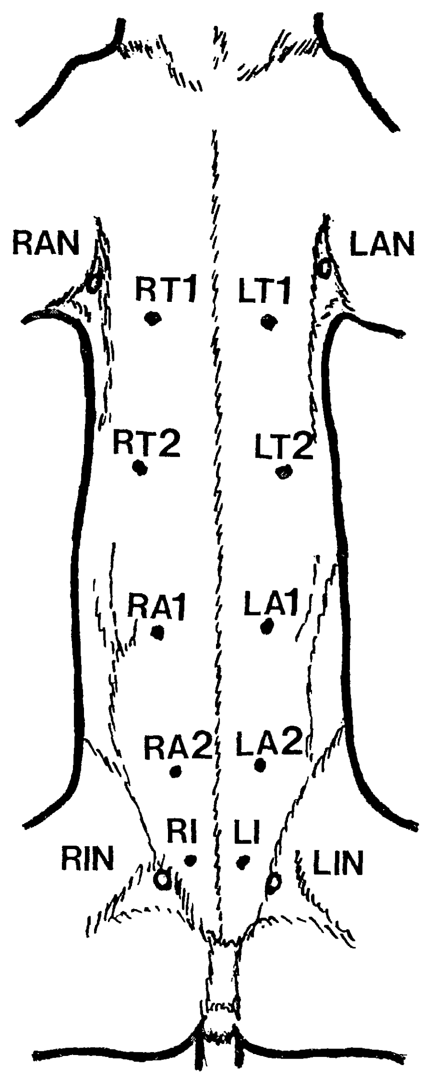
RAN
LAN
RT1
LT1
RT2
LT2
RA1
LA1
RA2
LA2
RI
LI
RIN
LIN

5.3 Results

A total of 238 mammary glands and 111 regional lymph nodes (56 axillary and 55 superficial inguinal) in 28 bitches were scanned within a seven month period. Of the 28 bitches, 21 (75%) had 10 mammary glands and seven (25%) had eight mammary glands. Seventeen mammary glands and one regional lymph node were found to be missing in a total of nine bitches during the first examination. Of the 17 missing glands, 10 had been removed due to past history of mammary gland tumours in three bitches. The remaining seven missing glands were from six bitches who had no previous history of tumours. Twenty-two bitches (78.6%) involved in this study were intact females and the remaining six (21.4%) were neutered females.

The breed and age incidence of the 28 bitches involved in this study are given in table 5.1 and 5.2 respectively. Cross breed and German shepherd dogs were the most frequently encountered type in this study. The average age of the 28 bitches at the time of examination was 10.8 years (range from 2 years to 15 years) with the peak incidence at 11 to 14 years old.

Results of the ultrasonographic examination of the mammary glands and the regional lymph nodes are shown in table 5.3. Out of the 238 glands examined by both palpation and ultrasonography, a total of 92 (38.7%) mammary tumours was detected on ultrasonographic examination but only 79 (33.2%) mammary tumours were detected on palpation. Thirteen (5.5%) mammary tumours were not detected on physical examination but were detected by ultrasound. Of the 111 axillary and superficial inguinal lymph nodes examined by both palpation and ultrasonography, a total of 23 (20.7%) lymph nodes were found positive on ultrasonographic examination and only six (5.4%) were detected on palpation. Seventeen (15.3%) enlarged lymph nodes detected on ultrasonographic examination were not detected on palpation.

The distribution of the mammary tumours and the regional lymph node involvement of 28 bitches is given in table 5.4 and table 5.5 respectively. Of the 94 mammary gland tumours detected by ultrasonography, 56 (59.6%) tumours originated in caudal abdominal and inguinal glands on both sides, and 18 (19.1%) tumours originated in cranial thoracic and caudal thoracic glands on both sides. Twenty (21.3%) tumours originated in cranial abdominal glands on both sides. Of the 23 regional lymph nodes detected as positive on ultrasonographic examination, 18 (78.3%) involved the superficial inguinal lymph nodes on both sides and 5 (21.7%) involved the axillary lymph nodes on both sides.

Two bitches (cases 20 and 21) were presented in this study with suspicion of having mammary tumours but later were found to be free of mammary tumours by both palpation and ultrasonography. Case 20 was presented because there was a firm swelling at the xyphoid area but ultrasonographic examination found that it did not involve mammary tissue but demonstrated a well encapsulated firm swelling which produced an image of homogenous echotexture at the xyphoid area. Case 21 was presented with swollen masses between LA1 and LA2 and between RT2 and RA1 which were found not to involve mammary tissue on palpation and ultrasonographic examination. The swelling between LA1 and LA2 appeared cystic and well encapsulated with flocculent content and the mass between RT2 and RA1 appeared to have a more organised echotexture and be well encapsulated which suggested abscess formation (figure 5.2).

For the purpose of this study, the tumours found in the mammary gland were classified into three groups according to their ultrasonographic appearance. Group one was represented by areas of tumour tissue which appeared anechoic to hypoechoic (figure 5.3). The tumour masses were small and varied from 0.4 cm to 1.3 cm in diameter (average 0.8 cm) with an ill-defined margin. Group two was represented by areas of tumour tissue appearing as areas of mixed echotexture. They are hypoechoic relative to surrounding tissues but contain hyperechoic speckling scattered throughout the parenchyma (figure 5.4). They varied in size from 0.5 cm to approximately 5.0 cm in diameter. Group three was represented by areas of tumour tissue which were large and appeared hyperechoic (figure 5.5a). In many cases they contained discrete anechoic regions indicating cystic structures (figure 5.5b,c). The tumour masses were large and varied from 2.0 cm to approximately 5.0 cm in diameter with well-defined margins. Acoustic enhancement artefact was the most prominent feature for all groups of tumour masses as in figure 5.2 and 5.3. Tumour masses with calcification were found in cases 23 and 26, and appeared as disorganised hyperechoic accumulations with acoustic shadowing within the hypoechoic masses (figure 5.6). The incidence of mammary gland tumours classified ultrasonographically is given in table 5.6. Group one was the most commonly encountered tumour while group three was the least commonly encountered tumour in this study.

The normal axillary and superficial inguinal lymph nodes imaged ultrasonographically appeared as round hypoechoic to isoechoic structures relative to surrounding soft tissues (figure 5.7). The enlarged abnormal regional lymph nodes found in this study were varied in echogenicity from homogeneously hypoechoic structures (figure 5.8a,b), mixed echotexture (figure 5.8c) to more echogenic echotexture relative to surrounding soft tissues (figure 5.8d).

Of the 28 bitches originally scanned, 17 (60.7%) bitches were re-scanned at a later date. Seven bitches (25%) had died and four bitches (10.7%) failed to respond to the recall. Of the seven bitches which died, one (case 2) died on the same day as the examination due to the severity of the massive tumour spread. Six bitches were requested by the owner to be euthanased several weeks after the examination of which four of them (cases 3, 7, 10 and 13) were due to mammary tumour metastasis and two (cases 8 and 11) were due to unrelated complications. One bitch (case 11) was euthanased immediately after ultrasound examination due to massive tumour spread.

Results of the re-scan and time interval between first scan and re-scan are given in table 5.3. Out of the 17 bitches re-scanned, six bitches had not undergone surgery, and the results of the re-scan after approximately three to five months showed findings similar to the previous scan in four bitches, while in two bitches (cases 6 and 18) the findings were dissimilar. In case 6, tumour of the LA1 and LA2 had increased in size from 1.0 cm (LA1) and 0.5 cm (LA2) to 1.6 cm for LA1 and 0.8 cm for LA2 (figure 5.9a,b), and the superficial inguinal lymph node (RIN) was found to be enlarged on re-scan (figure 5.9c). In case 18, small new superficial tumour masses size 0.7 cm and 0.4 cm in diameter were found in LA2 and RA1 respectively by both palpation and ultrasonography (figure 5.10). Fourteen cases had undergone surgery to remove the mammary gland tumours and the results of the re-scan failed to demonstrate any new tumour tissue in 11 cases, while in three cases (19, 22 and 25) the tumour tissues were still detected on both palpation and ultrasound examination. In cases 19 and 22, not all of the mammary gland tumours detected ultrasonographically were removed during surgery, resulting in positive findings on the rescan. In case 25, all the mammary gland tumours were removed but not the enlarged RAN. The re-scan image showed that the RAN was increased in size and had become more echogenic (figure 5.8d).

The ultrasonographic images of the mammary tumour tissue not detected on palpation appeared hypoechoic with an ill-defined margin (figure 5.11). They were small in size (0.4 cm to 1.3 cm) and were classified as being of group one type. Six regional lymph nodes which were found to be enlarged and hypoechoic with an ill defined margin on the first scan were found to be negative on re-scan after the mammary gland tumours had been removed. The approximate time taken for scanning each dog was 15 minutes with a major portion of time being spent on imaging the axillary and superficial inguinal lymph nodes.

Table 5.1 Breed incidence of 28 bitches with mammary gland neoplasm

Breed	No.
Cross breed	6
German shepherd	6
Border Collie	5
Yorkshire Terrier	3
Labrador	3
Whippet	1
Jack Russell Terrier	1
Doberman	1
Staffordshire Bull Terrier	1
Cairn Terrier	1
Total	28

Table 5.2 Age incidence of 28 bitches with mammary gland neoplasm

Age (years)	No. of bitches
2	2
5	2
7	1
9	3
10	1
11	4
12	5
13	5
14	4
15	1
Total	28

Table 5.3 The positive mammary glands and regional lymph nodes found on first scan and on re-scan, the glands and regional lymph nodes removed, and time interval between the first scan and re-scan

Case no.	Positive glands and regional lymph nodes found on first scan	Glands and lymph nodes removed	Positive glands and regional lymph nodes found on re-scan	Time interval between first and re-scan	outcome
1	LIN, RA1, RA2, RI, RIN	no surgery			alive
2	LT2, LA1, LA2, LI, LIN RT2, RA1, RA2, RI, RIN				died
3	LAN, LA1, LA2, LI, LIN RAN, RT1, RT2, RA1, RA2, RI,RIN				euthanased
4	RA2, RI, RIN	RA2, RI, RIN	-	5 months	alive
5	LT1, LT2, LA1, LA2, LI, LIN RA1, RA2, RI, RIN,	All glands were removed	-	5 months	alive
6	LA1, LA2, LI, LIN, RI	no surgery	LA1, LA2, LI, LIN, RI,RIN	5 ½ months	alive
7	LT2, LA1, LA2 RT1*, RT2, RA1				euthanased

* The glands that were negative on palpation but positive on ultrasonography

Table 5.3 continued

case no.	Positive glands and regional lymph nodes found on first scan	Glands and lymph nodes removed	Positive glands and regional lymph nodes found on re-scan	Time interval between first and re-scan	remarks
8	LI, RI*				euthanased
9	LI	LI	-	5 ½ months	alive
10	LAN, LT1, LT2, LA1*,LA2,LI RAN, RA1*, RA2, RI, RIN				euthanased
11	LT1, RA2, RIN				euthanased
12	LA1, LA2, RT1*, RA2, RI	no surgery	LA1, LA2, RT1*, RA2, RI	4 months	alive
13	LT2*, LA1, LA2, LI				euthanased
14	LA1, LI, RI	RA2, RI, LA1, LI	-	4 months	alive
15	LIN, RA2*	RA2, RI	-	3 months one week	alive
16	LA1*, LI, RA2	no surgery	LA1*,LI, RA2	4 ½ months	alive

* The glands that were negative on palpation but positive on ultrasonography

Table 5.3 continued

case no.	Positive glands and regional lymph nodes found on first scan	Glands and lymph nodes removed	Positive glands and regional lymph nodes found on re-scan	Time interval between first and re-scan	remarks
17	LA1, LI	LA1, LA2, LI	-	3 months one week	alive
18	LA1	no surgery	LA1, LA2, RA1	4 months one weeks	alive
19	LA2, LI*, RA2, RI*, RIN	LA2, LI	RA2, RI*	3 months one week	alive
20	-	no surgery	-	4 months	alive
21	-	no surgery			alive
22	LIN, LA2, RI	LA2, LI, LIN	RI	1 ½ months	alive
23	LA1*, LI	LA1, LA2, LI	-	3 months three weeks	alive
24	LA2, RT1*, RT2*, RA2, RIN	no surgery	LA2, RT1*, RT2* RA2,RIN	2 ½ months	alive
25	RAN, RA1, RI	RT2, RA1, RA2, RI	RAN	2 ½ months	alive
26	RA2, RI	RA2, RI			alive
27	LA2, LI, LIN	LA2, LI	-	2 months	alive
28	LA2, LI, LIN, RT2	LA2, LI			alive

* The glands that were negative on palpation but positive on ultrasonography

Table 5.4 Distribution of tumours in 28 bitches with mammary gland neoplasm

Gland	No. of tumours	Gland	No. of tumours	Total
LT1	3	RT1	4	7
LT2	5	RT2	6	11
LA1	13	RA1	7	20
LA2	14	RA2	13	27
LI	15	RI	14	29
Total	50		44	94

Table 5.5 Distribution of the regional lymph node involvement in 28 bitches with mammary gland neoplasm

Lymph node	No.	Lymph node	No.	Total
LAN	2	RAN	3	5
LIN	9	RIN	9	18
Total	11		12	23

Table 5.6 The incidence of tumours in 28 bitches with mammary gland neoplasm classified ultrasonographically

Group	Number of incidence (%)
1	45 (47.9%)
2	37 (39.4%)
3	12 (12.8%)
Total	94

Figure 5.2 Ultrasonographic appearance of the masses (**a**) between LA1 and LA2, and (**b**) between RT2 and RA1 in one and half year old bitch (case 22). Note the mass between LA1 and LA2 appears cystic and well encapsulated and the mass between RT2 and RA1 appears to have more organised echotexture and is well encapsulated which suggests abscess formation. **s**, skin, **c**, cyst, **abc**, abscess

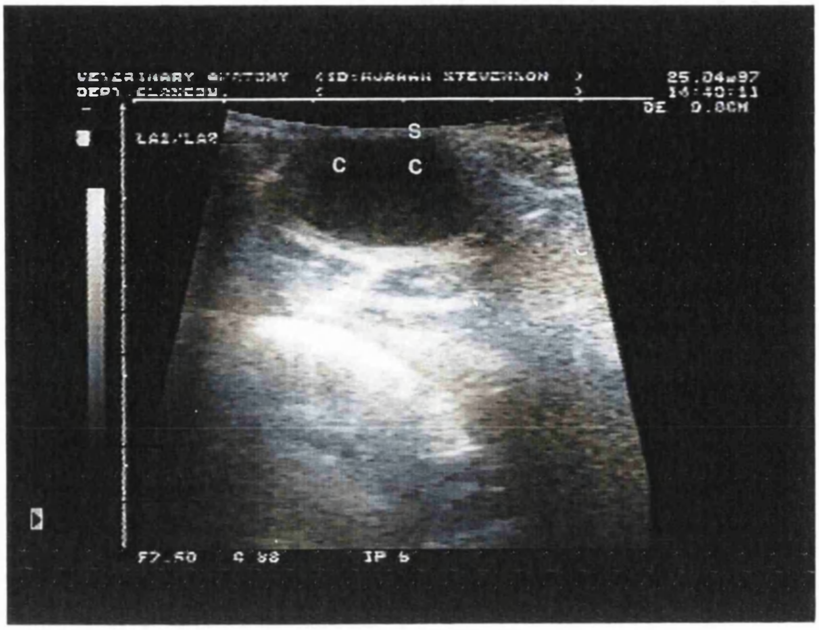

Figure 5.2a

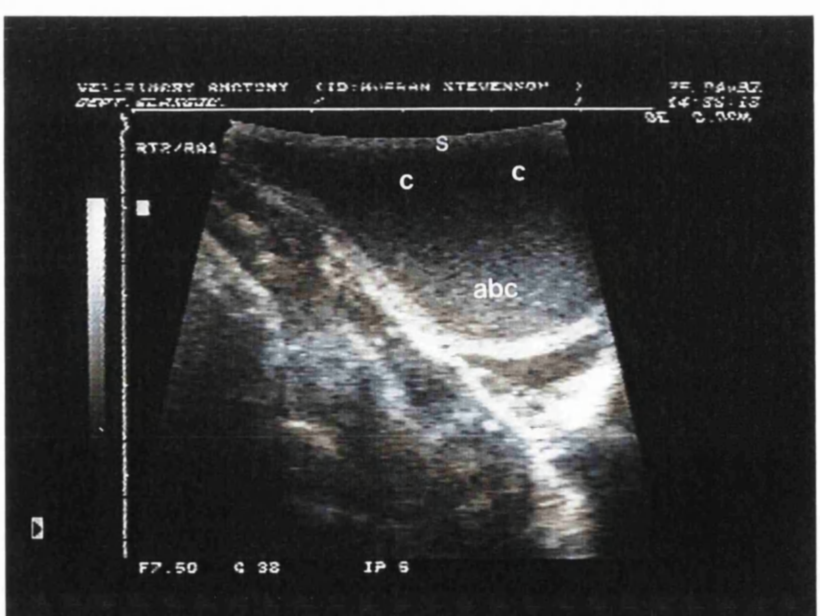

Figure 5.2b

Figure 5.3 Ultrasonographic appearance of the mammary tumours representing group one (**a**, **b**, **c**). The areas of tumour tissue are small and appear anechoic to hypoechoic with ill-defined margins. They produce acoustic enhancement artefact (arrow heads). **s**, skin, **ab**, abdominal muscle, **m**, tumour tissue.

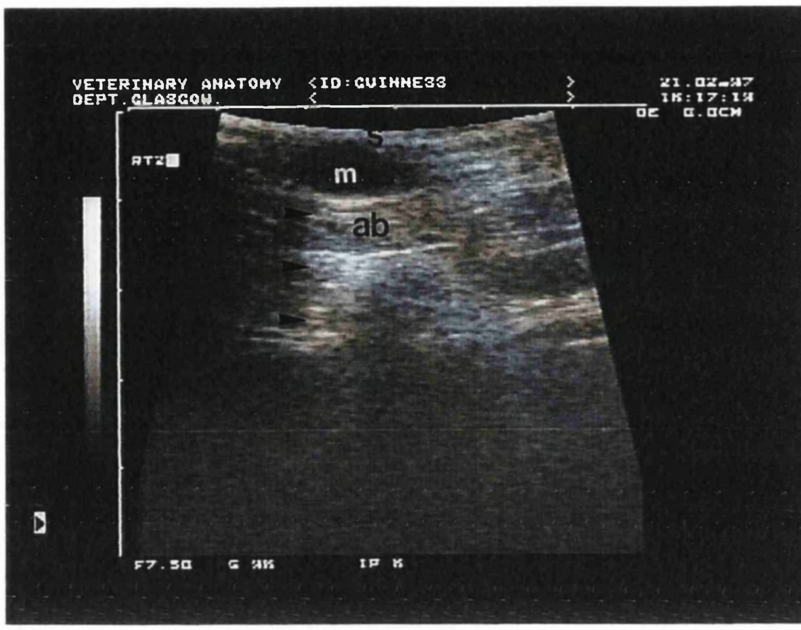

Figure 5.3a

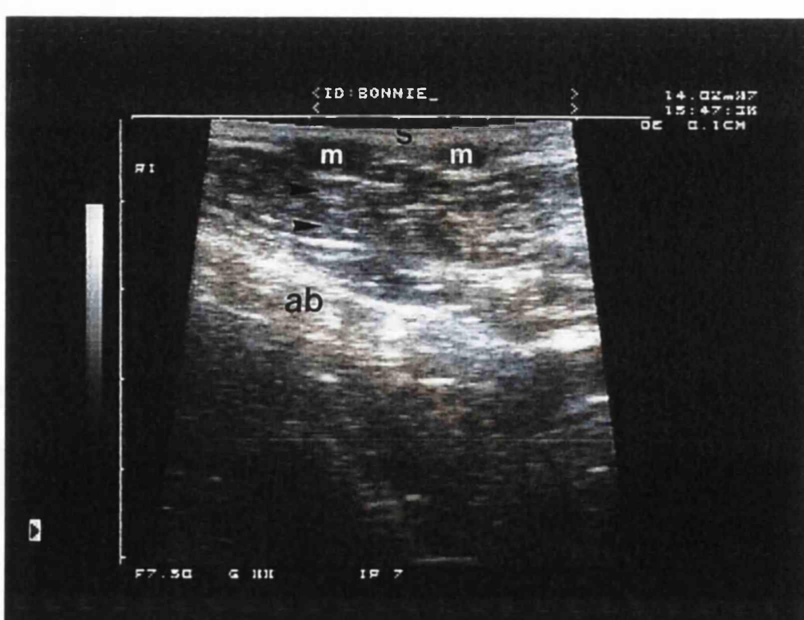

Figure 5.3b

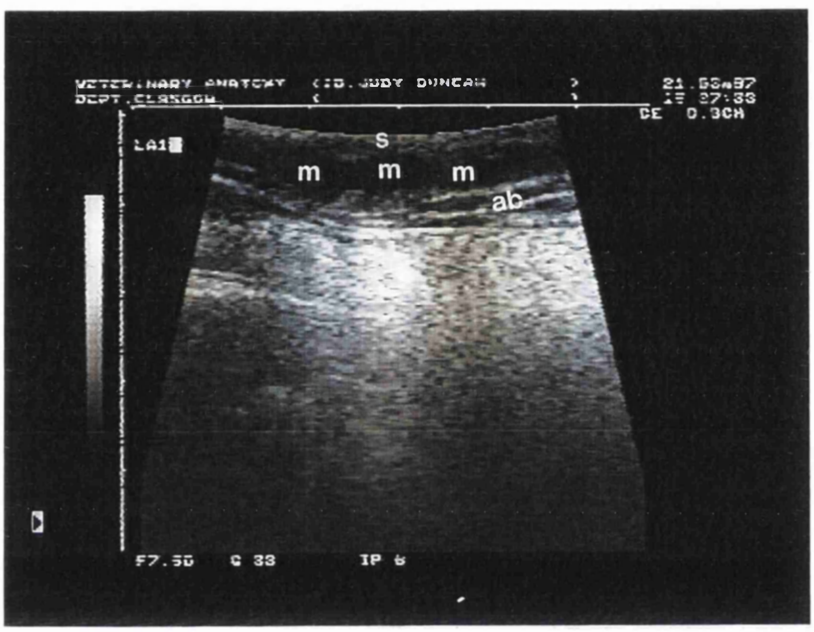

Figure 5.3c

Figure 5.4 Ultrasonographic appearance of the mammary tumours representing group two (**a**, **b**, **c**). The areas of tumour tissue are large and appear as areas of mixed echotexture. They are hypoechoic relative to the surrounding tissues but contain hyperechoic speckling scattered throughout the parenchyma. Note also that the tumour tissue produces acoustic enhancement artefact (arrow heads). **s**, skin, **m**, tumour tissue, **ab**, abdominal muscle.

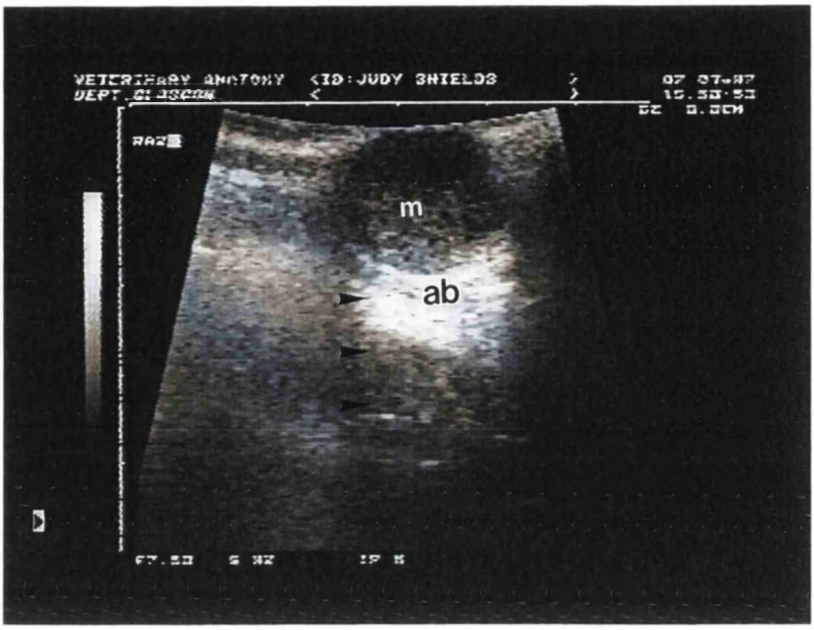

Figure 5.4a

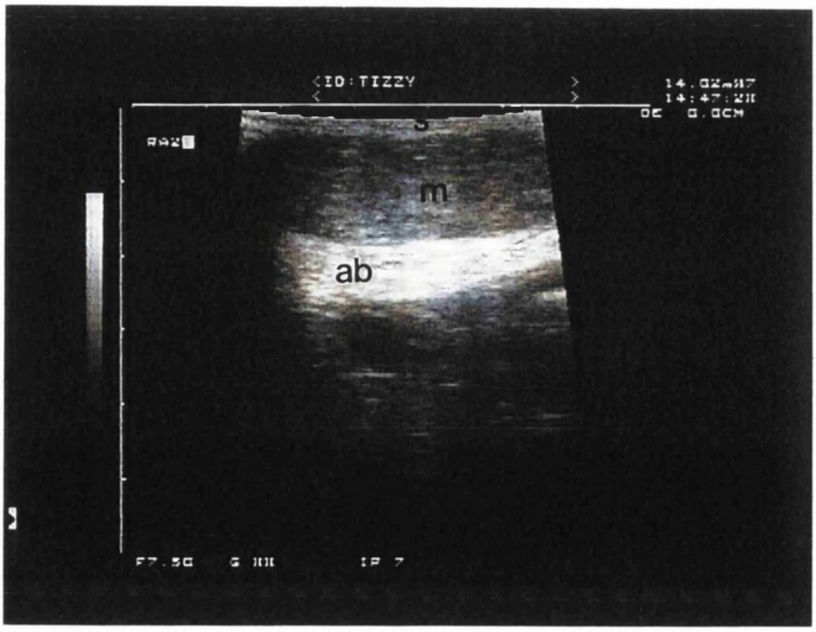

Figure 5.4b

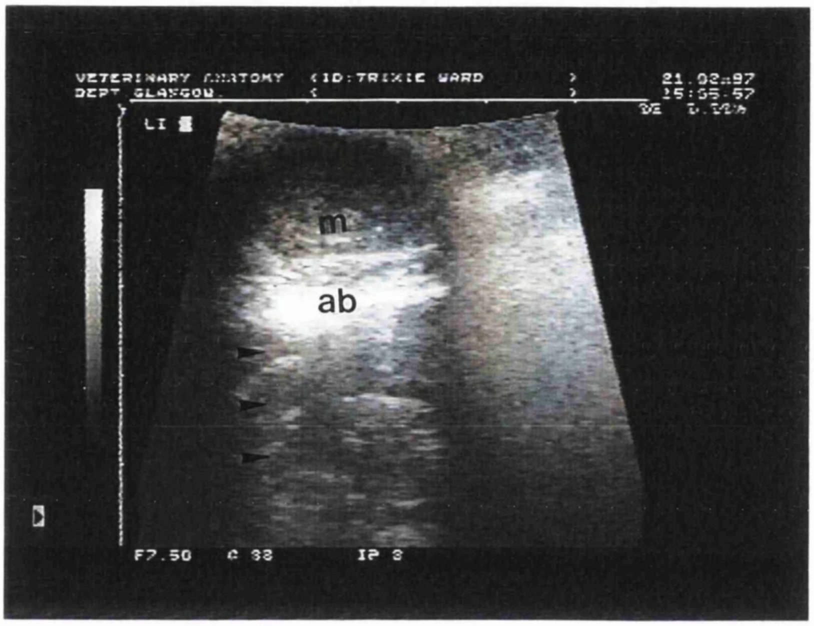

Figure 5.4c

Figure 5.5 Ultrasonographic appearance of the mammary tumours representing group three (**a**, **b**, **c**). The areas of tumour tissue are large and appear hyperechoic. In many cases they contained discrete anechoic regions indicating cystic structures. **s**, skin, **m**, tumour tissue, **c**, cyst.

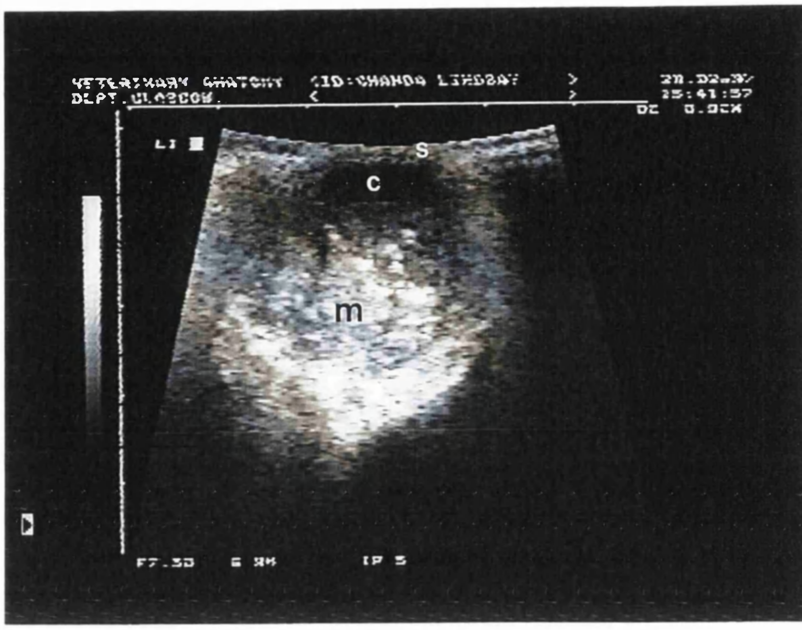

Figure 5.5a

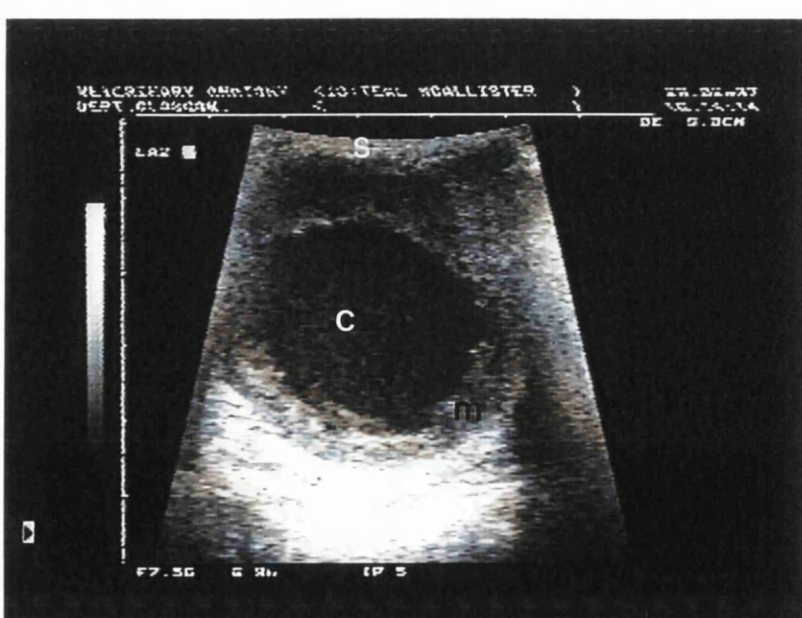

Figure 5.5b

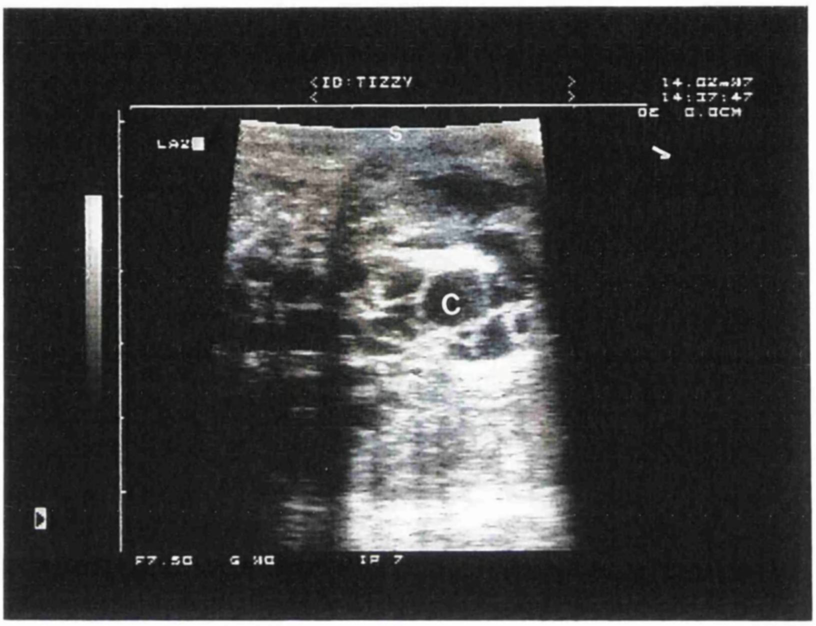

Figure 5.5c

Figure 5.6 Ultrasonographic images of (**a**) tumour of the left inguinal mammary gland in case 23, and (**b**) tumour of the right caudal abdominal mammary gland in case 26. Note the hyperechoic accumulations of calcified tumour tissue (arrow) with acoustic shadowing within the hypoechoic parenchyma mass (arrow heads). The mammary tumours were removed by surgery in both cases. The rescan result three months later showed no tumour mass was found in case 23. Unfortunately, case 26 failed to return for a rescan. **s**, skin, **m**, tumour tissue, **ab**, abdominal muscle.

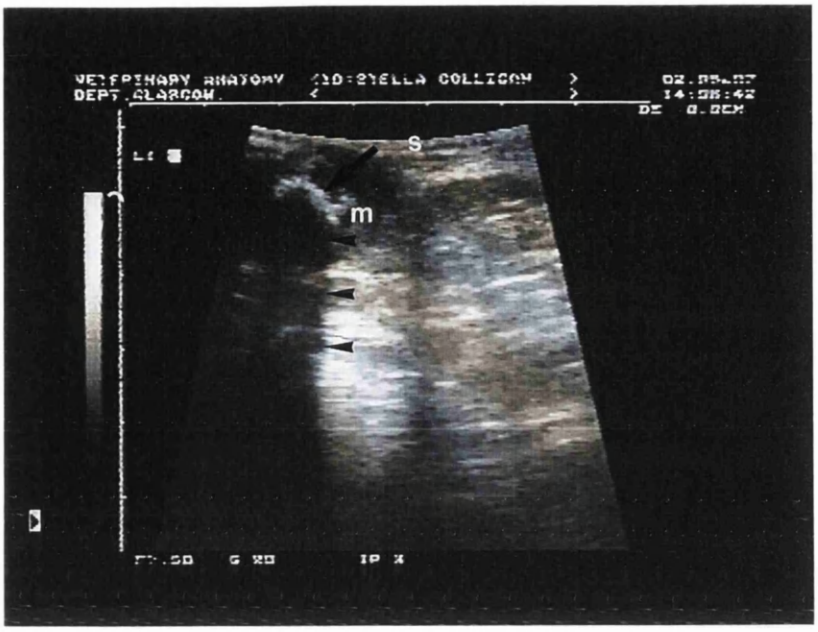

Figure 5.6a

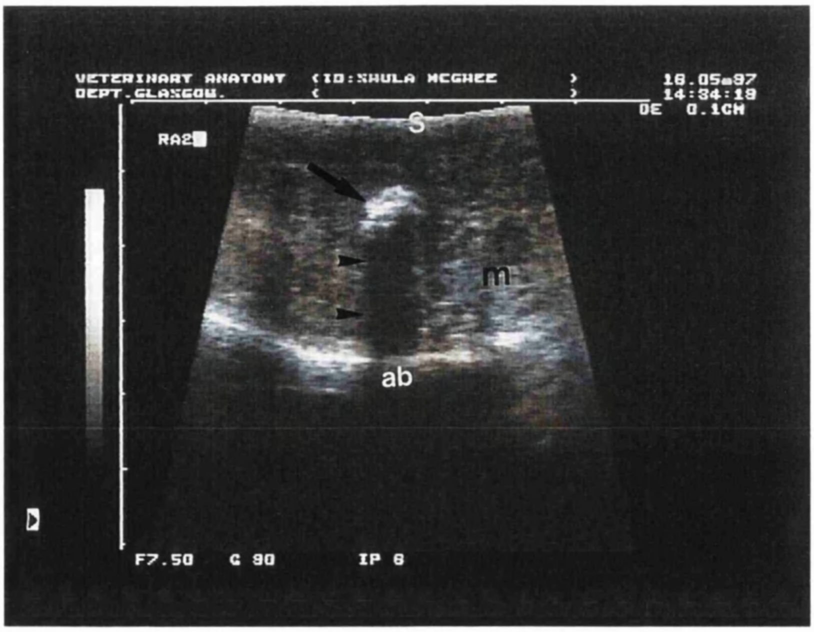

Figure 5.6b

Figure 5.7 Ultrasonographic images of the normal (**a**) right axillary lymph node, RAN in case 19, and (**b**) left superficial inguinal lymph nodes, LIN in case 17. The normal superficial lymph nodes appear rounded and isoechoic to hypoechoic structures relative to the surrounding soft tissue (arrow heads). **s**, skin, **pm**, pectoral muscle.

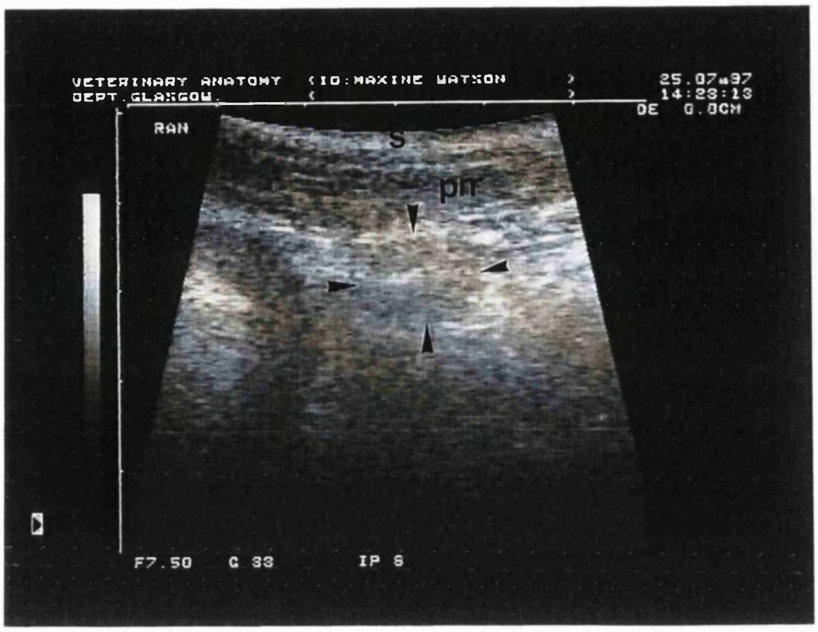

Figure 5.7a

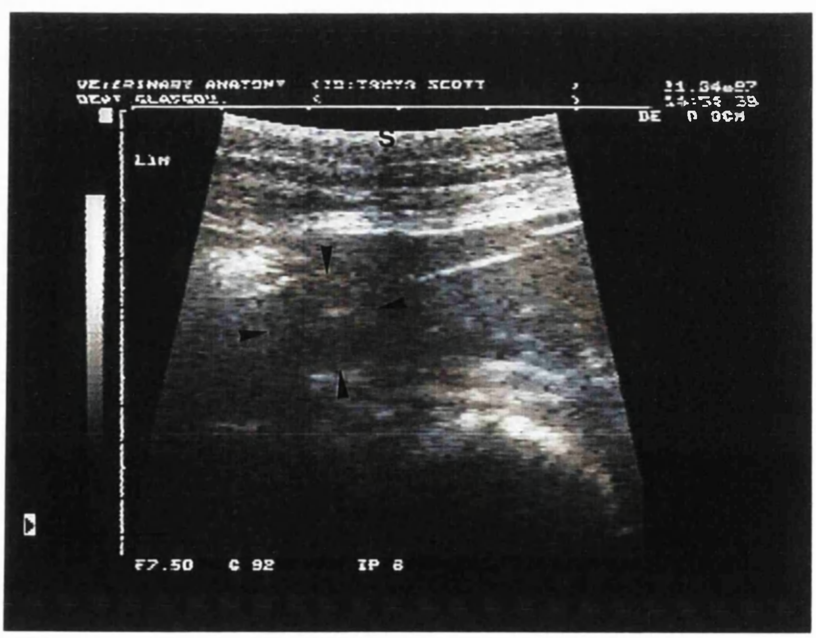

Figure 5.7b

Figure 5.8 Ultrasonographic images of the abnormal enlarged left axillary lymph nodes, LAN in case 3 (**a**) and left superficial inguinal lymph node, LIN in case 6 (**b**). They appear as homogeneously hypoechoic structures relative to surrounding tissue. The right axillary lymph node, RAN in case 24 (**c**) appears to have a mixed echotexture with some anechoic areas, and the right superficial inguinal lymph node, RIN in case 25 (**d**) appears to have a more echogenic echotexture relative to its surroundings. **s**, skin, **aa**, axillary artery, **ep**, external pudendal artery.

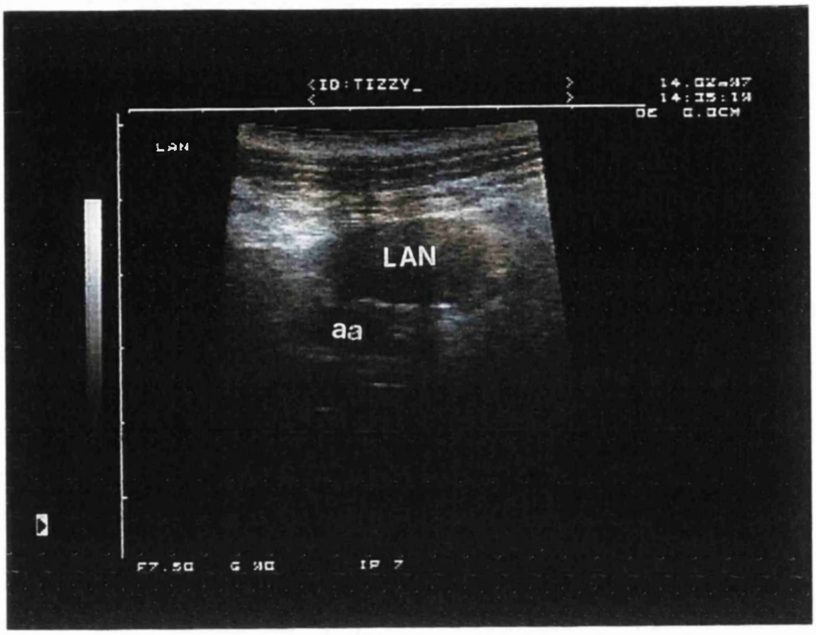

Figure 5.8a

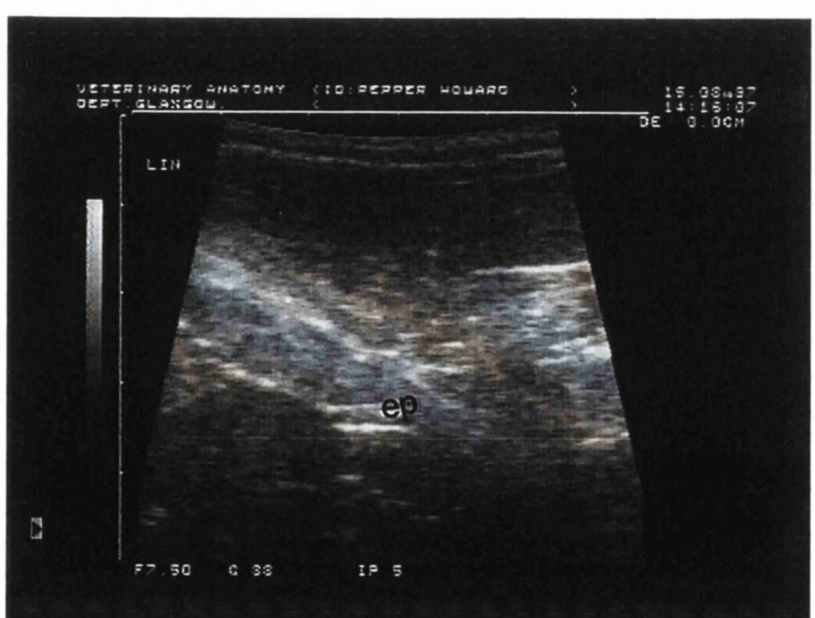

Figure 5.8b

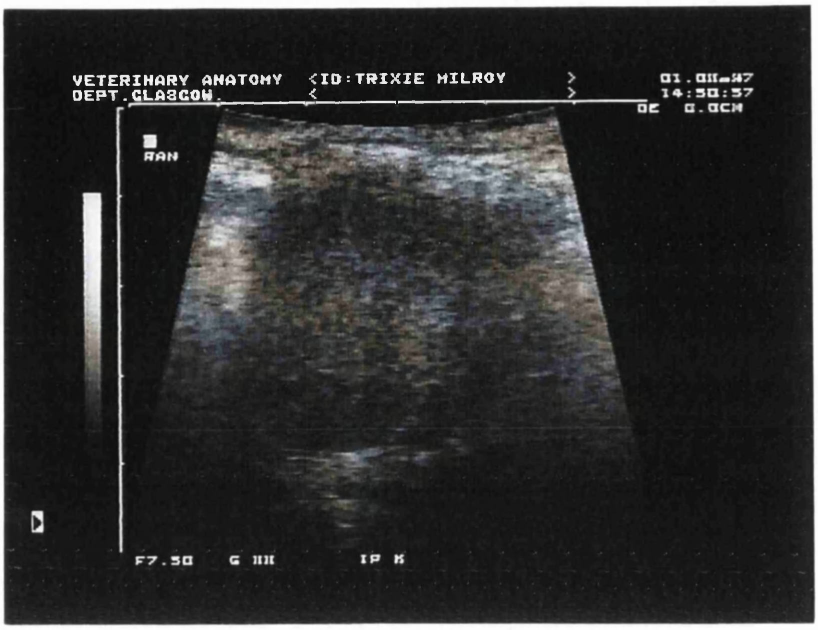

Figure 5.8c

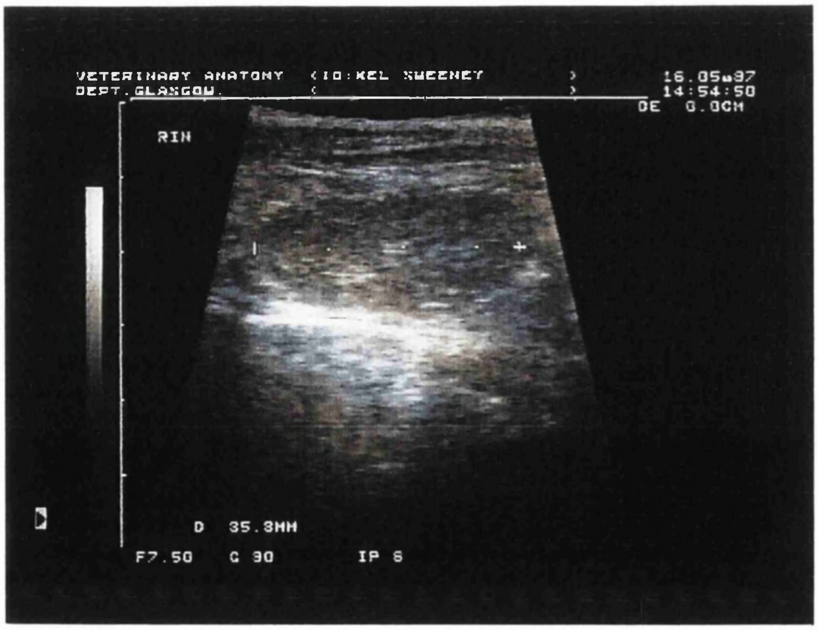

Figure 5.8d

Figure 5.9 Ultrasonographic images of the left cranial abdominal mammary gland, LA1 (**a, a1**), left caudal abdominal mammary gland, LA2 (**b, b1**) and right superficial inguinal lymph node, RIN (**c, c1**) in a 12 year old cross breed dog with clinical evidence of mammary gland tumours (case 6). The tumour tissues have increased in size on the rescan from 1.0 cm (**a**) to 1.6 cm (**a1**) in LA1, and from 0.5 cm (**b**) to 0.8 cm (**b1**) in LA2 (arrow head). The echogenicity has not changed. The RIN is normal (1.4 cm in diameter) on the first scan (**c**) but is found to be enlarged (2.5 x 1.0 cm) (**c1**) on the rescan and appearing homogeneously hypoechoic with an ill defined margin. **s**, skin, **ab**, abdominal muscle.

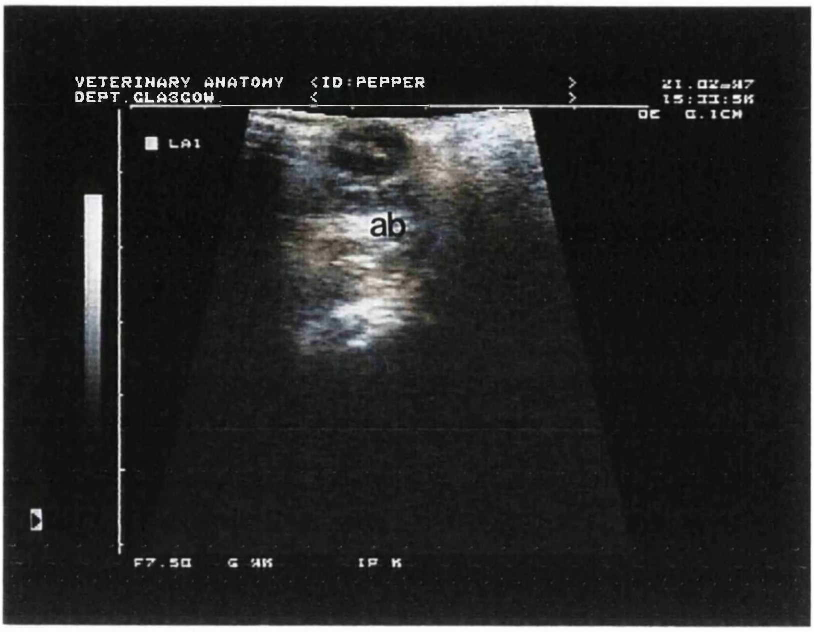

Figure 5.9a

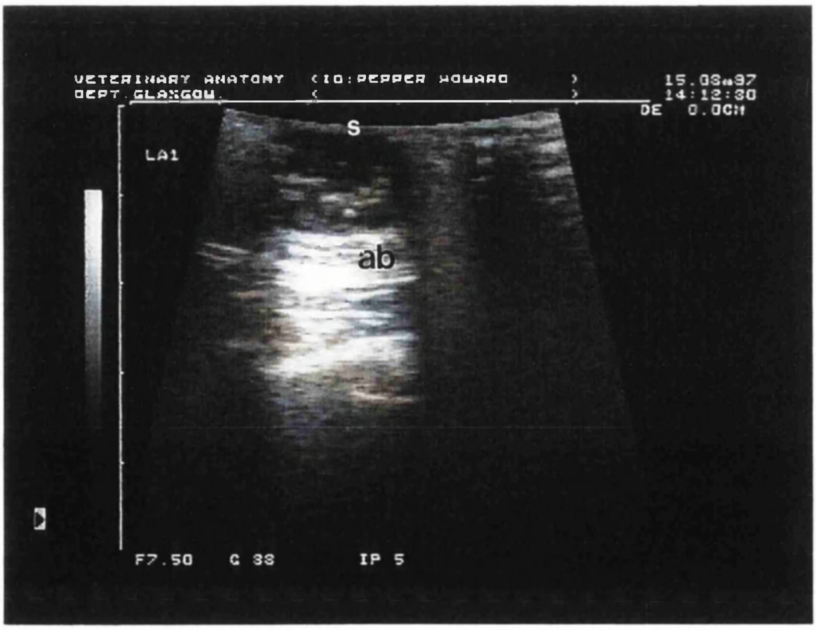

Figure 5.9a1

Figure 5.9b

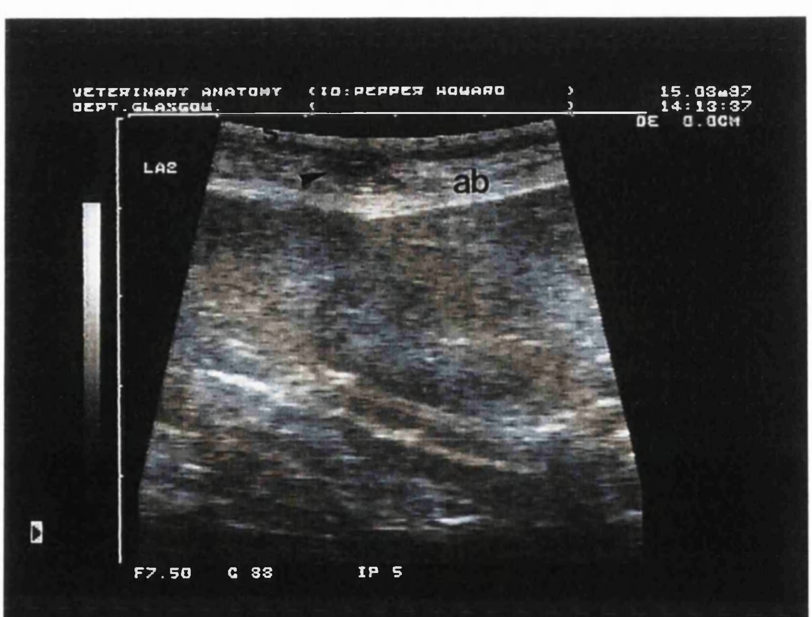

Figure 5.9b1

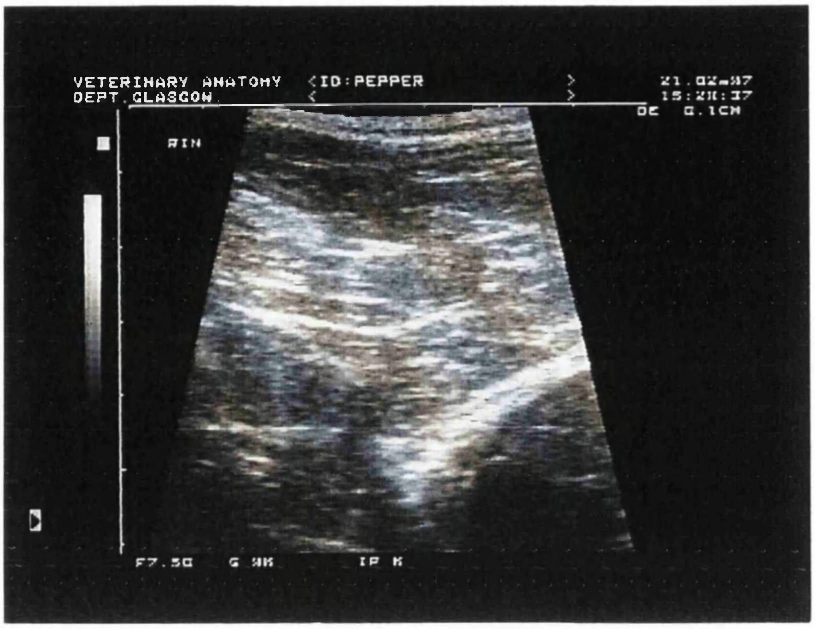

Figure 5.9c

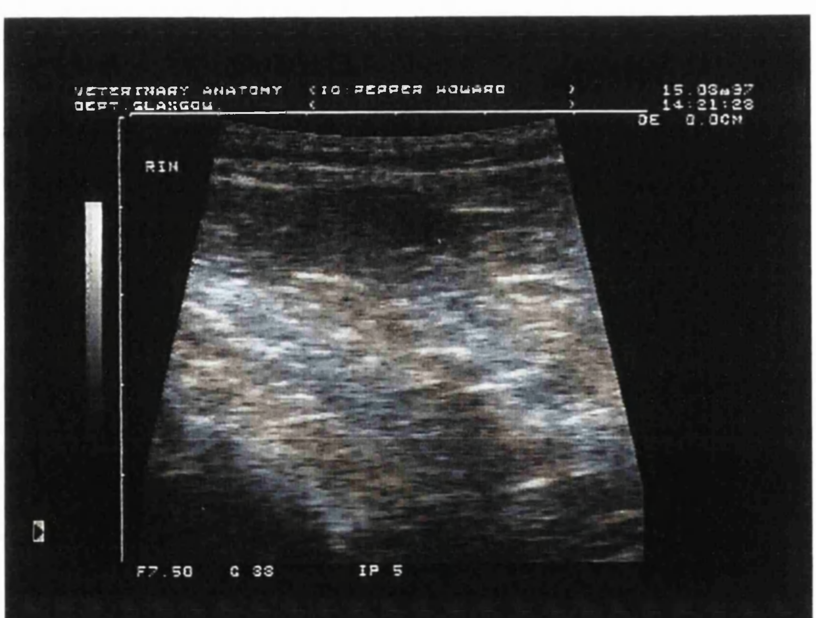

Figure 5.9c1

Figure 5.10 Ultrasonographic images of the tumour tissues in the left caudal abdominal mammary gland, LA2 (**a**) and the right cranial abdominal mammary gland, RA1 (**b**) in a nine year old bitch (case 18). Small areas of tumour tissue (arrow head) were detected on the rescan and appearing hypoechoic with an ill-defined margin. **s**, skin, **ab**, abdominal muscle.

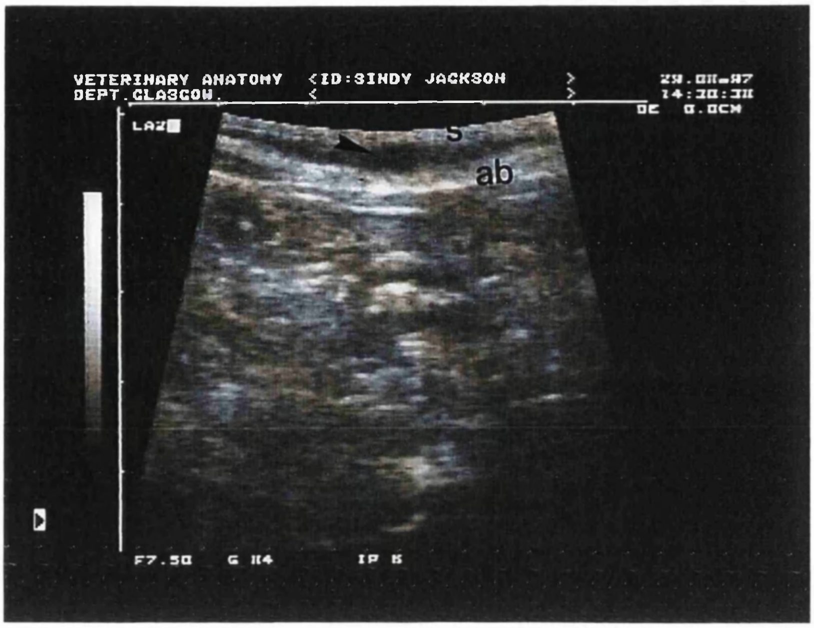

Figure 5.10a

Figure 5.10b

Figure 5.11 Ultrasonographic images of the tumour tissues in the left cranial abdominal mammary gland, LA1 in case 16 (**a**) and the right cranial abdominal mammary gland, RA1 in case 10 (**b**) which were not detected by palpation. Note the areas of tumour tissue are small (arrow head) and appear hypoechoic with an ill-defined margin. **s**, skin, **ab**, abdominal muscle.

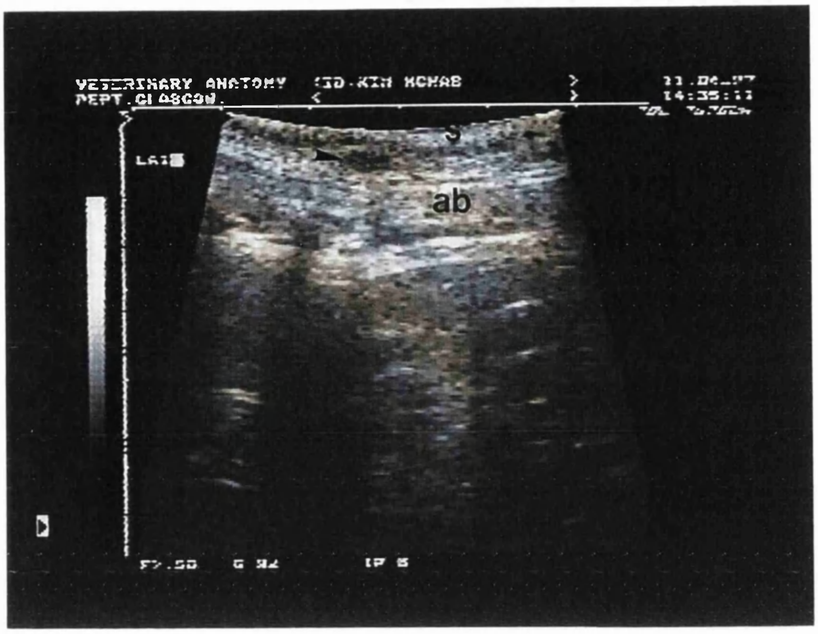

Figure 5.11a

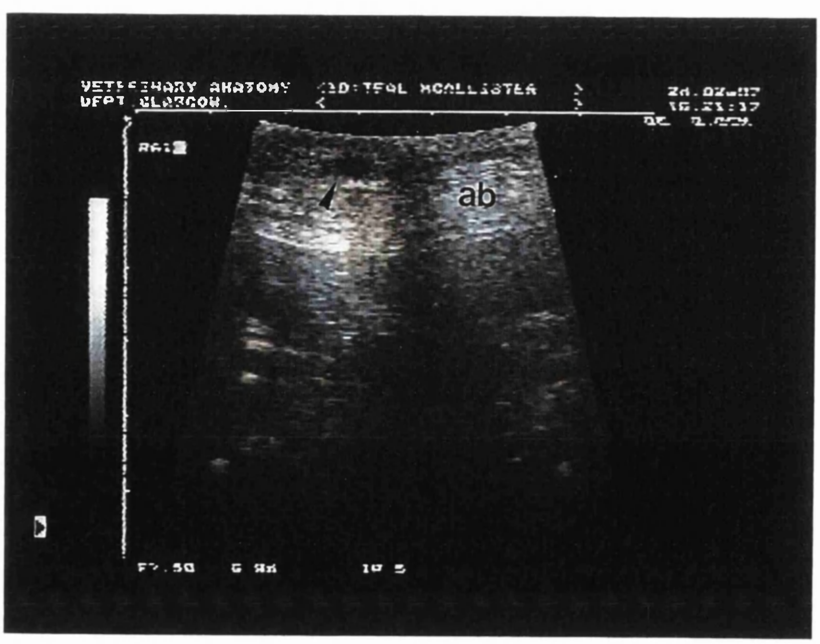

Figure 5.11b

5.4 **Discussion**

The present study was carried out with the aim of ascertaining the reliability of high resolution ultrasonography in evaluating mammary gland tumour and tumour spread to regional lymph nodes in bitches. Most of the ultrasonographic findings on canine mammary gland tumour in the present study were compared with human ultrasonography.

Ultrasonography has been shown to be an excellent modality for diagnosing soft tissue tumours in small animals (Harcke *et al.*, 1988; Craychee, 1995; Kramer *et al.*, 1997). They can be differentiated into solid against cystic forms. The echotexture of solid tumours is variable and ranges from homogenous to inhomogenous and practically anechoic to hyperechoic (Kramer *et al.*, 1997). The tumour tissue is more distinct if the difference in echogenicity from the surrounding tissue is large (Kramer *et al.*, 1997). However, there are no ultrasonographic criteria which give any information regarding the aggressiveness or type of a tumour (Kramer *et al.*, 1997). The only exception is lipoma, which has a characteristic ultrasonographic appearance of anechoic background with diffuse hyperechoic foci and wide spread lines (Kramer *et al.*, 1997). In the human, ultrasonography of the mammary gland has evolved tremendously and gained clinical acceptance over the decades. Its use in detecting breast tumour lesions has became a routine procedure (Hayashi *et al.*, 1985; Stavros *et al.*, 1995; Kolb *et al.*, 1998). Contrary to the previously held belief that ultrasound is only capable of detecting advanced breast cancer, with improvement in technology ultrasonography can now identify not only early tumours under one cm in diameter but also intraductal tumour components using a high-resolution real-time system (Fornage *et al* 1990). Although the use of ultrasonography in evaluation of breast tumour in humans is well documented (Schneider *et al.*, 1969; Schneider, 1970; Hayashi *et al.*, 1985; Richter *et al.*, 1997), its use in the evaluation of mammary gland tumour in bitches has never been reported. The use of high-resolution ultrasound with a transducer of 7.5 MHz frequency in this study has resulted in imaging well defined mammary tumour tissue masses. With a high frequency transducer, however, a marked reduction in the depth of imaging occurs as a result of absorption, thus confining the use of such transducers to only a few centimetres superficially. Current real-time high resolution linear array transducer as used in this study have optimal images in terms of resolution, contrast, and speckle pattern, and this allows small lesions under 1 cm to be visualised.

The normal canine mammary glands consist of epithelial glandular tissue, connective tissue, and the covering skin (Evans and Christensen, 1993). The great majority of the mammary region is occupied by dense stroma and fat (Silver 1966). The secretory tissue is present to a significant degree only during pregnancy, pseudopregnancy, the period of lactation when pups are nursing, and for 40 to 50 days following weaning (Evans and Christensen, 1993). During oestrus the duct of the mammary gland grows rapidly and the alveolar system develops (Evans and Christensen, 1993). The size of the mammae is greatly reduced approximately 10 days after parturition. By 40 days the lobule-alveolar system is largely degenerated, and the ducts are shrunken. After cessation of lactation, the mammary gland in the dog regresses to a simple duct system (Evans and Christensen, 1993), though this is usually slightly more extensive than in the young animal (Silver, 1966). The majority of the bitches involved in this study were in a stage of anestrus, and in addition six bitches had already been neutered. Thus, in most cases the mammary gland tissue was in a regression stage and the glands were small.

The number of mammary glands in bitches involved in this study varied in individuals. It is well known that the number of mammary glands in bitches varies from 8 to 12 glands with 10 glands being the most commonly encountered (Evans and Christensen, 1993). The usual pairs of glands are from caudal to cranial, one inguinal, two abdominal (caudal and cranial abdominal) and two thoracic (caudal and cranial thoracic) which are established in early embryological development. Anomalies in position and number may also arise at this time such as uneven spacing, failure of nipple development or complete aplasia (Silver, 1966). The majority of the bitches encountered in the present study (75%) had 10 mammary glands; none of them had 12 mammary glands. Seventeen missing mammary glands in a total of nine bitches were noticed during examination. Ten missing mammary glands in a total of three bitches had a previous history of being removed due to mammary gland tumours. The remaining seven missing mammary glands consisted of four cranial thoracic mammary glands, one caudal thoracic mammary gland and two cranial abdominal mammary glands in a total of six bitches which had no previous history of surgery. It is strongly believed that the remaining seven missing mammary glands were due to either regression of the cranial glands, failure of nipple development or due to complete aplasia. The most cranial mammary glands in the majority of the bitches in this study were small and flat due to regression of the lobular alveolar system of the gland itself. Thus, they were sometimes difficult to find during examination.

The optimum age group for the peak incidence of mammary gland tumour in dog has been reported to be in a range between 6-10 years old (Jabara, 1960), 9-10 years old (Priester, 1979), and 10-12 years old (Fidler and Brodey, 1967). In the present study, the optimum age of incidence was found to be between 9-14 years old. Thus, it is slightly higher than Jabara (1960) and Priester (1979), but similar to Fidler and Brodey (1967). The big range of age incidence encountered in the present series is most probably due to the small number of bitches involved.

Mammary gland tumour has been reported to constitute more than 50% of all neoplasms in bitches (Bostock 1986). About 40% of mammary tumour tissue has been found in the inguinal region, the remaining being equally distributed between the four cranial glands (Bostock 1977). The highest incidence of mammary tumour was encountered in the most caudal gland and the lowest incidence was in the most cranial gland (Anderson and Jarrett, 1966; Fidler and Brodey, 1967; Bostock, 1977, 1986). In the present study, the highest incidence of the mammary tumours (30%) was found in the most caudal mammary glands (inguinal mammary gland) and the occurrence declined cranially with the lowest incidence (7%) in the most cranial mammary gland (cranial thoracic mammary gland). Thus, the results are in accord with the previous studies.

Previous studies showed that canine mammary tumours occur independent of breed (Jabara, 1960; Else and Hannant 1979). However, there is a study showing that mammary tumour incidence in dogs has been shown to be greatest in sporting breeds (Priester, 1979). Although there was an indication of breed prevalence in this study, there was not representation of all breeds in the study area. This is because of the small size of sample encountered in this series. A study of a large number of animals would be required in order to predict the breed prevalence in a particular area.

It is well known that mammary glands tumours occur primarily in female dogs. The result in this study is consistent with the above fact where all the dogs with a suspicious of having mammary gland tumour referred to the PDSA in a period of 7 months were female. However, mammary gland tumour could happened in male dogs and it has been shown by Priester (1979) in a study using a large number of dogs.

The aetiology of tumour of the mammary gland is still unknown (Evans and Christensen, 1993), but a good deal of circumstantial evidence indicates that the development of the neoplastic process is influenced by the female sex hormones (Evans and Christensen, 1993). Neutering is the greatest protection if done before oestrus cycles begin. It is understood that ovariectomy before puberty will almost completely prevent the development of mammary neoplasia, whilst spaying after puberty becomes progressively less protective with time (Schneider *et al* 1969). It has been reported that the relative risk for bitches spayed before oestrus is 0.05%, 8% after the first cycle and 26% after the second or more oestrus cycles, and neutering after 2 and half years of age did not influence mammary cancer risk (Schneider *et al.,* 1969). However, the abnormal oestrus cycles, pseudopregnancy, parity, age at birth of first litter, stillbirth experience, and fecundity had no influence on mammary tumour development (Schneider *et al.*, 1969). It has been postulated that during the first few cycles small clones of pre-neoplastic epithelial cells are established which may develop into true neoplasms after many years (Brodey *et al.,* 1983).

In a very recent study, Morris and co-workers (1998) have found that ovariohysterectomy when mammary tumours are removed does not have a significant effect on the progression of malignant disease. They also found that there were more benign than malignant mammary tumours. In addition, the development of a mammary tumour in bitch is an event programmed in early life which is not predominantly influenced by the removal of hormonal stimulation in maturity. Many of the malignant mammary tumours appear to have become independent of hormonal stimulation. Early spaying seems to be the only way to prevent the hormonal fluctuations which undoubtedly influence the development of such tumours (Morris *et al.*, 1998).

Tumours which are so invasive that either a unilateral or bilateral mammary strip is required to excise them will almost certainly reappear within a few weeks and it is very ambiguous whether surgical intervention is justified in these animals (Bostock 1986). Since most tumours are behaviourally benign, and there is little evidence that initially benign neoplasms undergo subsequent malignant transformation, there may be a few occasions when surgery is not appropriate. This is particularly true in very old dogs with several, slowly growing, hard mammary nodules, where surgery would be distressing to the animal and would be unlikely to increase life span to any significant extent (Bostock 1986).

The most common ultrasonographic features of mammary tumours in humans have been described as consisting of an hypoechoic tumour nidus, a surrounding hypoechoic halo and distal acoustic shadowing (Harper *et al* 1983; Cole-Beuglet *et al.,* 1983). The larger tumours tend to show a heterogenous internal echo pattern, with variable through transmission. There may be either shadowing, enhancement, or no effect. With ultrasonography, the smallest cyst identified was 3 mm, whereas the smallest malignancy detected was 7 mm in diameter (Yang *et al.,* 1996). Ultrasonographic appearance of the areas of mammary tumour tissue encountered in the present study were varied from anechoic to hyperechoic structures. The divergence in ultrasonographic appearance of the areas of tumour tissue seemed to depend on the severity of the development of the tumour. Group one type which consisted of areas of tumour tissue and appeared anechoic to hypoechoic was the most commonly encountered while group three type which consisted of areas of tumour tissue and appeared hyperechoic with the presence of cysts in many of them was the least commonly encountered. Vincent (1988) has demonstrated that most of the soft tissue tumours of the extremities imaged ultrasonographically appeared hypoechoic relative to its surroundings. A similar appearance has also been demonstrated in human breast tumours (Hayashi *et al.*, 1985; Yang *et al.*, 1996). The echotexture of solid soft tissue tumours has been described as variable and ranges from anechoic to hyperechoic structures (Kramer *et al.*, 1997). The presence of cysts within the tumour masses was suggestive of a benign type of tumour and they appeared as anechoic structures with the proximal wall highlighted by a strong echo and there was marked enhancement distal to the cyst (Kramer *et al.*, 1997). Thus, the present findings are an accord with the previous studies. The ultrasonographic appearance of mammary gland tumours shown in this study had similar characteristics compared to soft tissue tumours in other organs.

Ultrasonography was found to be superior to palpation in detecting mammary tumour nodules in this study. Of the 92 mammary gland tumours detected, 13 had failed to be detected by palpation. The detection of the mammary tumour tissues appeared to be dependent on size and consistency of the tumour itself. Areas of mammary tumour tissue as small as 0.4 cm when solid and hard in consistency were able to be detected by both palpation and ultrasonography. Conversely, when the area of tumour tissue was small and soft in consistency, palpation failed to detect it. This is in agreement with Yang *et al.* (1996) who reported that ultrasonography was more sensitive than clinical palpation in detecting human breast lesions. They also suggested that the combination of ultrasonography and clinical palpation was more specific than other diagnostic measures. This is in accord with the result of the present study.

The spread of mammary tumour tissue through the mammary gland is believed to be via the lymphatic connections. Each mammary gland has a network of lymph vessels which joins similar networks in the subcutis and parenchyma (Silver, 1966). These link up by larger channels either to the networks of adjacent glands or directly to the local lymph node. In a recent study, the lymphatic connection between the caudal abdominal and inguinal glands was shown to be indirect (Patsikas and Dessiris, 1996b). Their connection was demonstrated to be via the superficial inguinal lymph node. The cranial thoracic and inguinal mammary glands always drain only to the axillary and superficial inguinal lymph node respectively, while the caudal thoracic, cranial and caudal abdominal glands drain to both the axillary and superficial inguinal lymph nodes (Sautet *et al.*, 1992). No lymphatic connection has been shown between the two rows of the mammary glands (Sautet *et al.*, 1992; Patsikas and Dessiris, 1996a). The involvement of regional lymph nodes in mammary tumour metastases is dependent on which mammary glands are affected (Fidler and Brodey, 1967). In the present study, the highest incidence (59.6%) of mammary gland tumours was emanating from the caudal abdominal and inguinal mammary glands on both sides. Consequently, the majority (78.3%) of the enlarged regional lymph nodes were also found in superficial inguinal lymph node on both sides. Thus, it is in agreement with the previous studies.

Ultrasonographic appearance of normal and abnormal lymph nodes has been described in humans (Ying *et al.*, 1996) and in small animals (Marchal *et al.*, 1985; Rubaltelli *et al.*; 1990; Saunders *et al.*, 1992; Pugh, 1994). It is understood that high resolution ultrasound plays an important role in the assessment of lymph nodes both in human and small animals. A transducer of 7.5 MHz frequency has been used to evaluate the superficial lymph nodes (Vasallo *et al.,* 1992) and cervical lymph nodes (Bruneton *et al.,* 1984) and has been proved to be of particular diagnostic value for investigating metastatic nodal disease associated with breast cancer and ENT (ear, nose, throat) cancer respectively in humans. Normal axillary and superficial inguinal lymph nodes are relatively small, and therefore high resolution ultrasonography is required for their evaluation. A clear understanding of the distribution and ultrasonographic appearance of normal axillary and superficial inguinal lymph nodes is necessary in differentiating normal lymph nodes from pathologic ones. In one report, the canine regional cervical lymph nodes were characterised as round to oval hypoechoic structures (Wisner *et al.*, 1991). However, not all the normal lymph nodes can be visualised ultrasonographically. Normal lymph nodes are often indistinct due to their small size and echogenicity similar to the surrounding soft tissue (Pugh, 1994). Often it varies from hypoechoic to isoechoic relative to the surrounding fatty tissue. Lymph nodes which have changed due to infiltrative or inflammatory processes may become visible due to enlargement or altered echogenicity (Pugh, 1994). The major vascular hilus appears as an hyperechoic linear structure within a lymph node and is continuous with the surrounding connective tissue (Pugh, 1994). The normal appearances of axillary and superficial inguinal lymph nodes found in this study were characterised as oval to round hypoechoic to isoechoic structures. A similar appearance has been described in canine regional cervical lymph nodes (Wisner *et al.*, 1991), and canine abdominal lymph nodes (Cartee and Mahaffey, 1995). They were imaged as hypoechoic structures within the relatively hyperechoic mesentery (Cartee and Mahaffey, 1995).

In the human, lymph nodes are ultrasonographically evaluated relative to their size, shape, echopattern, and vascularity (Nagano *et al.*, 1991). Shape has also been stated to be a useful criterion in differentiating normal or reactive nodes from malignant nodes (Vasallo *et al.*, 1992; Ying *et al.*, 1996). In small animals, size is normally the major criterion for diagnosis (Cartee and Mahaffey, 1995). The shape is not an important criterion in small animals as the nodes tend to be oval to round in shape for both the normal and enlarged lymph nodes as shown in this study. Therefore, the size is very important in evaluating the abnormal or diseased lymph nodes in small animals as they become enlarged in disease and can be detected ultrasonographically.

Results in this study show that enlarged lymph nodes can be recognised ultrasonographically and differentiated from surrounding soft tissue. Most of the enlarged lymph nodes found in the present study appeared hypoechoic with an ill defined margin. The enlargement of regional lymph nodes in mammary gland tumours with an hypoechoic appearance did not always indicate metastatic spread of tumour tissue. It could sometimes be due to other factors such as lymphoid hyperplasia consequent upon tumour breakdown or due to lymphadenitis (Saunders *et al.,* 1992; Pugh, 1994). This has been demonstrated in the present study where six regional lymph nodes which were found to be enlarged and have an hypoechoic appearance on the first scan, later were found to be negative (normal) on the rescan after the mammary gland tumours had been removed. Thus, it was suggestive that the enlargement of six regional lymph nodes found in the first scan was most probably due to inflammatory reaction. However, the presence of two enlarged regional lymph nodes in case 24 and case 25 which appeared more echogenic was suggestive of metastasis tumour spread. These two enlarged lymph nodes were not removed during surgery. The rescan examination on these cases after approximately two and half months showed that the enlarged lymph nodes had further increased in size but the echogenicity was not changed. Thus, this finding strongly suggested that the metastasis tumour had spread into the regional lymph nodes in these cases.

Seven bitches that did not undergo surgery in this study were treated thus for various reasons. Due to involvement of the regional lymph node, LIN and RIN in case 6 and case 24 respectively, the surgeon decided that surgery would do more harm than good to the animal. In case 12, permission was not given by the owner because the dog was too old. In case 16, the surgeon decided not to perform surgery unless the tumour size increased on the next examination. In case 18, only one gland was involved and the tumour tissue was very small. In case 20 and 21, there was no mammary tumour tissue found during examination.

Of the seven bitches that did not undergo surgery, in only one bitch (case 6) the size of the tumour tissue area increased slowly over a period of approximately 3 - 5 months. The mammary tumour tissue in the five remaining bitches had not increased in size. This was suggestive of a benign type of tumour. The finding of the presence of cysts in the group three type of mammary tumour, suggested that most of the mammary gland tumours encountered in this group were of a benign type. This is an accord with Cotchin (1958), Owen (1966) and Yager and Scott (1993). In a series of 424 bitches with mammary tumours, 41% appeared malignant histologically but only about 10% proved themselves to be malignant by metastasising (Cotchin, 1958). With benign conditions, the most easily recognised feature is cysts or other liquid filled areas (Kramer *et al.,* 1997). However, there was evidence that suggested the presence of malignant type of mammary gland tumours as found in cases 2, 3, 7, 10 and 13 with massive tumour spread among the mammary glands and the enlargement of regional lymph nodes (axillary and /or superficial inguinal lymph node). Unfortunately, the rescan examination on these cases was not attained because all of them were euthanased as a result of massive tumour spread in accordance with the request of the owner. The presence of enlarged lymph nodes with more homogenous echogenic appearance in case 24 and case 25 on the first scan also suggested a malignant type of tumour. The rescan images on these cases after approximately two and half months showed the enlarged lymph nodes had further increased in size with a similar echogenicity. The evidence of new tumour tissue detected on the rescan in case 18 after approximately three and half months also suggested the presence of a malignant type of tumour in this study. However, the definitive diagnosis of benign and malignant type of tumour by ultrasound examination alone is unlikely because their characteristics may be similar (Wisner *et al.*, 1994).

One bitch presented in this study with a suspicion of having mammary tumour was later found to have a well encapsulated homogenous echogenic structure with more organised echotexture suggestive of abscess formation. This structure did not involve mammary tissue. The ultrasonographic appearance of abscesses has been shown to vary from anechoic and cyst-like to an echogenic solid appearing mass, depending on the character of the purulent material (Craychee, 1995).

Mastectomy is always the operation of choice in the treatment of mammary gland tumours (Owen,1966). Mammotomy is not the best solution because it leads to recurrence from implantation of tumour cells from the scalpel blade and other instruments (Owen, 1966). Moreover cells in the remaining part of the clinically normal mammary gland may be in a pre-malignant state and produce tumours later (Owen, 1966). In the case of multiple tumours complete mastectomy of a whole side may be necessary. This was done in case 5 in this study. It has been suggested that caudal abdominal and inguinal mammary glands should be excised together even if tumours only occur in one gland because of the lymphatic drainage connection (Owen, 1966). If both sides are affected with tumour it is sometimes possible to remove all the caudal glands at one operation (Owen, 1966). If this is not possible because of extensive skin loss a second operation becomes necessary later (Owen, 1966).

A number of studies have been carried out in an attempt to differentiate malignant and benign lesions in human breast tumours using ultrasonographic criteria (Cole-Beuglet *et al.,* 1983; Fleischer *et al.,* 1983; Hayashi *et al.,* 1985; Stavros *et al.,* 1995; Yang *et al.,* 1996; Richter *et al.,* 1997; Kolb *et al.,* 1998). One of the most difficult problems in breast imaging is the differentiation of benign from malignant solid masses (Jackson, 1995). Malignant breast tumour has been characterised as an intensely hyperechoic mass, an ellipsoid shape with a thin echogenic capsule, or two or three gentle lobulations plus a thin echogenic capsule (Stavros *et al.,* 1995). Histological study has shown that benign tumours are more frequently encountered than malignant tumours (Stavros *et al.,* 1995). Malignant nodules also have characteristics of anechoic spiculations and angular margins, distal shadowing and an hypoechoic centre when compared with fat (Stavros *et al.,* 1995). In a study by Yang *et al.* (1996), malignant breast tumour (carcinoma) has been diagnosed correctly by ultrasonography with 97% sensitivity in patients with a proven malignancy. It was found that ultrasonography did not miss any tumour lesions. A malignant tumour less than one centimetre in diameter was imaged as an irregular hypoechoic structure with an increased depth to width ratio (Yang *et al.,* 1996). In small animals, the benign superficial neoplasms are usually clearly circumscribed with no invasion of surrounding tissues (Barr, 1990b). Malignant superficial neoplasms also have a very variable ultrasonographic architexture. Large masses in particular are often heterogenous, with anechoic areas of necrosis and haemorrhage, and echogenic patches representing fibrosis and calcification (Barr, 1990b). Most malignant neoplasms are poorly circumscribed, with no clear boundaries between normal and abnormal tissue (Barr, 1990b). It is not possible, however, to determine the histological type of most neoplasms by the ultrasonographic appearance alone. Potentially, ultrasound may be used for the detection of small nonpalpable masses (Barr, 1990b).

Although ultrasonographic evaluation of lymph nodes cannot definitely discriminate between malignant and benign neoplasms, there are suggestive patterns. Lymph nodes associated with malignant disease are generally larger and more numerous than in benign disease (Smeeth *et al.,* 1990; Homco, 1996). Lymph nodes associated with malignant disease are more hypoechoic than those associated with benign disease (Smeeth *et al.,* 1990). Most lymph nodes involved in malignant disease tend to develop a rounded shape, but in benign disease, they tend to retain their original oval or spindle shape despite an increase in size (Smeeth *et al.,* 1990; Homco, 1996). Most disease of the lymph nodes, whether inflammatory or neoplastic results in some degree of node enlargement. Because most normal lymph nodes are flat and ovoid or spindle shape, any changes toward a rounded appearance should suggest disease (Smeets *et al.*, 1990).

In the human, the signs most used in vivo to detect lymph node metastases are lymph node enlargement, variation in shape, and loss of hypoechoic hilus (Vasallo *et al.,* 1992). The mass effect of metastatic tissue that infiltrates a lymph node causes the node to be round (Vasallo *et al.,* 1992). The cortex is composed mainly of lymphoid tissue without sinuses and appears as an hypoechoic zone. Changes in the thickness or shape usually represent metastasis but sometimes can be due to an increase in the density of lymphoid tissue. The reactive nodal changes begin in the cortex, where lymphoid proliferation increases the size of the cortex (Vasallo *et al.,* 1992), but metastasis also reaches the cortical zone of the lymph node via afferent lymphatic vessel. Hence, diagnosis can be confusing and lead to false positives. Both inflammatory and malignant diseases reach the lymph node via afferent lymphatic vessels that drain into the peripheral sinuses located in the subscapular regions of the node. Thus, early malignant and benign lesions primarily involve the cortex (Vasallo *et al.,* 1992). In malignant disease, however, the changes occurring within the lymph node are somewhat different in nature. The process involves infiltration of the node by malignant tissue, which is more likely to result in early distortion of internal nodal architecture with invasion (narrowing or loss) of the hilus. In addition, the mass effect of infiltrating tumour, which may not be equal at all points within the node, may lead to a change in nodal shape (Vasallo *et al.,* 1992). However, Bruneton *et al.* (1984) and Hajeck *et al.* (1986) found that ultrasound has not been helpful in differentiation between malignant infiltration and enlargement due to inflammatory process. Similarly in this study, the enlarged lymph nodes were not be able to be differentiated whether it was due to lymphadenitis or tumour tissue infiltration.

In conclusion ultrasonographic evaluation of the canine mammary gland tumours and their regional lymph nodes has been found to be useful in determining the extent and spread of the tumour tissues. This could greatly help the surgeon in making a proper diagnosis and deciding on treatment.

AN ULTRASONOGRAPHIC STUDY OF MUSCULOSKELETAL INJURIES AND MAMMARY GLAND TUMOUR IN SMALL ANIMALS

A thesis submitted to the Faculty of Veterinary Medicine,
University of Glasgow.
For the Degree of Doctor of Philosophy

by

MD ZUKI ABU BAKAR@ZAKARIA.
D.V.M. (Putra University of Malaysia)

Division of Veterinary Anatomy,
Department of Veterinary Preclinical Studies,
School of Veterinary Medicine,
University of Glasgow,
March, 1999

VOLUME 2(i)

CONTENTS -VOLUME 2(i)

LIST OF TABLES

LIST OF FIGURES

ABBREVIATIONS

K-wires	Kirschner wires
PDS	Polydioxanone (suture material)
DCP	Dynamic Compression Plate
ESF	External Skeletal Fixator
POP	Plaster of Paris

CHAPTER 6

AN ULTRASONOGRAPHIC STUDY OF THE PROGRESS OF BONE HEALING AFTER ORTHOPAEDIC SURGERY IN SMALL ANIMALS

6.1 **Introduction and aim of the study**

Evaluation of the healing of bone fractures in small animals is by far accomplished by radiography (Newton and Hohn, 1974; Cocke and Norton, 1974; Braden and Brinker, 1976; Chawla, *et al.*, 1983; Wu, *et al.*, 1984; Lewallen, *et al*, 1984; Pettine *et al*, 1993). Histological studies of the fracture healing process have also been carried out (Rahn, *et al.*, 1971; Aro and Chao, 1993). The healing of fracture is one of the most remarkable of all the repair processes in the body since it results, not in a scar, but in the actual reconstruction of the injured tissue in something very similar to its original form.

Traditionally, the major role of musculoskeletal ultrasonography has been evaluation of soft-tissue structures of the extremities (Kaplan, *et al.* 1990). Because of its high acoustic impedance, bone is a natural barrier to the high frequency sound from the bone boundary. Ultrasonography is therefore, capable of revealing only the bone surface. Some investigators have reported successful ultrasonographic evaluation of bone and bony abnormalities. High resolution ultrasonography has shown to be more sensitive than plain radiographs for detection of new bone formation at the distraction site in Ilizarov limb-lengthening procedures (Young *et al.* 1990). Its also has been used in the detection of occult femoral and clavicular fractures in two infants with symptoms of fracture in whom plain radiographs were normal (Graif *et al.* 1988). Recently, it has been suggested that rotator cuff ultrasonography may help to detect and define fracture of the greater tuberosity of the humerus (Patten *et al.* 1992).

Despite the limitation on bone evaluation, diagnostic ultrasonography has been demonstrated to be a useful diagnostic tool in the assessment of bone fracture in animals and humans (Reef, 1992; Ricciardy, *et al.*, 1993; Smith and Webbon, 1994), and its healing process (Young *et al.*, 1990; Mahaisavariya, *et al*, 1991; Ricciardy, *et al.*, 1992; Maffuli, *et al.*, 1992; Eyres, *et al.*, 1993; Smith and Webbon, 1994; Hamanishi, *et al.*, 1994). In humans, ultrasound has successfully predicted fracture healing and delayed healing and it was able to predict fracture healing before it was radiographically evident (Moed, *et al.*

1995). Even fine osteophytes can be detected, appearing as hyperechoic, rough, irregular structures (Kramer *et al.*, 1997). Previous researchers agree that ultrasound has a significant value in evaluating the progress of bone fracture healing especially in the early stage where radiography cannot reveal the changes at the fracture site at this stage (Derbyshire and Simpson, 1992; Mahaisavariya and Laupattarakasem, 1993; Hendrich, *et al.*, 1995; McClellan, 1995; Sarazin, *et al.*, 1996). Initially, the unmineralised callus can be identified between the two ends of bone. They can be seen as echogenic islands which became aligned longitudinally and progressively increased to fill the fracture gap (Eyres, *et al.*, 1993). As healing progresses, mineralised callus is identified casting an acoustic shadow (Smith and Webbon, 1994). Because the immature callus can be seen ultrasonographically before it is visible radiographically, ultrasound can be used to measure bone distraction, and it has been suggested that the use of ultrasound in human patients undergoing limb lengthening could reduce their exposure to radiation (Maffuli, *et al.*, 1992). However, ultrasound could only measure the gap distance during the early stages of distraction when the edges of the corticotomies were still well defined (Eyres, *et al.*, 1993). In the assessment of pelvic fracture in the horse, the fracture site is shown as bony discontinuity on the ultrasound image (Reef, 1992). Multiple fragments with areas of muscle disruption and haemorrhage surrounding the fracture can also be detected.

Most of the previous studies on ultrasonographic examination of the bone fracture and its healing process were produced artificially (Ricciardy, *et al.*, 1993; Claes, *et al.*, 1997). This in turn produced the desired fracture according to the experimental protocol. However, this is not totally comparable with the clinical cases which were used in the present study. The type of fractures were different in the clinical case compared to those produced artificially in the experimental study. There was less soft tissue trauma in artificial fractures and rarely does a natural fracture occur at right angles to the long axis of the shaft. Also comminution is quite common in traumatic fracture cases. These factors predispose to displacement and to the likelihood of much more movement than occurs in an experimentally produced fracture.

Ultrasound has been demonstrated to be able to detect osteomyelitis (Steiner and Sprigg, 1992; Kramer *et al.*, 1997), soft tissue damage surrounding fracture site (Maffuli and Thornton, 1995) and foreign bodies such as metal implants, wood, bone fragments, pencil graphite and glass (Shah, *et al.*, 1992; Manthey, *et al.*, 1996; Jacobson, *et al.*, 1998).

Plain radiography is relatively insensitive and does not detect new bone production until a considerable quantity has been laid down (Peretti *et al.* 1988; Young *et al.* 1990). Thus, it cannot be used to determine the rate of bone formation especially in the early stage. A precise and accurate non-invasive method of quantifying new bone formation would be valuable in the assessment of bone healing after fracture. Although ultrasonography has been demonstrated to be a useful diagnostic tool in evaluation of bone fracture healing, there are still very few articles documented on this particular subject in small animals. This may be due to the limitation of ultrasound in the evaluation of the skeletal system. Thus, the purpose of the present prospective study is to evaluate the usefulness of ultrasonography in the evaluation of the progress of bone fracture healing after orthopaedic surgery. This is intended to observe and define the ultrasonographic changes at the fracture site, and to compare the results of ultrasonography with routine radiography procedure. In the mean time the muscle damage is also evaluated ultrasonographically as well as the healing process.

6.2 **Materials and Methods**

Animals

Twenty four animals (twenty canine and four feline) with fracture of the long bones (involving either femur, humerus or tibia) or fracture of the pelvic bones were included in the study. All these animals were selected from orthopaedic cases referred to the Glasgow University Small Animal Clinics (GUSAC) from June 1996 to February 1998. The identification, type of fracture and method of reduction used in the animals involved are given in tables 6.1 and 6.2 respectively. Animals with fractures which were treated with additional external bandaging were not included in the study. This is because it cannot be monitored ultrasonographically especially in the early stages of the healing process as the ultrasound beam cannot penetrate through the bandaging material. All these animals had undergone orthopaedic surgery which was done by a group of experienced surgeons in the small animal clinic. Radiographs were obtained before and immediately after surgery for fracture repair and then when the animals were referred for assessment. The suture materials used to close the wound were 3/0 - 2/0 vicryl for muscle and 3/0 - 2/0 Ethilon for skin depending on the animals.

Of the 24 animals involved, seventeen animals were entire male, three animals were entire female, two animals were neutered male and two were neutered female. The breed incidence encountered in this study is given in table 6.3 of which the Border Collie was the highest incident breed involved in the study. Thirteen different breeds and four cats (three DSH and one Burmese) were involved. The age of animals involved varied from 7 months to 10 years old. Of the 20 dogs, 15 were large size (18-40 kg.), three were medium size (11-13 kg.) and two were small size (3-7 kg.). The frequency of the bones involved in this study is given in table 6.4 of which the highest incidence of bone involved is the femur whilst the least incidence was tibia/fibula.

Scanning technique

For ultrasonographic examination, the conscious animal was placed on the table in lateral recumbency with the fractured leg in a relaxed position. On occasions cases were examined in a standing or sitting position. An assistant was required to restrain the animal during examination. The skin preparation that was carried out prior to surgery has facilitated the process of ultrasound scanning during the first few days post-operation without the need for clipping hair. However, in this study, the technique of scanning without clipping the hair was applied during the follow up ultrasound examination. With this technique, the area to be scanned was first damped with tap water by using paper tissue, then a large amount of ultrasound gel was applied. In some circumstances, a comb was used to part the hair especially in long haired animals, thus exposing the skin surface before scanning.

Ultrasonographic examination was performed using a real-time B-mode ultrasound scanner (Capasee TOSHIBA) connected with a 7.5 MHz linear array transducer. The same machine was used throughout the study. Ultrasonographic scanning was done where possible on lateral and medial aspects, and sagittal plane for the femoral and humeral fractures. For pelvic fractures scanning was performed on the dorsal aspect. All fracture sites were examined both in longitudinal and transverse planes. Scanning directly over the incision site in the first few days after surgery was avoided. All scanned images were recorded on super VHS tape using a Panasonic video recorder during each examination for later review. Thermal prints of the best images were produced during review and labelled.

The first scanning was carried out approximately 24 hours post-operation when the animal was in a stable condition and then at day two and day three if the animal was still in hospital. When the animal was unstable, the first scan was done at day three to day five post operation. Five cases (cases 15, 21, 25, 26 and 28) were first scanned when the animals returned for assessment four to six weeks after the operation. The follow up scans were done when the animal returned for assessment approximately 4-6 weeks after the operation and then at 2-3 months after the operation. Five cases (cases 5, 13, 14, 24 and 27) failed to return for assessment at the Glasgow University Veterinary Clinics. Case 6 was scanned immediately before the implant removal, and then approximately 24 hours after the implant removal where the fracture site had already completely healed.

Table 6.1 Small animals orthopaedic cases involved in the study

No.	Species	Breed	sex	age	weight
1.	Canine	Eng. Pointer	M	1.3 years	n/a
2.	Canine	Border Collie	F	3.7 years	19 kg
3.	Canine	GSD	M	3 years	28 kg
4.	Canine	Doberman	F	1.1 years	25.5 kg
5.	Canine	Border Collie	M	3.3 years	18.5 kg
6.	Canine	Cross	M	1.2 years	31.0 kg
7.	Canine	JRT	M	3.1 years	11.1 kg
8.	Canine	Collie	M	7 months	12 kg
9.	Feline	Burmese	M	1.6 years	4.5 kg
10.	Canine	Border Collie	M	1.4 years	n/a
11.	Canine	Cross	F	1.2 years	15 kg
12.	Canine	Collie	FN	5.1 years	12.5 kg
13.	Canine	Mastiff Neopolitan	M	8 months	37 kg
14.	Canine	Cross	M	n/a	n/a
15.	Canine	Spaniel Cocker	M	8 years	22 kg
16.	Feline	DSH	MN	4 years	4.5 kg
17.	Canine	Border Collie	M	n/a	25 kg
18.	Feline	DSH	MN	17 months	4.0 kg
19.	Canine	Labrador	M	6 months	19 kg
20.	Canine	Akita	M	3 years	40 kg
21.	Feline	DSH	MN	1 year	n/a
22.	Canine	Labrador	M	1 year	33 kg
23.	Canine	Lakeland	M	10 years	7.34 kg

Table 6.2 Type of fracture and method of reduction used in the animals involved in the study.

Case number	Type of fracture	Method of reduction
1	Comminuted fracture of the mid shaft of the left femur	Bone plating + lag screws
2	Comminuted fracture of the midshaft of the right femur	Bone plating + lag screws
3	Comminuted and segmented fracture of the left femur	Bone plating + cerclage wires
4	Comminuted pelvis fracture	Bone plating
5	Comminuted fracture of proximal half of the right femoral shaft	Bone plating
6	Humerus fracture at distal half	IM pinning
7	Non-union of femoral fracture	Bone plating
8	Comminuted pelvis fracture	Bone plating
9	Comminuted fracture of the midshaft of left femur	IM pinning + cerclage wires + external fixation
10	Oblique fracture of distal humerus	Bone plating
11	Comminuted fracture of midshaft of the tibia and fibula	IM pinning + external fixation
12	Transverse fracture of the midshaft of the left humerus	IM pinning + bone plating
13	Y-shape fracture of distal humerus	Bone plating + cerclage wires + lag screws
14	Comminuted fracture of the right pelvis Femoral neck fracture	Bone plating Cancellous screws + K wires

Table 6.2 continued

Case number	Type of fracture	Method of reduction
15	Comminuted fracture of distal shaft of the left humerus	External fixation
16	Comminuted midshaft fracture of the right femur	IM pinning + external fixation
17	Comminuted fracture of left femur	IM pinning + external fixation
18	Humerus fracture	IM pinning + external fixation
19	Tibia/fibula fractures	IM pinning + external fixation
20	Comminuted humerus fracture	IM pinning + external fixation
21	Multiple pelvic fracture	Bone plating
22	Transverse fracture of the tibia/fibula	External fixation
23	Transverse mid-shaft fracture of the left humerus	IM pinning + external fixation

IM intramedullary pin

K wire Kirschner wire

Table 6.3 Breed incidence involved in the study.

A. Canine

Breed	frequency
Akita	1
Border Collie	4
Doberman	1
English Pointer	1
German Shepherd	1
Jack Russel Terrier	1
German Shepherd Dog	1
Labrador	2
Lakeland Terrier	1
Mastiff Neopolitan	1
Mongrel	3
Spaniel Cocker	1

B. Feline

Breed	Frequency
Burmese	1
Domestic Short Hair	3

Table 6.4 The frequency of bone fractures involved in this study

	canine	feline	total
Femur	7	2	9
Humerus	6	1	7
Pelvis	3	1	4
Tibia/fibula	3	-	3

6.3 Results

Case 1

A 16 month old male English Pointer was referred to the Glasgow University Veterinary School with a suspicion of sustaining a femoral fracture after a road traffic accident one week previously. Radiographs taken following physical examination demonstrated that a comminuted fracture of the mid-shaft of the left femur had been sustained with caudo-proximal displacement of the distal fragment (figure 6.1.1). Radiographs obtained immediately after fracture repair showed that the comminuted fracture was stabilised using a 12 holes bone plate with 11 screws (figure 6.1.2). One hole at the fracture site was left open. One lag screw was used in addition to the bone plate. One small bone fragment remained, being craniomedially displaced, while two smaller bone fragments adjacent to each other also remained, being caudally displaced. The fracture gap was clearly visible. There was a large haematoma which developed within the muscle at the fracture site caudal to the femur.

Ultrasonographic examination

Day one after fracture repair

On day one examination, a large haematoma was found within the muscle. It appeared hypoechoic with some hyperechoic material present at the base of the haematoma which may represent the connective tissue fascias (figure 5.1.3). The haematoma had developed after fracture repair. The ruptured blood vessel within the haematoma was identified and was pulsating during examination (figure 6.1.4). Suture materials within the muscle appeared hyperechoic and produced acoustic shadowing (figure 6.1.5). The fracture site imaged on ultrasound appeared as a discontinuity of the smooth bone surface on longitudinal scan from the cranial aspect (figure 6.1.6). There was a small gap present at the fracture site. The lag screw used in the bone reduction was imaged near the fracture site. There was no periosteal or soft tissue reaction detected at the fracture site. The fracture site was unable to be located ultrasonographically from caudal aspect because of a large haematoma. The two small bone fragments seen radiographically placed caudally in the muscle were identified and appeared as one small hyperechoic area with acoustic shadowing artefact (figure 6.1.7). The bone plate with screws appeared as an intermittent hyperechoic line with comet tail artefact (figure 6.1.8).

Day two after fracture repair

The fracture site with a piece of bone fragment was recognised on the day two examination when scanned on the caudal aspect (figure 6.1.9). The bone appeared highly hyperechoic which was likely due to the high gain setting. The large haematoma was still persisting but with some echogenic material present within (figure 6.1.10). There was no evidence of the pulsating blood vessel found on the day two examination. The two small bone fragments placed caudal to the femur appeared as two hyperechoic areas adjacent to each other with acoustic shadowing artefacts. They appeared smaller than on the day one examination (figure 6.1.11).

Day three after fracture repair

There was still no periosteal reaction to be seen at the fracture site on day three post-operation when imaged from the cranial aspect (figure 6.1.12). The ultarsonographic image appeared as in the previous examination. However, the image from the caudal aspect showed that the fracture site appeared to have some periosteal tissue reaction as shown by an hyperechoic area at the fracture site (figure 6.1.13). The haematoma had become more organised with the presence of an echogenic area (figure 6.1.14). The two small bone fragments evident on day two had became much smaller and appeared as two small hyperechoic dots placed adjacent to each other with acoustic shadowing artefact (figure 6.1.15). The hypoechoic areas surrounding the two small bone fragments indicated the process of bone lysis.

Three weeks after fracture repair

Radiographic examination

Radiographs obtained on day 21 (three weeks) after fracture repair revealed that the callus was forming at the distal end of the fracture site, particularly caudally where the proliferative appearance was suggestive of local periosteal elevation and was associated with local soft tissue swelling (figure 6.1.16). A small amount of poorly defined periosteal reaction was present proximo-cranially some distance from the fracture site. The fracture had apparently healed with minimal callus formation at the fracture site. The fracture line was visible. No evidence of implant loosening or instability was seen.

Ultrasonographic examination

On day 21 after fracture repair, ultrasonographic examination showed periosteal tissue reaction with some soft callus formation at the fracture site scanned from the cranio-medial aspect (figure 6.1.17). On the caudal aspect, periosteal and soft tissue reactions were seen at the fracture site as shown by the hyperechoic area (figure 6.1.18). An area of muscle over the fracture site had lost its normal ultrasonographic characteristics and appeared as a disorganised hyperechoic structure. The callus formation at the distal end of the femur was demonstrated as an uneven rough surface of the femur on both longitudinal and transverse scans (figure 6.1.19). The haematoma had not persisted.

Six weeks after fracture repair

Radiographic examination

Radiographs obtained on day 43 (six weeks) after fracture repair showed the callus was beginning to obliterate the fracture line and the areas of periosteal reaction seen on third week post-op had became well defined in appearance with the exception of a small area cranially which still had poorly defined margins (figure 6.1.20). The fracture line was still visible.

Ultrasonographic examination

On day 43 after fracture repair, ultrasonographic examination revealed that there was still no callus formation to be seen bridging the fracture site (figure 6.1.21a). However, the fracture gap appeared smaller than the previous examination and there were some echogenic materials present. The longitudinal scan from the cranial aspect demonstrated the fracture site in which it appeared that the distal fragment was more elevated than the proximal fragment (figure 6.1.21b). The callus formation was found some distance away at a position distal and proximal to the fracture site (figure 6.1.22). The soft callus formation was detected as woven echogenic material attached to the more mature callus (figure 6.1.23).

Seven weeks after fracture repair

Radiographic examination

Radiographs obtained on day 48 (seven weeks) after fracture repair demonstrated the fractured bone plate at the level of the empty screw hole and femoral fracture site, giving overriding of the fragments (figure 6.1.24). Radiographs obtained immediately after fracture re-alignment showed the replacement of the bone plate with a larger 11 holes plate and screws (figure 6.1.25). A large haematoma was present at the fracture site.

Ultrasonographic examination

On day 48 after fracture repair, ultrasonographic examination demonstrated an hyperechoic straight line protruding into the muscle cranially as shown in figure 6.1.26. The hyperechoic area at the end of the fragment indicated the periosteal and soft tissue reactions. This was in effect the broken plate which protruded into the muscle as shown by radiographs taken after ultrasound examination. The bone plate was imaged as discontinuity of the hyperechoic straight line with the distal portion overriding the proximal portion when scanned from the lateral aspect (figure 6.1.27). This indicate that the plate had broken off. A big gap was revealed when scanned from the medial aspect as a result of the broken plate (figure 6.1.28).

Day two after fracture re-alignment

Ultrasonographic examination on day two after fracture re-alignment showed an excessive callus formation at the distal end (figure 6.1.29). The fractured bone was well apposed and aligned so that the ultrasonographic examination failed to reveal the fracture site. It was also due to the excessive callus formation which made ultrasonographic examination of the fracture site difficult. A bone graft had been placed at the fracture site to enhance the fracture healing process. The holes on the bone surface were seen as notches indicating the site of the screws which had been in place before the plate had broken off (figure 6.1.30). An hyperechoic layer on the femoral surface (periosteum) was detected which indicated the soft tissue reaction. The presence of blood in the area of muscle damage was evidenced by the anechoic areas within the muscle.

Six weeks after fracture re-alignment

Radiographic examination

Radiographs taken at day 40 (six weeks) after fracture re-alignment showed the extensive periosteal reaction which was variable in thickness (figure 6.1.31). Callus formation was not visible at the fracture site.

Ultrasonographic examination

Ultrasonographic examination on day 40 after fracture re-alignment showed excessive callus formation (figure 6.1.32). The fracture site was more easily located on a longitudinal scan from the medial aspect (figure 6.1.33). It appeared as a large notch on the rough femoral surface with some hyperechoic materials on it. No fracture gap could be seen ultrasonographically as was seen on the radiograph. The femur had become larger than normal with an uneven surface on transverse scan and it had lost its normal appearance of a straight hyperechoic line on longitudinal scan (figure 6.1.34). The muscle was still lacking its normal ultrasonographic characteristic. The bone plate appeared as an hyperechoic straight line (figure 6.1.35).

Eleven weeks after fracture re-alignment

Radiographic examination

Radiographs taken at day 75 (11 weeks) after fracture re-alignment showed that the fracture line was still visible (figure 6.1.36). However, there was quite marked new bone deposition, but, little of this was near the fracture ends. The distal screw had fractured and the fifth screw looked as though it was coming loose.

Ultrasonographic examination

On day 75 after fracture re-alignment, ultrasonographic examination showed that the femoral surface appeared as an uneven rough surface (figure 6.1.37). The fracture site was detected and was completely bridged over by mature callus. Radiographically, the fracture gap was still visible. A transverse scan over the distal part still showed excessive callus formation on the femur.

138 days after fracture re-alignment

Radiographic examination

Radiographs obtained at day 138 after fracture re-alignment showed a satisfactory healing process where the callus had bridged the fracture gap (figure 6.1.38). However, the fracture gap was still visible but the size was reduced. The screws were in place.

Ultrasonographic examination

On day 138 after fracture re-alignment, ultrasonographic examination showed that the femoral surface had become less irregular than previous scans (figure 6.1.39). The fracture site could still be recognised as shown by a small notch. The femoral surface appeared nearly smooth. The muscle structure had returned to its normal ultrasonographic characteristic. The fracture site was satisfactorily healed and the remodelling process was continuing at this stage.

Figure 6.1.1 A 16 months old English Pointer was hit by a car. There is a comminuted fracture involving the mid-shaft of the left femur with caudo-proximal displacement of the distal fragment.

Figure 6.1.2 Radiographs obtained immediately after fracture repair, **a**, cranial view, and **b**. lateral view, show that the comminuted fracture has been repaired using one lag screw in addition to a bone plate and 11 screws. One small fragment remains cranio-medially displaced. There is a small gap at the fracture site.

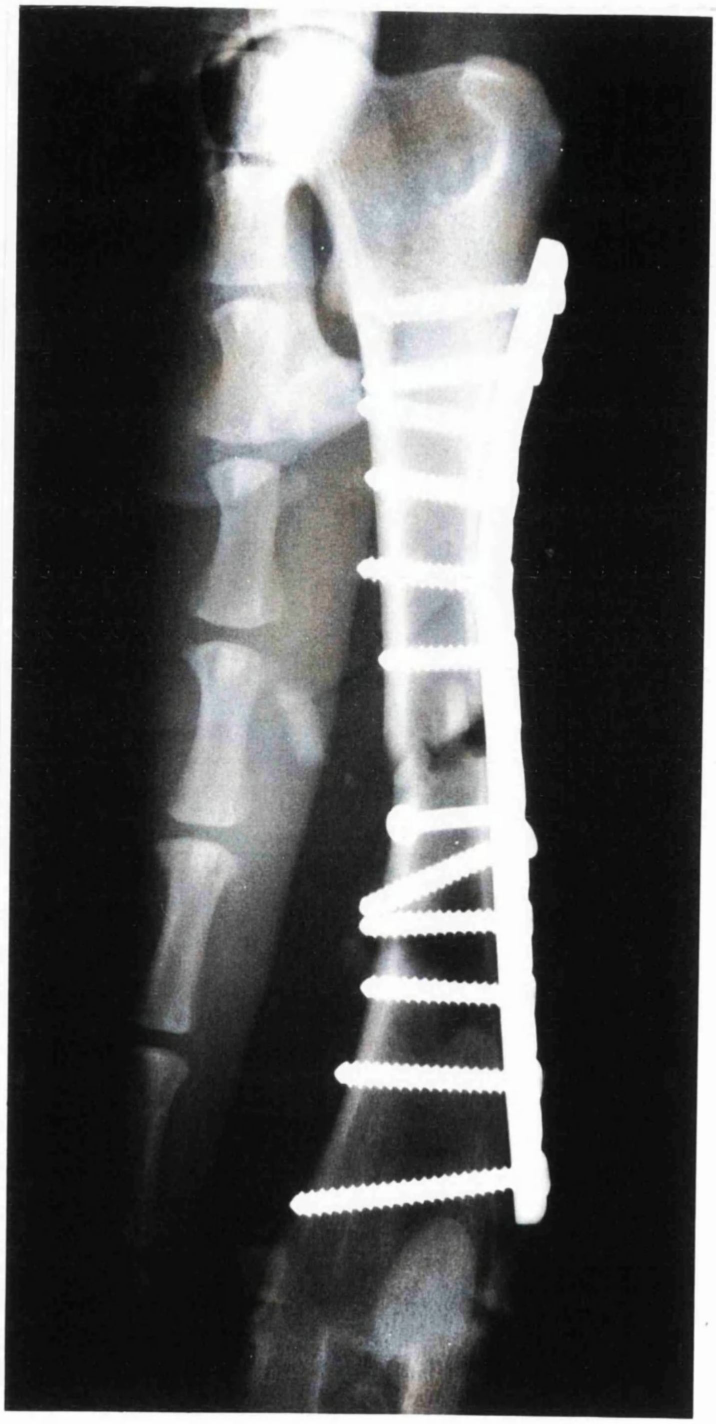

a

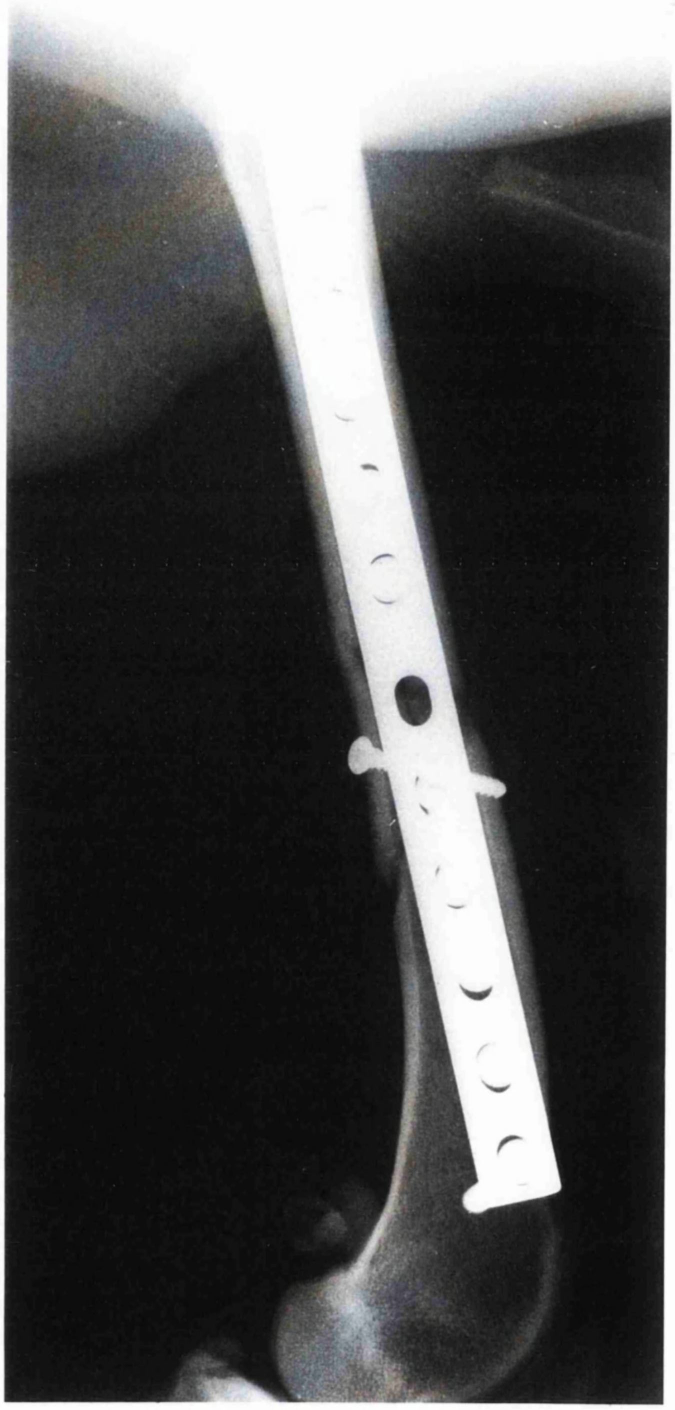

b

Figure 6.1.3 A large haematoma within the muscle caudal to the femur imaged 24 hours after surgery. Ultrasonographic examination revealed a large hypoechoic area with some hyperechoic dots present at the base of the haematoma which may represent the connective tissue fascias.

Figure 6.1.4 The ruptured blood vessel (arrow) can be seen within the large haematoma imaged 24 hours after surgery and was pulsating during scaning. **F**, femur

Figure 6.1.3

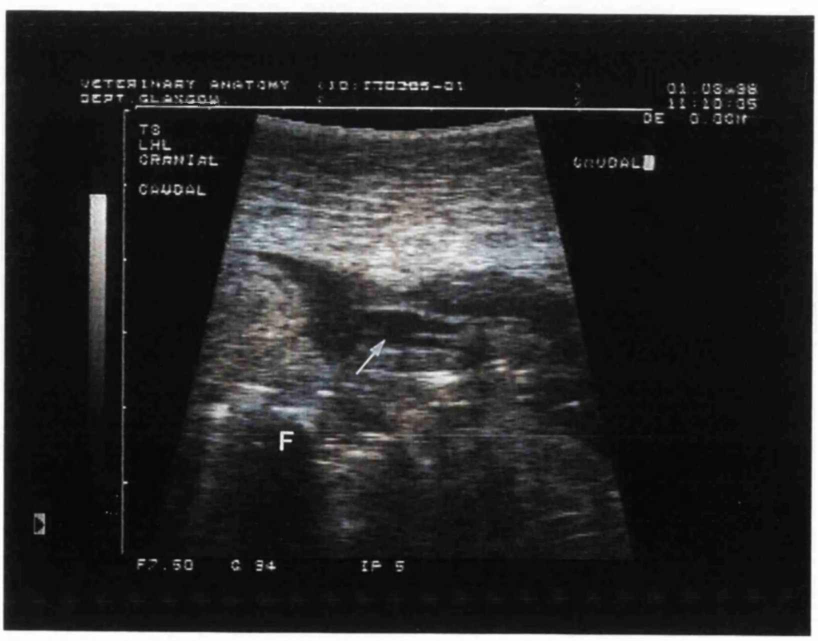

Figure 6.1.4

Figure 6.1.5 Suture materials within the muscle near the skin surface scanned on day one after surgery appear as thin hyperechoic lines (arrow heads) and produce acoustic shadowing artefacts. Note also the hyperechoic bone plate attached to the femur (arrow). **F**, femur

Figure 6.1.6 Longitudinal scan from the cranial aspect of the femur 24 hours after surgery demonstrates the fracture site which appears as discontinuity of the smooth bone surface (arrow). A small gap is present at the fracture site. The screw is also imaged some distance away from the fracture site (arrow head).

Figure 6.1.5

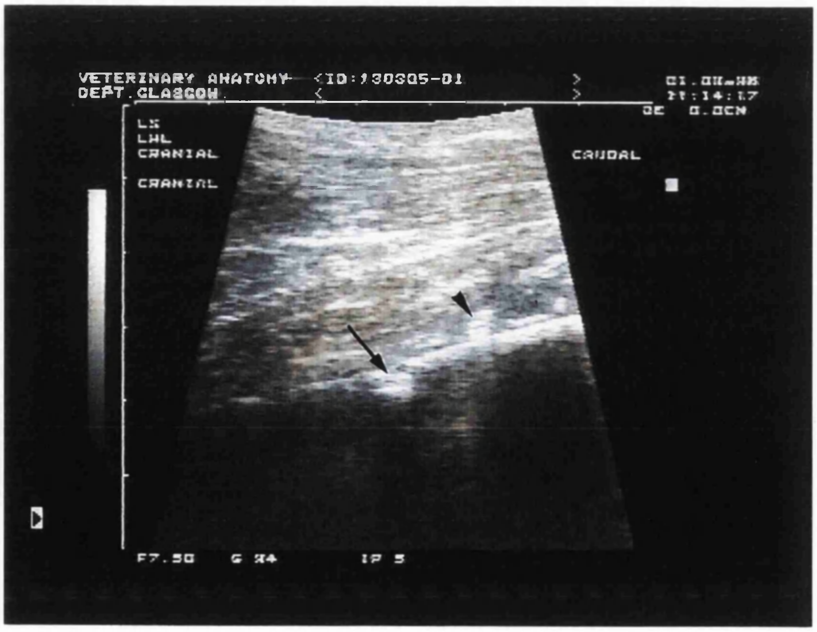

Figure 6.1.6

Figure 6.1.7 The small bone fragment within the muscle placed caudal to the femur (arrow head) imaged 24 hours after surgery appears hyperechoic and is producing acoustic shadowing artefact. **F**, femur

Figure 6.1.8 Longitudinal scan from the caudal aspect of the femur 24 hours after surgery demonstrates the intermittent hyperechoic line which represents the screws used in the bone fracture reduction.

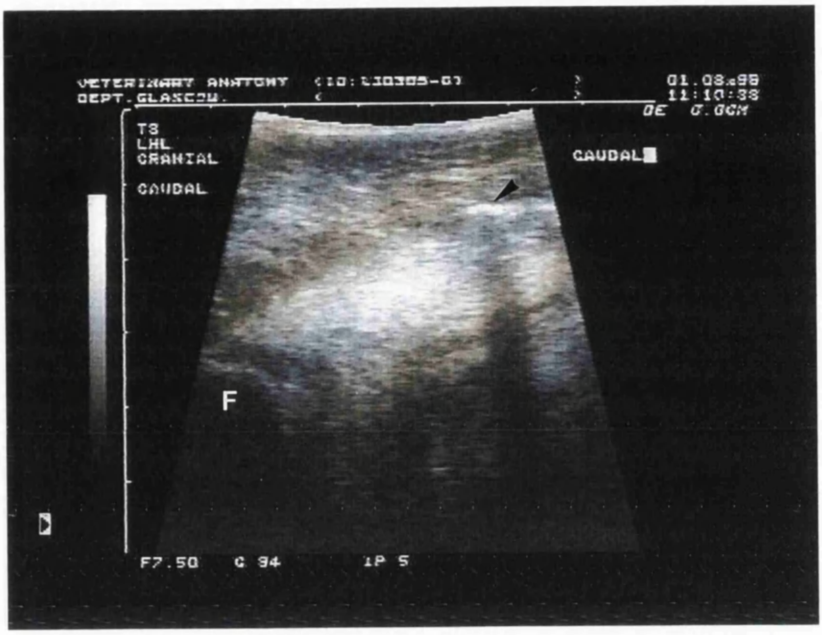

Figure 6.1.7

Figure 6.1.8

Figure 6.1.9 Longitudinal scan from the caudal aspect of the femur 48 hours after surgery demonstrates the fracture site which appears hyperechoic. The overall hyperechoic appearance of the femoral surface is likely due to the high gain setting. Note also the bone fragment, attached to the main bone, can be recognised (arrow heads).

Figure 6.1.10 The large haematoma within the muscle scanned on day two post-operation appears as a disorganised hypoechoic area with the presence of echogenic material within the haematoma area.

Figure 6.1.9

Figure 6.1.10

Figure 6.1.11 Transverse scan from the caudal aspect of the femur 48 hours post-operation demonstrates the two small bone fragments placed caudal to the femur (arrow heads). Note that the two small bone fragments appear hyperechoic with acoustic shadowing artefacts. They also appear smaller than on the day one examination. **F**, femur

Figure 6.1.12 Longitudinal scan from the cranial aspect of the femur on day three post-operation demonstrates the fracture site (arrow) which still has no periosteal reaction detected.

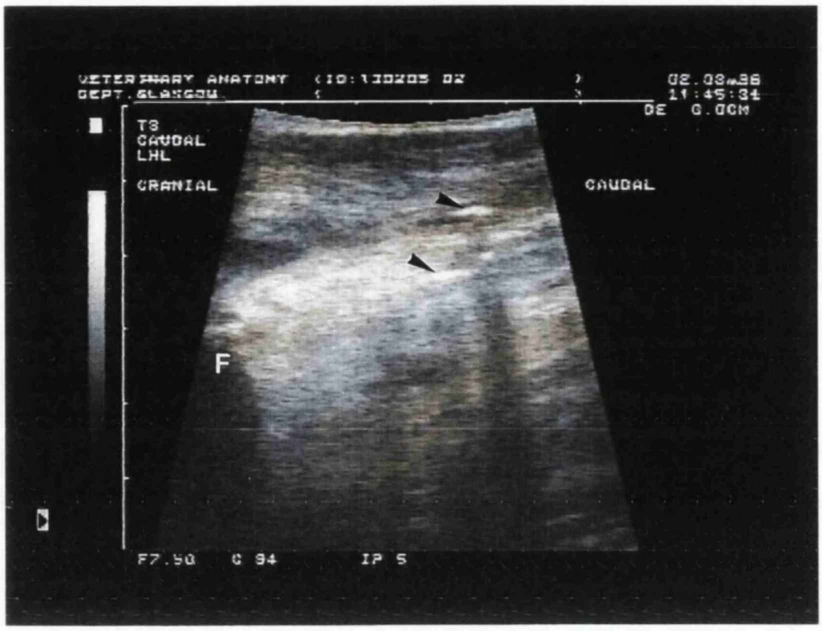

Figure 6.1.11

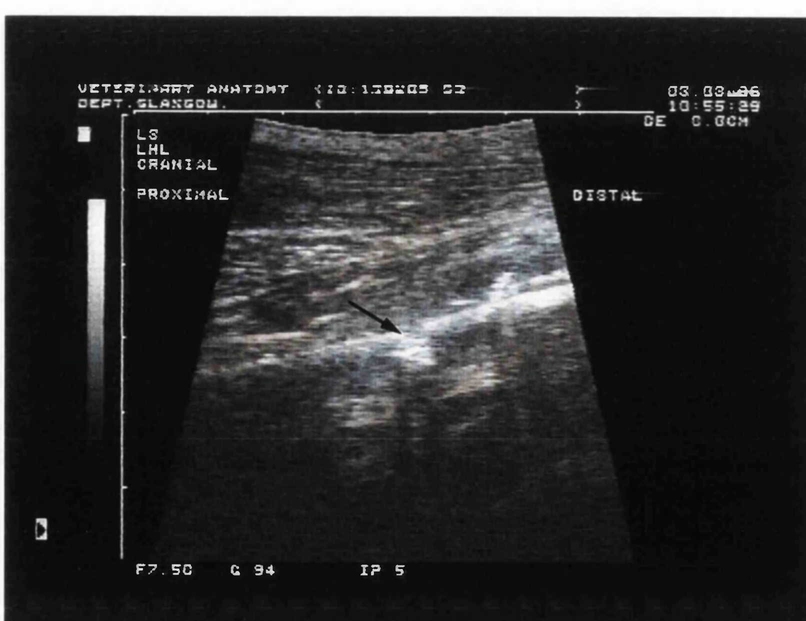

Figure 6.1.12

Figure 6.1.13 Longitudinal scan from the caudal aspect of the femur on day three post-operation demonstrates the fracture site which appears to have some periosteal reaction as shown by the hyperechoic appearance (arrow). Note also the area of muscle damage above the femur that appears disorganised and has lost its normal ultrasonographic characteristics.

Figure 6.1.14 Ultrasonographic image of the haematoma within the muscle on day three post-operation. Note the haematoma has become more organised with the presence of more echogenic areas.

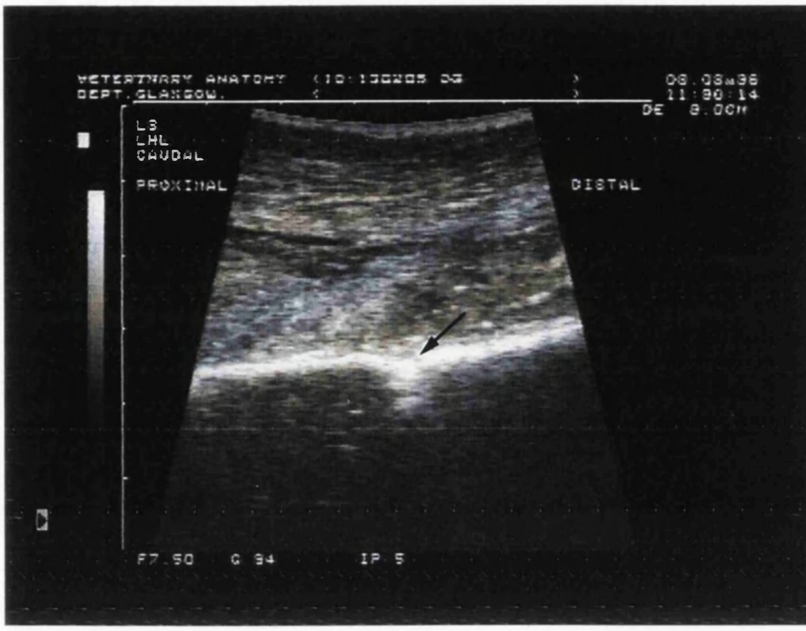

Figure 6.1.13

Figure 6.1.14

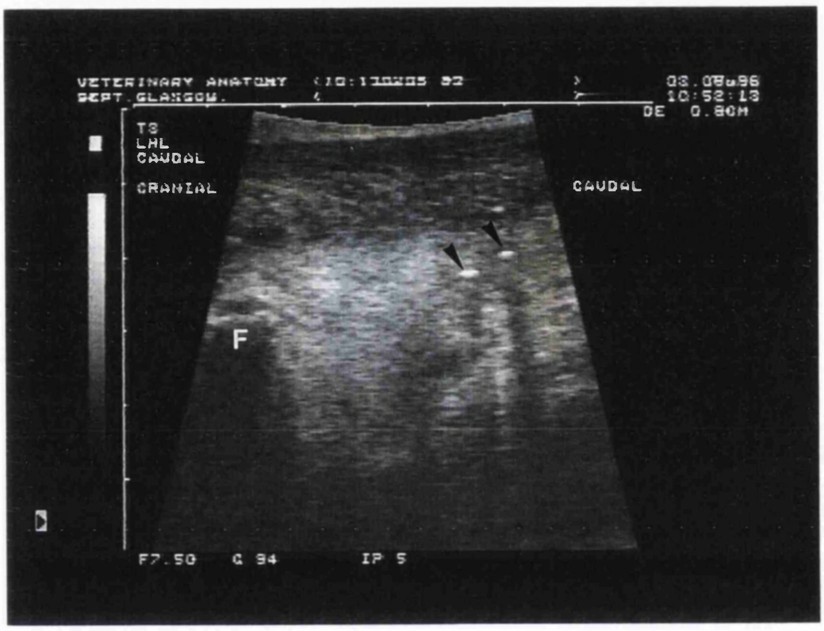

Figure 6.1.15 Ultrasonographic image from the caudal aspect of the femur on day three post-operation demonstrates the two small bone fragments (arrow heads) which appear as hyperechoic dots with acoustic shadowing artefacts. They appear smaller than on the day two examination. Note also the hypoechoic area surrounding the two small bone fragments which indicate the lysis process. **F**, femur

Figure 6.1.16 Radiographs obtained at day 21 (three weeks) after fracture repair, **a**, cranial view, **b**, lateral view. The fracture has apparently healed with minimal callus formation at the fracture site. Callus is forming mostly at the distal end of the fracture site, particularly caudally where the proliferative appearance is suggestive of local periosteal reaction associated with local soft tissue swelling. A small amount of poorly defined periosteal reaction is present proximo-cranially some distance away from the fracture site. No evidence of implant loosening or instability is seen.

a

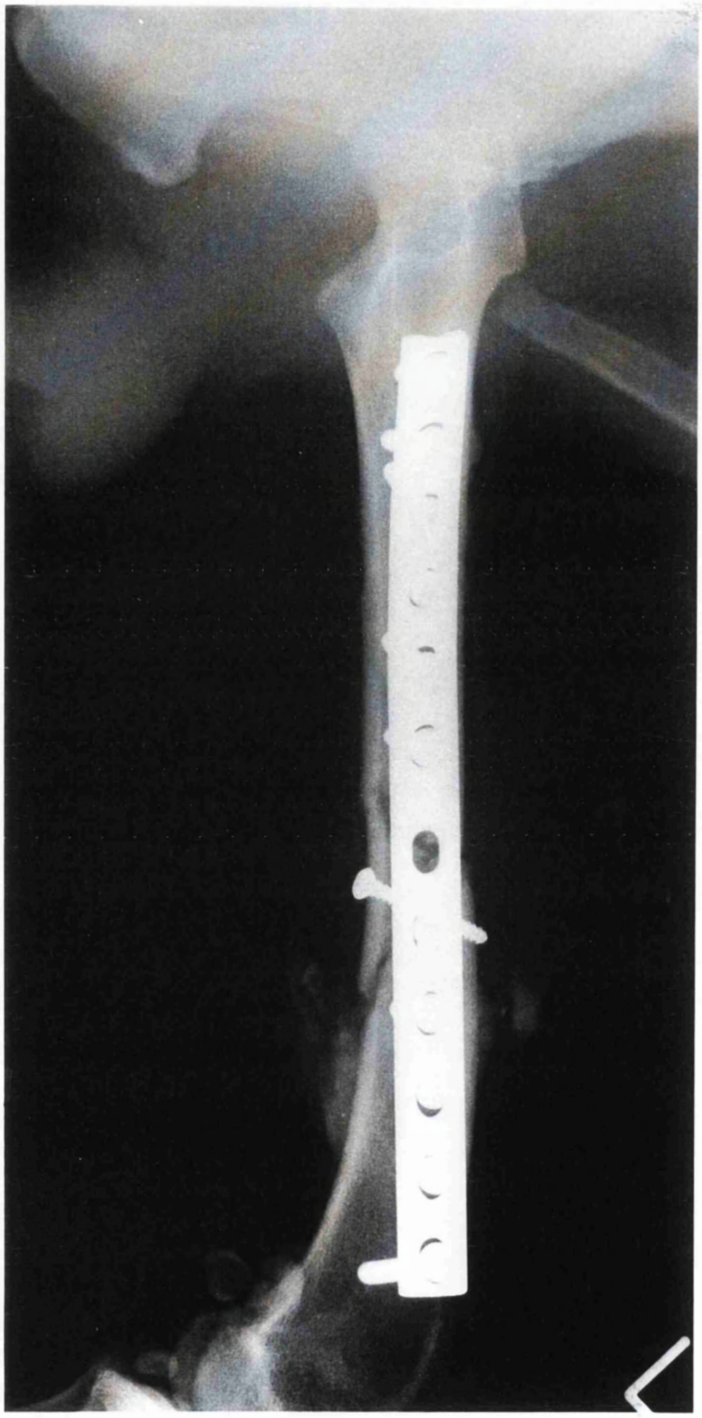

b

Figure 6.1.17 Longitudinal scan from the cranio-medial aspect of the femur on day 21 post-operation demonstrates the fracture site with some periosteal reaction. Soft callus formation is detected on both sides of the fracture site (arrow heads) and gives a characteristic hyperechoic appearance.

Figure 6.1.18 Longitudinal scan from the caudal aspect of the femur on day 21 post-operation shows the hyperechoic area at the fracture site which indicate the periosteal and soft tissue reactions. Note also the muscle damage above the femur appearing as a disorganised hypoechoic area.

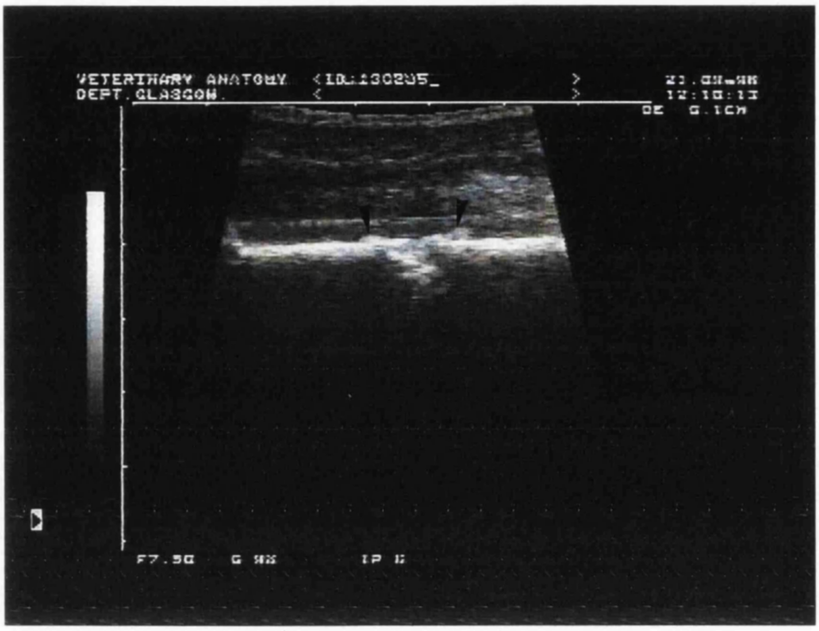

Figure 6.1.17

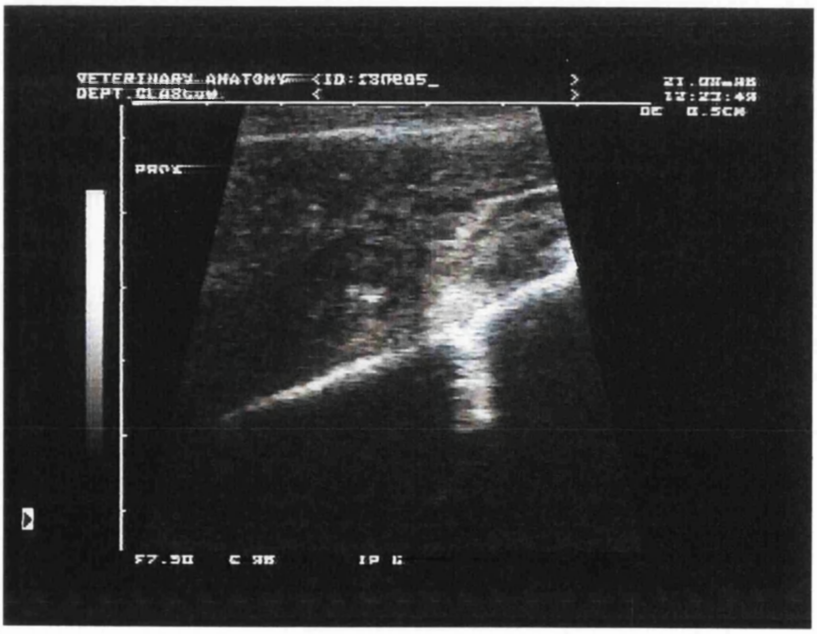

Figure 6.1.18

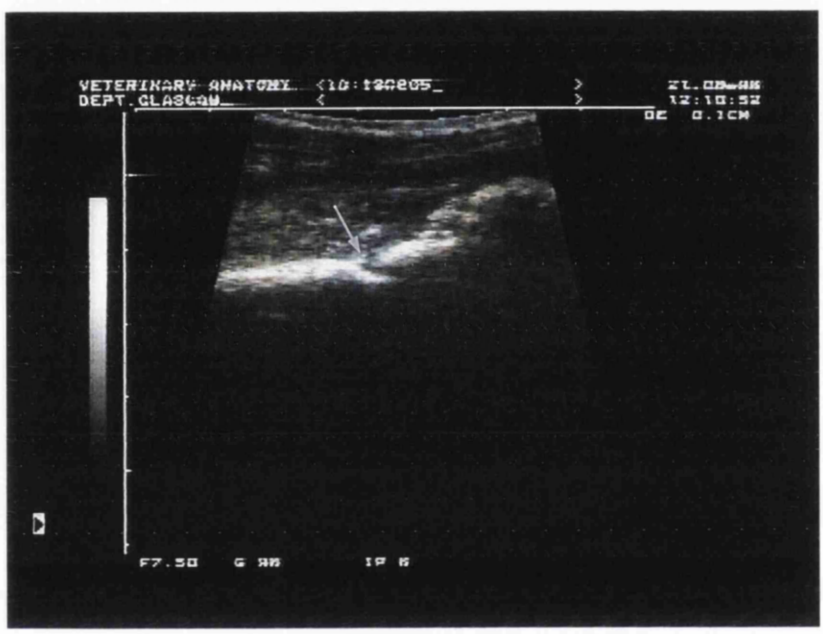

Figure 6.1.19 Longitudinal scan from the caudal aspect of the femur on day 21 after fracture repair demonstrates the callus formation which appears as bulging hyperechoic material. Note also the fracture site can be seen as a notch on the femoral surface (arrow).

Figure 6.1.20 Radiographs obtained at day 43 (six weeks) after fracture repair, **a**, cranial view, **b**, lateral view. Callus is beginning to obliterate the fracture lines and the areas of periosteal reaction seen on the third week have became well defined in appearance with the exception of a small area craniodistally which still has poorly defined margins.

b

Figure 6.1.21 Longitudinal scan of the femur on day 43 post-operation. A small gap could still be seen at the fracture site on caudal aspect image (**a**). However, some echogenic material can be detected within the fracture gap. The distal fragment appeared slightly more elevated than the proximal fragment on cranial aspect scan (**b**).

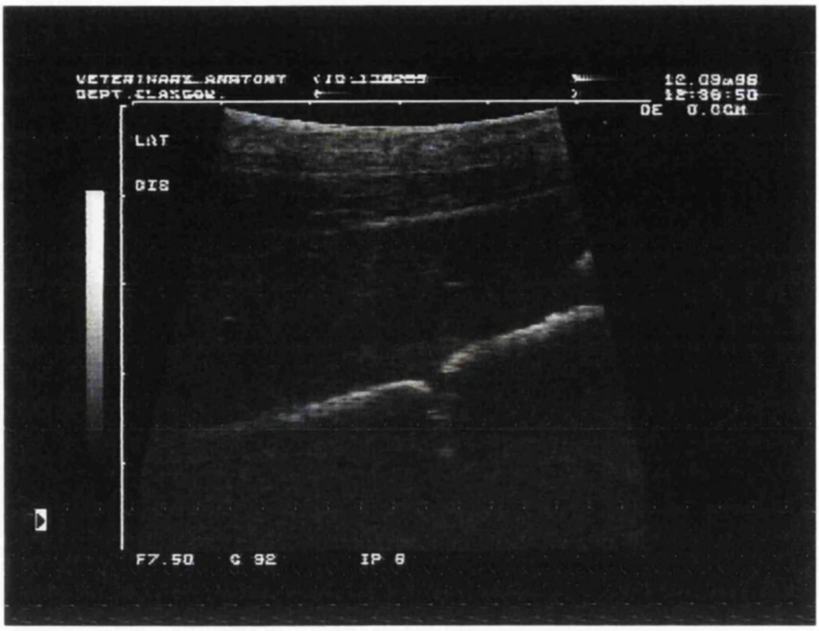

Figure 6.1.21a

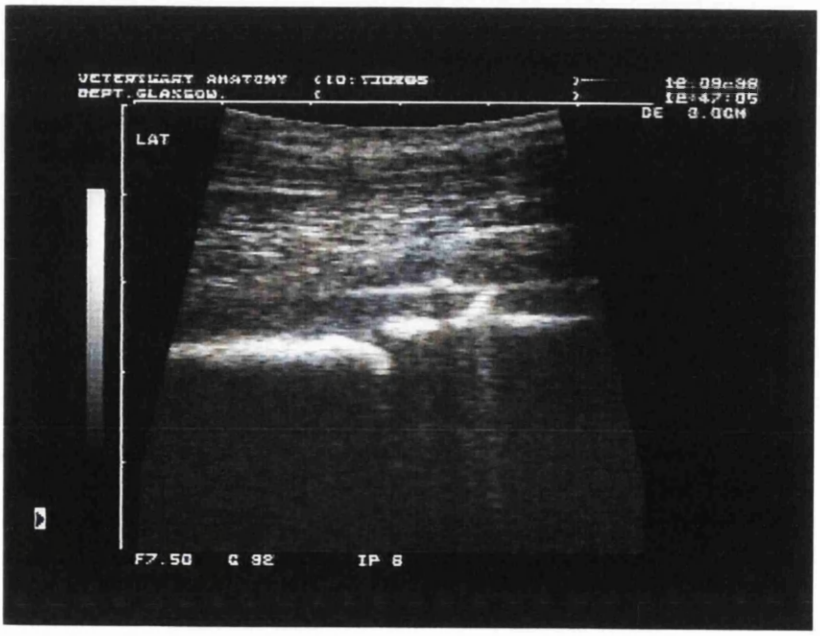

Figure 6.1.21b

Figure 6.1.22 Longitudinal scan from the caudal aspect of the femur on day 43 post-operation demonstrates the hyperechoic appearance of the callus formation. **a**, proximal and **b**, distal portions. Note also that the mature callus has formed some distance away from the fracture site on both sides.

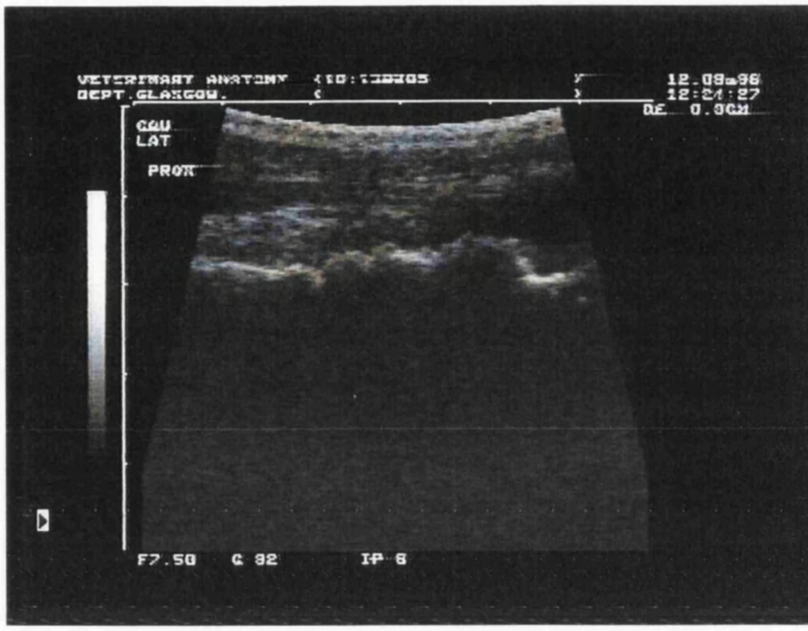

Figure 6.1.22a

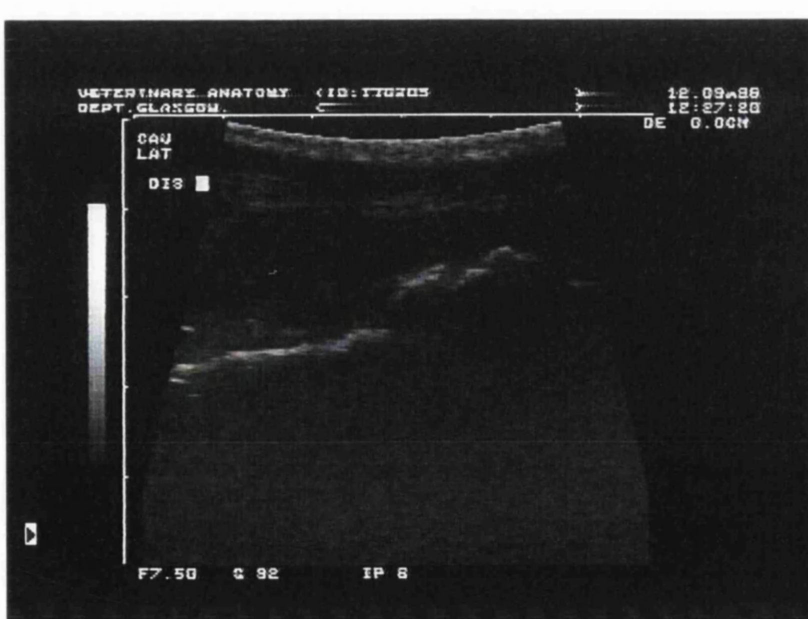

Figure 6.1.22b

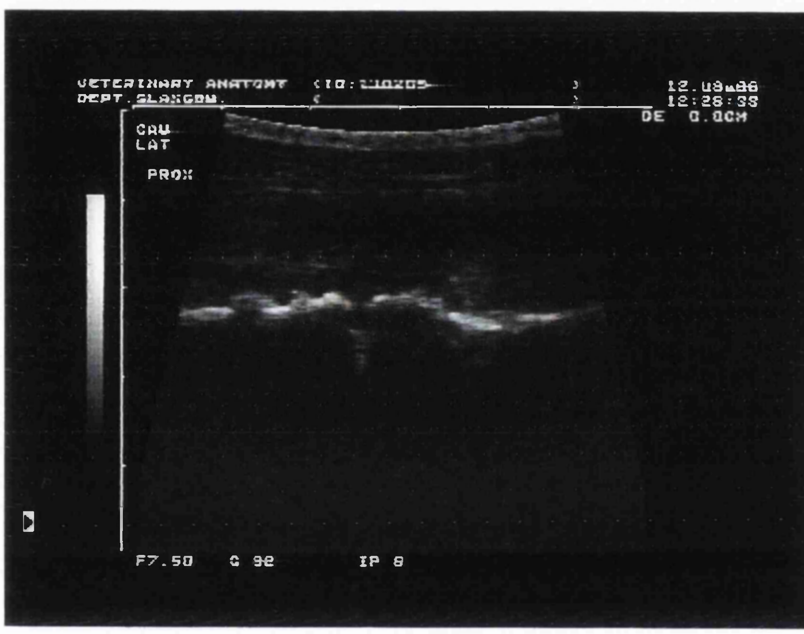

Figure 6.1.23 Longitudinal scan from the caudal aspect of the femur on day 43 post-operation. Note there was soft callus formation present at the fracture site which appears as a woven hyperechoic material adhered to the femoral surface. Fracture gap is still visible.

Figure 6.1.24 Radiographs obtained at day 48 (seven weeks) after fracture repair, **a**, cranial view, **b**, lateral view,. The bone plate has fractured at the level of the empty screw hole and fracture site, giving overriding of the fragments.

a

b

Figure 6.1.25 Radiographs obtained immediately after fracture re-alignment, **a**, cranial view, **b**, lateral view show the repair has been performed with a larger 11 holes plate and 11 screws. The repair results in good reduction. A large haematoma is present at the fracture site.

a

b

Figure 6.1.26 Longitudinal scan from the cranial aspect of the femur on day 48 post-operation demonstrates the proximal fragment with the plate attached to it protruding into the muscle cranially. The hyperechoic area at the end of the fragment (arrow) indicates the periosteal and soft tissue reactions.

Figure 6.1.27 Longitudinal scan from the lateral aspect of the femur on day 48 post-operation demonstrates the discontinuity of the hyperechoic straight line with the distal portion (arrow head) appearing to override the proximal portion (arrow).

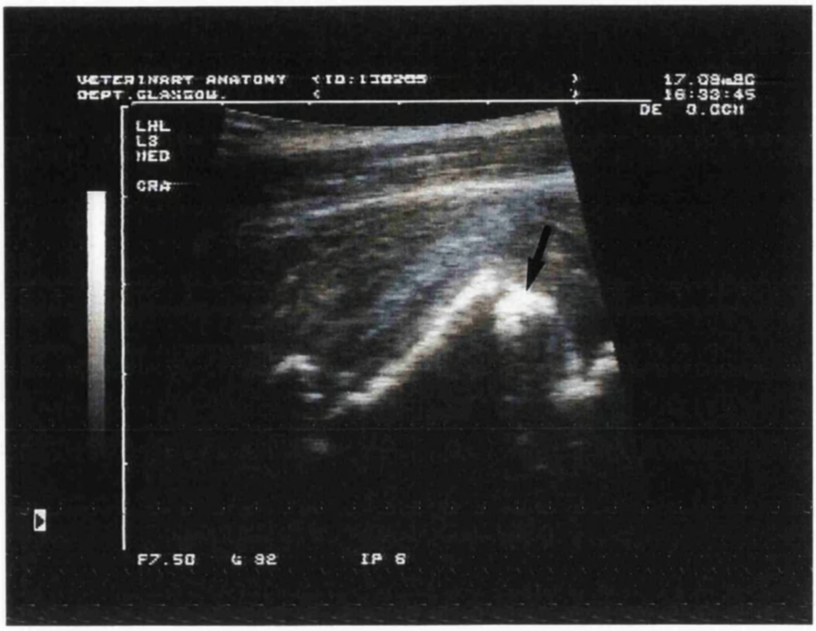

Figure 6.1.26

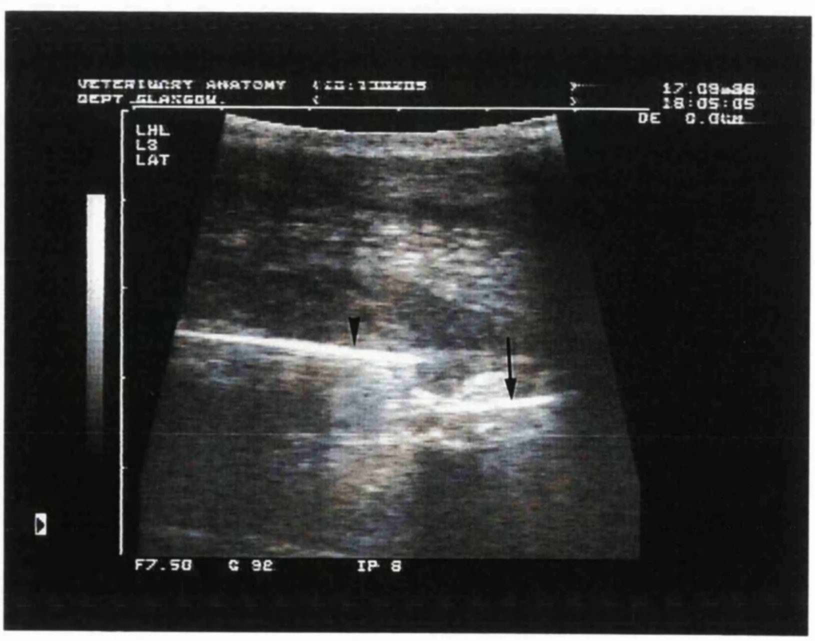

Figure 6.1.27

Figure 6.1.28 Longitudinal scan from the medial aspect of the femur on day 48 post-operation reveals the large gap in between the two fragments. There is massive callus formation at the end of both fragments.

Figure 6.1.29 Longitudinal scan from the lateral aspect of the femur on day two after fracture re-alignment demonstrates the excessive callus formation at distal part of the femur. Note also the area of soft tissue reaction and the area of muscle damage which appears hyperechoic and disorganised hypoechoic respectively.

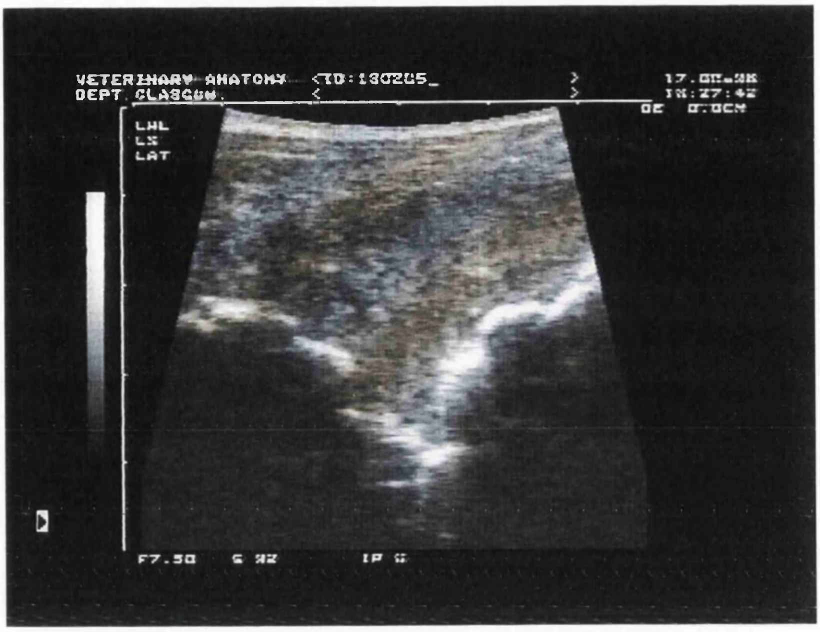

Figure 6.1.28

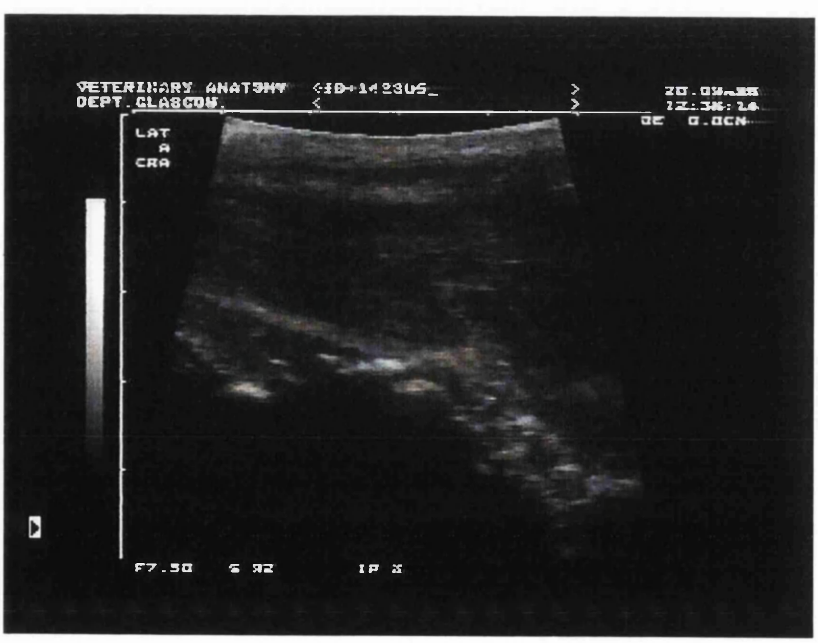

Figure 6.1.29

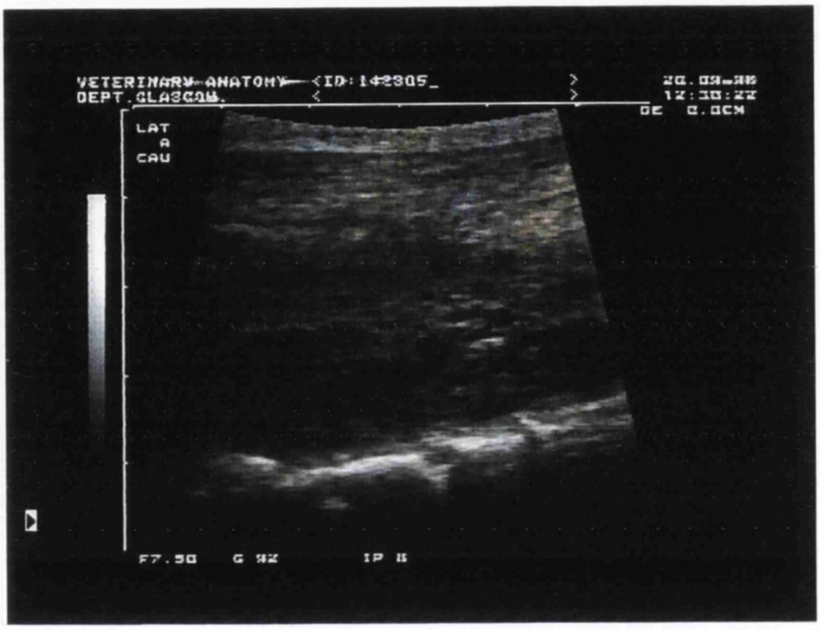

Figure 6.1.30 Longitudinal scan from the caudo-lateral aspect of the femur on day two after fracture re-alignment demonstrates the femoral surface with a few notches indicating the site of the screws which had been placed before the plate had broken off. Note also the area of muscle tissue damage above the femur appearing as disorganised hypoechoic areas. A hyperechoic layer on the femoral surface (periosteum) can be seen which indicates the soft tissue reaction.

Figure 6.1.31 Radiographs obtained at day 40 (six weeks) after fracture re-alignment, **a**, cranial view, **b**, lateral view. The implant is intact, but is associated with subtle areas of lucency around the screws. The periosteal reaction is so extensive and variable in thickness that this could be artificial. Bony callus is not visible at the fracture site.

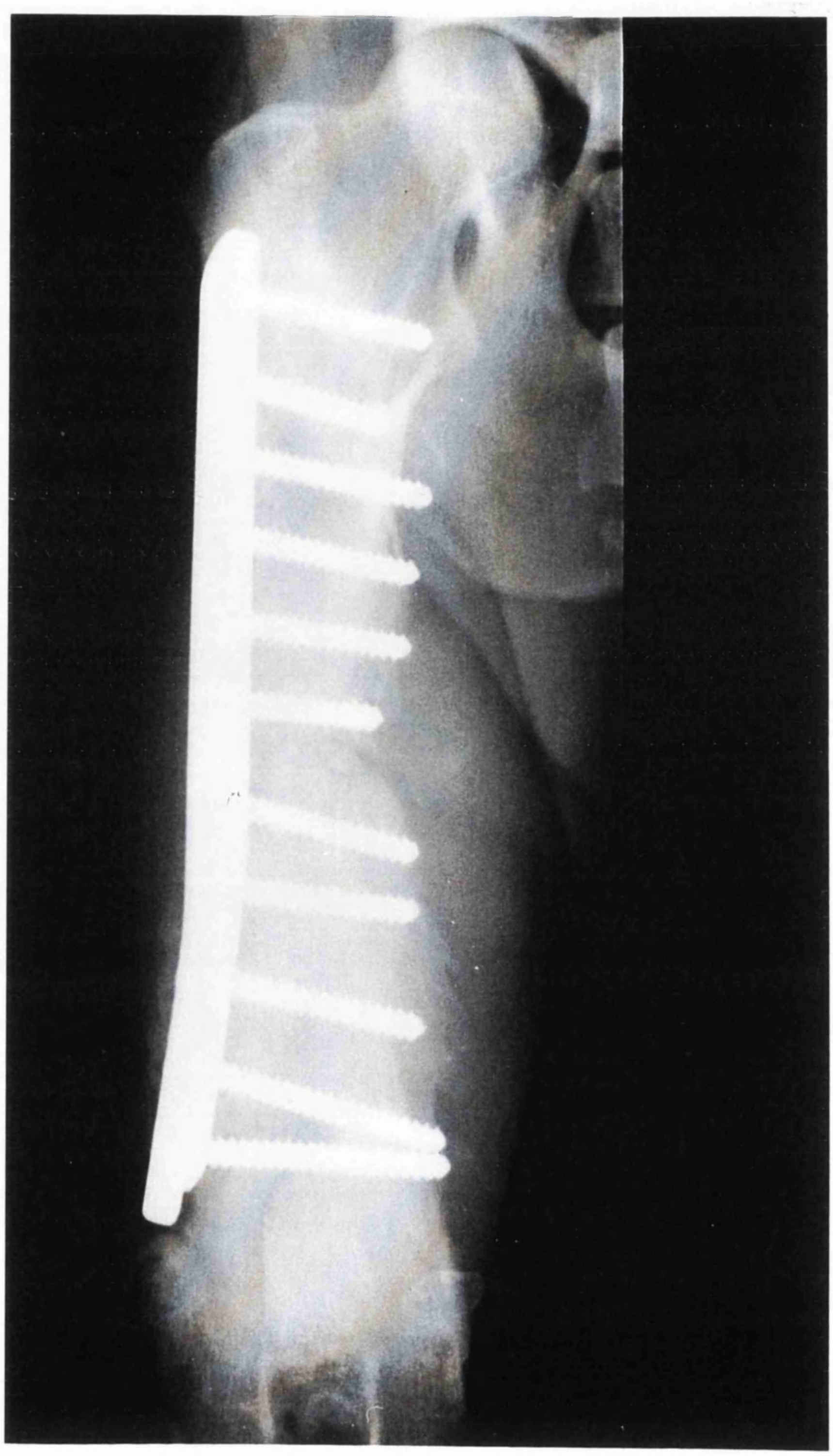

a

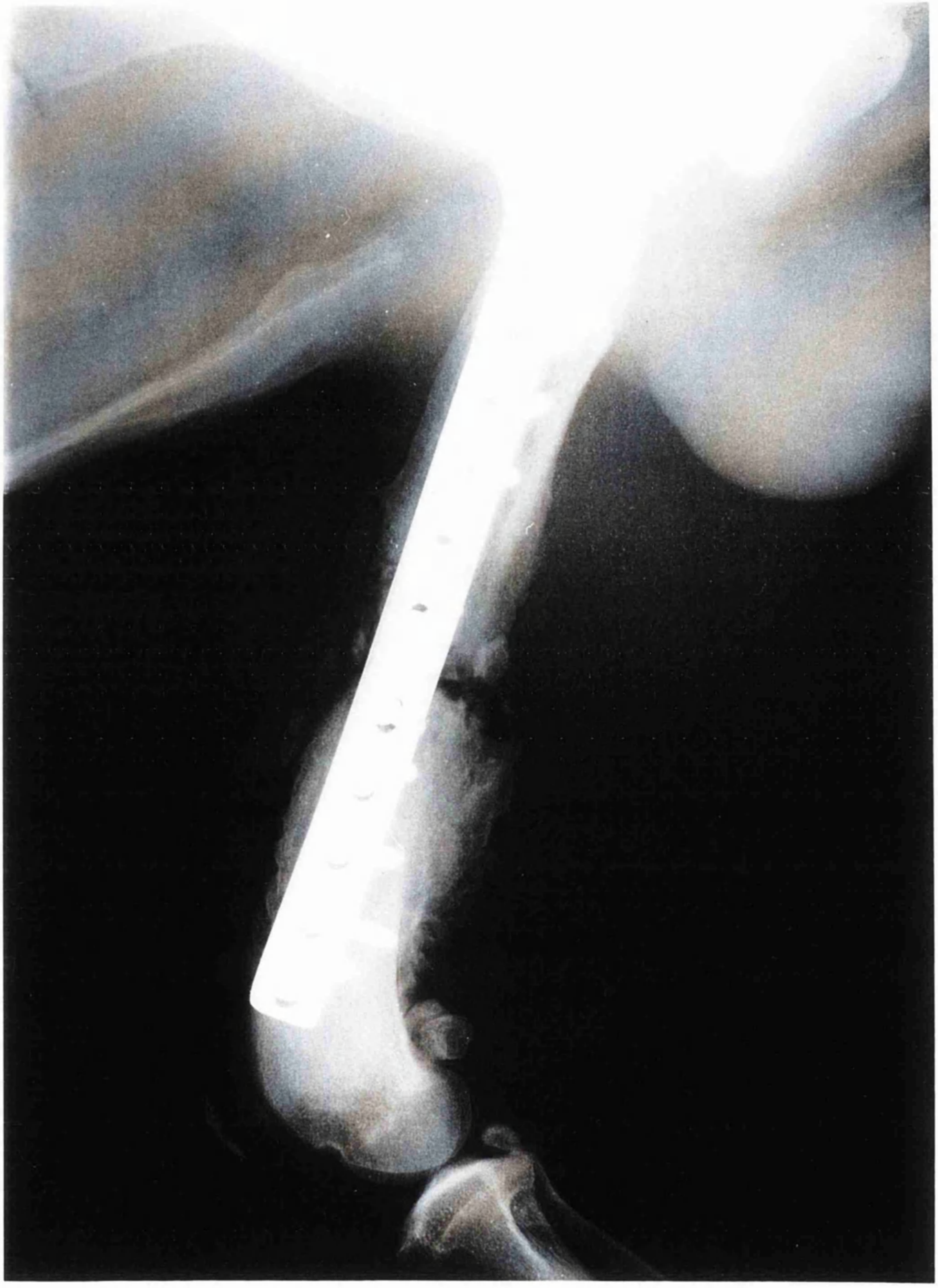

b

Figure 6.1.32 Longitudinal scan from the caudo-lateral aspect of the femur on day 40 after fracture re-alignment demonstrates the excessive callus formation which appears hyperechoic so that nothing could be seen distally.

Figure 6.1.33 Longitudinal scan from the medial aspect of the femur on day 40 after fracture re-alignment demonstrates the fracture site (arrow) which has already been bridged by mature callus. Note also there are some hyperechoic materials present at the fracture site.

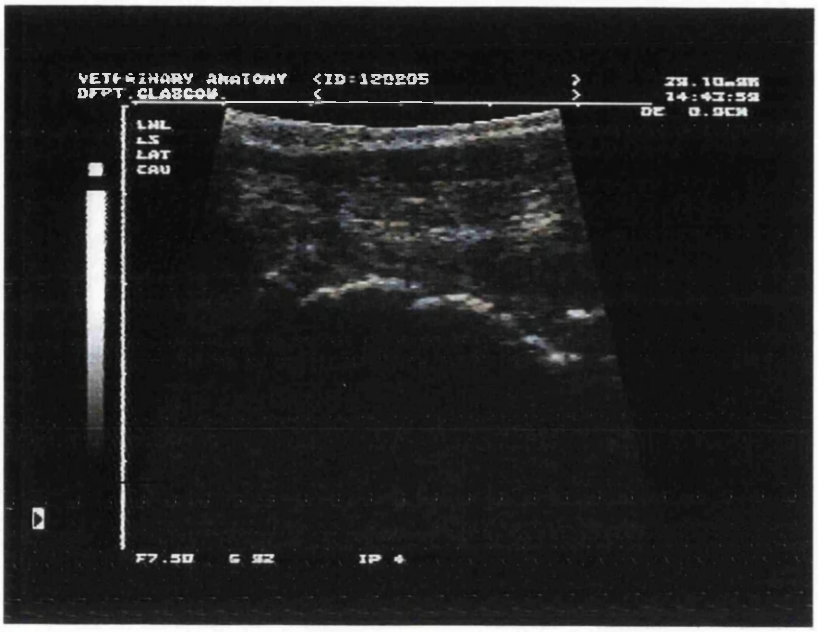

Figure 6.1.32

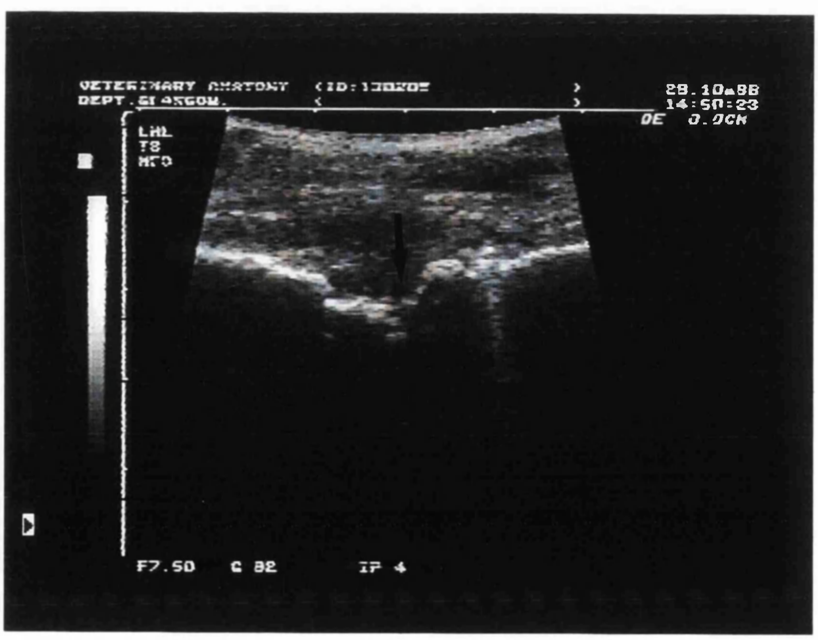

Figure 6.1.33

Figure 6.1.34 Longitudinal and transverse scans from the lateral aspect of the femur on day 40 after fracture re-alignment demonstrates the excessive callus formation. Note that the diameter of the femur appears enlarged on transverse scan (**a**), and the uneven femoral surface on longitudinal scan (**b**). Area of muscle damage appears as a disorganised hypoechoic pattern. **F**, femur.

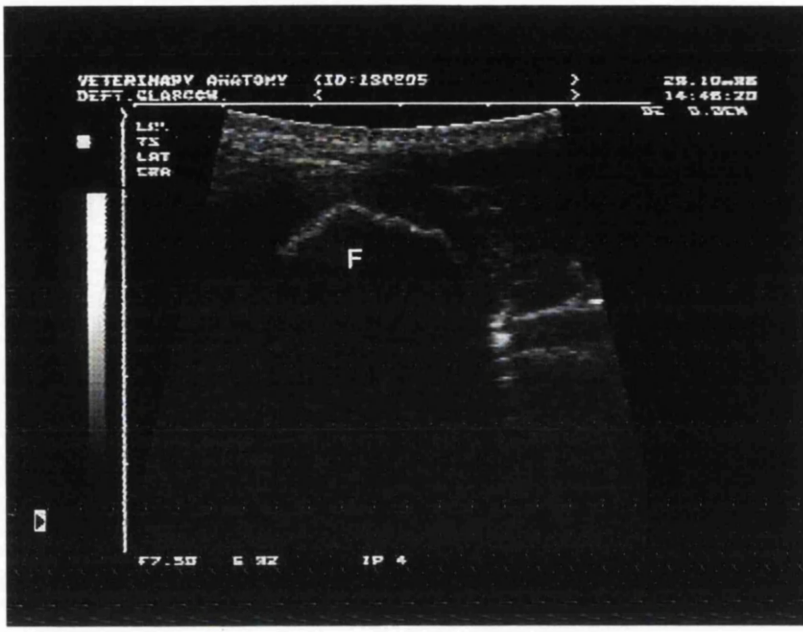

Figure 6.1.34a

Figure 6.1.34b

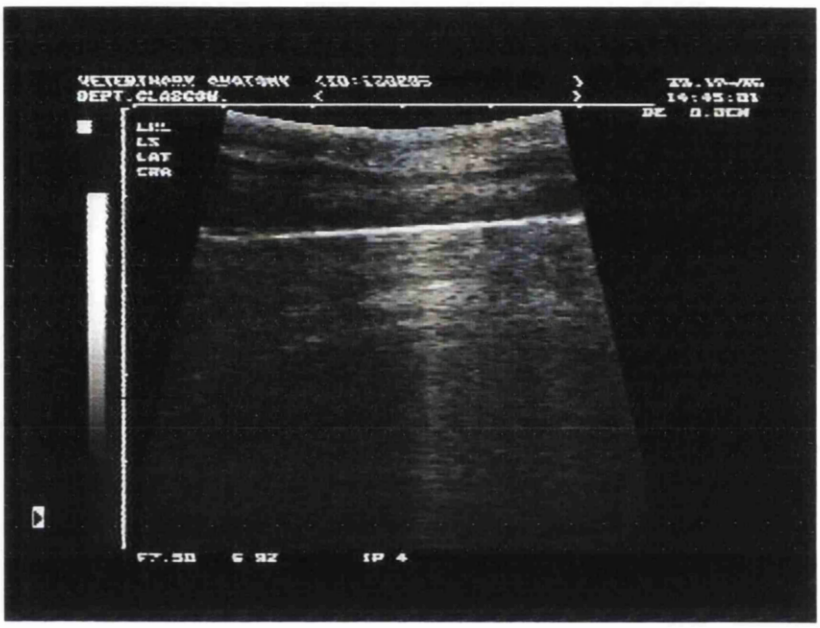

Figure 6.1.35 Longitudinal scan from the lateral aspect of the femur on day 40 after fracture re-alignment. Note that the bone plate adhered to the femur appears as a straight hyperechoic line.

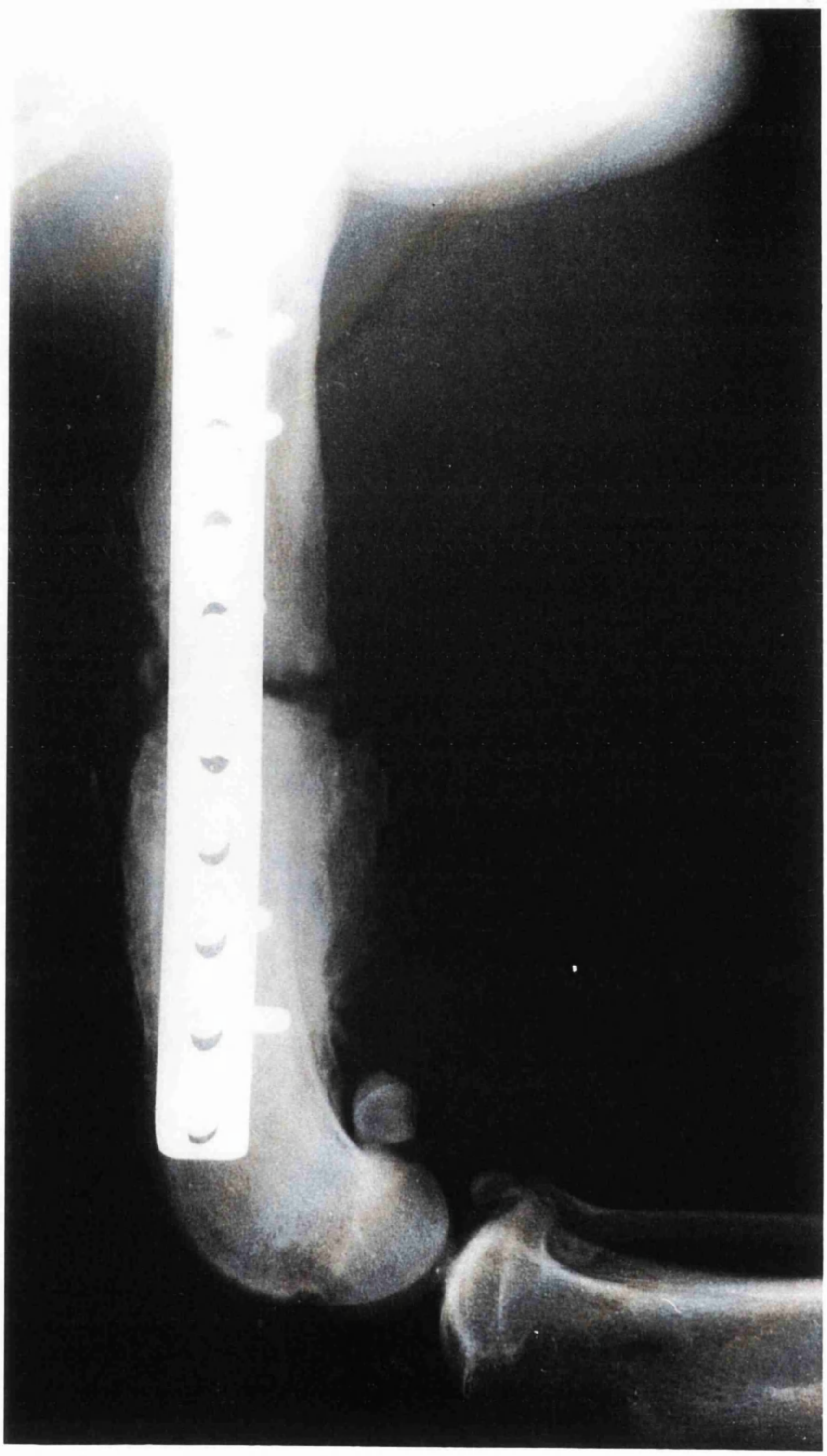

b

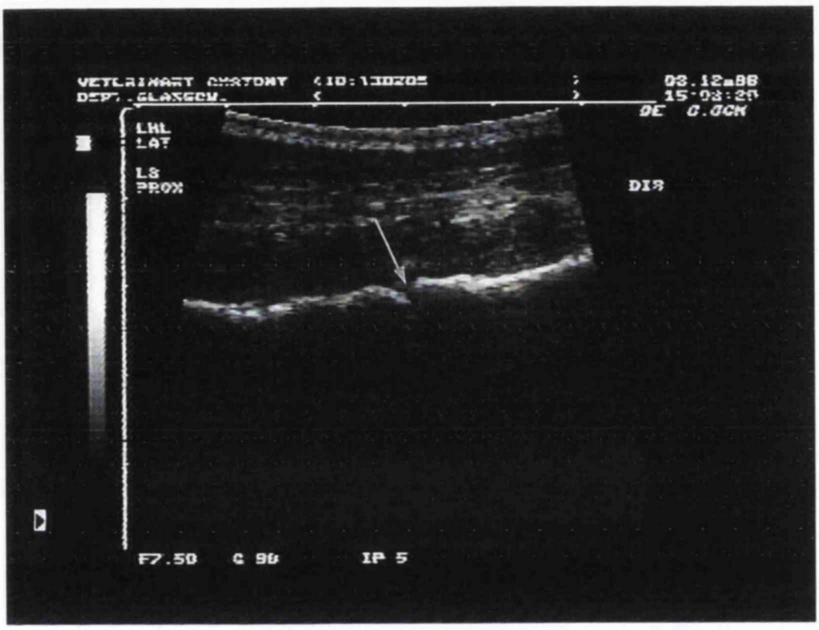

Figure 6.1.37 Longitudinal scan from the lateral aspect of the femur on day 75 after fracture re-alignment shows the uneven continuous femoral surface. The fracture site is recognised as a notch on the femoral surface (arrow) and has already been bridged over by mature callus. No gap can be seen. The area of muscle damage can still be seen near the femoral surface as the disorganised hypoechoic structures. The remodelling process is taking place at this stage.

Figure 6.1.38 Radiographs obtained at day 138 after fracture re-alignment show a satisfactory healing process where the callus has bridged the fracture gap. **a**, cranial view, **b**, lateral view. However, the fracture gap is still visible but the size is reduced. The screws are in place.

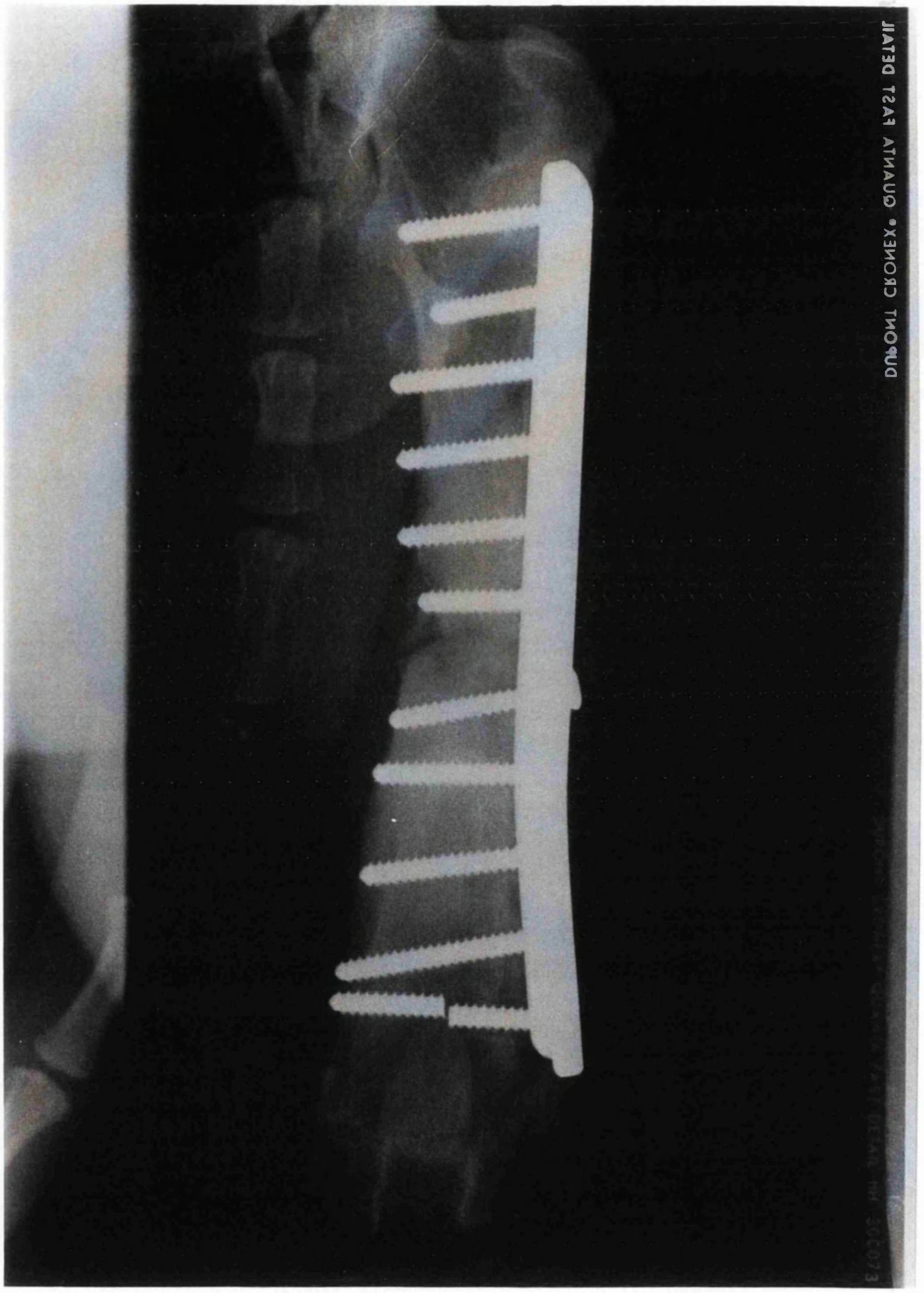

a

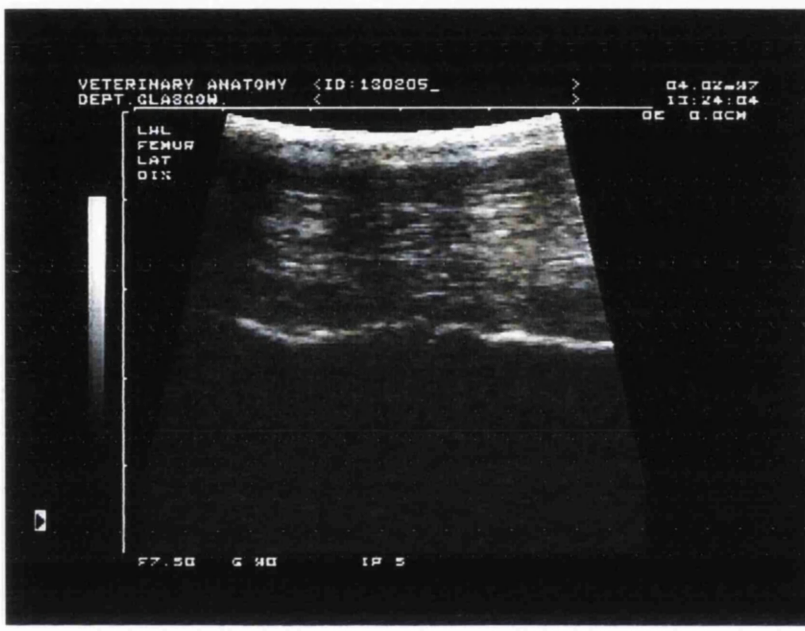

Figure 6.1.39 Longitudinal scan from the lateral aspect of the femur on day 138 post-operation demonstrates the femoral surface which has become much smoother. The fracture site can still be recognised as a small notch (arrow). Note that the muscle structure has returned to its normal ultrasonographic characteristic. The shadowing artefacts within muscle are due to the hair on the skin surface.

Case 2

A 3.7 year old female Border collie, weight 20 kg, with a suspicion of having femoral fracture was referred to the Glasgow University Veterinary Hospital. The dog had been involved in a road traffic accident and had been taken to the clinic immediately after the accident. The dog had been struck from behind on the right side and was unconscious for a while after the accident. Upon physical examination the dog was pale and tachycardiac and had no pedal withdrawal on the right limb and was in extreme pain. Radiographs taken following physical examination demonstrated a complete closed fracture of the mid-shaft of the right femur (figure 6.2.1). There was a comminuted fracture with a large butterfly fragment.

Surgery was performed on the following day to repair the fractured bone with lateral approach to the right femur. Comminuted femoral fracture was identified and there was a large proximal butterfly fragment where the whole cylinder fragment attached to the adductor muscle. There were also small bone fragments distally. The fracture was stabilised using a 10 holes bone plate with eight screws of 3.5 mm. Holes four and seven were left open. The bone plate was placed on the lateral aspect of the femur. Two lag screws size 2.0 mm were also used to fix the large fragment in place. The repair process resulted in good reduction. The incision site was closed in the standard manner. The deep muscle layer was closed using simple interrupted stitches of 3 metric vicryl 3. The muscle aponeurosis of the biceps femoris was closed using simple interrupted sutures of 3 metric PDS 1. The deep and superficial layers were closed using a continuous pattern of 3 metric ethilon 4 in a simple interrupted fashion.

Radiographs taken immediately after the fracture repair showed good alignment with the fracture lines clearly visible (figure 6.2.2). There was a small bone fragment left in the muscle caudal to the distal femur. Blood accumulation (haematoma) was present near the fracture site which had developed after the surgery. The less dense area at the fracture site on cranial view may indicate a space left on the cranial aspect of the femur.

Ultrasonographic examination

Day one after fracture repair

Ultrasonographic examination demonstrated a large haematoma within the muscle near the fracture site on both longitudinal and transverse scans as shown by the hypoechoic area (figure 6.2.3a,b). The bone with the plate attached appeared as a short hyperechoic line on transverse scan and produced comet tail artefact (figure 6.2.3b). The small bone fragment within muscle caudal to the distal femur appeared hyperechoic with acoustic shadowing (figure 6.2.4). The fracture site at the distal third of the femur was difficult to locate on day one after operation because of the large haematoma formation near the fracture site. Suture materials used to close the muscle appeared as hyperechoic short lines on longitudinal scans of the femur (figure 6.2.5a), and as intermittent lines on transverse scans of the femur on the day two examination (figure 6.2.5b). They produced comet tail artefacts.

Day two after fracture repair

The fracture site at the proximal end of the femur was imaged on the day two examination. There was some periosteal reaction which could be seen at the fracture site as demonstrated by the area of increased echogenicity (figure 6.2.6). The two lag screws used to fix the large fragment were imaged on the day two examination and appeared hyperechoic with comet tail artefacts (figure 6.2.6). Only the screws head were imaged on the cranio-lateral scan. The fracture site at the distal third of the femur was imaged but no area of periosteal reaction could be detected. A small, irregular and well defined hypoechoic area casting acoustic enhancement artefact was detected at the distal third of the femoral fracture site as shown in figure 6.2.7. There was a gap left at the distal third of the femoral fracture site as shown by the discontinuity of the femoral surface as scanned longitudinally on caudo-lateral aspect of the femur (figure 6.2.7). This had been shown by a less dense area at the distal third of the femoral fracture site on the cranio-caudal view radiograph. A small bone fragment was identified cranial to the femur within the biceps femoris muscle, but was not demonstrated on radiographs (figure 6.2.8). It appeared as a hyperechoic area with acoustic shadowing artefact. The bone plate that adhered to the femur appeared as an hyperechoic straight line and produced reverberation artefact when the sound beam was directly perpendicular to the plate's long axis (figure 6.2.9a). Sometimes it appeared as intermittent hyperechoic lines with distal comet tail artefacts (figure 6.2.9b). The haematoma appeared hypoechoic with some faint echogenic materials present (figure 6.2.10).

Day three after fracture repair

The ultrasonographic image of the fracture site at the proximal end from the cranial aspect appeared as in day two examination (figure 6.2.11). The haematoma was slowly becoming more echogenic as compared to the previous scans (figure 6.2.12). The small bone fragment placed within the biceps femoris muscle cranial to the femur appeared hyperechoic with acoustic shadowing artefact (figure 6.2.13). There was an hypoechoic area surrounding the small bone fragment which indicated the lysis process. The small bone fragment appeared smaller than on the day two examination. The small, irregular and well defined hypoechoic area seen in day two at the distal third of the femoral fracture site had increased in size and appeared as an ill-defined hypoechoic area (figure 6.2.14).

Day 42 after fracture repair

Radiographic examination

Radiographs taken on day 42 (six weeks) after fracture repair demonstrated the exuberant smooth callus formation bridging the fracture gap (figure 6.2.15). The fracture lines at the proximal and distal third of the femur were still visible radiographically. The wispy periosteal reaction proximal and distal to the fracture site at distal third of the femur may represent damage to the periosteum at surgery. There was no evidence of implant instability.

Ultrasonographic examination

Ultrasonographic examination on day 42 (six weeks) after fracture repair demonstrated the exuberant callus formation at the fracture site both on transverse and longitudinal scans (figure 6.2.16). No fracture line could be detected at this stage, but the fracture site at the distal third of the femur could still be recognised as shown by a small notch on the callus formation at the fracture site (figure 6.2.17). Mature callus had bridged the fracture gap at this stage. The mature callus appeared hyperechoic with an uneven rough surface and produced acoustic shadowing. It has ultrasonographic characteristics similar to normal bone tissue. There was no haematoma detected in the muscle. The muscle structure had returned to its normal characteristic. Ultrasonographically, the fractured bone was healed satisfactorily with no complication.

Figure 6.2.1 A three years old female Border Collie was hit by a car. There is a comminuted fracture involving the mid-shaft of the femur with a large butterfly fragment. This is a complete closed fracture.

Figure 6.2.2 Radiographs obtained immediately after fracture repair. **a**, cranial view, **b**, lateral view. The comminuted fracture has been repaired with a 10 holes plate and eight screws plus two lag screws. There is blood accumulation in the muscle caudo-distally. The fracture lines are clearly visible.

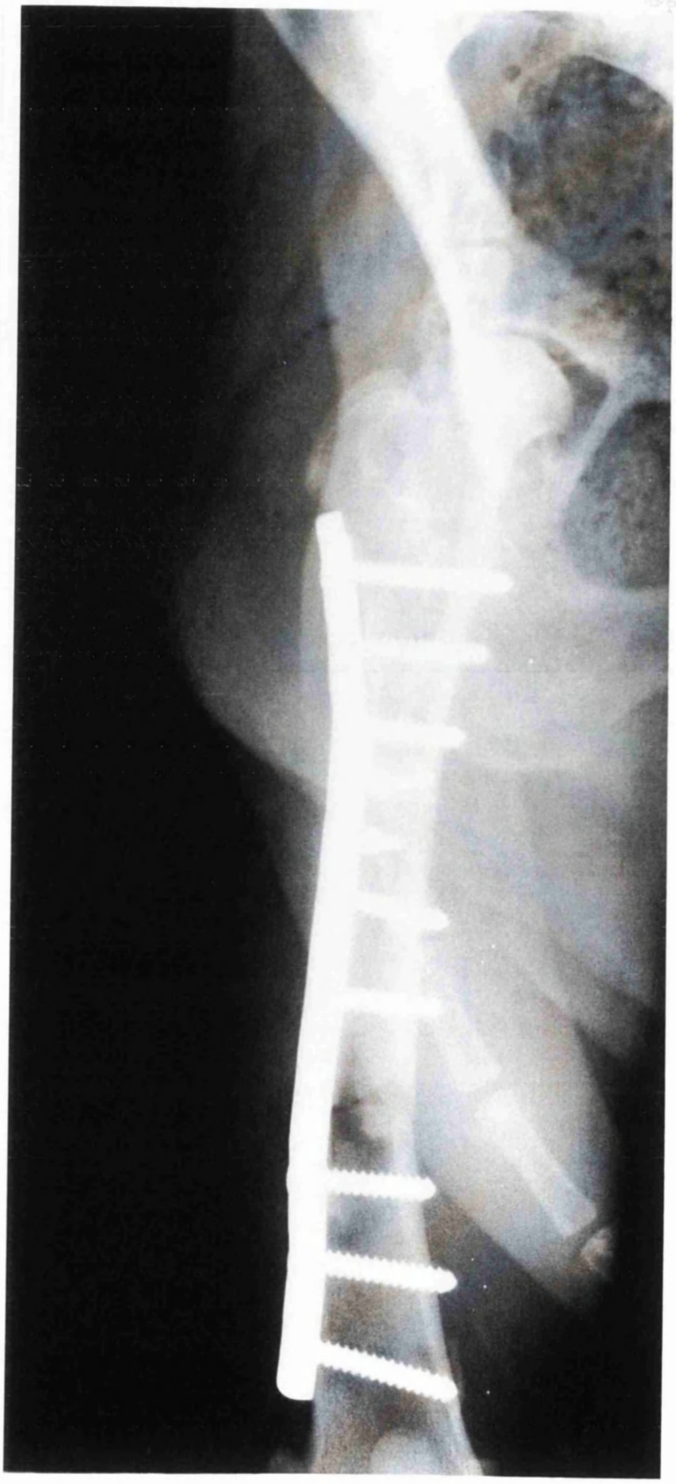

a

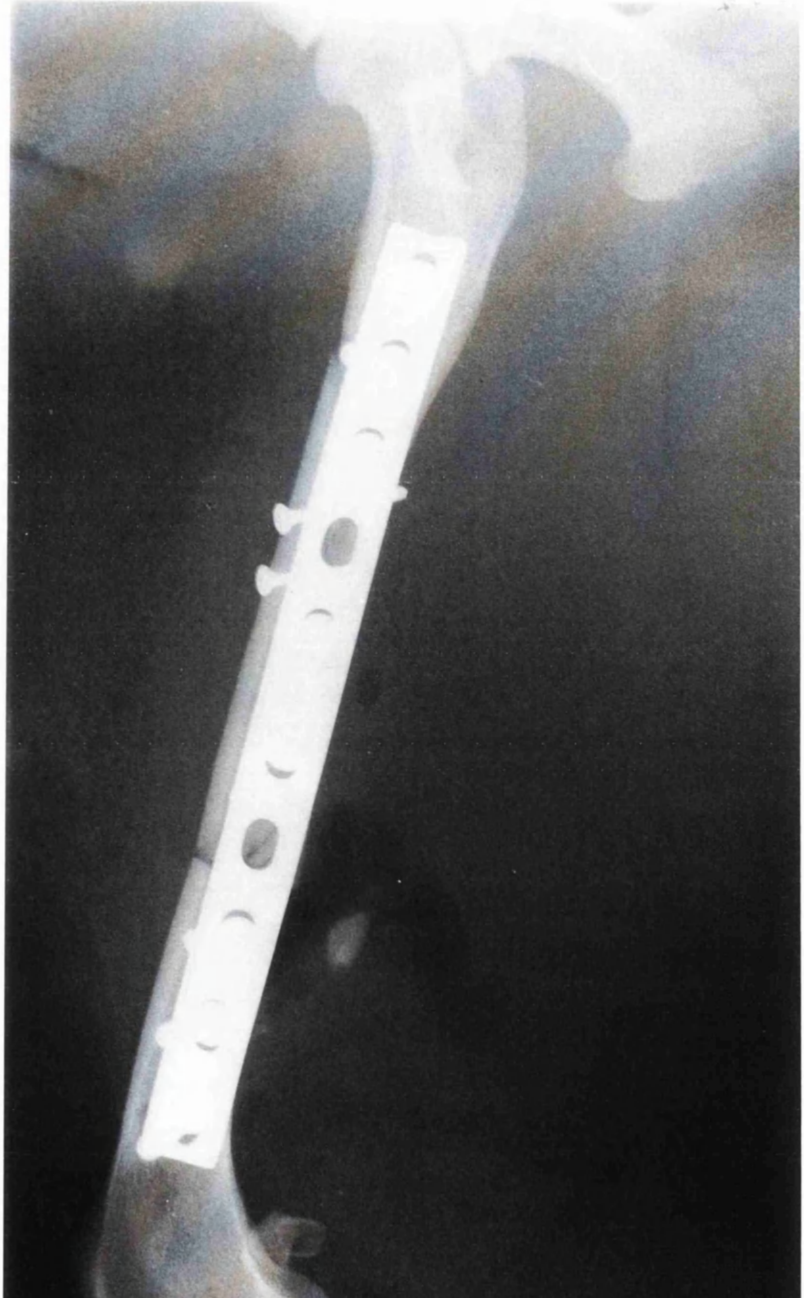

b

Figure 6.2.3 Ultrasonographic images of the large haematoma within the muscle near the fracture site which developed 24 hours after surgery. **a**, longitudinal scan and **b**, transverse scan. The haematoma within the muscle appears hypoechoic with acoustic enhancement artefact. Note also the plate adhering to the bone appears hyperechoic producing comet tail artefact (**b**). **F**, femur

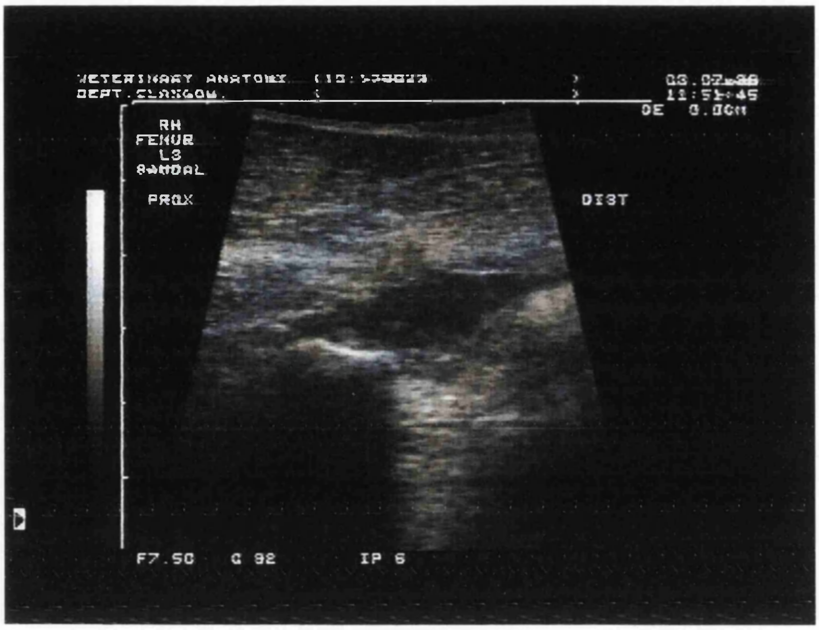

Figure 6.2.3a

Figure 6.2.3b

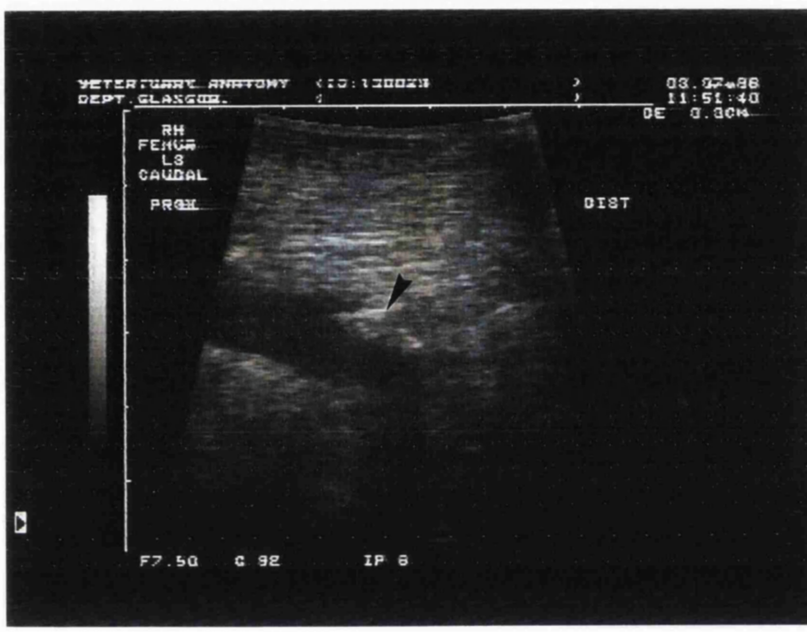

Figure 6.2.4 The bone fragment remaining in the muscle (arrow head) imaged 24 hours after surgery appears hyperechoic with acoustic shadowing artefact. Note the haematoma area on the left side of the fragment.

Figure 6.2.5 Suture material within the muscle (arrow heads) imaged ultrasonographically appears as an hyperechoic short line on the longitudinal scan (**a**), and as an intermittent hyperechoic line on a transverse scan (**b**). They are producing comet tail artefacts.

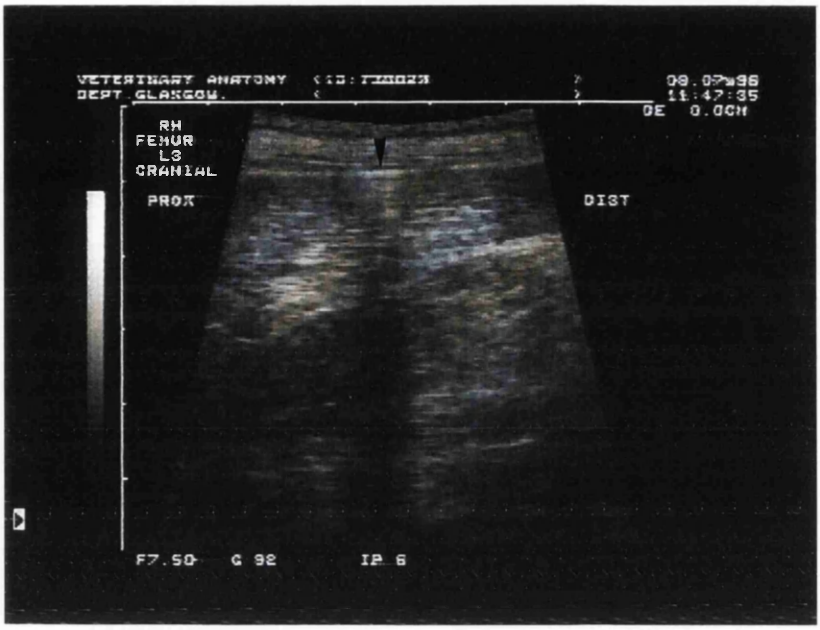

Figure 6.2.5a

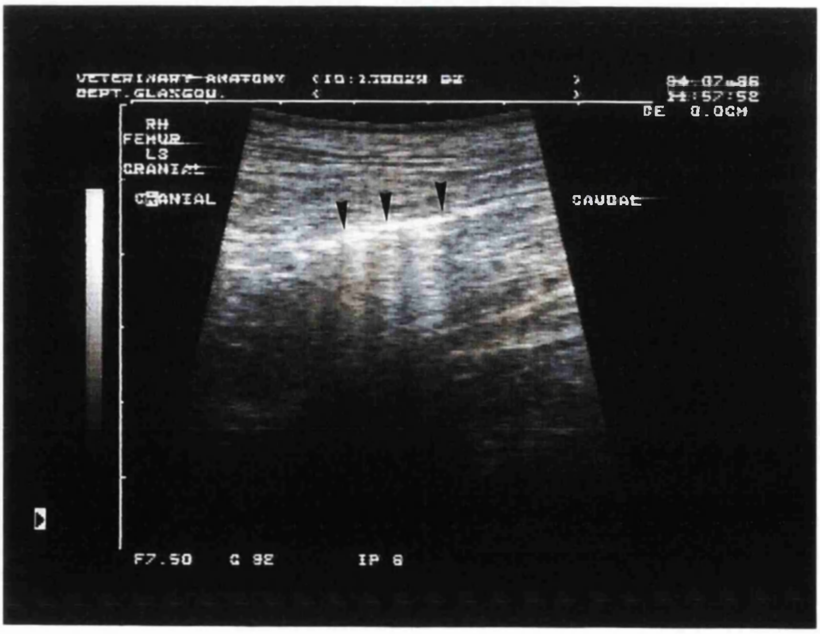

Figure 6.2.5b

Figure 6.2.6 Longitudinal scan from the cranial aspect of the femur on day two post-operation demonstrates the fracture site (arrow) with an hyperechoic appearance indicating soft tissue and periosteal reactions. The two screws (arrow heads) used to fix the large fragment in place appear hyperechoic with comet tail artefact some distance from the fracture site.

Figure 6.2.7 Longitudinal scan from the caudal aspect of the femur on day two post-operation demonstrates a small, irregular and well defined hypoechoic area (arrow head) with acoustic enhancement artefact at the end of the proximal fragment. The hyperechoic straight line (arrow) is the bone plate. Note also the discontinuity of the proximal fragment which indicates the presence of a gap at the fracture site.

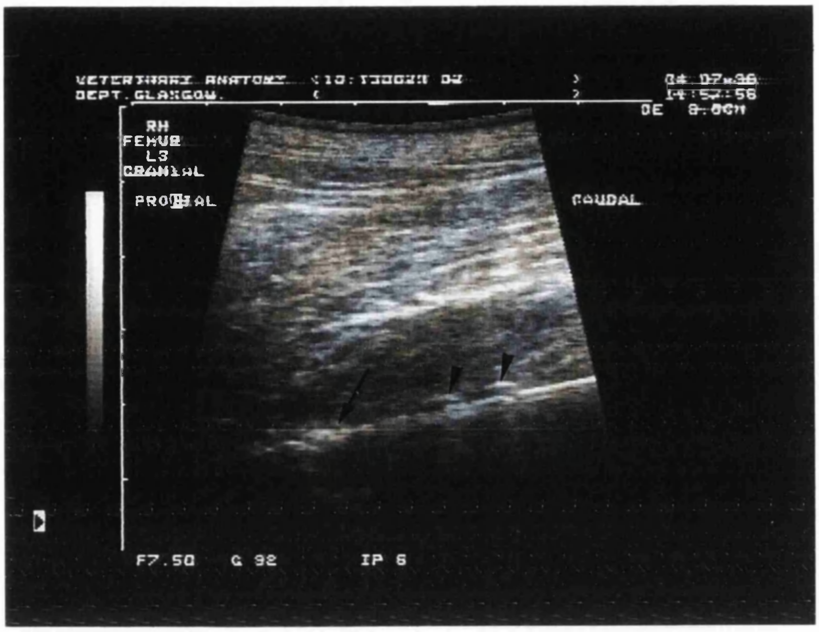

Figure 6.2.6

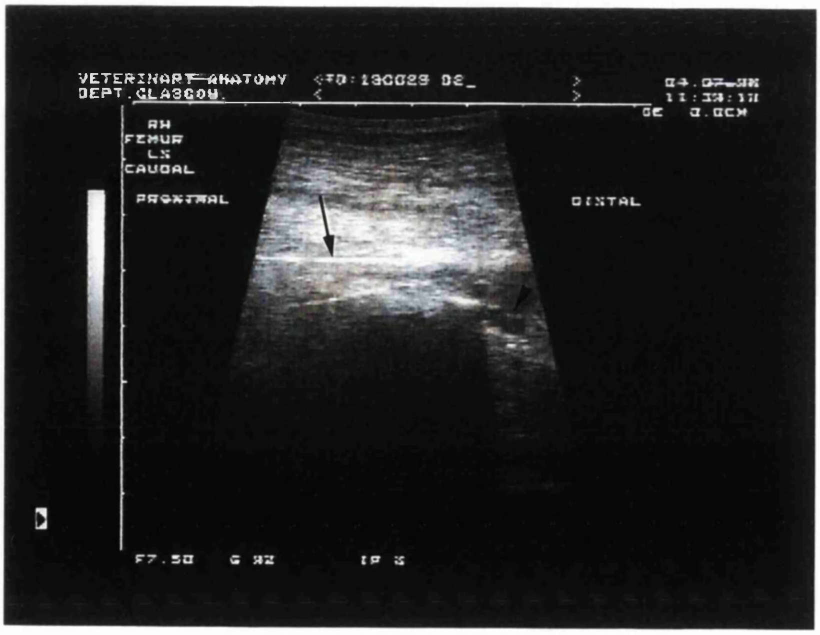

Figure 6.2.7

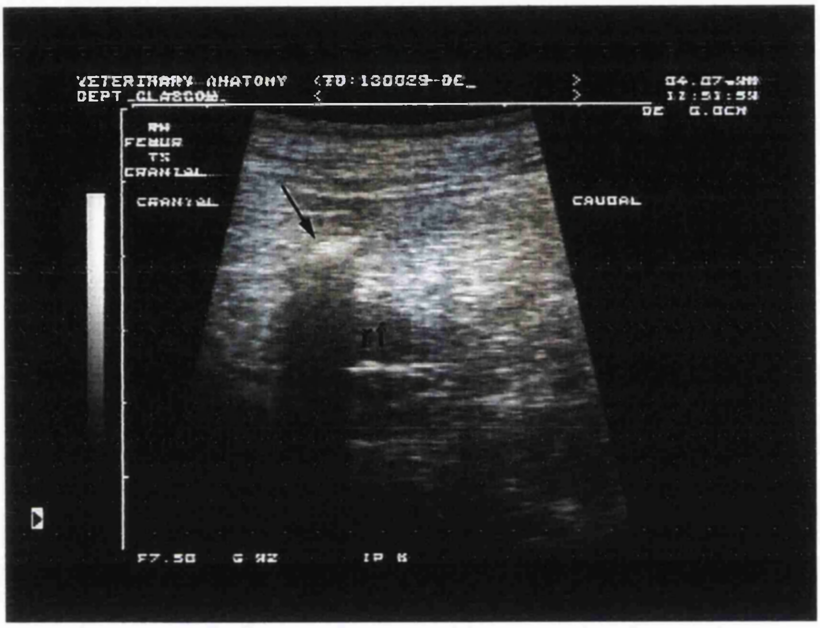

Figure 6.2.8 The small bone fragment (arrow) placed cranial to the femur within the biceps femoris muscle imaged 48 hours after the surgery appears hyperechoic and is producing acoustic shadowing artefact. This small fragment was not visualised on radiography. **rf**, m. rectus femoris

Figure 6.2.9 Longitudinal scans from the lateral aspect (**a**) and from caudal aspect (**b**) of the femur demonstrate the bone plate with screws that attach to the femur. The bone plate appears as an hyperechoic straight line producing reverberation artefact on the lateral aspect image (**a**), and appears as an intermittent hyperechoic line with comet tail artefact on the caudal aspect image (**b**).

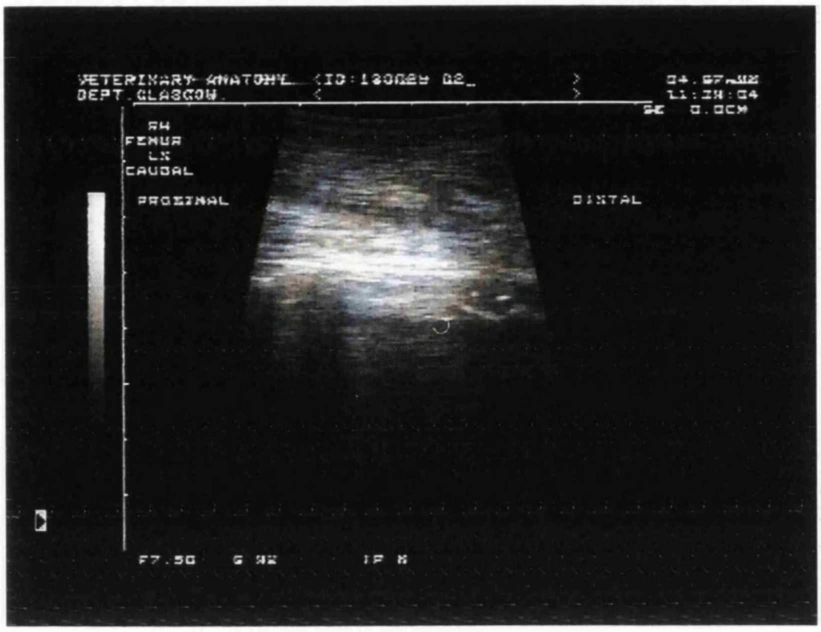

Figure 6.2.9a

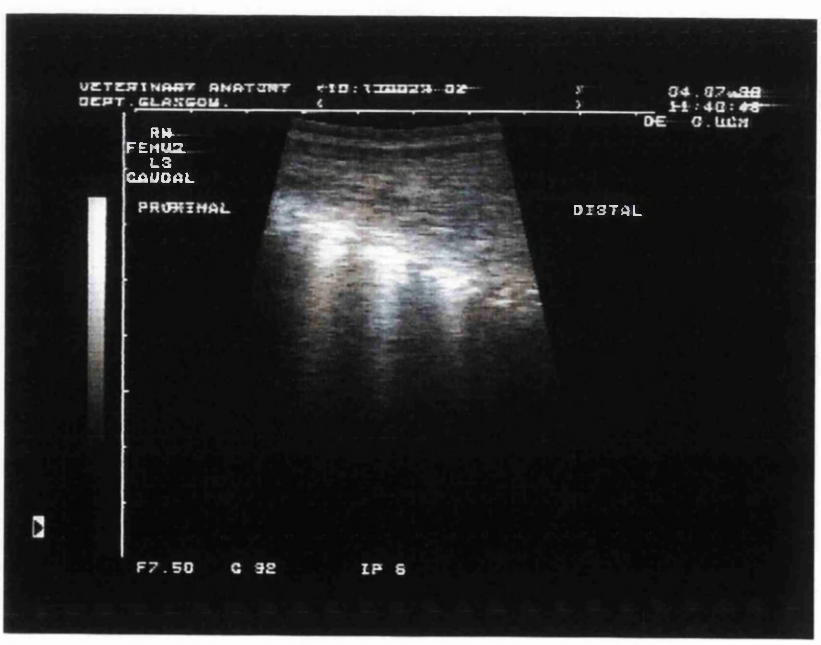

Figure 6.2.9b

Figure 6.2.10 The haematoma within the muscle near fracture site imaged 48 hours after surgery appears as an hypoechoic area with some echogenic material present. **F**, femur.

Figure 6.2.11 Longitudinal scan from the cranial aspect of the femur on day three post-operation demonstrates the fracture site (arrow). Note that the hyperechoic appearance at the fracture site and the presence of some echogenic material indicates periosteal and soft tissue reactions.

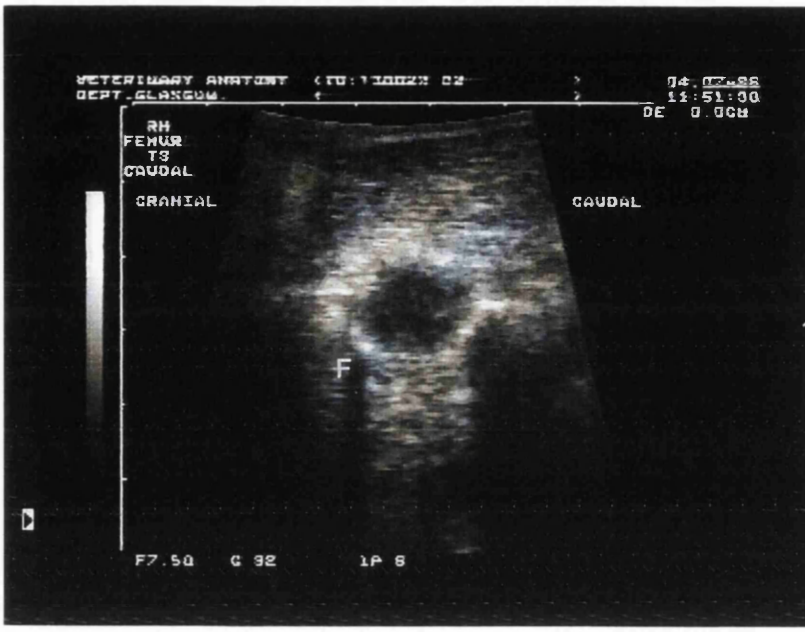

Figure 6.2.10

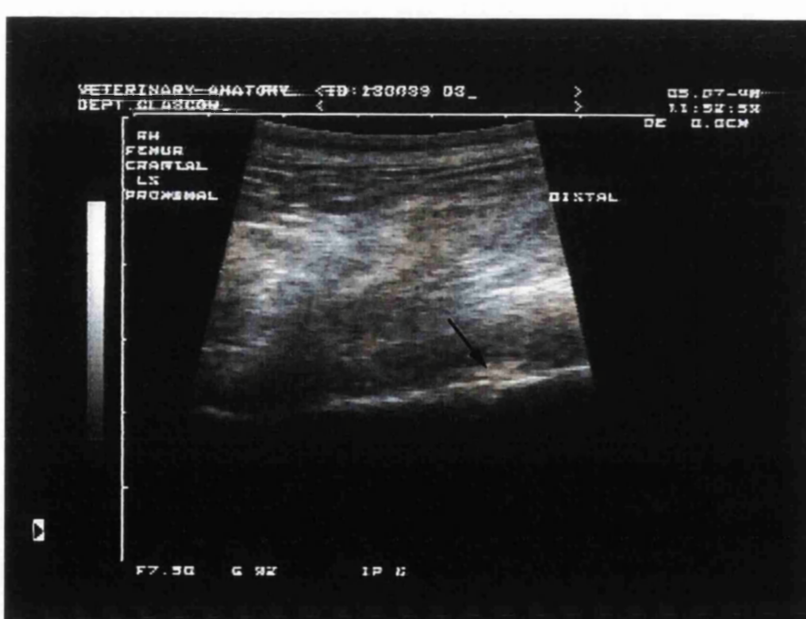

Figure 6.2.11

Figure 6.2.12 The large haematoma within the muscle near the fracture site scanned on day three post-operation appears hypoechoic with the content becoming more echogenic than on the day two examination. This indicates that the haematoma is resolving.

Figure 6.2.13 A small bone fragment (arrow) is lying within the biceps femoris muscle cranial to the femur as scanned on day three post-operation. Note the bone fragment appears hyperechoic with acoustic shadowing artefact and has become smaller than on the day two examination. The hypoechoic area surrounding the bone fragment indicates a lysis process. **rf**, m. rectus femoris.

Figure 6.2.12

Figure 6.2.13

Figure 6.2.14 Longitudinal scan from the caudal aspect of the femur on day three post-operation demonstrates an ill-defined hypoechoic area (arrow head) which appears bigger than on the day two examination.

Figure 6.2.15 Radiographs obtained at six weeks after fracture repair. **a**, cranial view, **b**, lateral view. Callus formation is bridging the fracture gap. The fracture lines at both the distal third and proximal end of the femur are still visible. The wispy periosteal reaction proximal and distal to the distal third fracture site may represent damage to the periosteum at surgery. There is no evidence of implant instability.

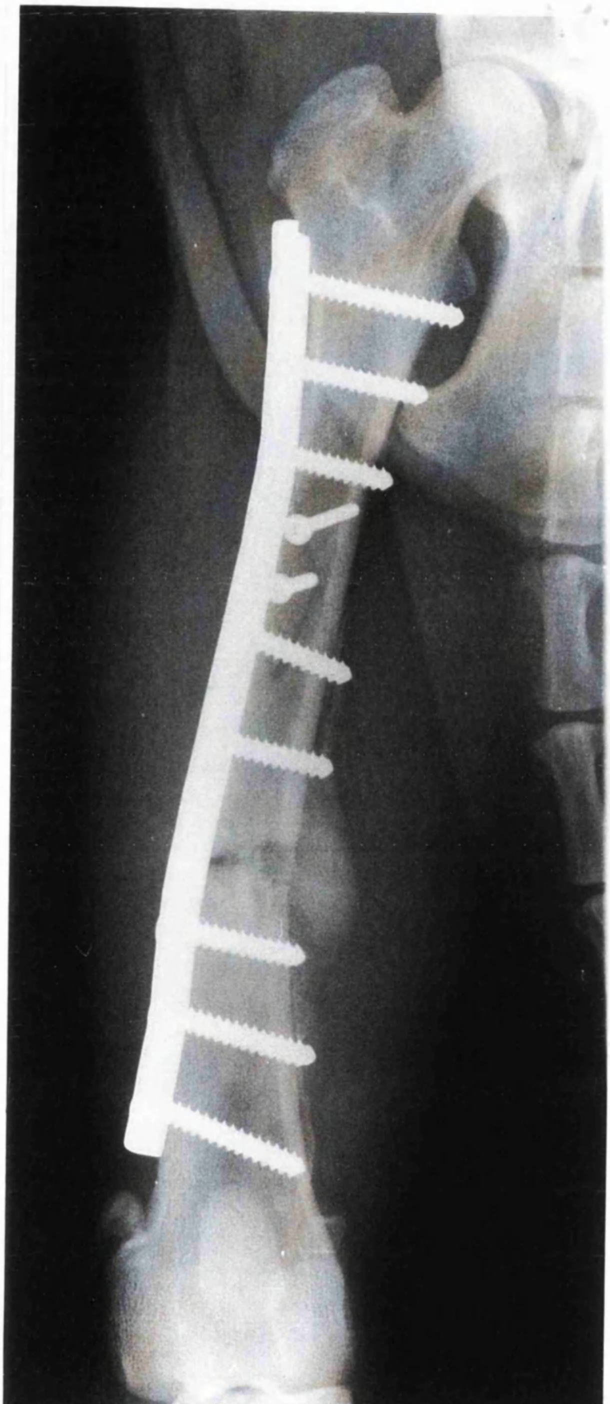

a

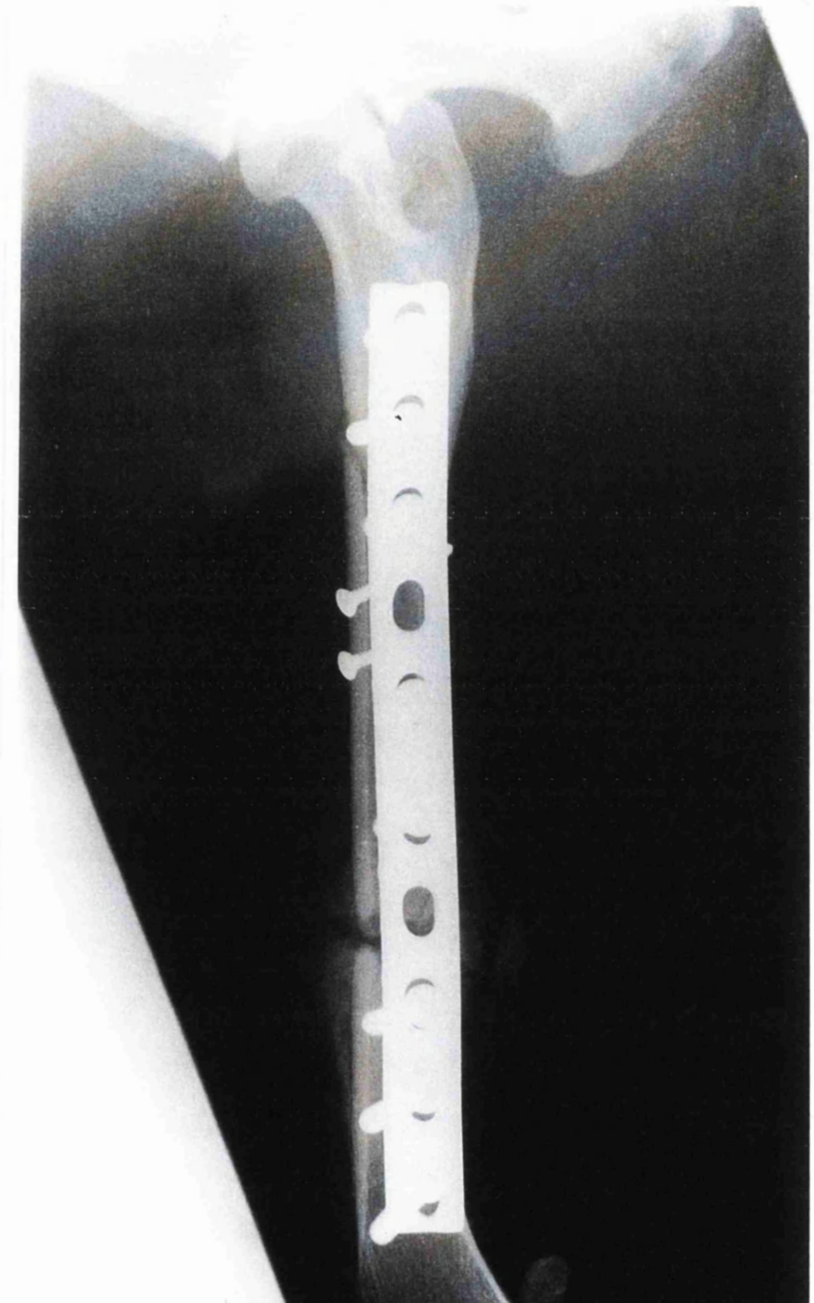

b

Figure 6.2.16 Transverse scan from the lateral aspect of the femur on day 42 post-operation shows extensive callus formation on both sides of the bone plate. Note also that the bone plate and screw that are adhering to the femur appears hyperechoic and are producing comet tail artefacts.

Figure 6.2.17 Longitudinal scan from the cranial aspect of the femur on day 42 post-operation demonstrates the bulging femoral surface which is due to the mature callus. Note also that the fracture site can still be identified as a small notch (arrow). The fracture site has been completely bridged by the mature callus. The remodelling process is in progress at this stage.

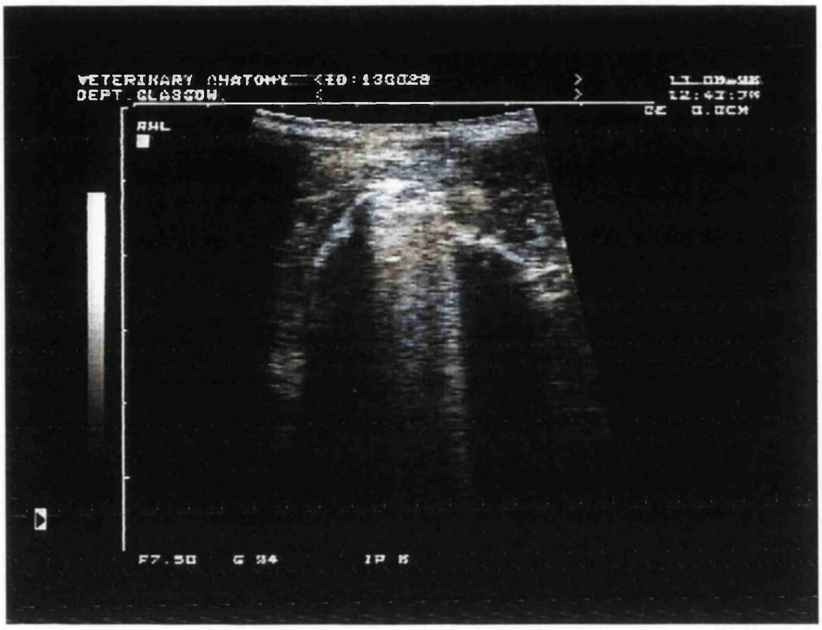

Figure 6.2.16

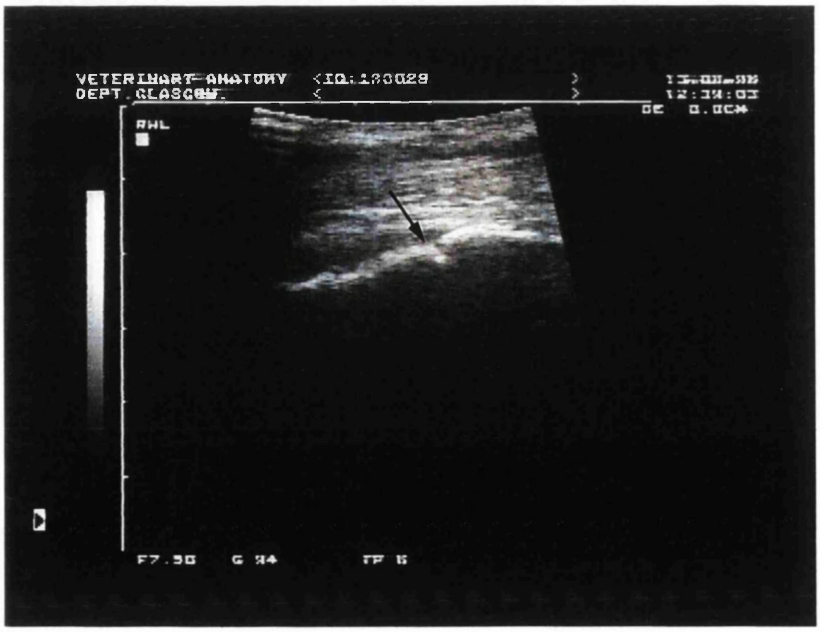

Figure 6.2.17

Case 3

A three year old male German Shepherd, weight 28 kg, with a suspicion of having a femoral fracture was admitted to the Glasgow University Veterinary Hospital. The dog had been hit from behind in a road traffic accident one week previously. Radiographic examination carried out before the fracture repair was done showed a multiple comminuted and segmented fracture of the left femur (figure 6.3.1). The fracture had been sustained with a significant displacement of the fragments. There was also a marked tissue reaction.

Surgery had been carried on the day following admission. A standard approach on the lateral aspect of the femur was made. A large haematoma and new callus formation were found during surgery. The callus was then removed from the site. Three large fragments of bone were also found and were placed in saline. A standard 4.5 mm 10 holes plate was used to stabilise the fracture following transverse osteotomies both at the proximal and distal fracture sites. Two lag screws and two cerclage wires were used in addition to the bone plate to fix the middle fragments in place. These were introduced to provide a good reduction of the fracture. The wound was closed in the standard fashion. The deep muscle layer was closed using simple interrupted sutures of 3 metric PDS 1. The deep and superficial fascial layers were closed using a continuous pattern of 3 metric vicryl 3. The skin was closed with 2 metric ethilon 4 with a simple interrupted suture pattern.

Radiographs taken immediately after the fracture reduction showed the repair process had resulted in a good reduction but a number of small fragments remained in the muscle (figure 6.3.2).

Ultrasonographic examination

Day one after fracture repair

Ultrasonographic examination revealed a large haematoma within the muscle which appeared as a large, clear anechoic area (figure 6.3.3a). There was a "bell clapper" sign at the upper wall of the haematoma suggesting a muscle tear. One small bone fragment was found within the muscle near the haematoma area and appeared hyperechoic with acoustic shadowing artefact (6.3.3b). The metal plate adherent to the bone appeared as a straight hyperechoic line and produced a reverberation artefact (figure 6.3.4). The screw used in the fracture reduction appeared hyperechoic and produced a comet tail artefact. The fracture site at the distal third scanned longitudinally from the cranial aspect appeared as a vertical hyperechoic line across the femur with the presence of a small gap (figure 6.3.5a). The soft tissue reaction could be seen at the fracture site appearing as an hyperechoic area. The fracture site at the proximal third of the femur appeared as discontinuity of the hyperechoic straight line of the bone but there was no gap present (figure 6.3.5b). The small bone fragment lying superficial to the femur appeared hyperechoic with acoustic shadowing artefact. The fracture site was clearly seen from the medial aspect scan with the presence of a fracture gap (figure 6.3.6). There was also a bone fragment immediately superficial to the fracture site which appeared as an hyperechoic short line structure. The soft tissue and periosteal tissue reactions were detected at the fracture site and in the nearby area and appeared as an hyperechoic area. The muscle had lost its normal ultrasonographic appearance and appeared as a disorganised hypoechoic region. The screws used to fix the fragment near the fracture site appeared hyperechoic with comet tail artefacts. The screws were protruding into the muscle on medial aspect of the femur. Soft tissue reactions were detected around the screws and appeared as disorganised hyperechoic areas (figure 6.3.7). The area of muscle damage above the femur appeared as a disorganised hypoechoic region relative to the area of normal muscle on a transverse scan (figure 6.3.8). The fracture site imaged on a transverse scan appeared as a 'V'-shape fracture gap present on the femoral surface (figure 6.3.9). The ruptured blood vessel within the large haematoma was detected (figure 6.3.10). It was pulsating during ultrasonographic examination. A small blood vessel within the muscle imaged in cross section appeared as a small, well defined round hypoechoic area with edge shadowing artefacts (figure 6.3.11).

Day 3 after fracture repair

The large haematoma evident with a clear margin within the muscle still persisted on the day three examination and appeared anechoic but with some echogenic materials present (figure 6.3.12). The periosteal tissue reaction could be seen on the femoral surface as an hyperechoic area. The fracture site imaged from medial aspect of the femur demonstrated the disorganised hyperechoic structure area on the femoral surface and around the fracture site suggesting the presence of soft tissue and periosteal tissue reaction (figure 6.3.13). The soft callus formation could be seen within the fracture gap appearing hyperechoic and trying to bridge the gap. The area of extensive muscle damage caudal to the femur appeared as a disorganised mixture of anechoic and echogenic areas on the caudo-medial aspect scan (figure 6.3.14). Soft callus formation was detected at the distal third fracture site on a cranial aspect scan and appeared as hyperechoic material adherent to the bone surface adjacent to the fracture site (figure 6.3.15). The periosteal tissue reaction could also be seen on the femoral surface around the fracture site. The small fracture gap had become shallow due to callus formation. The femur appeared slightly bent at the area of the proximal third fracture site on a longitudinal scan from the caudal aspect (figure 6.3.16). The hyperechoic layer on the femoral surface suggested a periosteal tissue reaction. The fracture site at the distal third of the femur imaged on a transverse scan showed a fracture gap which appeared hyperechoic due to periosteal tissue reaction (figure 6.3.17). Soft callus formation could be seen as an hyperechoic structure adhered to the bone surface. The gap appeared smaller than on the day one examination. The area of muscle damage had slowly returned to its normal ultrasonographic appearance. The femur appeared abnormal on a transverse scan with a rough hyperechoic surface (figure 6.3.18). The bone fragment within the muscle appeared hyperechoic with acoustic shadowing artefact (figure 6.3.19). Suture materials within the muscle appeared hyperechoic and produced comet tail artefact.

Day 34 after fracture repair

Ultrasonographic examination at the mid shaft of the femur demonstrated the excessive callus formation both on transverse and longitudinal scans and appeared as a rough hyperechoic surface with acoustic shadowing artefact (figure 6.3.20a and 6.3.20b). The femur has lost its normal smooth hyperechoic appearance. The fracture site at the distal third of the femur could still be seen when scanned from the cranio-lateral aspect and appeared as a notch on the bone surface (figure 6.3.21). The fracture site appeared to have been bridged by the mature callus and a fracture gap was no longer detectable on a longitudinal scan from the cranio-lateral aspect. The femoral surface appeared smooth at both sides of the fracture site seen from the cranio-lateral aspect and suggested a remodelling process had occurred. A transverse scan of the proximal fracture site from the cranio-lateral aspect showed the fracture gap which still persisted and appeared hyperechoic (figure 6.3.22). On the medial aspect, the fracture gap could still be seen as discontinuity of the femoral surface (figure 6.3.23). However, the fracture gap had become shallow due to callus formation. A large hyperechoic structure casting a complete acoustic shadowing artefact was found adjacent to the femur on a transverse scan from the lateral aspect (figure 6.3.24a and 6.3.24b). This structure was apparent some distance away from the mid-femur, and it came to lie closer to the femur distally (figure 6.3.24b). The bone plate that adhered to the femur appeared hyperechoic and produced reverberation artefact, while the screws appeared hyperechoic and produced comet tail artefact (figure 6.3.25). The muscle structure had returned to its normal ultrasonographic appearance. Suture materials within the muscle appeared as hyperechoic straight lines and produced comet tail artefacts.

Day 62 after fracture repair

Radiographic examination

Radiographs taken on day 62 (9 weeks) after fracture repair showed that the fracture line was still visible, and the most proximal screw was coming adrift which indicate the failure of the implant at the proximal end. On the cranial view the callus formation was found at the medial side of the mid femoral shaft (figure 6.3.26).

Ultrasonographic examination

Ultrasonographic examination demonstrated the fracture site which had been bridged completely by the mature callus (figure 6.3.27). The fracture site could still be detected as a defect on the bone surface. A transverse scan of the mid shaft of the femur revealed the excessive callus formation around the femur which resulted in a rough and uneven femoral surface (figure 6.3.28). On the medial aspect, the fracture site appeared as a disorganised hypoechoic area with a mottled hyperechoic structure indicating callus formation (figure 6.3.29). The area of muscle damage had returned to its normal ultrasonographic appearance. Ultrasonographically, the fracture healing was occurring satisfactorily.

Figure 6.3.1 A three year old German Shepherd with a comminuted fracture of the left femur. The femur fracture had been sustained with significant displacement of the fragments after a road traffic accident one week previously.

Figure 6.3.2 Radiographs obtained immediately after fracture repair. The repair process has resulted in good fracture reduction. **a**, lateral view, **b**, cranial/caudal view. A standard 4.5 mm 10 holes plate was used to stabilise the fracture following transverse osteotomy both at proximal and distal fracture sites. Two lag screws and two cerclage wires were used in addition to the bone plate. A number of small bone fragments remain in the muscle.

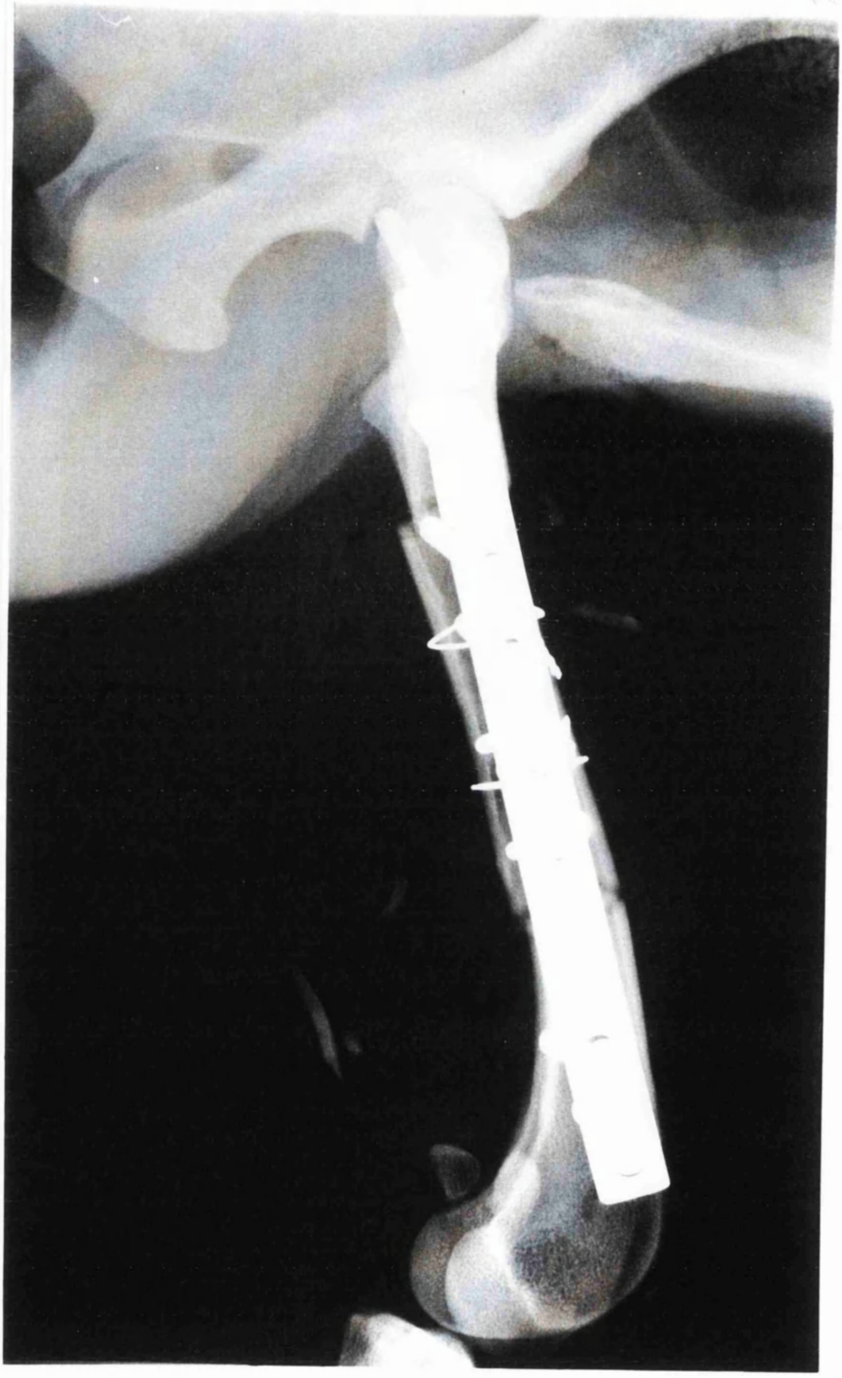

a

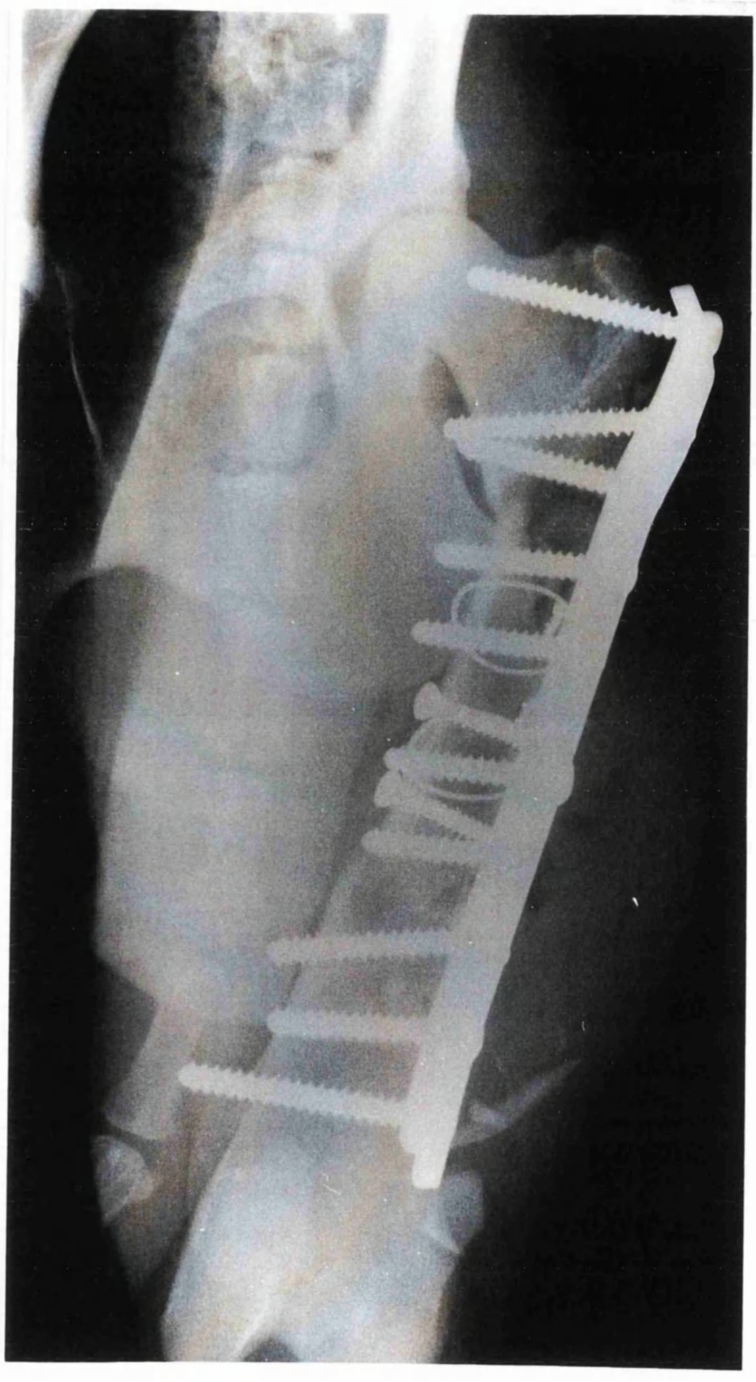

b

Figure 6.3.3 Longitudinal scan of the thigh from the lateral aspect 24 hours after fracture repair demonstrating a large, clear anechoic area within the muscle which represents the area of haematoma (**a**). Note also the presence of "bell clapper" sign (arrow) in (**a**) which indicate the muscle tear. The small bone fragment remaining in the muscle (arrow) appears hyperechoic with acoustic shadowing artefact (**b**).

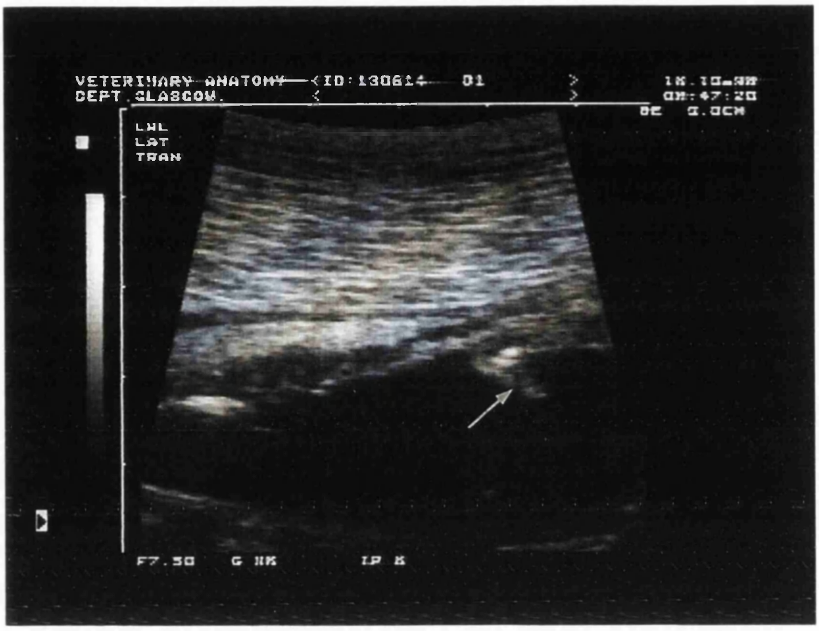

Figure 6.3.3a

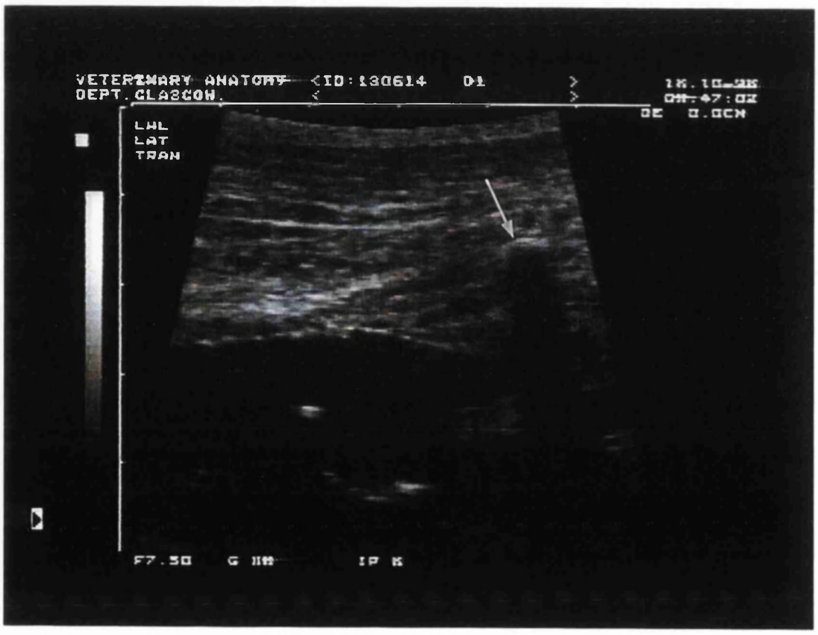

Figure 6.3.3b

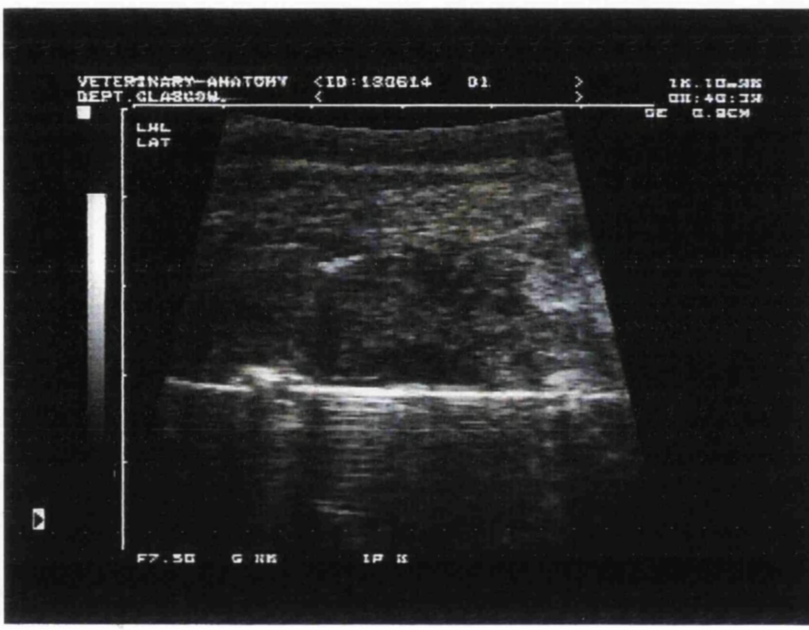

Figure 6.3.4 The bone plate adhering to the femur appears as a straight hyperechoic line and produces reverberation artefact on the longitudinal scan. Note also the area of muscle damage overlying the bone plate appearing as a disorganised hypoechoic region of the imaged muscle.

Figure 6.3.5 Longitudinal scans from the cranial aspect of the femur 24 hours post-operation show the fracture site (arrow) at the distal third of the femur (**a**) and at the proximal third of the femur (**b**). The distal third fracture site appears as a hyperechoic line with the presence of a small gap, and the proximal third fracture site appears as discontinuity of the femoral surface. The hyperechoic area at the fracture site in (**a**) suggests a soft tissue reaction. The area of muscle damage above the femur appears as a disorganised hypoechoic region. One small bone fragment (arrow head) imaged superficial to the femur appears hyperechoic with acoustic shadowing (**b**).

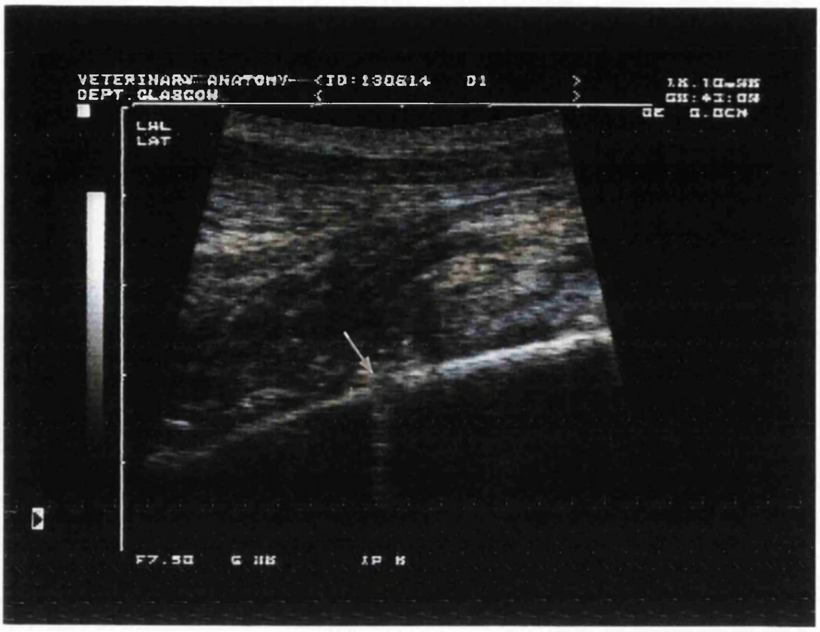

Figure 6.3.5a

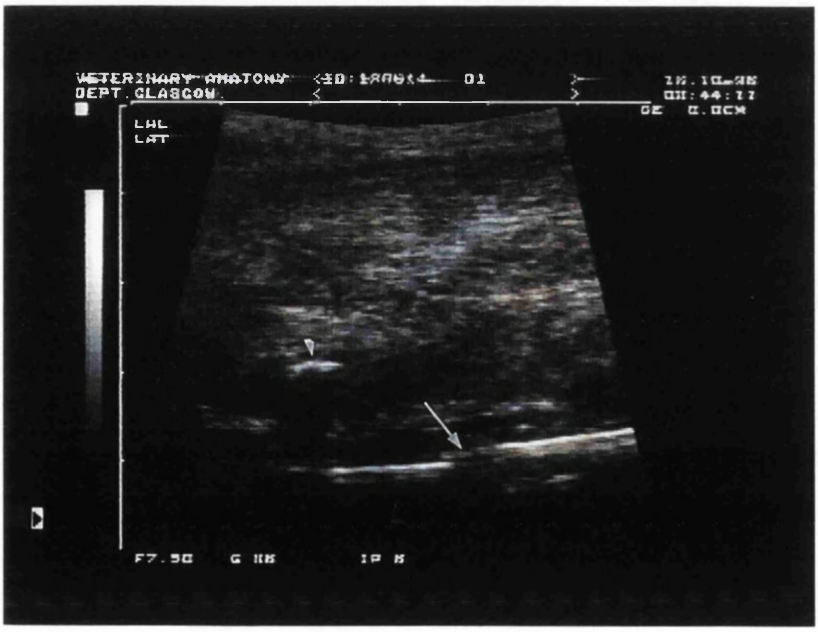

Figure 6.3.5b

Figure 6.3.6 Longitudinal scan from the medial aspect of the femur 24 hours post-operation shows the fracture site with the presence of a gap. Note also the small hyperechoic bone fragment at the fracture site. The area of soft tissue and periosteal tissue reactions appear as disorganised hyperechoic regions at the fracture site and nearby area.

Figure 6.3.7 Longitudinal scan of the femur from the medial aspect shows the area of soft tissue reaction around the screws which appear as disorganised hyperechoic regions.

Figure 6.3.6

Figure 6.3.7

Figure 6.3.8 Transverse scan of the femur from the lateral aspect 24 hours post-operation demonstrates the area of muscle damage which appears as a disorganised hypoechoic region (DM) as compared to the normal muscle (M). Note also the bone plate (arrow) adherent to the femur appearing as an hyperechoic structure with reverberation artefact. **M**, normal muscle, **DM**, damage muscle, **Ha**, haematoma area, **F**, femur.

Figure 6.3.9 A fracture site imaged on a transverse scan 24 hours post-operation shows the fracture gap which appears as a 'V' shape. The area of muscle damage above the femur appears as disorganised hypoechoic structure. **F**, femur.

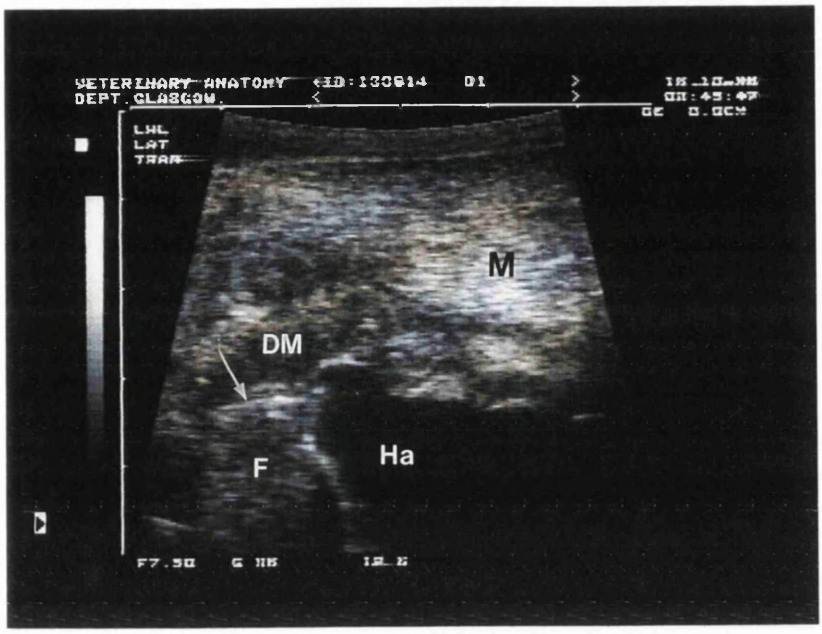

Figure 6.3.8

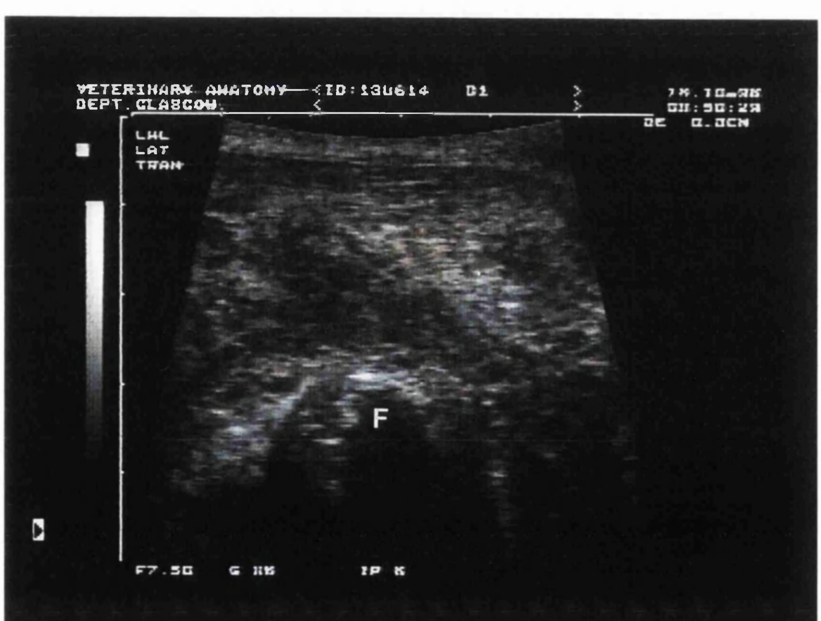

Figure 6.3.9

Figure 6.3.10 The ruptured blood vessel can be seen within the large haematoma 24 hours post-operation (arrow). It was pulsating during examination. **Ha**, haematoma area.

Figure 6.3.11 The small blood vessel (arrow head) on transverse scan appears hypoechoic with edge shadowing artefact.

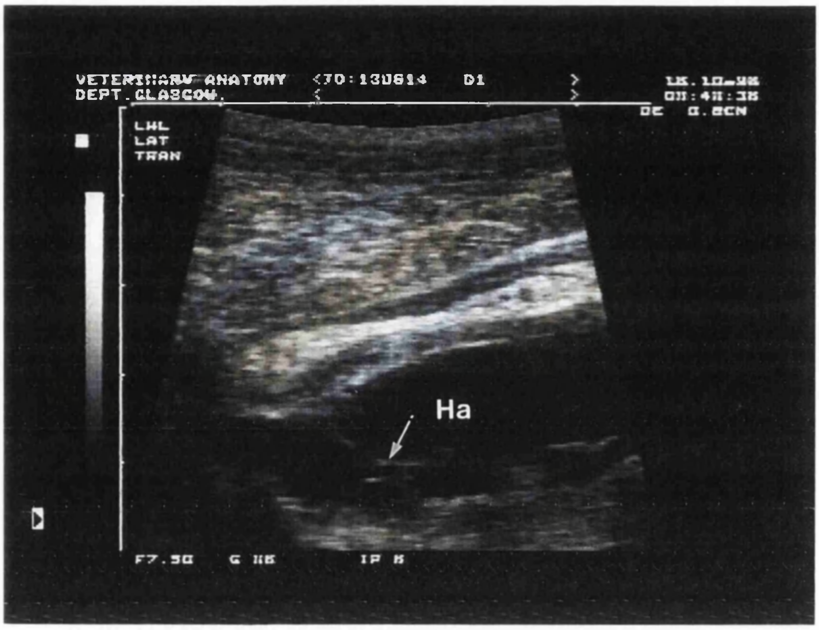

Figure 6.3.10

Figure 6.3.11

Figure 6.3.12 A large haematoma imaged on day three post-operation appears anechoic with the presence of some echogenic material inside.

Figure 6.3.13 Ultrasonographic image of the fracture site from the medial aspect on day three after fracture repair demonstrates the fracture gap with the presence of soft callus formation. The presence of a disorganised hyperechoic area around the screws and on the femur suggests an area of soft tissue and periosteal reaction. The screw (arrow head) appears hyperechoic with comet tail artefact.

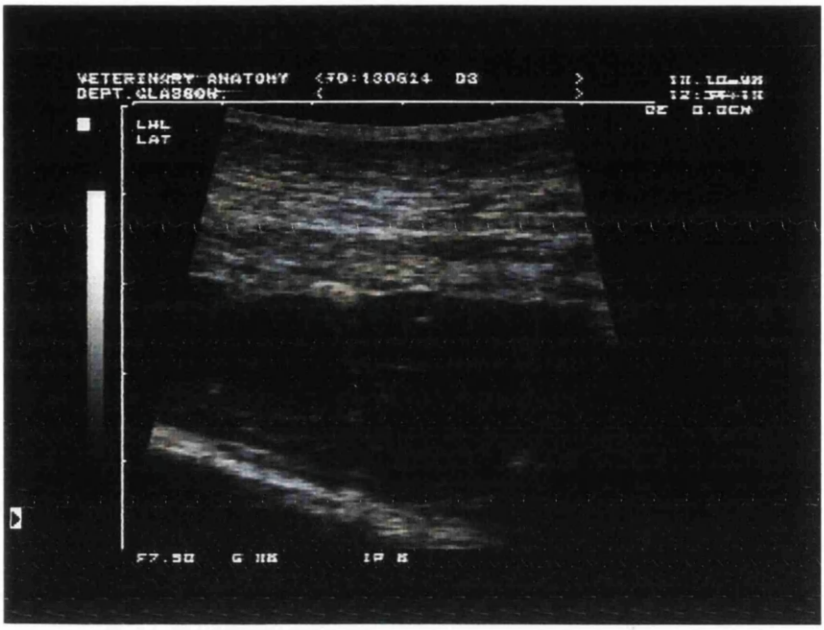

Figure 6.3.12

Figure 6.3.13

Figure 6.3.14 The mixture of anechoic and echogenic structures represents the area of extensive muscle damage imaged from the medial aspect of the thigh on day three after fracture repair.

Figure 6.3.15 Longitudinal scan from the cranial aspect of the femur on day three after fracture repair shows the fracture site at the distal third of the femur with the soft callus formation (arrows). Note that the soft callus formation appears as hyperechoic material adhering to the femoral surface adjacent to the fracture site. There is also a layer of periosteal tissue reaction on the femoral surface which appears hyperechoic. The fracture gap is becoming shallow due to the callus formation.

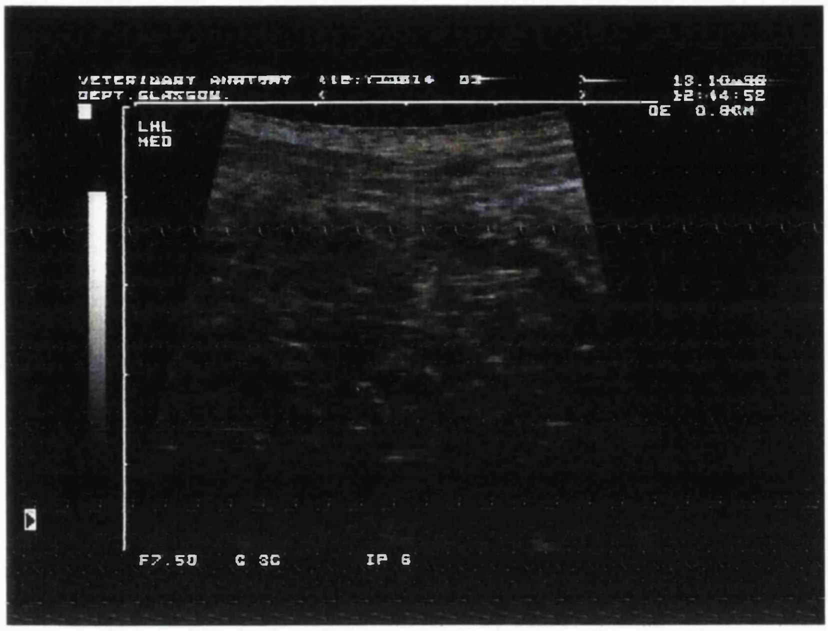

Figure 6.3.14

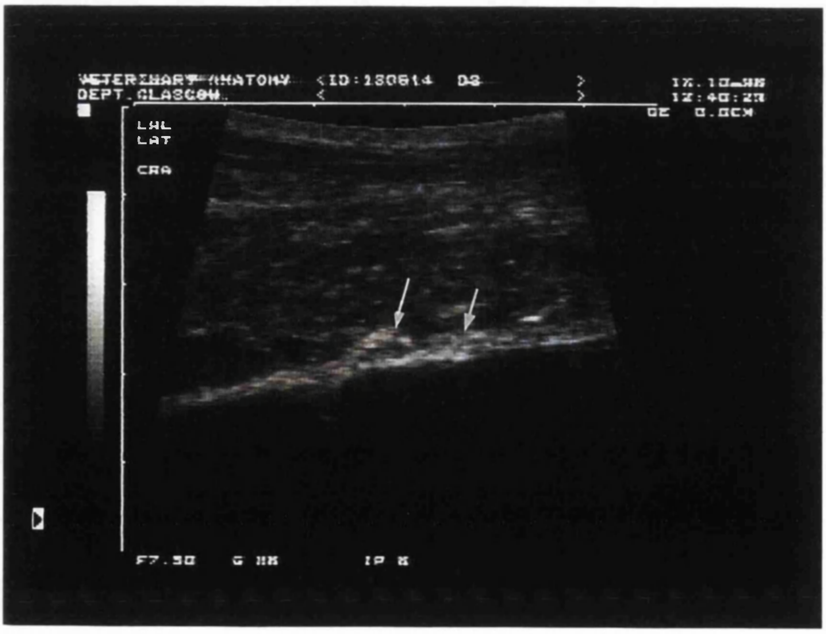

Figure 6.3.15

Figure 6.3.16 Longitudinal scan from the caudal aspect of the femur on day three after fracture repair shows the femur which is slightly bent at the proximal third fracture site (arrow head). Note also the hyperechoic area on the femoral surface suggesting a periosteal tissue reaction.

Figure 6.3.17 Transverse scan of the distal third fracture site from the cranial aspect of the femur on day three post-operation shows the fracture site which appears hyperechoic due to periosteal tissue reaction and soft callus formation. The soft callus formation appears as hyperechoic material adhering to the bone surface on the cranial side of the femur (arrow heads). The fracture gap appears smaller than on the previous examination. The bone plate with screw (arrow) appears hyperechoic with comet tail artefact.

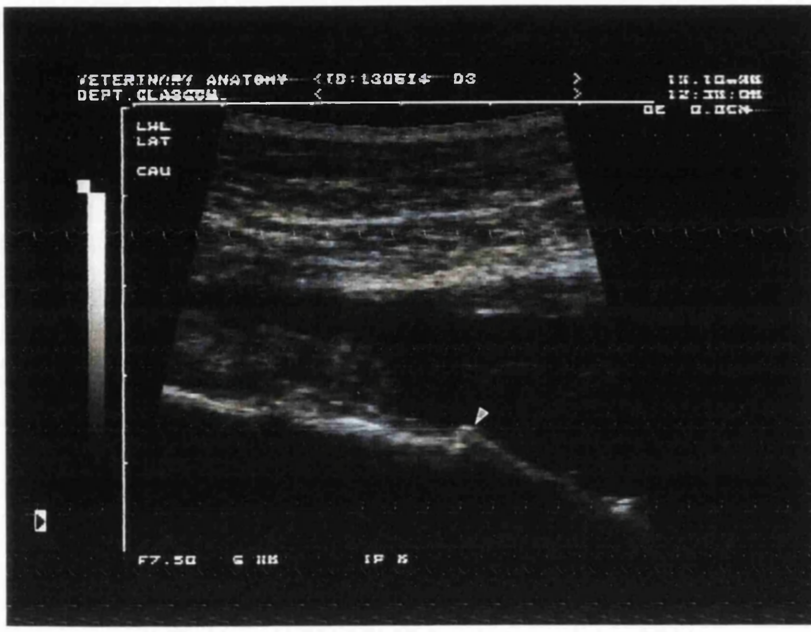

Figure 6.3.16

Figure 6.3.17

Figure 6.3.18 Transverse scan of the femur from the lateral aspect on day three post-operation shows the abnormal, enlarged and roughened surface of the femur. The bone plate (arrow) appears hyperechoic producing reverberation artefact.

Figure 6.3.19 Longitudinal scan from the caudal aspect of the femur on day three post-operation demonstrates the bone fragment (arrow head) which remains in the muscle and appears hyperechoic with clear acoustic shadowing artefact.

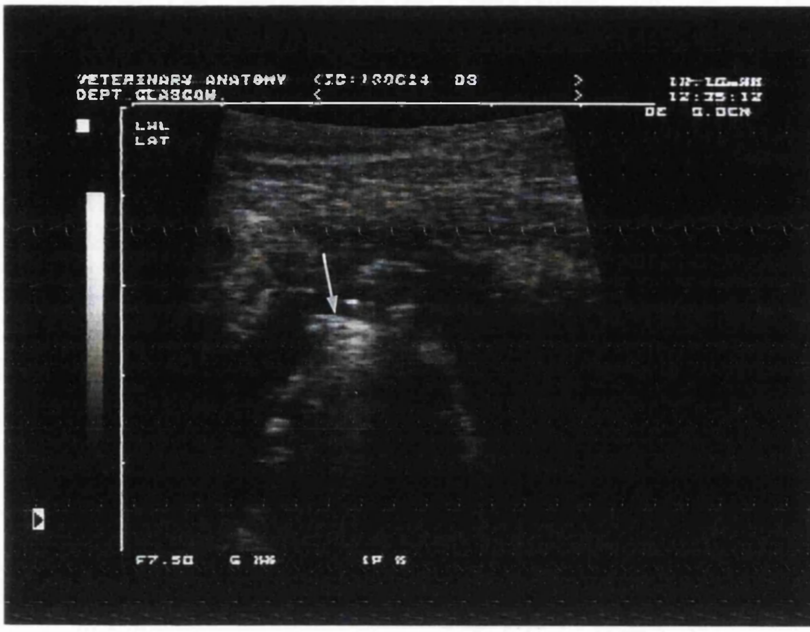

Figure 6.3.18

Figure 6.3.19

Figure 6.3.20 Ultrasonographic examination of the femur on day 34 post-operation demonstrate the excessive callus formation both on transverse (**a**) and longitudinal (**b**) scans. The mature callus appears hyperechoic and produces acoustic shadowing artefact. **F**, femur.

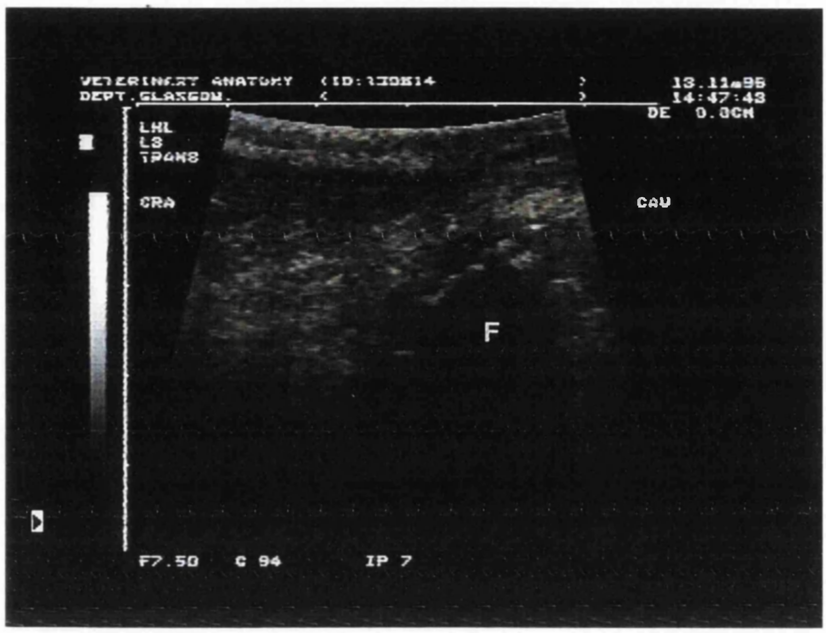

Figure 6.3.20a

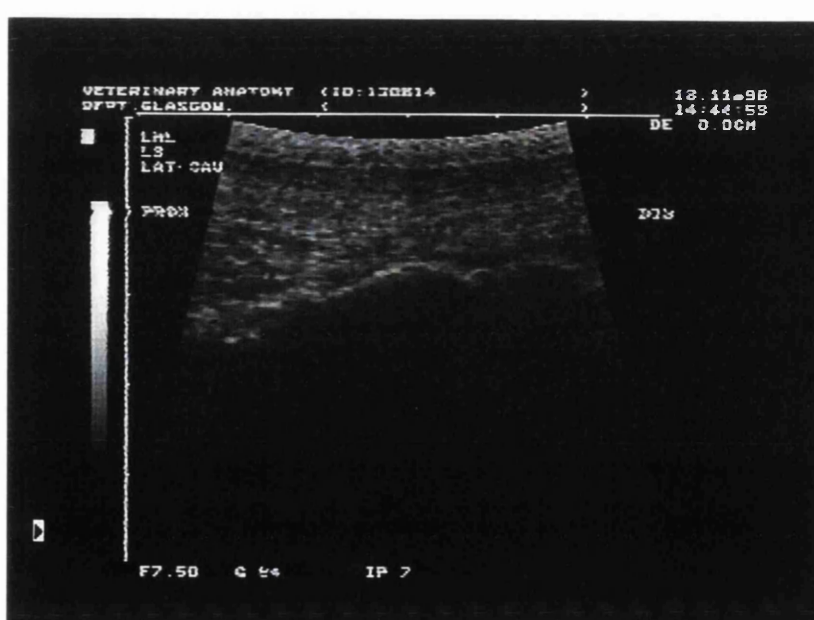

Figure 6.3.20b

Figure 6.3.21 Longitudinal scan from the cranio-lateral aspect of the femur on day 34 post-operation shows the distal third fracture site (arrow head) which has been completely bridged by the bony callus. It appears as a small notch on the bone surface. No fracture gap can be seen on cranio-lateral aspect.

Figure 6.3.22 Transverse scan on the cranial aspect of the femur on day 34 post-operation shows the fracture site which still persists and appears hyperechoic. The fracture site has become smaller than in the previous scans.

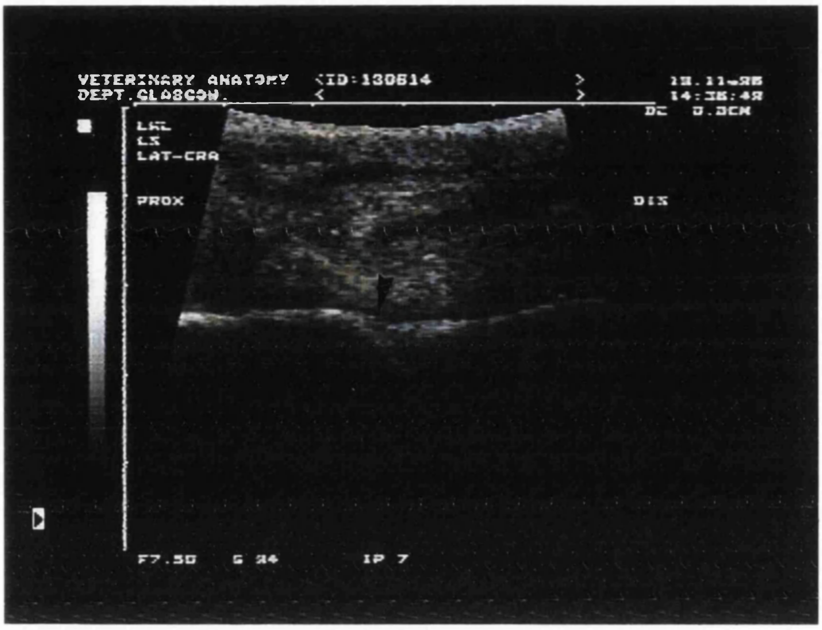

Figure 6.3.21

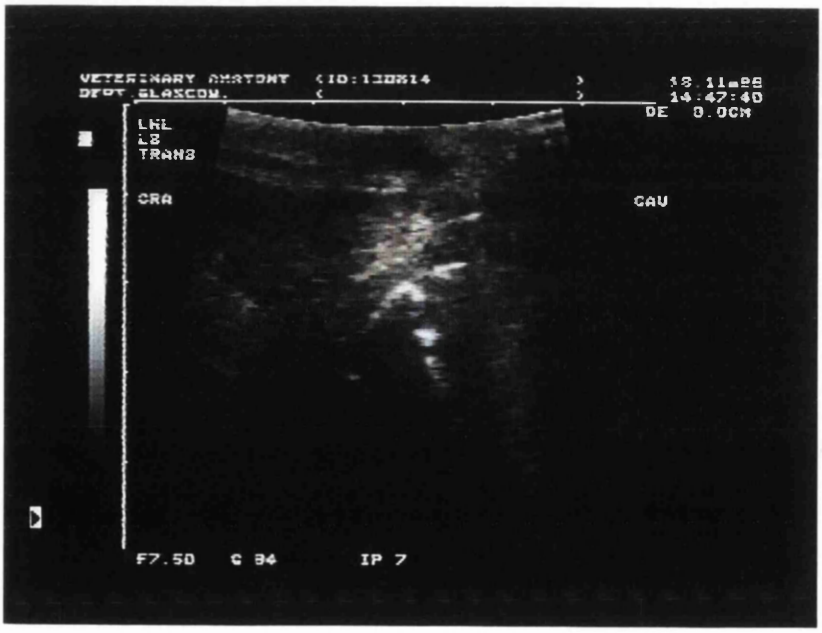

Figure 6.3.22

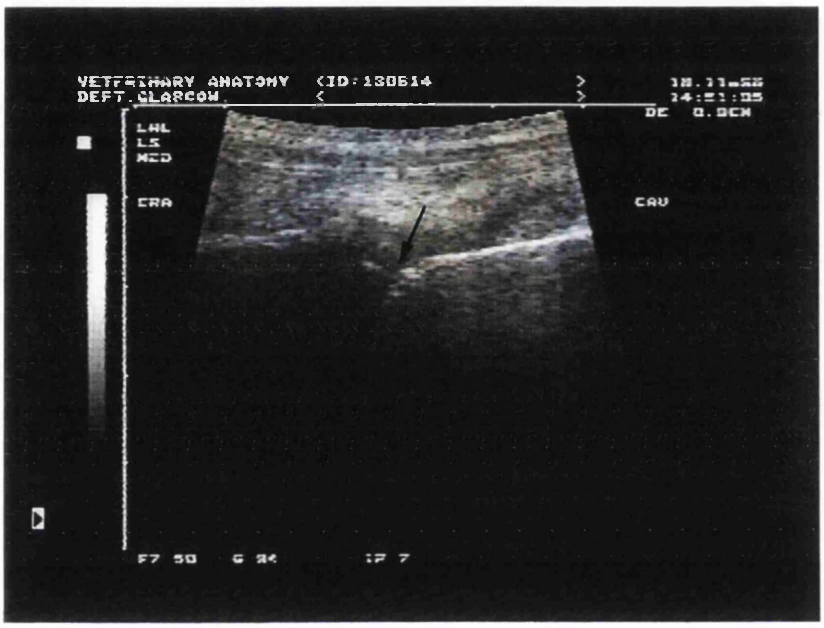

Figure 6.3.23 Longitudinal scan of the femur from the medial aspect on day 34 post-operation demonstrates the fracture gap (arrow) which has become shallow due to the callus formation.

Figure 6.3.24 Transverse scans from the lateral aspect of the femur on day 34 post-operation demonstrate the hyperechoic material (arrow) which casts an acoustic shadow near the mid shaft of the femur (**a**). The structure appears bigger and closer to the femur when the transducer is moved distally (**b**). **F**, femur.

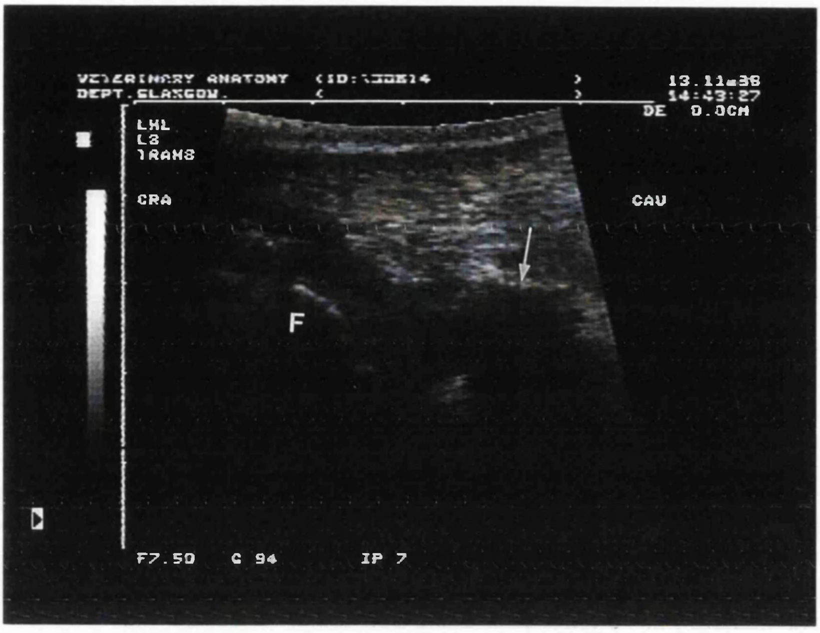

Figure 6.3.24a

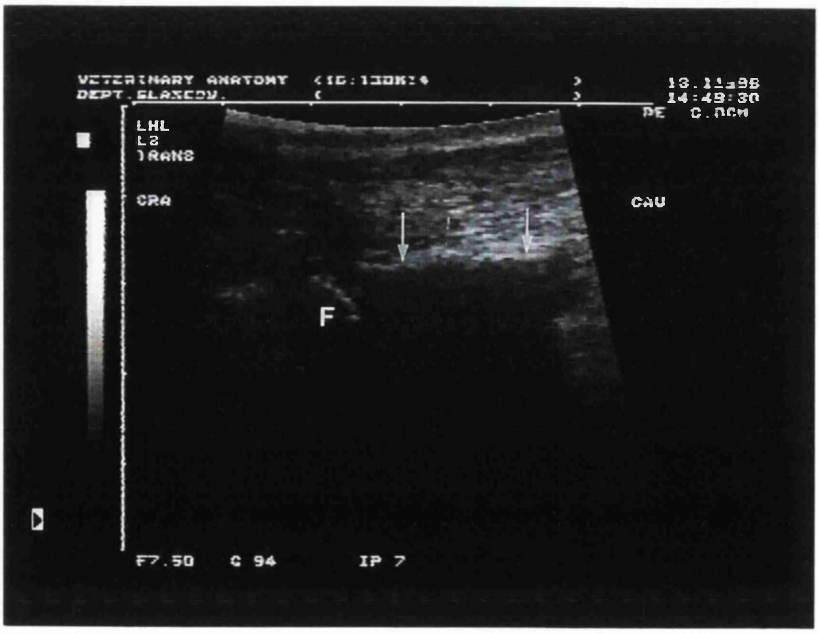

Figure 6.3.24b

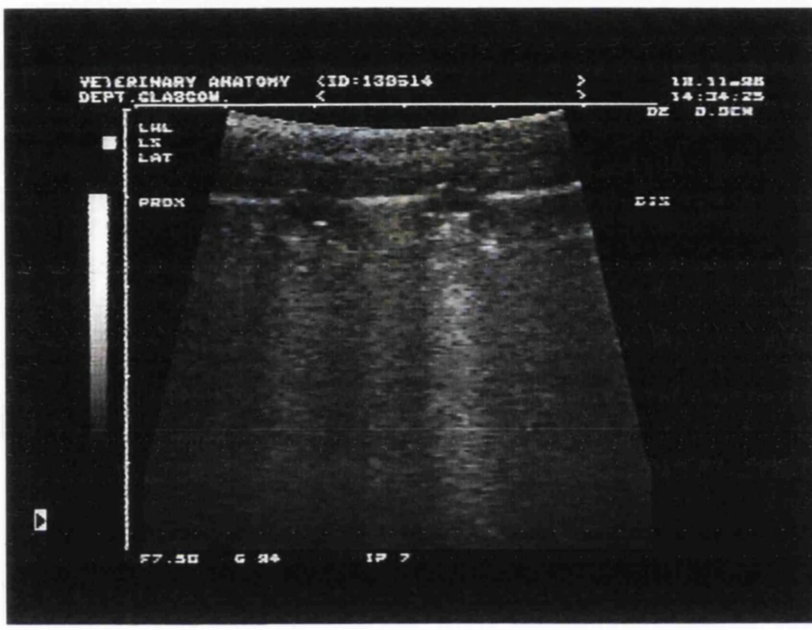

Figure 6.3.25 The bone plate adhering to the femur appears hyperechoic with reverberation artefact while the screws appear hyperechoic and produce comet tail artefacts.

Figure 6.3.26 Radiographs obtained at day 62 after fracture repair. **a**, lateral view, **b**, cranial view. The fracture line is still visible radiographically, and the most proximal screw is coming adrift which indicates the failure of the implant at the proximal end. Callus formation is found at the medial side of the mid-femoral shaft

a

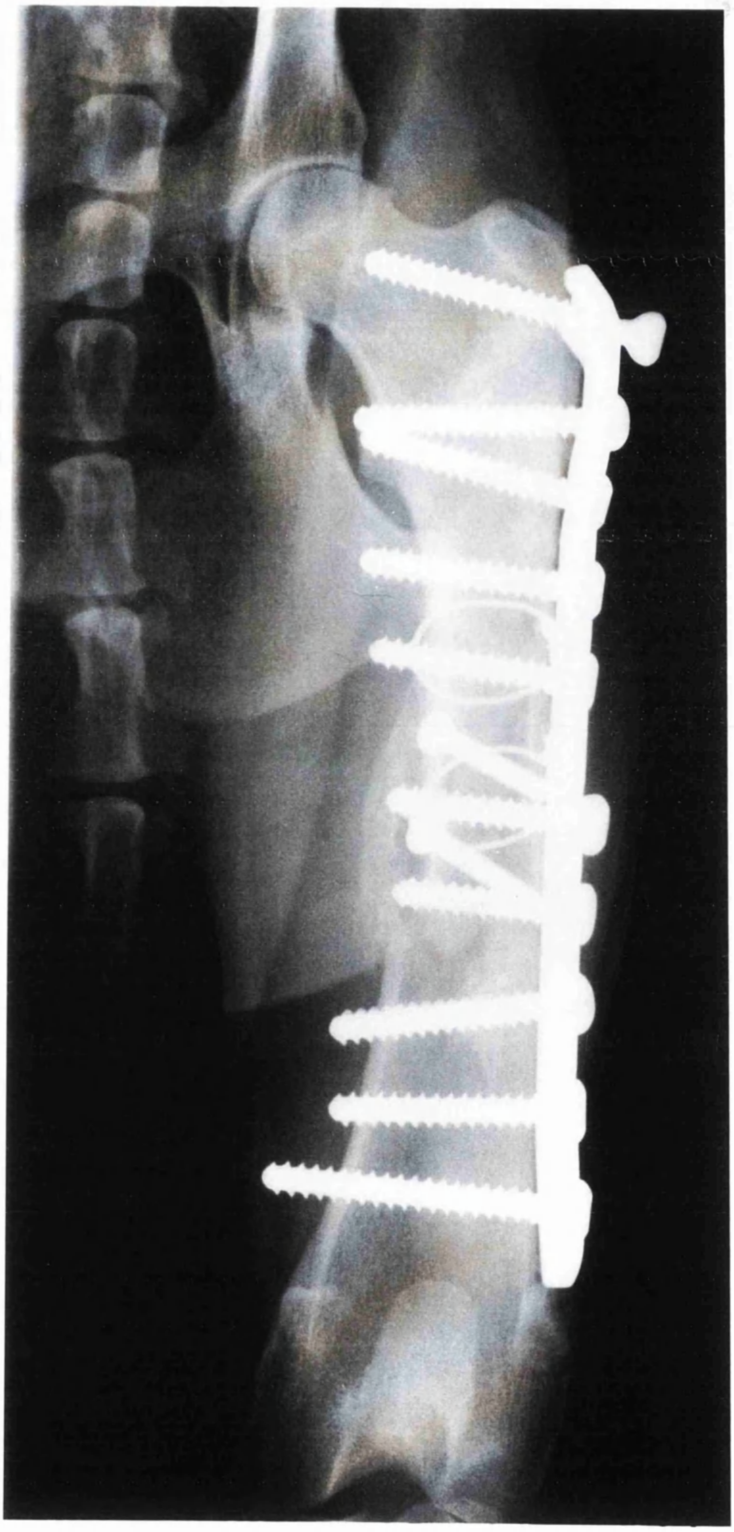

b

Figure 6.3.27 Longitudinal scan of the femur from the medial aspect on day 62 after fracture repair shows the fracture site (arrow head) which can still be recognised as a small notch. The fracture gap has already been bridged by the mature callus.

Figure 6.3.28 Transverse scan at the mid-femur from the medial aspect on day 62 after fracture repair shows the excessive callus formation which appears as a rough and uneven femoral surface.

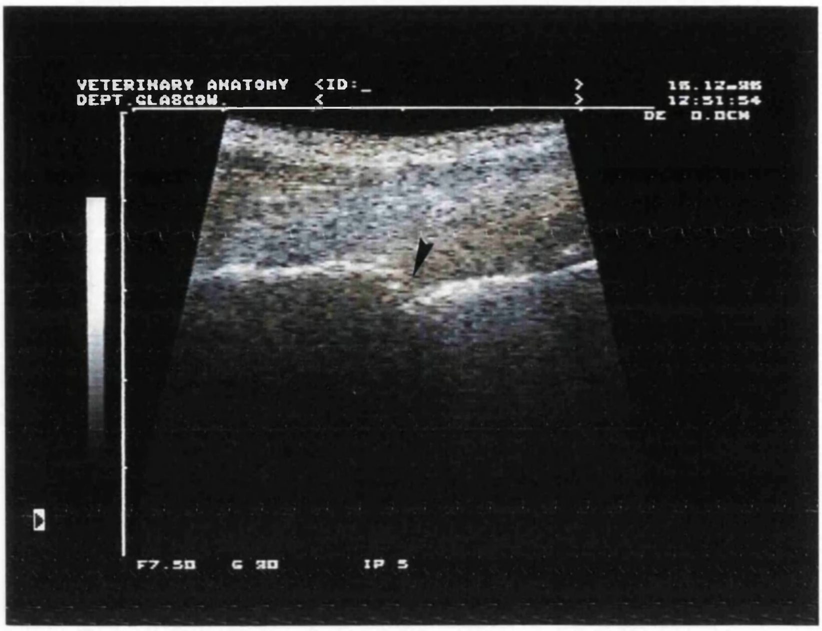

Figure 6.3.27

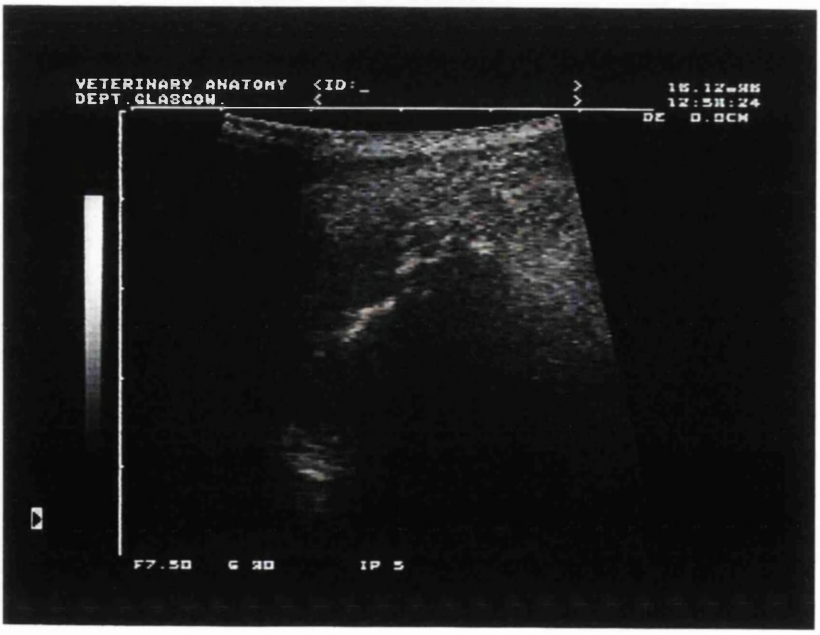

Figure 6.3.28

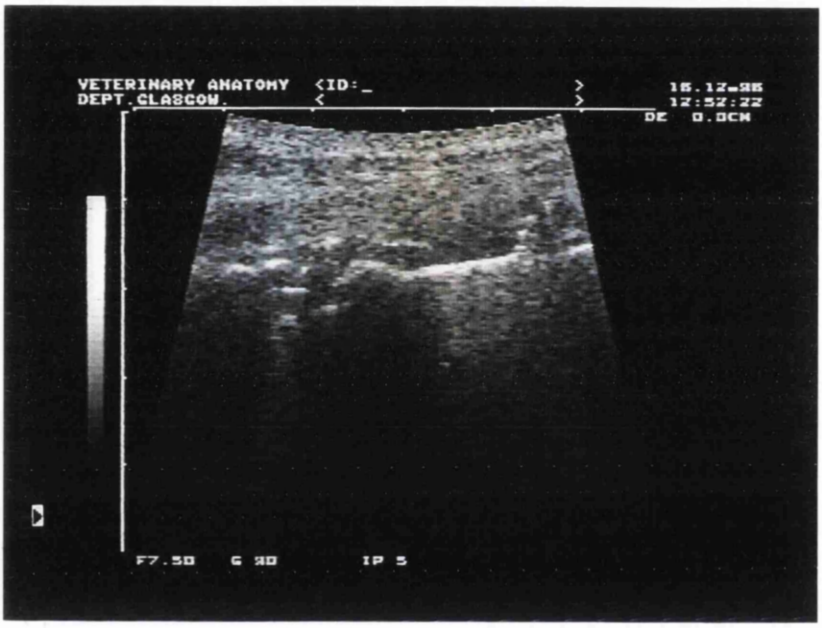

Figure 6.3.29 Longitudinal scan from the medial aspect of the femur on day 62 after fracture repair shows the fracture site area which appears as a disorganised hypoechoic area with a mottled hyperechoic texture suggesting the bony callus formation.

Case 4

A one year old female Doberman, weight 25.5 kg, was admitted to the Glasgow University Veterinary Hospital with severe shock after being involved in a road traffic accident. The animal's mucous membranes was very pale and was given an intravenous (IV) drip of 500 ml of Haemacell and one litre of Hartmans. The animal was not able to walk on its hind legs.

Radiographic examination showed that the right side of the ilium was fractured with severe over-riding and reduction of the pelvic canal diameter (figure 6.4.1). The fracture was comminuted and difficult to reduce. Surgery was performed by a lateral approach to the ilial shaft with the aim of reducing the fracture and increasing the pelvic canal diameter. A skin incision was made along the length of the right ilium. The gluteal muscles were separated and after dissection down to the ilial shaft the gluteals were retracted and the proximal and distal segments were levered together. A Dynamic Compression Plate (DCP) was used in this case. The DCP was applied to the contour of the bone. A successful result was obtained using a 6 holes 2.7 DCP and the pelvic diameter was returned to normal. Three screws were placed on either side of the fracture. To close the wound, vicryl 2.0 was used to close the fascia in a continuous pattern. The subcutaneous tissue was closed in a continuous pattern using vicryl 2.0, and the skin was closed using ethilon 2.0 in a simple interrupted pattern.

Radiographs taken immediately after the fracture repair showed the ilial fracture had been stabilised using a 6 holes DCP and 6 screws (figure 6.4.2). A triangular fracture was present cranioventrally.

Ultrasonographic examination

Day one after fracture repair

Ultrasonographic examination on day one after fracture repair demonstrated the fracture site both on longitudinal and transverse scans. The fracture site appeared as discontinuity of the ilial shaft with the presence of a fracture gap on longitudinal scan (figure 6.4.3a). On transverse scan, the fracture site could be recognised as a defect on the ilial shaft surface which appeared as a hole near to the bone plate (figure 6.4.3b). This could be compared with the normal part of the ilial shaft bone which appeared as a smooth hyperechoic surface (figure 6.4.3c). There was no periosteal tissue reaction detected at this stage. The bone plate and screws adhering to the ilial shaft appeared hyperechoic and produced comet tail artefacts. The area of muscle damage above the ilium appeared as a disorganised hypoechoic structure relative to the surrounding normal muscle (figures 6.4.4a and 6.4.4b). Suture materials within the muscle appeared as intermittent hyperechoic lines with comet tail artefacts (figure 6.4.5).

Day two after fracture repair

Ultrasonographic examination on day two post-operation demonstrated the fracture site which appeared as on the day one examination both on longitudinal and transverse scans (figure 6.4.6a and 6.4.6b). The fracture sites on both planes were clearly seen with no changes detected. The area of muscle damage above the ilial shaft still persisted and appeared as a disorganised hypoechoic structure. The haematoma above the ilial bone surface appeared homogenously hypoechoic (figure 6.4.7). The bone plate and screws appeared as an intermittent hyperechoic line and produced comet tail artefacts (figure 6.4.8). Suture materials within the muscle appeared as intermittent hyperechoic lines with comet tail artefacts as seen on the day one examination.

Day 40 (6 weeks) after fracture repair

Radiographic examination

Radiographs taken at day 40 after fracture repair showed that the fracture site had healed satisfactorily (figure 6.4.9). The callus formation had bridged the fracture gap. There was no indication of implant loosening. The plate was in place and was secure.

Ultrasonographic examination

Ultrasonographic examination demonstrated the excessive callus formation on the ilial shaft (figure 6.4.10). The fracture site could not be detected at this stage largely due to the excessive callus formation at the fracture site area which resulted in a bulging and uneven surface of the ilial shaft. The muscle structure has returned to its normal ultrasonographic appearance. The bone plate was still in placed and appeared hyperechoic with reverberation artefact (figure 6.4.11). Ultrasonographically, the fracture site appeared to have healed satisfactorily.

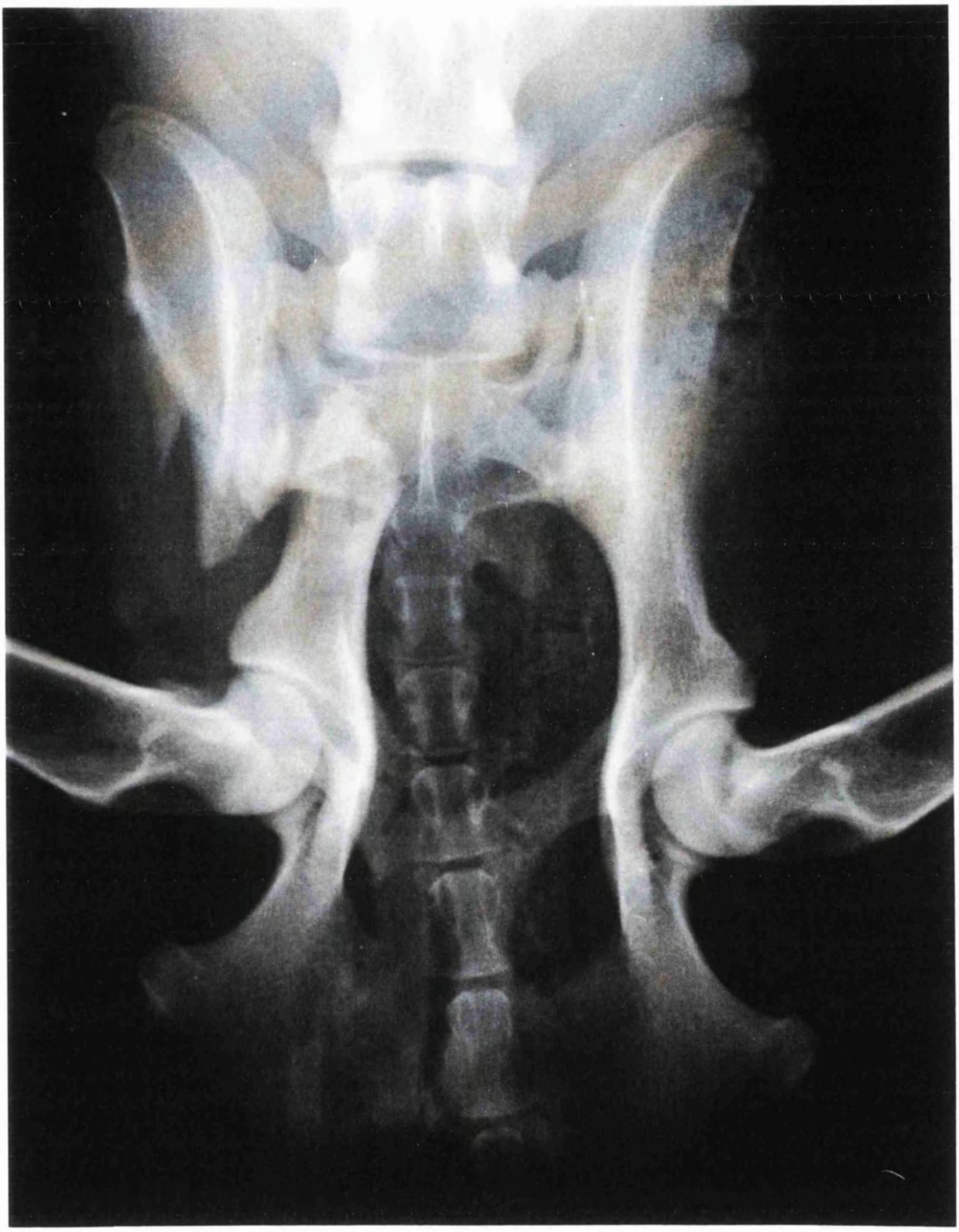

Figure 6.4.1 Radiograph of the one year old Doberman having a comminuted pelvic fracture involving the pubis, ilium and ischium. There is some medial displacement of the caudal part of the ilium. This animal was also suffering from pneumothorax and pneumomediastinum.

Figure 6.4.2 Radiographs obtained immediately after fracture repair. **a**, lateral view, **b**, ventral view. The ilial shaft fracture has been stabilised using a six hole plate and screws. The fracture line is clearly visible. A triangular fragment is present cranioventrally in **b**.

b

Figure 6.4.3 Ultrasonographic images of the shaft of ilium 24 hours post-operation demonstrate the fracture site. **a**, longitudinal scan **b**, transverse scan, **c**, transverse scan of the normal part of ilium. The fracture site appears as discontinuity of the bone surface with the presence of the fracture gap in **a**. The fracture site appears as a hole on the ilial shaft surface near to the bone plate in **b**. Note also the bone plate which is adhering to the bone appears hyperechoic with reverberation artefact in **b**. The normal part of the ilum appears as a smooth hyperechoic surface in **c**.

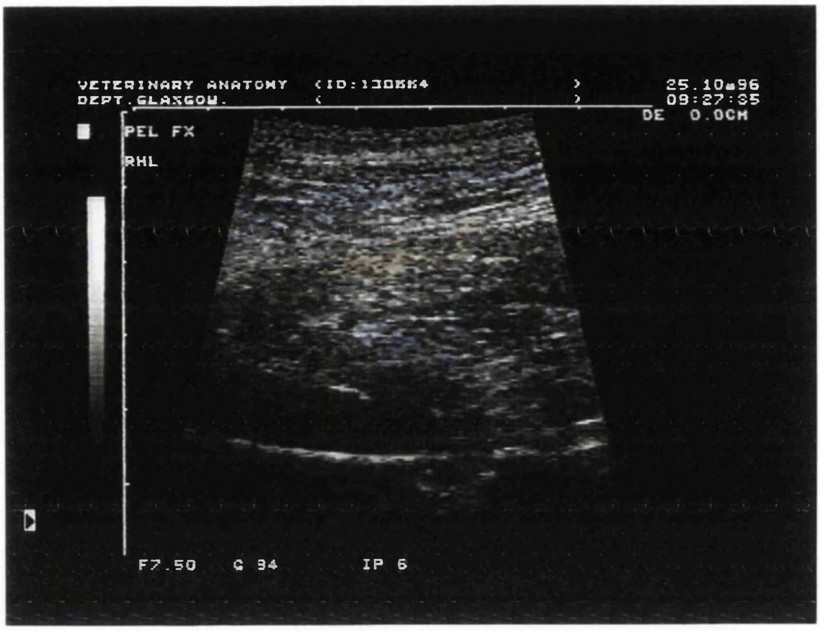

Figure 6.4.3a

Figure 6.4.3b

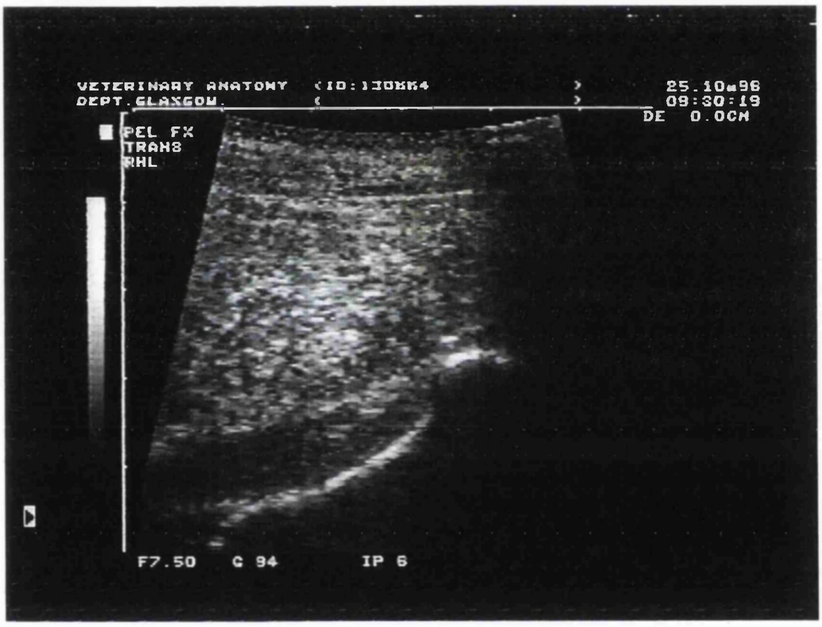
VETERINARY ANATOMY
DEPT. GLASGOW.
25.10.96
09:30:19
DE 0.0CM
PEL FX
TRANS
RHL
F7.50
G 94
IP 6

Figure 6.4.3c

Figure 6.4.4 The area of muscle damage imaged ultrasonographically 24 hours after fracture repair appears as a disorganised hypoechoic structure (arrow) both on longitudinal (**a**) and transverse (**b**) scans. Note also the fracture site with the presence of a gap on both images which appears as discontinuity of the bone.

Figure 6.4.4a

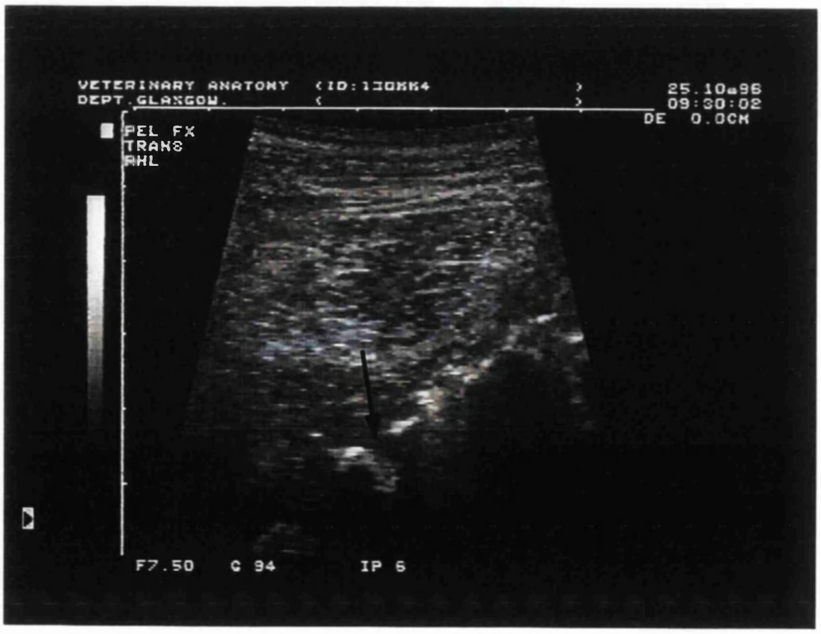

Figure 6.4.4b

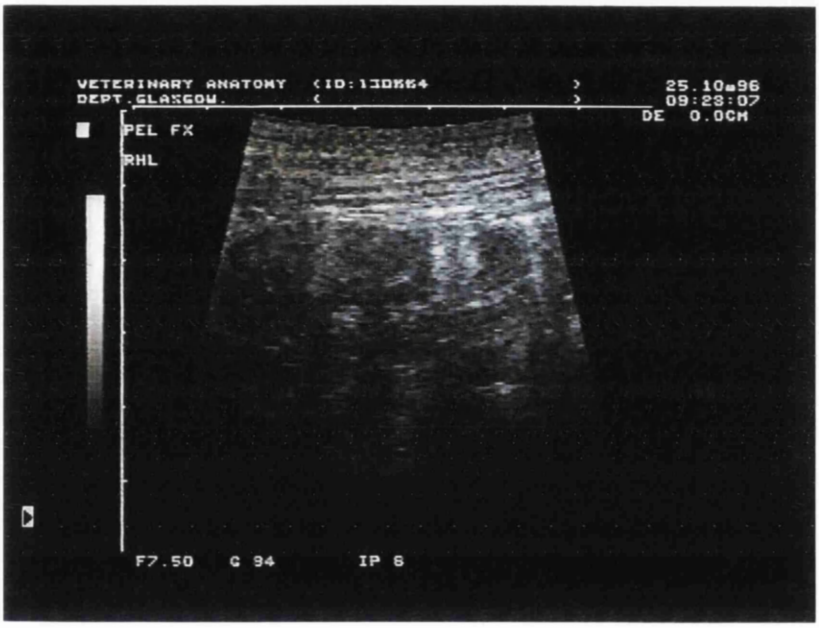

Figure 6.4.5 Suture materials within the muscle imaged ultrasonographically 24 hours after fracture repair appear hyperechoic with comet tail artefacts.

Figure 6.4.6 The fracture site imaged on day two after fracture repair both on longitudinal (**a**) and transverse (**b**) scans appears similar to the day one examination. The fracture site is clearly seen with no changes detected. The area of muscle damage still persists and appears as a disorganised hypoechoic structure.

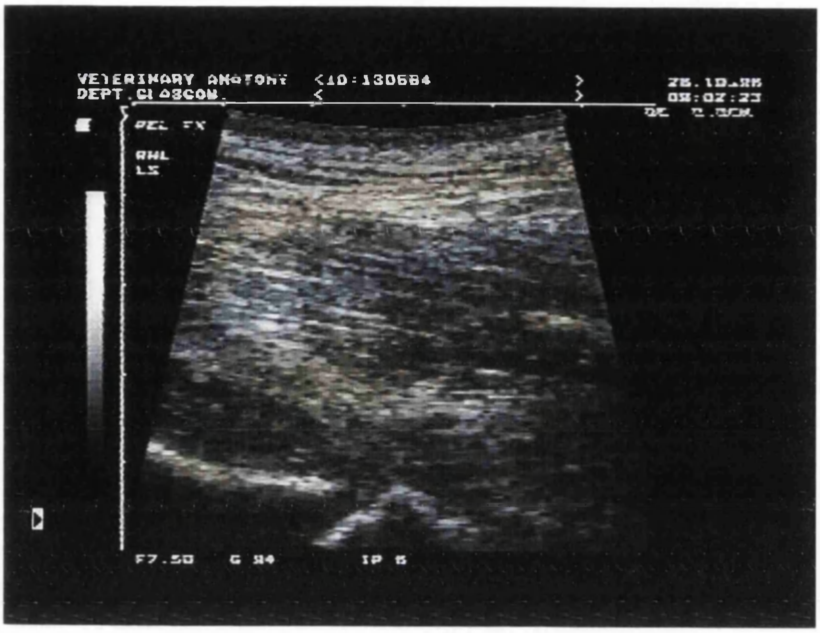

Figure 6.4.6a

Figure 6.4.6b

Figure 6.4.7 Longitudinal scan on the ilial shaft on day two after fracture repair shows the haematoma area which appears homogenous hypoechoic above the ilial bone.

Figure 6.4.8 The bone plate with screws attached to the ilium appears as an intermittent hyperechoic line with comet tail artefacts on longitudinal scan. Note also the area of muscle damage appears as a disorganised hypoechoic structure.

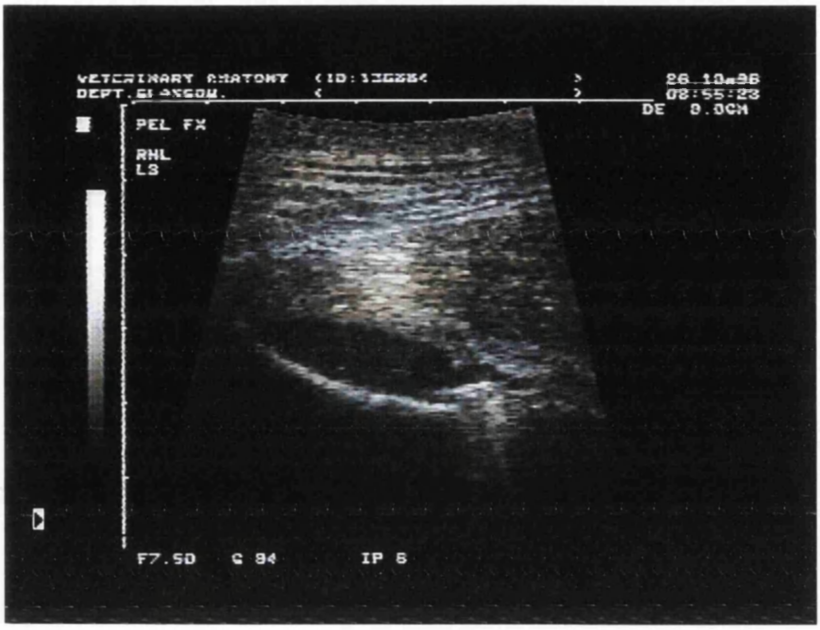

Figure 6.4.7

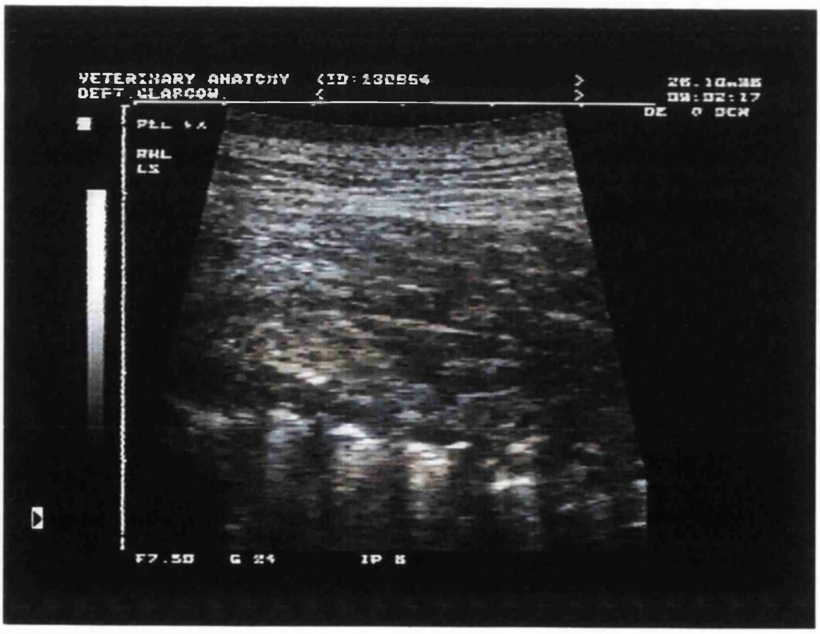

Figure 6.4.8

Figure 6.4.9 Radiographs taken at day 40 after fracture repair show that the fracture site is satisfactorily healed. **a**, lateral view, **b**, ventro-dorsal view. Callus formation is bridging the fracture gap. There is no indication of implant loosening. The plate is in place and secure.

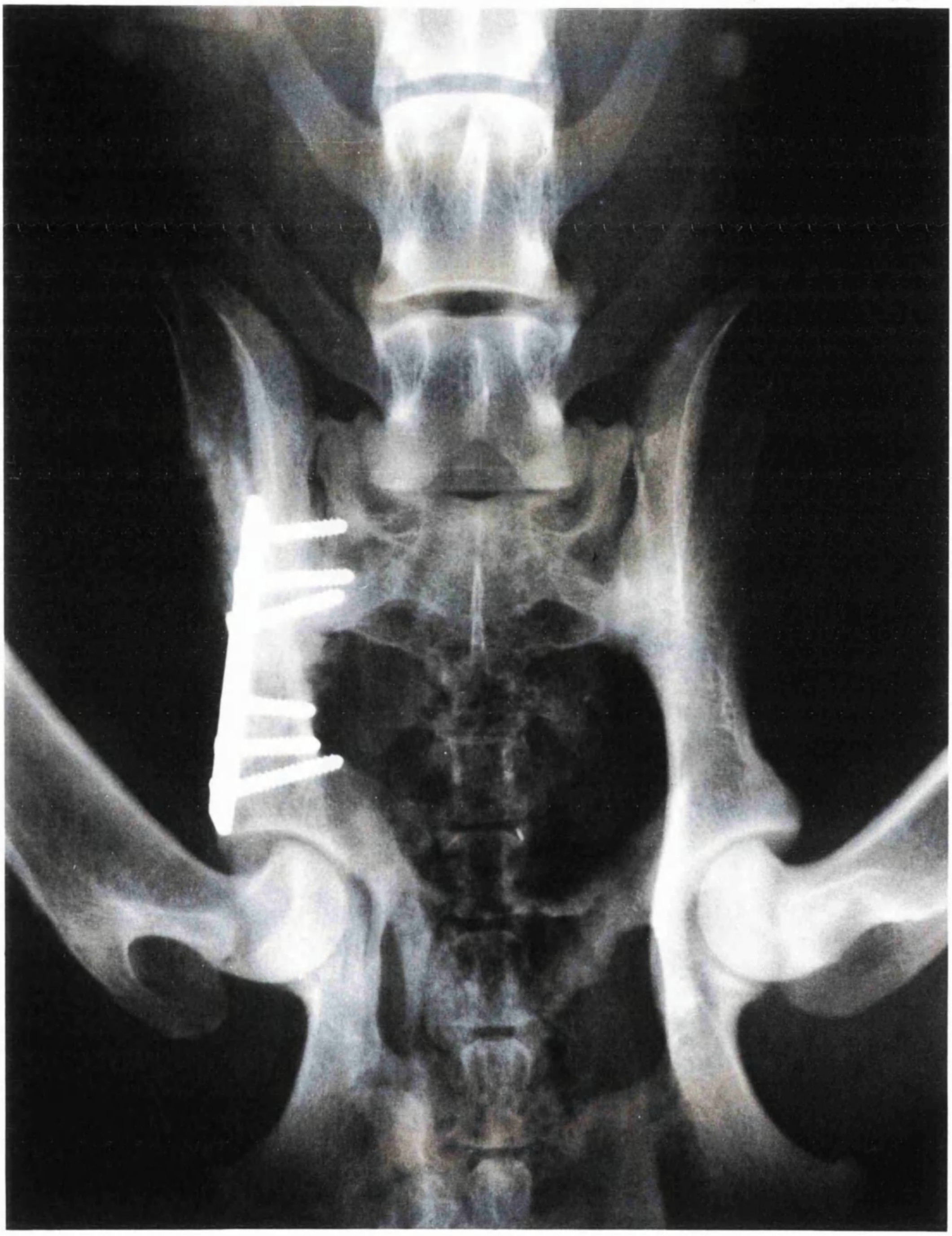

b

Figure 6.4.10 Longitudinal scan of the shaft of ilium on day 40 after fracture repair demonstrates the excessive callus formation which appears hyperechoic with a rough and uneven surface of the ilium. The actual fracture site has already been bridged by the mature callus and can no longer be detected largely due to the excessive callus formation at the fracture site area. The acoustic shadowing appearing in the image is due to air trapped in the hair on the skin surface.

Figure 6.4.11 Longitudinal scan of the shaft of ilium on day 40 after fracture repair shows the bone plate (arrow heads) which appears hyperechoic with reverberation artefact.

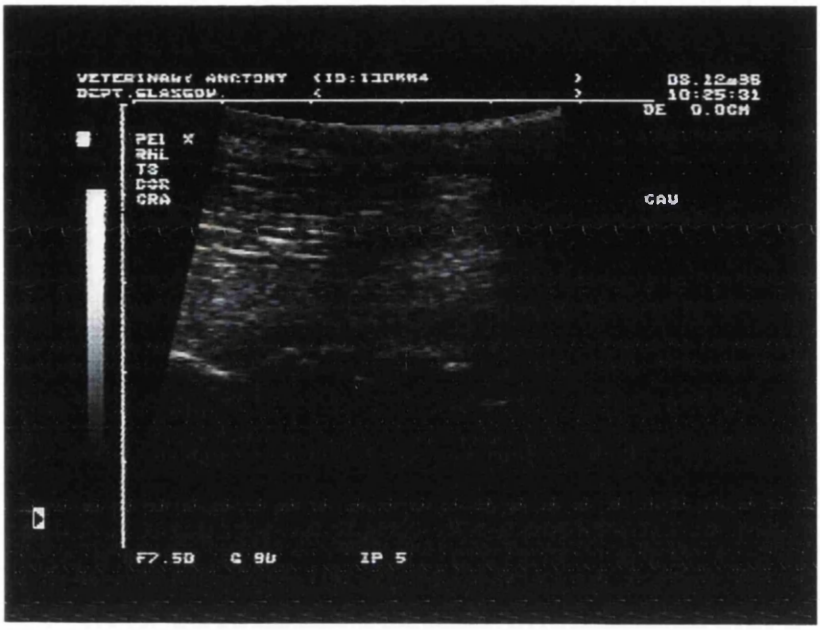

Figure 6.4.10

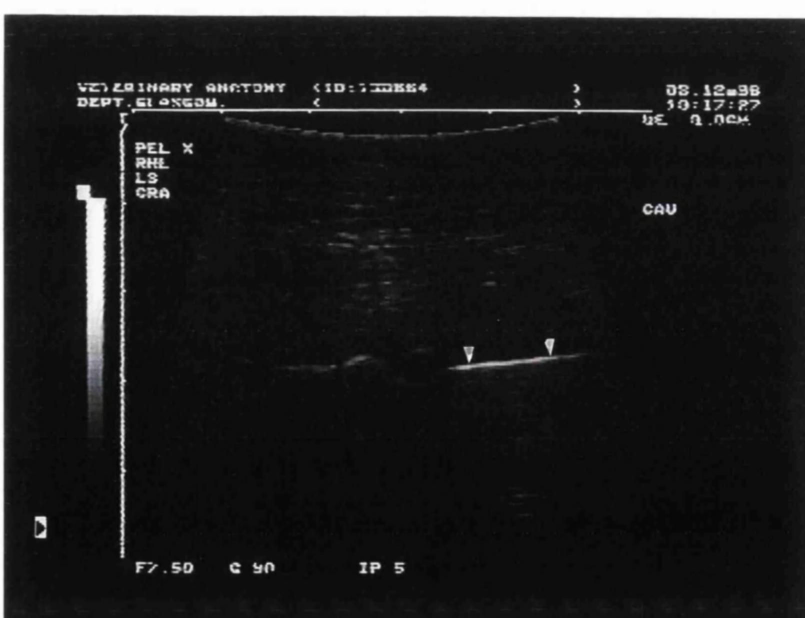

Figure 6.4.11

Case 5

A three year old male, Border Collie, weighing 18.5 kg was presented for assessment of a right femoral shaft fracture. The fracture repair had been carried out approximately seven and a half months previously. Radiographic examination at approximately seven and a half months after fracture repair showed the femoral fracture which was completely healed (figure 6.5.1). There was no fracture site to be seen on the radiographs. The femur had returned to its normal structure and clinically the affected leg can be considered to be normal. The bone plate was removed after the radiographic examination through a lateral approach. In day one after implant removal the dog started using the limb. There was good improvement and the dog was not lame while walking. Ultrasonographic examination was carried out a day before implant removal and at day two after implant removal.

Ultrasonographic examination

Approximately seven and half months after fracture repair (a day before implant removal)

Ultrasonographic examination at seven and half months post-operation (prior to implant removal) demonstrated the smooth hyperechoic bone surface (figure 6.5.2). The fracture could not be recognised anymore and the bone had returned to its normal ultrasonographic appearance. The bone plate and screws that attached to the femur appeared hyperechoic with reverberation and comet tail artefacts respectively (figure 6.5.3a and 6.5.3b). A longitudinal scan from lateral aspect revealed that the screws at the proximal part of the plate appeared higher than the plate level (figure 6.5.3a), and that the screws at the distal part of the plate appeared almost at the same level as the bone plate (figure 6.5.3b). This was actually due to the fact that the screws used at the proximal part of the plate (from second to fourth holes) were larger (45 mm) than the distal ones (35 mm) as shown on the radiograph (figure 6.5.1). The femur appeared smooth with a rounded surface on transverse scan (figure 6.5.4). The plate was seen adherent to the surface. The callus had become smooth at this stage due to the remodelling process. There was also an hyperechoic area detected within the muscle nearby the femur when imaged from the lateral aspect both on transverse and longitudinal scans which suggested an area of muscle atrophy.

Day two after implant removal

Ultrasonographic examination demonstrated the femur which appeared as an hyperechoic straight line with the presence of holes in it (figure 6.5.5). The holes on the femur were actually the previous sites of the screws before the implant was removed. The hyperechoic appearance around and within the holes suggested periosteal tissue reaction. Some soft callus formation was detected and appeared as an hyperechoic structure on the bone surface. Suture materials within the muscle appeared as intermittent hyperechoic lines with comet tail artefacts (figure 6.5.6). The area of muscle damage appeared as a disorganised hypoechoic area relative to the surrounding normal appearance of muscle. A transverse scan of the femur in this case did not produce much additional information. However, the hole on the femoral surface could be seen as a small notch (figure 6.5.7) The area of muscle damage appeared hypoechoic relative to the surrounding tissue. The muscle near the femur appeared hyperechoic suggested an area of muscle atrophy. Clinically, the animal was showing good use of the affected limb and the implant removal was successful.

Figure 6.5.1 Radiographs obtained at approximately seven and a half months after fracture repair. **a**, lateral view and **b**, cranial view. The femur has become smooth and the fracture line is no longer visible. There is no evidence of implant instability and cortical remodelling is occurring. The screws in the proximal plate from the second to the fourth holes are larger (45 mm) than the distal ones (35 mm) (**b**).

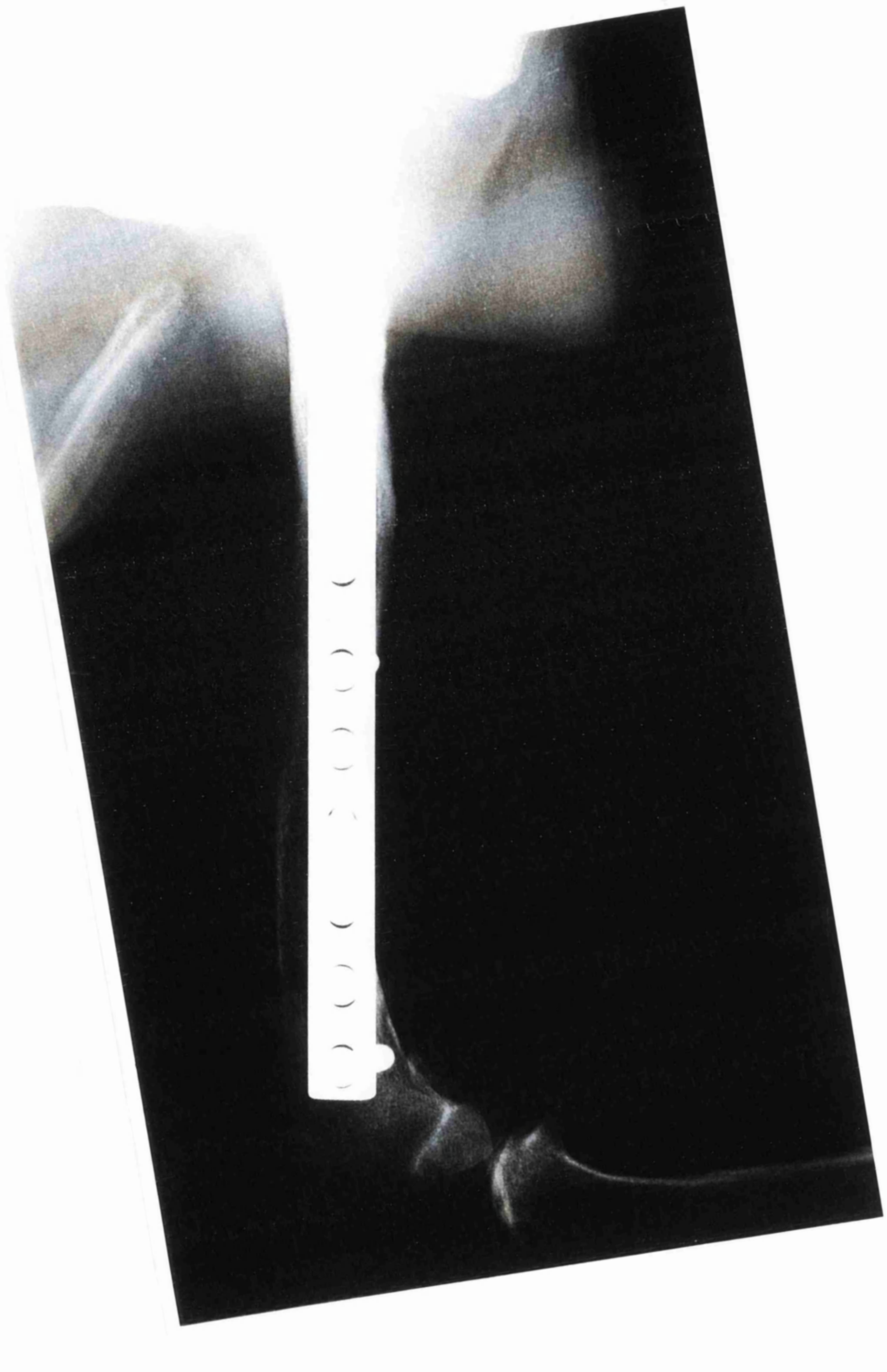

a

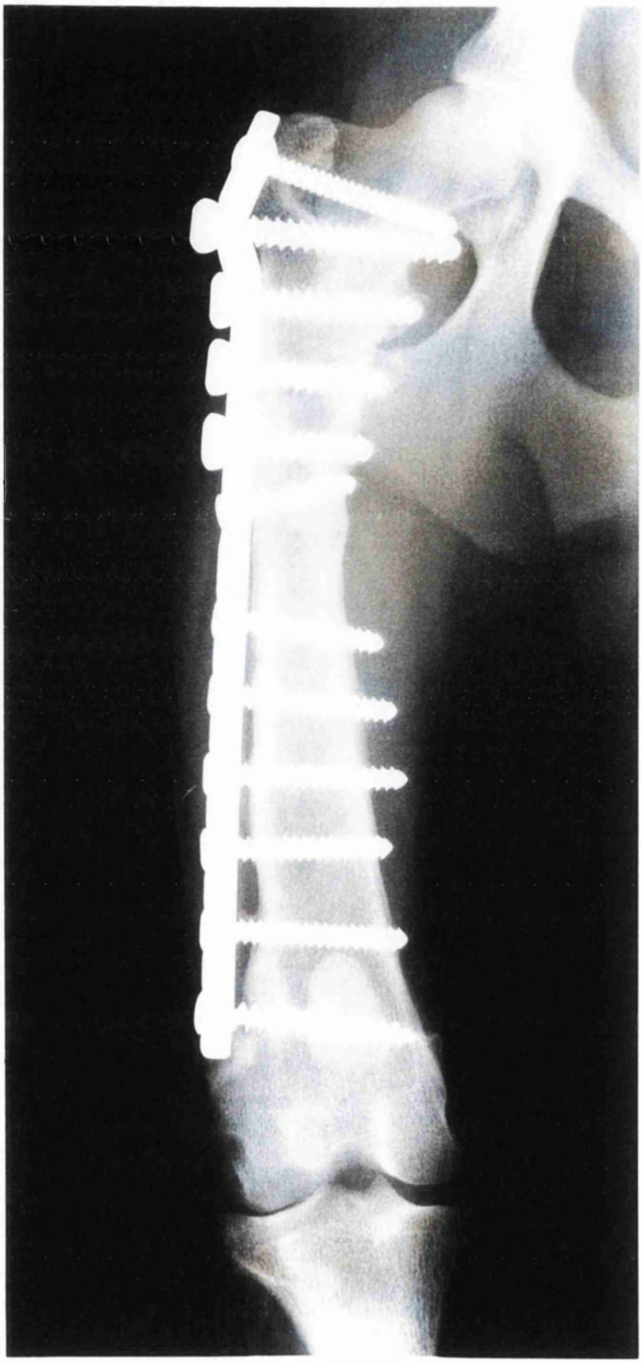

b

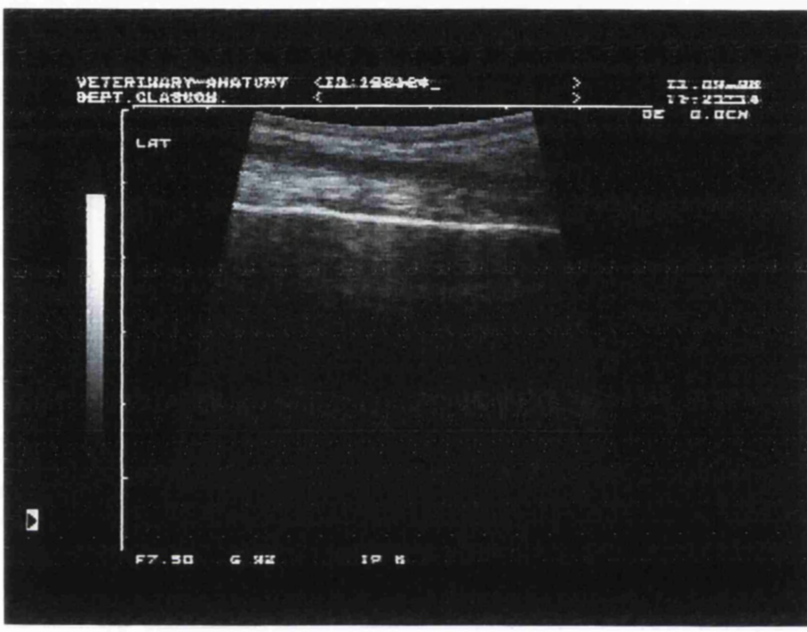

Figure 6.5.2 Longitudinal scan of the femur at approximately seven and a half months after fracture repair demonstrates the smooth hyperechoic bone surface. The fracture site is undetectable.

Figure 6.5.3 Longitudinal scans of the femur from the lateral aspect one day before implant removal demonstrate the bone plate with screws. **a**, proximal part, **b**, distal part. Both are hyperechoic but the bone plate produces reverberation artefact while the screws produce comet tail artefacts. The screws at the proximal part appear higher than the plate level (**a**), and appear almost the same level with the plate (**b**). This is because the screws used at the proximal part of the plate (from hole two to hole four) are larger than at the distal one.

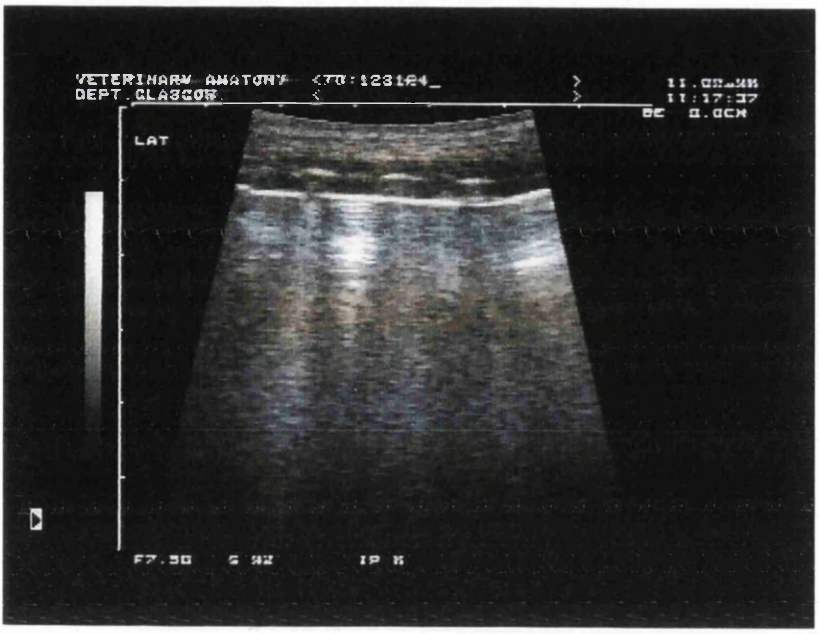

Figure 6.5.3a

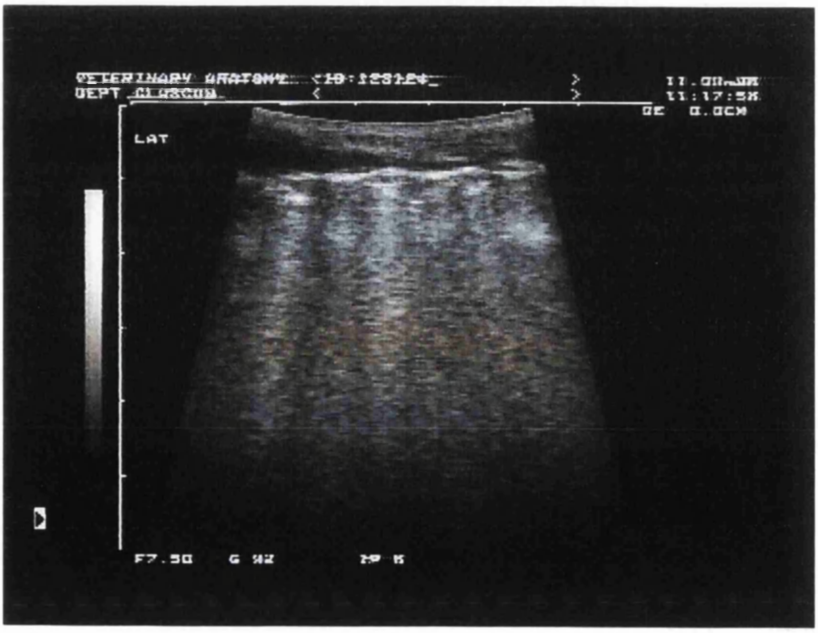

Figure 6.5.3b

Figure 6.5.4 Transverse scan of the femur from the cranio-lateral aspect one day before implant removal shows a round, smooth hyperechoic femoral surface with the bone plate on the lateral side (arrow). Note also the hyperechoic area of muscle beside the femur which suggests an area of muscle atrophy. There are hypoechoic areas in the muscle as well.

Figure 6.5.5 Longitudinal scan of the femur from the caudo-lateral aspect on day two after implant removal shows the femoral surface with a number of holes in it. These holes actually represent the site of the screws before the implant was removed. The holes and the surrounding area appear hyperechoic which suggests periosteal reaction. Some soft callus formation can be seen as an hyperechoic structure on the bone surface (arrow).

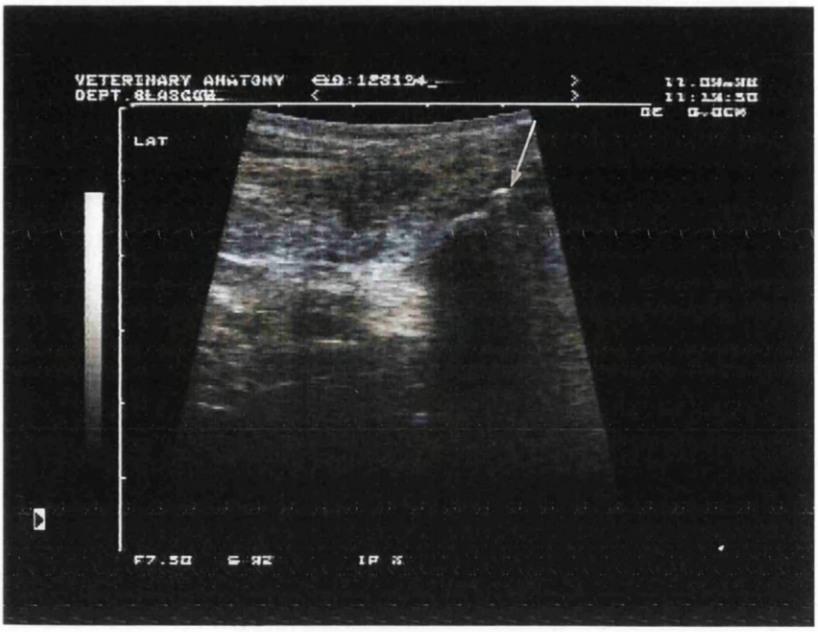

Figure 6.5.4

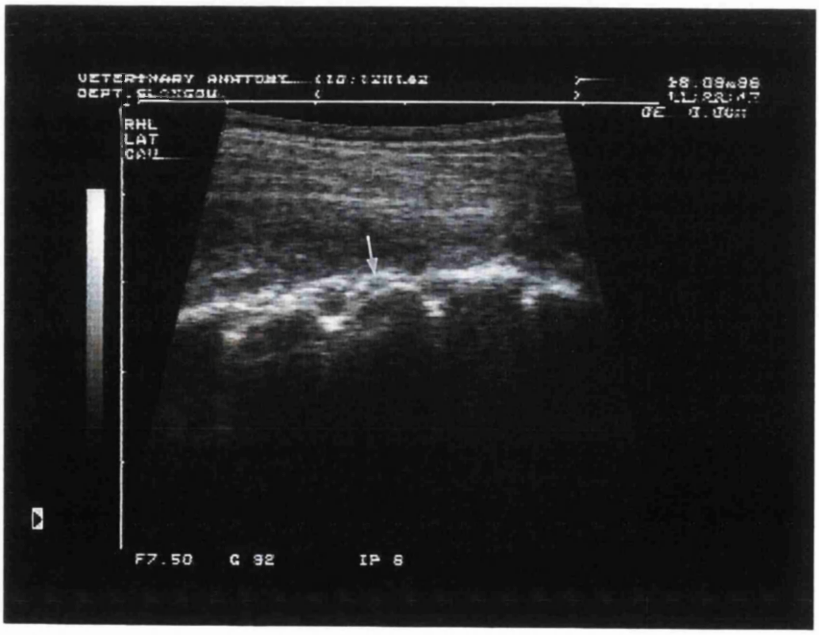

Figure 6.5.5

Figure 6.5.6 Suture material within the muscle imaged on day two after implant removal appears as hyperechoic intermittent lines with comet tail artefacts. Note also the area of muscle damage appearing as a disorganised hypoechoic structure.

Figure 6.5.7 Transverse scan from the caudo-lateral aspect of the femur on day two after implant removal shows the femur with a small hole on its surface. The area of muscle damage above the femur appears as a disorganised hypoechoic structure. The hyperechoic appearance of the muscle (semitendinosus) beside the femur suggests an area of muscle atrophy (arrow heads).

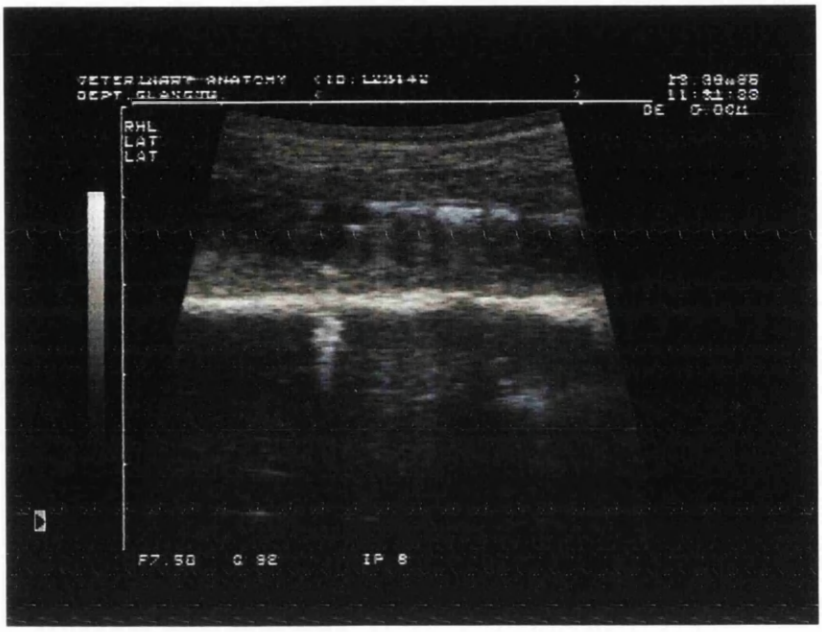

Figure 6.5.6

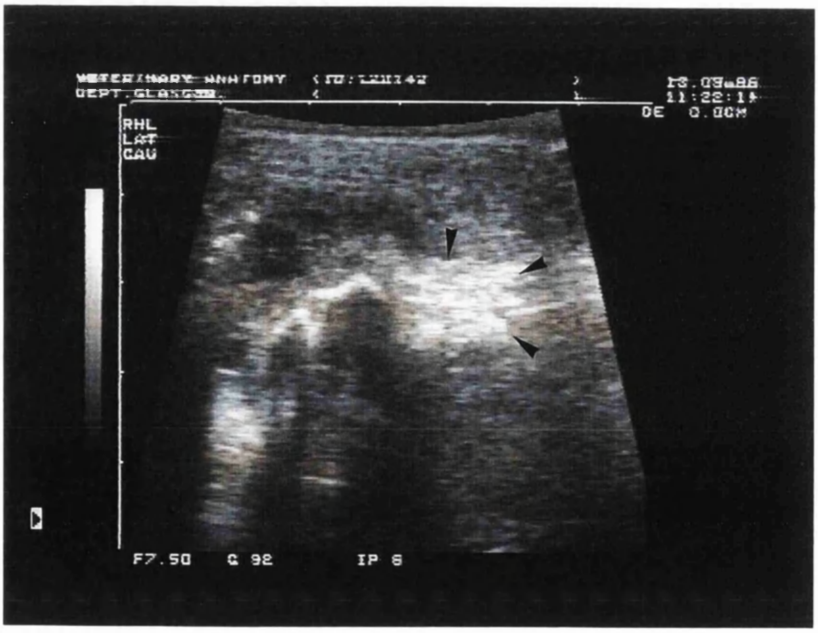

Figure 6.5.7

Case 6

A one year old cross breed dog, weight 31.0 kg, was presented to the Glasgow University Veterinary Hospital for management of a transverse fracture of the distal third of right humerus after having been involved in a road traffic accident. Clinical examination revealed tachypnea and excessive panting. Radiographic examination of the thoracic identified a significant pneomothorax. Radiographs of the right forelimb obtained before the repair process was carried out demonstrated that a transverse fracture of the distal third of the right humerus had been sustained (figure 6.6.1). Radiographs taken after fracture reduction showed the fracture fragments have been stabilised with an intramedullary pin and tied in to a five pins lateral type I ESF (figure 6.6.2). The fracture repair resulted in a reasonable reduction with the humerus being slightly misaligned at the fracture site.

Ultrasonographic examination

Day one after fracture repair

Ultrasonographic examination of the humeral fracture demonstrated the fracture site which was not well aligned (figure 6.6.3). The distal fragment appeared elevated compared to the proximal fragment. During scanning, the transducer was carefully adjusted to image the fracture site. There was no fracture gap present at the fracture site. The area of muscle damage scanned longitudinally appeared as a disorganised hypoechoic region relative to the surrounding normal muscle structure (figure 6.6.4). Fluid accumulation within the muscle which had resulted from surgical interference appeared anechoic. A transverse scan of the humerus demonstrated an hyperechoic image surrounding the fracture site which suggested an area of periosteal and soft tissue reaction (figure 6.6.5). On transverse scan the humerus has lost its normal rounded appearance at the area of the fracture site. The area of muscle damage appeared as disorganised with a mixture of hypoechoic and hyperechoic structures superficial to the humerus. Longitudinal image of the brachial muscles showed the normal ultrasonographic appearance of the triceps muscle which produced a "feather-like" appearance (figure 6.6.6).

Day 44 (6 weeks) after fracture repair

Radiographic examination

Radiographs taken at day 44 after fracture repair showed that the callus formation had bridged the fracture site and the periosteal reaction had stimulated new bone that was already showing evidence of remodelling (figure 6.6.7). However, the fracture line was still visible radiographically.

Ultrasonographic examination

Ultrasonographic examination demonstrated the fracture site which had been bridged by the bony callus (figure 6.6.8a). No excessive callus formation was found on the humerus. The humerus appeared as a smooth hyperechoic bone surface with a small notch and a slight bend of the bone at the fracture site on longitudinal scan from the caudo-lateral aspect. The fracture site scanned from the medial aspect appeared as a small notch on the hyperechoic humeral surface (figure 6.6.8b). On the lateral aspect, the proximal fragment appeared elevated from the distal fragment. The area of muscle damage had returned to its normal ultrasonographic appearance.

Day 73 (10 weeks) after fracture repair

Radiographic examination

Radiographs taken at day 73 after fracture repair showed that the fracture line has been completely bridged by the new bone tissue (figure 6.6.9). Thus, the fracture line was no longer visible. There was a mild lysis around some of the pins. The healing process had not resulted in a straight bone because of the early defect at the fracture site which resulted during the repair process. However, the fracture was completely healed. The intramedullary pin and external fixator were removed at this time.

Ultrasonographic examination

Ultrasonographic examination demonstrated a smooth surface of the humerus both on longitudinal and transverse scans (figure 6.6.10a and 6.6.10b) suggesting a successful remodelling process. The humeral surface appeared smoother than on the day 44 examination. The humerus appeared slightly bent at the fracture site area on longitudinal scan from the lateral aspect. The muscle structure appeared to have a normal ultrasonographic characteristic. The fractured bone had healed satisfactorily.

Figure 6.6.1 Radiograph of the one year old Cross bred dog with transverse fracture of the distal third of the right humerus. This is a complete closed fracture of the humerus.

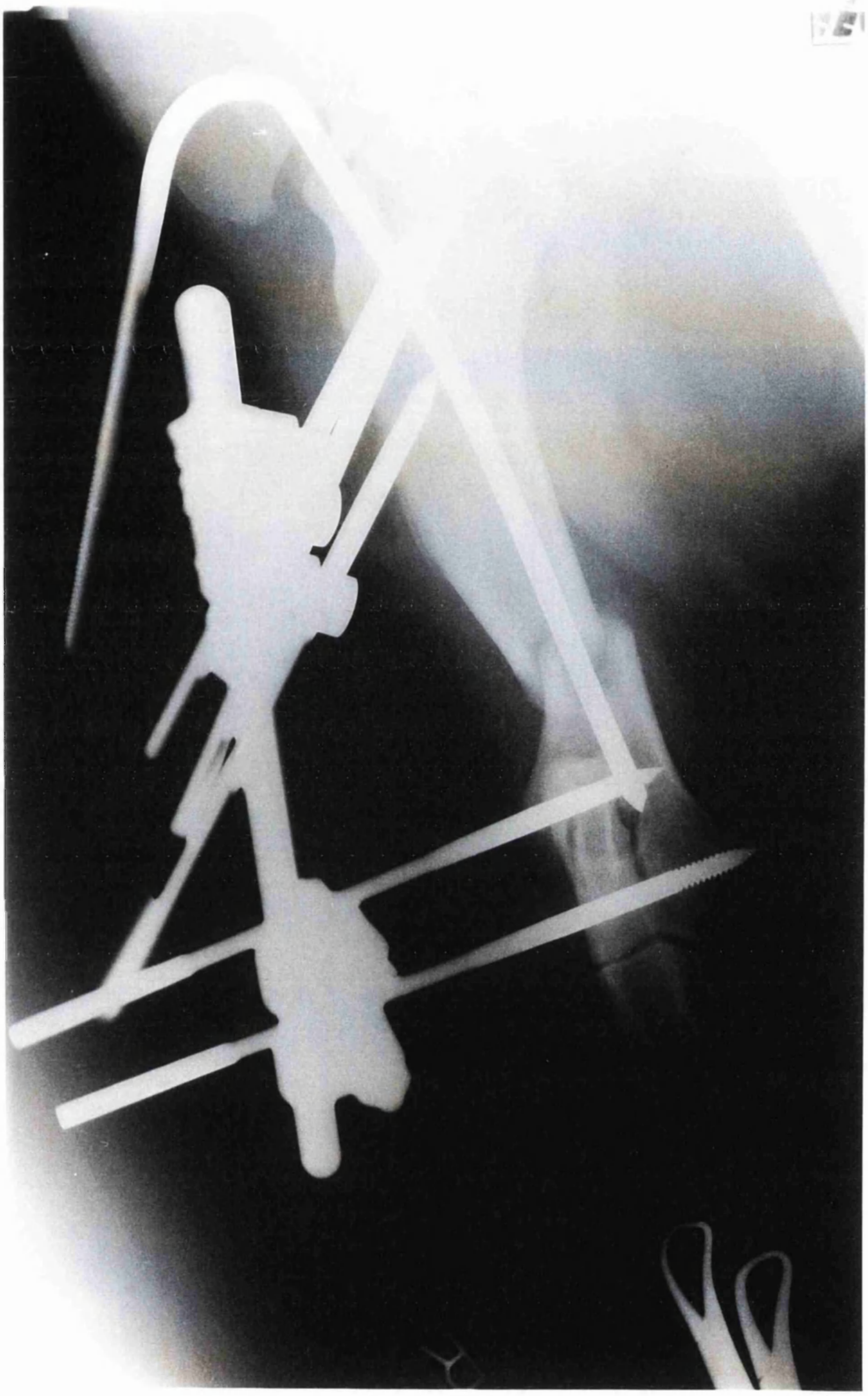

Figure 6.6.2 Radiograph obtained immediately after fracture repair shows the fracture has been stabilised with an intramedullary pin and tied in to a five pins lateral type I ESF. The repair process is resulting in reasonable reduction with the humerus only slightly misaligned at the fracture site.

Figure 6.6.3 Longitudinal scan of the humerus from the cranial aspect 24 hours after fracture repair shows the fracture site which appears as if there are two levels of bone. The proximal and distal fragments are not well aligned. Note that the distal fragment (large arrow head) appears elevated compared to the proximal fragment (small arrow head).

Figure 6.6.4 The area of muscle damage imaged ultrasonographically 24 hours after fracture repair appears as disorganised hypoechoic area as compared to the normal muscular regions.

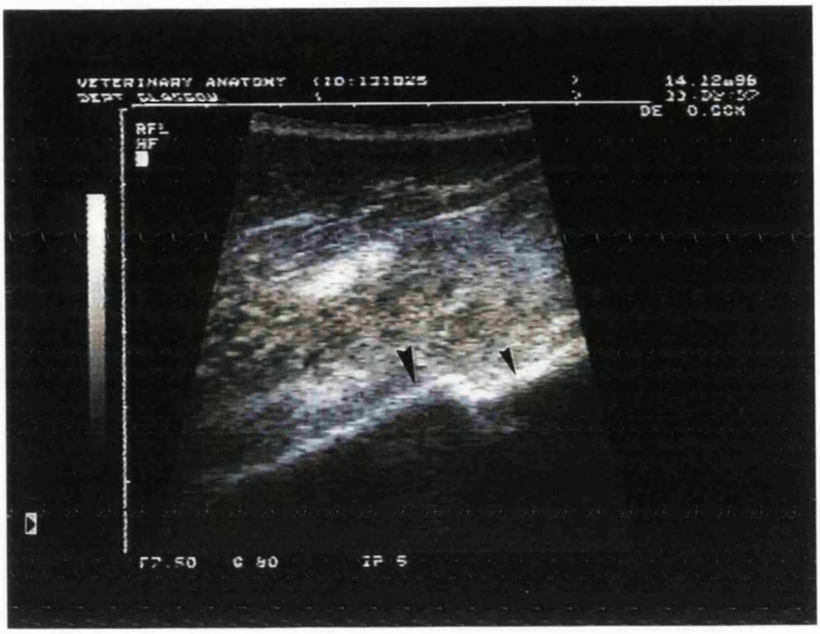

Figure 6.6.3

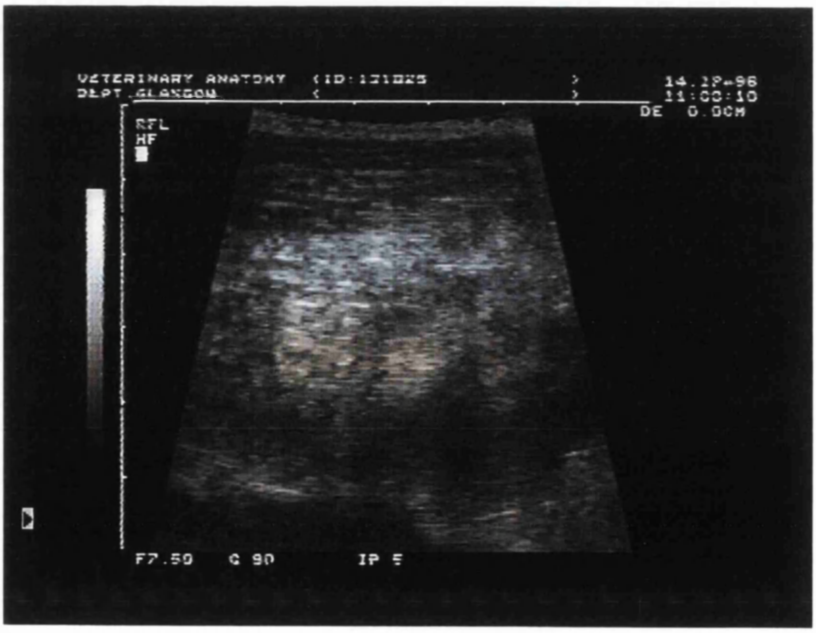

Figure 6.6.4

Figure 6.6.5 Transverse scan of the humerus from the cranial aspect 24 hours after fracture repair demonstrates the fracture site which appears as a defect on the bone surface. The humerus has lost its normal rounded appearance. The area of hyperechoic appearance surrounding the humerus suggests periosteal and soft tissue reaction. The area of muscle damage appears as a disorganised mixture of hypoechoic and hyperechoic structures superficial to the humerus.

Figure 6.6.6 Longitudinal scan of the brachial muscle demonstrates the normal ultrasonographic appearance of the triceps muscle which produces a "feather - like" appearance.

Figure 6.6.5

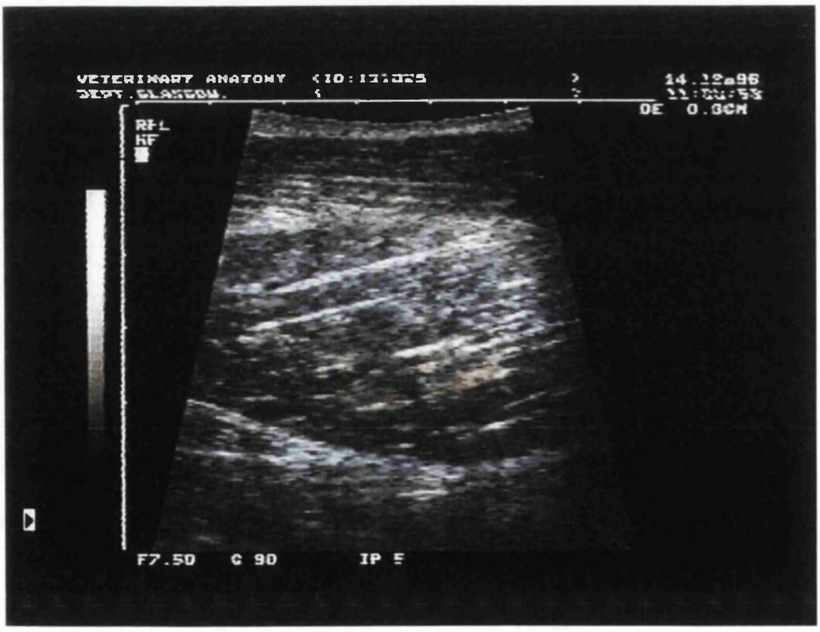

Figure 6.6.6

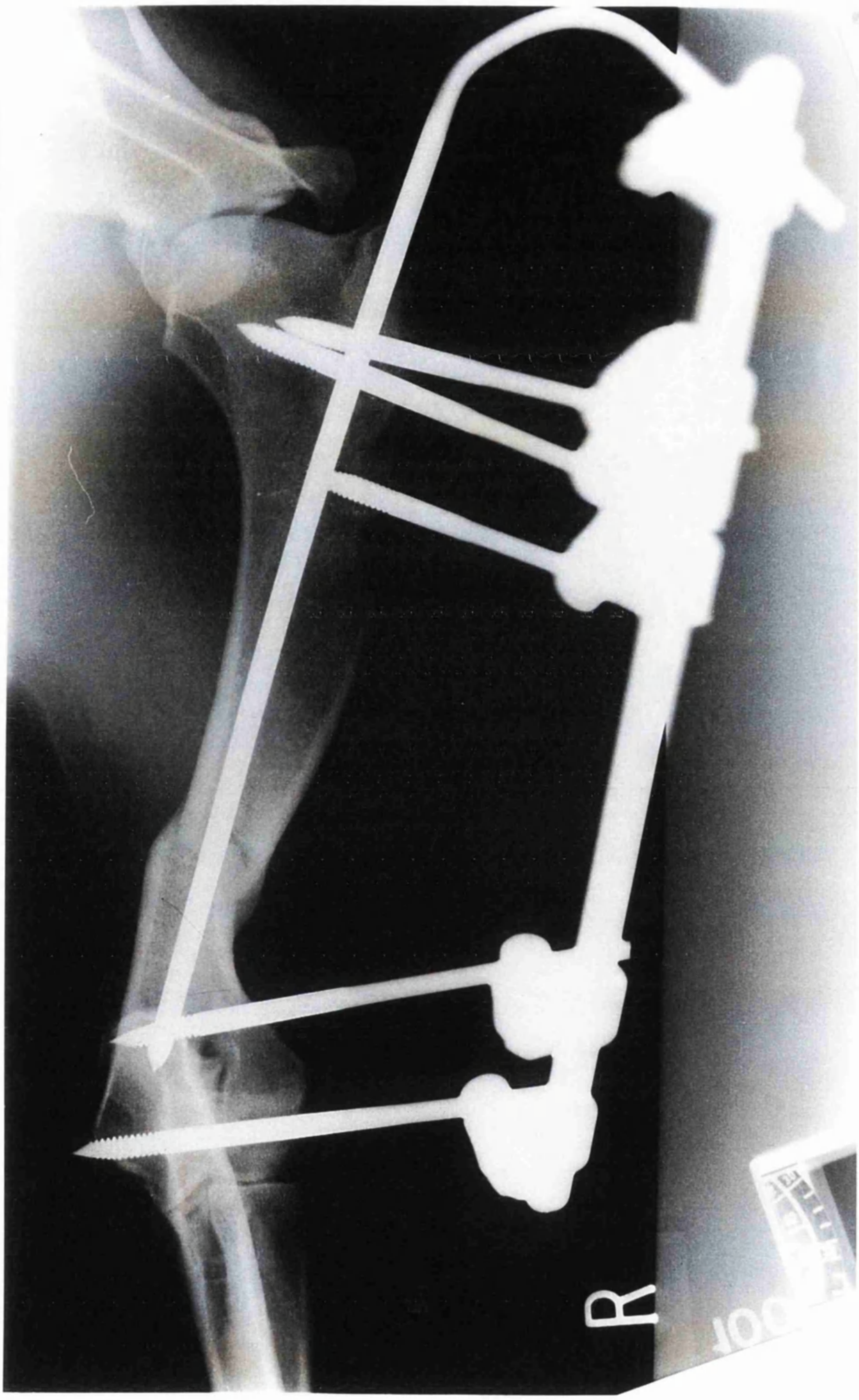

Figure 6.6.7 Radiograph taken at day 44 after fracture repair shows the callus formation is bridging the fracture site and the periosteal reaction has stimulated new bone that is already showing evidence of remodelling. The fracture line is still visible radiographically.

Figure 6.6.8 Longitudinal scans of the humerus from the caudo-lateral aspect (**a**) and the medial aspect (**b**) on day 44 after fracture repair show the smooth, hyperechoic humeral surface. The fracture site has been bridged by the bony callus and appears as a defect on the bone surface (arrow head). Note also the area of muscle damage has returned to its normal ultrasonographic appearance.

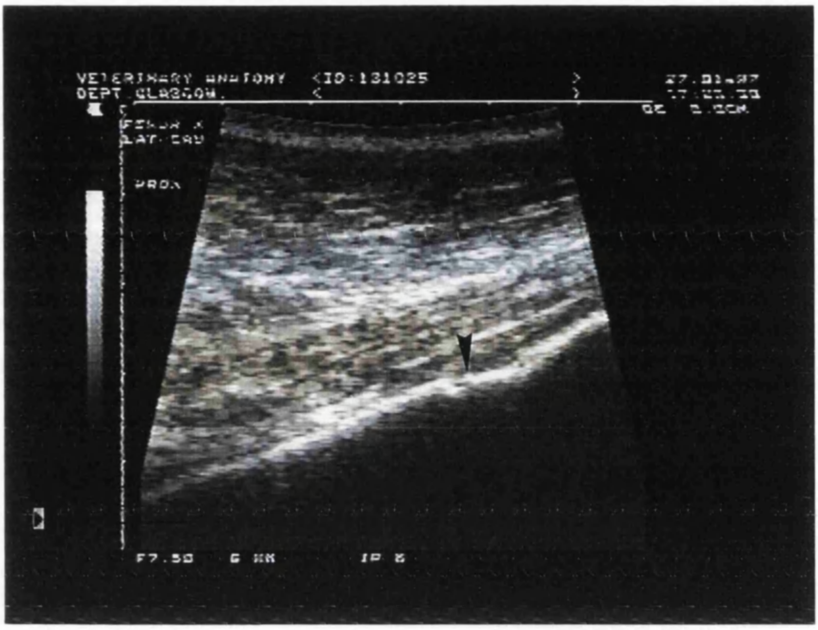

Figure 6.6.8a

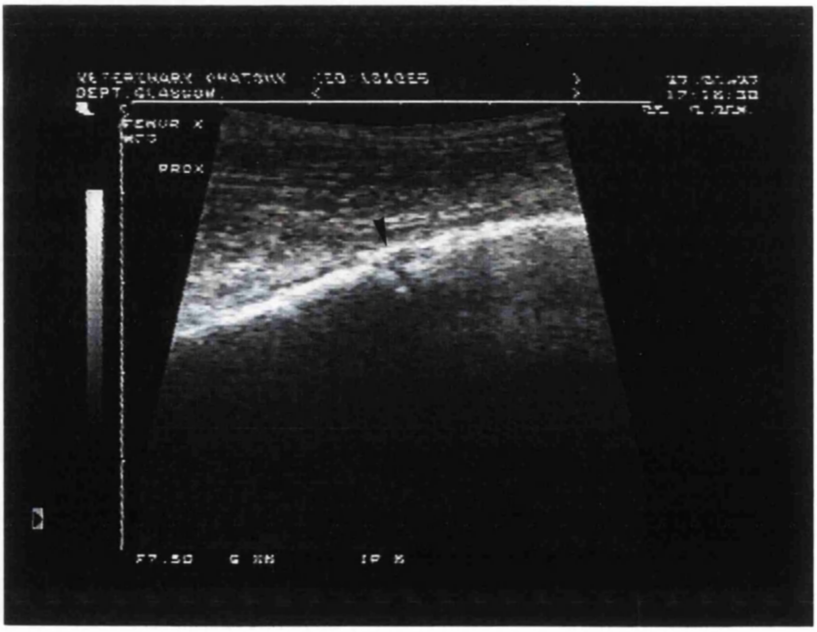

Figure 6.6.8b

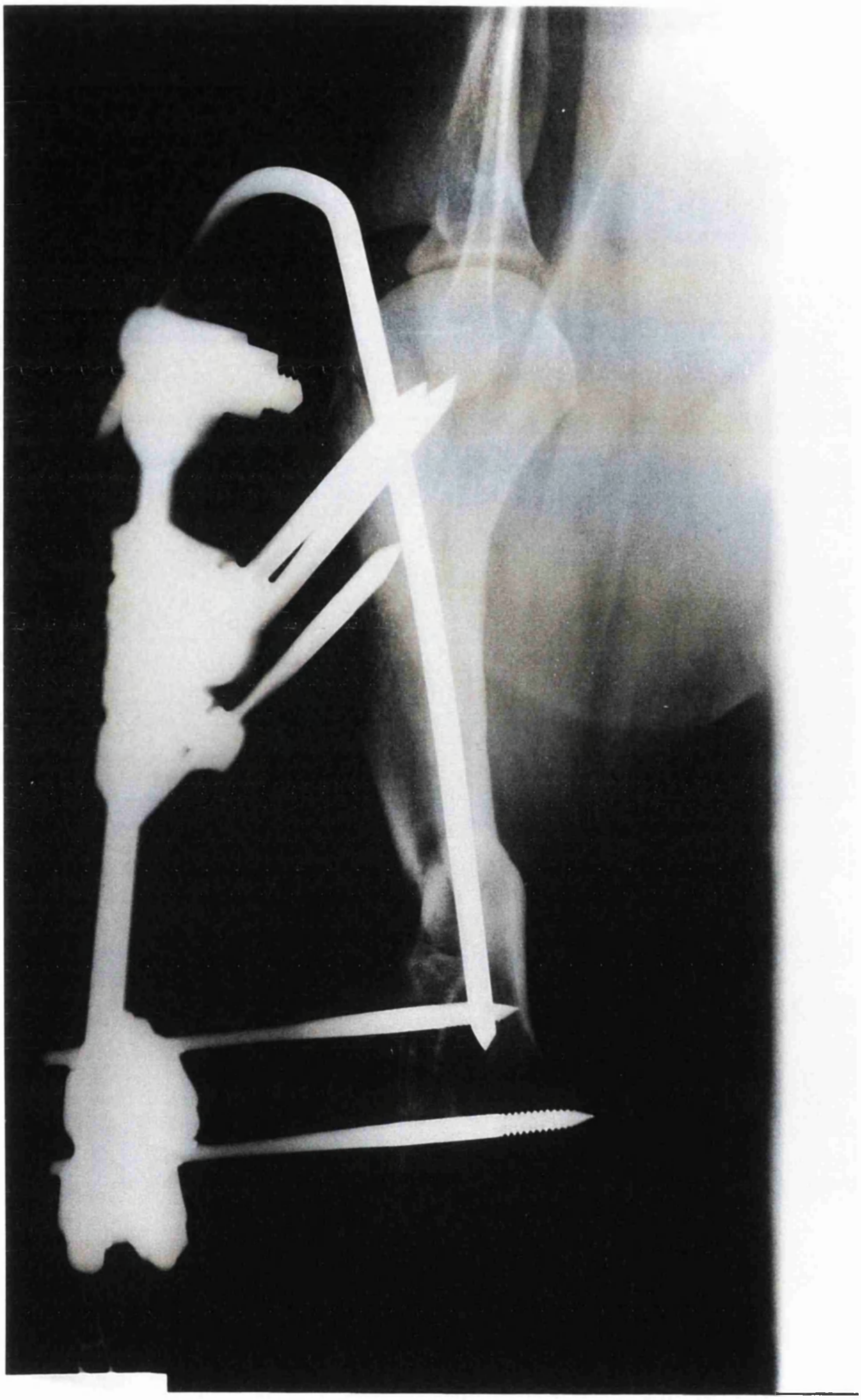

Figure 6.6.9 Radiograph taken at day 73 after fracture repair shows the fracture line which has been completely bridged by the new bone tissue. The fracture line is no longer visible. There is a mild lysis around some of the pins. The healing process has not resulted in a straight bone because of the early defect at the fracture site during the repair process.

Figure 6.6.10 Ultrasonographic examination of the humerus on day 73 after fracture repair. **a**, longitudinal image, **b**, transverse image. The humerus has returned to its normal ultrasonographic appearance in both images with a slight bend at the fracture site on a longitudinal scan. **H**, humerus.

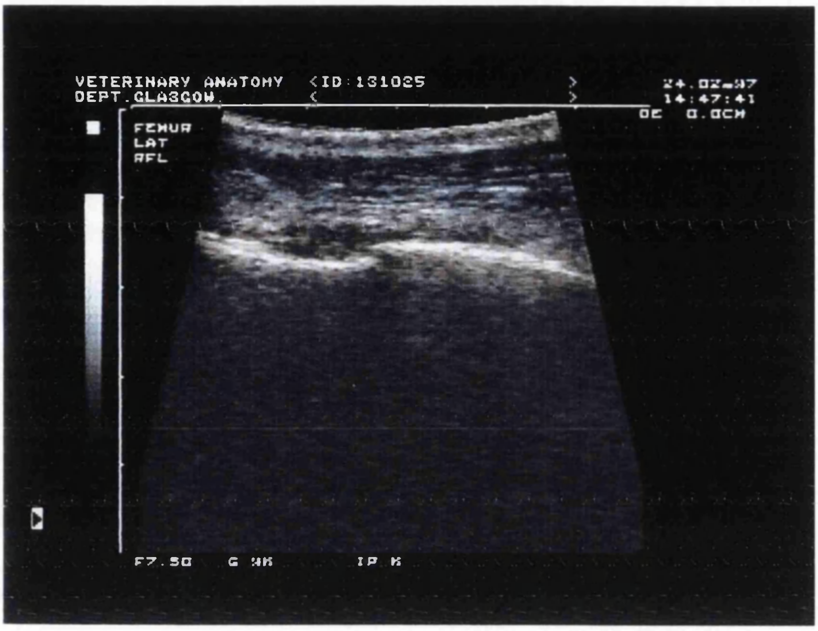

Figure 6.6.10a

Figure 6.6.10b

Case 7

A three year old male Jack Russell Terrier, weight 11.0 kg, was admitted to the Glasgow University Veterinary Hospital after exhibiting right hind limb lameness following a fracture repair attempt five months previously. Upon examination, it was found to have a fibrous non-union fracture of the mid-femoral shaft. There was a loose cerclage wire and a 90 degree angulation of the femur (figure 6.7.1). Stifle flexion was also restricted due to a fibrotic quadriceps contracture. An osteotomy and corrective plating was carried out approximately one month after referral.

A ten centimetre elliptical incision was made through the lateral surface of the right hind limb from the greater trochanter to about 2 cm proximal to the stifle. A large amount of scar tissue was revealed. The scar tissue was cut through and the femur exposed. A bone saw was used to make the two ends of the cortex flush. An eight holes DCP (Dynamic Compression Plate) was applied on the lateral side of the femur. The bone was aligned on the cranial surface but was not fully aligned caudally. The overlying muscle was closed with PDS suture material in a simple interrupted pattern. The scar tissue and the surrounding subcutaneous tissue were closed in simple continuous pattern. The skin was closed in a simple continuous suture pattern.

Surgery had resulted in straightening of the femur. This in turn had led to additional tension on the quadriceps muscle. This muscle may relax as the animal adapts to its new situation. The muscle damage presented the main problem affecting the prognosis. The dogs leg had also been shortened considerably to allow apposition and minimise the effect of the short quadriceps muscle.

Radiographs taken immediately after fracture repair showed that the fracture has been reduced and fixed with a plate and screws (figure 6.7.2). There was no fracture gap present as the two fragments were well apposed. The proliferation of new bone was present around the femur.

Ultrasonographic examination

Day one after fracture repair

Ultrasonographic examination demonstrated the fracture site which appeared as a shallow notch on a bulging surface (figure 6.7.3). The excessive callus formation around the fracture site before the reunion process had been carried out produced the image of an uneven and bulging bone surface. The bone plate was evident as it adhered to the femur when scanned transversely, appearing hyperechoic with reverberation artefact. The fracture site was not imaged on the cranial aspect scan due to the excessive callus formation which had developed after the repair process had been first carried out. The image only showed the bony callus bulging up from the femoral surface and it appeared hyperechoic with acoustic shadowing artefact (figure 6.7.4). A longitudinal scan from the medial aspect revealed the femur as slightly bent at the fracture site (figure 6.7.5). The femur appeared abnormal on a transverse scan, it was big and flat due to the excessive callus formation (figure 6.7.6). The bone plate appeared hyperechoic with reverberation artefact.

Day 27 (four weeks) after fracture repair

Radiographic examination

Radiographs taken at day 27 after fracture repair showed that the healing process appeared to be progressing satisfactorily (figure 6.7.7). No evidence of implant loosening or instability could be seen.

Ultrasonographic examination

Ultrasonographic examination from the medial aspect demonstrated the rough and uneven femoral surface due to callus formation (figure 6.7.8). The fracture site could still be recognised as a shallow notch on the uneven and rough femoral surface. It had been completely bridged by the mature callus. On the cranio-lateral scan, the femoral surface appeared less uneven and the fracture site was no longer detected (figure 6.7.9). This indicated the remodelling process was taking place. The bone plate appeared hyperechoic and produced reverberation artefact (figure 6.7.10a and 6.7.10b).

Day 61 after fracture repair

Ultrasonographic examination demonstrated the fracture site which had been completely bridged by the mature callus (figure 6.7.11). The fracture site could still be recognised ultrasonographically and appeared as a shallow notch on the femoral surface. The bulging bone area had reduced in size and appeared smoother than the previous scan suggesting a remodelling process. On the medial aspect scan, the femur appeared slightly bent at the fracture site area as seen on day one after reunion process (figure 6.7.12). The bone plate and screws appeared hyperechoic with reverberation artefacts. The distal part of the plate appeared slightly elevated from the femoral surface (figure 6.7.13). This could suggest that the screws were loosening at the distal portion. Muscle tissue had a normal ultrasonographic appearance. Ultrasonographically, the fracture site had healed satisfactorily.

Figure 6.7.1 A three year old Jack Russell Terrier with a nonunion fracture of the mid shaft femur with proliferative new bone and a cerclage wire.

Figure 6.7.2 Radiographs obtained immediately after the reunion process show the fragments have been fixed with a plate and screws. **a**, lateral view, **b**, cranial view. The osteotomy and corrective plating was carried out approximately one month after referral. There was no fracture gap present and the two fragments were well apposed. Proliferation of new bone was present around the femur.

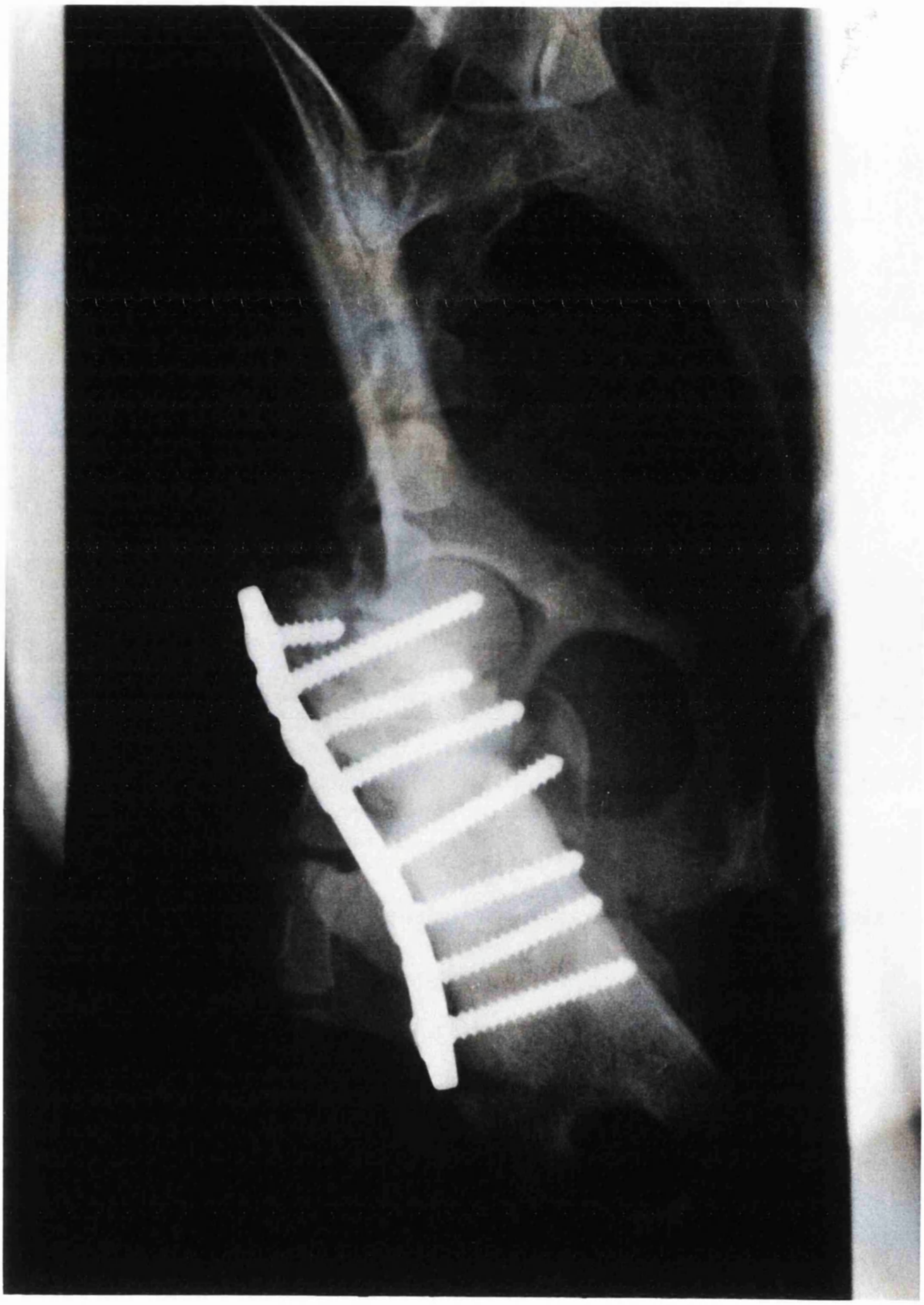

b

Figure 6.7.3 Longitudinal scan of the femur from the caudal aspect 24 hours after reunion shows the fracture site which appears as a shallow notch on a bulging bone surface (arrow).

Figure 6.7.4 Longitudinal scan of the femur from the cranial aspect 24 hours after reunion shows the bony callus is bulging up from the bone surface and appears hyperechoic with acoustic shadowing artefact.

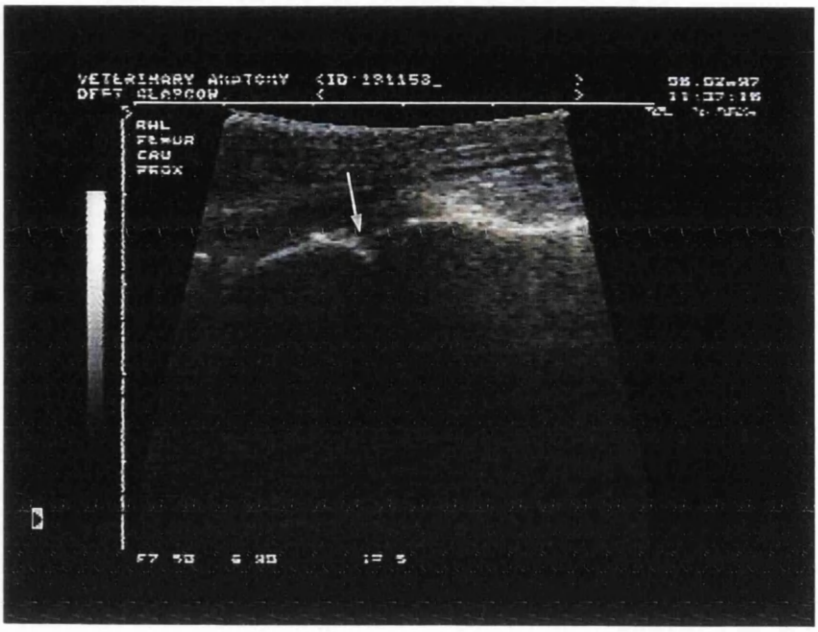

Figure 6.7.3

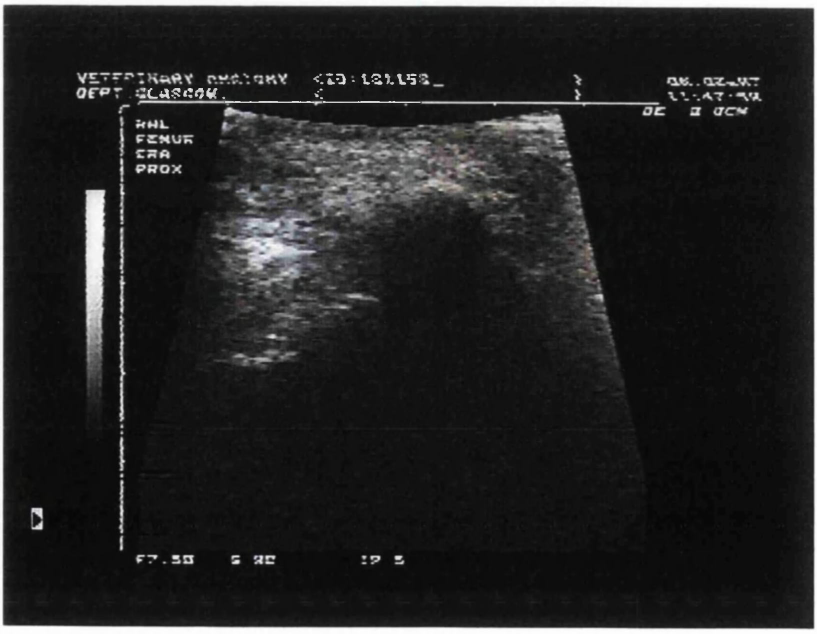

Figure 6.7.4

Figure 6.7.5 Longitudinal scan of the femur from the medial aspect 24 hours after reunion demonstrates the femur which is slightly bent at the fracture site (arrow head).

Figure 6.7.6 Transverse scan of the femur from the medial aspect 24 hours after reunion shows the femur with a hyperechoic flat bone surface with acoustic shadowing artefact. The abnormal appearance of the femoral surface is due to the excessive callus formation. **F**, femur.

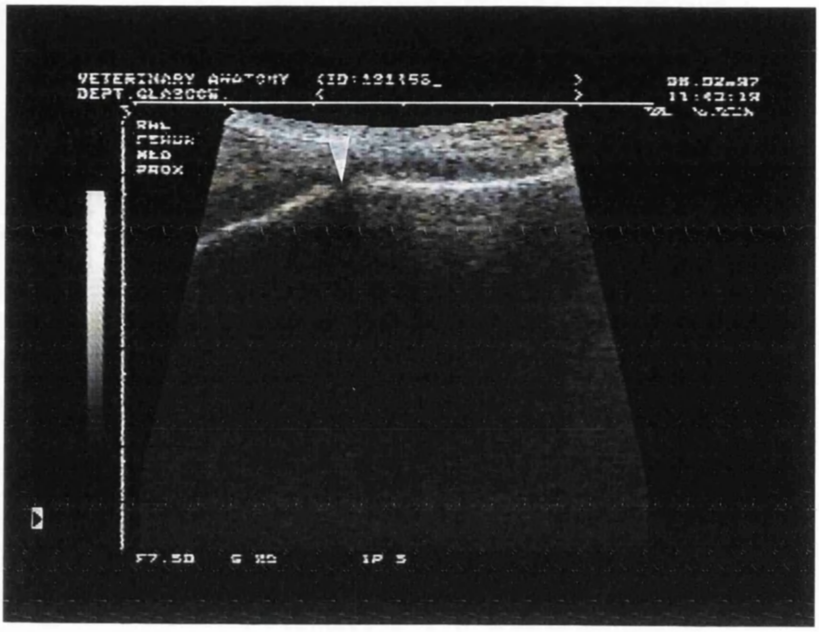

Figure 6.7.5

Figure 6.7.6

Figure 6.7.7 Radiographs obtained at day 27 after fracture repair show that the healing process appears to be progressing satisfactorily. **a**, lateral view, **b**, cranial view. No evidence of implant loosening or instability can be seen.

b

Figure 6.7.8 Longitudinal scan of the femur from the medial aspect on day 27 after reunion demonstrates the femur with a rough and uneven surface due to callus formation. Note that the fracture site can be recognised as a shallow notch (arrow).

Figure 6.7.9 Longitudinal scan of the femur from the cranio-lateral aspect on day 27 after reunion shows the femoral surface which appears less uneven, and the fracture site is no longer detected. This indicates the remodelling process is taking place.

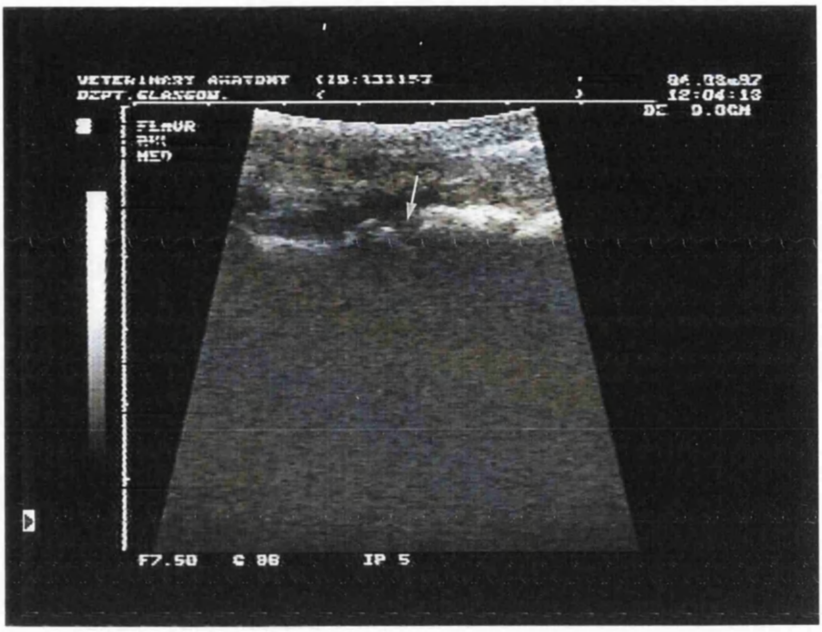

Figure 6.7.8

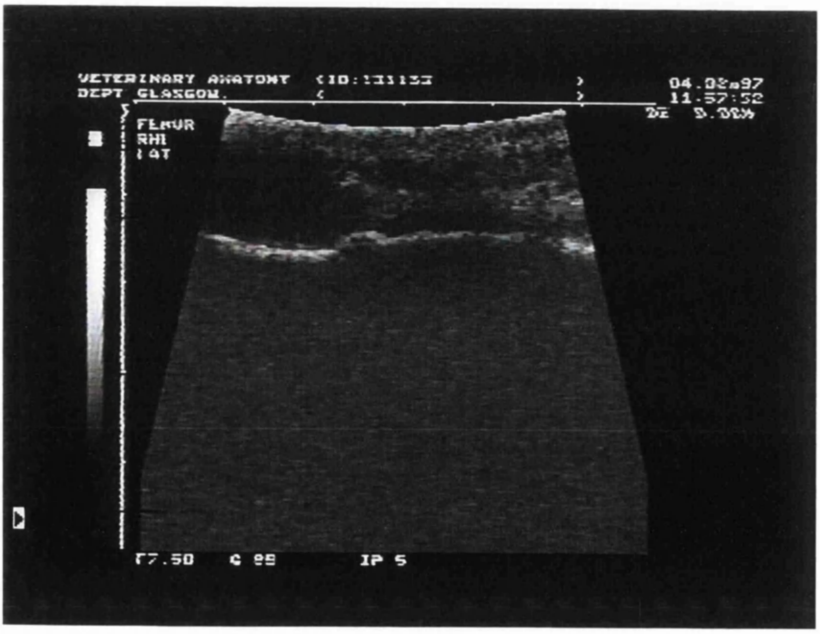

Figure 6.7.9

Figure 6.7.10 The bone plate appears hyperechoic on an ultrasonographic scan and produces reverberation artefact. **a**, longitudinal scan, **b**, transverse scan.

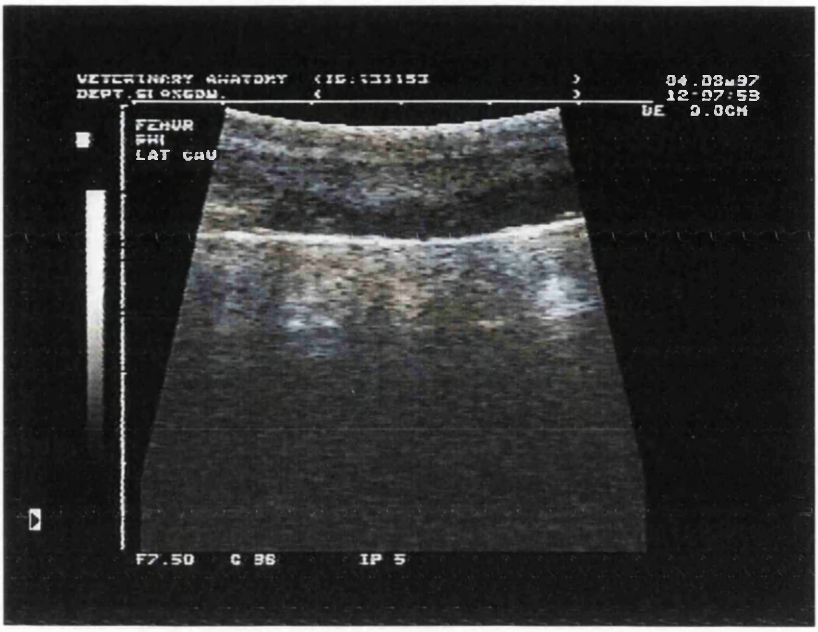

Figure 6.7.10a

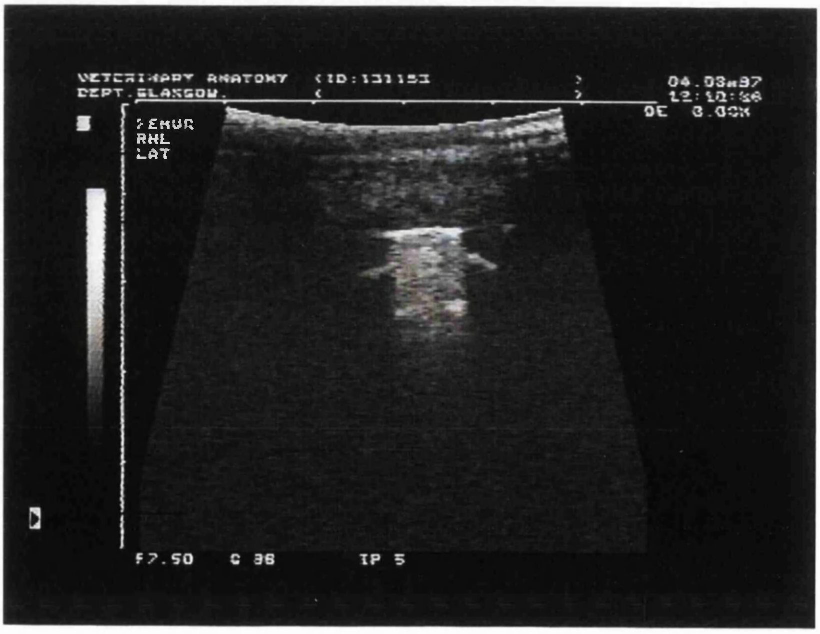

Figure 6.7.10b

Figure 6.7.11 Longitudinal scan of the femur from the lateral aspect on day 61 after reunion demonstrates the fracture site which appears as a shallow notch on the femoral surface. The mature callus is bridging the fracture site completely.

Figure 6.7.12 Longitudinal scan of the femur from the medial aspect on day 61 after reunion shows the femur which appears slightly bent at the fracture site area.

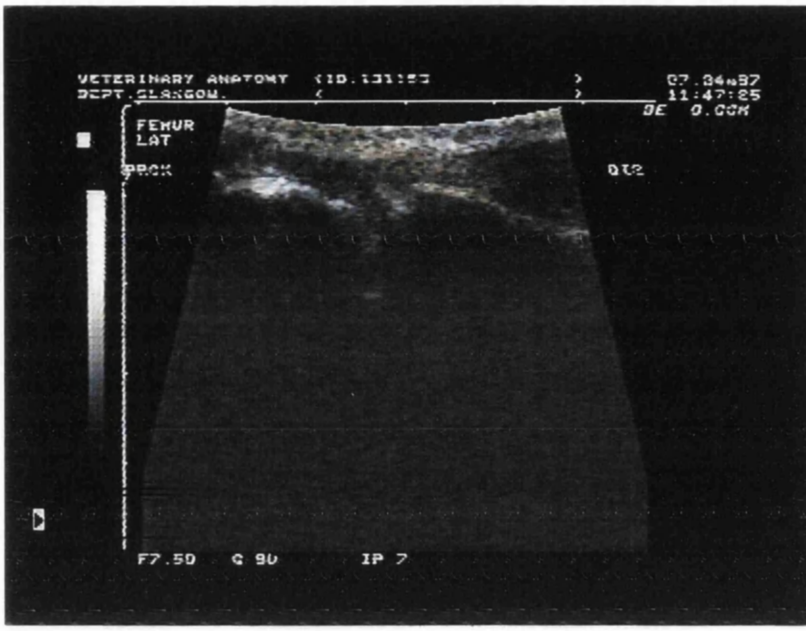

Figure 6.7.11

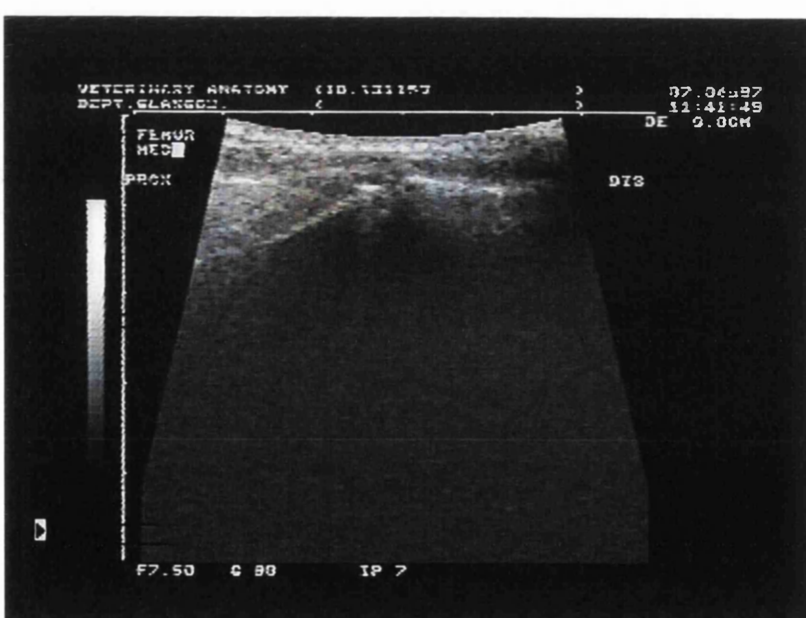

Figure 6.7.12

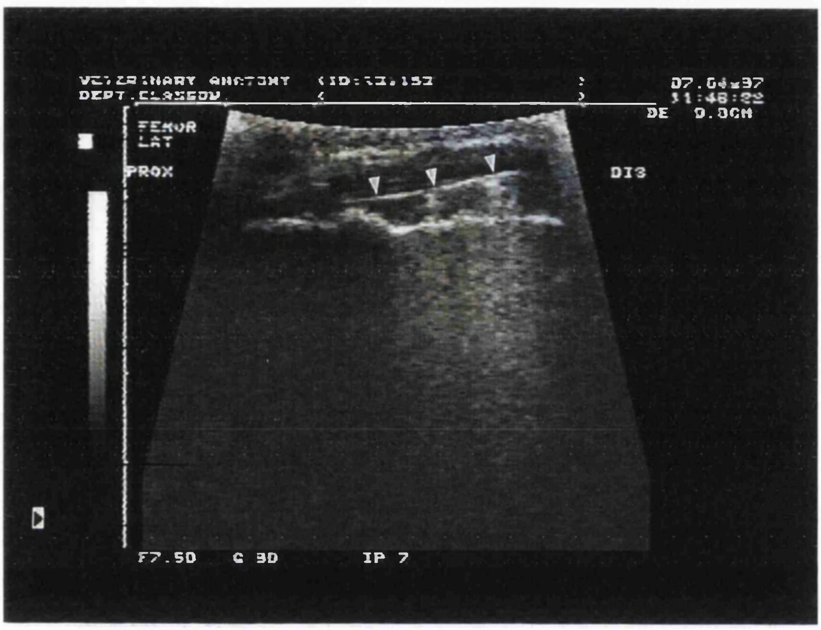

Figure 6.7.13 Longitudinal scan of the femur from the lateral aspect on day 61 after reunion demonstrates the distal part of the plate (arrow heads) which appears elevated from the femoral surface. This may indicate the screws loosening at the distal portion.

Case 8

A seven month old male Border Collie, weight 12 kg, was referred to the Glasgow University Veterinary Hospital after having been involved in a road traffic accident. The dog had fractures of the right hemipelvis and a sacroiliac luxation of the left hemipelvis. On clinical examination the animal showed a poor anal reflex and poor anal tone but apparently normal urinary control. A sciatic nerve deficit was identified in the left limb. Radiographs taken before fracture repair showed the right acetabular fragment to be "free" and markedly impacted into the pelvic canal (figure 6.8.1).

A standard lateral approach to the right ilium was made with the deep gluteal muscle being elevated and displaced ventrally, and the middle gluteal muscle transected and elevated dorsally. With the aid of bone holding forceps and Holfman retractors the fracture was reduced and a 2.7 cm eight holes DCP (Dynamic Compression Plate) was aligned on the ilium. The caudal iliac fragment was first drilled, taped and screwed (4 screws in total), then the cranial fragment attached to the plate by 3 screws. The fourth hole was left open as it lay over the fracture site.

The middle gluteal muscle was closed with 3 metric PDS in a simple interrupted pattern, and the deep gluteal muscles repositioned by simple interrupted PDS sutures. The overlying muscle and tissue layers were closed with 3 metric vicryl in a continuous pattern. A subcutaneous layer of simple interrupted 3 metric vicryl was also put in place. The skin was closed with 3 metric ethilon in a simple interrupted pattern.

The right ilium had been plated with an eight hole 2.7 mm DCP (Dynamic Compression Plate). Reduction of the fracture was good, although post-operation radiographs showed an under-reduction of the ischial fracture due to slight under-contouring of the plate (figure 6.8.2). The acetabular fragment had been pulled back into a more normal position.

Ultrasonographic examination

Day three after fracture repair

Ultrasonographic examination of the ilial shaft on a transverse scan demonstrated the fracture site with the presence of a small gap near to the bone plate (figure 6.8.3). It appeared as discontinuity of the shaft of the ilium when imaged in cross section. The fracture site could be seen as a defect on the ilial shaft on a longitudinal scan. The presence of soft callus formation was detected and appeared as an hyperechoic structure in the area of the fracture (figure 6.8.4). The bone plate with screws appeared hyperechoic and produced comet tail artefacts. The disorganised hyperechoic structure area superficial to the ilium suggested an area of soft tissue reaction (figure 6.8.5). The area of muscle damage appeared disorganised and hypoechoic.

Day five after fracture repair

Ultrasonographic examination demonstrated the fracture site of the ilial shaft both on transverse and longitudinal scans. The fracture site imaged on a transverse plane still demonstrated the small gap as seen on the day three examination (figure 6.8.6). However, the fracture site appeared hyperechoic suggesting the presence of periosteal tissue reaction. The area over the bone surface level appeared hyperechoic which suggested soft tissue reaction. The bone plate near the fracture site appeared hyperechoic and produced reverberation artefact. The area of muscle damage was still present and appeared as a disorganised hypoechoic structure as seen on the day three examination. The fracture site imaged on longitudinal plane appeared as on the day three examination. The small fracture gap was clearly evident with the presence of hyperechoic material suggesting soft callus formation (figure 6.8.7). A longitudinal scan of the dorsal part of the ilial shaft demonstrated the fracture site with the proximal fragment appearing higher than the caudal fragment (figure 6.8.8). The echogenic area at the proximal end fragment suggested the soft tissue reaction.

Day seven after fracture repair

Ultrasonographic examination revealed the fracture site which appeared as on the day five examination. There was still no soft callus formation to be seen at the fracture site on the transverse scan. The small fracture gap imaged on the transverse scan appeared hyperechoic which suggested periosteal tissue reaction. The soft tissue reaction superficial to the ilial surface appeared as a disorganised hyperechoic structure as seen on the day five examination. The fracture site imaged on a longitudinal scan at the dorsal part of the ilial shaft appeared as on the day five examination. The area of muscle damage could still be detected appearing as a disorganised hyperechoic region.

Day 10 after fracture repair

Ultrasonographic examination demonstrated the formation of the periosteal callus which developed some distance away from the fracture site both on transverse and longitudinal scans (figure 5.8.9a and 6.8.9b). The callus formation appeared as clumping hyperechoic structures emerging from the bone surface and produced acoustic shadowing artefact. Thus, the excessive amount of callus formation resulted in a rough, uneven surface of the bone. The soft callus formation was also detected and appeared as a disorganised hyperechoic structure with an irregular margin and produced no artefact. The bone surface underneath could still be seen. The soft callus was gradually maturing with time and appeared hyperechoic with acoustic shadowing artefact. However, as it became mature only the surface could be imaged. The mature callus appeared ultrasonographically similar to the bone tissue but it had an irregular surface. The area of muscle damage had returned to its normal ultrasonographic appearance. The bone plate with screws attached to the shaft of the ilium appeared hyperechoic and produced reverberation artefact. This case failed to return for the reassessment. Thus, follow up scans were not available.

Figure 6.8.1 A seven months old male Border Collie with fractures of the right hemipelvis and the sacroiliac luxation of the left hemipelvis. Note that the right acetabular fragment appears to be "free" and markedly impacted into the pelvic canal.

Figure 6.8.2 Radiographs taken immediately after the fracture repair show that the medial displacement of the iliac shaft has been corrected and the pelvic canal reopened. **a**, lateral view, **b**, ventral view. The fracture is reduced using a 2.7 cm eight holes DCP (Dynamic Compression Plate) aligned on the ilium. The caudal iliac fragment has been first drilled, taped and screwed (4 screws in total), then the cranial fragment attached to the plate by 3 screws. The fourth hole has been left open as it lies over the fracture site. The medial displacement of the ilial shaft has been corrected reopening the pelvic canal.

b

Figure 6.8.3 Transverse scan of the shaft of ilium on day three after fracture repair demonstrates the fracture site with a small fracture gap (arrow) near to the bone plate (arrow head). There is no soft callus formation detected.

Figure 6.8.4 Longitudinal scan of the shaft of ilium on day three after fracture repair shows the fracture site which appears as a defect of the ilial shaft surface. Note the hyperechoic material at the fracture site suggesting the presence of soft callus formation. The area of muscle damage appears disorganised and hypoechoic.

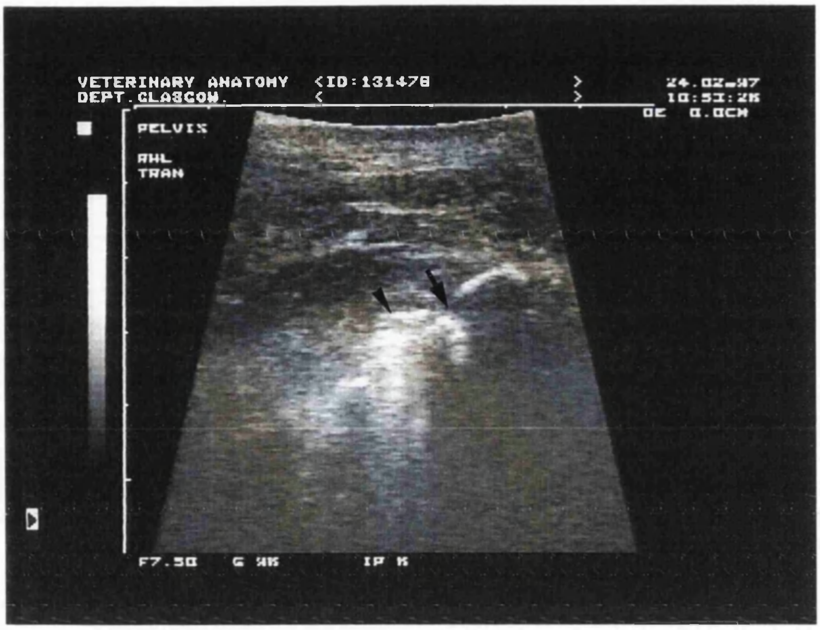

Figure 6.8.3

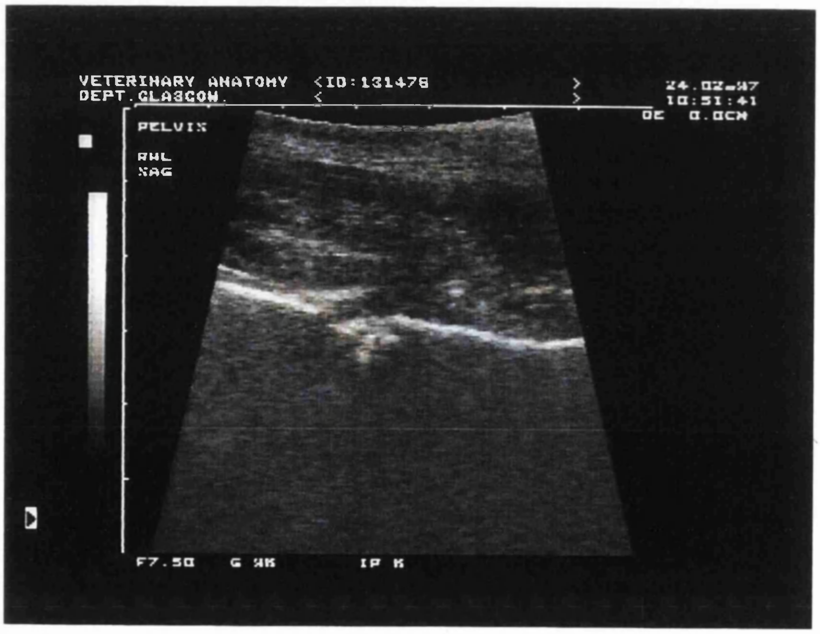

Figure 6.8.4

Figure 6.8.5 Longitudinal scan of the ilial shaft on day three after fracture repair shows the bone plate with screws which appear hyperechoic with reverberation artefact. Note also the area of disorganised hyperechoic structure superficial to the bone surface suggesting soft tissue reaction.

Figure 6.8.6 Transverse scan of the shaft of ilium on day five after fracture repair shows the fracture site with the presence of a small gap near the bone plate (arrow) which casts reverberation artefact. The hyperechoic appearance at the fracture site suggests the presence of periosteal tissue reaction. The area over the bone surface appears hyperechoic which may suggest an area of soft tissue reaction. The area of muscle damage appears as a disorganised hypoechoic structure.

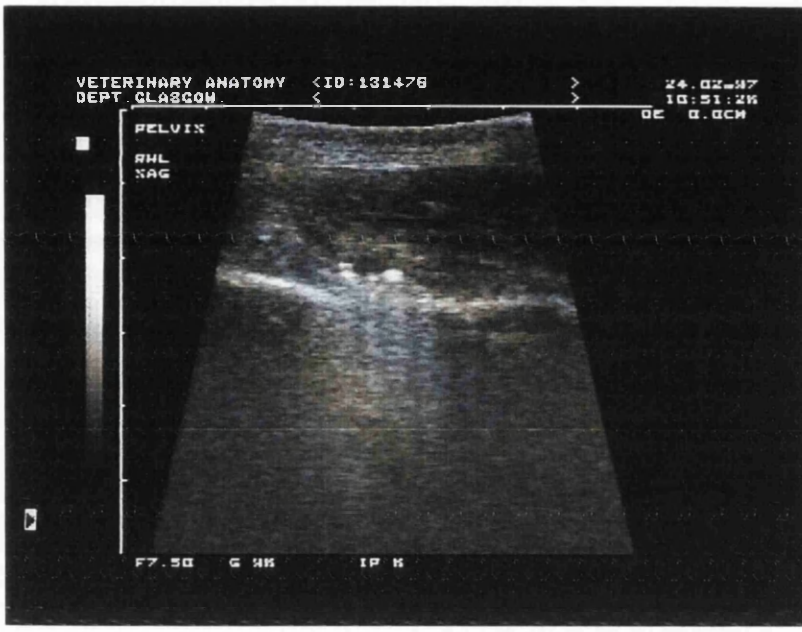

Figure 6.8.5

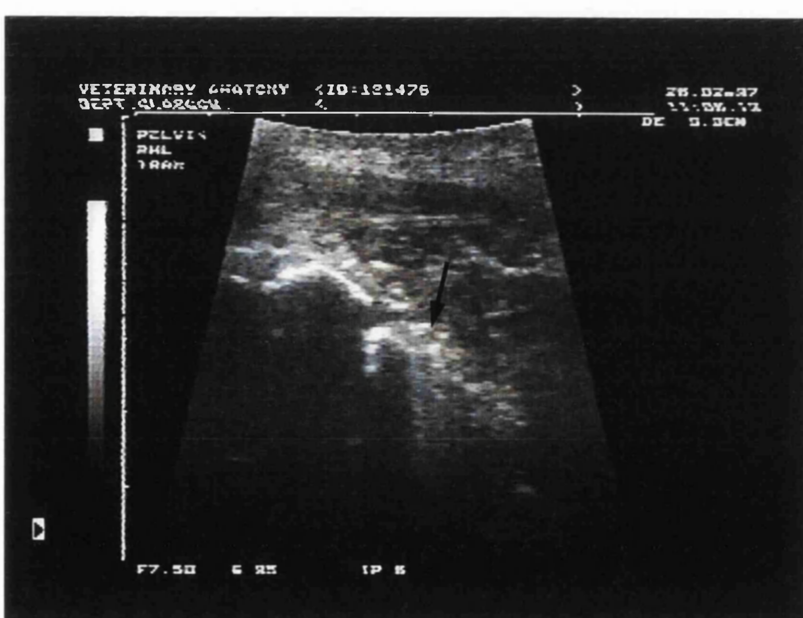

Figure 6.8.6

Figure 6.8.7 Longitudinal scan of the ilium on day five after fracture repair shows the fracture site with a small gap. The hyperechoic material at the fracture site suggests soft callus formation.

Figure 6.8.8 Longitudinal scan of the dorsal side of the shaft of ilium on day five after fracture repair demonstrates the fracture site with the proximal fragment appearing elevated from the distal fragment. There is no fracture gap seen at this site. The echogenic area at the proximal end fragment (arrow) suggests soft tissue reaction.

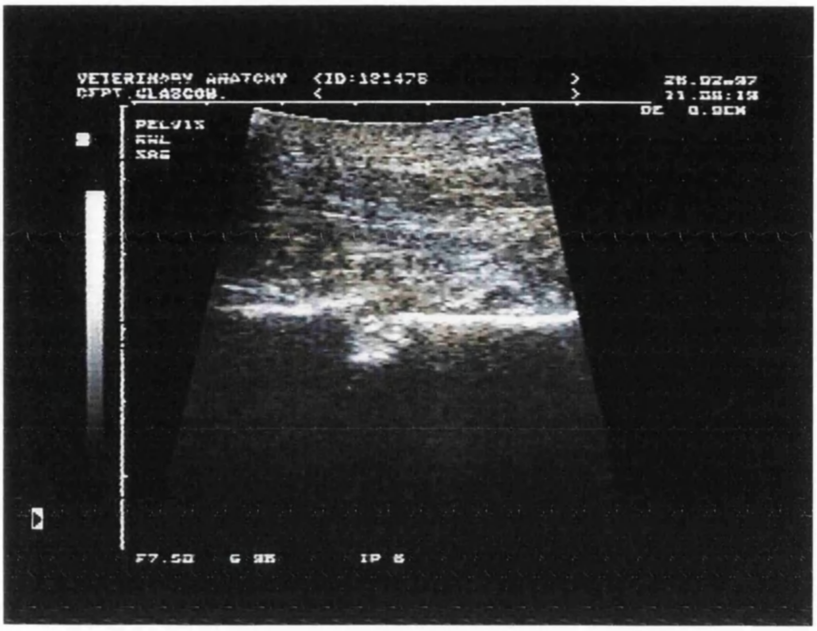

Figure 6.8.7

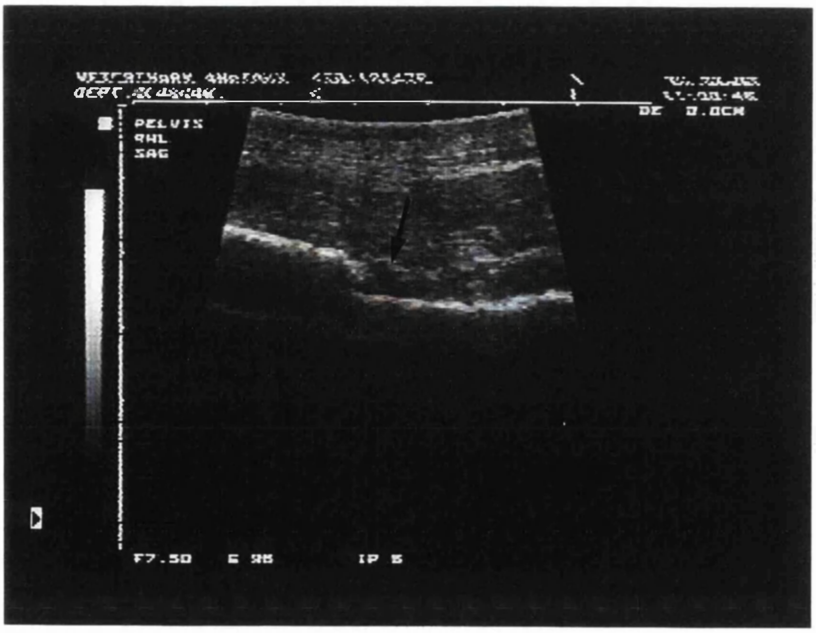

Figure 6.8.8

Figure 6.8.9 Ultrasonographic examination of the ilial shaft on day 10 after fracture repair. **a**, transverse scan, **b**, longitudinal scan. Both images demonstrate the presence of periosteal callus formation which is developing some distance away from the fracture site. The callus formation appears as clumping hyperechoic structures emerging from the bone surface and casting acoustic shadowing artefact. The soft callus formation seen on a transverse scan (**a**) appears as a disorganised hyperechoic structure with an ill-defined margin (arrow head) and produces no artefact. The bone surface underneath the soft callus formation in **b** (arrow heads) is still visible. The maturing callus appears similar to the bone tissue but it has an irregular surface and produces an abnormal image outline of the bone.

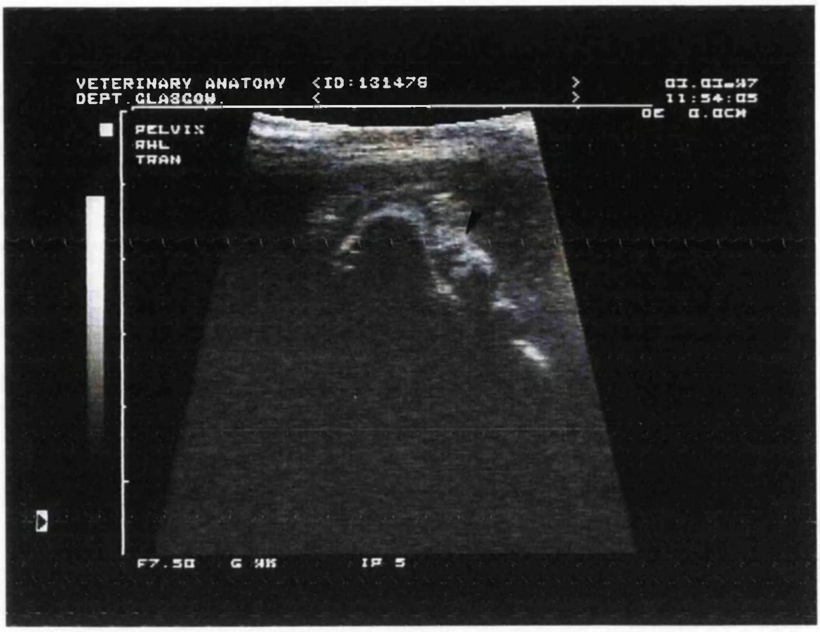

Figure 6.8.9a

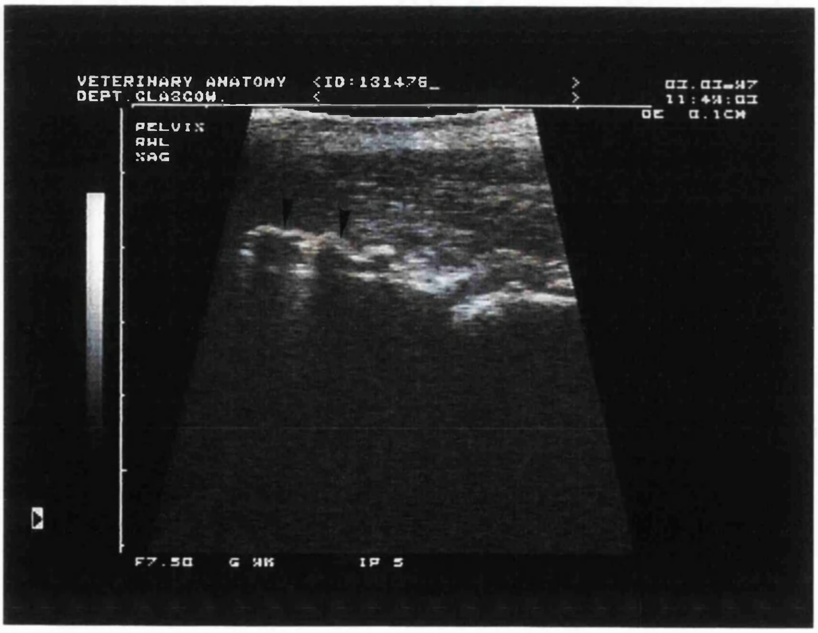

Figure 6.8.9b

Case 9

A twenty one month old male Burmese cat, weight 4.5 kg, was presented to the Glasgow University Veterinary Hospital after having been involved in a road traffic accident one day previously. Radiographic examination revealed that a comminuted fracture of the mid-shaft of the left femur had been sustained.

Fracture repair was carried out on the day following admission. The animal was laid in right lateral recumbency during the operation. A skin incision was made over the lateral aspect of the femur and the fracture was revealed. A large haematoma was also identified. The fissure in the femur was stabilised using two cerclage wires. These were parallel, through holes made in the adductor muscle, passed around the femur and tightened laterally. The twisted ends were bent down to lie flat against the lateral femur. An intramedullary femoral pin was placed in a normograde direction using a hand-chuck. Two transfixion pins were inserted at both ends of the femur, passing through both cortices of the bone. These were connected using clamps and a connecting bar. Two more pins were placed in between the outer pins using two middle clamps as guides ensuring that all pins were lying in the same plane.

The muscle layers and subcutaneous tissue were closed using 2/0 vicryl in a continuous pattern. The skin was closed using 2/0 Ethilon in a simple interrupted pattern.

Radiographs taken immediately after fracture repair showed that the comminuted femoral fracture had been reduced and aligned with an intramedullary pin and I/E external fixator tied in (figure 6.9.1). A piece of bone fragment was remaining in the muscle, being caudal to the fracture site. A small fragment of bone was seen lying across the femur at the fracture site area on lateral view.

Ultrasonographic examination

Day one after fracture repair

Scanning directly onto the lateral aspect of the femur could not be carried out because the external fixator was placed on the lateral aspect. Ultrasonographic examination from the caudal aspect of the femur revealed a piece of bone fragment lying caudal to the fracture site (figure 6.9.2). The fragment appeared as an hyperechoic short line and produced acoustic shadowing artefact. Thus, scanning from the caudal aspect failed to image the fracture site. However, the fracture site was imaged on cranio-lateral aspect and appeared well aligned with no fracture gap present (figure 6.9.3). A small hyperechoic structure was seen protruding into the muscle from the bone surface at the fracture site. This was actually a small bone fragment as shown in the radiographs. The two cerclage wires used in the fracture reduction appeared as two small hyperechoic spots on the femoral surface (figure 6.9.3). The area of extensive muscle damage caudal to the femur appeared as a large, round hyperechoic region with an hypoechoic centre on a longitudinal scan (figure 6.9.4a), and appeared as a round, mixture of hyperechoic and hypoechoic structures on a transverse scan (figure 6.9.4b). The fracture site imaged on a transverse scan from the caudal aspect showed the bone fragment which lay caudal to the bone and appeared hyperechoic with acoustic shadowing artefact. The intramedullary pin imaged in cross section appeared as a small hyperechoic region with comet tail artefact. The fracture site imaged on a longitudinal scan from the caudo-lateral aspect revealed a large fracture gap (figure 6.9.5). Only the proximal or the distal fragment could be imaged at one time. The two main fragments were connected by the intramedullary pin which appeared as an hyperechoic straight line and produced reverberation artefact. The area of damaged muscle above the femur appeared as a disorganised hyperechoic structure.

Day two after fracture repair

Ultrasonographic examination demonstrated the fracture site which appeared as on the day one examination. No soft callus formation was detected at this stage. The bone fragment lying caudal to the fracture site appeared as an hyperechoic short line above the proximal fragment (figure 6.9.6). The fracture site on transverse scan appeared as on the day one examination. No significant changes were seen. The area of extensive muscle damage caudal to the femur had become more echogenic but still appeared as a round, disorganised hyperechoic structure as seen on the day one examination (figure 6.9.7).

Day 45 (6 weeks) after fracture repair

Radiographic examination

Radiographs taken at day 45 after fracture repair showed the callus formation has bridged the fracture site and around the femoral shaft (figure 6.9.8). This was suggestive of fracture healing. The fracture site was still visible radiographically. The bone fragment lying caudal to the femur had coalesced with the main fragment by bony callus.

Ultrasonographic examination

Ultrasonographic examination from caudo-lateral aspect demonstrated the femur with callus formation (figure 6.9.9a). The fracture site was imaged and appeared as a vertical hyperechoic line which had been occupied by the soft callus (figure 6.9.9b). The large fracture gap seen on the day two examination was no longer detected. The femoral surface appeared uneven and rough at the area of fracture site both on longitudinal and transverse scans (figure 6.9.10a and

6.9.10b). The femur appeared bigger than normal with a rough, rounded surface on a transverse scan. The fracture site could still be seen with the presence of a small gap which appeared hyperechoic suggesting the presence of periosteal tissue reaction. The loose bone fragment lying caudal to the fracture site as seen on the day one and two examinations had now coalesced with the main fragment by means of the mature callus. Thus, the large fracture gap was no longer visible. The area of muscle damage had returned to its normal muscle structure but with an increased hyperechoic appearance (figure 6.9.11a and 6.9.11b). This hyperechoic appearance was suggestive of the presence of fibrous tissue within the muscle. The muscle thickness had reduced in size as compared to the day two examination. This was shown by the decreased distance between the skin surface and the femur. Ultrasonographically, the fracture site was healing satisfactorily.

Figure 6.9.1 Radiographs obtained immediately after fracture repair show the comminuted femur fracture has been reduced and aligned with an intramedullary pin and I/E external fixator tied in. **a**, lateral view, **b**, cranial view. A piece of bone fragment remains, lying caudal to the femur at the fracture site. A small fragment of bone is seen positioned across the femur at the fracture site area on a lateral view.

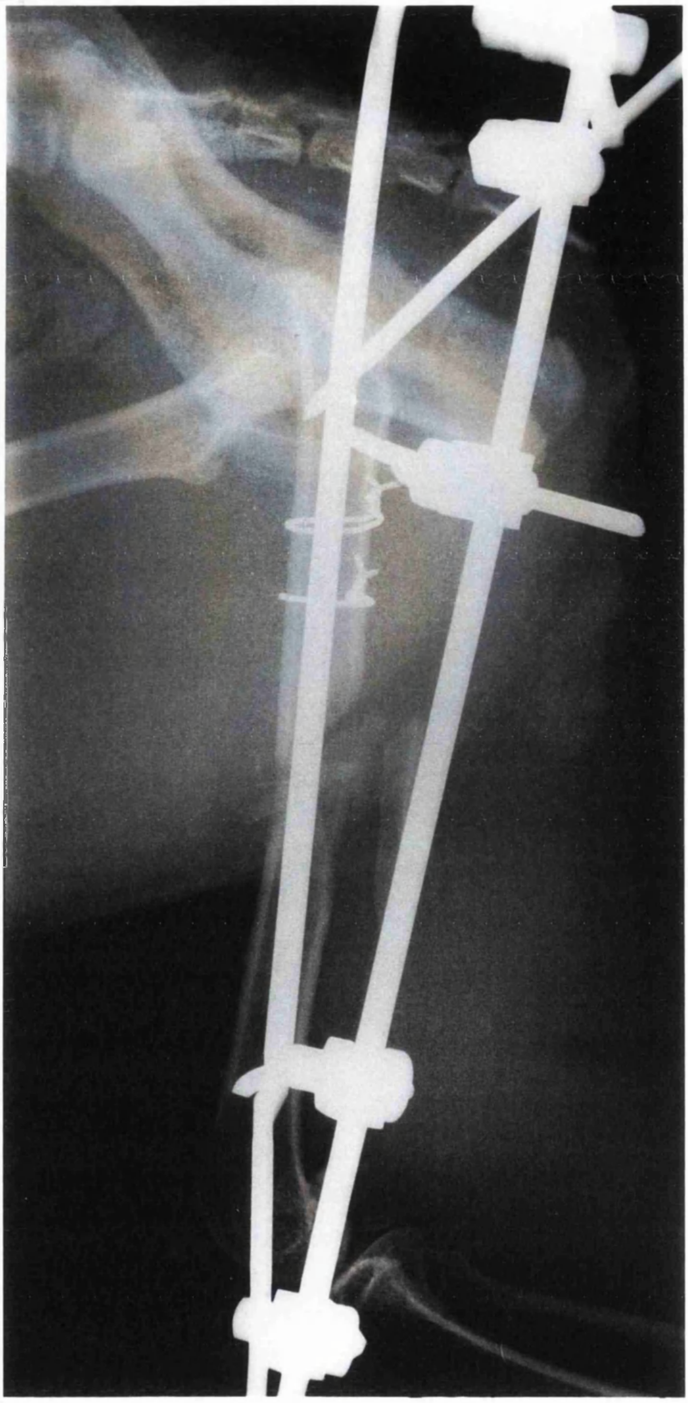

a

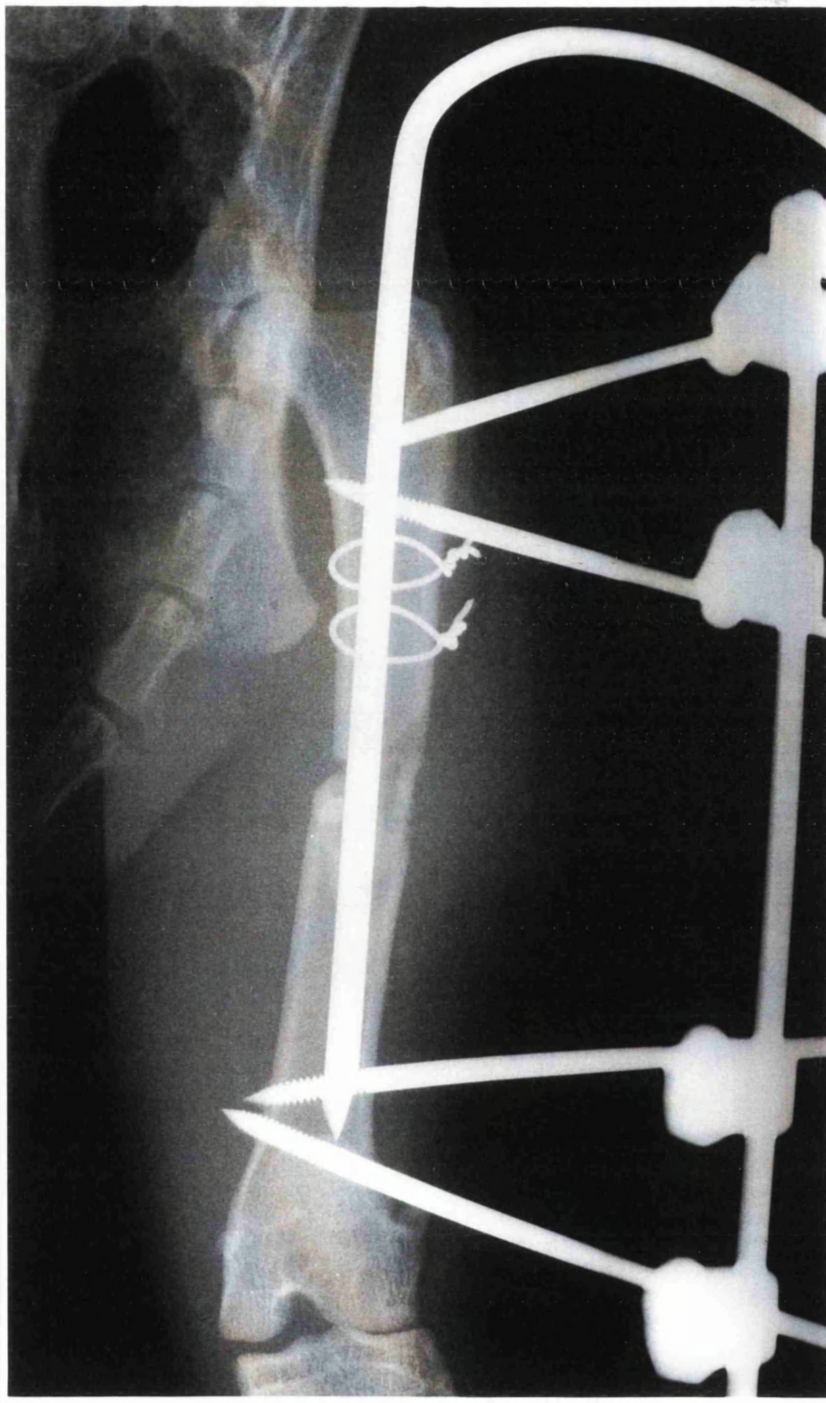

b

Figure 6.9.2 Longitudinal scan of the femur from the caudal aspect 24 hours after fracture repair shows the piece of bone fragment lying caudal to the fracture site. It appears as a straight hyperechoic line and produces acoustic shadowing artefact. This bone fragment is blocking out the image of the fracture site on the caudal aspect scan of the femur.

Figure 6.9.3 Longitudinal scan of the femur from the cranial aspect 24 hours after fracture repair demonstrates the fracture site (long arrow) which is well aligned and no significant fracture gap is present. The small hyperechoic structure (short arrow) protruding into the muscle from the bone surface at the fracture site is actually a small bone fragment. Note also that the two small hyperechoic spots are representing the cerclage wires (arrow heads).

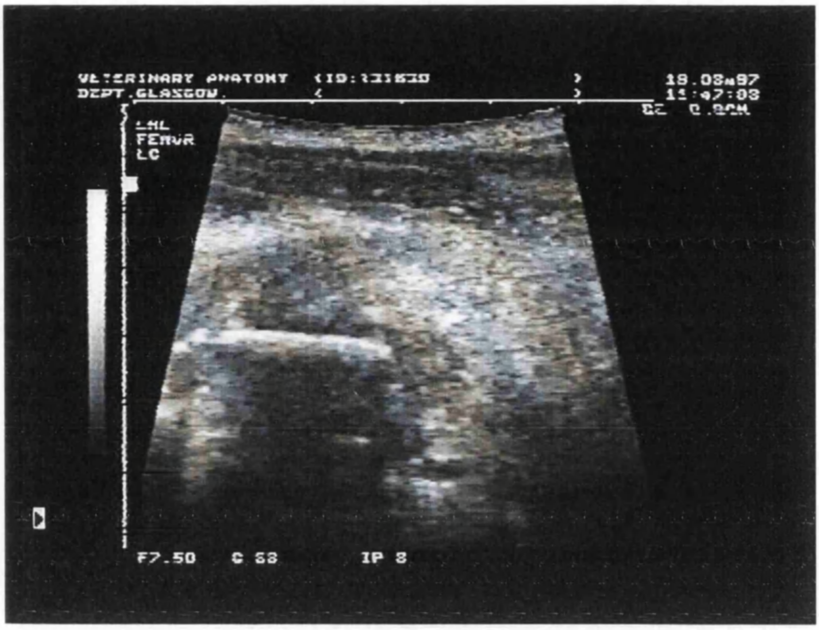

Figure 6.9.2

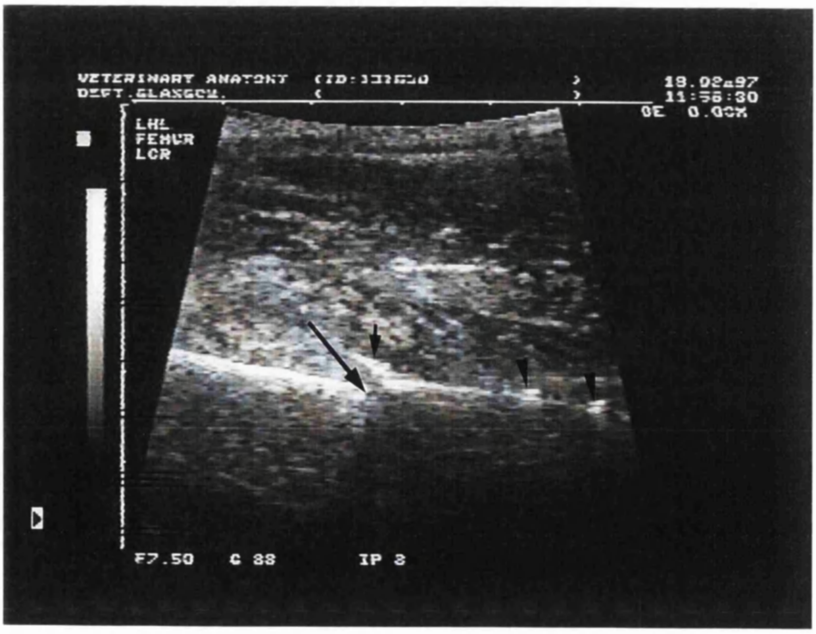

Figure 6.9.3

Figure 6.9.4 Ultrasonographic images of the area of extensive muscle damage caudal to the femur 24 hours after fracture repair. **a**, longitudinal scan from lateral aspect, **b**, transverse scan from caudal aspect. The area of muscle damage appears as a large, round hyperechoic structure with hypoechoic centre on longitudinal scan, and appears as a round area with a mixture of hyperechoic and hypoechoic structures on a transverse scan. Note also the fracture site area on the transverse scan (**b**), the bone fragment lying caudal to the fracture site (arrow head) appears hyperechoic with acoustic shadowing artefact.

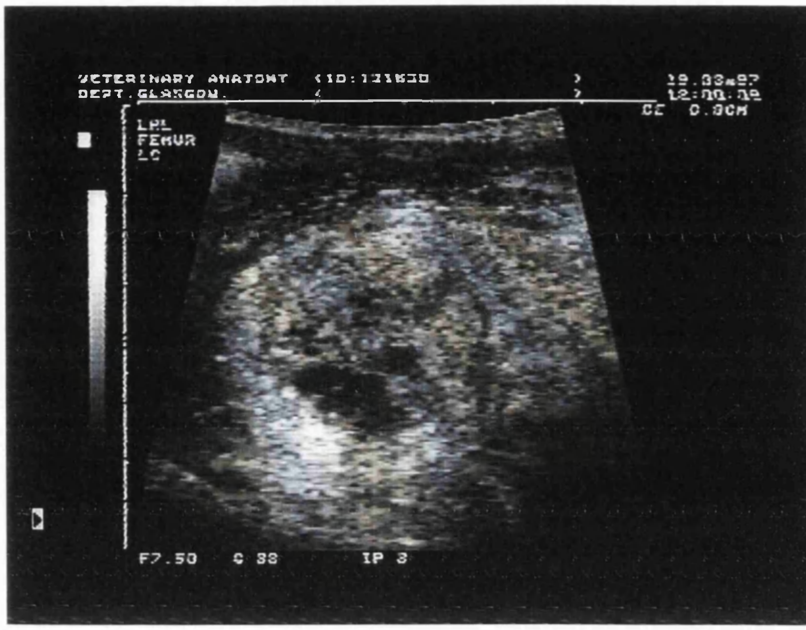

Figure 6.9.4a

Figure 6.9.4b

Figure 6.9.5 Longitudinal scan of the femur from the caudo-lateral aspect 24 hours after fracture repair demonstrates the intramedullary pin (arrow heads) which appears as a straight hyperechoic line and produces reverberation artefact. There is a large gap between the two fragments at the fracture site through which runs the intramedullary pin. The area of muscle damage superficial to the femur appears as disorganised hyperechoic structure.

Figure 6.9.6 Longitudinal scan of the femur from the caudal aspect on day two after fracture repair demonstrates the piece of bone fragment (arrow heads) which appears as an hyperechoic line lying above the proximal fragment with acoustic shadowing artefact.

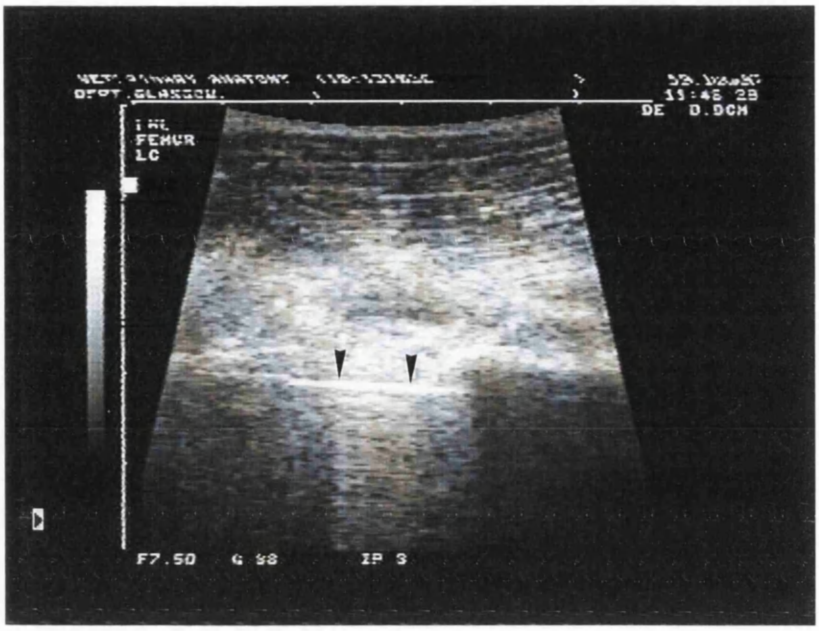

Figure 6.9.5

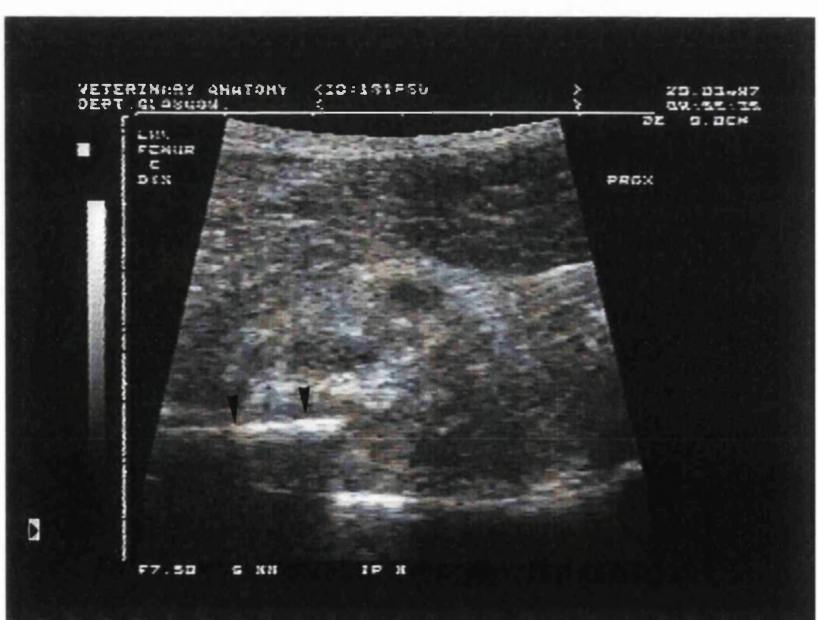

Figure 6.9.6

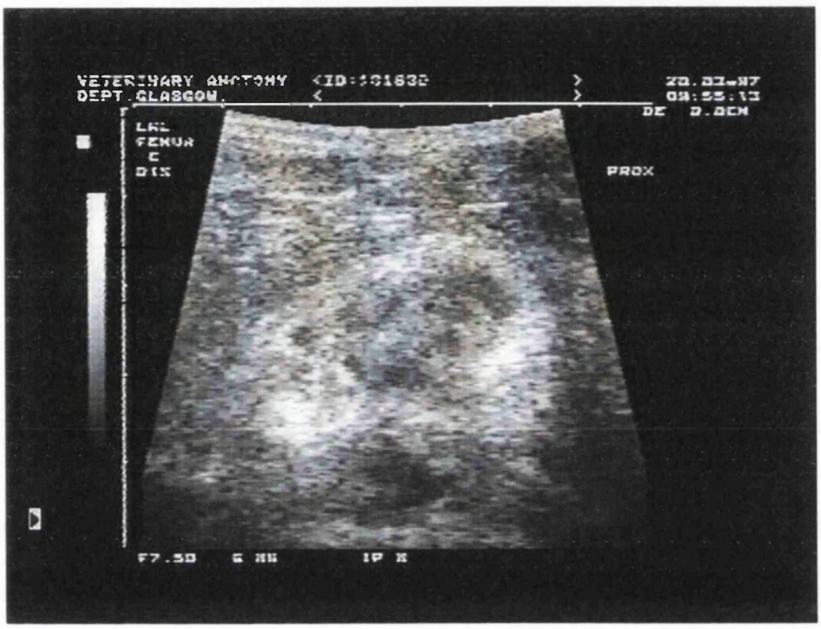

Figure 6.9.7 The area of muscle damage caudal to the femur scanned transversely on day two after fracture repair appears more echogenic and smaller than on the day one examination, but still remains round, disorganised and hyperechoic.

Figure 6.9.8 Radiographs taken at day 45 after fracture repair show the callus formation is bridging the fracture site and around the femoral shaft. **a**, cranial view, **b**, lateral view. This is suggestive of fracture healing. The fracture site is still visible. The bone fragment lying caudal to the femur has coalesced with the main fragment by bony callus.

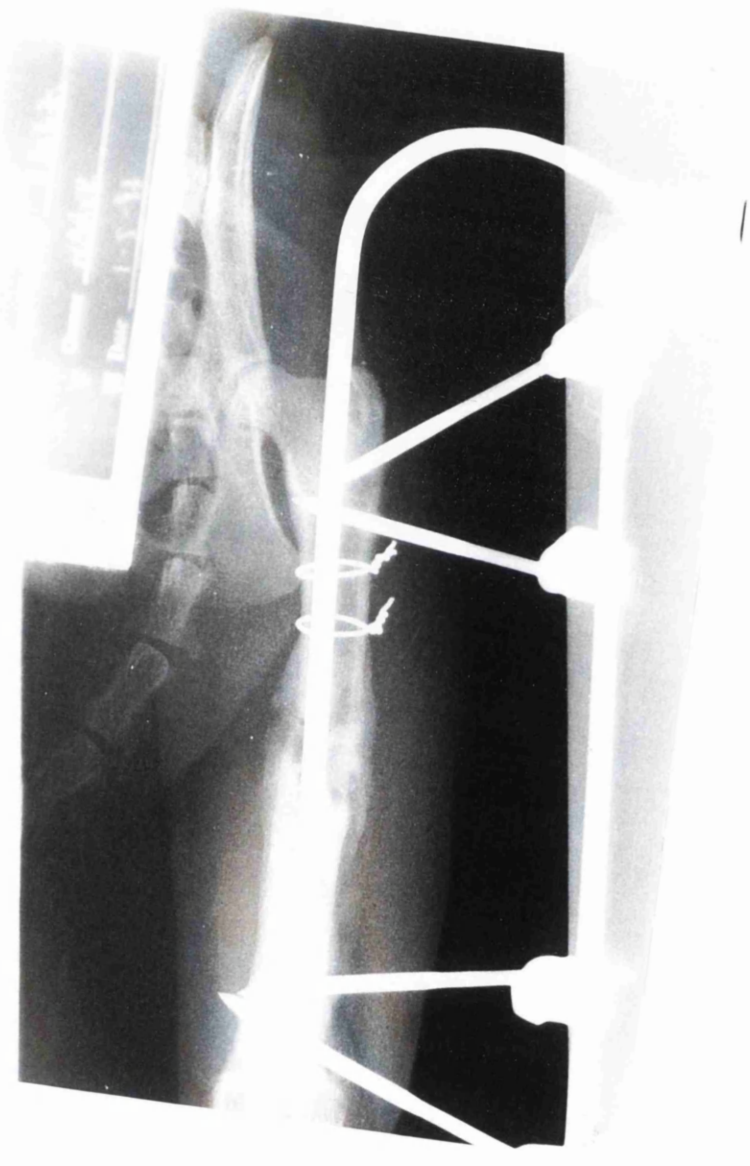

a

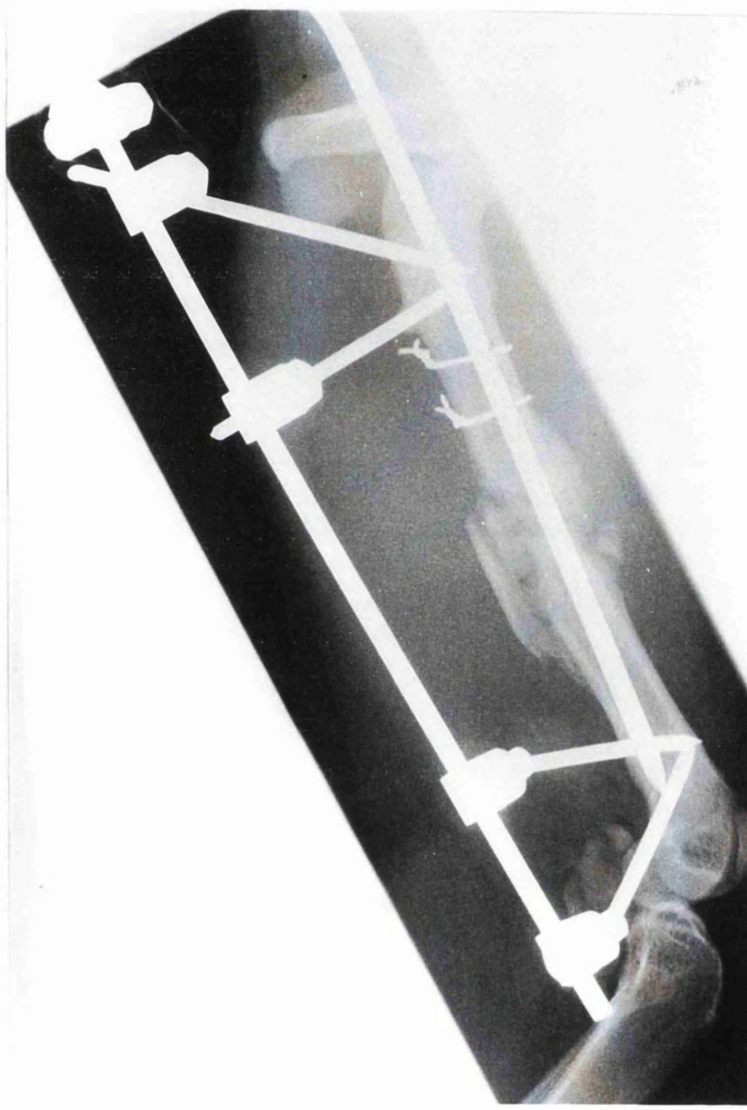

b

Figure 6.9.9 Longitudinal scans of the femur on day 45 after fracture repair demonstrate the femur with callus formation. **a**, lateral aspect, **b**, caudo-lateral aspect. The fracture site (arrow) still can be seen and appears as a vertical hyperechoic line and is occupied by the soft callus (**b**). The big fracture gap seen on the day two examination is no longer visible. The muscle structure has returned to its normal ultrasonographic structural appearance but is hyperechoic suggesting residual fibrosis.

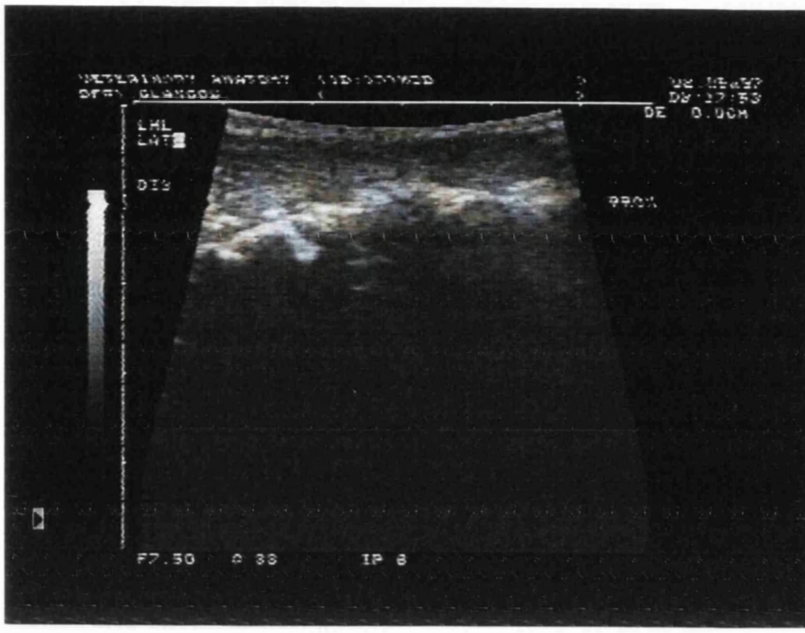

Figure 6.9.9a

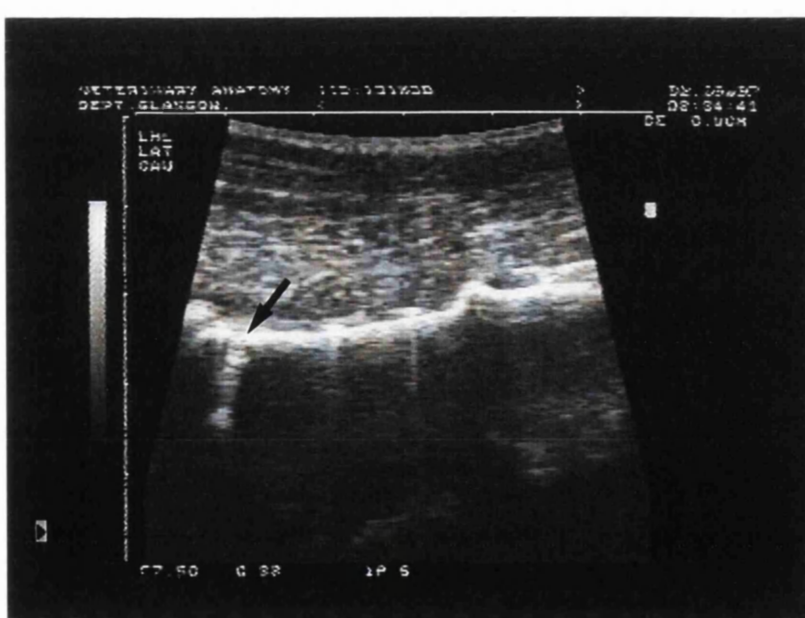

Figure 6.9.9b

Figure 6.9.10 Ultrasonographic images of the femur at the fracture site area on day 45 after fracture repair show the femoral with an uneven and rough hyperechoic surface due to callus formation. **a**, longitudinal scan, **b**, transverse scan. The femur appears bigger than normal on the transverse scan. The fracture site still can be seen with the presence of a small gap which appears hyperechoic suggesting the presence of periosteal tissue reaction on a transverse scan.

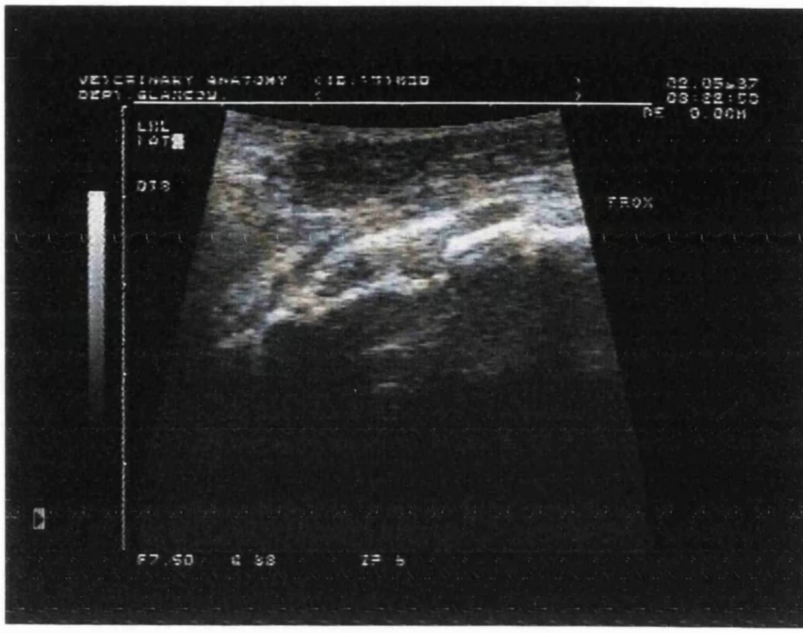

Figure 6.9.10a

Figure 6.9.10b

Figure 6.9.11 Ultrasonographic images of the muscle on day 45 after fracture repair demonstrate the previous area of muscle damage which has now returned to its normal muscle structure but has an hyperechoic appearance. **a**, longitudinal scan, **b**, transverse scan. The hyperechoic appearance is suggesting the presence of fibrous tissue within the muscle.

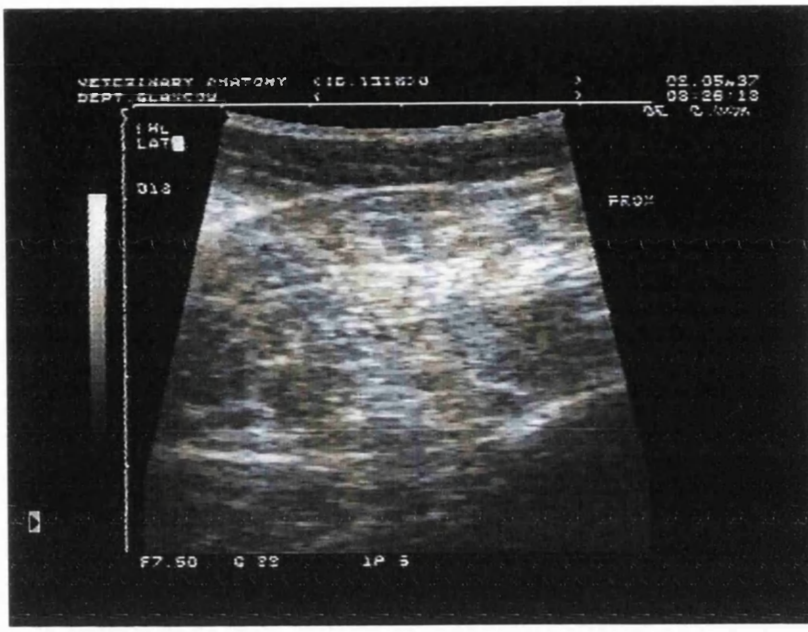

Figure 6.9.11a

Figure 6.9.11b

Case 10

A one year old male Border Collie was presented to the Glasgow University Veterinary Hospital after having been involved in a road traffic accident. Radiographic examination showed that an oblique fracture of the distal humerus had been sustained. Radiographs taken immediately after fracture repair demonstrated a humeral fracture which had been reduced and immobilised with a plate and screws (figure 6.10.1). The plate was placed on the medial aspect of the humerus. The fracture repair resulted in a good union and alignment. There was no fracture gap present and the fracture line was hardly visible radiographically.

Ultrasonographic examination

Day three after fracture repair

Ultrasonographic examination demonstrated the fracture site which appeared as a short hyperechoic vertical line on a longitudinal scan from the cranial aspect (figure 6.10.2). The two fragments were well united and there was no obvious gap present. A disorganised hyperechoic area imaged above the humerus suggested a soft tissue reaction. Soft tissue reactions were also found around the screws and appeared as disorganised hyperechoic structures (figure 6.10.3). The fracture site imaged from the caudo-lateral aspect appeared hyperechoic which suggested the presence of periosteal tissue reaction (figure 6.10.4). At this stage no callus formation could be detected at the fracture site. The area of soft tissue reaction imaged on a transverse scan appeared as a disorganised hyperechoic structure as previously seen on the longitudinal scan (figure 6.10.5). The fracture site was not clearly seen on a transverse scan but it could be recognised by the defective or abnormal appearance of the humerus.

Day five after fracture repair

Ultrasonographic examination demonstrated the humerus with some soft callus formation . The soft callus appeared as hyperechoic material adhering to the bone surface at the fracture site area (periosteum) (figure 6.10.6a and 6.10.6b). The short hyperechoic vertical line seen at the fracture site on the day three examination had disappeared. Soft callus formation was developing at the fracture site but produced no shadow artefact. The soft tissue reaction around the screws seen on the day three examination had become more distinct and appeared as disorganised hyperechoic structures (figure 6.10.7). An area of soft tissue reaction still appeared as a disorganised hyperechoic structure on the transverse scan as had been seen on the day three examination.

Day 52 (approximately 8 weeks) after fracture repair

Radiographic examination

Radiographs taken on day 52 after fracture repair showed there was no fracture line visible. The fracture site had been bridged by the mature callus which was remodelling. There was no evidence of lucency around the screws and the healing process was good (figure 6.10.8).

Ultrasonographic examination

Ultrasonographic examination demonstrated the smooth, straight hyperechoic surface of the humerus with only a slight uneven bone surface on caudo-lateral aspect (figure 6.10.9). Callus formation that normally results in a rough bone surface was not seen at this stage. This suggested that the bone had been remodelled. There was no more soft tissue reaction within the muscle and the muscle appeared to have normal ultrasonographic characteristics (figure

6.10.10). The size of the brachial muscle had reduced as shown by the decreased distance between the skin surface and the humerus. This was suggestive of muscle atrophy. Ultrasonographically, the healing process was good.

Figure 6.10.1 Radiographs obtained immediately after fracture repair demonstrate the fracture which has been reduced and immobilised with a plate and screws. **a**, lateral view, **b**, cranial view. The repair process has resulted in a good union and alignment of the fracture. There is no fracture gap present and the fracture line is hardly visible.

b

Figure 6.10.2 Longitudinal scan of the humerus from the cranial aspect on day three after fracture repair shows the fracture site which appears as a short hyperechoic vertical line across the humerus (arrow). The two fragments are well united and there is no obvious gap present. Note also an area of soft tissue reaction appearing disorganised and hyperechoic.

Figure 6.10.3 Longitudinal scan of the humerus from the lateral aspect on day three after fracture repair shows the soft tissue reaction around screws which appears disorganised and hyperechoic. The screws appear hyperechoic with comet tail artefacts.

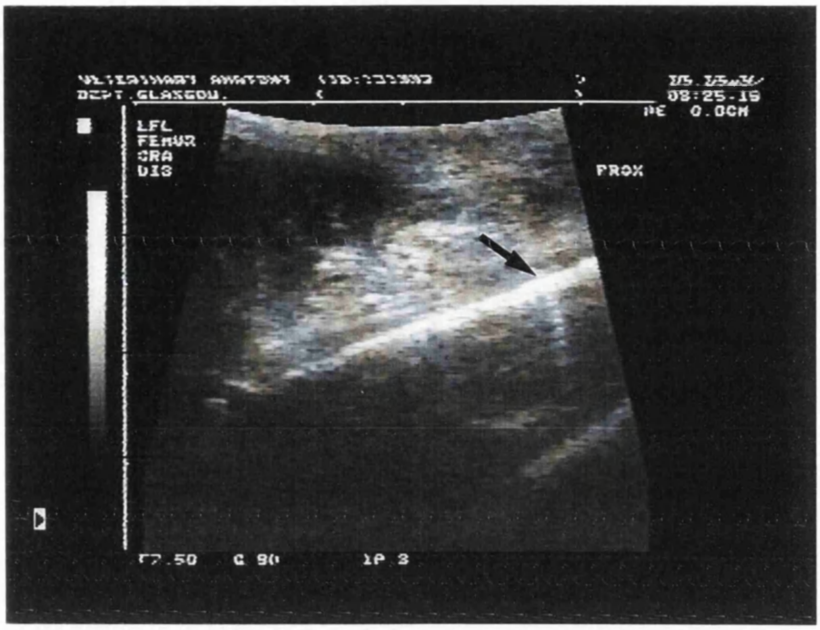

Figure 6.10.2

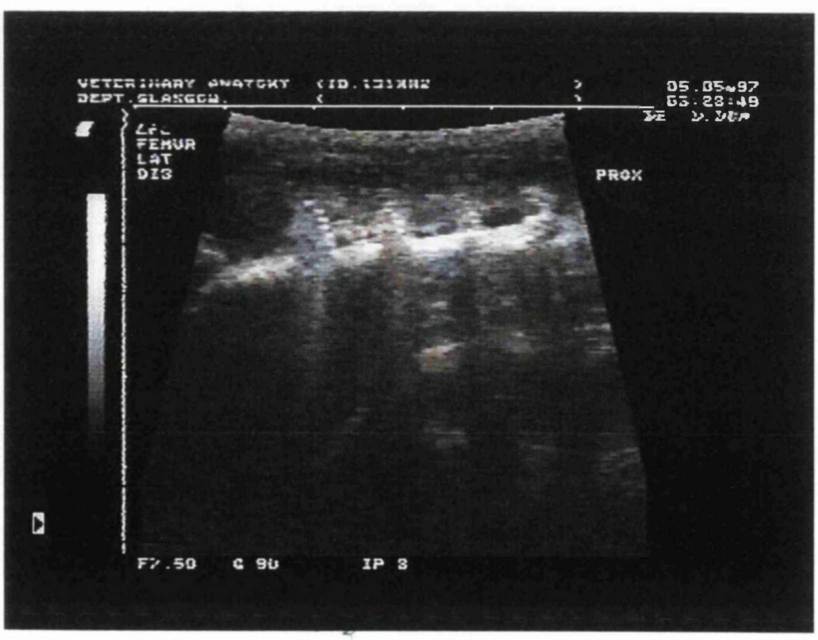

Figure 6.10.3

Figure 6.10.4 Longitudinal scan of the humerus from the caudo-lateral aspect on day three after fracture repair shows the fracture site (arrow) which appears hyperechoic suggesting the presence of periosteal tissue reaction. At this stage no callus formation can be detected at the fracture site.

Figure 6.10.5 Transverse scan from the caudal aspect on day three after fracture repair shows the area of soft tissue reaction which appears as a disorganised hyperechoic structure. The fracture site is not clearly seen on a transverse scan but it can be recognised by the abnormal appearance of the humerus. **H**, humerus.

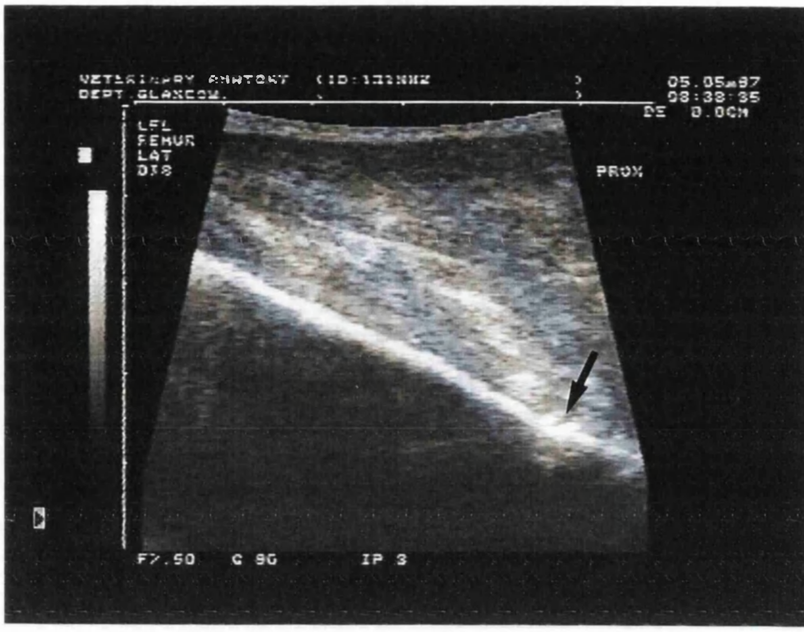

Figure 6.10.4

Figure 6.10.5

Figure 6.10.6 Ultrasonographic examination of the humerus on day five after fracture repair, **a**, longitudinal scan from the caudo-lateral aspect, **b**, transverse scan from the cranio-lateral aspect demonstrates soft callus formation (arrow head) which appears as hyperechoic material adhering to the periosteum at the fracture site area. The short hyperechoic vertical line at the fracture site as seen on the day three examination has disappeared. Note also that there is no shadow artefact produced by the soft callus.

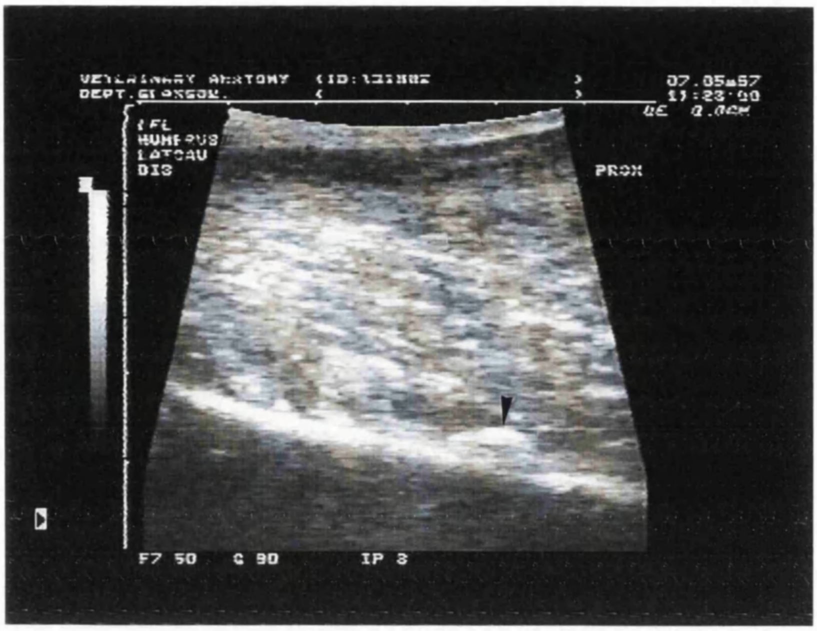

Figure 6.10.6a

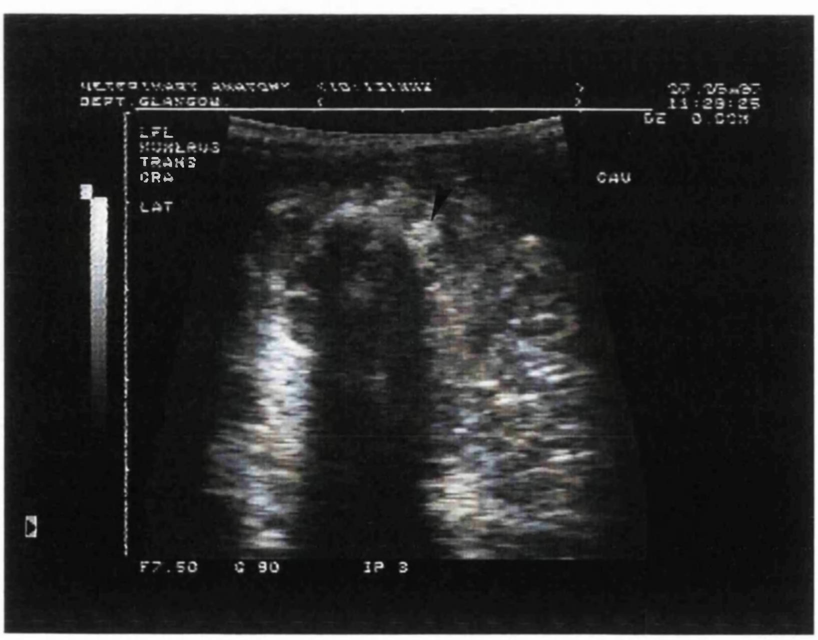

Figure 6.10.6b

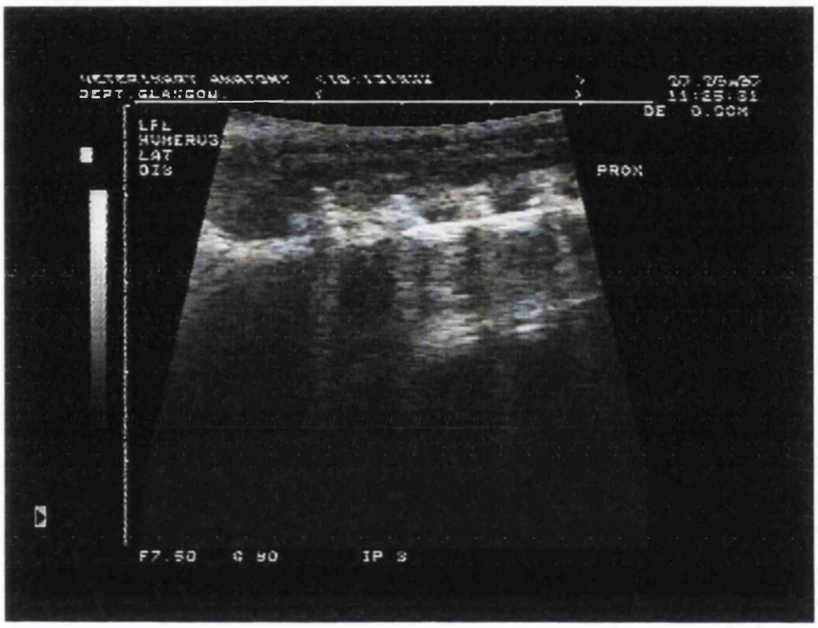

Figure 6.10.7 Longitudinal scan of the humerus from the lateral aspect on day five after fracture repair shows the soft tissue reaction around the screws appearing disorganised and hyperechoic.

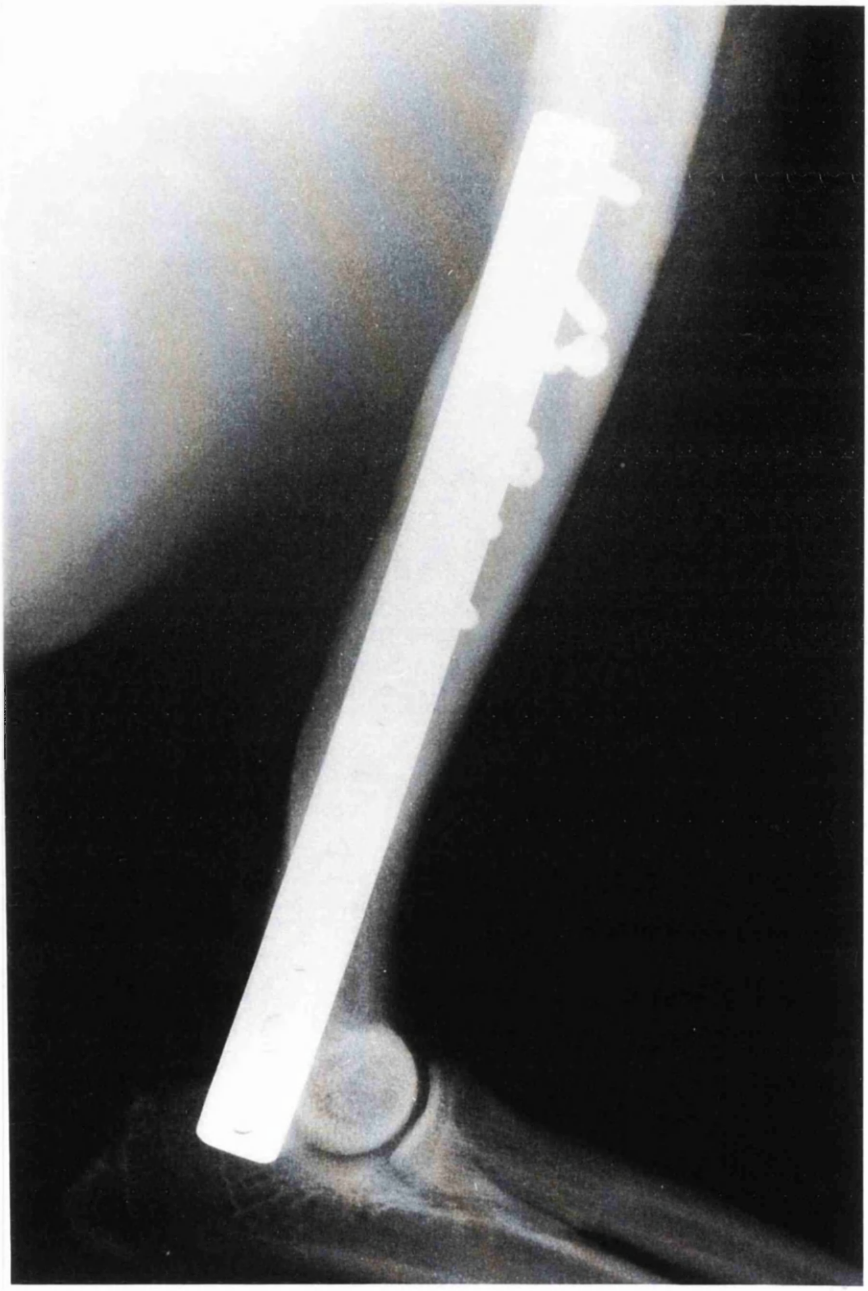

Figure 6.10.8 Radiograph taken on day 52 after fracture repair shows there is no more fracture line visible. The fracture site has been completely bridged by the mature callus which is remodelling. There is no evidence of lucency around the screws and the healing is excellent.

Figure 6.10.9 Longitudinal scan from the caudo-lateral aspect of the humerus on day 52 after fracture repair demonstrates the smooth, straight hyperechoic humerus with only a slight uneven bone surface which suggest that the bone is remodelling.

Figure 6.10.10 Transverse scan from the caudo-lateral aspect on day 52 after fracture repair shows the normal appearance of the muscle. There is no more soft tissue reaction found in the muscle. **H** humerus.

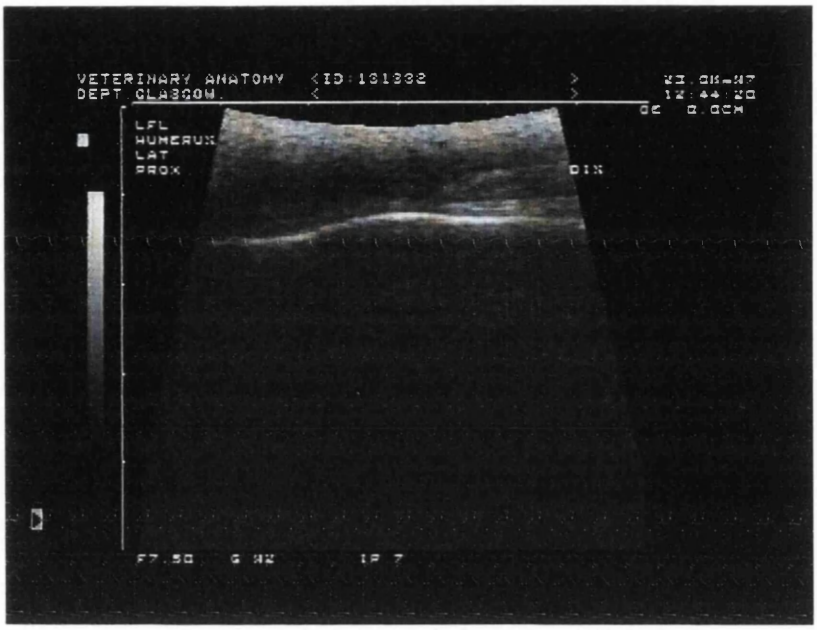

Figure 6.10.9

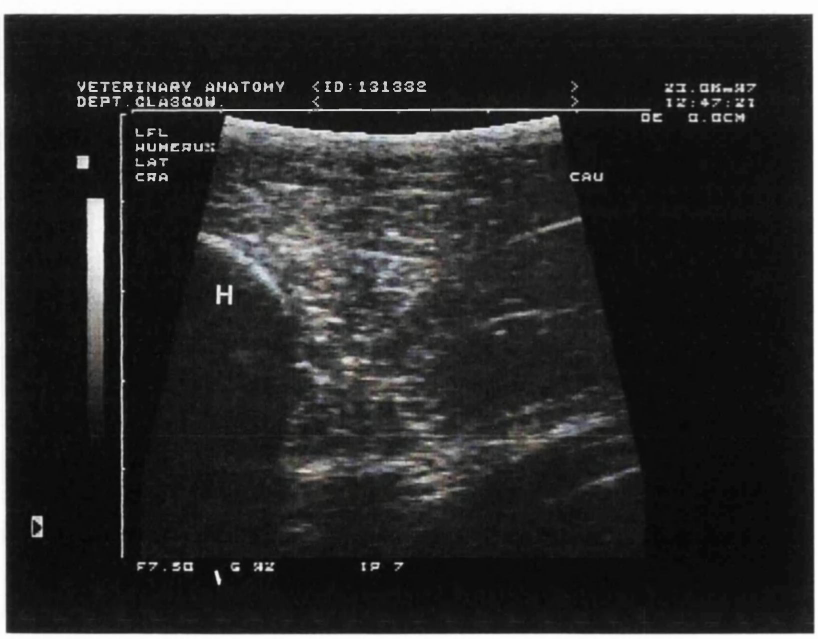

Figure 6.10.10

AN ULTRASONOGRAPHIC STUDY OF MUSCULOSKELETAL INJURIES AND MAMMARY GLAND TUMOUR IN SMALL ANIMALS

A thesis submitted to the Faculty of Veterinary Medicine,
University of Glasgow.
For the Degree of Doctor of Philosophy

by

MD ZUKI ABU BAKAR@ZAKARIA.
D.V.M. (Putra University of Malaysia)

Division of Veterinary Anatomy,
Department of Veterinary Preclinical Studies,
School of Veterinary Medicine,
University of Glasgow,
March, 1999

VOLUME 2(ii)

CONTENTS -VOLUME 2(ii)

LIST OF FIGURES

Case 11

A 15 year old female cross breed dog, weight 15 kg, was presented to the Glasgow University Veterinary Hospital after having been involved in a road traffic accident. Radiographic examination revealed that a comminuted oblique fracture of the mid-shaft of the left tibia/fibula had been sustained. There were also fractures of the second and third metatarsal bones but they were not included in this study. Surgery was carried out on the following day after the admission. The fracture site was opened via a medial approach and revealed an oblique comminuted fracture with one fragment from the distal bone impacted into the distal medullary cavity. This fragment was then extracted. An intramedullary pin was inserted normograde from the stifle joint to align the fracture fragments. An external fixator was then applied to restrict movement and shearing forces. The external fixator consisted of two transfixing pins proximal to the fracture and two pins distal to the fracture. Overall, the fracture was well aligned and the prognosis was good. The muscle was closed with 2/0 vicryl in a subarticular pattern.

Radiographs taken immediately after fracture repair showed the tibial fracture had been reduced and stabilised with an intramedullary pin and I/E fixator (figure 6.11.1). The fracture line was clearly visible. The repair process had resulted in a good alignment.

Ultrasonographic examination

Day three after fracture repair

Ultrasonographic examination on the lateral aspect of the tibia demonstrated the fracture site which appeared well aligned (figure 6.11.2). There was a hyperechoic layer on the bone surface which suggested a periosteal tissue reaction. The muscle structure imaged on a longitudinal scan appeared to have normal ultrasonographic characteristic. The fracture site imaged on transverse scan revealed the presence of a gap (figure 6.11.3). There was no indication of soft callus formation to be found on the transverse scan.

Day five after fracture repair

Ultrasonographic examination of the tibia on the lateral aspect demonstrated the fracture site which had the appearance of the proximal fragment overriding the distal fragment (figure 6.11.4). This had not been evident on the day three examination. No callus formation was found at this stage. On the medial aspect, the distal fragment appeared slightly elevated from the proximal fragment (figure 6.11.5), and the fracture gap could be seen at the fracture site. The hyperechoic area seen at the fracture site suggested the present of periosteal tissue reaction. A transverse scan of the tibia showed that the fracture gap still persisted as demonstrated on the day three examination but this time it appeared hyperechoic due to the periosteal tissue reaction (figure 6.11.6).

Day 56 (8 weeks) after fracture repair

Radiographic examination

Radiographs taken at day 56 after fracture repair showed that the callus formation had completely bridged the fracture site (figure 6.11.7). The fracture line was much less evident at this stage seen on a lateral view. A slight curve of the shaft in a cranial direction was noted. Union of the fibula fracture was also evident. The implant was removed at this time.

Ultrasonographic examination

Ultrasonographic examination immediately after the implant removal demonstrated the smooth hyperechoic appearance of the tibia (figure 6.11.8a). The fracture site had been completely bridged by the mature callus and remodelled. Thus, it was not found during examination. One hole was found on the bone surface distally and appeared hyperechoic which was believed to be due to soft tissue reaction (figure 6.11.8b). This hole was actually the site where the external fixator pin was placed before being removed. The tibia imaged on a longitudinal scan from the lateral aspect appeared slightly bent at the fracture site area (figure 6.11.9). A transverse scan from caudal aspect of the tibia showed the area of the fracture site with no gap present. Ultrasonographically, the healing process was satisfactory.

Figure 6.11.1 Radiographs taken immediately after fracture repair, **a**, cranial view, **b**, lateral view, show the tibial fracture which has been reduced and stabilised with an intramedullary pin and I/E fixator. The external fixator consists of two transfixing pins proximal to the fracture and two pins distal to the fracture. The fracture line is clearly visible. The repair process had resulted in good alignment.

a

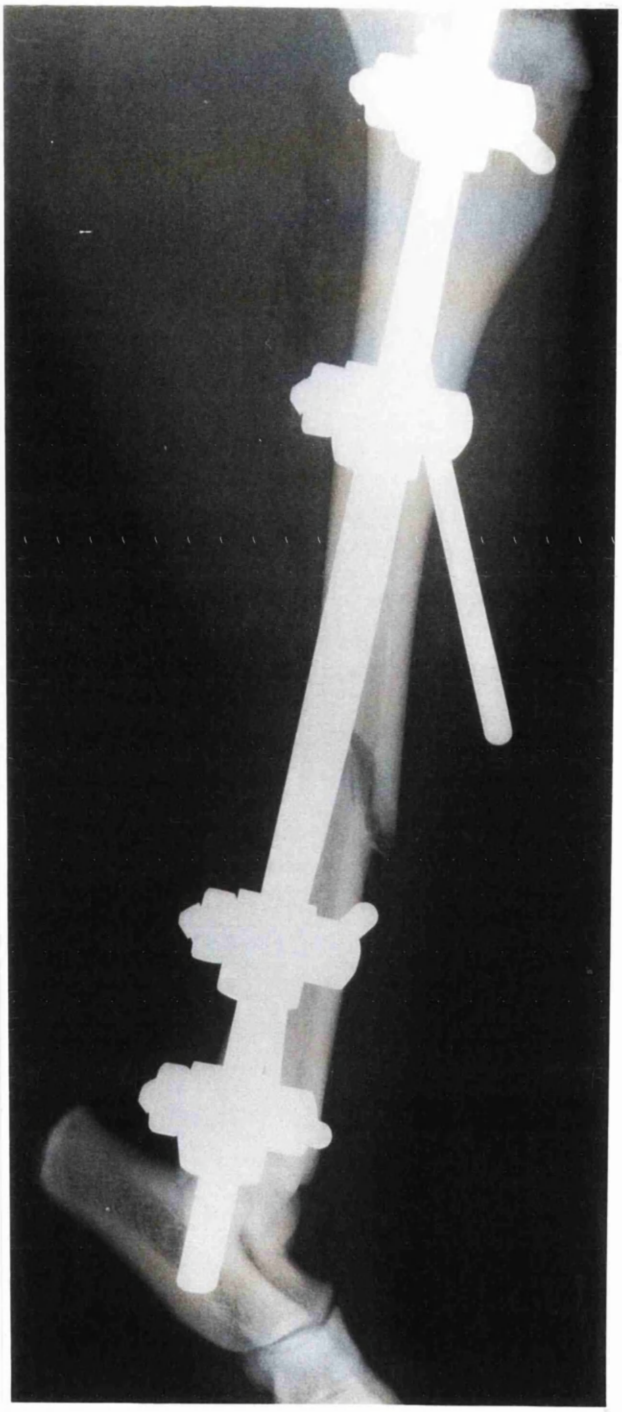

b

Figure 6.11.2 Longitudinal scan of the tibia from the lateral aspect on day three after fracture repair shows the fracture site (arrow head) which appears well aligned. There is a hyperechoic layer on the bone surface which indicates the presence of some periosteal tissue reaction.

Figure 6.11.3 Transverse scan of the tibia from the lateral aspect on day three after fracture repair shows the tibia at the fracture site area with the presence of a gap. **T**, tibia.

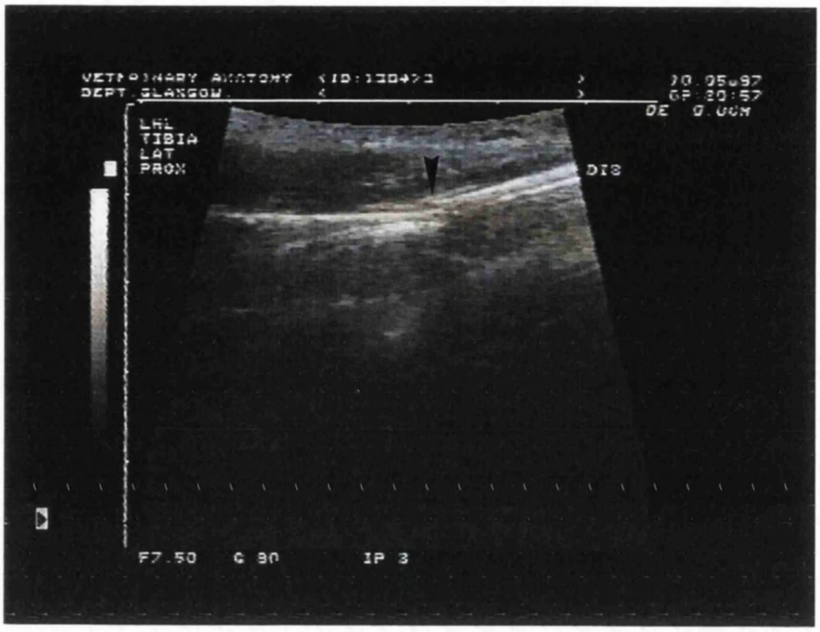

Figure 6.11.2

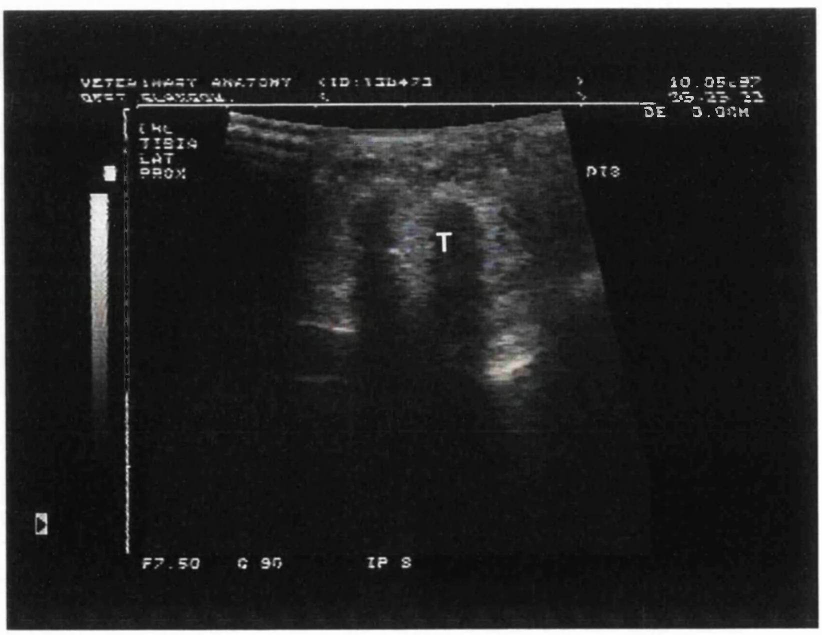

Figure 6.11.3

Figure 6.11.4 Longitudinal scan of the tibia from the lateral aspect on day five after fracture repair demonstrates the fracture site which appears as having the distal fragment overriding the proximal fragment. No callus formation is to be found.

Figure 6.11.5 Longitudinal scan of the tibia from the medial aspect on day five after fracture repair shows the presence of fracture gap at the fracture site. The hyperechoic area of the fracture site suggests the present of periosteal tissue reaction. Note also that the distal fragment (arrow head) appears slightly elevated from the proximal fragment which is in agreement with the previous image.

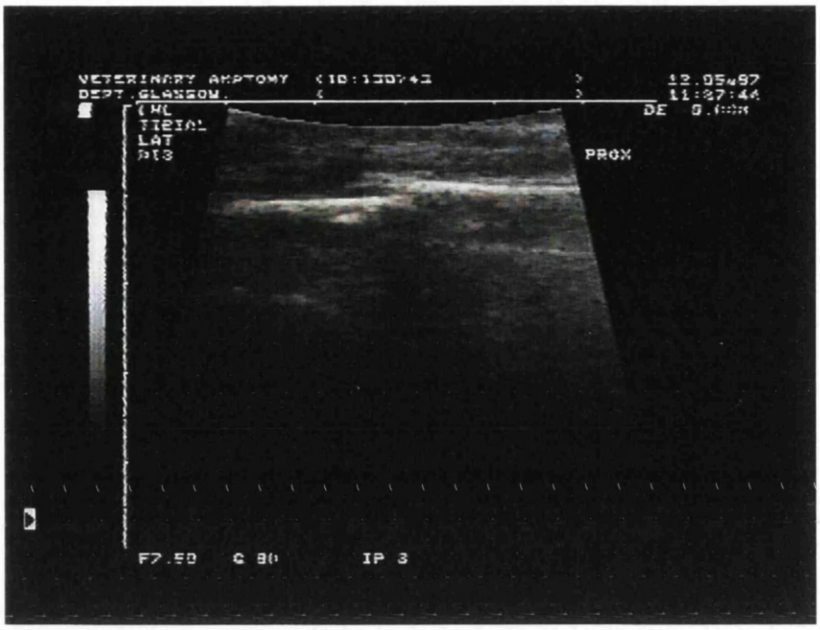

Figure 6.11.4

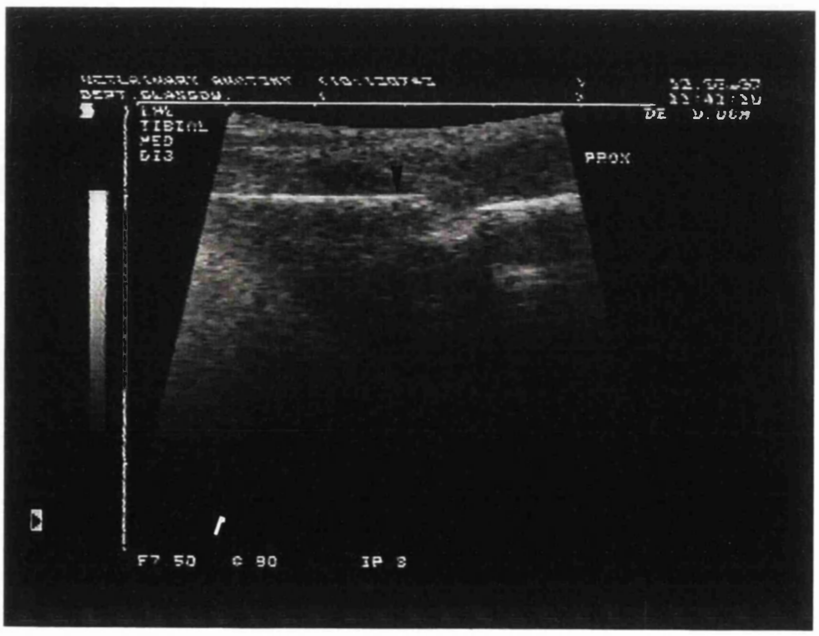

Figure 6.11.5

Figure 6.11.6 Transverse scan of the tibia from the lateral aspect on day five after fracture repair shows the fracture site with an hyperechoic appearance suggesting the periosteal tissue reaction. The fracture gap is still present. **T**, tibia.

Figure 6.11.7 Radiographs taken at day 56 after fracture repair show that the callus formation has completely bridged the fracture site. **a**, lateral view, **b**, cranial view. The fracture line is much less evident at this stage (**a**). A slight curve of the shaft in a cranial direction is noted. Union of the fibula fracture is also evident.

a

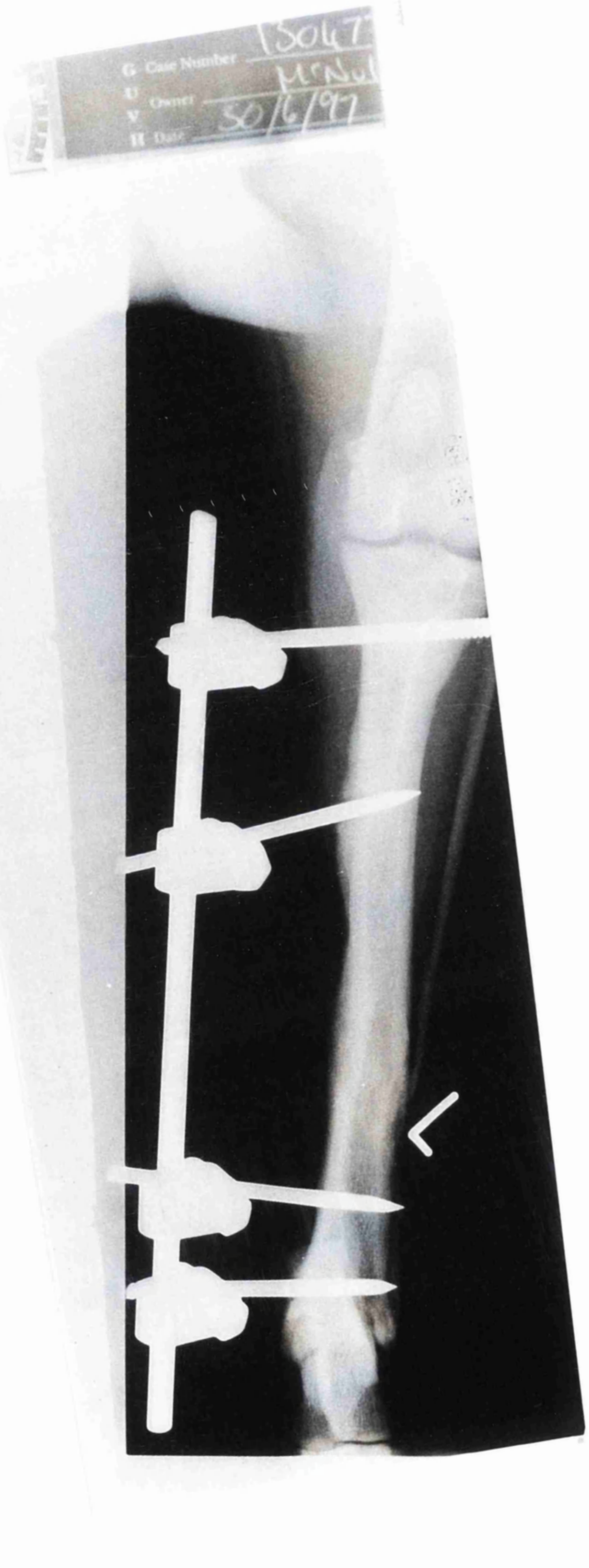

b

Figure 6.11.8 Longitudinal scans of the tibia from the lateral aspect on day 56 after fracture repair (immediately after implant removal) demonstrate the tibia with a smooth hyperechoic appearance (**a**). There is no fracture site to be found during examination. The fracture site has been completely bridged by the mature callus and remodelled. One hole was found on the medial aspect of the tibia distally (**b**) and appears hyperechoic which suggest a soft tissue reaction. This hole is actually the site where the external fixator pin was placed before being removed.

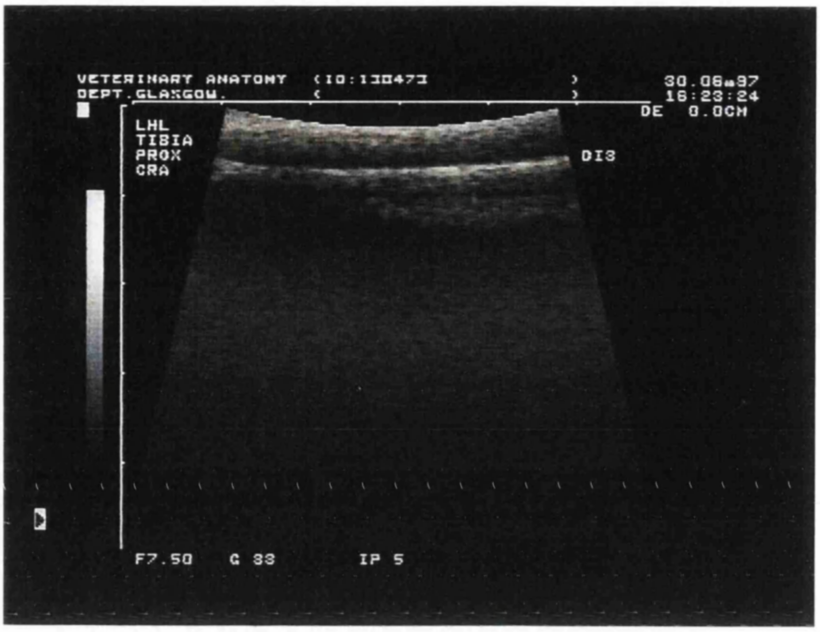

Figure 6.11.8a

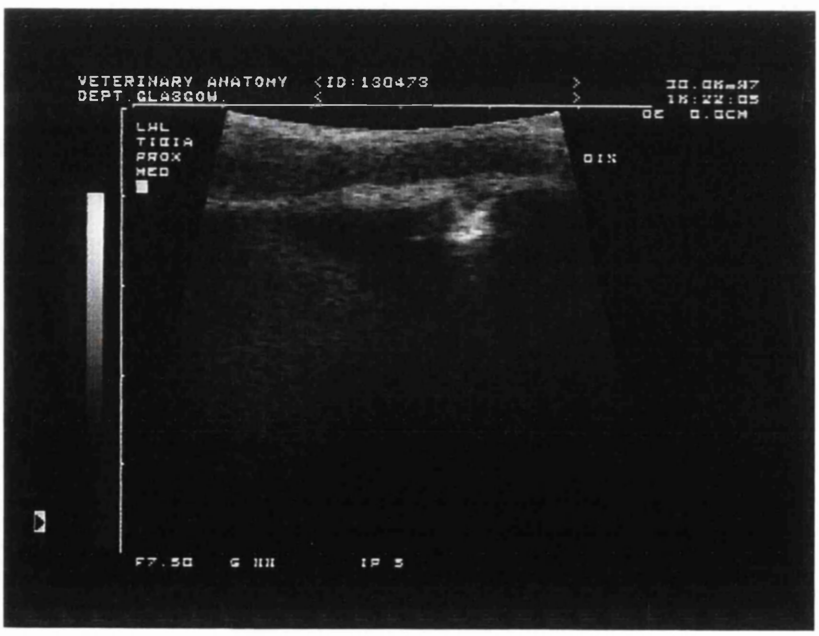

Figure 6.11.8b

Figure 6.11.9 Longitudinal scan of the tibia from the caudal aspect on day 56 after fracture repair shows the tibia which appears slightly bent at the fracture site area.

Figure 6.11.10 Transverse scan of the tibia from the caudal aspect on day 56 after fracture repair shows the tibia at the fracture site area. The fracture gap is no longer present. The tibia appears as a normal round hyperechoic structure. Note also that the fibula on lateral side of the tibia appears hyperechoic with acoustic shadowing artefact. **T**, tibia, **Fi**, fibula.

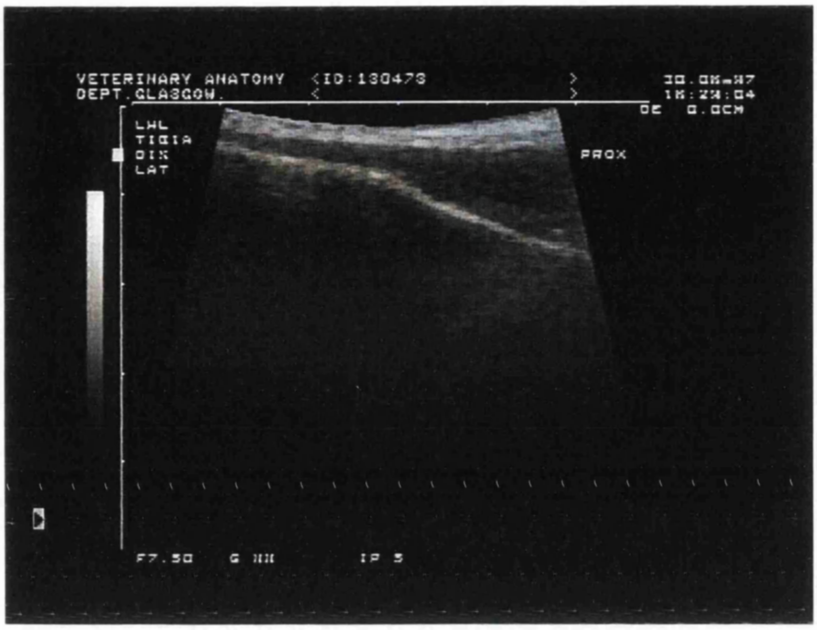

Figure 6.11.9

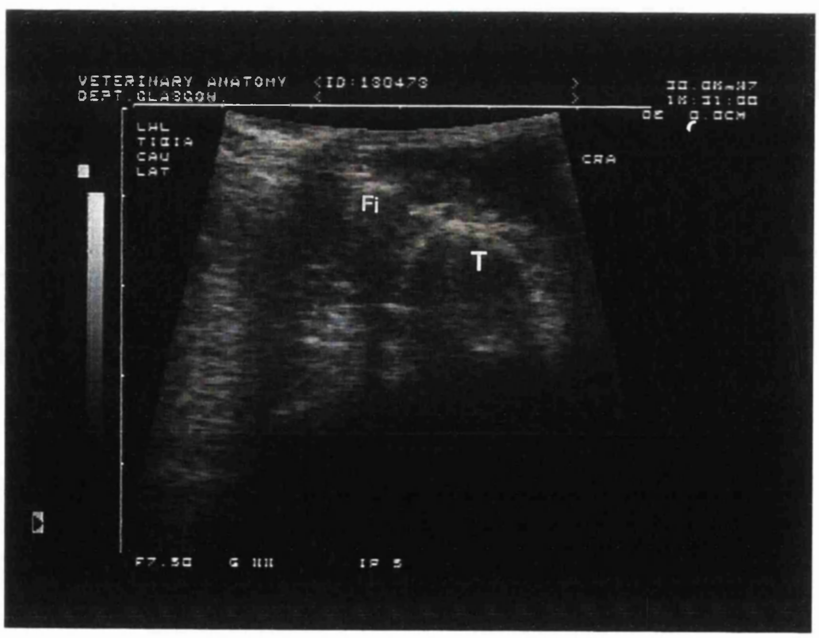

Figure 6.11.10

Case 12

A five year old female neutered Border Collie, weight 12.5 kg, was presented to the Glasgow University Veterinary Hospital with the complaint of left forelimb lameness after being kicked three days previously. Clinically, the animal had an obvious left forelimb lameness during examination and was holding the limb flexed. A fracture of the left humerus was palpable. Radiographs taken before repair showed that the dog had sustained a simple oblique fracture of the mid-shaft of the left humerus. Surgery was carried out and the fracture stabilised with a normograde intramedullary pin plus an eight hole 2.7 mm plate applied to the lateral side of the humerus using monocortical screws. Post-operation radiographs showed that the repair had resulted in a good alignment (figure 6.12.1). There was an open fracture gap medially.

Ultrasonographic examination

Day two after fracture repair

Ultrasonographic examination of the humerus scanned from the medial aspect demonstrated the fracture site which appeared as discontinuity of the bone surface with the presence of a fracture gap (figure 6.12.2). The hyperechoic structure at the fracture site suggested an area of soft tissue reaction. The fracture gap appeared smaller on the cranial side of the femur than on the medial side (figure 6.12.3a), and the gap was not shown on the caudal side of the femur (figure 6.12.3b). The distal fragment appeared slightly elevated from the proximal fragment on the caudal aspect scan. One screw was imaged some distance away from the fracture site with some periosteal tissue reaction at the screw base which appeared as hyperechoic material (figure 6.12.4). A transverse scan at the fracture site on the medial aspect showed the humeral bone surface with a space (fracture gap) and hyperechoic material which produced comet tail artefact (figure 6.12.5). The hyperechoic material was actually the intramedullary pin that was used in the fracture reduction. The animal failed to return for a follow up check and no follow up ultrasonographic scans are available.

Figure 6.12.1 Radiographs obtained immediately after the fracture repair show the repair process resulting in a good alignment. **a**, lateral view, **b**, cranial view. The fracture is stabilised with an intramedullary pin plus an eight hole 2.7 mm plate applied to the lateral side of the humerus using monocortical screws. There is an open fracture gap medially.

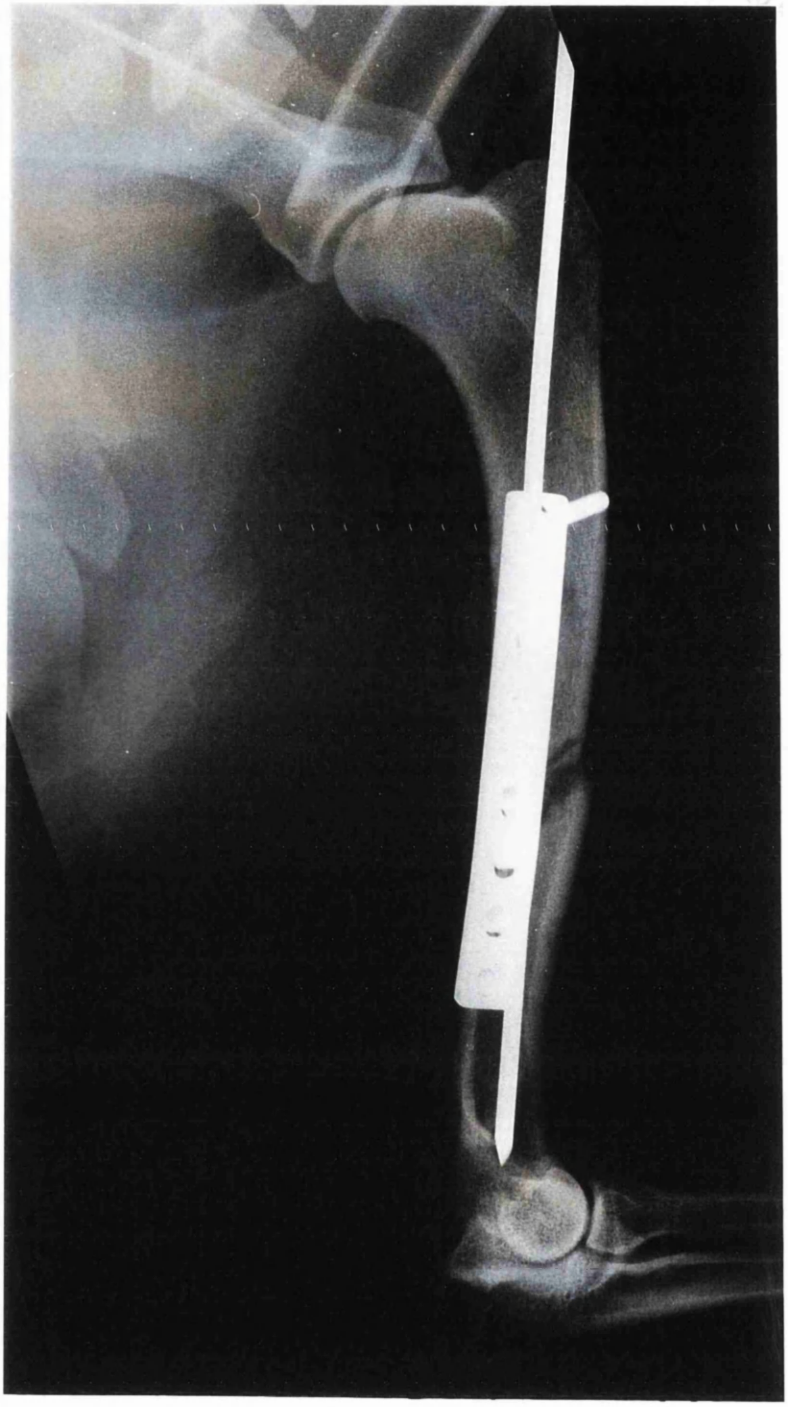

a

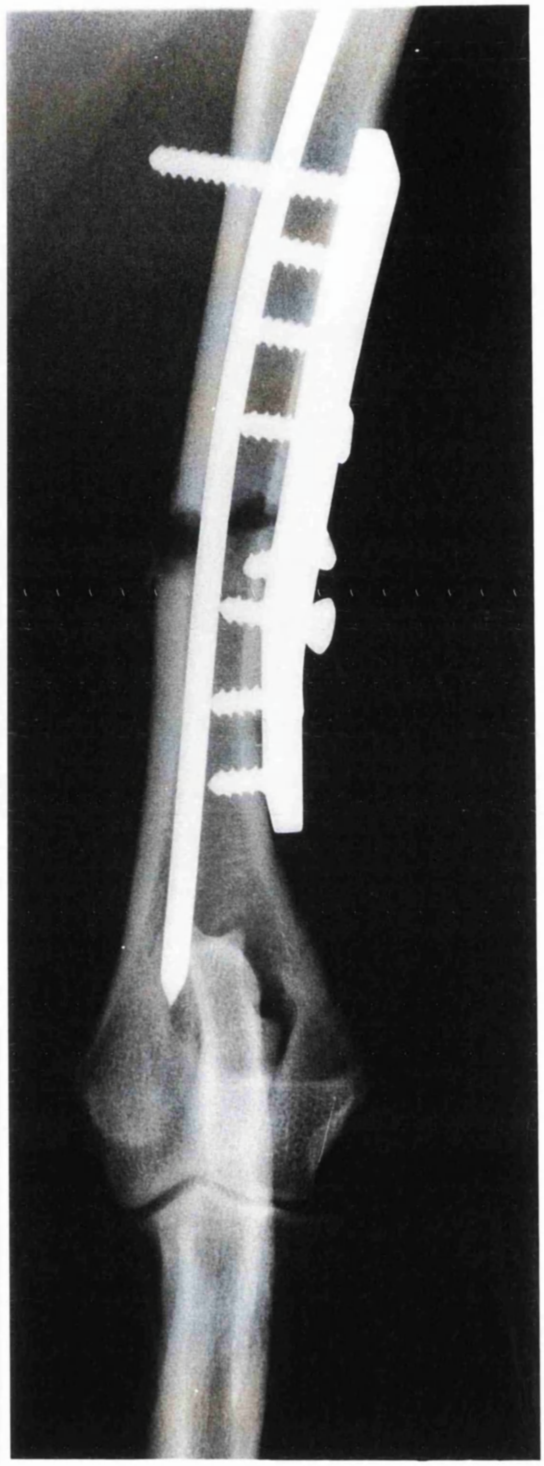

b

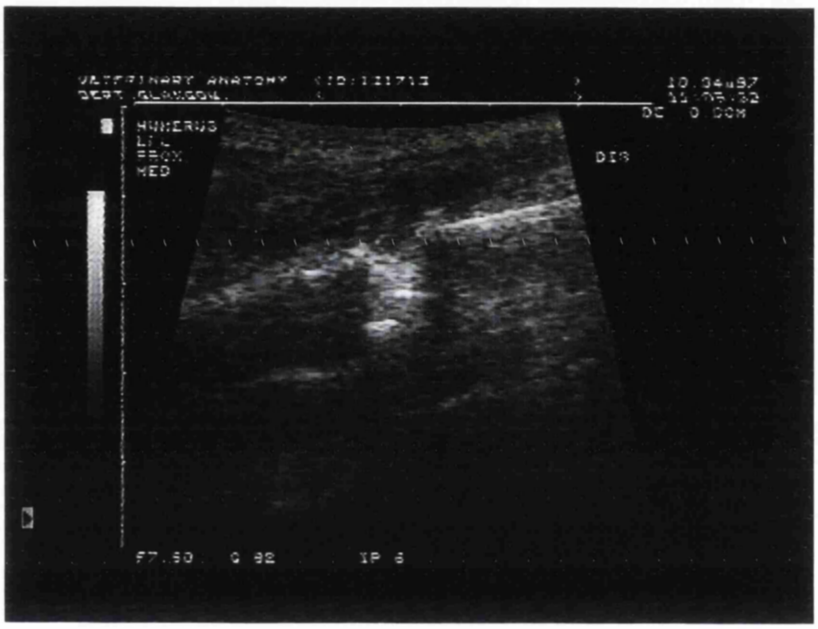

Figure 6.12.2 Longitudinal scan of the humerus from the medial aspect 48 hours after fracture repair demonstrates the fracture site which appears as discontinuity of the bone surface. There is a fracture gap present. The hyperechoic structure at the fracture site may indicate soft tissue reaction.

Figure 6.12.3 Longitudinal images of the humerus from the cranial aspect 48 hours after fracture repair demonstrate the fracture site with a small gap (arrow head). **a**, cranial aspect, **b**, caudal aspect. The fracture gap on the cranial side of the humerus appears smaller than on the medial side, and there is no gap present on the caudal side of the femur. Note also that the proximal fragment (arrow head) appears slightly elevated from the proximal fragment on the caudal aspect scan (**b**).

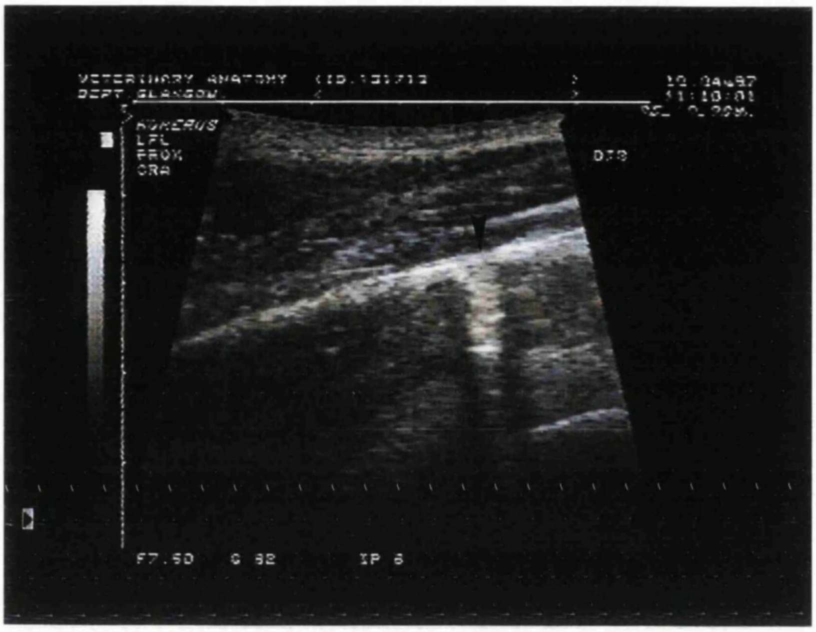

Figure 6.12.3a

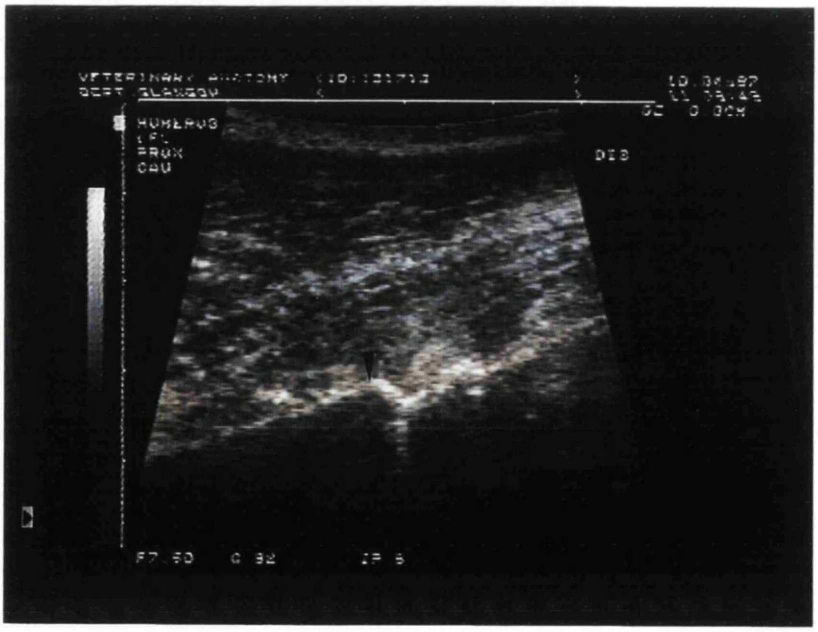

Figure 6.12.3b

Figure 6.12.4 Longitudinal scan of the humerus from the medial aspect 48 hours after fracture repair shows a screw (arrow head) some distance away from the fracture site (arrow) with some periosteal reaction detected at the screw base appearing as hyperechoic material.

Figure 6.12.5 Transverse scan of the humerus from the medial aspect 48 hours after fracture repair shows the fracture site which appears hyperechoic suggesting a periosteal tissue reaction. The hyperechoic material (arrow head) with comet tail artefact is actually the intramedullary pin that was used in the fracture reduction. **H**, humerus.

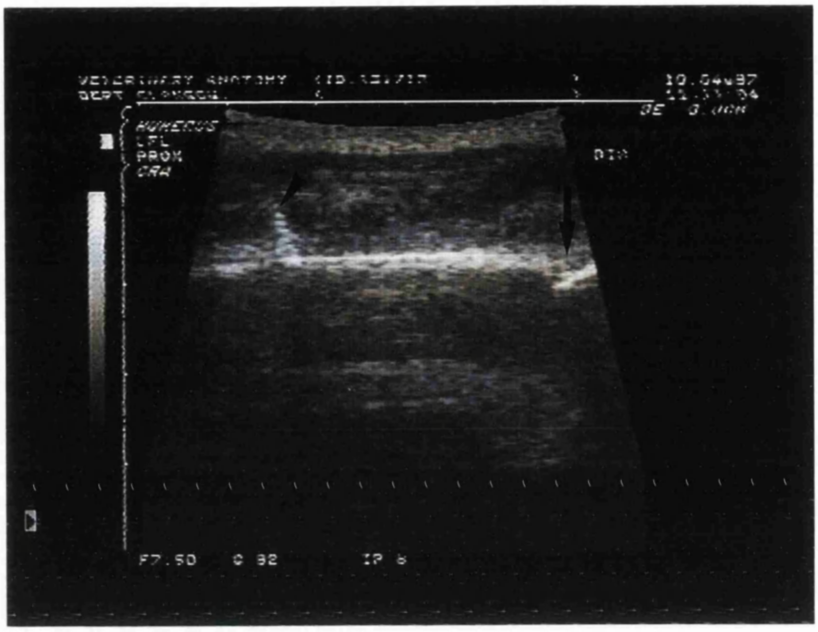

Figure 6.12.4

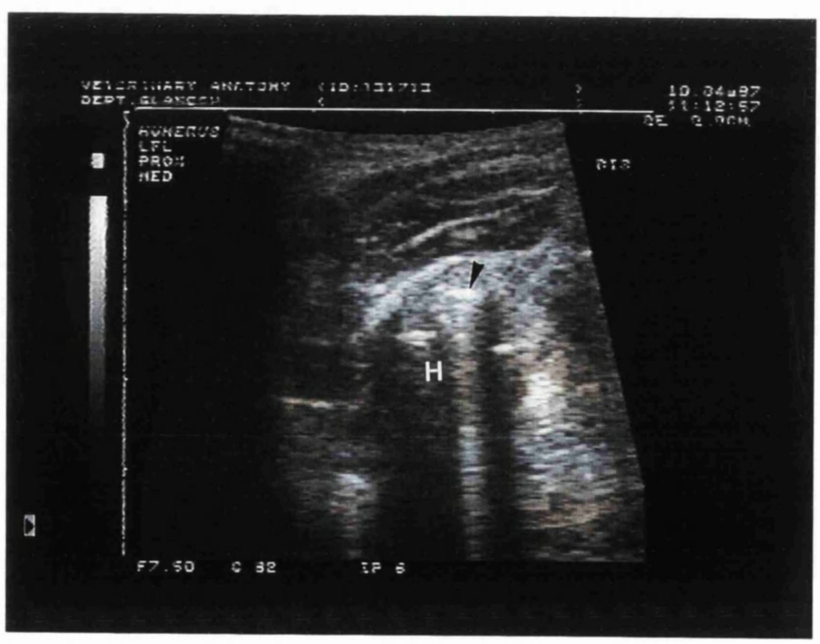

Figure 6.12.5

Case 13

An eight month old male Mastiff Neopolitan, weight 35 kg, was presented to the Glasgow University Veterinary Hospital with the suspicion of having an humeral fracture after it had been involved in a road traffic accident. Clinical and radiographic examination revealed that a Y-shape fracture of the right distal humerus had been sustained. The fracture was repaired using a trans-olecranon approach by a combination of lag screw, Kirschner wires and a 7 hole 3.5 mm Dynamic Compression Plate (DCP). The limb had been bandaged for 10 - 14 days. The dog was on a routine course of antibiotics and pain killers. Unfortunately, this dog also had a lateral luxation of the left patella as a consequential finding. This caused a definite clinical problem as it made it difficult for the dog to stand and ambulate since it was unable to bear weight at all on the right foreleg. Since the humerus was bandaged with Plaster of Paris (POP) after the surgery the post-operation ultrasonographic examination could not be carried out because the ultrasound beam could not penetrate the bandaging material. The animal came for an assessment approximately one month later. On examination the animal was non-ambulatory without support due to a complicating left hind limb lateral patella luxation. The right elbow had a very limited range of motion and showed marked thickening. Radiographic examination showed good progression of the fracture healing (figure 6.13.1).

Given the degree of disability that the animal was suffering with the multiple limb problems it was decided to perform surgery to stabilise the left patella. Initially it was decided to relocate the tibial tuberosity and perform a capsular overlap on the medial tissues. After surgery marked stifle swelling was apparent, which could be due to the failure of capsular overlap.

Ultrasonographic examination

Day 38 after fracture repair

Ultrasonographic examination of the fracture site area demonstrated the rough and uneven bone surface due to excessive callus formation (figure 6.13.2). The muscle structure appeared to have a normal ultrasonographic appearance. The fracture site was not detected which suggested that it had already been bridged by the bony callus. The bone plate adhering to the bone appeared as hyperechoic straight lines (figure 6.13.3).

Day 61 after fracture repair

Radiographic examination

Radiographic examination on day 61 after fracture repair showed the proliferative callus had bridged the fracture site in the distal humerus. A minimal amount of lucency was noted under the distal part of the plate and around the second most distal screw. Fracture lines were no longer visible (figure 6.13.4).

Ultrasonographic examination

Ultrasonographic examination on day 63 after fracture repair demonstrated the humeral surface which appeared smooth on lateral, cranial and medial scans (figure 6.13.5a, 6.13.5b and 6.13.5c). The smooth appearance of the bone surface compared to the day 38, was suggestive of a successful remodelling process. However, on the caudal aspect scan of the fracture site area, the callus formation could still be seen appearing as an hyperechoic, uneven rough bone surface (figure 6.13.6). The bone plate was imaged from the caudal aspect and appeared hyperechoic with reverberation artefact. The disorganised hyperechoic structure area of muscle suggested an area of muscle damage.

Clinically, there was a marked extracapsular soft tissue swelling and effusion associated with the left stifle. On ultrasound, the soft tissue swelling appeared as disorganised hyperechoic structures with some hypoechoic areas representing fluid (figure 6.13.7).

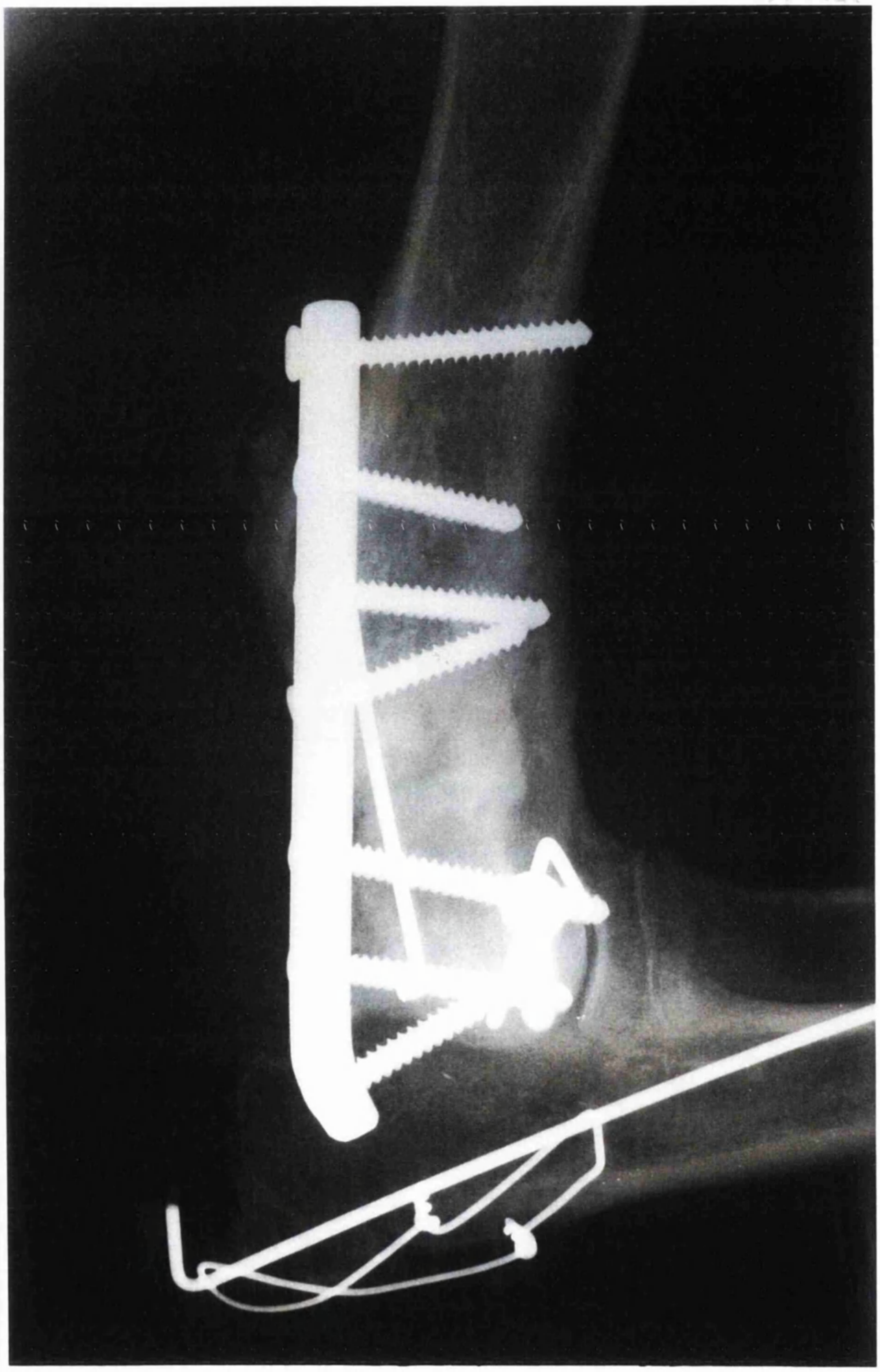

Figure 6.13.1 Radiographs obtained at day 32 after fracture repair demonstrate that the healing of the distal humerus fracture is progressing well with the presence of excessive callus formation.

Figure 6.13.2 Longitudinal scan of the distal femur from the caudal aspect on day 38 after fracture repair demonstrates the rough and uneven bone surface which is due to excessive callus formation. Note also the muscle appears to have a normal ultrasonographic appearance.

Figure 6.13.3 The bone plate adhering to the distal humerus appears as an hyperechoic straight line (arrow heads). The shadow appearing on the image is due to the hair on the skin.

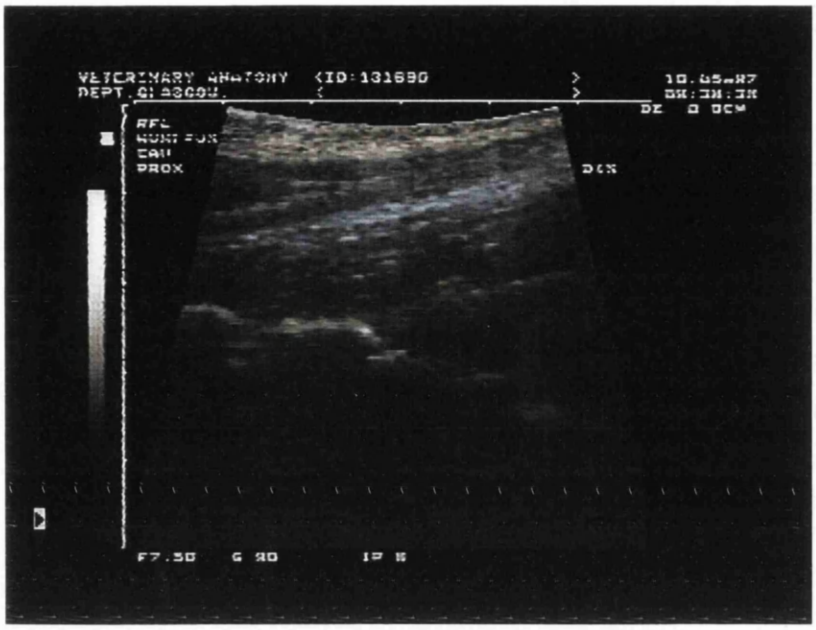

Figure 6.13.2

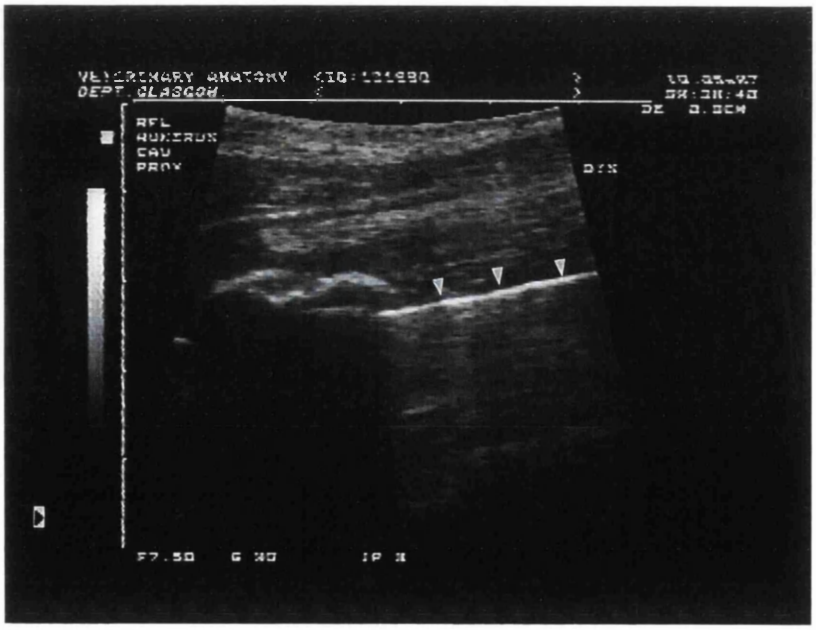

Figure 6.13.3

Figure 6.13.4 Radiographs obtained on day 61 after fracture repair show the proliferative callus has bridged the fracture site at the distal humerus. A minimal amount of lucency is noted under the distal part of the plate and around the second most distal screw. Fracture lines are no longer visible. **a**, lateral view, **b**, cranial view.

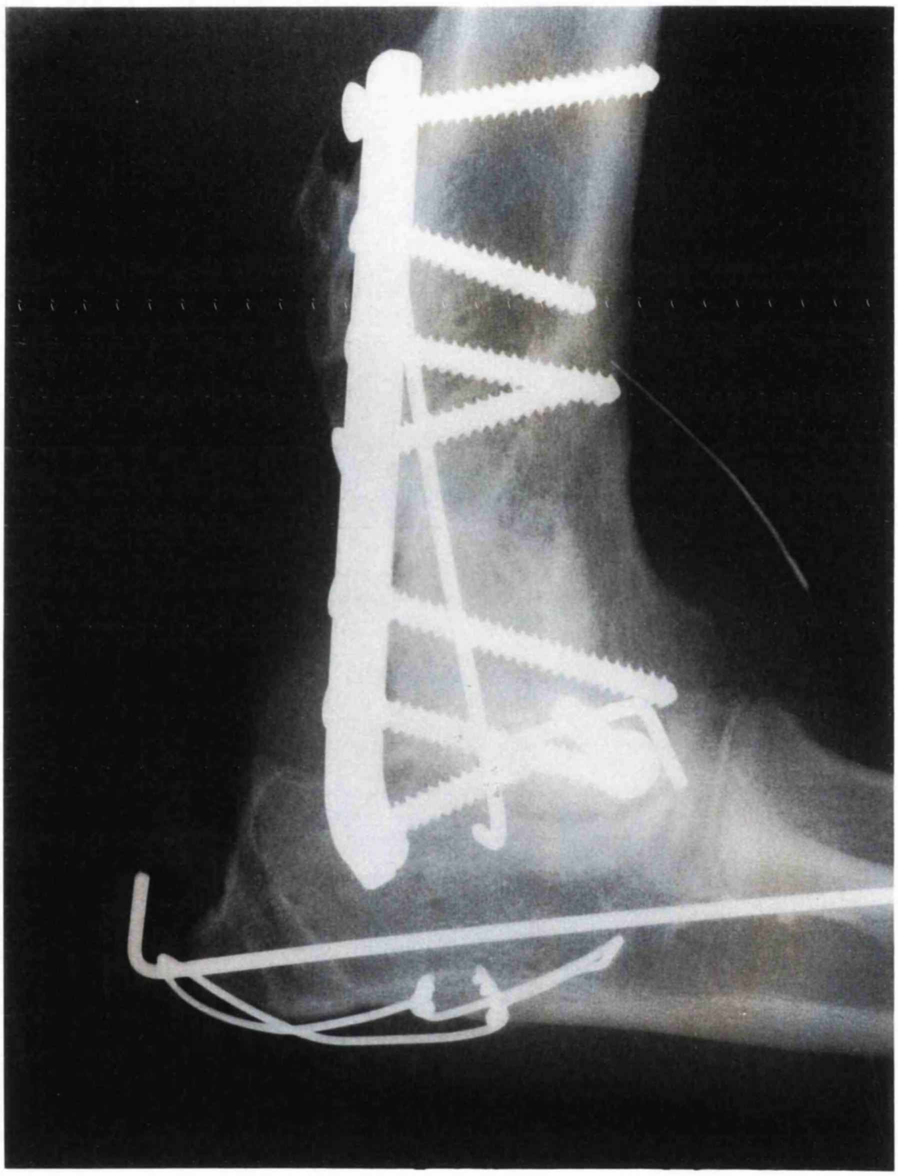

a

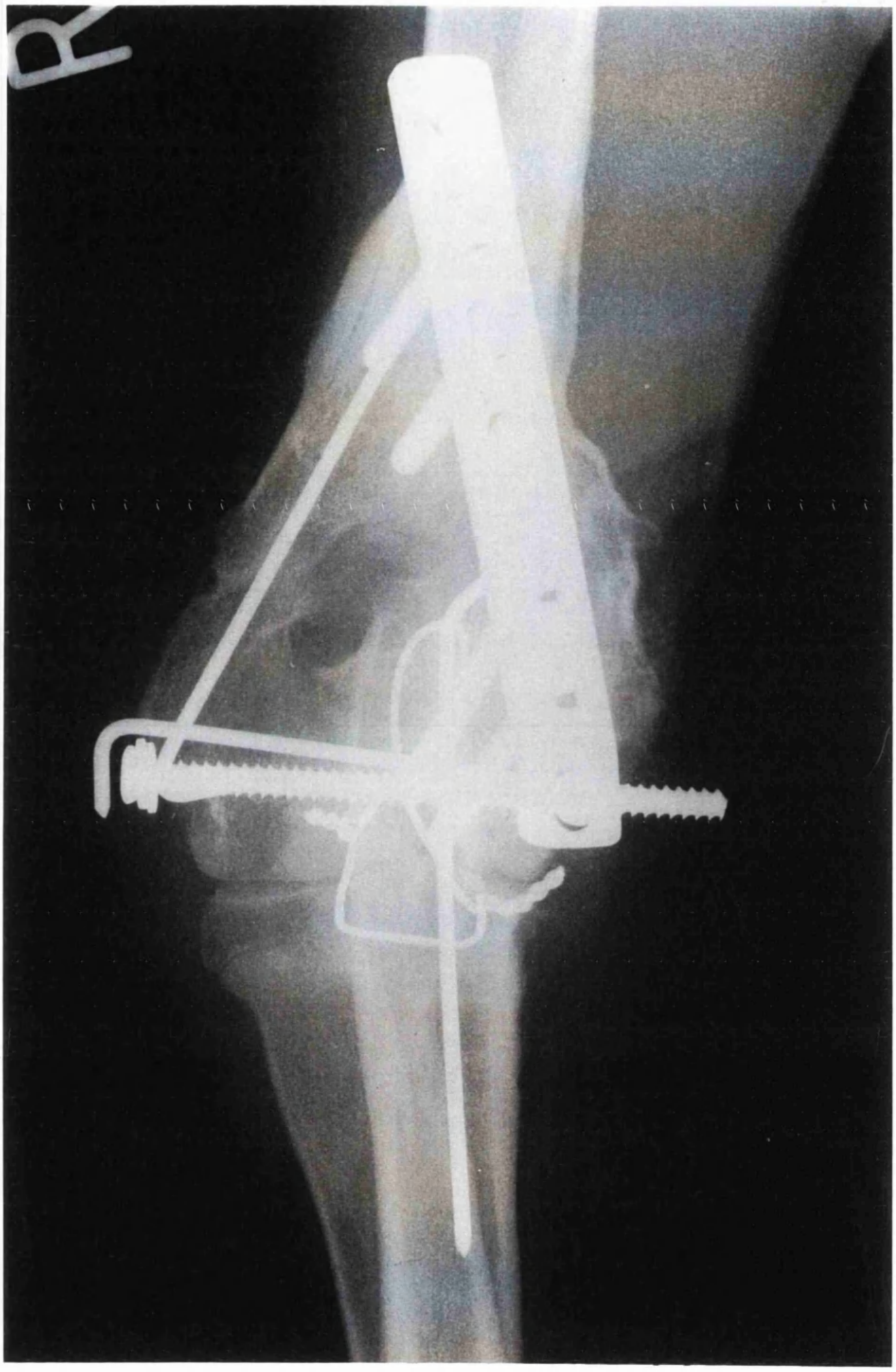

b

Figure 6.13.5 Longitudinal scans of the distal humerus at the fracture site area on day 63 after fracture repair demonstrate the smooth bone surface. **a**, lateral aspect, **b**, cranial aspect, and **c**, caudal aspect. The smooth appearance of the bone surface compared to the scan of 36 days is suggestive of a successful remodelling process.

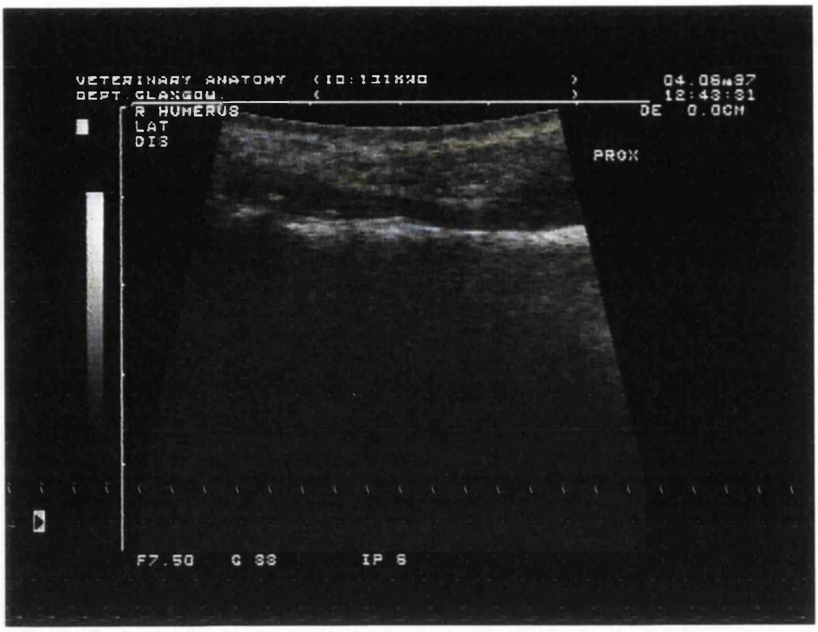

Figure 6.13.5a

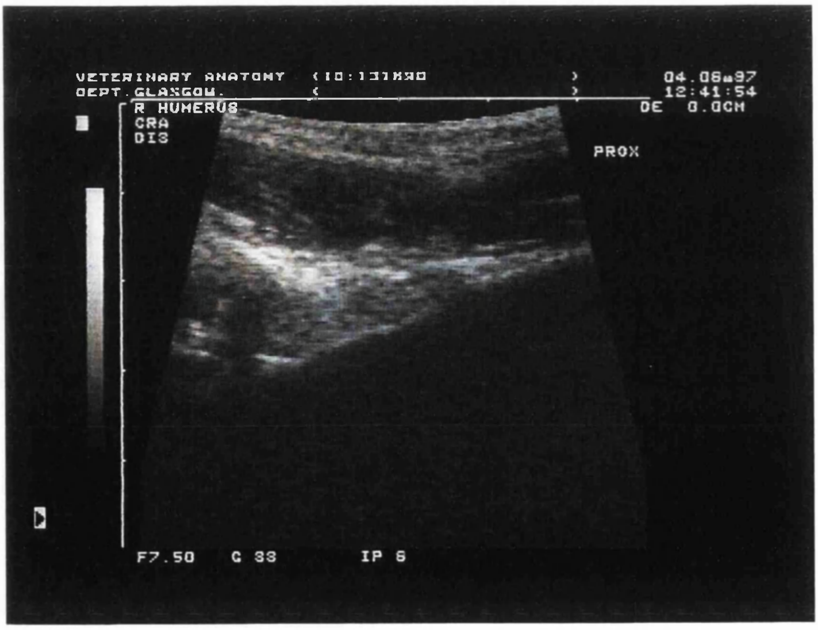

Figure 6.13.5b

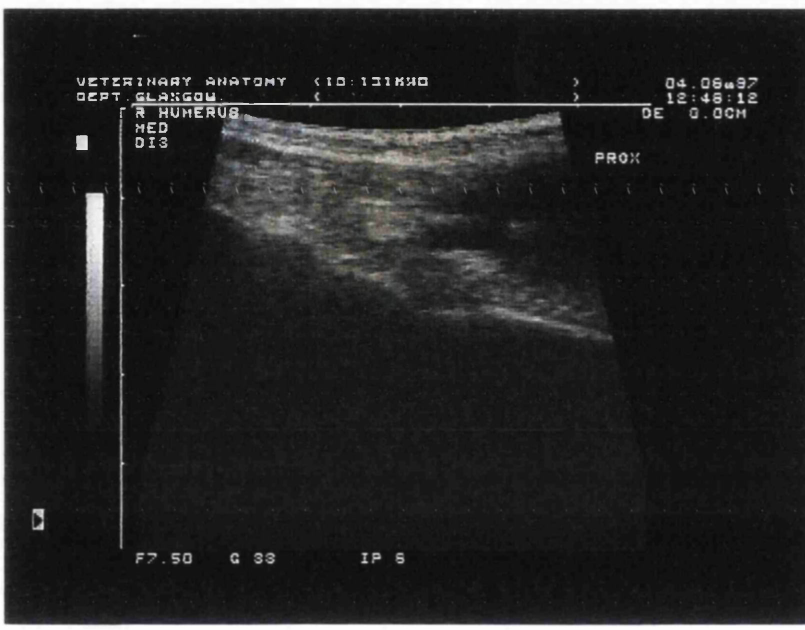

Figure 6.13.5c

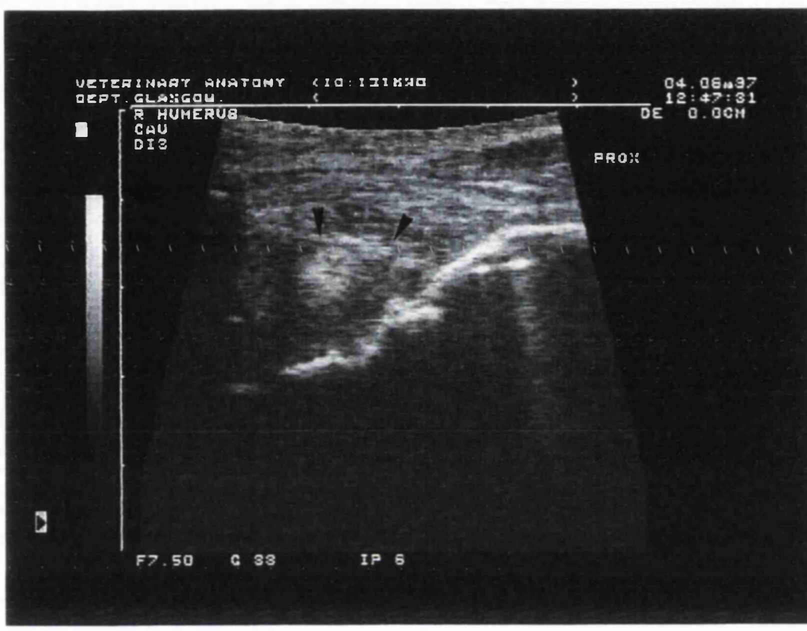

Figure 6.13.6 Longitudinal scan of the fracture site area from the caudal aspect on day 63 after fracture repair shows the callus which appears as an hyperechoic, uneven and rough bone surface. The disorganised hyperechoic structure area of muscle (arrow heads) may suggest an area of muscle damage.

Figure 6.13.7 Ultrasonographic examination of the marked extracapsular soft tissue swelling and effusion on the left stifle showing a disorganised hyperechoic structures with some hypoechoic areas. **a**, longitudinal scan, **b**, transverse scan. The hypoechoic areas represent fluid filled regions.

Figure 6.13.7a

Figure 6.13.7b

Case 14

A male cross bred dog was presented to the Glasgow University Veterinary Hospital after having been involved in a road traffic accident. The dog was unable to stand during examination. Radiographic examination showed that a comminuted fracture of the right side of the ilium and the ischium had been sustained. There was also an oblique fracture of the right femoral neck with possibly one small fragment seen.

Surgery was carried out and the pelvic fracture was reduced using a seven holes plate and screws. The fracture of the right femoral neck was reduced using TBW, K wires and screws. The radiographs obtained immediately after fracture repair were not available because the owner claimed possession of them.

Ultrasonographic examination

Day four after fracture repair

Ultrasonographic examination of the pelvis demonstrated the fracture site which appeared as discontinuity of the bone of the ilial body (figure 6.14.1). The fracture gap was clearly seen. The fracture site appeared hyperechoic suggesting the presence of periosteal tissue reaction. The area of muscle damage above the ilium appeared as a disorganised hypoechoic structure relative to the surrounding region. The bone plate adhering to the ilium, scanned longitudinally, appeared as an hyperechoic straight line with reverberation artefact (figure 6.14.2). The fracture site appeared as discontinuity of the shaft of the ilium on a transverse scan image (figure 6.14.3). The area of muscle damage imaged on a transverse scan appeared as a disorganised hypoechoic area similar to that seen on the longitudinal scan.

Day seven after fracture repair

Ultrasonographic examination showed the fracture site which appeared as on the day four examination. There was no indication of callus formation. The fracture site appeared hyperechoic suggesting periosteal tissue reaction. The area of muscle damage above the ilium seen on the day four examination still appeared as an hypoechoic structure but had become more organised. The bone plate appeared as a straight hyperechoic line with reverberation artefact. The fracture site imaged on a transverse scan from the dorsal aspect appeared as a "V" shape gap and no callus formation was detected (figure 6.14.4).

Day eleven after fracture repair

Ultrasonographic examination demonstrated the fracture site with the gap still present both on longitudinal and transverse scans. The fracture site still appeared hyperechoic with no indication of callus formation on the longitudinal scan (figure 6.14.5a). However, there was hyperechoic material within the fracture gap on the transverse scan which could suggest the early formation of a periosteal callus (figure 6.14.5b). The area of muscle damage could still be seen on the transverse scan and appeared as a disorganised hypoechoic area. The bone plate and screws adherent to the ilium appeared hyperechoic and produced reverberation and comet tail artefacts respectively.

Day 14 after fracture repair

Ultrasonographic examination demonstrated the fracture gap with the presence of hyperechoic material within the gap which suggested soft callus formation (figure 6.14.6). There was no artefact seen distal to the hyperechoic material. Soft callus formation was detected on the bone surface near to the fracture site appearing as hyperechoic structures. The area of muscle damage above the ilium still appeared as a disorganised hypoechoic area. The bone plate appeared hyperechoic with reverberation artefact and was slightly elevated from the ilial shaft surface at the caudal end (figure 6.14.7). A transverse scan of the ilium demonstrated soft callus formation at the fracture site which appeared hyperechoic (figure 6.14.8). The area of muscle damage still appeared hypoechoic but with more organised structure on the transverse scan.

Day 17 after fracture repair

Ultrasonographic examination demonstrated the fracture site with the gap still able to be seen but it appeared smaller than in the previous scan due to the callus formation (figure 6.14.9). The soft callus formation on the bone surface near to the fracture site imaged on the day 14 examination had become enlarged and appeared as an hyperechoic structure (figure 6.14.10). It was more distinct than in the previous scan. The bone plate adherent to the ilium appeared hyperechoic with reverberation artefact as seen on day 14 after fracture repair. The area of muscle damage had become smaller and appeared hypoechoic with a more organised structure.

Day 47 after fracture repair

Radiographic examination

Radiographs taken at day 47 after fracture repair showed there was a fracture gap present with the middle screw appearing to lie in the fracture site. The fifth screw extended 0.5 cm medial to the ilium. The fracture margins were indistinct and a callus was evident. The fracture line of the femoral neck was barely visible (figure 6.14.11).

Ultrasonographic examination

Ultrasonographic examination demonstrated the fracture site with the fracture gap still evident but it appeared smaller and more shallow than the previous scan (figure 6.14.12). Callus formation could be seen at the fracture site and at the area near to the fracture site. The callus formation at the fracture site appeared like a 'collar'. The area of disorganised muscle damage had returned to its normal structure producing a normal ultrasonographic appearance of the muscle. The animal failed to return for the check up and thus, the follow up scans were not available.

Ultrasonographic examination of the femoral neck fracture

Day four after fracture repair

Ultrasonographic examination failed to detect the fracture site at the femoral neck. The fact that site of the fracture was at the base of the femoral neck and the fracture site which was very well aligned with the fracture line was barely visible on radiograph helped to explain why ultrasonographic examination of this site failed to show the line of the fracture. However, ultrasonographic examination in this area demonstrated the Kirschner wires and screws used in the reduction procedure. These materials appeared hyperechoic and produced comet tail artefacts (figure 6.14.13). A large haematoma was found caudal to the proximal femur on the lateral aspect scans (figure 6.14.14a and 6.14.14b). The haematoma appeared anechoic with some echogenic material present within the area.

Day seven after fracture repair

Ultrasonographic examination showed that the large area of the haematoma had reduced considerably in size and appeared as a small hypoechoic area surrounded by the hyperechoic image of the muscle both on longitudinal and transverse scans (figure 6.14.15a and 6.14.15b).

Day eleven after fracture repair

Ultrasonographic examination of the site of the haematoma in the muscle had returned to its normal ultrasonographic appearance both on transverse and longitudinal scans (figure 6.14.16a and 6.14.16b).

Day 14 after fracture repair

Ultrasonographic examination of the site of the haematoma in the muscle showed that it had returned to its normal ultrasonographic appearance on the transverse scan (figure 6.14.17). The metal materials used in the femoral neck fracture reduction appeared hyperechoic and produced comet tail artefact (figure 6.14.18).

Day 17 after fracture repair

Ultrasonographic examination revealed that the area of haematoma had returned to the normal muscle structure and had now become hyperechoic on the transverse scan (figure 6.14.19). This suggested the presence of fibrous tissue within the muscle as a consequence of the muscle damage.

Figure 6.14.1 Longitudinal scan of the shaft of the ilium from the dorsal aspect on day four after fracture repair demonstrates the fracture site with the presence of a fracture gap. Note that the fracture site appears hyperechoic suggesting the presence of periosteal tissue reaction. The area of muscle damage above the ilium appear as a disorganised hypoechoic structure relative to the surrounding area.

Figure 6.14.2 Longitudinal scan of the ilium on day four after fracture repair shows the bone plate which appears as an hyperechoic straight line and produces reverberation artefact.

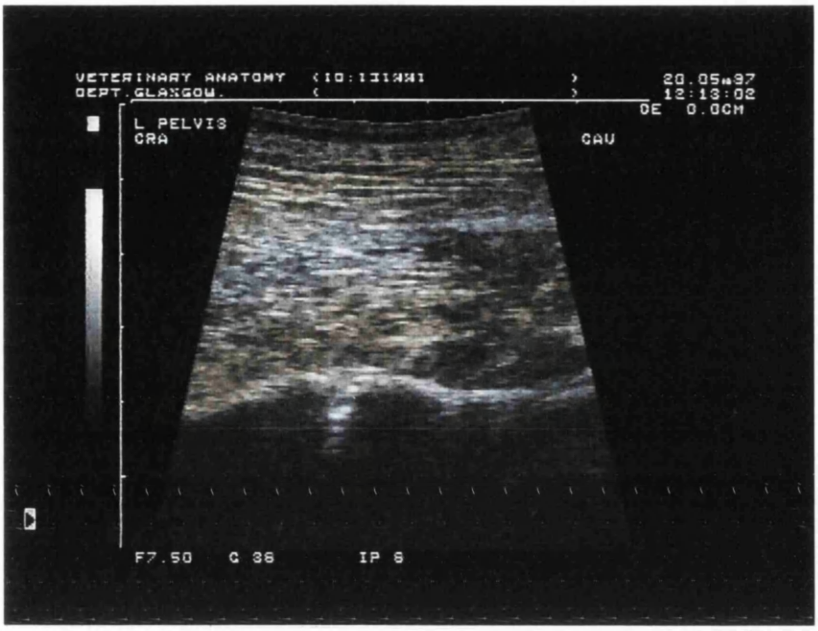

Figure 6.14.1

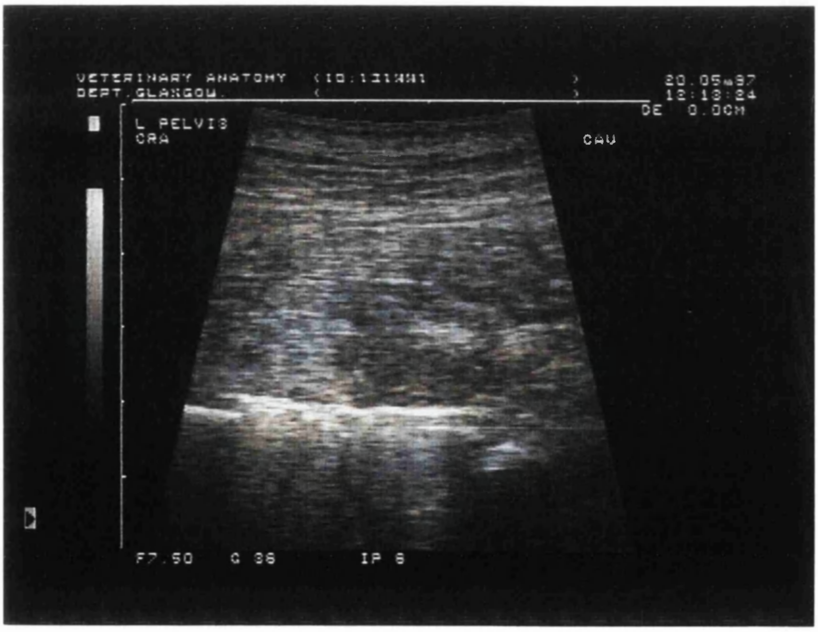

Figure 6.14.2

Figure 6.14.3 Transverse scan of the ilium on day four after fracture repair shows the fracture site (large arrow head) which appears as discontinuity of the bone in cross section. The area of muscle damage (small arrow heads) appears as a disorganised hypoechoic region relative to the surrounding. The bone plate and screws adhering to the ilium (arrow) appear hyperechoic with reverberation artefact.

Figure 6.14.4 The fracture site imaged on a transverse scan from the dorsal aspect on day seven after fracture repair appears as a "V" shape gap (arrow head) No callus formation can be detected.

Figure 6.14.3

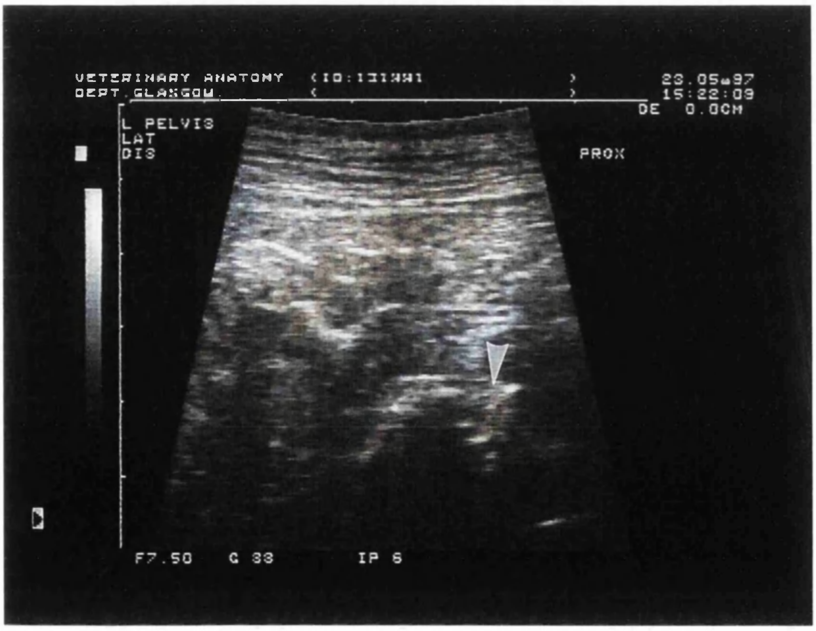

Figure 6.14.4

Figure 6.14.5 Ultrasonographic examination of the ilium on day 11 after fracture repair demonstrates the fracture site with the gap still present both on (**a**) longitudinal and (**b**) transverse scans. The fracture site still appears hyperechoic with no indication of callus formation on a longitudinal scan. However, there is hyperechoic material within the fracture gap on the transverse scan which may suggest the early formation of periosteal callus. The area of muscle damage still appears as a disorganised hypoechoic area on transverse scan. The bone plate and screws are adherent to the ilium and appear hyperechoic producing reverberation and comet tail artefacts.

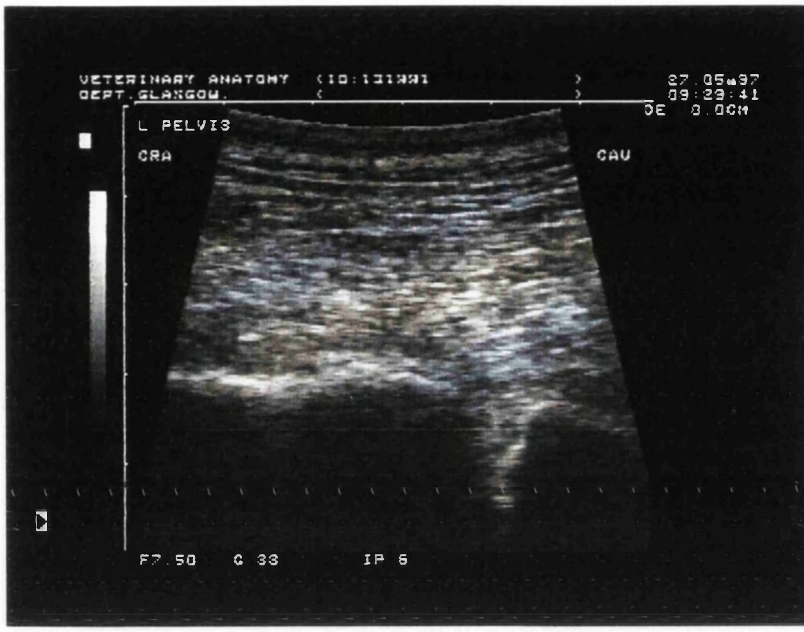

Figure 6.14.5a

Figure 6.14.5b

Figure 6.14.6 A longitudinal scan of the ilium on day 14 after fracture repair demonstrates the fracture gap with the presence of hyperechoic material within the gap which suggests soft callus formation. Soft callus formation is also detected on the bone surface near to the fracture site appearing as an hyperechoic structure (arrow head). The area of muscle damage above the ilium still appears as a disorganised hypoechoic region.

Figure 6.14.7 The hyperechoic bone plate with reverberation artefact (arrow heads), appears slightly elevated from the ilial shaft surface at the caudal end on a longitudinal scan on day 14 after fracture repair.

Figure 6.14.6

Figure 6.14.7

Figure 6.14.8 Transverse scan of the ilium on day 14 after fracture repair demonstrates the soft callus formation at the fracture site which appears as hyperechoic material (large arrow head). Note that the area of muscle damage still appears hypoechoic but with a more organised structure (small arrow heads).

Figure 6.14.9 Longitudinal scan of the ilium on day 17 after fracture repair demonstrates the fracture site with the gap still clearly seen (arrow head) but it appears smaller than the previous scan which is due to the callus formation.

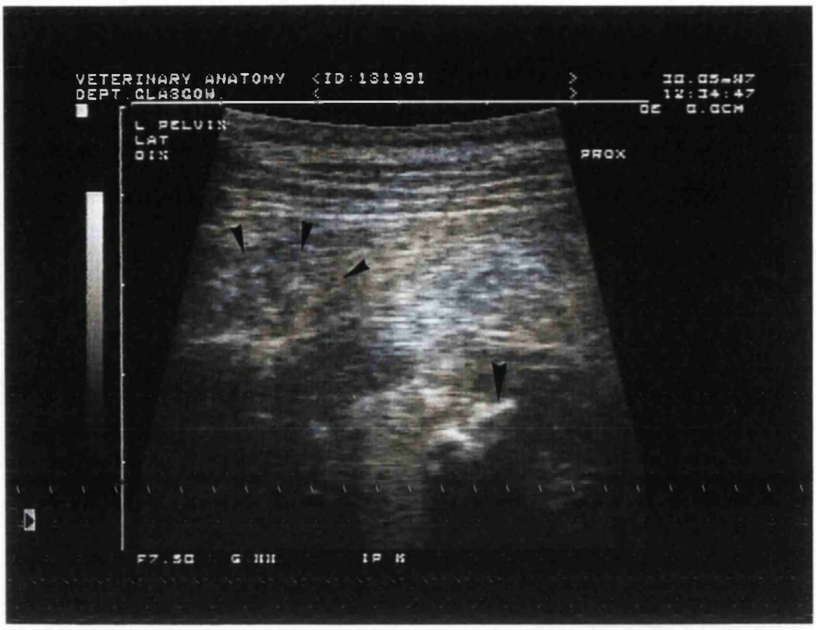

Figure 6.14.8

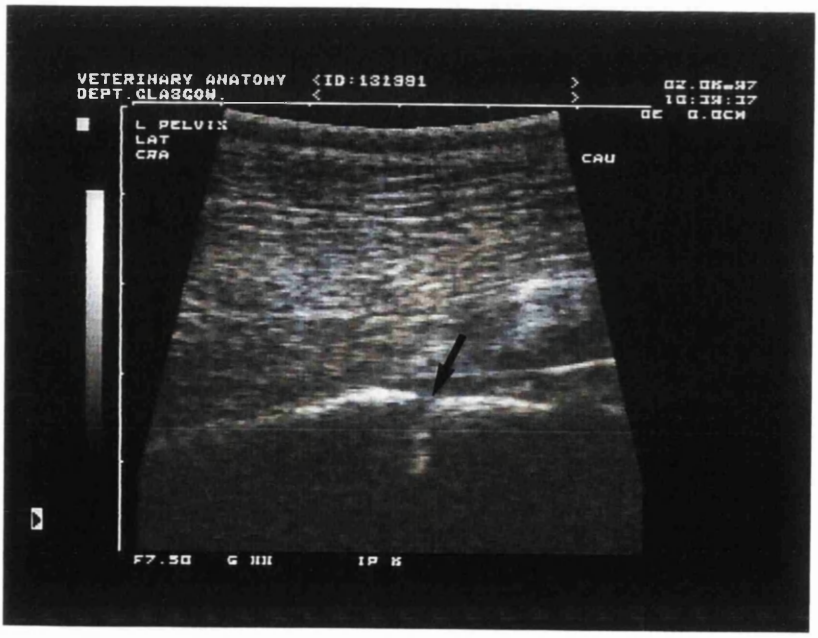

Figure 6.14.9

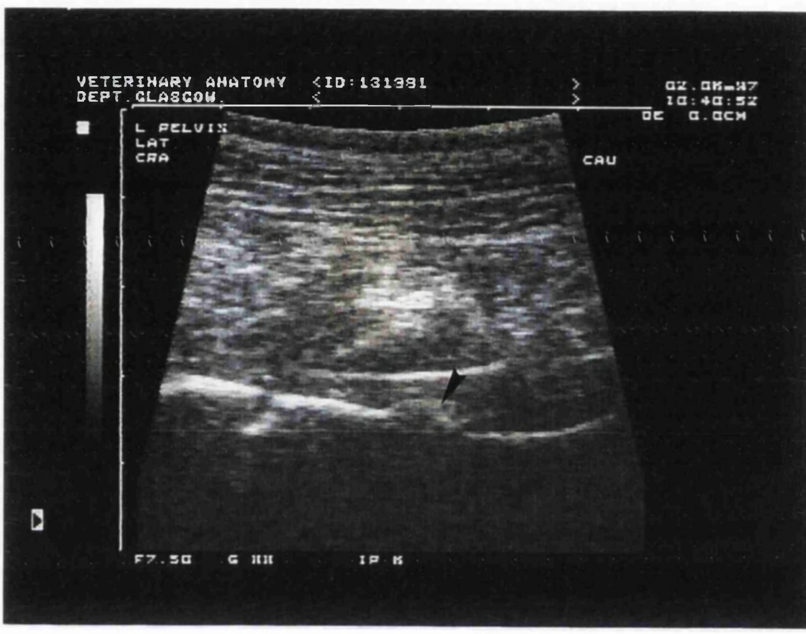

Figure 6.14.10 Longitudinal scan of the ilium on day 17 after fracture repair demonstrates soft callus formation on the bone surface near to the fracture site (arrow). It has enlarged and appears as a hyperechoic structure. It is clearer than in the previous image. The area of muscle damage has become smaller and appears hypoechoic with a more organised structure.

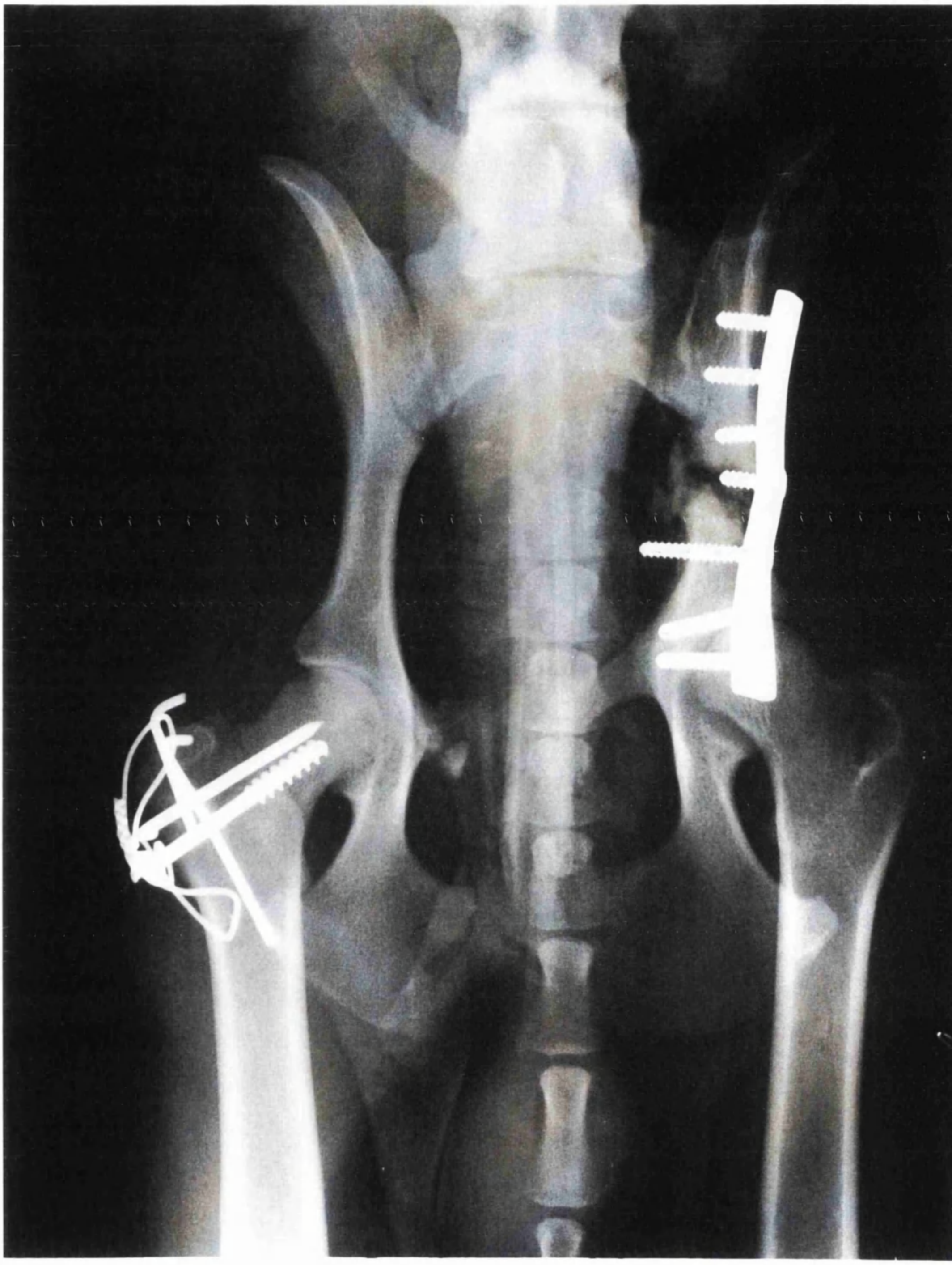

Figure 6.14.11 Radiographs taken at day 47 after fracture repair show there is a fracture gap present with the middle screw appearing to lie in the fracture site. The fifth screw extends 0.5 cm medial to the ilium. The fracture margins are indistinct and callus is evident. The fracture line of the femoral neck is seen with difficulty.

Figure 6.14.12 Longitudinal scan of the ilium on day 47 after fracture repair demonstrates the fracture site with the fracture gap still present but appears small and shallow (arrow). The callus formation can be seen at the fracture site and at the area near to the fracture site. The callus formation at the fracture site appears like a 'collar'. The muscle structure appears to have a normal ultrasonographic appearance.

Figure 6.14.13 Longitudinal scan of the proximal end of the femur on day four after fracture repair demonstrates the hyperechoic material with the comet tail artefacts which represents the Kirschner wires and screws that had been used in the reduction procedure.

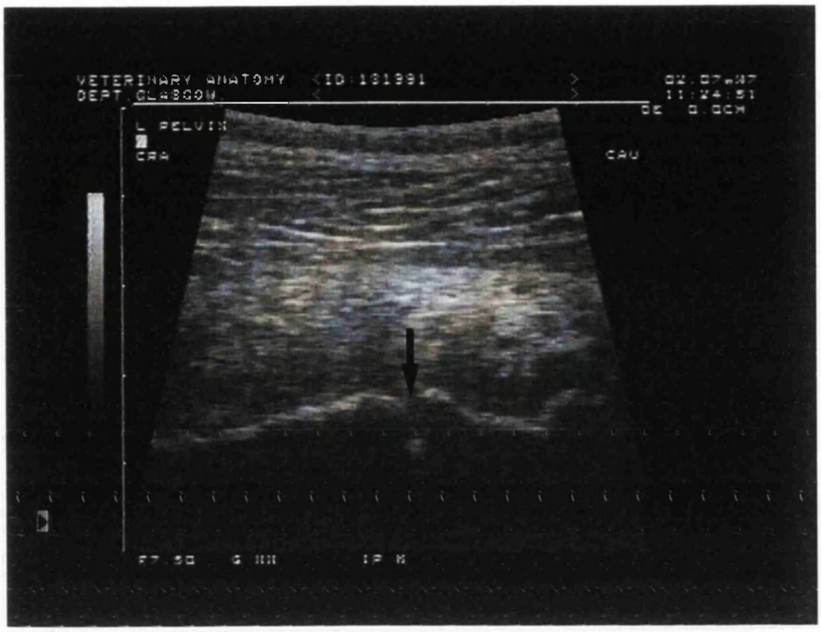

Figure 6.14.12

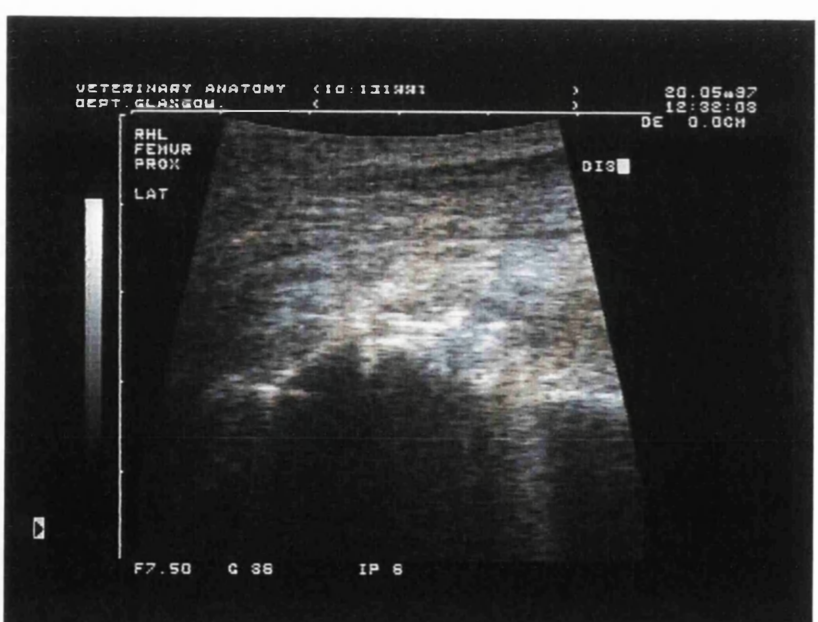

Figure 6.14.13

Figure 6.14.14 A large haematoma caudal to the proximal femur, imaged on day four after fracture repair , **a**, longitudinal plane, **b**, transverse plane. Note that the area of the haematoma appears anechoic with some echogenic material present within. **F**, femur

Figure 6.14.14a

Figure 6.14.14b

Figure 6.14.15 Ultrasonographic images of the site of the haematoma on day seven after fracture repair show a small hypoechoic area (arrow head) surrounded by the hyperechoic structure area of the muscle. **a**, longitudinal scan, **b**, transverse scan. The haematoma has reduced to the extent that it has disappeared. **F**, femur.

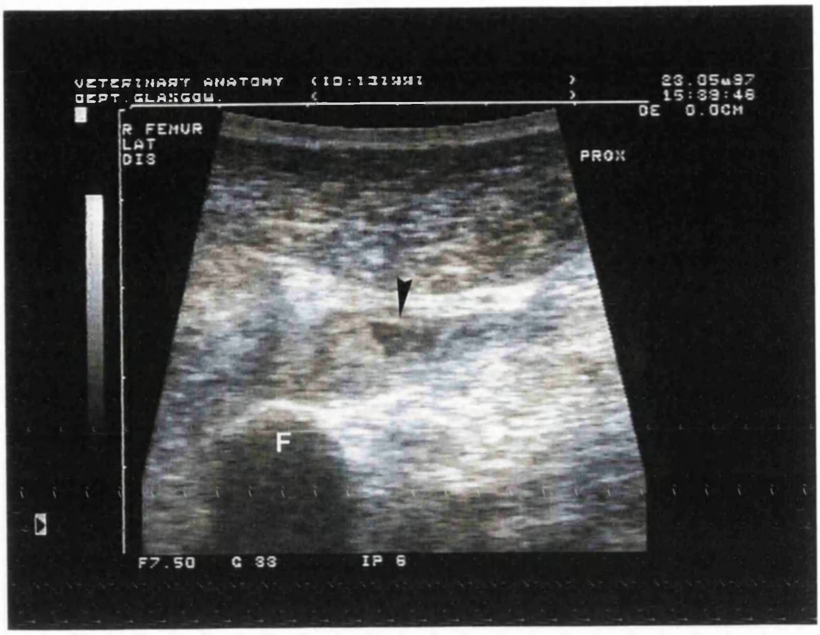

Figure 6.14.15a

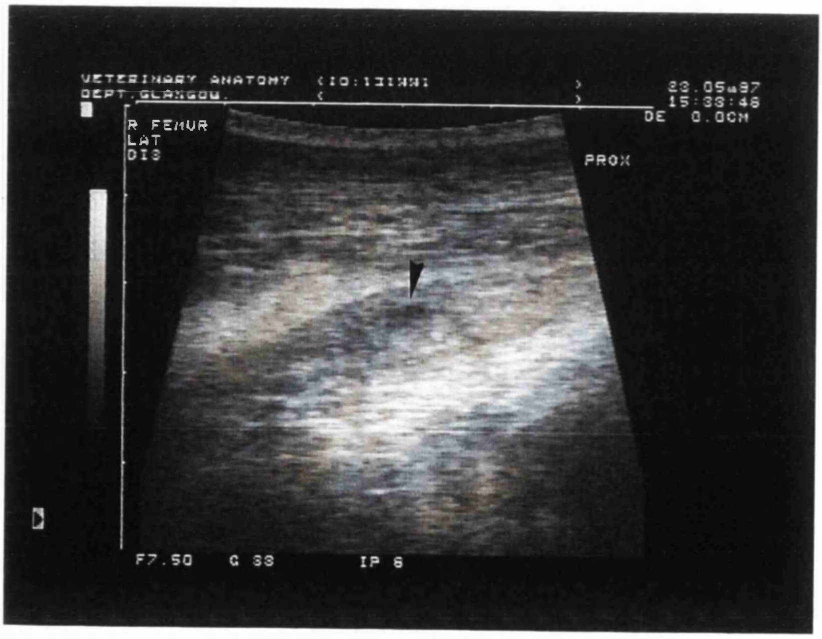

Figure 6.14.15b

Figure 6.14.16 Ultrasonographic images of the site of the muscle haematoma on day 11 after fracture repair demonstrate the normal ultrasonographic appearance of the muscle structure. **a**, longitudinal scan, **b**, transverse scan. **F**, femur

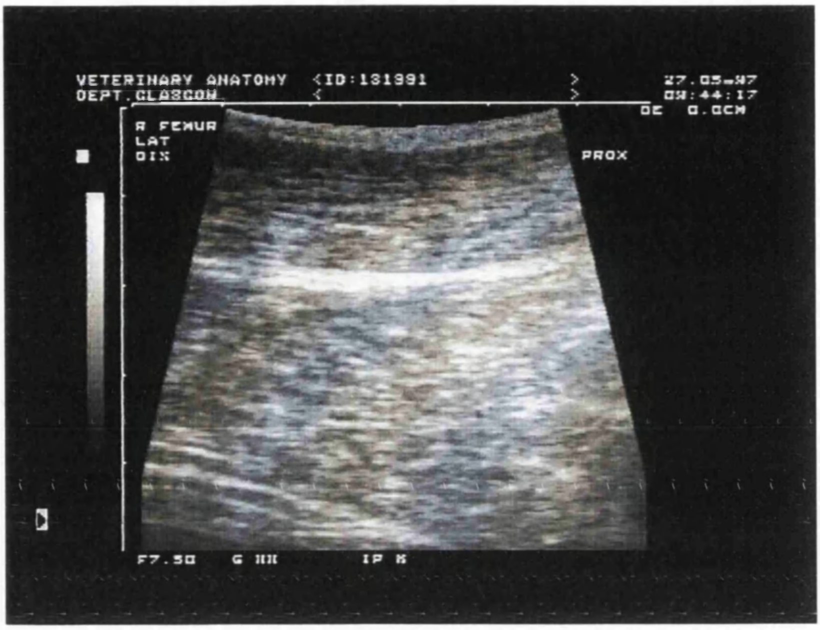

Figure 6.14.16a

Figure 6.14.16b

Figure 6.14.17 Transverse scan of the proximal femur at the site of muscle haematoma on day 14 after fracture repair demonstrates the normal ultrasonographic appearance of muscle. **F**, femur

Figure 6.14.18 Ultrasonographic image of the metal material used in femoral neck fracture reduction appears hyperechoic and produces comet tail artefact.

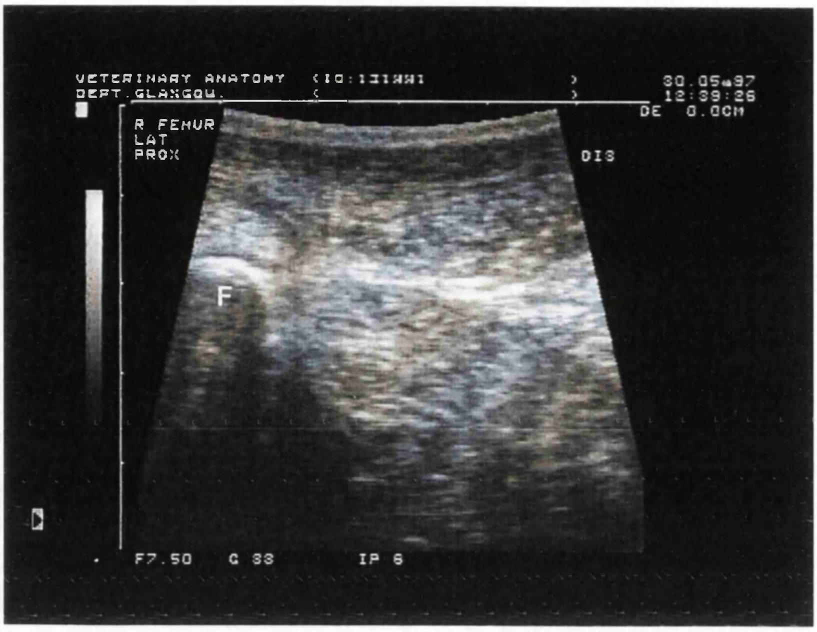

Figure 6.14.17

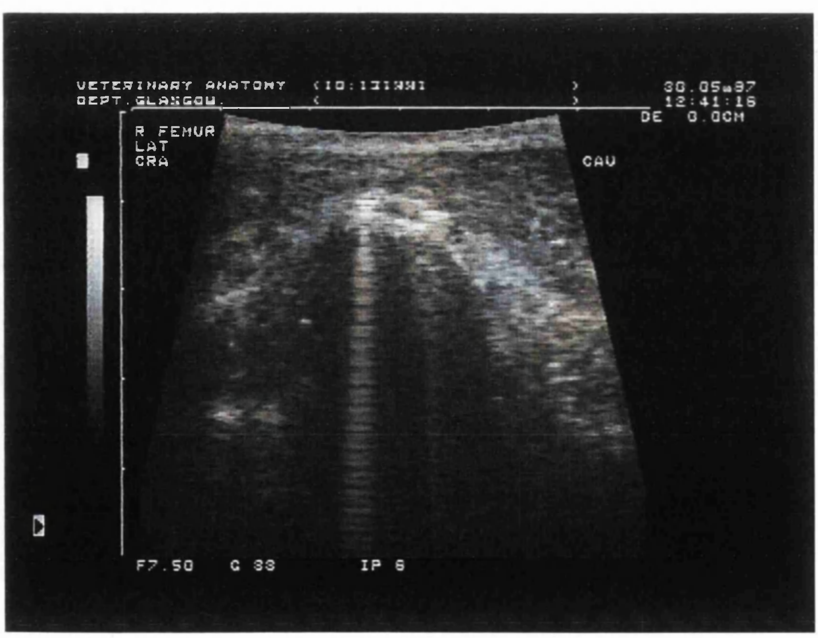

Figure 6.14.18

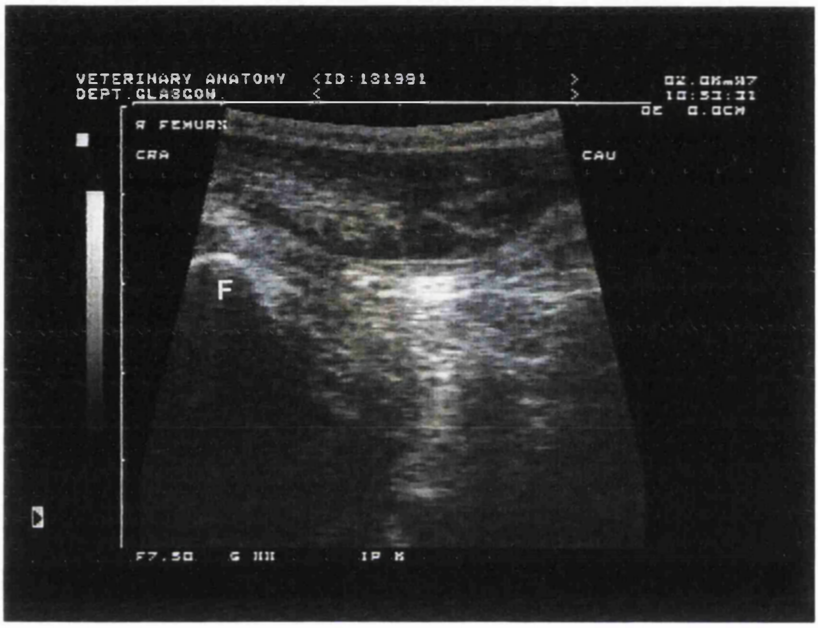

Figure 6.14.19 Transverse scan of the proximal femur at the site of muscle haematoma demonstrates the hyperechoic area. This appearance may be due to the presence of fibrous tissue within muscle. **F**, femur

Case 15

An eight year old male Cocker Spaniel was presented to the Glasgow University Veterinary Hospital with a suspicion of having a humeral fracture, cause unknown. Radiographic examination revealed that a severely comminuted fracture of the distal shaft of the left humerus had been sustained, which was intracondylar and intra-articular. The distal portion of the fracture was caudoproximally displaced. Repair had been carried out using a combination of two external fixators with four pins in the proximal humerus, two in the lateral condyle and one in the medial condyle. The repair process had resulted in a good alignment (figure 6.15.1).

Ultrasonographic examination

Day four after fracture repair

Ultrasonographic examination of the distal humerus at the fracture site area demonstrated a large bone fragment which appeared hyperechoic with a smooth surface (figure 6.15.2). The proximal fragment of the humerus was imaged as not continuous with the distal fragment (figure 6.15.3). A transverse scan at the fracture site area demonstrated the humerus with the bone fragments caudally (figure 6.15.4). The disorganised hyperechoic structure of the muscle around the fracture site area suggested an area of soft tissue reaction. The suture material within the muscle was imaged and appeared hyperechoic with reverberation artefact (figure 6.15.5).

Day 55 (approximately 8 weeks) after fracture repair

Radiographic examination

Radiographs taken at day 55 after fracture repair showed there was evidence of callus bridging the fracture gap between the two fragments (figure 6.15.6). Proximally, there was some periosteal reaction and some lucency associated with the pin, indicating pin loosening due to infection or implant instability.

Ultrasonographic examination

Ultrasonographic examination of the distal humerus from the lateral aspect demonstrated the bone fragment which appeared as in the day four examination (figure 6.15.7). The distal humerus was found to be continuous on a caudo-lateral scan with no gap detected (figure 6.15.8). One pin was seen at the fracture site area with soft callus formation detected around the pin. This soft callus formation suggested that some pin movement had occurred. The bulging bone was suggestive of a healing process with callus formation. This suggested that the healing process was progressing well. However, the fracture site was detected on a lateral scan and appeared as a large notch (figure 6.15.9). There was no excessive callus formation detected at the fracture site. The muscle structure appeared to have a normal ultrasonographic appearance.

Day 96 (approximately 14 weeks) after fracture repair

Radiographic examination

Radiographs taken at day 96 showed the healing process was progressing satisfactorily (figure 6.15.10).

Ultrasonographic examination

A transverse scan at the fracture site area still showed the rough bone surface which was due to callus formation (figure 6.15.11a). The distal humerus had lost its normal shape as compared to the normal proximal humerus (figure 6.15.11b). Scanning on the caudo-lateral aspect of the fracture site area showed the uneven bone contour, but the bone surface showed that the remodelling process was taking place as it appeared to be becoming smoother (figure 6.15.12). The hyperechoic area in the muscle at the fracture site area suggested the presence of fibrous tissue within the muscle. The dog was not seen since then, and according to the clinician, the fixation device had been removed at the local veterinary clinic and the fractured humerus was healed satisfactorily.

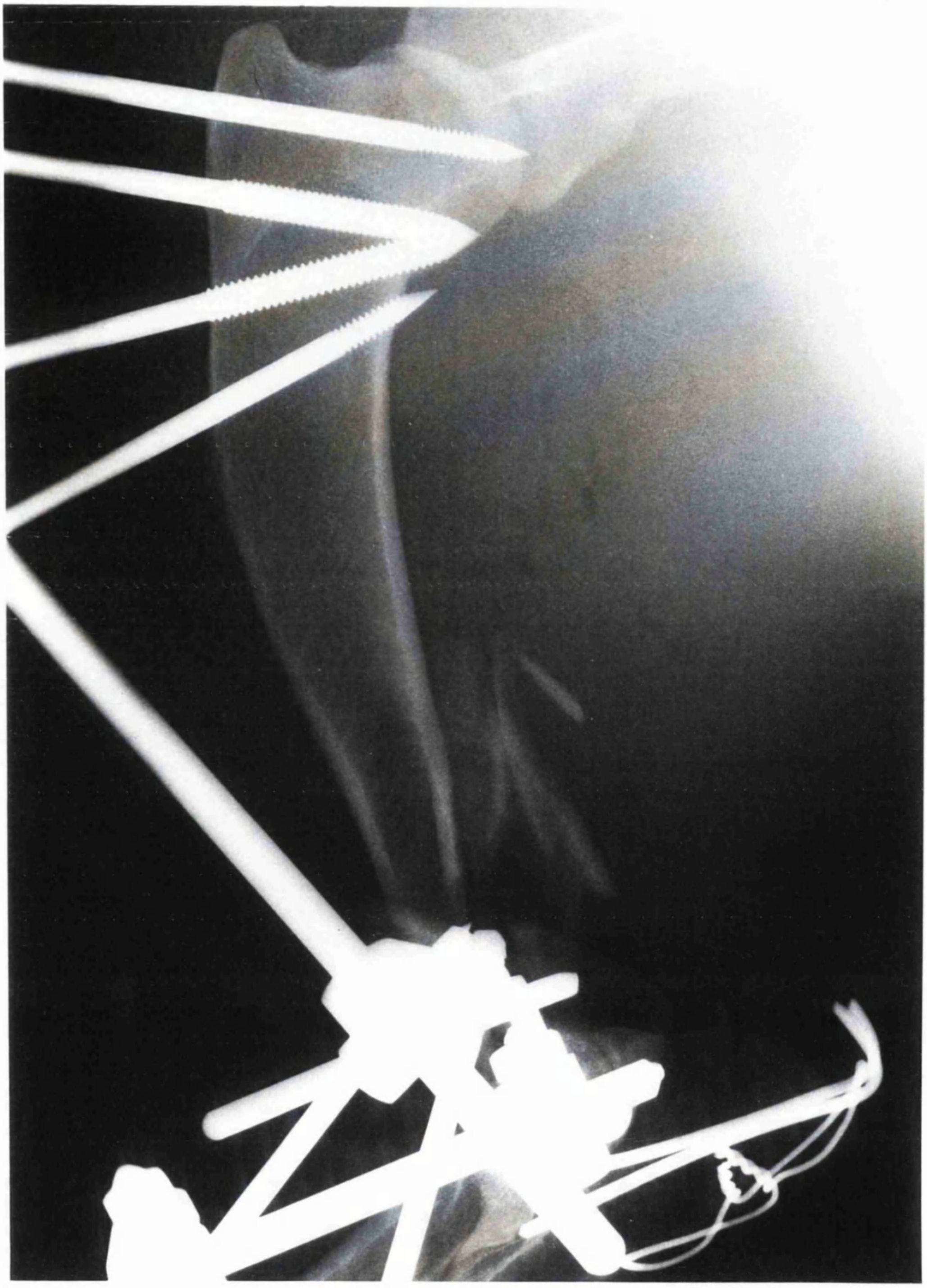

Figure 6.15.1 Radiograph obtained immediately after fracture repair shows the repair has been carried out using a combination of two external fixators with four pins in the proximal humerus, two in the lateral condyle and one in the medial condyle. The repair process is resulting in a good alignment.

Figure 6.15.2 Longitudinal scan of the distal humerus at the fracture site area on day four after fracture repair shows a large bone fragment which appears hyperechoic with a smooth surface. There is no indication of callus formation.

Figure 6.15.3 Longitudinal scan of the humerus from the lateral aspect on day four after fracture repair shows the proximal fragment (arrow head) and there is no continuity with the distal fragment (blank arrow).

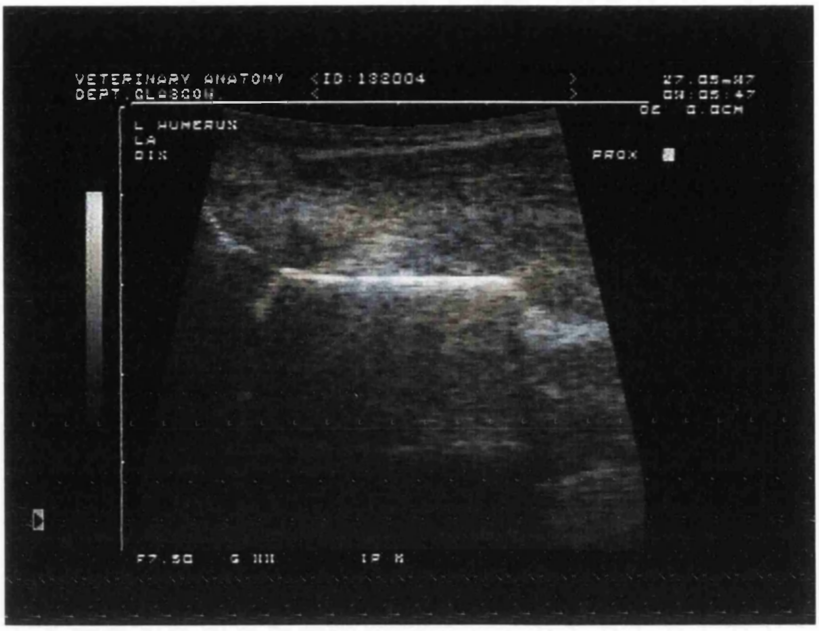

Figure 6.15.2

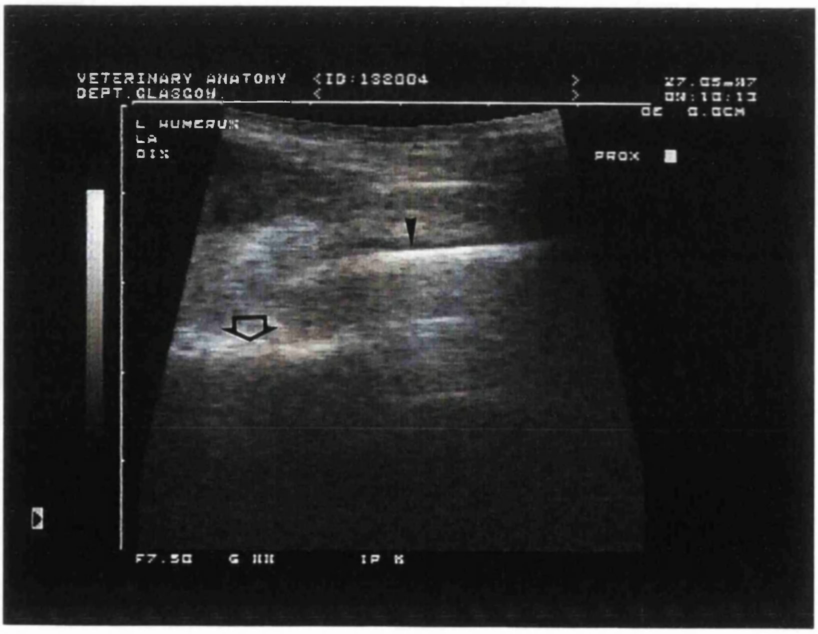

Figure 6.15.3

Figure 6.15.4 Transverse scan at the fracture site area from the lateral aspect on day four after fracture repair demonstrates the humerus with the bone fragments caudally (arrow head). Note also the disorganised hyperechoic structure of the muscle around the fracture site area suggesting an area of soft tissue reaction. **H**, humerus.

Figure 6.15.5 The suture material within the muscle (arrow head) appears hyperechoic with reverberation artefact.

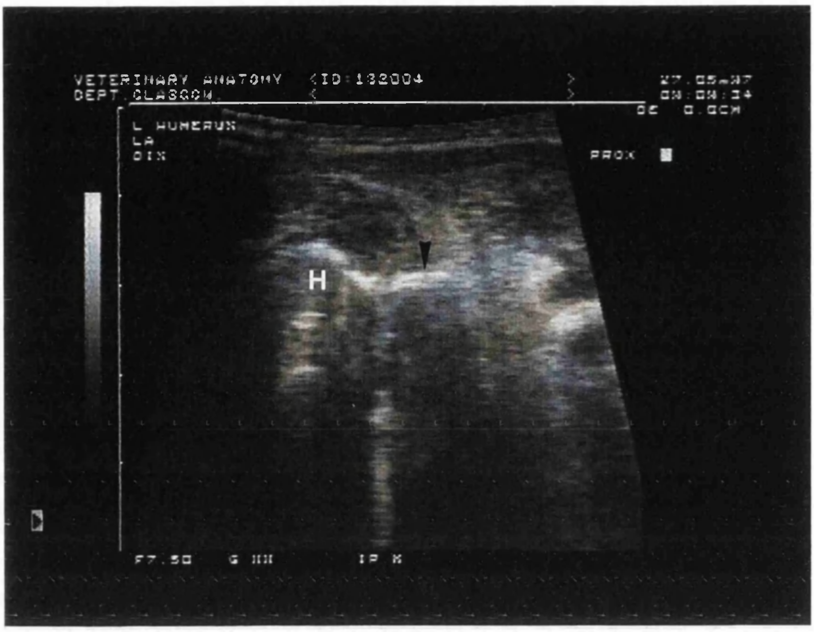

Figure 6.15.4

Figure 6.15.5

Figure 6.15.6 Radiograph taken at day 55 after fracture repair shows there is evidence of callus bridging the fracture gap between the two fragments. Proximally, there is some periosteal reaction and some lucency associated with the pin, indicating pin loosening due to infection or implant instability.

Figure 6.15.7 Ultrasonographic examination of the distal humerus from the lateral aspect on day 55 after fracture repair demonstrates the bone fragment which appears as in the day four examination.

Figure 6.15.8 Longtiudinal scan of the distal humerus from the lateral aspect on day 55 after fracture repair shows the bulging bone surface at the fracture site area. One pin is seen (arrow) and soft callus formation is detected around the pin (arrow head) which suggests there is some pin movement involved. The bulging bone is suggestive of a healing process with callus formation.

Figure 6.15.7

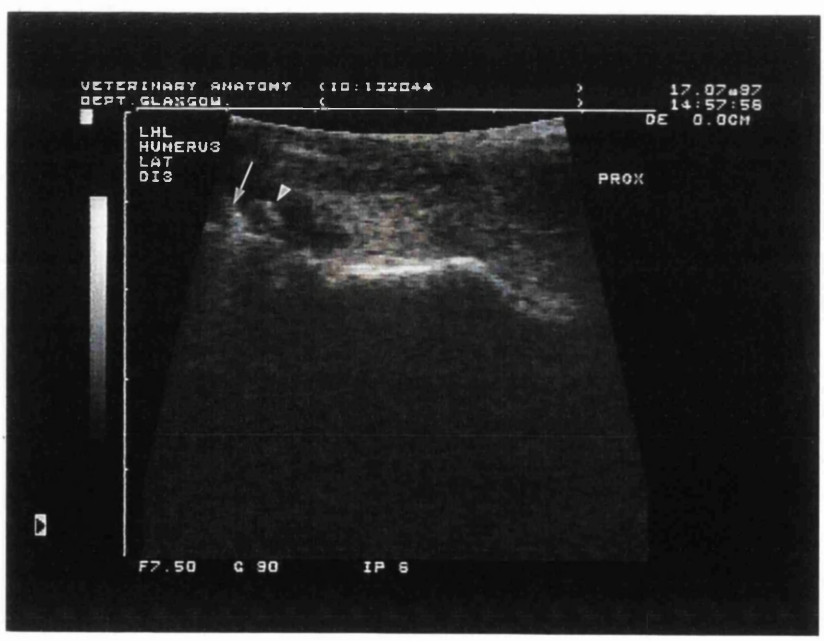

Figure 6.15.8

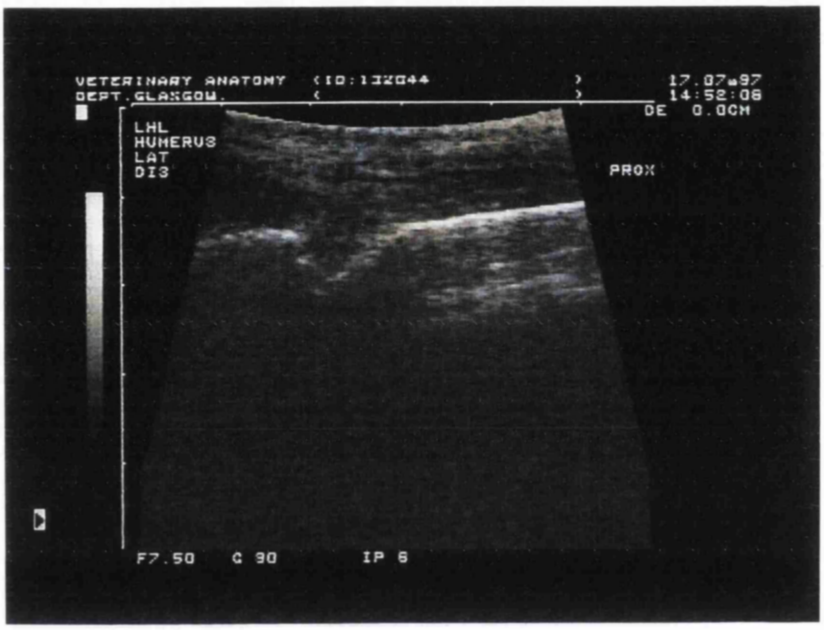

Figure 6.15.9 Longitudinal scan of the distal humerus on day 55 after fracture repair shows the fracture site which appears as a large notch. There is no excessive callus formation detected at the fracture site.

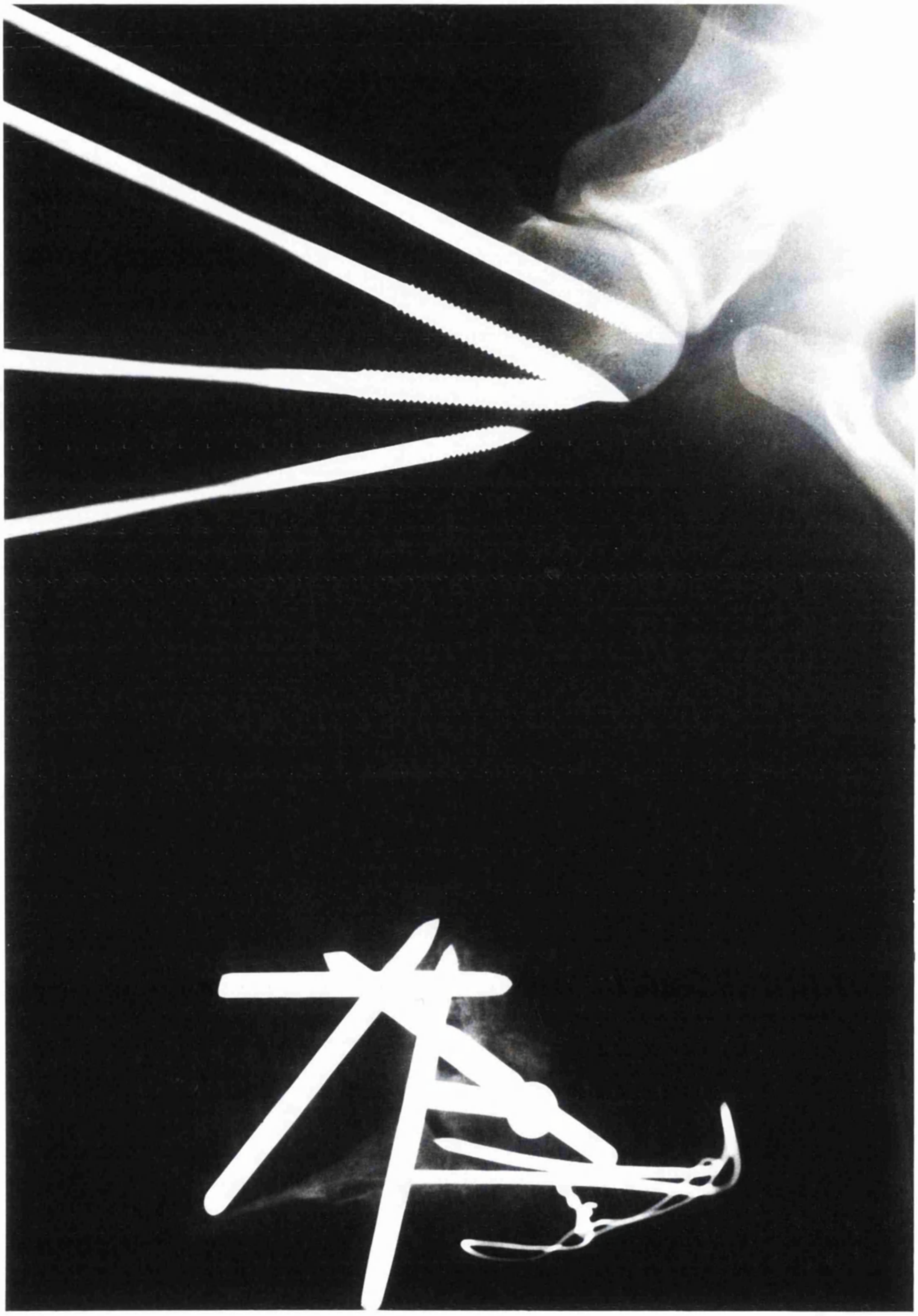

Figure 6.15.10 Radiograph taken at day 96 after fracture repair shows the healing process is progressing satisfactorily.

Figure 6.15.11 Transverse scan at the fracture site area on day 96 after fracture repair still shows the rough bone surface which is due to callus formation (**a**). The distal humerus has lost its normal shape as compared to the normal proximal humerus (**b**).

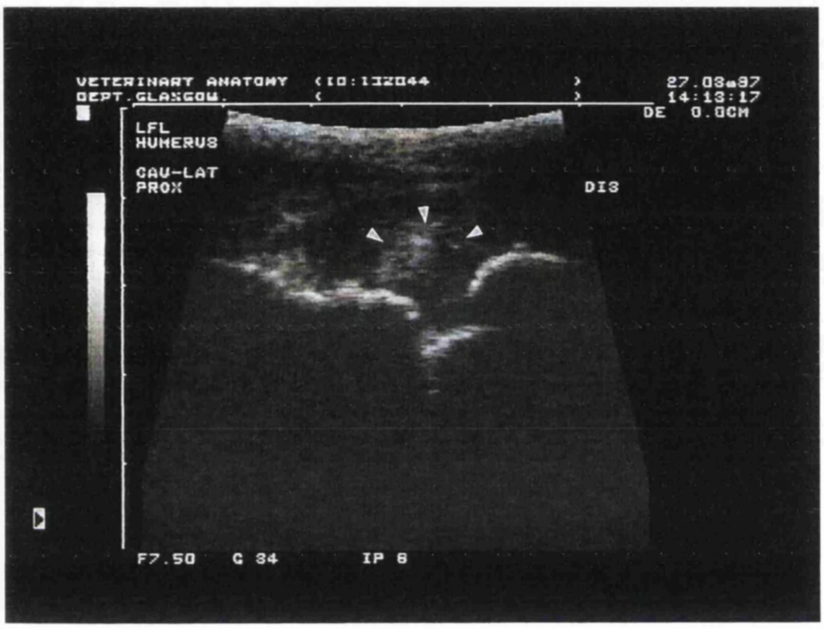

Figure 6.15.12 Longitudinal scan of the distal humerus on the caudo-lateral aspect of the fracture site area on day 96 after fracture repair shows the uneven bone contour, but the bone surface shows that a remodelling process is taking place as it is becoming smoother. The hyperechoic structure area in the muscle at the fracture site area (arrow heads) suggests the presence of fibrous tissue within the muscle.

Case 16

A four year old domestic short hair neutered male cat, weight 4.5 kg, was presented to the Glasgow University Veterinary Hospital after having been involved in a road traffic accident four days previously. Radiographic examination revealed a comminuted mid shaft fracture of the right femur with proximocaudal displacement of the distal segment. A fissure line was seen running vertically within the proximal fragment. The fracture was stabilised with an intramedullary pin which was augmented with a tied-in type one external fixator. Post operation radiographs showed this to have been enclosed in a cerclage wire (figure 6.16.1). The two main fragments remained loose.

Ultrasonographic examination

Day two after fracture repair

Ultrasonographic examination demonstrated the fracture site area which appeared hyperechoic suggesting periosteal tissue reaction (figure 6.16.2). The area of hyperechoic structure surrounding the fracture site suggested an area of soft tissue reaction. One fragment which appeared hyperechoic with acoustic shadowing artefact was imaged at the fracture site area. A large fracture gap was revealed when scanned longitudinally from the cranial aspect. It appeared as discontinuity of the two bone fragments (figure 6.16.3). The hyperechoic area at the fracture site and above the femur suggested the area of soft tissue reaction. On cranio-lateral scan, the large fracture gap was imaged connected by the intramedullary pin which appeared hyperechoic with reverberation artefact (figure 6.16.4). The loose bone fragment at the fracture site imaged on the medio-caudal aspect appeared as hyperechoic material with acoustic shadowing artefact and was protruding into the muscle (figure 6.16.5). The surrounding hyperechoic area suggested an area of soft tissue reaction. The large fracture gap also showed on the lateral aspect scan. The hyperechoic area on the bone surface at the fracture site suggested periosteal tissue reaction, and the hyperechoic appearance of the area surrounding the fracture site suggested a soft tissue reaction (figure 6.16.6). No callus formation was detected at this stage.

Day 31 after fracture repair

Radiographic examination

Radiographs taken at day 31 after fracture repair showed a good alignment of the fracture fragments, with less definition of the fracture edges (figure 6.16.7). Some implant reaction around the distal pin was seen as a subtle periosteal reaction and lucency. The soft tissue swelling had resolved. A fissure line running vertically within the proximal fragment was still visible on a lateral view.

Ultrasonographic examination

Ultrasonographic examination demonstrated the fracture site with an oblique bone fragment within the fracture gap. There was a small hyperechoic area on the bone fragment which suggested soft callus formation (figure 6.16.8). The intramedullary pin used in the fracture reduction was imaged connecting the two main fragments and appeared hyperechoic with reverberation artefact (figure 6.16.9). There was no callus formation detected on the bone surface at the fracture site area on the lateral side. A transverse scan on the lateral aspect revealed the fracture site with the bone fragment and an intramedullary pin. The intramedullary pin in cross sectioned appeared as a small hyperechoic image with comet tail artefact (figure 6.16.10). The bone fragment appeared hyperechoic with acoustic shadowing. The soft callus formation was detected on the transverse scan and appeared as an hyperechoic area (figure 6.16.11). The muscle area adjacent to the femur appeared hyperechoic.

Day 66 after fracture repair

Radiographic examination

Radiographs taken at day 66 after fracture repair showed that there was still no significant callus at the fracture site; however, the two small fragments seem less well defined than on the day 31 post-operation. The density of the more distal fragment aroused suspicion of a possible sequestrum forming although the position of the fragment relative to the beam may be responsible. A small amount of reaction was seen around the lateral end of the distal pin and minimal lucency was noted around the proximal pin at the level of greater trochanter (figure 6.16.12). Clinically, the animal was already bearing weight on the fractured leg.

Ultrasonographic examination

Ultrasonographic examination demonstrated the fracture site with an intramedullary pin and a bone fragment caudal to the femur (figure 6.16.13). The bone fragment caudal to the femur at the fracture site area had started to coalesce with the main fragment. There was no excessive callus formation at the fracture site. The muscle structure appeared normal ultrasonographically. The muscle had reduced in size as shown by the small distance between the skin surface and the femur. The fracture gap was still present but the size had reduced slightly due to callus formation. On the cranial aspect scan, the fracture gap appeared small with callus formation at the end of both fragments which was trying to bridge the gap (figure 6.16.14). On the medial side, the bone fragment and the intramedullary pin were imaged (figure 6.16.15). No excessive callus formation was detected on the medial side.

Day 88 after fracture repair

Radiographic examination

Radiographs taken at day 88 after fracture repair showed the implant had been modified after previous radiographs with removal of the proximal femoral fixator pin. This was because the proximal pin of the external fixator had loosened. Reaction and lucency were noted around the distal fixator pin. Callus was bridging the fracture fragments caudally, but was limited cranioproximally (figure 6.16.16).

Ultrasonographic examination

Ultrasonographic examination on day 88 after fracture repair still demonstrated the fracture gap with the intramedullary pin connecting the two fragments on a lateral scan (figure 6.16.17). The fracture gap appeared smaller than on the day 66 examination scans made previously and showed the presence of callus formation on a cranial aspect scan (figure 6.16.18). The fragments were not fully united on the cranial side. Transverse scan at the fracture site on the lateral aspect showed the femur with minimal callus formation and the intramedullary pin (figure 6.16.19). The intramedullary pin appeared as a small hyperechoic area with comet tail artefact. The muscle structure appeared to have a normal hypoechoic texture. On the caudal aspect the fracture gap appeared smaller than on the day 66 examination and was connected by the intramedullary pin (figure 6.16.20).

Day 125 after fracture repair

Radiographic examination

Radiographs taken at day 125 after fracture repair showed there was non union and no significant callus formation at the fracture site. There was osteolucency around the pin. The external fixator had been removed at this time as the cat could use the leg and was bearing weight although there was no significant callus formation seen radiographically. It was believed that probably some weak callus had formed (figure 6.16.21).

Ultrasonographic examination

Ultrasonographic examination demonstrated the fracture site which was being bridged by the callus on the lateral side. A small fracture gap could still be seen (figure 6.16.22). This suggested that the callus formation was bridging the fracture site slowly with no excessive callus formation detected. The bone surface appeared smooth suggestive of the remodelling process. Ultrasonographically, the healing progress was good. The cat was not seen again, the owner informed that the cat was using its leg indicating that the fracture was satisfactorily healed.

Figure 6.16.1 Radiographs obtained immediately after fracture repair show the fracture is stabilised with an intramedullary pin which is augmented with a tied-in type I external fixator. A fissure line is seen running vertically within the proximal fragment. The two main fragments remain loose. **a**, lateral view, **b**, cranial view.

a

b

Figure 6.16.2 Longitudinal scan of the femur from the caudal aspect on day two after fracture repair demonstrates the fracture site area which appears hyperechoic suggestive of periosteal tissue reaction. The hyperechoic area surrounding the fracture site indicates an area of soft tissue reaction. One fragment with acoustic shadowing artefact (arrow head) is seen at the fracture site protruding into the muscle.

Figure 6.16.3 A big fracture gap is revealed on a longitudinal scan from the cranial aspect. It appears as discontinuity of the bone. The hyperechoic area at the fracture site and above the femur is suggestive of soft tissue reaction.

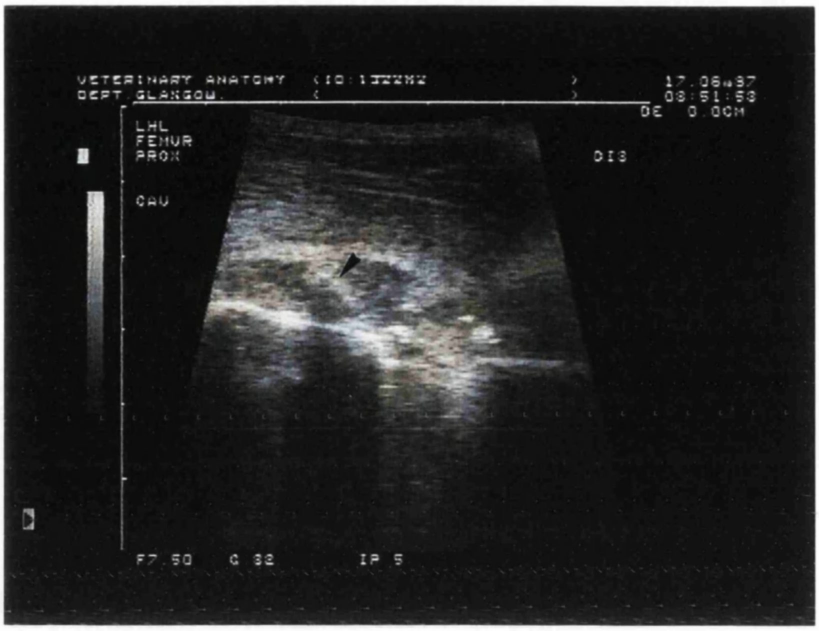

Figure 6.16.2

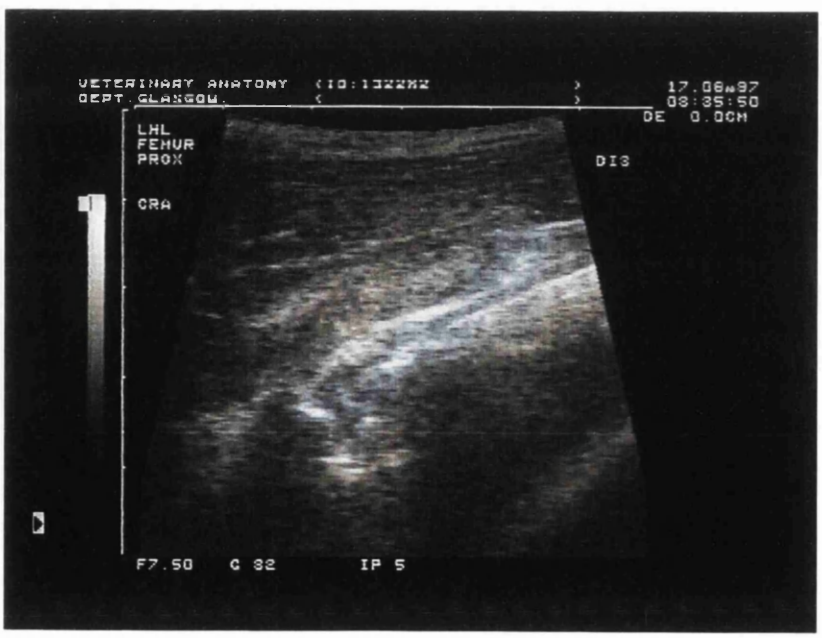

Figure 6.16.3

Figure 6.16.4 The large fracture gap connected by the hyperechoic straight lines with reverberation artefact is imaged on cranio-lateral scan. The hyperechoic straight lines with reverberation artefact is actually the intramedullary pin used in the fracture reduction.

Figure 6.16.5 The loose bone fragment at the fracture site appears as hyperechoic material with acoustic shadowing artefact protruding into the muscle on longitudinal scan 24 hours after fracture repair. Note also the surrounding area appears homogenously hyperechoic suggestive of soft tissue reaction.

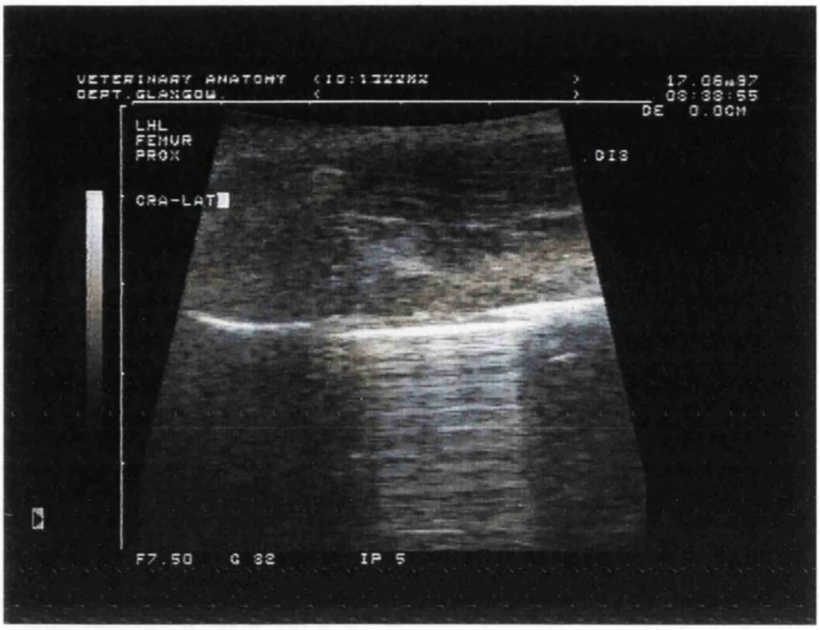

Figure 6.16.4

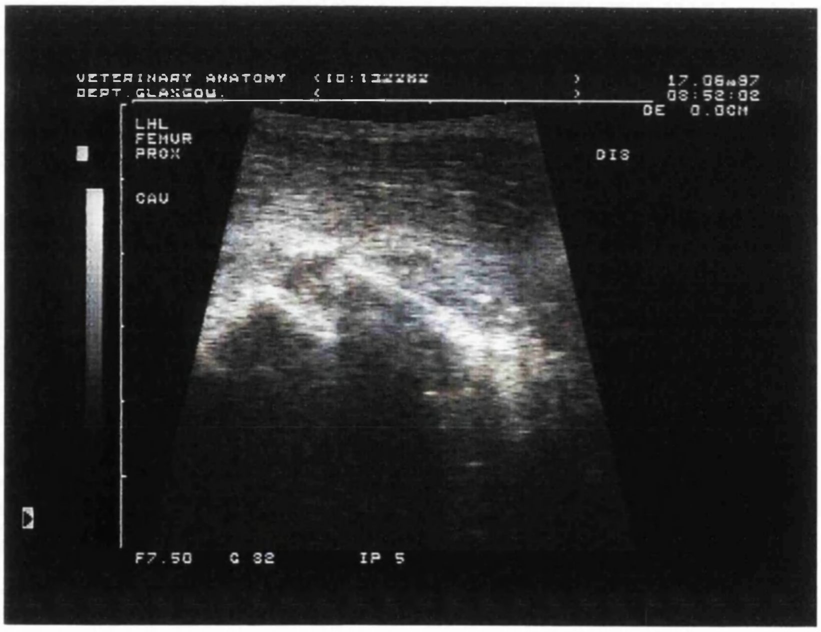

Figure 6.16.5

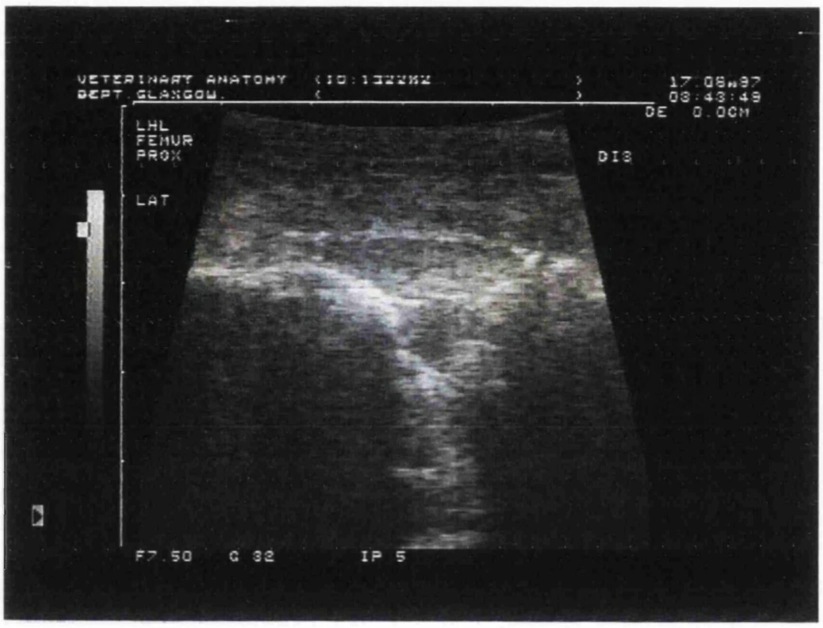

Figure 6.16.6 Longitudinal scan of the femur from the lateral aspect on day two after fracture repair shows the large fracture gap. The hyperechoic area on the bone surface at the fracture site is suggestive of periosteal tissue reaction, and the hyperechoic appearance of the area surrounding the fracture site suggests soft tissue reaction. No callus formation is seen at this stage.

Figure 6.16.7 Radiographs taken at day 31 after fracture repair show a good alignment of the fracture fragments, with less defined fracture edges. **a**, cranial view, **b**, lateral view. There is some implant reaction around the distal pin which is seen as a subtle periosteal reaction and lucency. The soft tissue swelling is resolved. A fissure line running vertically within the proximal fragment is still visible on the lateral view.

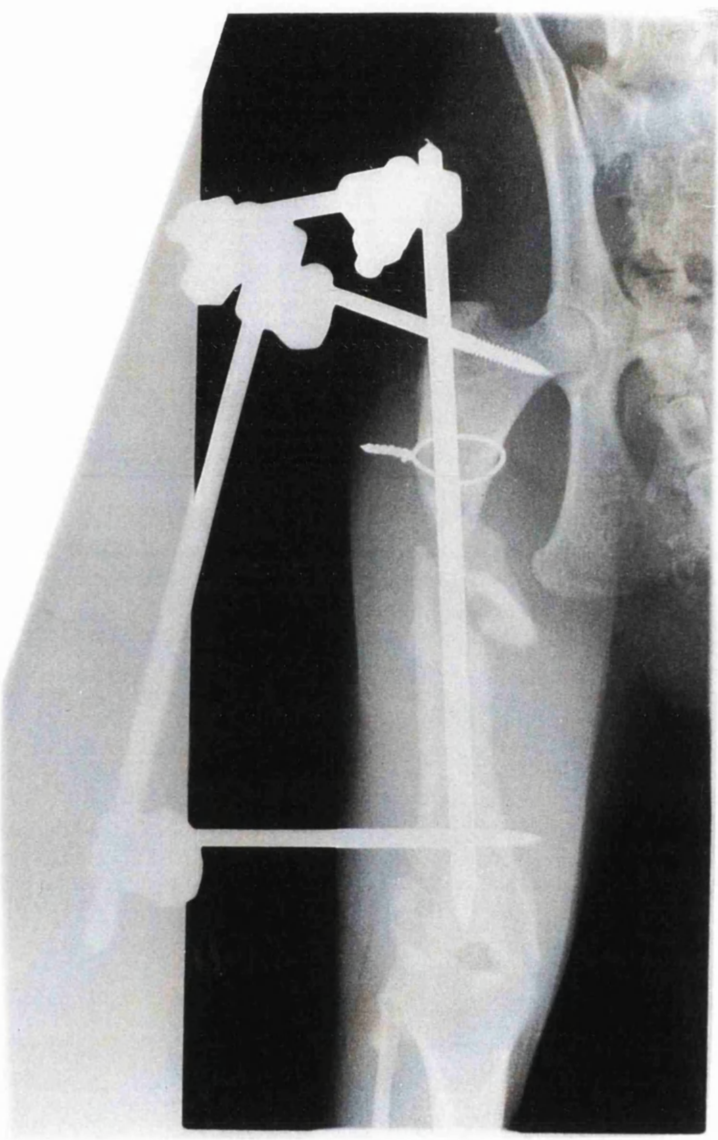

a

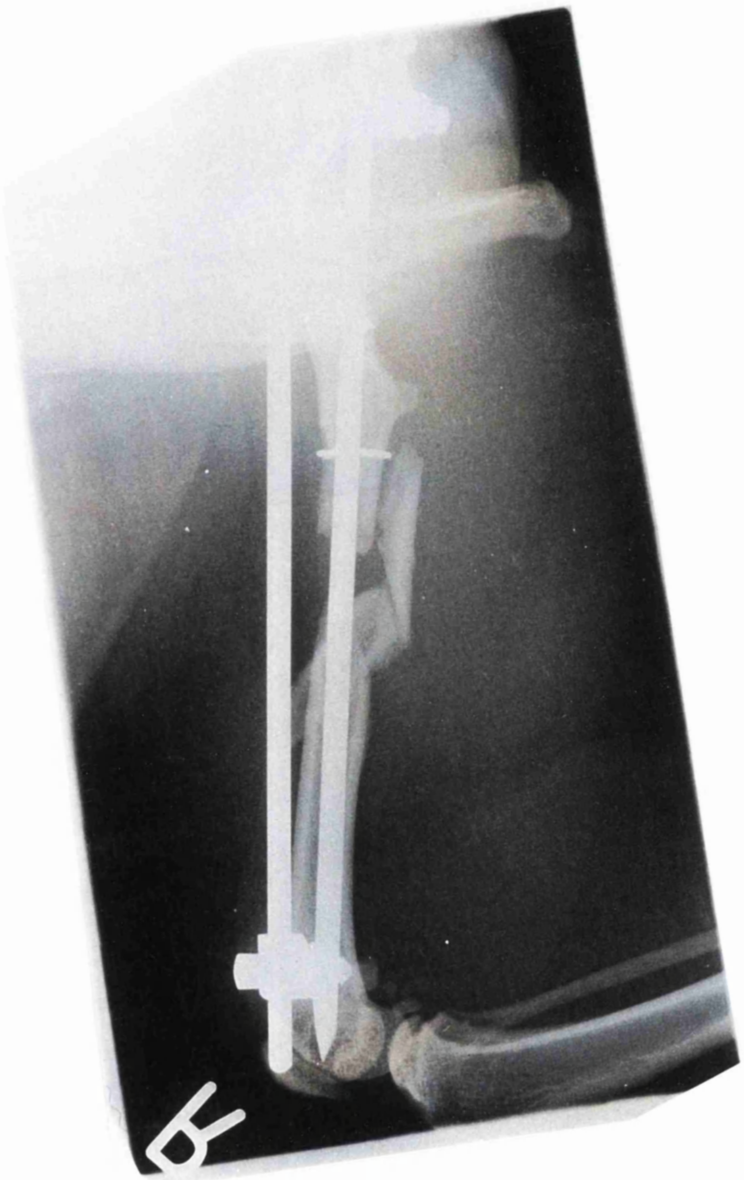

b

Figure 6.16.8 Longitudinal scan of the femur on day 31 after fracture repair shows the fracture site with an oblique bone fragment within the fracture gap. Note also that there is a small hyperechoic area on the bone fragment (arrow heads) which is suggestive of soft callus formation.

Figure 6.16.9 Longitudinal scan of the femur on day 31 after fracture repair shows the fracture gap with intramedullary pin which appears hyperechoic with typical reverberation artefact. The gap appears reduced in size but no excessive callus formation can be seen at the fracture site area and on the bone surface.

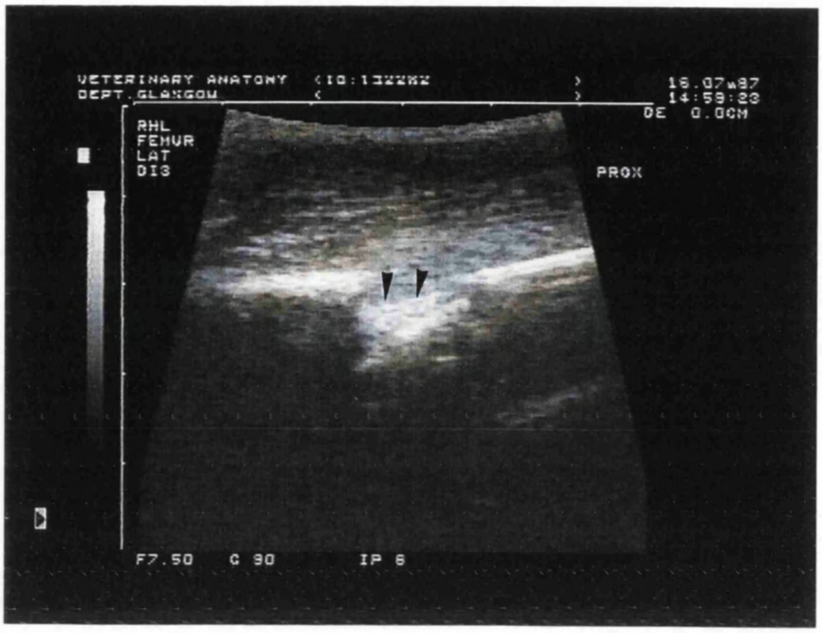

Figure 6.16.8

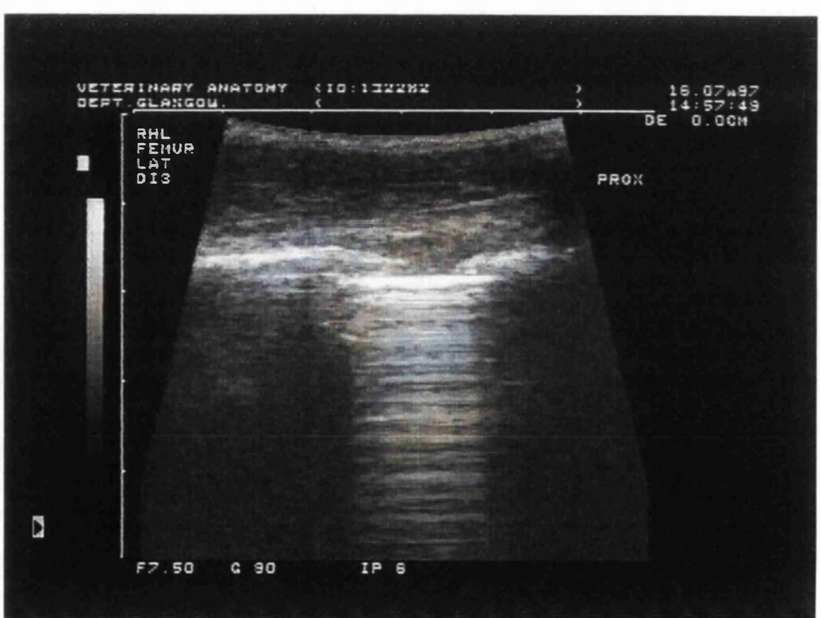

Figure 6.16.9

Figure 6.16.10 Transverse scan from the lateral aspect of the femur on day 31 after fracture repair shows the fracture site with the bone fragment and an intramedullary pin. The intramedullary pin scanned transversely appears as a small hyperechoic material (arrow) with comet tail artefact. **F**, femur.

Figure 6.16.11 The soft callus formation is detected on transverse scan at the fracture site area on day 31 after fracture repair and appears as a small hyperechoic materials (arrow heads). Note also the muscle area adjacent to the femur appears hyperechoic. **F**, femur.

Figure 6.16.10

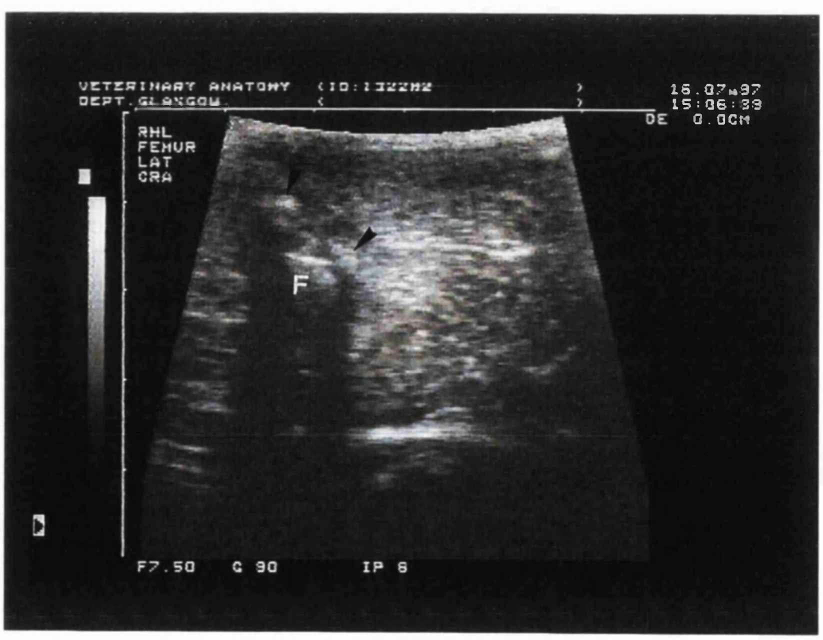

Figure 6.16.11

Figure 6.16.12 Radiographs taken at day 66 after fracture repair show that there is still no significant callus at the fracture site; however, the two small fragments seem less well defined than on the day 31 post operation. The density of the more distal fragment arouses suspicion of a possible sequestrum forming. A small amount of reaction is seen around the lateral end of the distal pin and minimal lucency is noted around the proximal pin at the level of the greater trochanter. Clinically, the animal could already bear weight on the fractured leg. **a**, lateral view, **b**, cranial view.

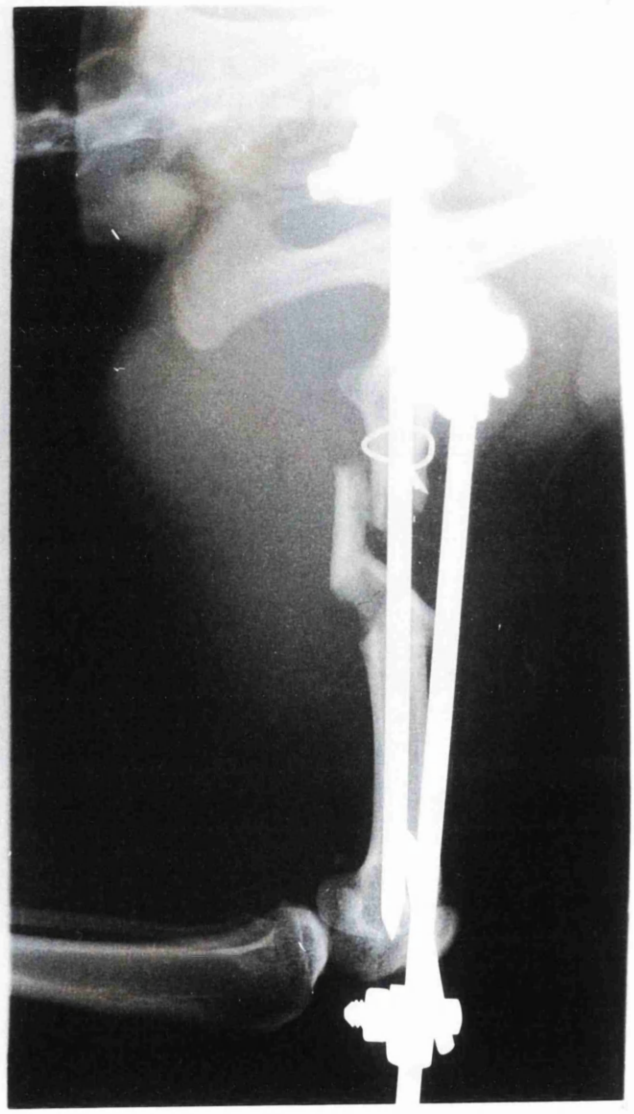

a

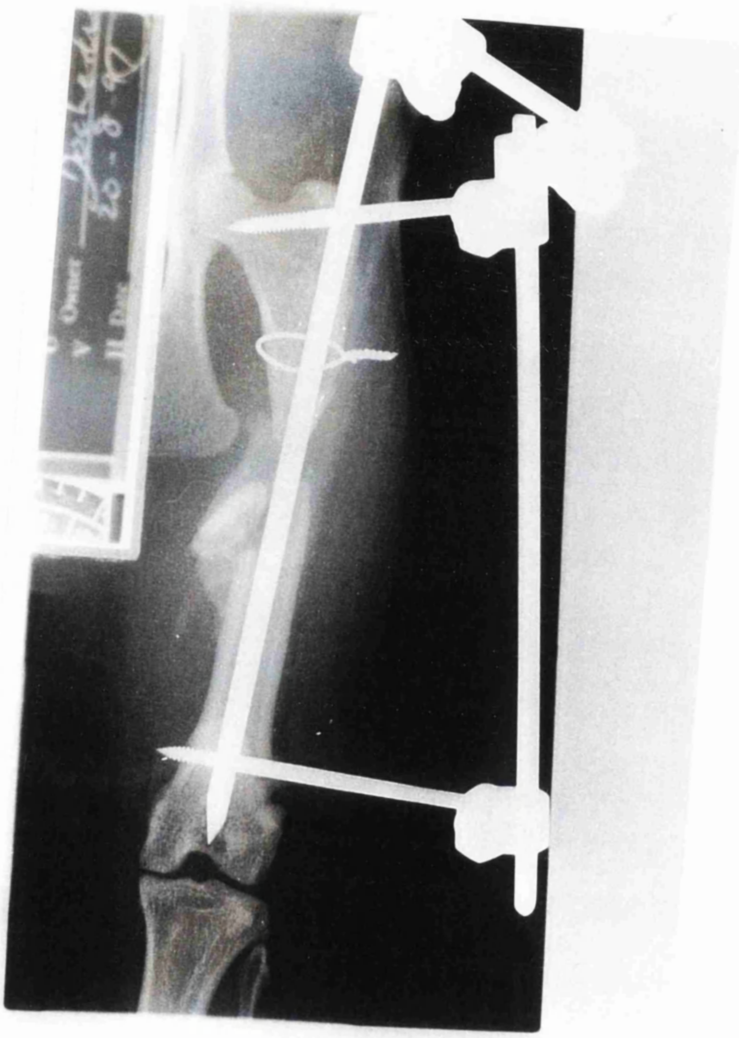

b

Figure 6.16.13 Longitudinal scan of the femur on day 66 after fracture repair demonstrates the fracture gap with an intramedullary pin and a bone fragment caudal to the femur (arrow heads). The intramedullary pin appears hyperechoic with reverberation artefact. There is no excessive callus formation at the fracture site.

Figure 6.16.14 Longitudinal scan of the fracture site from the cranial aspect on day 66 after fracture repair shows the fracture gap which has become smaller with the callus formation at the end of both fragments. The callus formation is trying to bridge the gap.

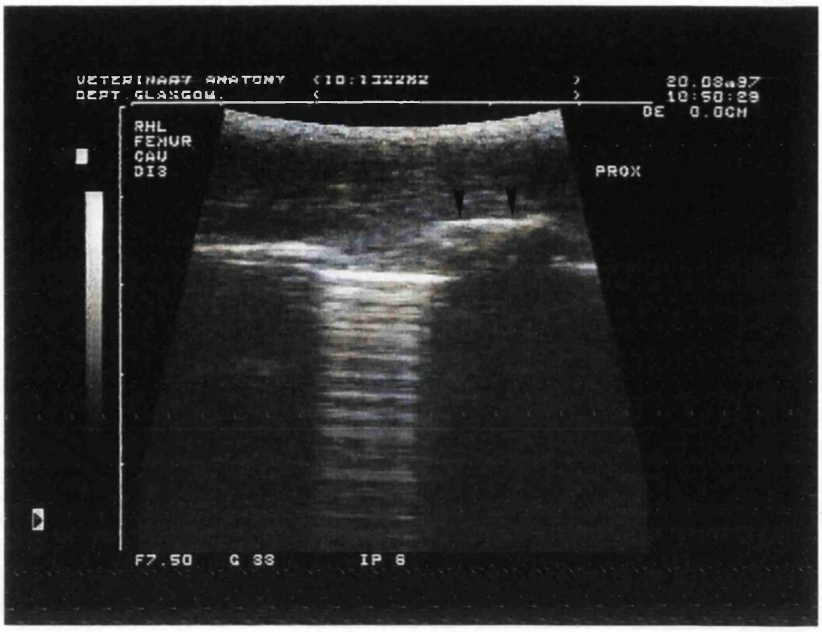

Figure 6.16.13

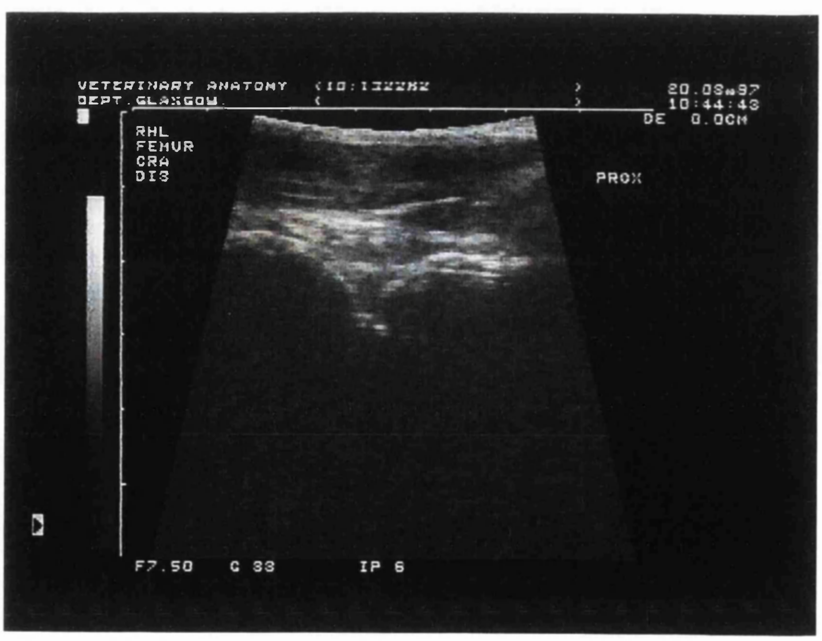

Figure 6.16.14

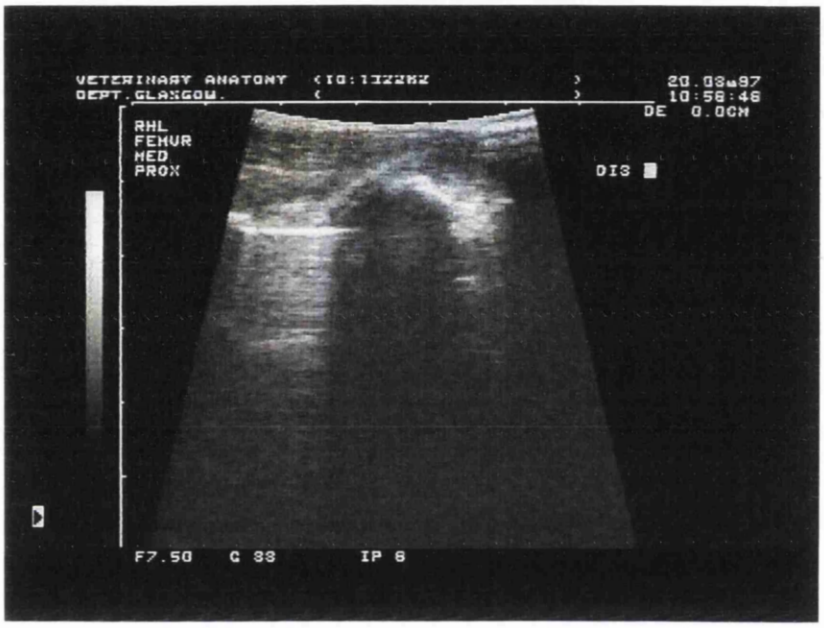

Figure 6.16.15 Longitudinal scan of the femur from the medial aspect on day 66 after fracture repair shows the fracture site area with the bone fragment and the intramedullary pin. There is no excessive callus formation detected.

Figure 6.16.16 Radiograph taken at day 88 after fracture repair shows the implant has been modified since previous radiographs with removal of the proximal femoral fixator pin. This is because the proximal pin of the external fixator had loosened. Reaction and lucency are noted around the distal fixator pin laterally. Callus formation is bridging the fracture fragments caudally, but is limited cranioproximally.

Figure 6.16.17 Longitudinal scan of the femur at the fracture site area on lateral scan at day 88 after fracture repair still shows the fracture gap with the intramedullary pin connecting the two fragments.

Figure 6.16.18 Longitudinal scan of the femur on cranial aspect on day 88 after fracture repair shows the fracture gap which is decreasing with the presence of callus formation within it.

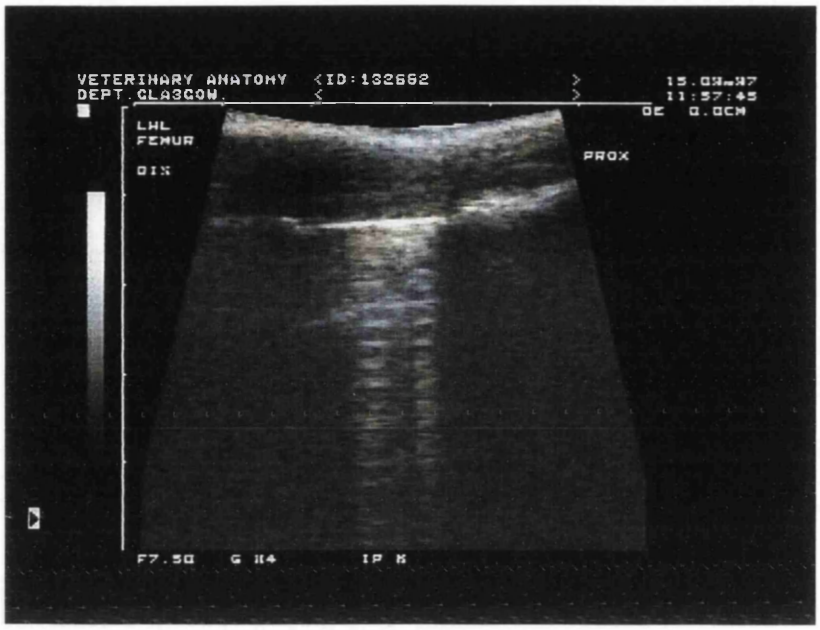

Figure 6.16.17

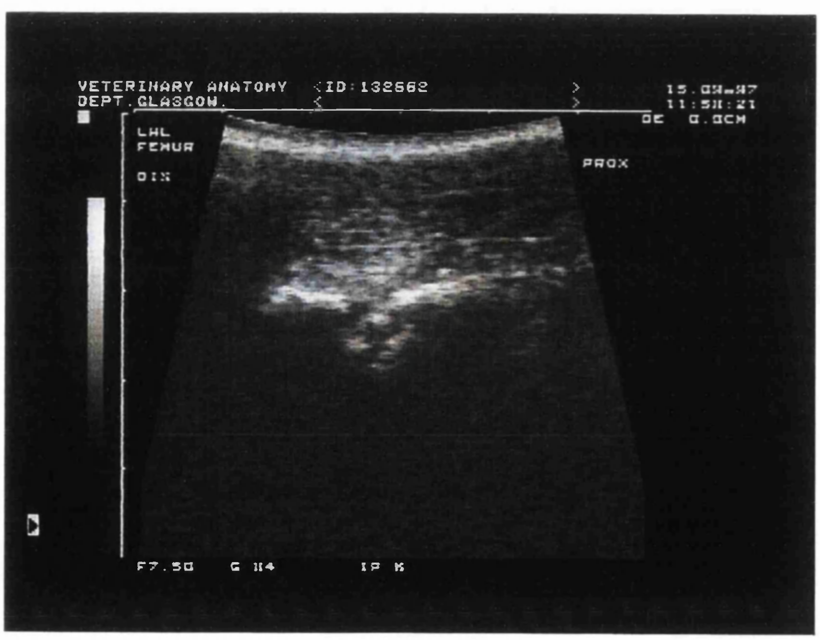

Figure 6.16.18

Figure 6.16.19 Transverse scan at the fracture site from the lateral aspect on day 88 after fracture repair shows the femur with minimal callus formation and the intramedullary pin (arrow). The intramedullary pin appears as a small hyperechoic mark with comet tail artefact. The muscle structure appears normal with an hypoechoic texture.

Figure 6.16.20 Longitudinal scan of the fracture site area from the caudal aspect on day 88 after fracture repair shows the fracture gap which appears smaller than in the previous scans. The intramedullary pin can still be seen.

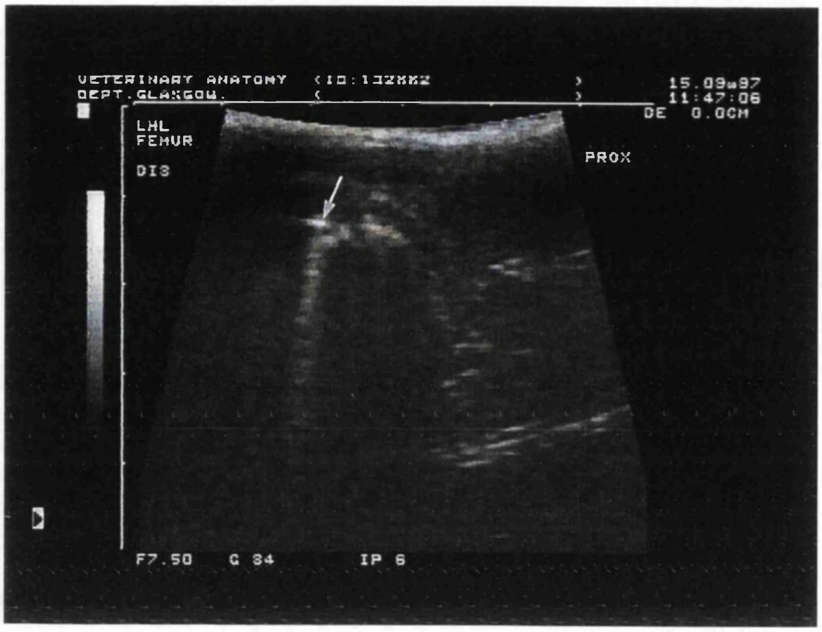

Figure 6.16.19

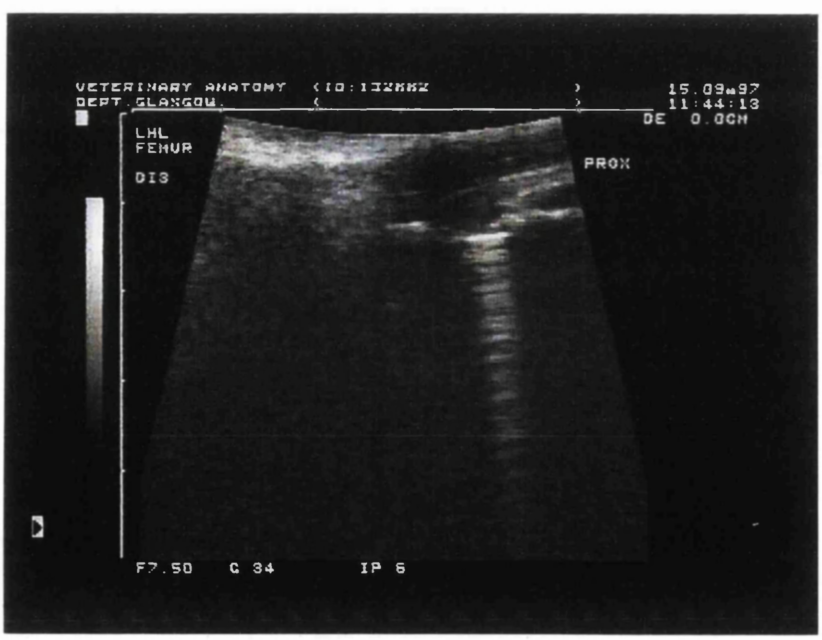

Figure 6.16.20

Figure 6.16.21 Radiographs taken at day 125 after fracture repair show there is non union and no significant callus formation at the fracture site. There is osteolucency around the pin. The external fixator has been removed at this time as the cat can used the leg and is bearing weight although there is no significant callus formation seen radiographically. It was believed that probably some weak callus had formed. **a**, lateral view, **b**, cranial view.

a

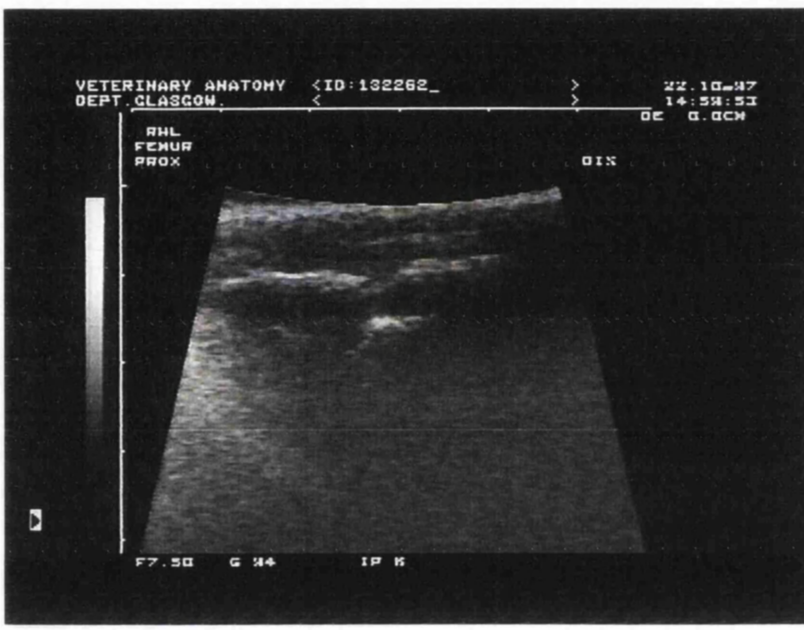

Figure 6.16.22 Longitudinal scan of the femur on day 125 after fracture repair demonstrates the fracture site which is being bridged by the callus on the lateral side. The small fracture gap can still be seen. This indicates that the callus formation is bridging the fracture site slowly. There is no excessive callus formation detected.

Case 17

A two year old male Border Collie, weight 25 kg, was referred to the Glasgow University Veterinary Hospital having been found to be lame. The animal had no owner and the accident was believed to be due to jumping over a fence or wall. Radiographic examination revealed that a severely comminuted fracture of the femoral mid shaft of the left hind limb had been sustained. Fracture repair was carried out on the following day after admission and the fracture was stabilised with an intramedullary pin tied in to a modified type two four pins external skeletal fixator. Radiographs taken immediately after the fracture repair showed that the repair process had resulted in good alignment of the fracture site (figure 6.17.1). At least two fragments remained in situ adjacent to the main bone segments.

Ultrasonographic examination

Day three after fracture repair

Ultrasonographic examination demonstrated the fracture site with the presence of a small fracture gap on the cranio-lateral aspect (figure 6.17.2). The fracture site appeared hyperechoic with no indication of soft callus formation being present. The muscle superficial to the fracture site appeared as a disorganised hypoechoic structure suggestive of an area of muscle damage. The fracture site scanned from the caudo-lateral aspect appeared as a defect on the bone surface but no significant gap was present (figure 6.17.3). The femur appeared smooth with no indication of soft callus formation on it, but the hyperechoic area at the fracture site was suggestive of early formation of the soft callus. A transverse scan from the cranio-lateral aspect revealed a small bone fragment caudal to the femur (figure 6.17.4). There were soft tissue and periosteal tissue reactions around the bone fragment beside the femur which appeared hyperechoic. The hyperechoic appearance of the area adjacent to the femur cranially was suggestive of an area of soft tissue reaction. The area of muscle damage appeared as a disorganised hypoechoic structure. The fracture site imaged on a transverse scan from the lateral aspect appeared as an abnormal femur with an hyperechoic appearance (figure 6.17.5). No callus formation was detected.

Day 54 after fracture repair

Radiographic examination

Radiograph taken at day 54 after fracture repair showed there was no bony callus formation, and there was insufficient reduction and alignment (figure 6.17.6).

Ultrasonographic examination

Ultrasonographic examination at the mid shaft of the femur on a transverse scan from the lateral aspect demonstrated the distal end of the bone fragment which was separated from the femur by a small space (figure 6.17.7a), and the fragment appeared to have coalesced with the femur toward the proximal end of the fragment (figure 6.17.7b). There was no excessive callus formation detected at the fracture site. The muscle structure appeared to have normal ultrasonographic characteristics. Similarly, on the medial aspect, a transverse scan of the mid femoral shaft showed that the distal end of the fragment was separate from the femoral shaft (figure 6.17.8a), and had coalesced with the femur toward the proximal end of the fragment (figure 6.17.8b). The intramedullary pin at the fracture site imaged from the medial aspect appeared hyperechoic with reverberation artefact, connecting the two bone fragments (figure 6.17.9). The distal fragment appeared elevated from the proximal fragment on the medial aspect scan. The femur appeared smooth and no callus formation was detected. However, some callus formation was detected at the fracture site on the medial aspect scan as shown by the rough femoral surface (figure 6.17.10).

Day 75 after fracture repair

Radiographic examination

Radiographs taken at day 75 after fracture repair showed that there was no improvement in the fracture healing process as compared to the previous radiographs (figure 6.17.11). The distal pin was removed at this time as it had become loose.

Ultrasonographic examination

Ultrasonographic examination of the fracture site area found that there was no excessive callus formation. The femoral surface appeared hyperechoic and smooth. The femur and the proximal portion of the bone fragment on the caudal side that had coalesced with the femoral shaft appeared smooth suggestive of a remodelling process (figure 6.17.12a). However, the distal end still appeared as nonunion with the femoral shaft (figure 6.17.12b), but soft callus formation which appeared hyperechoic attached to the femoral shaft on the caudal side could be seen within the space between them. This suggested that the healing process was in progress. The muscle structure appeared as having normal ultrasonographic characteristics. The distal pin of the external fixator had been removed after the radiographic examination. Thus, on the ultrasonographic scan one hole was found on the femur representing the former site of the pin. The hole appeared hyperechoic with soft tissue and perosteal tissue reactions around it (figure 6.17.13). The anechoic area with some echogenic material within lying above the hole is suggestive of blood or fluid accumulation. A transverse scan on the medial aspect of the femur showed the bone fragment on the caudal side as imaged on the day 54 after fracture repair. The intramedullary pin could still be seen, appearing hyperechoic with reverberation artefact on a longitudinal scan from the medial aspect (figure 6.17.14).

Day 98 after fracture repair

Radiographic examination

Radiographs taken at day 98 after fracture repair showed that there was evidence of bony callus formation as compared to the previous radiographs although this was not complete. There was also osteolucency around the remaining pin and the holes of the previous distal pin were still osteolucent (figure 6.17.15).

Ultrasonographic examination

Ultrasonograpic examination revealed the bulging but smooth bone surface which suggested a remodelling process (figure 6.17.16). The muscle structure appeared to have normal hypoechoic characteristics. A transverse scan of the femur on the caudo-lateral aspect at the fracture site area revealed an abnormal appearance with the bone fragment lying superficial to the femur (figure 6.17.17). The femur below the bone fragment appeared to have a smooth surface showing the remodelling process. The intramedullary pin could still be seen from the medial aspect connecting the two bone fragments. The intramedullary pin appeared hyperechoic with reverberation artefact. There was bulging bone at the end of both fragments which was due to callus formation, but appeared smooth suggestive of a remodelling process (figure 6.17.18).

Figure 6.17.1 Radiograph obtained immediately after fracture repair. The fracture is reduced with an intramedullary pin tied in to a modified type two four pins external skeletal fixator. The repair process has resulted in good alignment of the fracture site. One fragment can be seen in situ adjacent to the main bone segments.

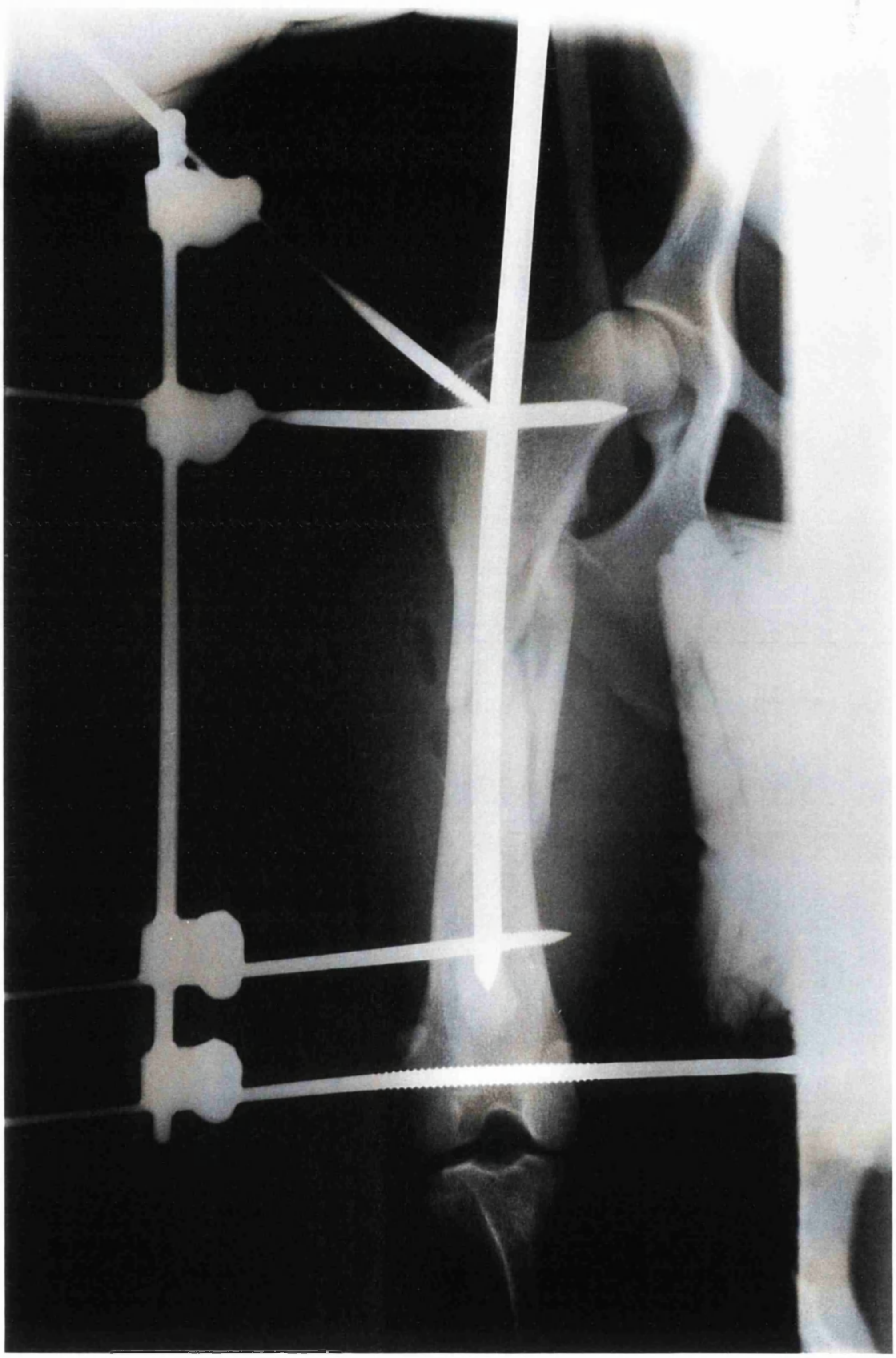

Figure 6.17.2 Longitudinal scan of the femur from the cranio-lateral aspect on day three after fracture repair demonstrates the fracture site with the presence of a small fracture gap. The fracture site appears hyperechoic with no callus formation present. Note also the area of muscle damage (arrow heads) lying above the fracture site which appears as a disorganised hypoechoic structure.

Figure 6.17.3 Longitudinal scan of the femur from the caudo-lateral aspect on day three after fracture repair shows the fracture site (arrow) which appears as a defect on the bone surface but no significant gap is present. Note also that the femur appears smooth with no indication of soft callus formation on it, but the hyperechoic area at the fracture site is suggestive of early formation of soft callus.

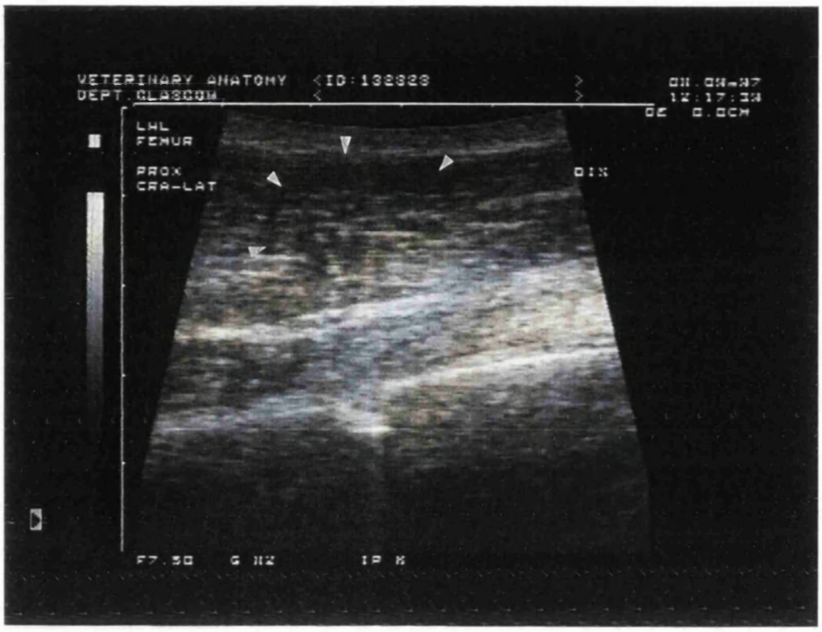

Figure 6.17.2

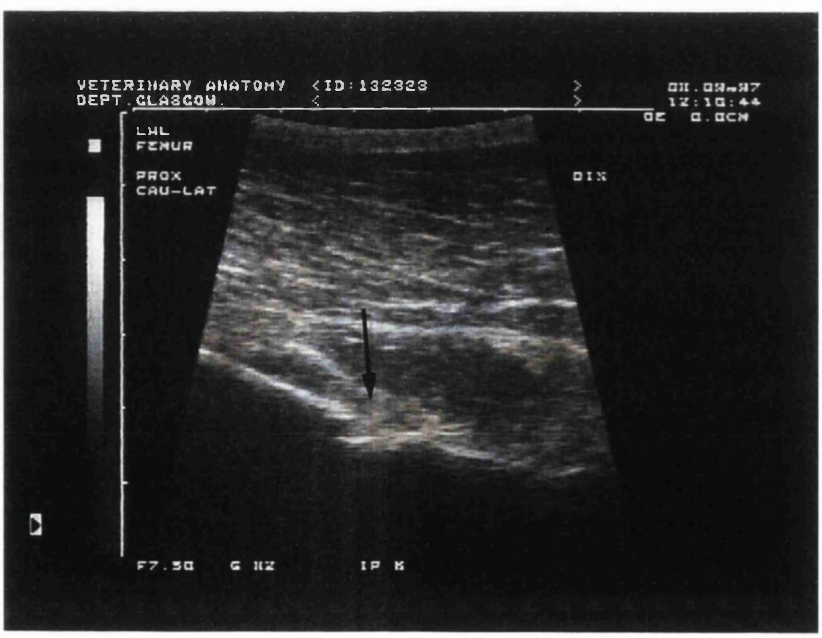

Figure 6.17.3

Figure 6.17.4 Transverse scan from the cranio-lateral aspect of the femur on day three after fracture repair demonstrates the femur and a small bone fragment (large arrow head) placed caudally near to the femur. There is soft tissue and periosteal tissue reactions around the bone fragment which appears hyperechoic. The area with an hyperechoic appearance adjacent to the femur cranially (small arrow heads) is suggestive of soft tissue reaction. Note also that the area of muscle damage appears as a disorganised hypoechoic structure superficial to the soft tissue reaction. **F**, femur.

Figure 6.17.5 Transverse scan from the lateral aspect at the fracture site area on day three after fracture repair shows an abnormal femur with an hyperechoic appearance. Note there is no callus formation present. **F**, femur.

Figure 6.17.4

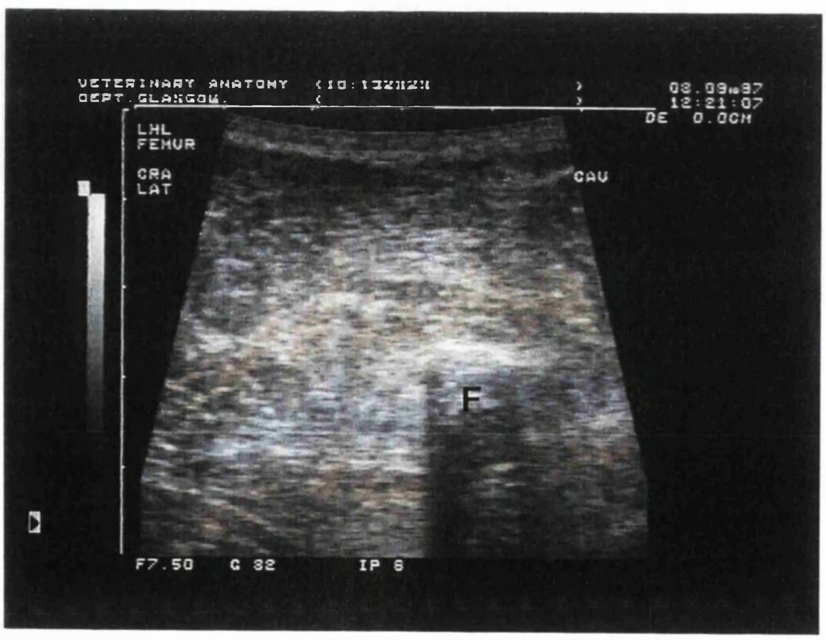

Figure 6.17.5

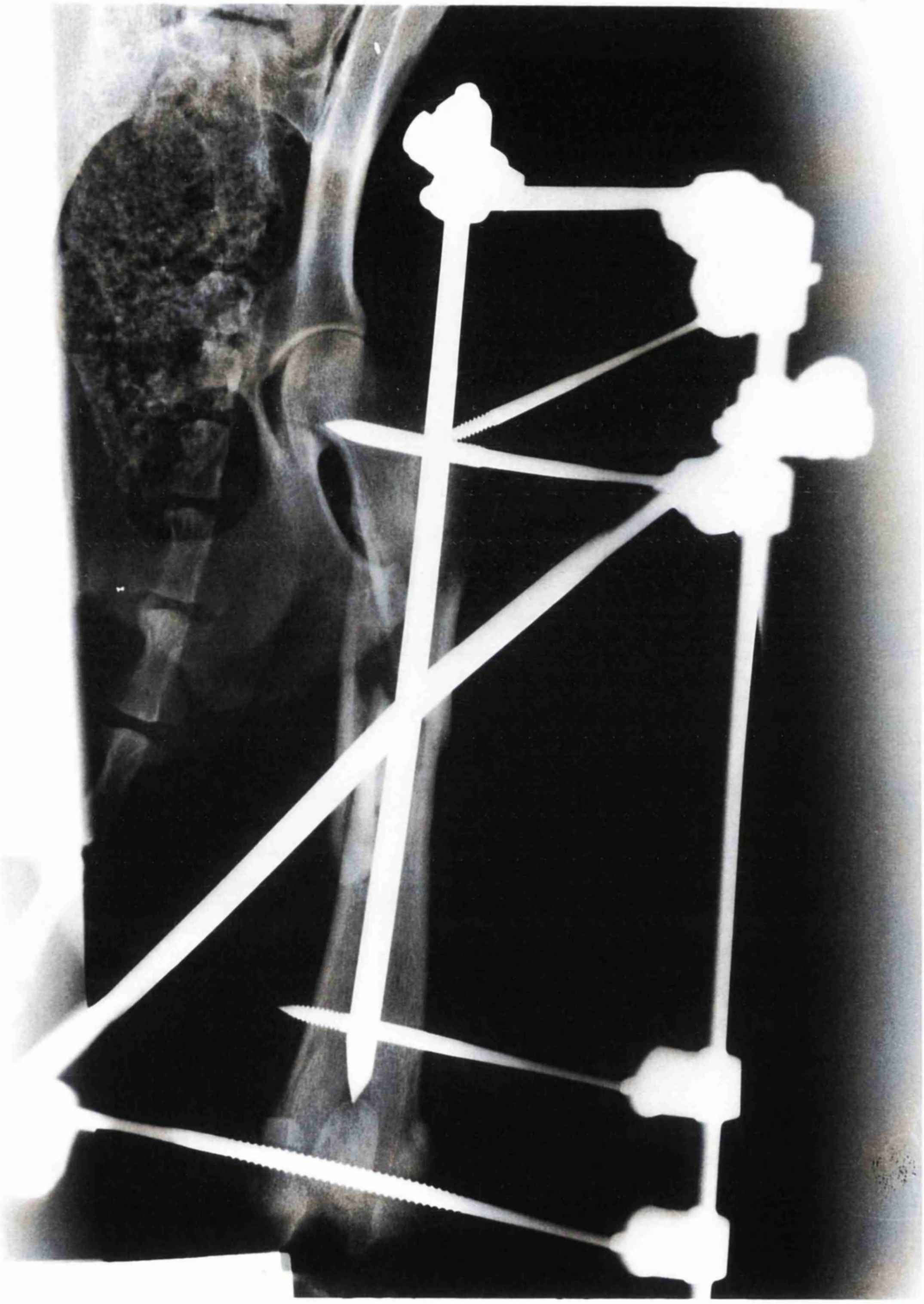

Figure 6.17.6 Radiograph taken at day 54 after fracture repair shows there is no bony callus formation, and there is insufficient reduction and alignment.

Figure 6.17.7 Transverse scans at the mid femoral shaft from the lateral aspect on day 54 after fracture repair demonstrate **a**, that the distal portion of the bone fragment on the caudal side (arrow head) is separated by a space, and **b**, that the fragment appears to coalesce with the femur toward the proximal end. Note also there is no excessive callus formation present at the fracture site. The overlying muscles have a normal ultrasonographic appearance. **F**, femur.

Figure 6.17.7a

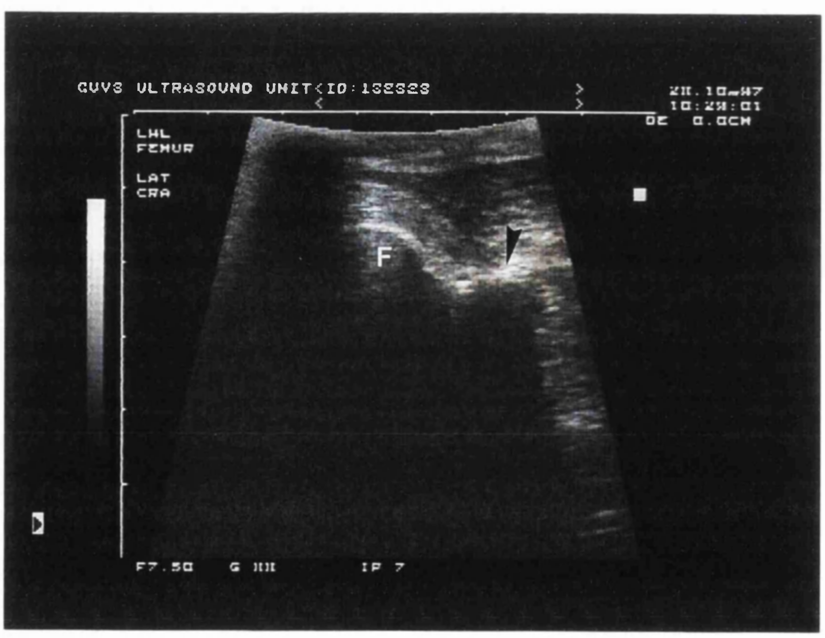

Figure 6.17.7b

Figure 6.17.8 Transverse scans of the mid femoral shaft from medial aspect on day 54 after fracture repair show the same bone fragment (arrow head) as in figure 18.7. The distal end of the fragment appears separate from the femoral shaft (**a**), and the proximal end appears to coalesce with the femur (**b**). **F**, femur.

Figure 6.17.8a

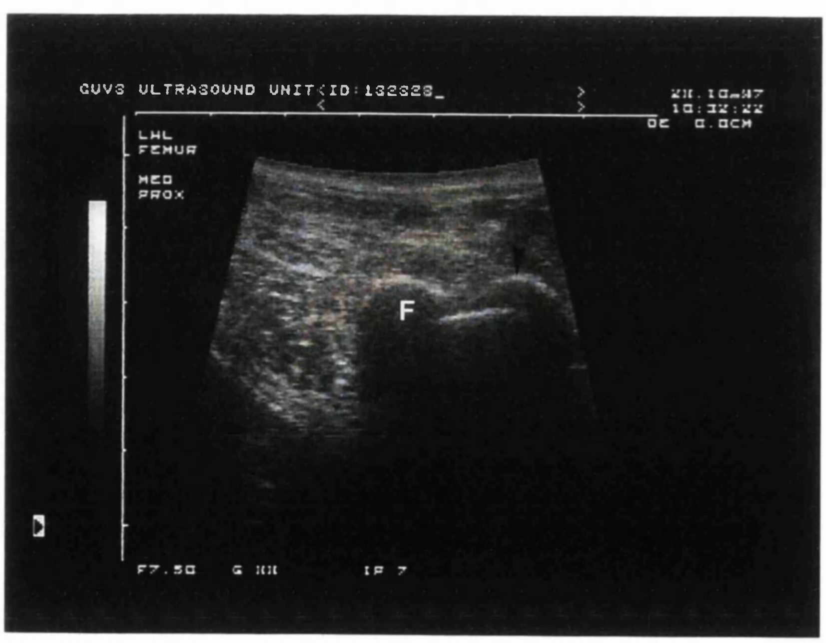

Figure 6.17.8b

Figure 6.17.9 Longitudinal scan of the femur at the fracture site area from the medial aspect on day 54 after fracture repair shows the intramedullary pin which connects the two bone fragments and appears hyperechoic with reverberation artefact. The distal fragment (arrow arrow) appears elevated from the proximal fragment. The femur appears smooth and no callus formation is detected.

Figure 6.17.10 Longitudinal scan of the fracture site from the medial aspect on day 54 after fracture repair shows some callus formation which appears as a rough surface.

Figure 6.17.11 Radiographs taken at day 75 after fracture repair show that there is no improvement in the fracture healing process as compared to the previous radiographs. **a**, caudolateral view, **b**, cranial view. The distal pin has been removed at this time as it had become loose.

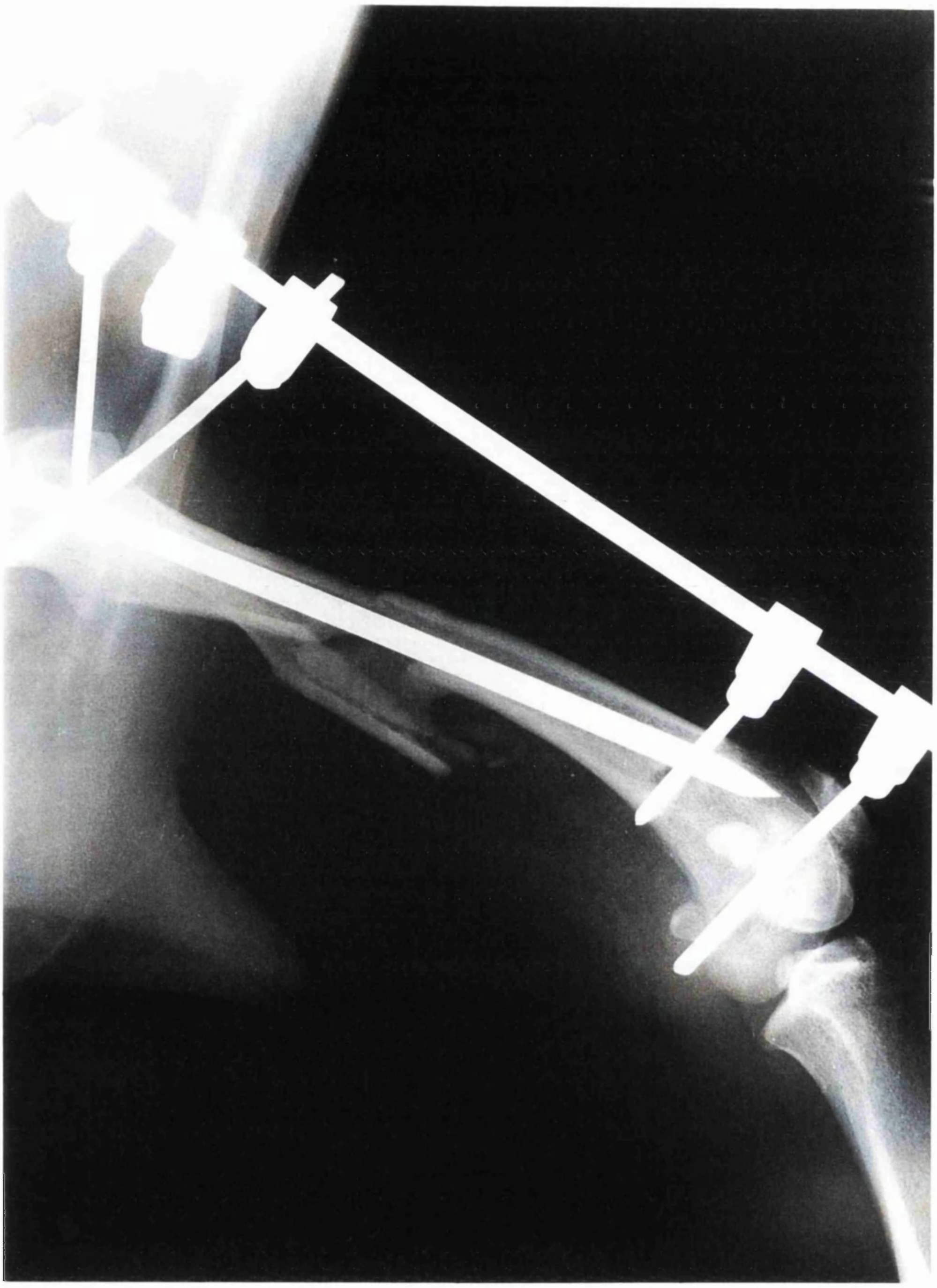

a

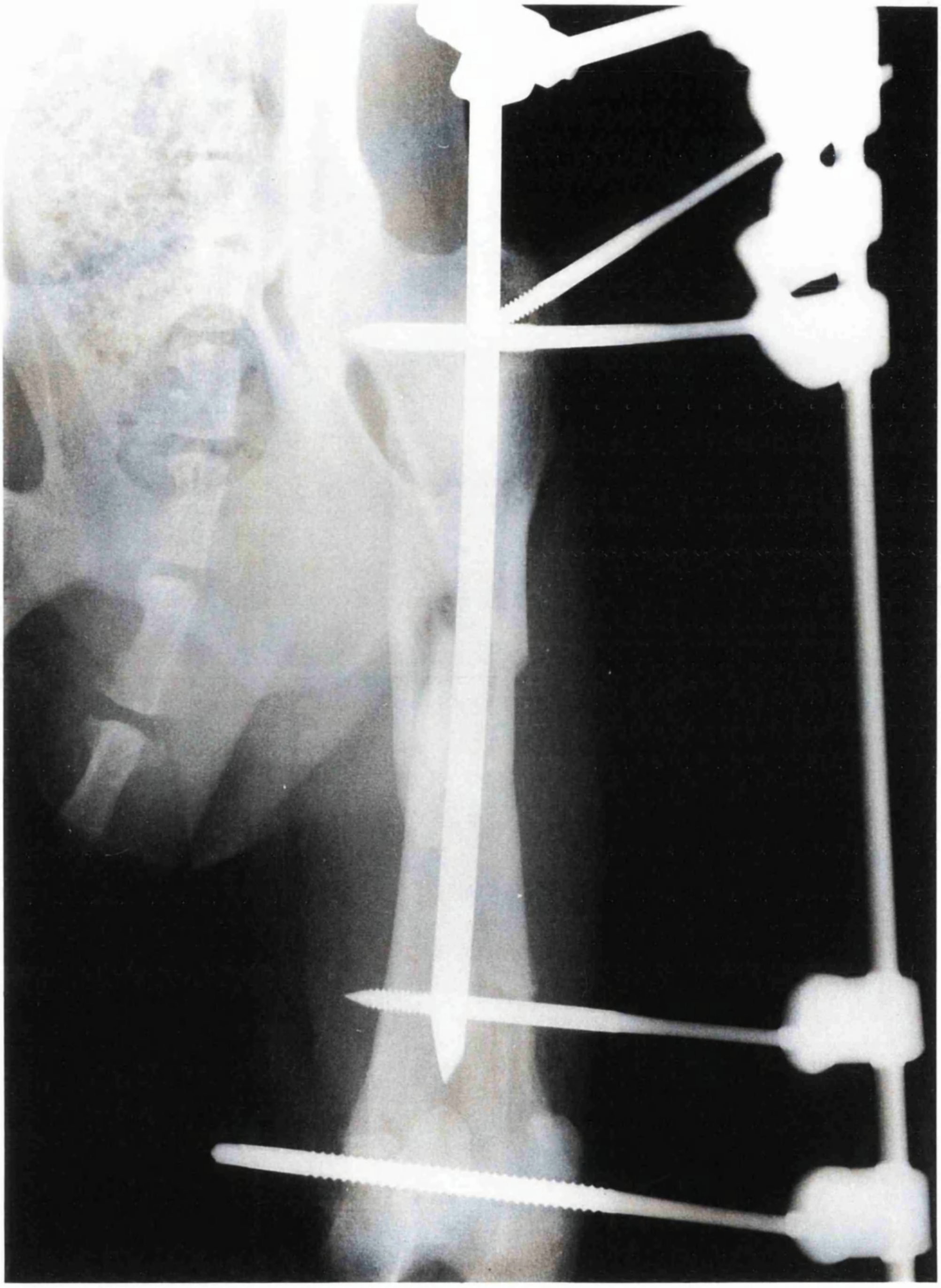

b

Figure 6.17.12 Transverse scans of the fracture site area from the lateral aspect on day 75 after fracture repair show the smooth bone surface with no excessive callus formation. **a**, the femur and the proximal portion of the bone fragment caudal to the femur appears smooth suggestive of a remodelling process. **b**, the distal end still appears as nonunion with the femur, but soft callus formation can be seen attached to the femur and appears hyperechoic. This indicates that the healing process is in progress.

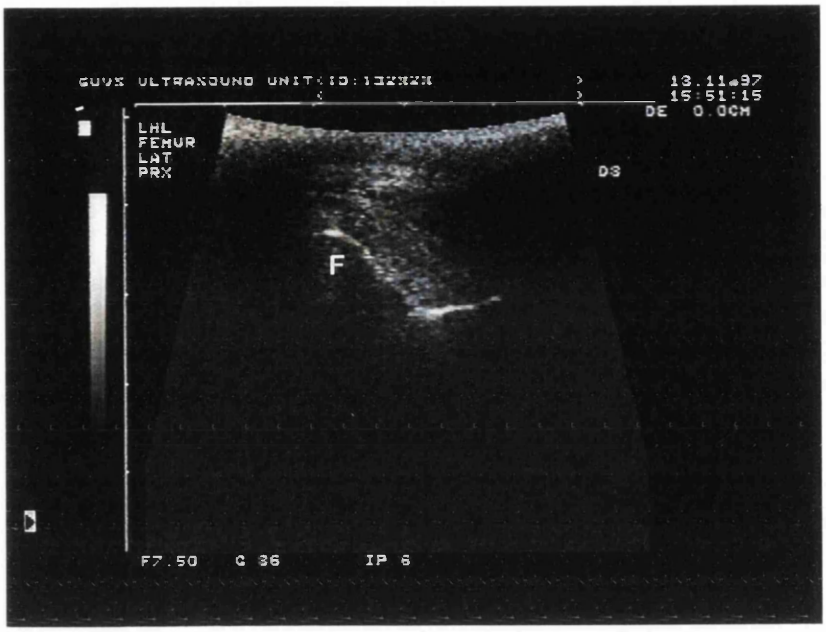

Figure 6.17.12a

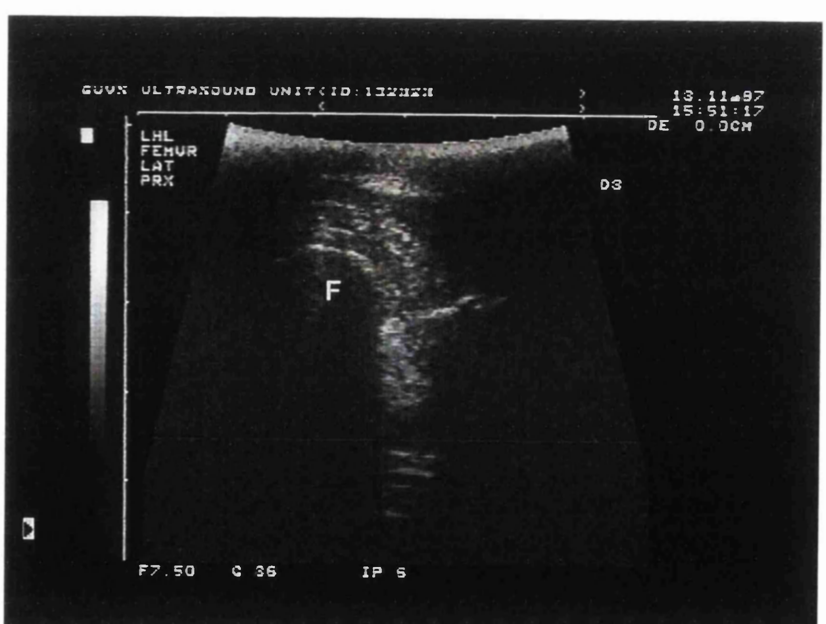

Figure 6.17.12b

Figure 6.17.13 Longitudinal scan of the distal femur after the distal pin of the external fixator has been removed demonstrates the hole in the femur. There are soft and periosteal tissues reactions around the hole. Note that the anechoic area with some echogenic material within above the hole is suggestive of blood or fluid accumulation.

Figure 6.17.14 Longitudinal scan of the femur from the medial aspect at the fracture site area on day 75 after fracture repair shows the intramedullary pin which can still be seen appearing hyperechoic with reverberation artefact.

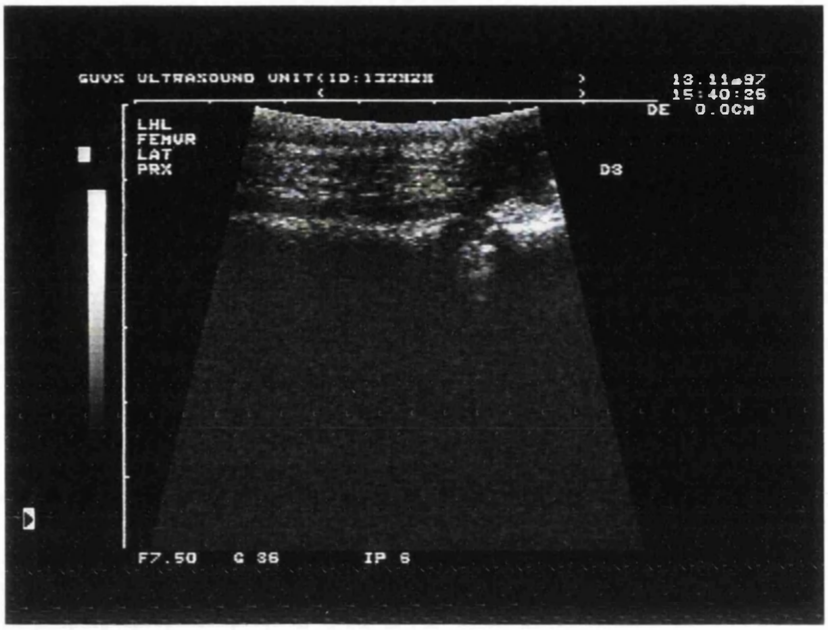

Figure 6.17.13

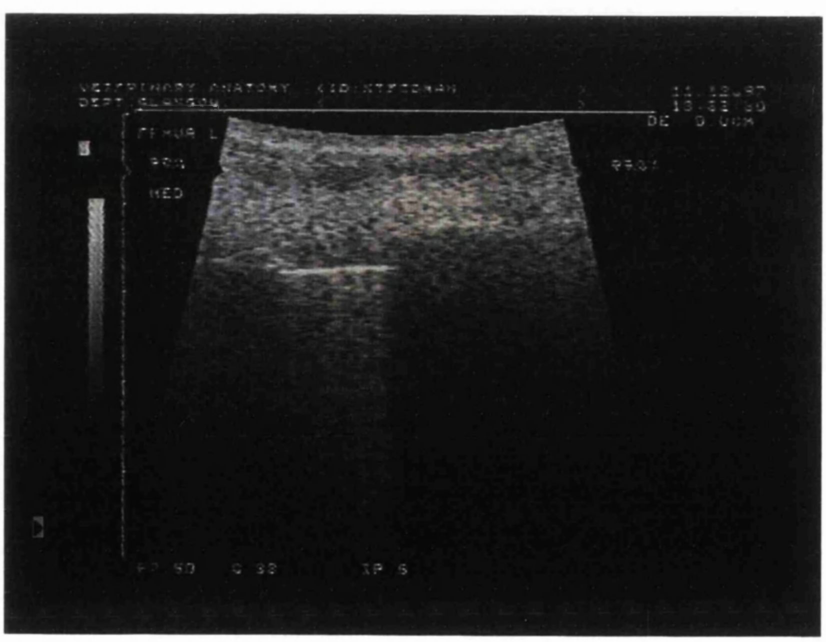

Figure 6.17.14

Figure 6.17.15 Radiographs taken at day 98 after fracture repair show that there is evidence of bony callus formation as compared with the previous radiographs although this is not complete. **a**, caudolateral view, **b**, cranial view. There is also osteolucency around the remaining pin and the holes of the previous distal pin are still osteolucent.

b

Figure 6.17.16 Longitudinal scan of the femur from the medial aspect on day 98 after fracture repair shows the bulging femoral surface with a smooth appearance suggestive of a remodelling process. The muscle structure appears to have normal hypoechoic characteristics.

Figure 6.17.17 Transverse scan of the fracture site area from the caudo-lateral aspect on day 98 after fracture repair shows the abnormal appearance of the femur. Note the bone fragment lying superficial to the femur (arrow head) appears hyperechoic with shadowing artefact. This causes incomplete imaging of the femur below it. The femur appears to have a smooth appearance showing a remodelling process.

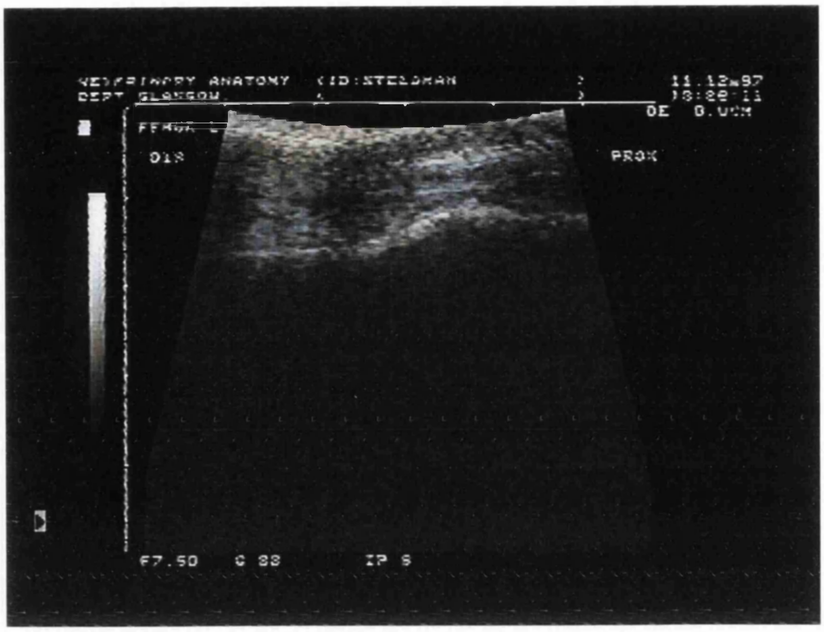

Figure 6.17.16

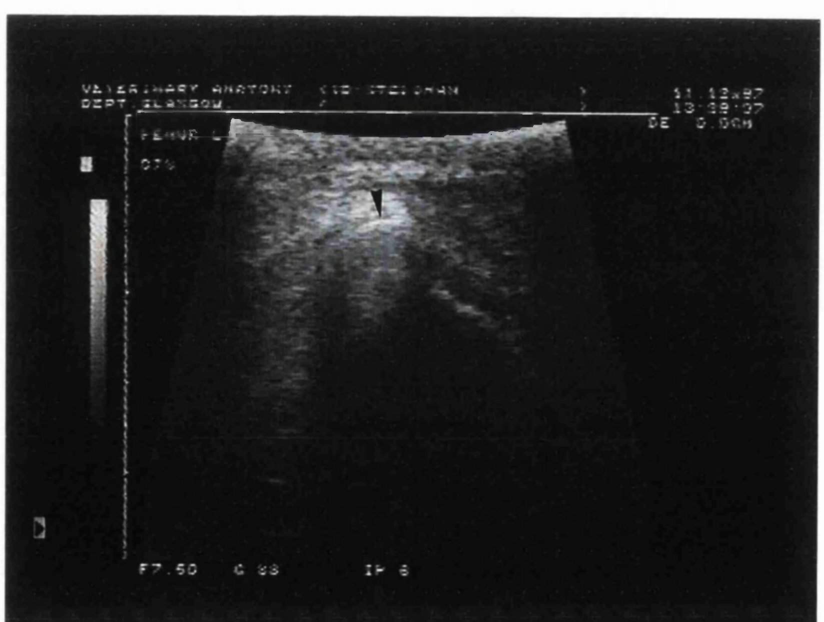

Figure 6.17.17

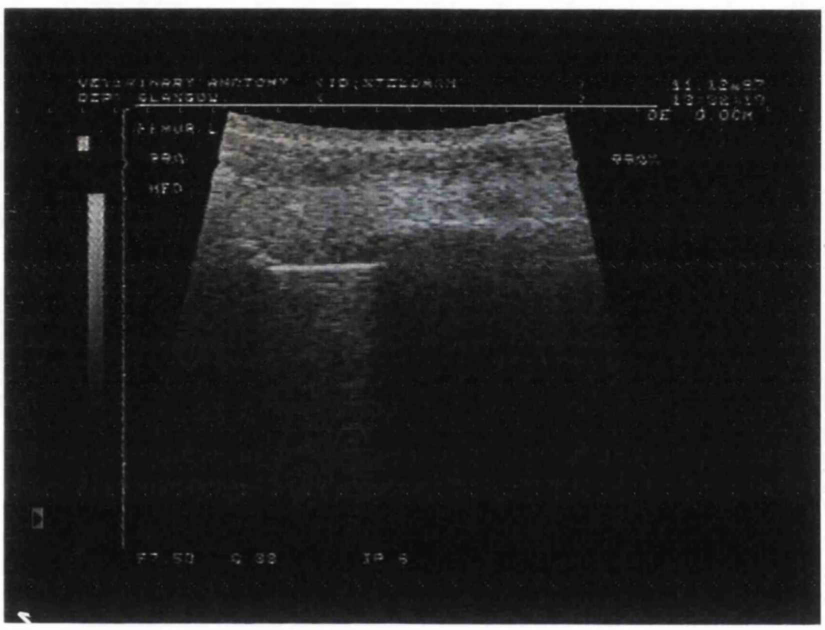

Figure 6.17.18 Longitudinal scan of the fracture site area on the medial aspect at day 98 after fracture repair shows the fracture gap with the intramedullary pin connecting the two bone fragments. The intramedullary pin appears hyperechoic with reverberation artefact. Note also there is bulging bone at the end of both fragments which is due to callus formation, but it appears smooth suggesting a remodelling process.

Case 18

A 17 month old male neutered Domestic Short Hair cat, weight 4.0 kg, was presented to the Glasgow University Veterinary Hospital with a fracture of the right humerus after having been involved in a road traffic accident. Radiographic examination of the right humerus showed that a simple oblique fracture of the distal third of the humeral shaft had been sustained. Radiographs taken immediately after fracture repair showed the fracture to have been reduced with an intramedullary pin and an external fixator two pin type one ESF. The ESF was used mainly to act against rotation and compression, as an adjunct to the pin. In addition, two cerclage wires were used in the reduction process. Radiographs taken immediately after fracture repair showed the fracture line was clearly visible (figure 6.18.1). The repair process resulted in satisfactory reduction and stabilization.

Ultrasonographic examination

Day three after fracture repair

Ultrasonographic examination demonstrated the fracture site which appeared well aligned with no fracture gap present on a lateral aspect scan (figure 6.18.2). The distal fragment appeared slightly elevated compared with the proximal one. The cerclage wires near the fracture site appeared as two small hyperechoic structures producing comet tail artefacts. By adjusting the transducer, the fracture site was imaged with a small portion of the proximal fragment being seen to over ride the distal fragment. There was no callus formation detected at the fracture site at this stage. However, the soft callus formation was detected on the bone surface at some distance from the fracture site. It developed at the area adjacent to the cerclage wires and appeared as two hyperechoic areas attached to the bone surface (figure 6.18.3). No artefact was produced by this hyperechoic material. The bone surface deep to the soft callus was still visible.

The femoral surface appeared hyperechoic and the area of soft tissue reaction above the femur appeared as a disorganised hyperechoic structure on transverse scan (figure 6.18.4). An area of muscle damage appeared as a disorganised hypoechoic area. A further transverse scan of the fracture site revealed an abnormal femur which had lost its normal rounded shape (figure 6.18.5).

Day 60 after fracture repair

Ultrasonographic examination on the lateral aspect demonstrated the area of the fracture site which had already been bridged by the mature callus. The two cerclage wires still appeared as small hyperechoic structures and produced comet tail artefact. The muscle had reduced in size and had become smaller than imaged on the day three examination as shown by the decreased distance between the skin surface and the femur. This could have been due to muscle atrophy. The two hyperechoic areas which were seen on day three after fracture repair being suggestive of soft callus formation were still present and appeared more echogenic than on the day three examination (figure 6.18.6). The fracture site with a small gap was imaged on the medial aspect (figure 5.18.7). The intramedullary pin could be seen within the fracture gap and appeared hyperechoic with comet tail artefact. The femur when scanned transversely appeared as a round hyperechoic structure with acoustic shadowing artefact. It has returned to the normal shape.

Ultrasonographically, the fracture site was not yet fully healed as the fracture site with the small gap could still be seen on the medial aspect even though the fracture site was no longer detected on the lateral side.

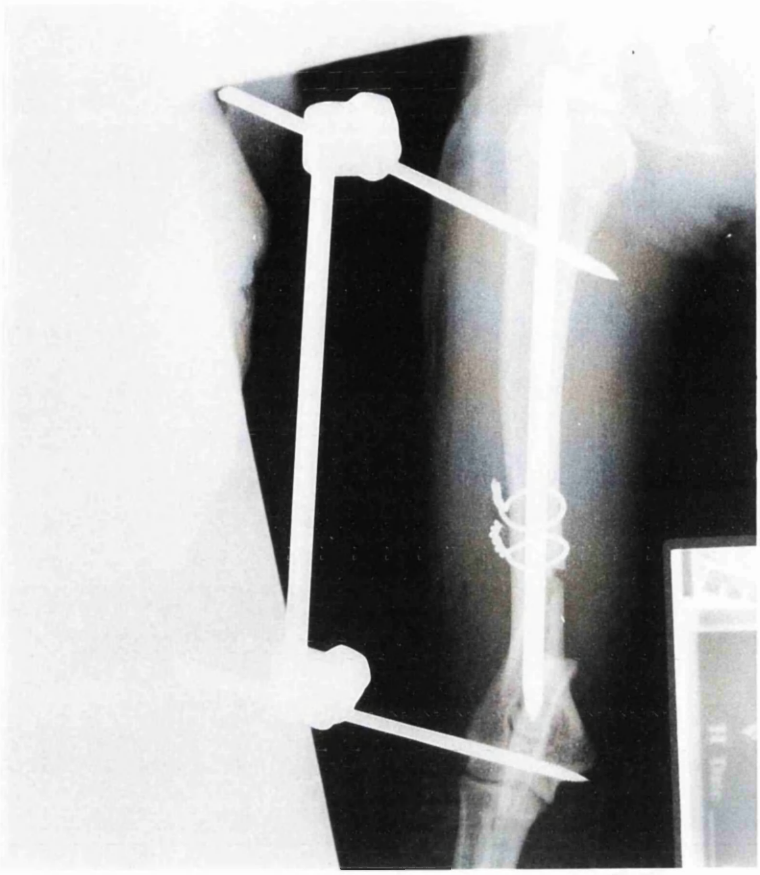

a

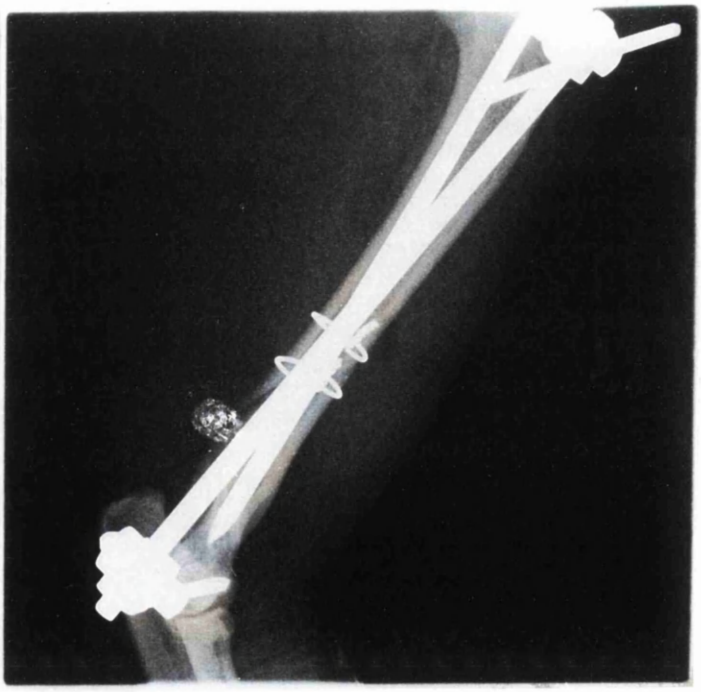

b

Figure 6.18.2 Longitudinal scan from the lateral aspect of the femur on day three after fracture repair demonstrates the fracture site (large arrow head) which appears well aligned with no fracture gap present. The distal fragment appears slightly elevated compared with the proximal one. Note also that the two cerclage wires (small arrow heads) near the fracture site appear as two small hyperechoic structures producing comet tail artefact.

Figure 6.18.3 Longitudinal scan of the femur on day three after fracture repair shows the fracture site (arrow) which appears as a small portion of the proximal fragment slightly overriding the distal fragment. Note also the soft callus formation some distance from the fracture site (arrow heads) which appears as two hyperechoic areas but with no shadow artefact produced. The bone deep to the soft callus is still clearly visible.

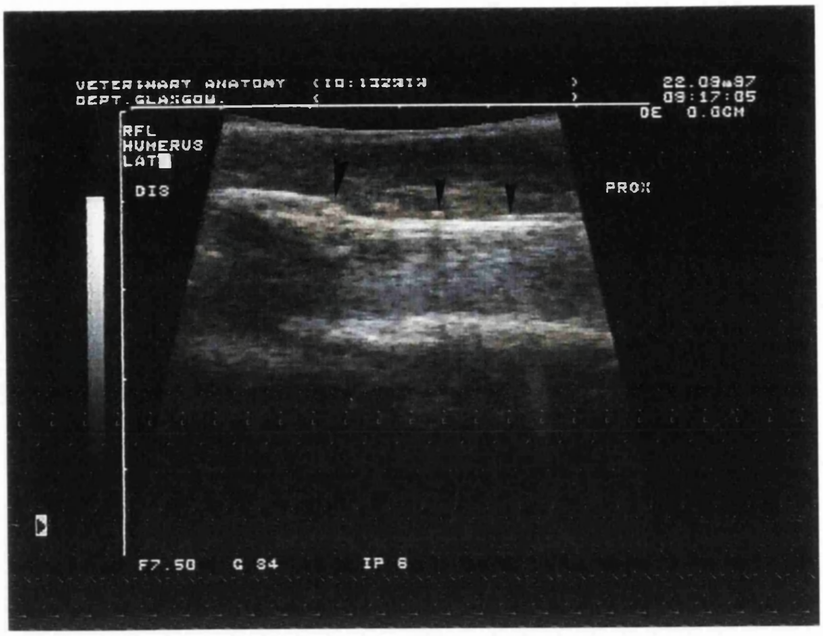

Figure 6.18.2

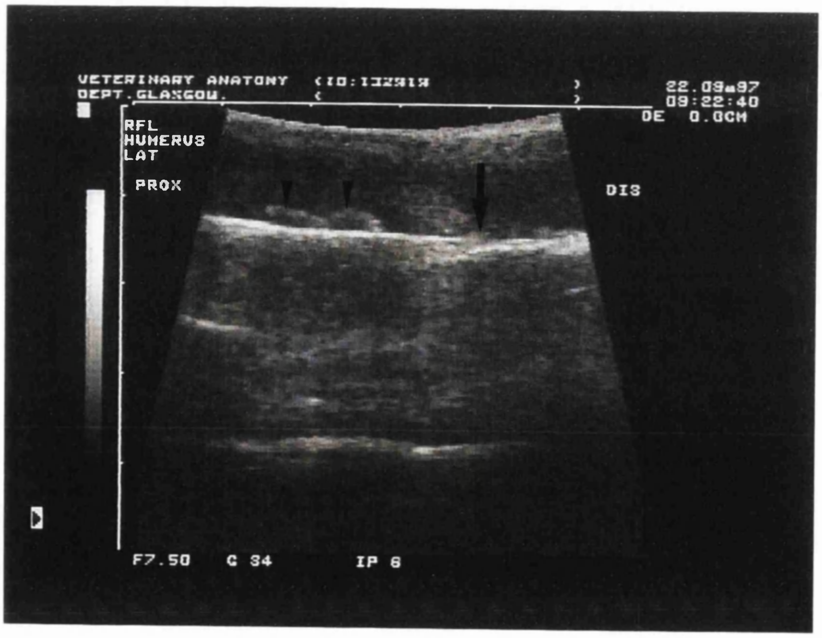

Figure 6.18.3

Figure 6.18.4 Transverse scan of the femur near the fracture site area on day three after fracture repair shows the femur which appears hyperechoic and the area of soft tissue reaction above the femur which appears as a disorganised hyperechoic structure. Note also that the area of muscle damage appears as a disorganised hypoechoic structure (arrow heads). **F**, femur.

Figure 6.18.5 The fracture site on transverse scan appears as an abnormal femur which has lost its normal rounded shape. **F**, femur.

Figure 6.18.4

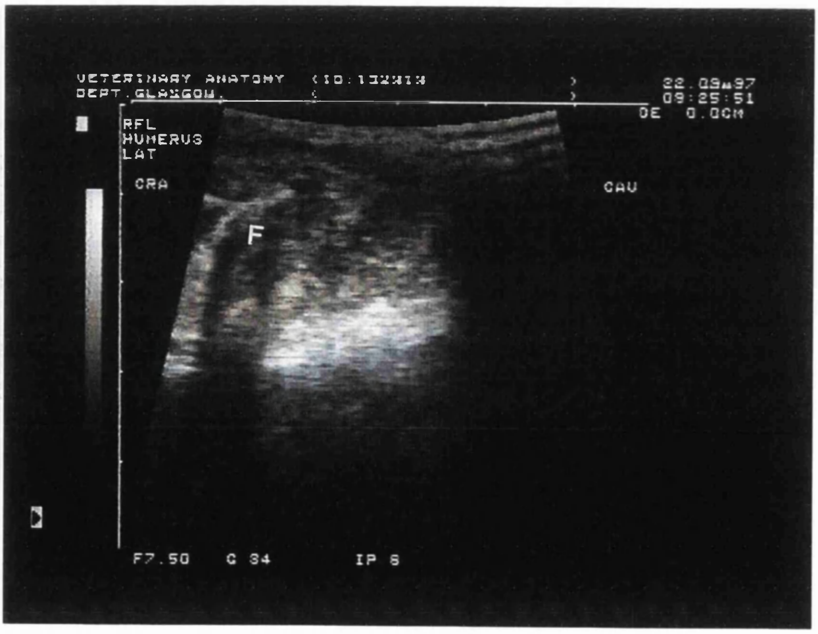

Figure 6.18.5

Figure 6.18.6 Longitudinal scan of the femur at the fracture site area from the lateral aspect on day 60 after fracture repair demonstrates a smooth bone surface. The fracture site is no longer detected. Note also the two hyperechoic areas suggestive of soft callus formation as seen on day three after fracture repair are still present and appear more echogenic than on the day three examination (arrow heads). The muscle has reduced in size as shown by a decrease in the distance between the skin surface and the femur which is due to muscle atrophy.

Figure 6.18.7 Longitudinal scan of the femur on the medial aspect on day 60 after fracture repair shows the fracture site with a small gap still present. Note that the intramedullary pin can be seen within the fracture gap appearing hyperechoic with comet tail artefact.

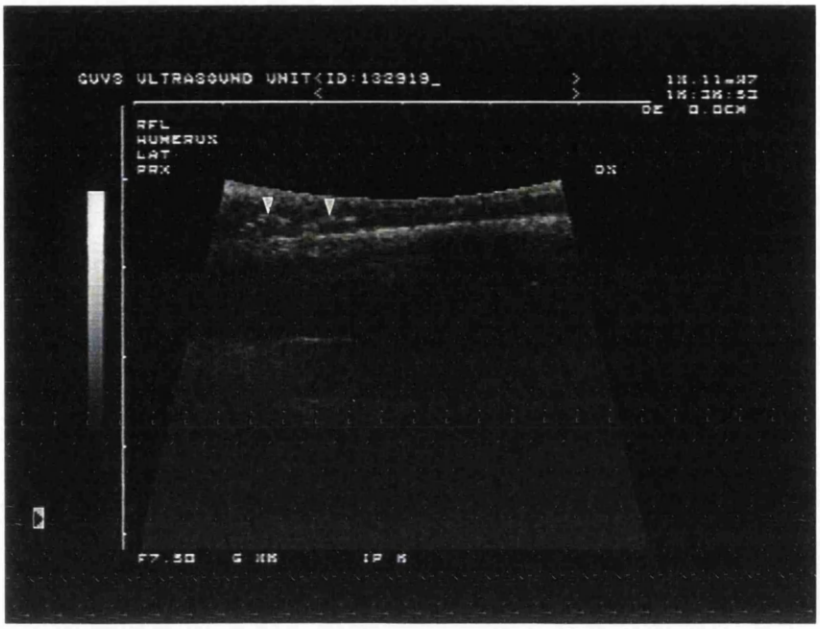

Figure 6.18.6

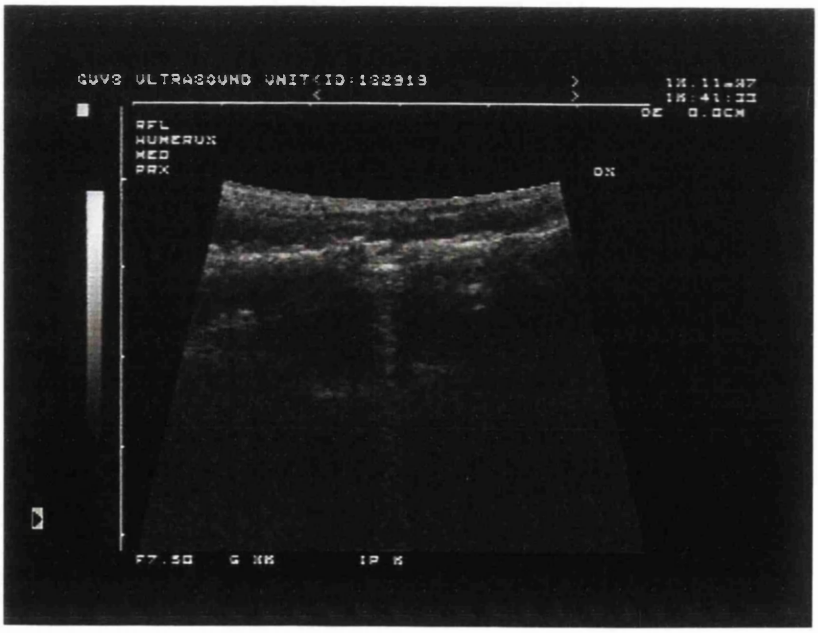

Figure 6.18.7

Case 19

A six month old male Labrador, weight 19 kg, was referred to the orthopaedic services at Glasgow University Veterinary Hospital for assessment and treatment of a tibial fracture after having been involved in a road traffic accident. Radiographic examination revealed a proximal comminuted fracture of the left tibia with four free fragments and a latero-cranial displacement of the distal tibial shaft had been sustained with moderate overriding present. A transverse mid shaft fracture of the fibula was also present. The fracture had been stabilised using a type 2 external skeletal fixator with 6 half pins. Radiographs taken immediately after fracture repair showed sufficient reduction and alignment, although slight valgus angulation and overriding was present (figure 6.19.1).

Ultrasonographic examination

Day one after fracture repair

Ultrasonographic examination at the fracture site area of the tibia on the lateral aspect demonstrated the fracture gap with a bone fragment at the fracture site (figure 6.19.2). The area of soft tissue reaction around the screw appeared as disorganised hyperechoic structure. The fracture site of the fibula was imaged from the lateral aspect and appeared as two bone segments poorly aligned (figure 6.19.3). The distal fragment of the fibula appeared elevated compared with the proximal fragment. The fracture site area imaged on a transverse scan showed a disorganised hyperechoic area around the fracture site which suggested soft tissue reaction (figure 6.19.4). The tibia and fibula had lost their normal appearance.

Day 43 (approximately 6 weeks) after fracture repair

Radiographs taken at day 43 after fracture repair showed marked callus formation at the fracture site but not complete. There was moderate valgus angulation and proximal displacement of the distal fracture element (figure 6.19.5). The external fixator device had been removed immediately after the radiographic examination and the animal was not expected to come again unless there was any problem.

Ultrasonographic examination

Ultrasonographic examination of the fracture site area from the lateral aspect demonstrated the presence of callus formation with a rough surface which appeared to bridge the fracture site completely (figure 6.19.6). A further examination on the lateral aspect demonstrated the bulging bone at the fracture site area which was due to callus formation (figure 6.19.7). The bulging hyperechoic surface appeared smooth suggesting a remodelling process. The fracture gap, however, could still be detected as a shallow notch. The fracture site was also detected on a caudo-lateral scan which appeared as a small notch on the bone surface (figure 6.19.8). The muscle tissue appeared to have normal ultrasonographic appearance. The fracture site of the fibula was imaged on a lateral scan and appeared to have been bridged completely by the mature callus. The fibula bone at the fracture site area appeared bulging due to callus formation but with a smooth surface appearance suggesting that a remodelling process was in progress (figure 6.19.9). A number of holes were detected on the proximal tibia on the medial aspect scan (figure 6.19.10). These holes were actually the site where the external fixator pins were placed previously. The bulging bone surface surrounding the holes due to callus formation suggested that some pin movement had occurred during the fixation period. The area of soft tissue reaction was present within the holes and appeared hyperechoic. One hole was also detected on the tibia distally on a caudo-lateral scan but there was no significant callus formation detected around it (figure 6.19.11). This suggested that the pin was rigidly fixed to the tibia. An area of muscle damage with some blood was detected above the hole which appeared as a disorganised hypoechoic structure mixed with an anechoic area. This muscle damage might have happened during pin distraction. Ultrasonographically, the fracture site was satisfactorily healed.

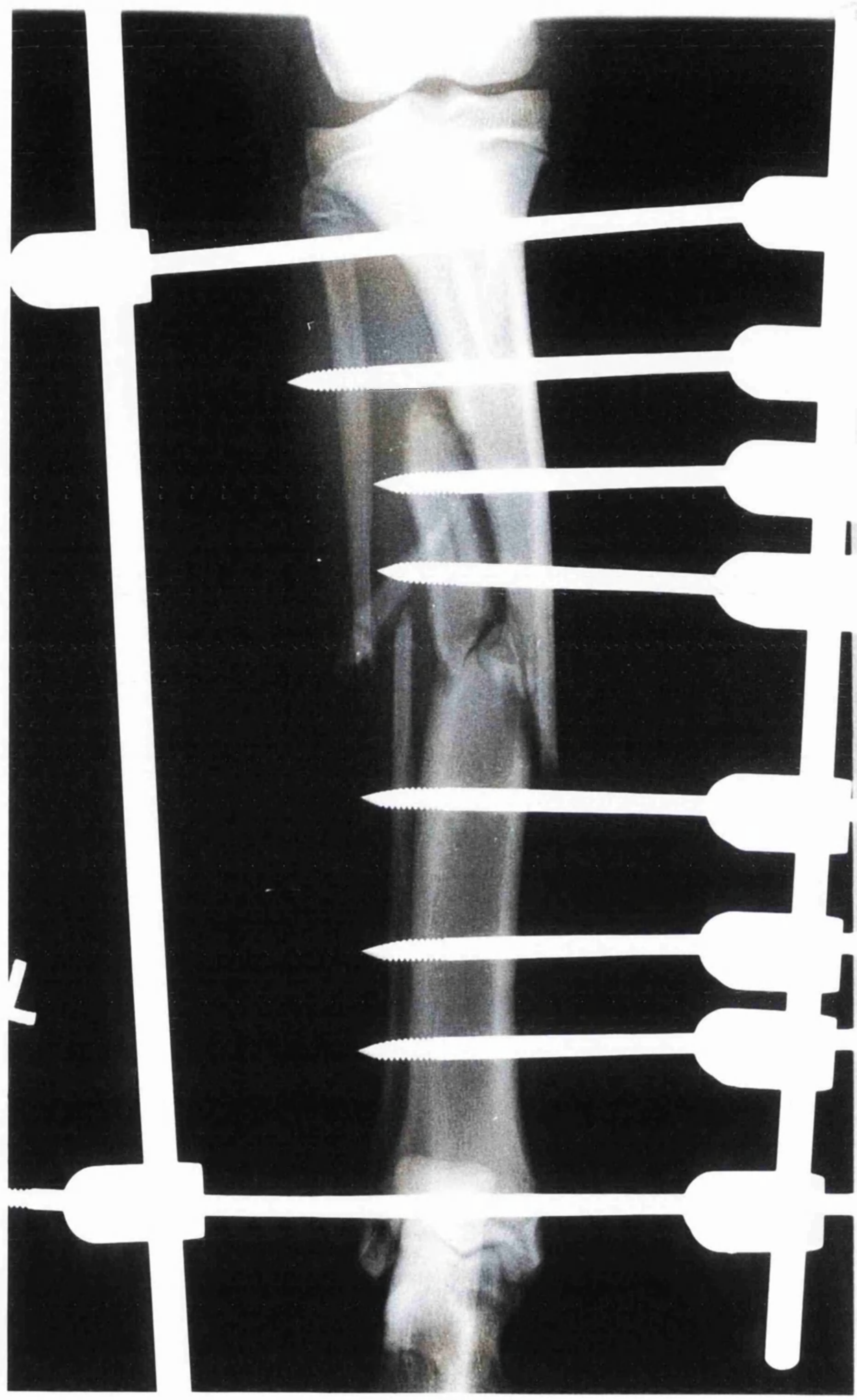

Figure 6.19.1 Radiograph taken immediately after fracture repair shows sufficient reduction and alignment, although slight valgus angulation and overriding is present. The fracture has been stabilised using type 2 external skeletal fixator with 6 half pins.

Figure 6.19.2 Longitudinal scan of the tibial shaft 24 hours after fracture repair demonstrates the fracture site with the presence of a small gap. One bone fragment (arrow head) is found at the fracture site area and appears hyperechoic. Note also the area of soft tissue reaction around the screw (arrow) appears as a disorganised hyperechoic structure.

Figure 6.19.3 Longitudinal scan of the fibula 24 hours after fracture repair demonstrates the fracture site which appears with the two segments poorly aligned. The distal fragment (large blank arrow) of the fibula appears elevated compared with the proximal fragment (small arrow head).

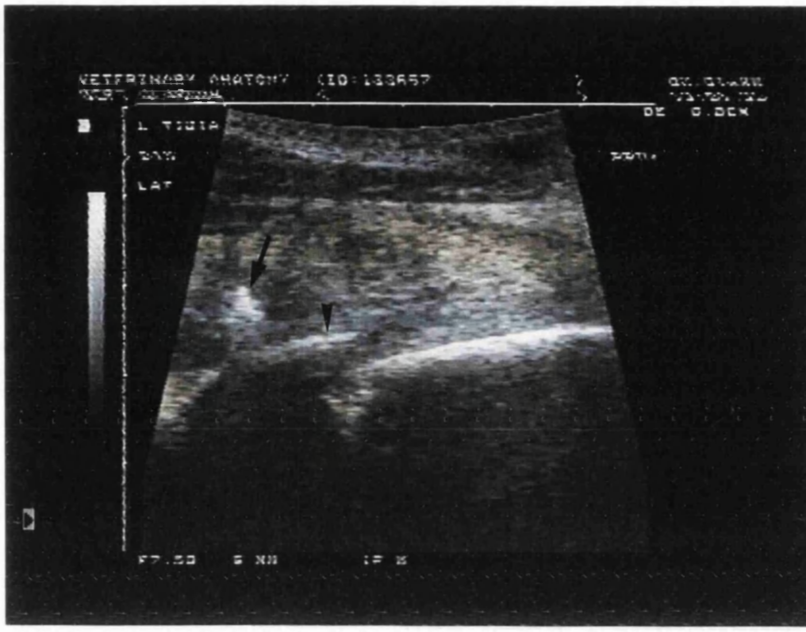

Figure 6.19.2

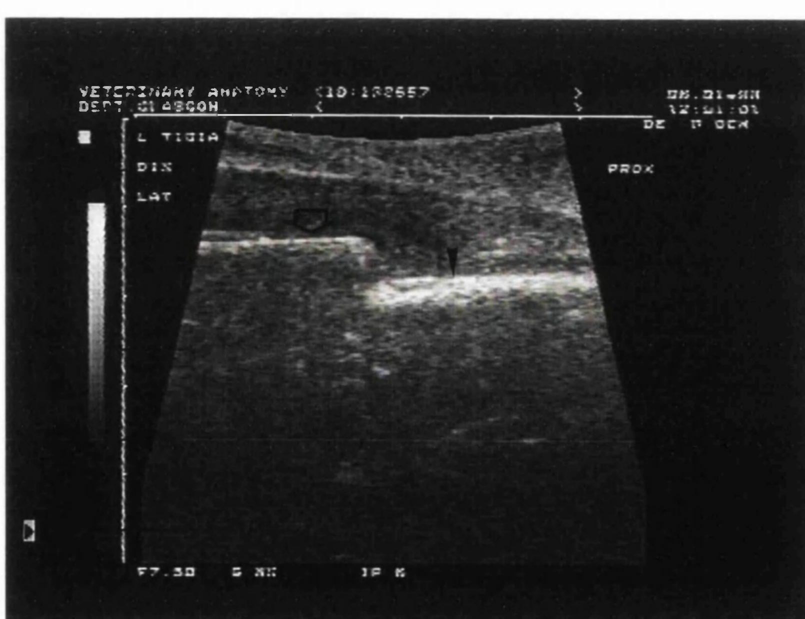

Figure 6.19.3

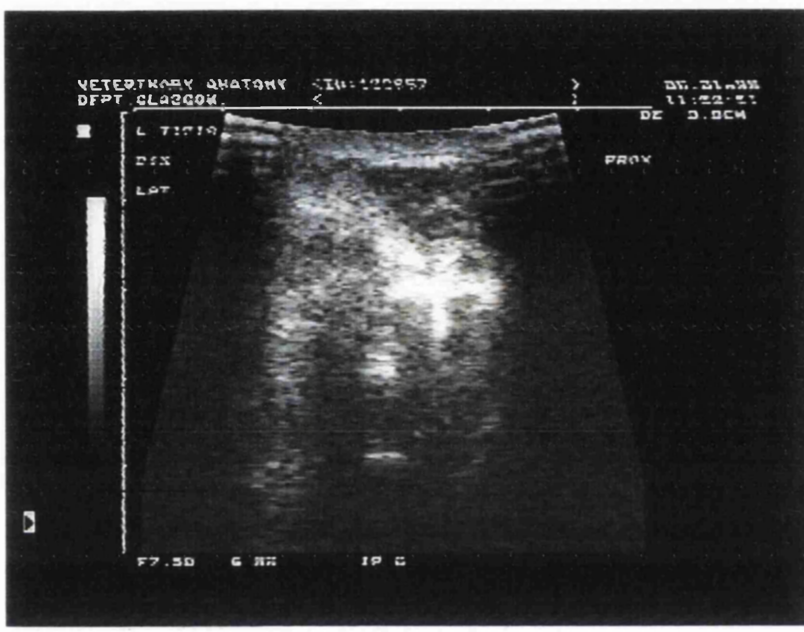

Figure 6.19.4 Transverse scan of the tibia and fibula at the fracture site area 24 hours after fracture repair shows a disorganised hyperechoic area which suggests the soft tissue reaction. The tibia and fibula have lost their normal ultrasonographic appearance.

Figure 6.19.5 Radiographs taken at day 43 after fracture repair show marked callus formation but it is not complete. Note also there is moderate valgus angulation and proximal displacement of the distal fracture element. **a**, lateral view, **b**, cranial view.

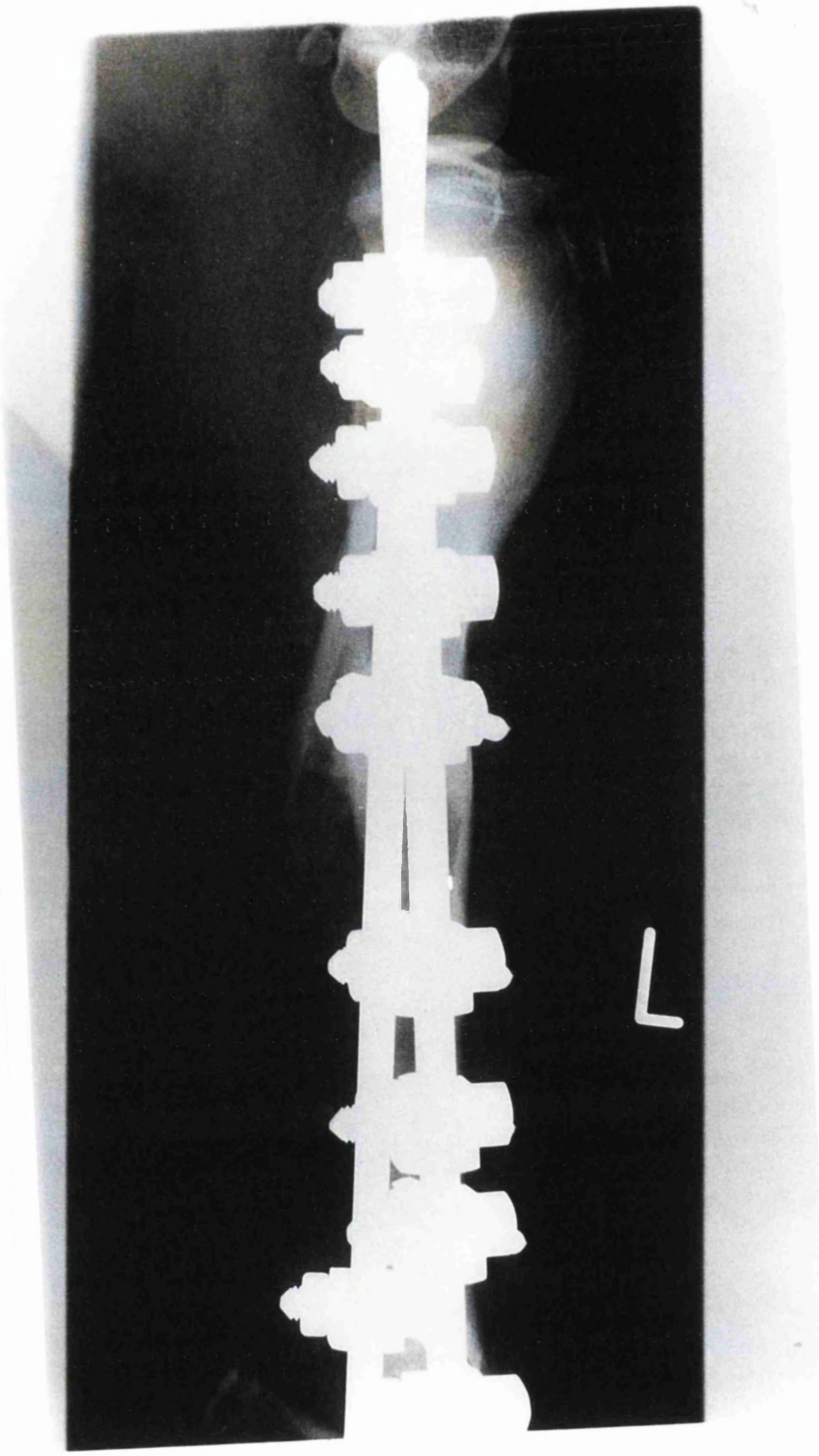

a

b

Figure 6.19.6 Longitudinal scan of the tibia at the fracture site area from the lateral aspect on day 43 after fracture repair demonstrates the presence of callus formation with a rough surface and it appears to bridge the fracture site completely.

Figure 6.19.7 Longitudinal scan of the tibia from the lateral aspect on day 43 after fracture repair demonstrates a bulging bone at the fracture site area which is due to callus formation. The bulging hyperechoic surface appears smooth suggesting a remodelling process. The fracture gap however can still be detected as a shallow notch (arrow).

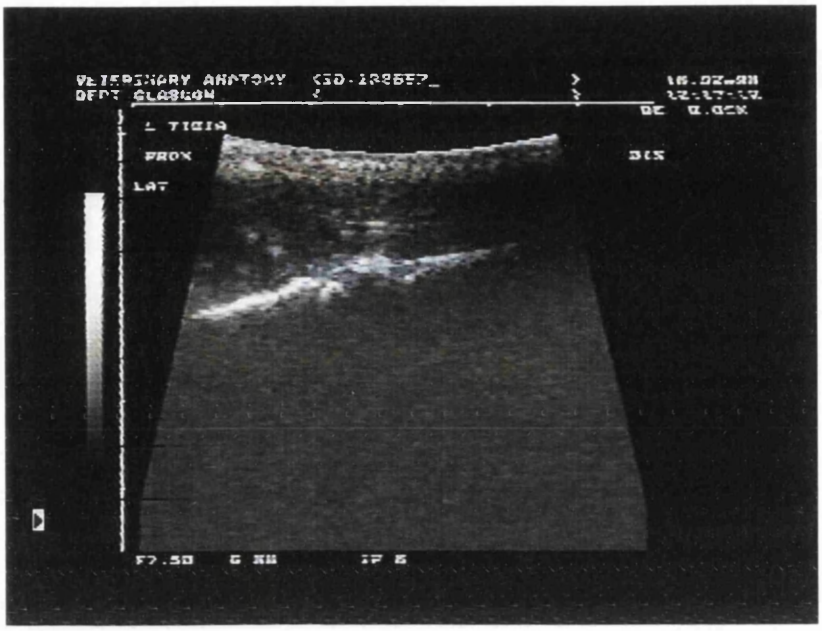

Figure 6.19.6

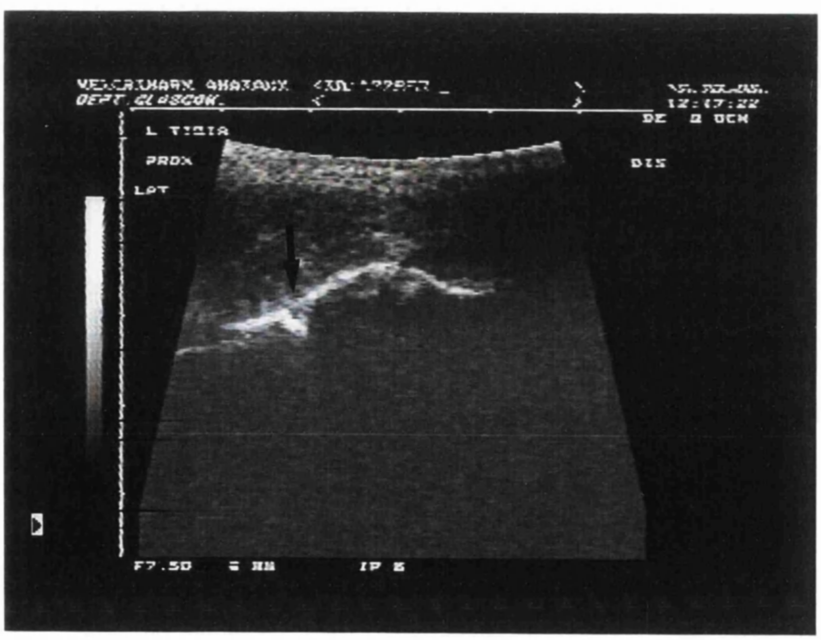

Figure 6.19.7

Figure 6.19.8 Longitudinal scan of the tibia from the caudo-lateral aspect on day 43 after fracture repair demonstrates the fracture site which appears as a small notch on the bone surface. Note that the muscle tissue appears to have a normal ultrasonographic appearance.

Figure 6.19.9 Longitudinal scan of the fibula from the lateral aspect on day 43 after fracture repair demonstrates the fracture site which appears to have been bridged completely by the mature callus. Note that the fibula at the fracture site area appears bulging due to callus formation but with a smooth surface appearance suggesting a remodelling process is in progress.

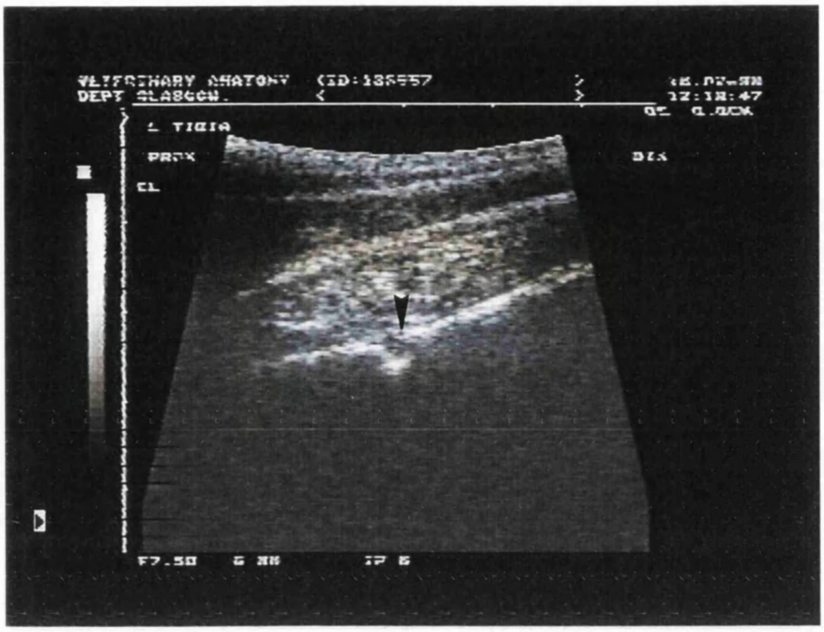

Figure 6.19.8

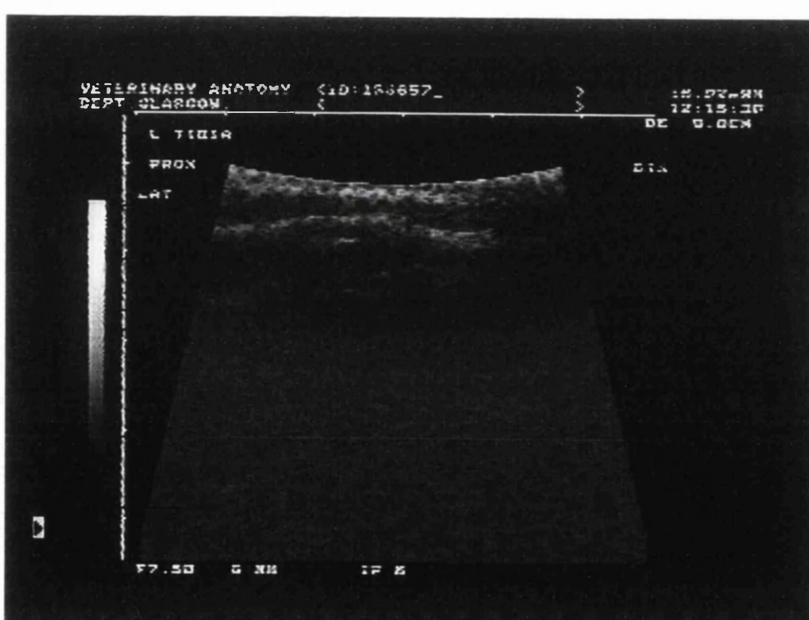

Figure 6.19.9

Figure 6.19.10 Longitudinal scan of the tibia from the medial aspect immediately after pin removal demonstrates a number of holes in the proximal tibia. These holes are actually the site of the external fixator pins before being removed. Note also the bulging bone surface surrounding the holes due to callus formation suggests that some movement of the pin had occurred during the fixation period. An area of soft tissue reaction is present within the holes and appears hyperechoic.

Figure 6.19.11 One hole is seen on the tibia distally on caudo-lateral scan with no significant callus formation around it (arrow). This suggests that the pin was rigidly fixed to the tibia. Note also that the area of muscle damage above the hole appears as a disorganised hypoechoic structure mixed with anechoic area (arrow heads) which represents blood. Muscle damage may have occurred during pin distraction.

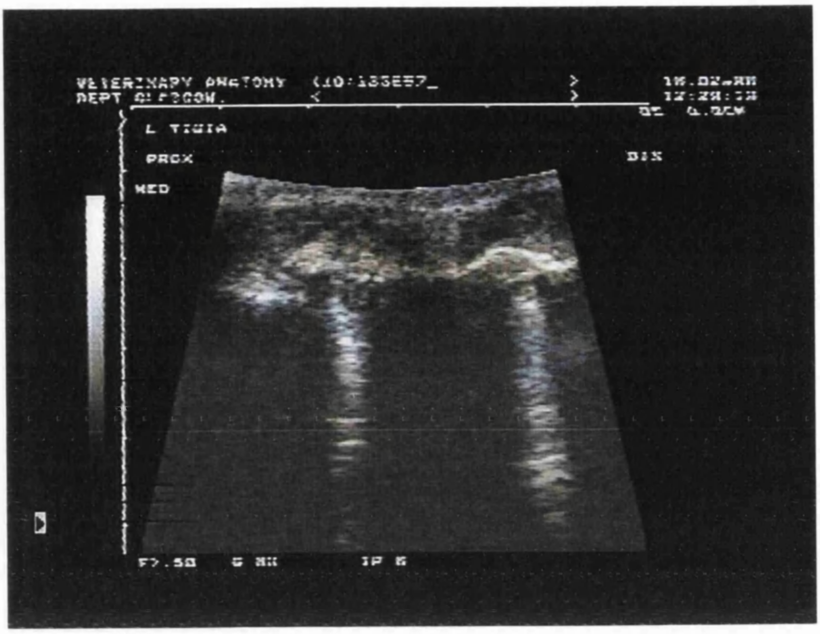

Figure 6.19.10

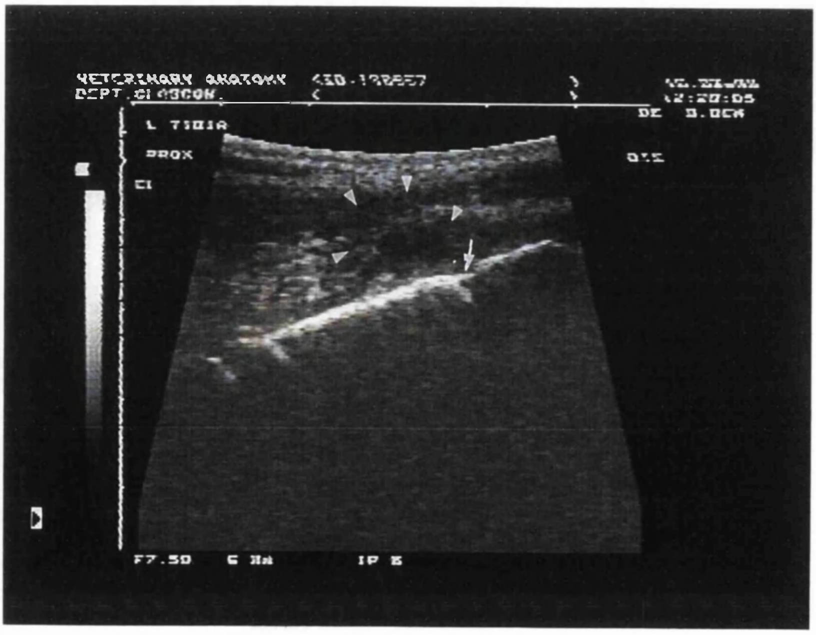

Figure 6.19.11

Case 20

A three year old male Akita, weighing 40 kg, was presented to the Glasgow University Veterinary Hospital after having been involved in a road traffic accident. The animal had suffered multiple injuries following the road traffic accident, including rupture of both eyes, avulsion of the muzzle from the maxilla, fracture of the right humerus, luxation of the hip and a fracture of the right talus. Radiographic examination of the right humerus showed that a comminuted oblique fracture of the right humerus had been sustained (figure 6.20.1).

The mid diaphyseal oblique fracture of the humerus was repaired with an intramedullary pin and external fixator. One pin was inserted through the humeral condyle to allow traction on the distal fragment to reduce the fracture. The fracture site was approached laterally and fluid drained from the site. The intramedullary pin was inserted retrograde. Three more pins were passed through the humerus: one distal and two proximal to the fracture site. The animal also had fractures of the lateral malleolus and talus of the right hock but these were not included in the study.

Radiographs taken immediately after fracture repair showed that the fragments were well aligned (figure 6.20.2). One bone fragment remained in the muscle, being caudal to the femur at the fracture site area. The fracture line was clearly visible. The small bone chips were also present.

Ultrasonographic examination

Day five after fracture repair

Ultrasonographic examination demonstrated the fracture site with the fragments appearing poorly aligned. The distal fragment appeared higher than the proximal fragment on the caudal aspect (figure 6.20.3a), and conversely, the proximal fragment appeared higher than the distal fragment on the cranial aspect (figure 6.20.3b). The area of muscle damage at the end of the proximal fragment appeared as a disorganised hypoechoic area. The hypoechoic area in the muscle suggested the present of blood or fluid within the muscle. No callus formation was detected. One large fragment caudal to the femur was detected both on longitudinal and transverse scans and appeared hyperechoic with acoustic shadowing artefact (figure 6.20.4a and 6.20.4b). The external fixator pin appeared as a straight hyperechoic line with reverberation artefact (figure 6.20.5).

Day seven after fracture repair

Ultrasonographic examination demonstrated the fracture site which appeared as on the day five examination. The bone fragment remained caudal to the femur and appeared as on the day five examination. Scanning from the cranial aspect only revealed the proximal fragment (figure 6.20.6). The distal fragment was not seen because the fragments were not well aligned. The area of muscle damage still appeared hypoechoic but with a more organised structure.

Day nineteen after fracture repair

Radiographic examination

Radiographs taken at 19 day after fracture repair showed a marked lucency around pin 2, 3 and 5, and bad alignment of the fragments with caudal overriding of the distal shaft fragment. Osteolysis was found around pin 2, 3 and 5, but there was no callus formation (figure 6.20.7).

Ultrasonographic examination

Ultrasonographic examination of the humerus demonstrated the fracture site but still no callus formation was detected. A large cystic structure with well defined margins was detected at the fracture site above the proximal end fragment and at the end of distal fragment on the caudal aspect scan (figure 6.20.8). The bone fragment caudal to the femur remained undisplaced but appeared smaller than on the previous scans. A transverse scan of the humerus also demonstrated the cystic structure with well defined margin above the proximal fragment (figure 6.20.9). The bone fragment superficial to the humerus appeared as on the previous scans. The muscle structure appeared as disorganised with a mixture of hypoechoic and hyperechoic structures. The cystic structure was not imaged on the cranial aspect scan. An area with an hyperechoic mottled appearance was detected at the end of the proximal fragment which was suggestive of soft callus formation (figure 6.20.10). Soft callus formation was also detected on the proximal fragment some distance away from the fracture site and appeared as an hyperechoic rough bone surface (figure 6.20.11). A transverse scan of the humerus showed the abnormal appearance of the humerus with a rough surface suggestive of callus formation (figure 6.20.12).

Day 25 after fracture repair

Ultrasonographic examination

Ultrasonographic examination of the fracture site showed there was no longer a cystic structure present, but that a well defined callus formation could still not be seen at the fracture site (figure 6.20.13). Callus formation was detected on the proximal fragment at some distance away from the fracture site and appeared as a rough femoral surface. A transverse scan on the proximal fragment showed the humerus with callus formation which appeared as an hyperechoic rough surface (figure 6.20.14). The muscle structure had returned to its normal ultrasonographic appearance.

Day 33 after fracture repair

Radiographic examination

Radiographs taken at day 33 after fracture repair showed that there was non alignment of the humeral fracture, overriding and no bridging callus formation. The external fixator had failed, so bone plating was performed instead. A Dynamic Compression Plate (DCP) was fixed with five cortex screws on each side resulting in satisfactory reduction and alignment. An osteotomy was performed at the end of the proximal fragment to stimulate new callus formation. The plate was placed on the medial side of the femur. There was abundant periosteal pallisade like callus formation around the humeral shaft. The realignment process resulted in a good alignment but there was a large gap on the caudal side. One bone fragment remained, being cranial to the femur at the fracture site area (figure 6.20.15).

Ultrasonographic examination

Ultrasonographic examination demonstrated the callus formation on the humerus some distance from the fracture site. The callus formation appeared hyperechoic and caused a rough bone surface appearance (figure 6.20.16). The fracture site was shown as a discontinuity of the bone on the lateral scan. The screws used in fracture reduction appeared hyperechoic with comet tail artefacts. The screw threads were shown and gave a typical characteristic appearance for the screws imaged ultrasonographically (figure 6.20.17). The area of muscle damage appeared as an hypoechoic region. A number of holes were found on the humerus which appeared hyperechoic with the presence of soft callus formation around them (figure 6.20.18). These holes were actually the site of external fixator pins placed before the recent realignment process. The fracture site with the presence of an hyperechoic area which was suggestive of soft tissue reaction was seen on the cranial aspect scan (figure 6.20.19). The bone fragment cranial to the femur appeared hyperechoic with acoustic shadowing artefact (figure 6.20.20). A transverse scan at the fracture site area showed an abnormal femur which appeared large with a rough surface (figure 6.20.21).

Day 54 after fracture repair

Radiographic examination

Radiographs taken at day 54 after fracture repair showed the major tubercle was laterally displaced relative to the acromion. The fracture site had been refixed by a larger plate, but one screw was broken. There was a caudal displacement of the distal humerus. No bridging bony callus was seen (figure 6.20.22).

Ultrasonographic examination

Ultrasonographic examination on day 54 after fracture repair showed the fracture site and demonstrated that the two bone fragments were poorly aligned (figure 6.20.23a). On the caudal aspect, only the proximal fragment was clearly imaged which appeared higher than the distal fragment (figure 6.20.23b). The callus formation could be detected by the rough bone surface. The muscle structure still appeared as a disorganised hypoechoic region suggesting an area of muscle damage. The holes on the bone appeared smaller than in the previous scan with callus formation bridging over the hole (figure 6.20.24). The fracture site imaged on the lateral aspect appeared as a groove and the bone fragments were completely bridged by the callus (figure 6.20.25). The bone surface appeared rough due to callus formation. The area of muscle damage could still be seen as disorganised and a mixture of hyperechoic and hypoechoic structures above the fracture site area. Several screws were also imaged at the fracture site area which appeared hyperechoic. Ultrasonographically, the healing of the fracture site was progressing satisfactorily.

Figure 6.20.1 Three years old male Akita with a comminuted oblique fracture of the right humerus. The fracture was sustained subsequent to a road traffic accident.

Figure 6.20.2 Radiographs taken immediately after fracture repair show that the fragments are well aligned. **a**, lateral view, **b**, cranial view. One bone fragment remains in the muscle, being caudal to the humerus at the fracture site area. The fracture line is clearly visible. There are also some small bone chips present in the muscle.

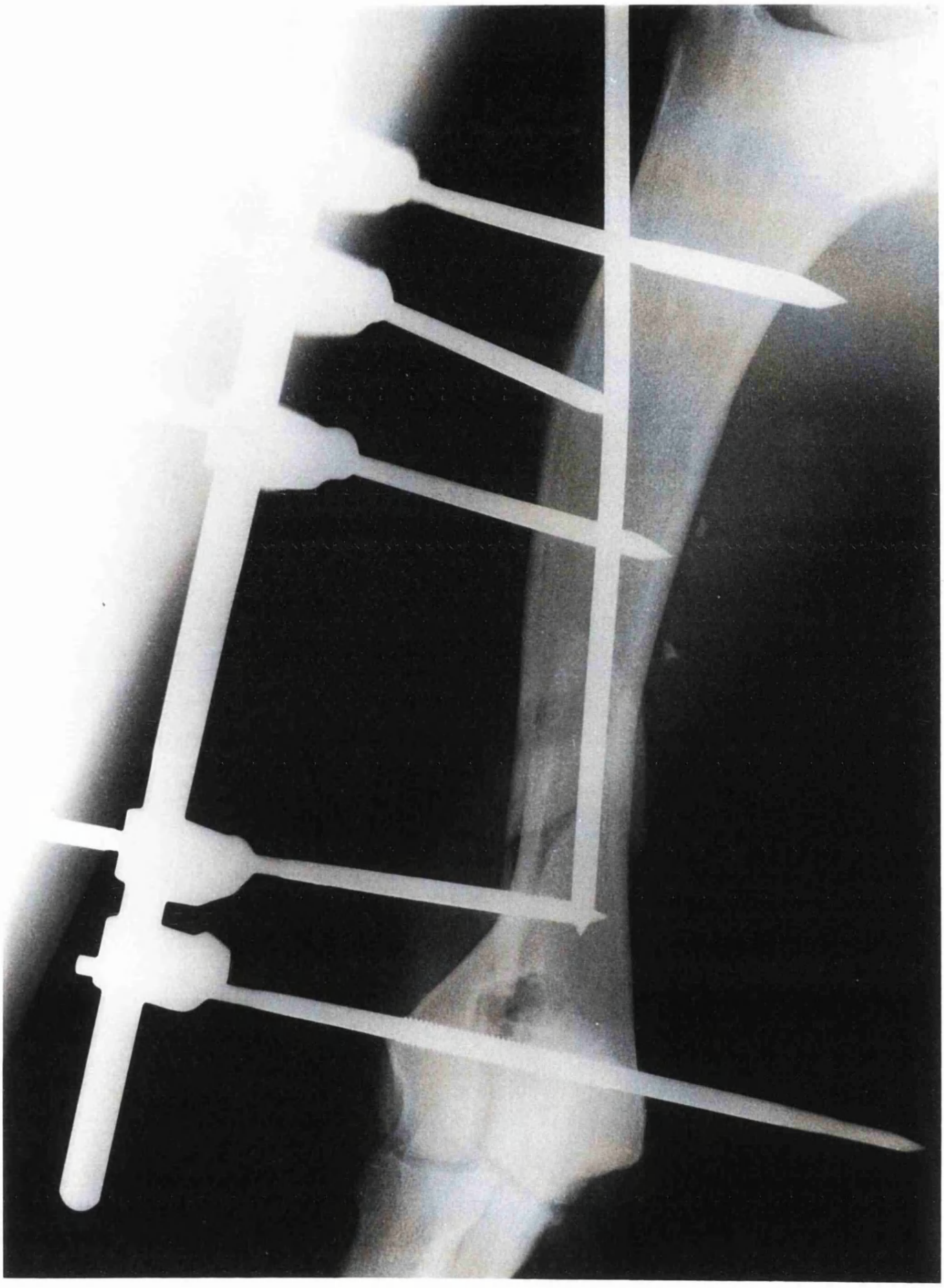

b

Figure 6.20.3 Longitudinal scans of the humerus on day five after fracture repair demonstrate the fracture site with the segments poorly aligned. **a**, caudal aspect, **b**, cranial aspect. The distal segment appears higher than the proximal segment in **a**, and conversely, the proximal segment appears higher than the distal segment in **b**. The area of muscle damage at the end of the proximal fragment appears as a disorganised hypoechoic area. The hypoechoic area in the muscle is suggestive of blood or fluid within the muscle. No callus formation is detected at this stage.

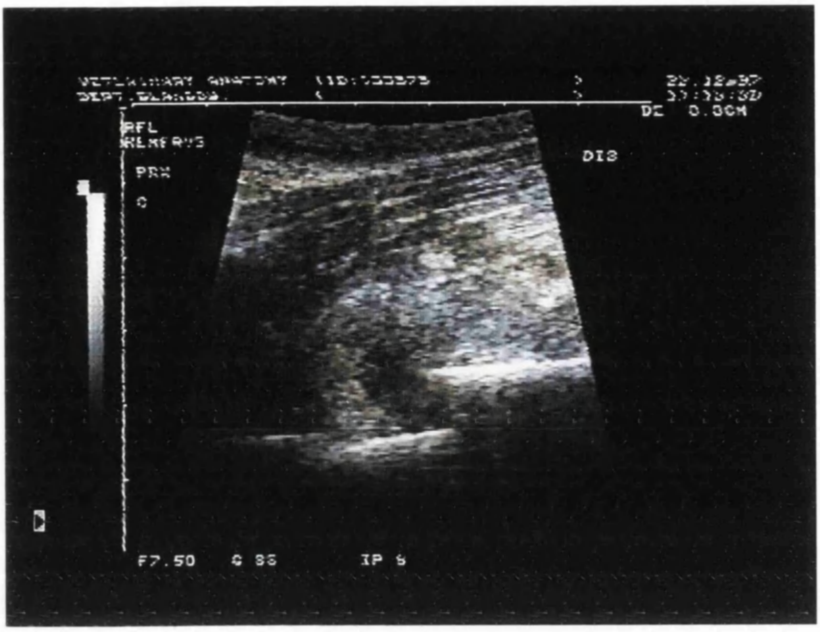

Figure 6.20.3a

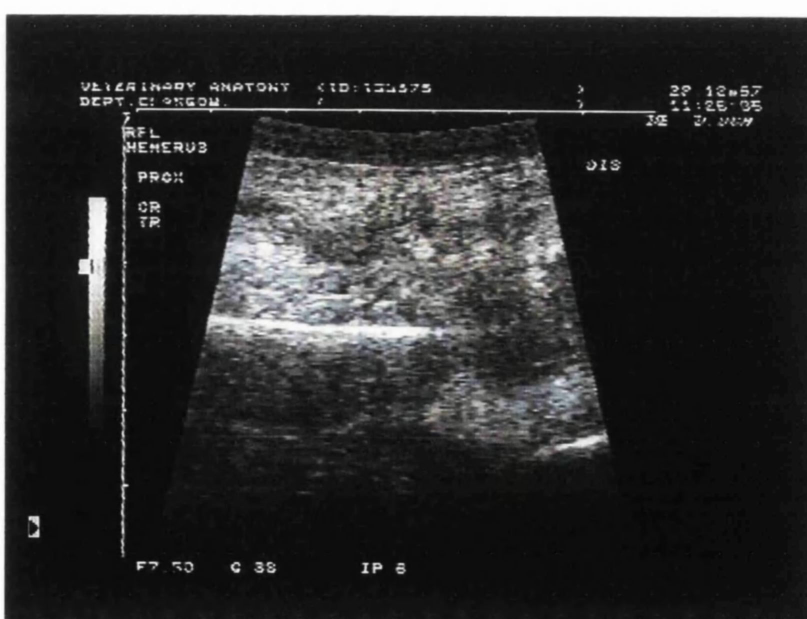

Figure 6.20.3b

Figure 6.20.4 Ultrasonographic examination of the humerus from the caudal aspect on day five after fracture repair **a**, longitudinal scan, **b**, transverse scan, shows a bone fragment caudal to the humerus which appears hyperechoic with acoustic shadowing artefact. Note that the femoral surface under the bone fragment is not imaged due to the shadow artefact. **H**, humerus.

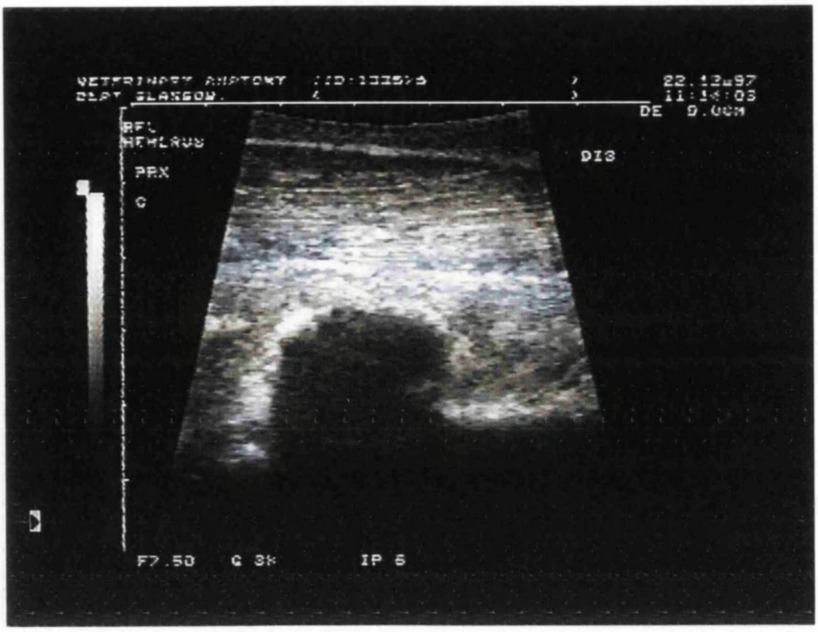

Figure 6.20.4a

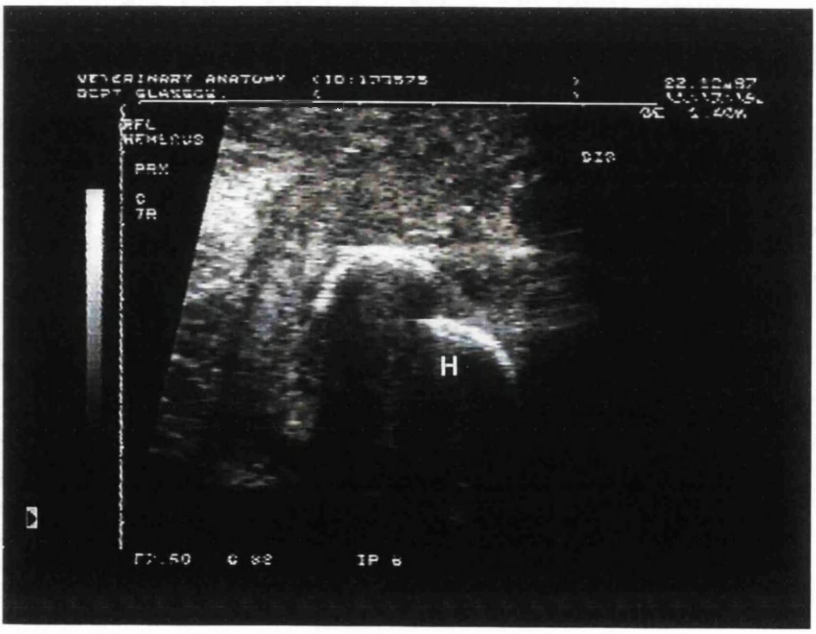

Figure 6.20.4b

Figure 6.20.5 Transverse scan of the humerus on the cranial aspect demonstrates the external fixator pin which appears as a straight hyperechoic line and is producing reverberation artefact. **H**, humerus.

Figure 6.20.6 Longitudinal scan of the humerus from the cranial aspect on day seven after fracture repair only demonstrates the proximal fragment. The distal segment is not seen because the segments are not well aligned. Note that the area of muscle damage still appears hypoechoic but with more organised structure.

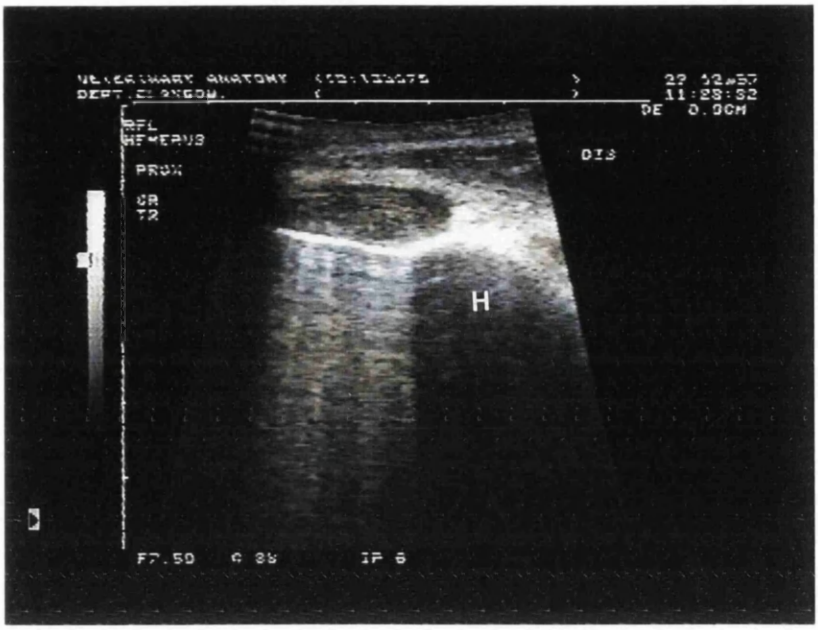

Figure 6.20.5

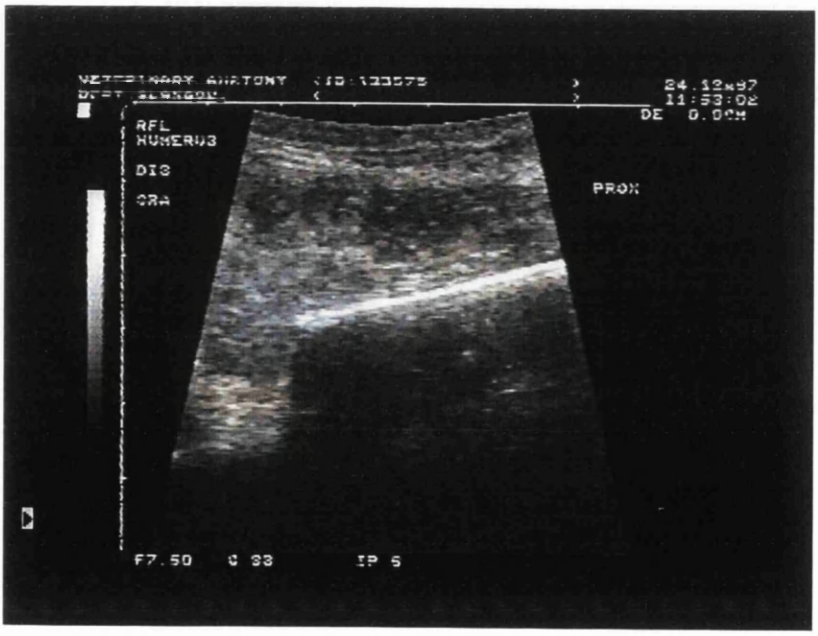

Figure 6.20.6

Figure 6.20.7 Radiographs taken at day 19 after fracture repair show a marked lucency around pin 2, 3 and 5, bad alignment of the fragments with caudal overriding of distal shaft fragment. Osteolysis is found around pin 2, 3 and 5, but no callus formation. **a**, lateral view, **b**, cranial view.

a

b

Figure 6.20.8 Longitudinal scan of the humerus from the caudal aspect on day 19 after fracture repair demonstrates a large cystic structure with well defined margin (blank arrow) at the fracture site above the proximal end segment and at the end of distal segment. The bone fragment caudal to the humerus (arrow head) remains undisplaced but appears smaller than on the previous scans. There is still no callus formation detected.

Figure 6.20.9 Transverse scan of the humerus from caudal aspect demonstrates the cystic structure on the proximal segment with a well defined margin (blank arrow). **H**, humerus.

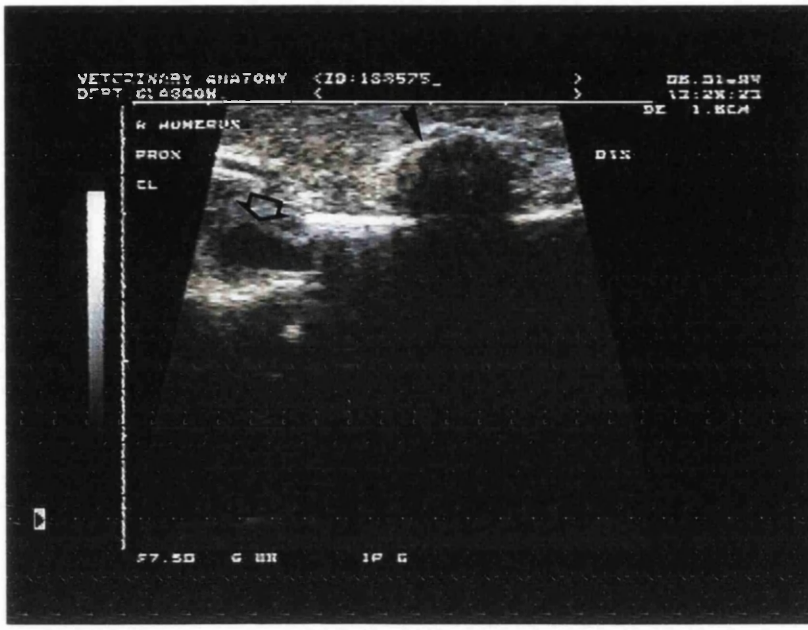

Figure 6.20.8

Figure 6.20.9

Figure 6.20.10 Longitudinal scan of the humerus from the cranial aspect on day 19 after fracture repair shows the fracture site but does not reveal the cystic structure. Note the soft callus formation at the end of the proximal fragment as shown by the hyperechoic mottled appearance.

Figure 6.20.11 Longitudinal scan of the humerus from the cranial aspect on day 19 after fracture repair demonstrates callus formation on the proximal segment at some distance away from the fracture site and appears as an hyperechoic rough bone surface.

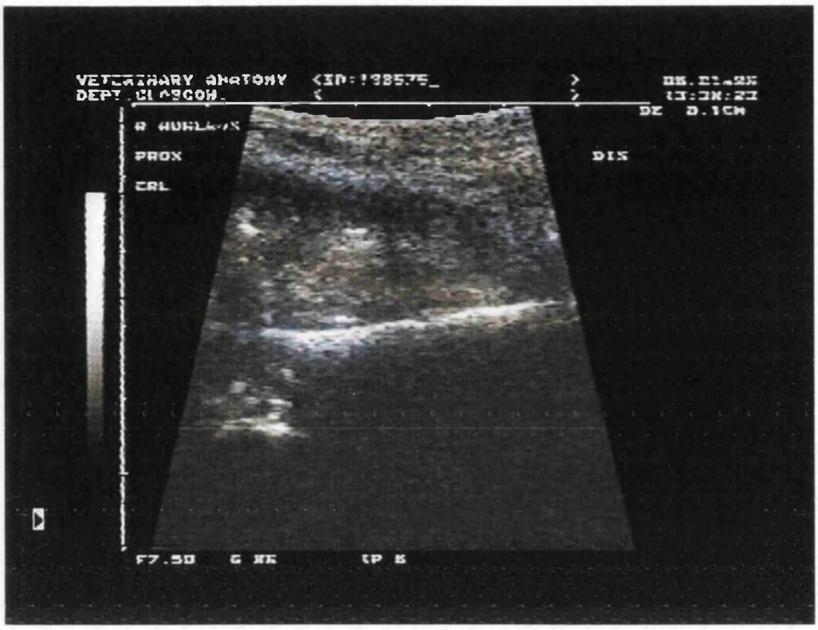

Figure 6.20.10

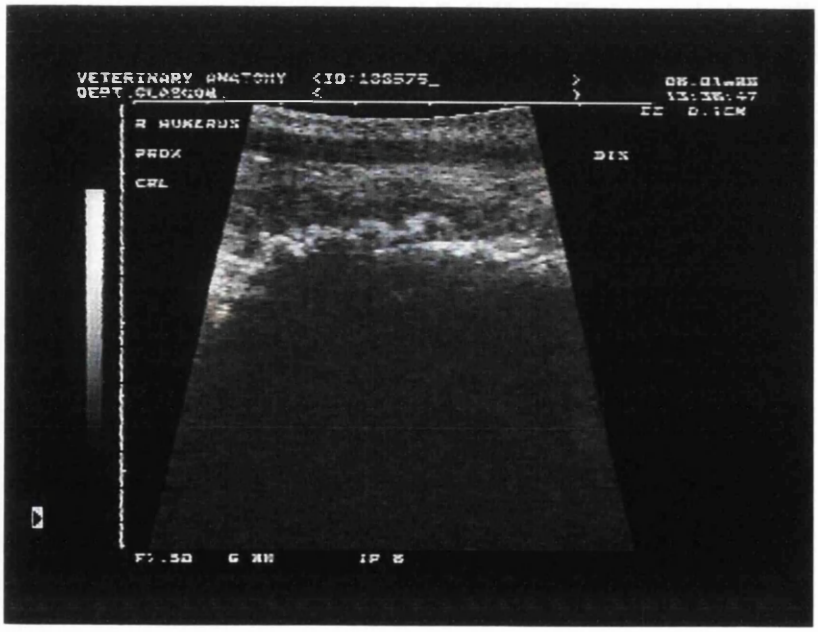

Figure 6.20.11

Figure 6.20.12 Transverse scan of the humerus on day 19 after fracture repair shows the abnormal appearance of the humerus with a rough surface suggestive of callus formation. **H**, humerus.

Figure 6.20.13 Ultrasonographic examination of the fracture site on day 25 after fracture repair shows there is no longer a cystic structure present. There is still no well defined callus formation to be seen at the fracture site. Callus formation could be seen on the proximal segment at some distance away from the fracture site appearing as a rough bone surface (arrow head).

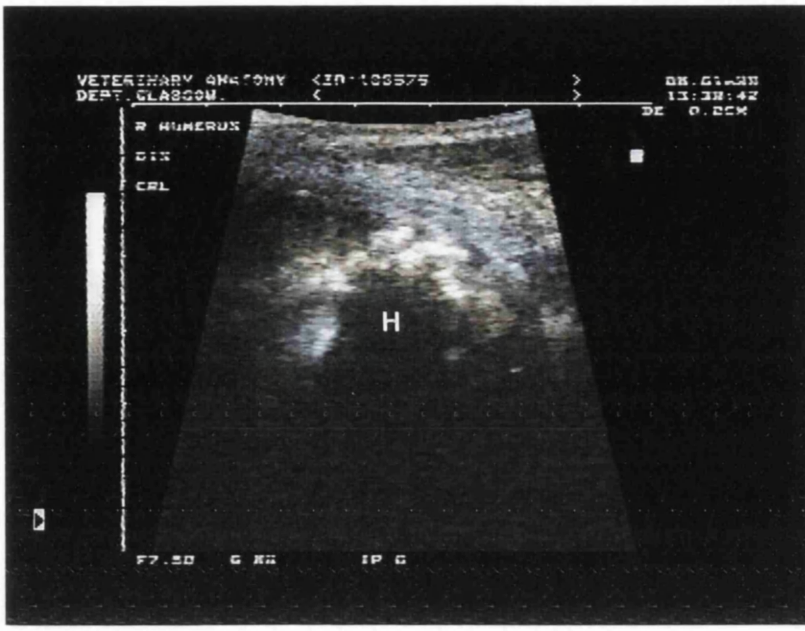

Figure 6.20.12

Figure 6.20.13

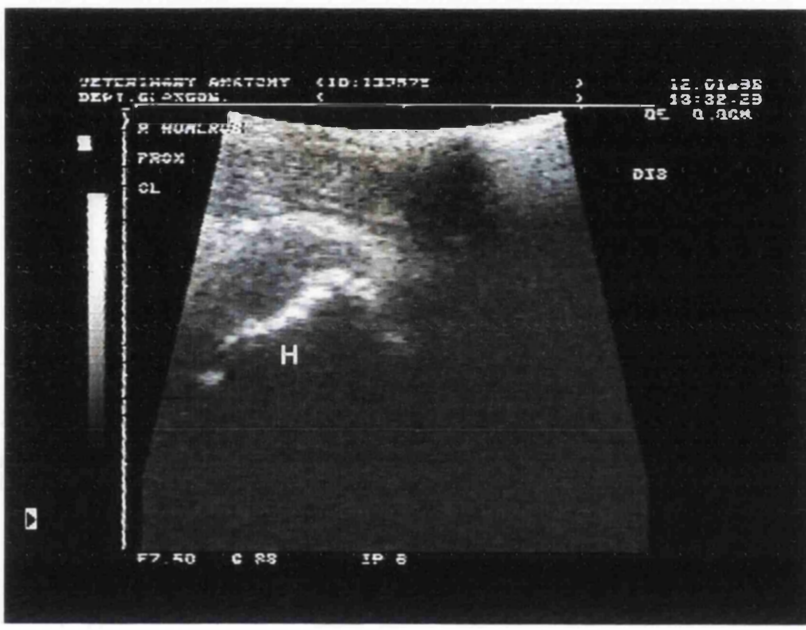

Figure 6.20.14 Transverse scan of the proximal fragment on day 25 after fracture repair shows the humerus with callus formation and appears as a hyperechoic rough bone surface. **H**, humerus.

Figure 6.20.15 Radiographs taken at day 32 after fracture repair shows the fracture has been realigned by a Dynamic Compression Plate (DCP). An osteotomy has been performed at the end of the proximal fragment to stimulate new callus formation. A DCP is fixed on the medial side of the humerus with five cortex screws on each side of the plate. The realignment process has resulted in satisfactory reduction and alignment.. There is abundant periosteal pallisade like callus formation around the humeral shaft. One bone fragment remains, being caudal to the femur at fracture site area.

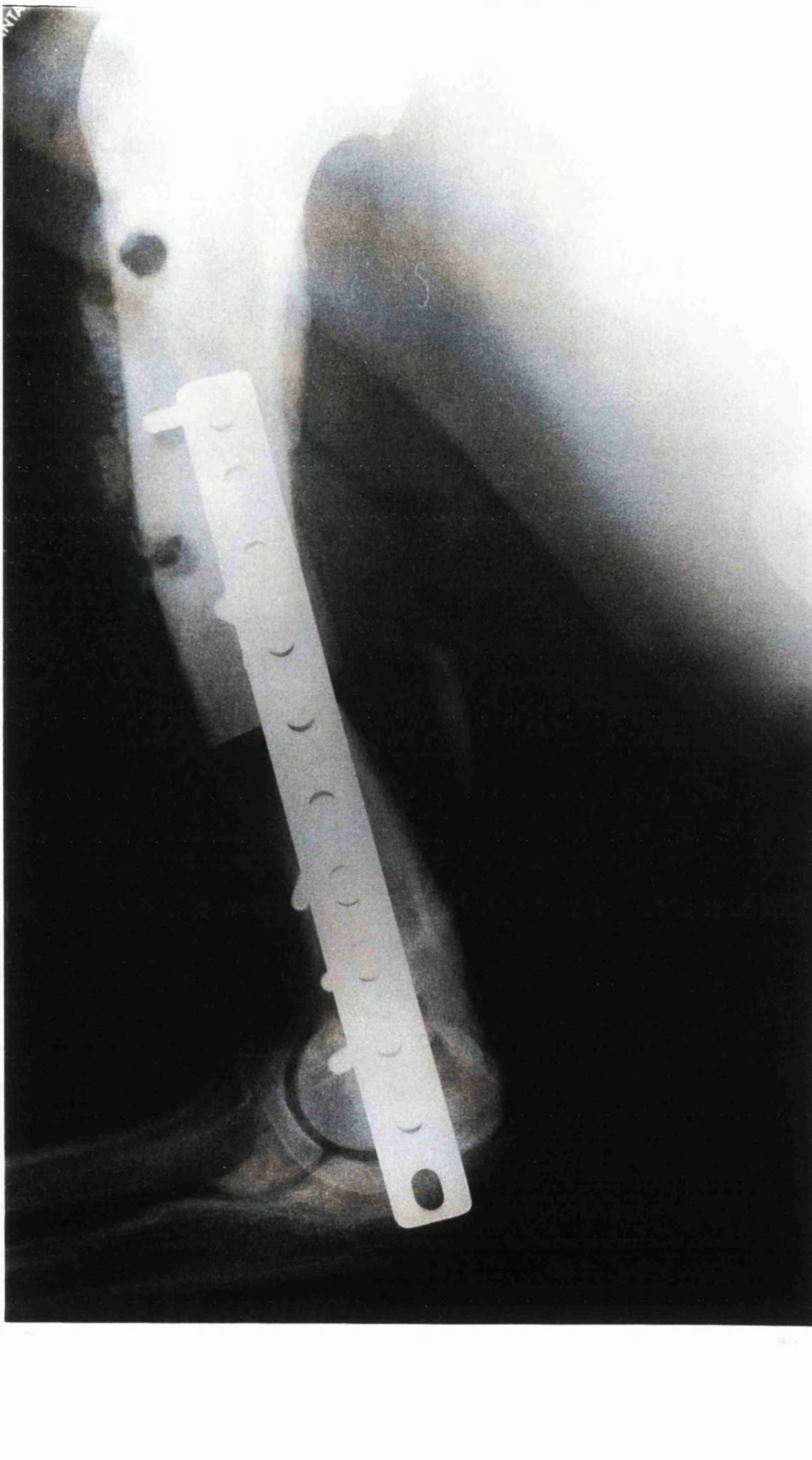

Figure 6.20.16 Longitudinal scan of the humerus from the caudal aspect on day 33 after fracture repair (24 hours after fracture realignment) demonstrates callus formation on the proximal segment some distance from the fracture site. The callus formation appears hyperechoic causing a rough bone surface appearance.

Figure 6.20.17 Longitudinal scan of the humerus from the lateral aspect 24 hours after fracture realignment demonstrates the fracture site (arrow) which appears as discontinuity of the bone. The screws used in fracture reduction appear hyperechoic and produce comet tail artefacts. The screw threads can be seen and give a typical characteristic appearance for screws imaged ultrasonographically (arrow heads). The area of muscle damage above the bone appears as a disorganised hypoechoic area.

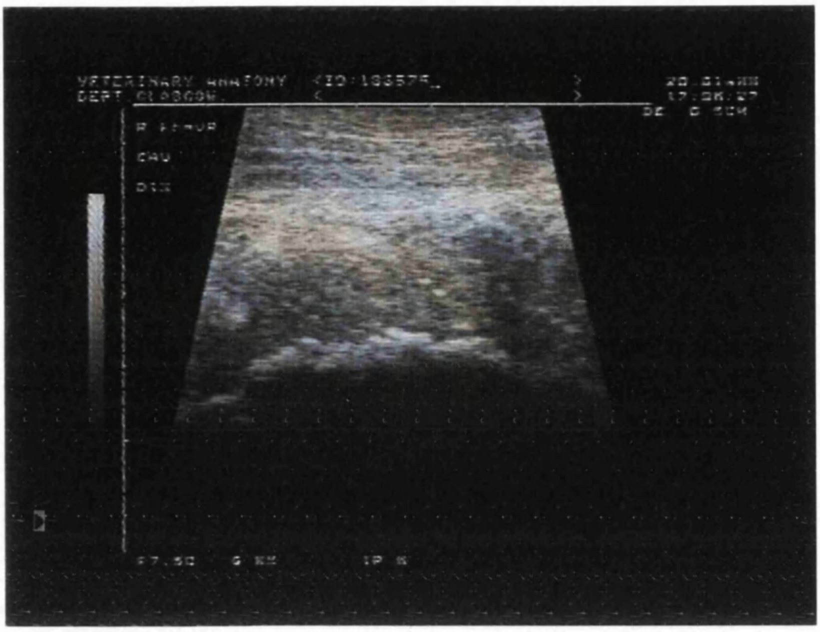

Figure 6.20.16

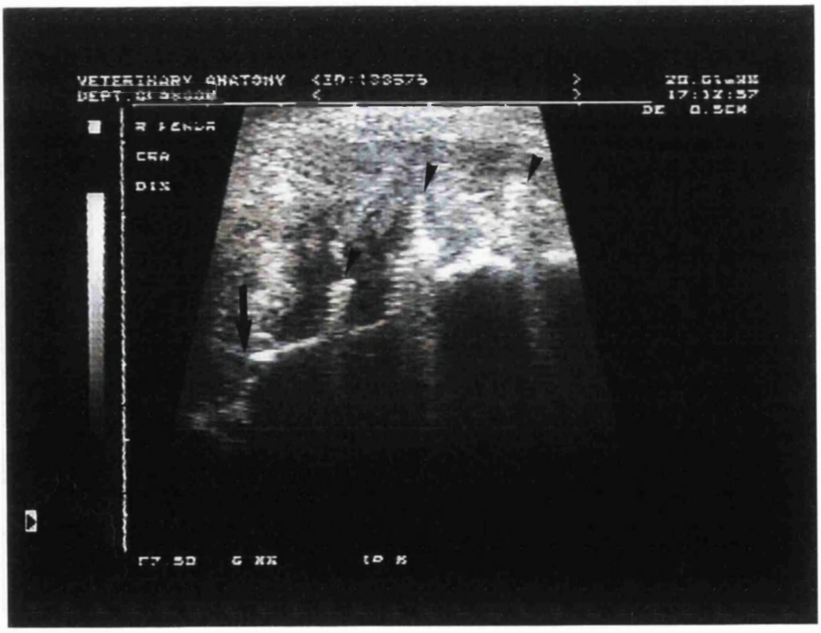

Figure 6.20.17

Figure 6.20.18 Longitudinal scan of the distal humerus from the cranial aspect 24 hours after realignment demonstrates a hole which appears hyperechoic with the presence of soft callus formation around it. Each hole is actually the previous site of an external fixator pin used before the recent realignment process.

Figure 6.20.19 Longitudinal scan of the humerus 24 hours after fracture realignment demonstrates the fracture site with the presence of hyperechoic material suggestive of soft tissue reaction (arrow head).

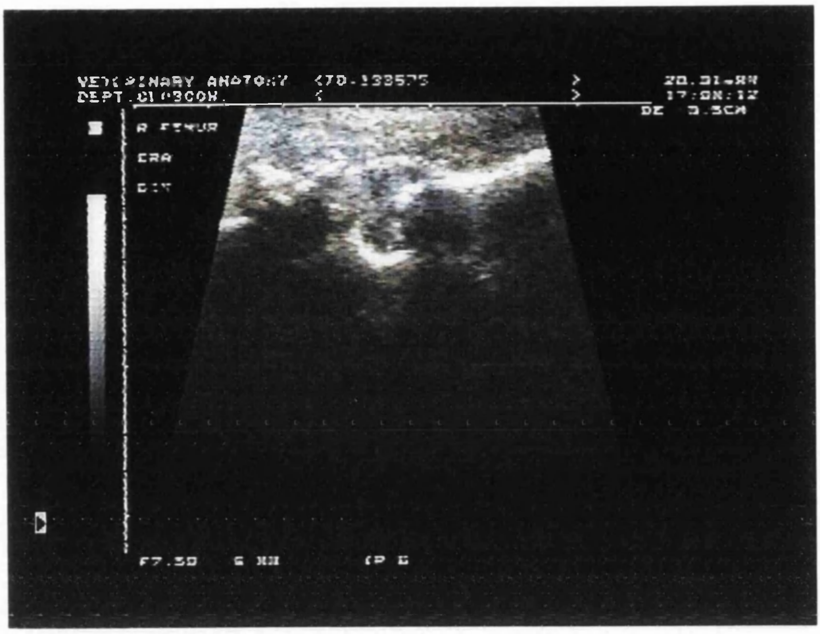

Figure 6.20.18

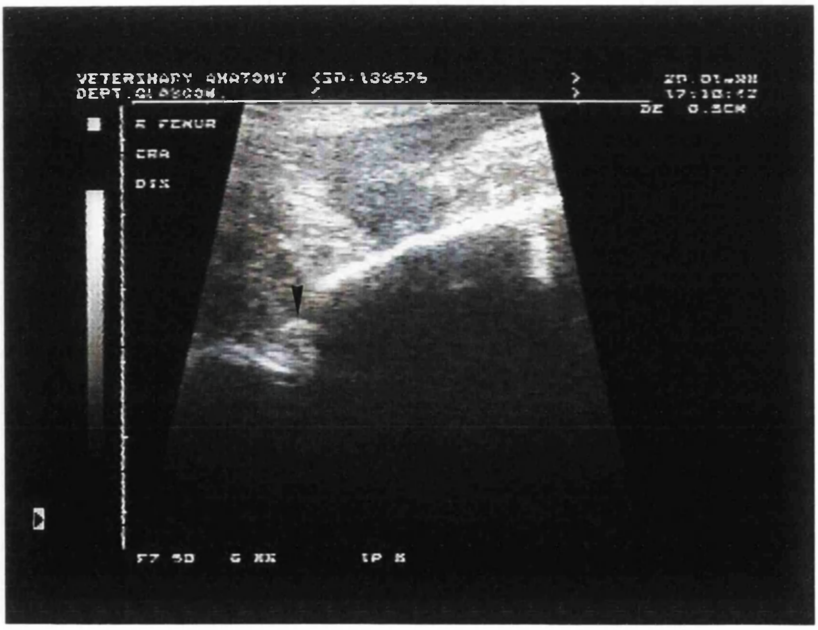

Figure 6.20.19

Figure 6.20.20 The bone fragment cranial to the humerus imaged from caudal aspect 24 hours after fracture realignment appears hyperechoic with acoustic shadowing artefact.

Figure 6.20.21 Transverse scan of the humerus 24 hours after fracture realignment shows the abnormal humerus which appears large with a rough surface. **H**, humerus.

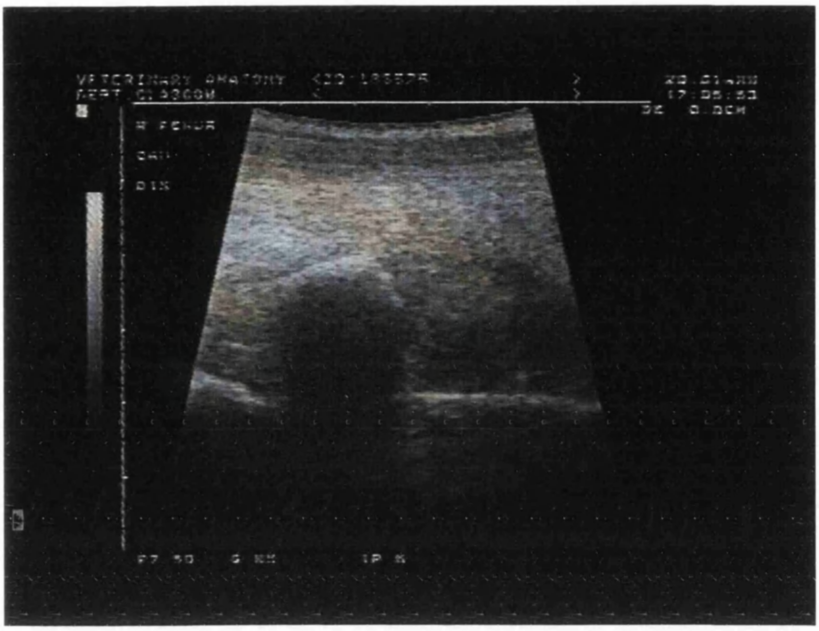

Figure 6.20.20

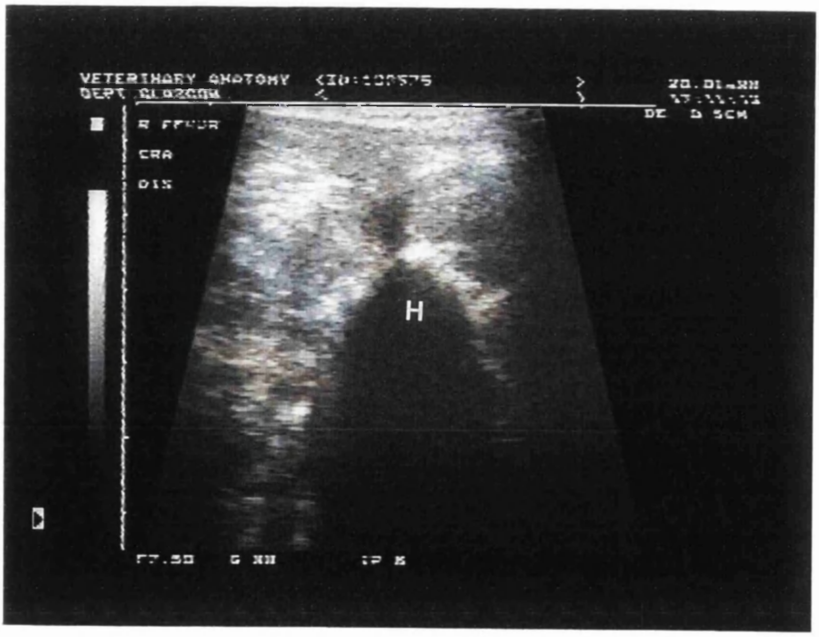

Figure 6.20.21

Figure 6.20.22 Radiograph taken at day 54 after fracture repair (day 22 after realignment) shows the major tubercle is laterally displaced relative to the acromion. The fracture site has been refixed by a larger plate, and one screw is broken as can be seen in cranial view (**b**). There is a caudal displacement of the distal humerus. No bridging bony callus is seen. **a**, lateral view, **b**, cranial view.

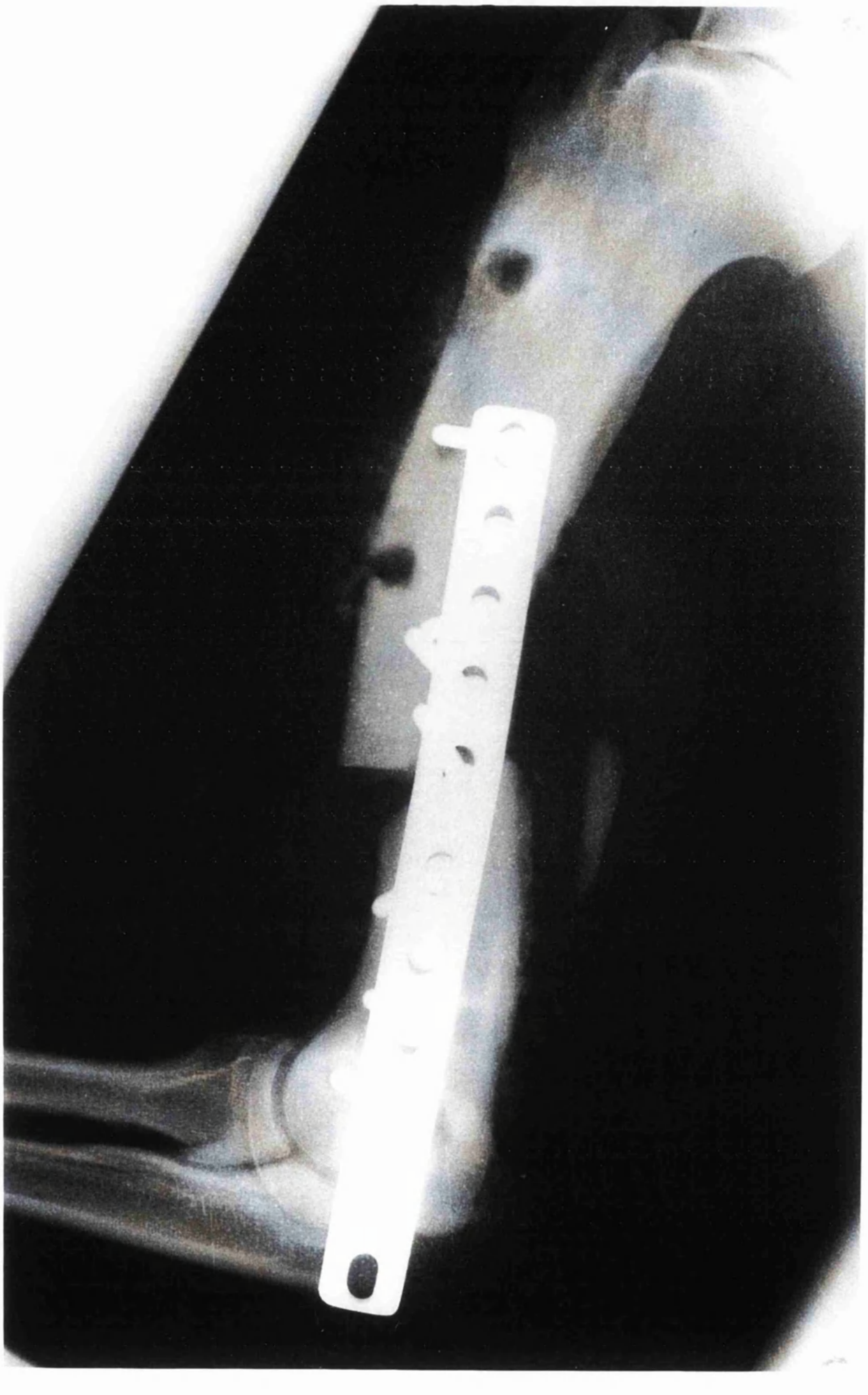

a

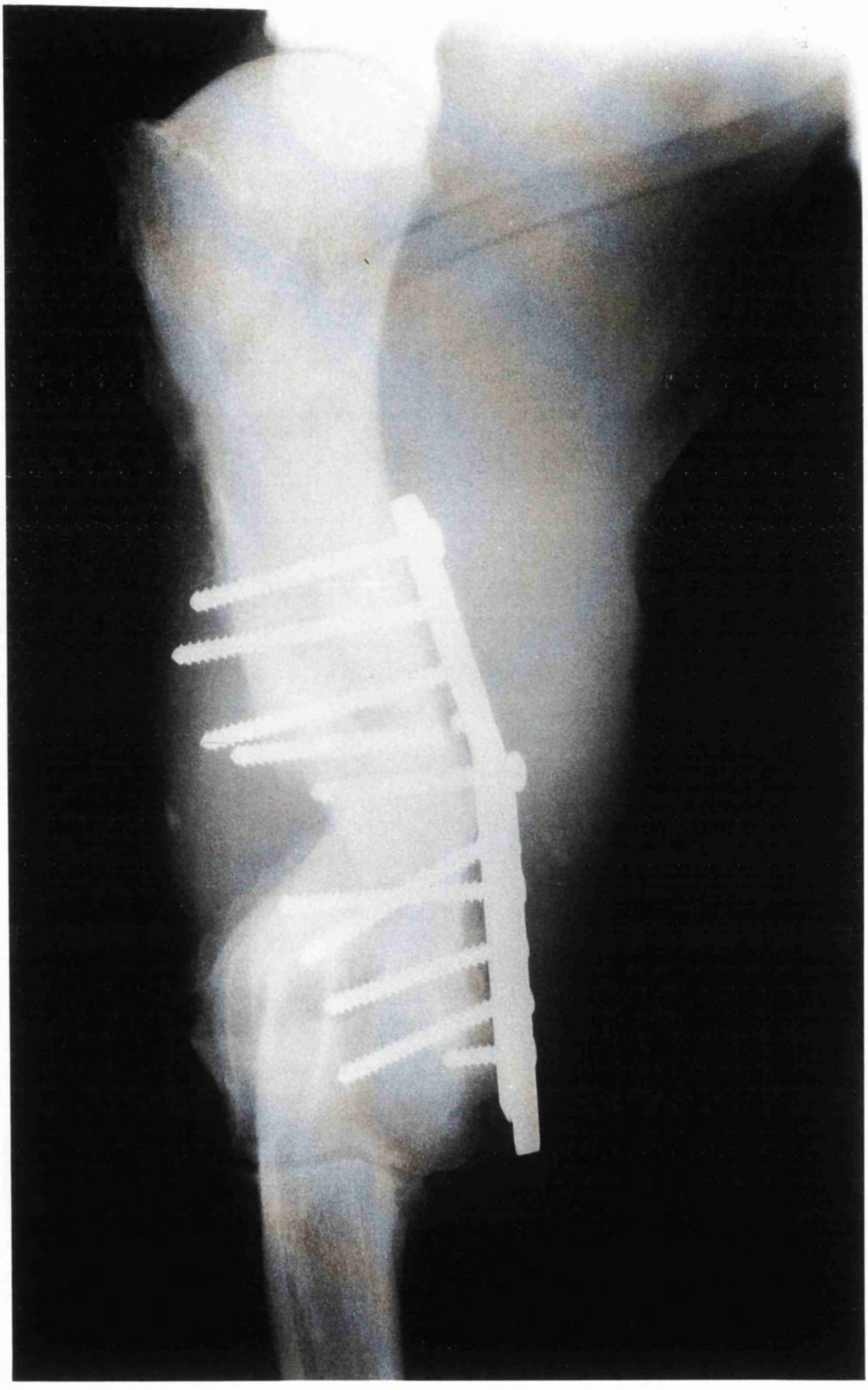

b

Figure 6.20.23 Longitudinal scans of the humerus on day 54 after fracture repair show the fracture site and demonstrate that the two bone segments are poorly aligned. **a**, cranial aspect, **b**, caudal aspect. The proximal segment appears higher than the distal one in **b**. Callus formation can be seen on the bone surface. The area of disorganised hypoechoic appearance in the muscle is suggestive of muscle damage.

Figure 6.20.23a

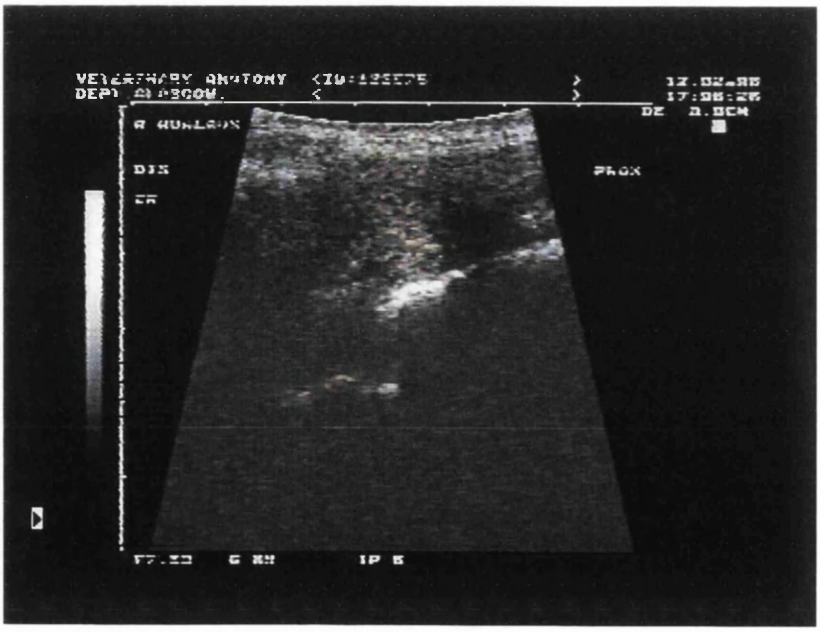

Figure 6.20.23b

Figure 6.20.24 Longitudinal scan of the distal humerus on day 21 after fracture realignment demonstrates the hole which appears smaller than in the previous scan. The callus formation is seen bridging over the hole.

Figure 6.20.25 The fracture site imaged on lateral aspect on day 21 after fracture realignment appears as a groove and the fragments are completely bridged by the callus. The bone surface appears rough due to callus formation. The area of muscle damage can still be seen as disorganised with a mixture of hyperechoic and hypoechoic structures above the fracture site area. A number of screws (arrow heads) are also imaged at the fracture site area appearing hyperechoic.

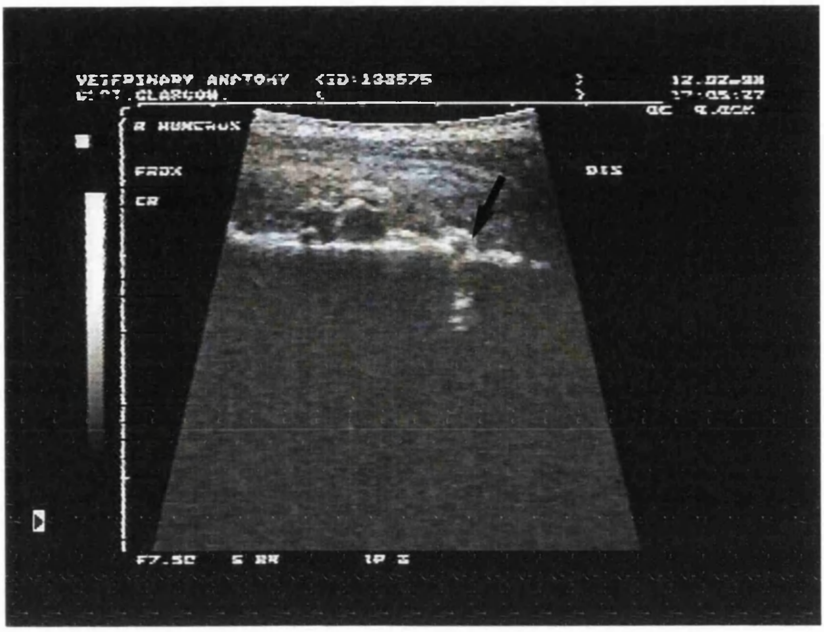

Figure 6.20.24

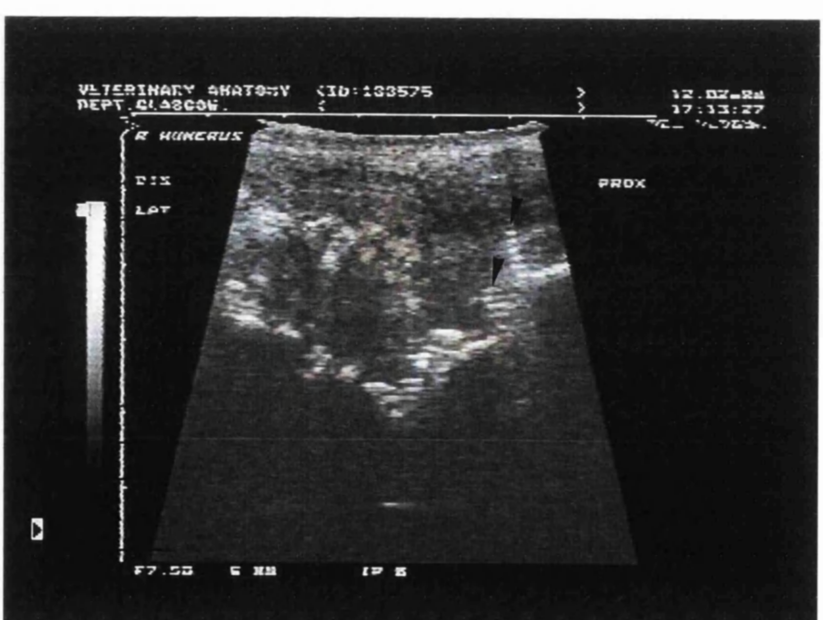

Figure 6.20.25

Case 21

A one year old male neutered domestic short hair cat was presented to the emergency service at Glasgow University Veterinary Hospital for stabilisation of injuries following a road traffic accident. Radiographic examination of the pelvis showed a displaced right ilial shaft fracture had been sustained. A sacroiliac luxation was also present on the left side. After temporary stabilisation over the weekend surgery was performed to stabilise the pelvic fracture. An eight hole 2.0 mm Dynamic Compression Plate (DCP) was contoured over the acetabulum with placement of six screws of two different diameters to repair the ilial fracture. Whilst the cat coped well with conservative management of the pelvic fractures the displaced nature of the caudal fragment on the right warranted surgery to prevent problems in the future with constipation. Radiographs taken immediately after the fracture repair showed satisfactory reduction and alignment and correct positioning of screws (figure 6.21.1).

Ultrasonographic examination

Day three after fracture repair

Ultrasonographic examination of the ilial fracture demonstrated the presence of disorganised hyperechoic material around the fracture site which was suggestive of soft tissue reaction (figure 6.21.2). There was some periosteal reaction present which appeared hyperechoic on the bone surface. The area of muscle damage appeared as disorganised hypoechoic material over the fracture site and was mixed with the area of soft tissue reaction. The bone plate attached to the ilial shaft appeared hyperechoic with reverberation artefact (figure 6.21.3).

Day seven after fracture repair

Ultrasonographic examination demonstrated the fracture site which appeared as a slight angulation of the ilium at the fracture site (figure 6.21.4). There was no callus formation detected. The bone plate appeared hyperechoic with reverberation artefact. The periosteal reaction was detected as on the day three examination. The cat failed to return for reassessment and following ultrasonographic examinations were not done.

Figure 6.21.1 Radiographs obtained immediately after fracture repair show that the fracture has been stabilised with an eight hole 2.0 mm DCP contoured over the acetabulum and with placement of six screws of two different diameters. The repair process is resulting in a satisfying reduction and alignment with correct positioning of the screws. **a**, lateral view, **b**, dorsal view.

b

Figure 6.21.2 Longitudinal scan of the ilial shaft on day three after fracture repair demonstrates the fracture site with the presence of disorganised hyperechoic structure around the fracture site suggestive of soft tissue reaction. There is some periosteal reaction present which appears hyperechoic on the bone surface. Note also the area of muscle damage which appears as disorganised hypoechoic material over the fracture site and is mixed with the area of soft tissue reaction.

Figure 6.21.3 Longitudinal scan of the ilial shaft on day three after fracture repair demonstrates the straight hyperechoic lines with reverberation artefact which represent the bone plate that is attached to the ilial shaft.

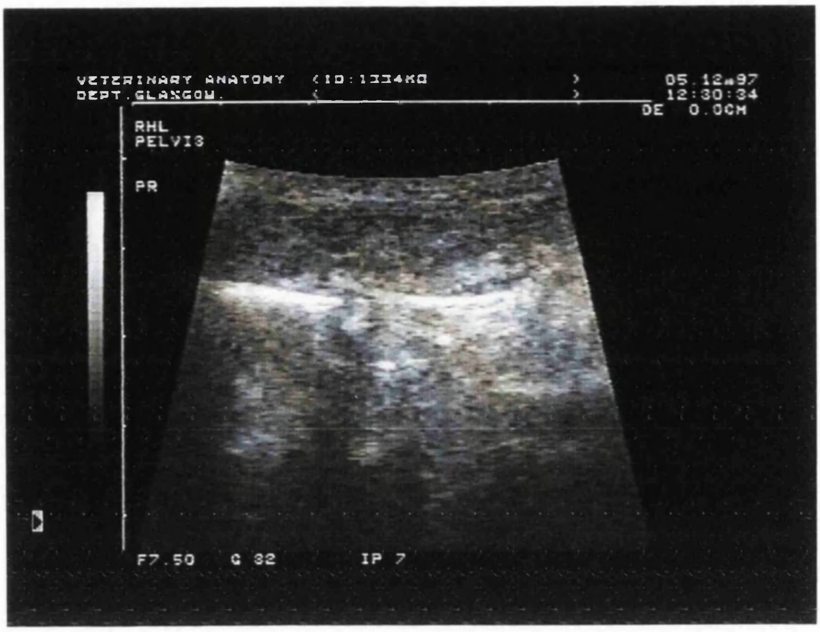

Figure 6.21.2

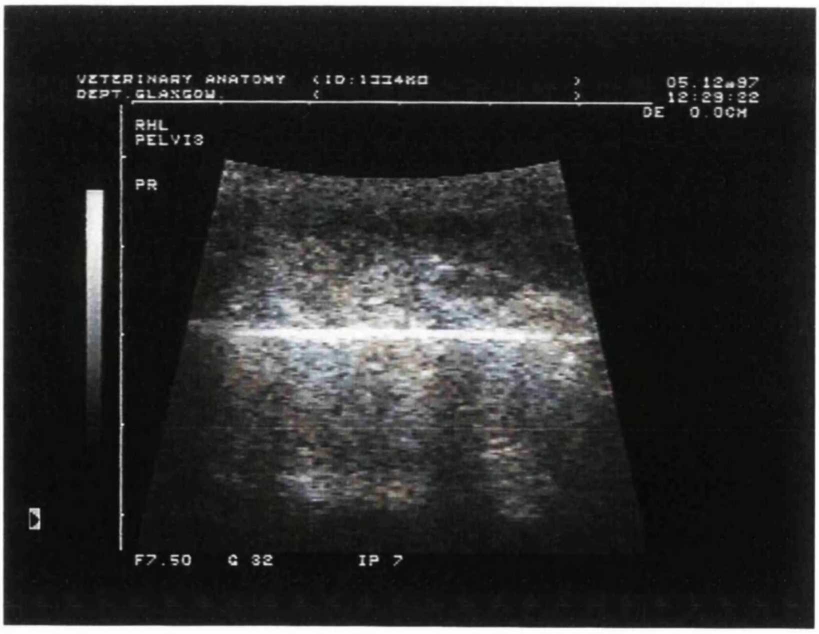

Figure 6.21.3

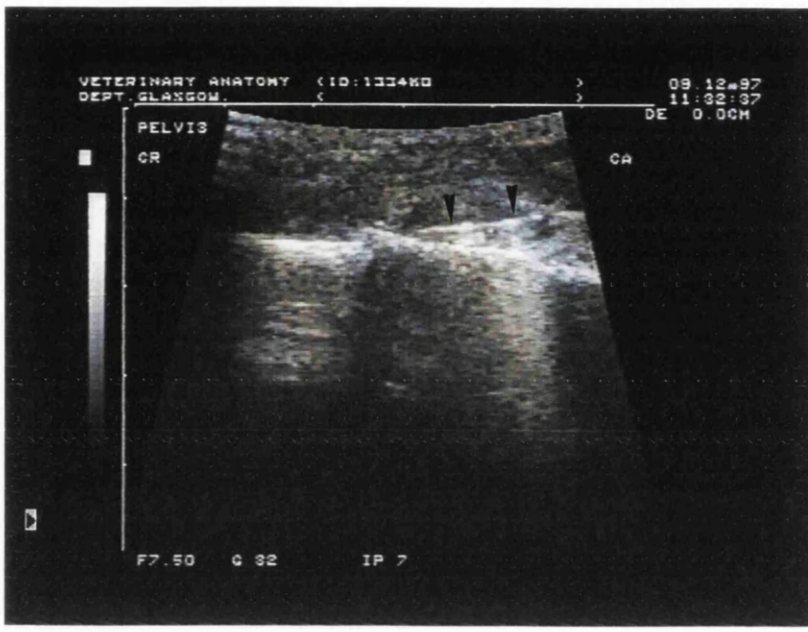

Figure 6.21.4 Longitudinal scan of the ilial shaft on day seven after fracture repair demonstrates the fracture site with a slight angulation of the ilial shaft. The bone plate can be seen over the cranial fragment (arrow heads). There is no callus formation detected.

Case 22

A one year old male Labrador Retriever, weight 33 kg, was presented to the Glasgow University Veterinary Hospital for assessment of the fracture healing of a tibial fracture. The animal had been involved in a road traffic accident and had sustained a transverse fracture at the proximal third of the tibia and fibula of the right hind limb.. The fracture had been repaired and stabilised with modified type II / type III external skeletal fixator (figure 6.22.1).

Clinical and radiographic assessment at day 28 after fracture repair showed the healing progress was very good (figure 6.22.2). On the cranio-caudal view there was one small fragment of bone that looked denser than the rest suggestive of sequestrum. The external skeletal fixator (ESF) had been scaled down to a modified type one frame at this time. The remainder of the frame was proposed to be removed in two to three weeks time.

Ultrasonographic examination

Day 28 after fracture repair

Ultrasonographic examination of the fracture site area demonstrated the presence of callus formation bridging the fracture site (figure 6.22.3). The callus formation appeared hyperechoic with a rough and uneven bone surface. The muscle structure appeared to have normal ultrasonographic characteristics. The normal part of the tibia appeared hyperechoic with a smooth bone surface. The fracture site detected on the lateral aspect scan appeared as a small shallow gap on the bulging and rough bone surface which was due to callus formation (figure 6.22.4). The fracture site of the fibula was also detected and had been bridged completely by the callus but the fragments were poorly aligned (figure 6.22.5) The fracture site appeared hyperechoic with a rough border.

Day 50 after fracture repair

Radiographs taken at day 50 after fracture repair showed satisfactory bony callus formation, good reduction but suboptimal alignment (figure 6.22.6). There was slight valgus angulation. The remaining part of the external fixator apparatus was removed at this stage.

Ultrasonographic examination

Ultrasonographic examination demonstrated the fracture site area which appeared uneven but with a reduction in the rough surface suggestive of a remodelling process (figure 6.22.7). A hole where the external fixator pin had been previously placed was detected and appeared hyperechoic. There was soft tissue reaction around the hole which appeared as disorganised and hyperechoic (figure 6.22.8). There was also blood accumulation above the hole which appeared anechoic. The fracture site of the fibula appeared as less bulging and the surface had become smooth suggestive of remodelling process (6.22.9). A transverse scan on the lateral aspect at the fracture site area demonstrated the enlarged fibula with a rough surface (figure 6.22.10). Half of the tibia was not visible due to shadowing artefact from the fibula. Ultrasonographically, the fracture site was healing satisfactorily, but was not yet complete.

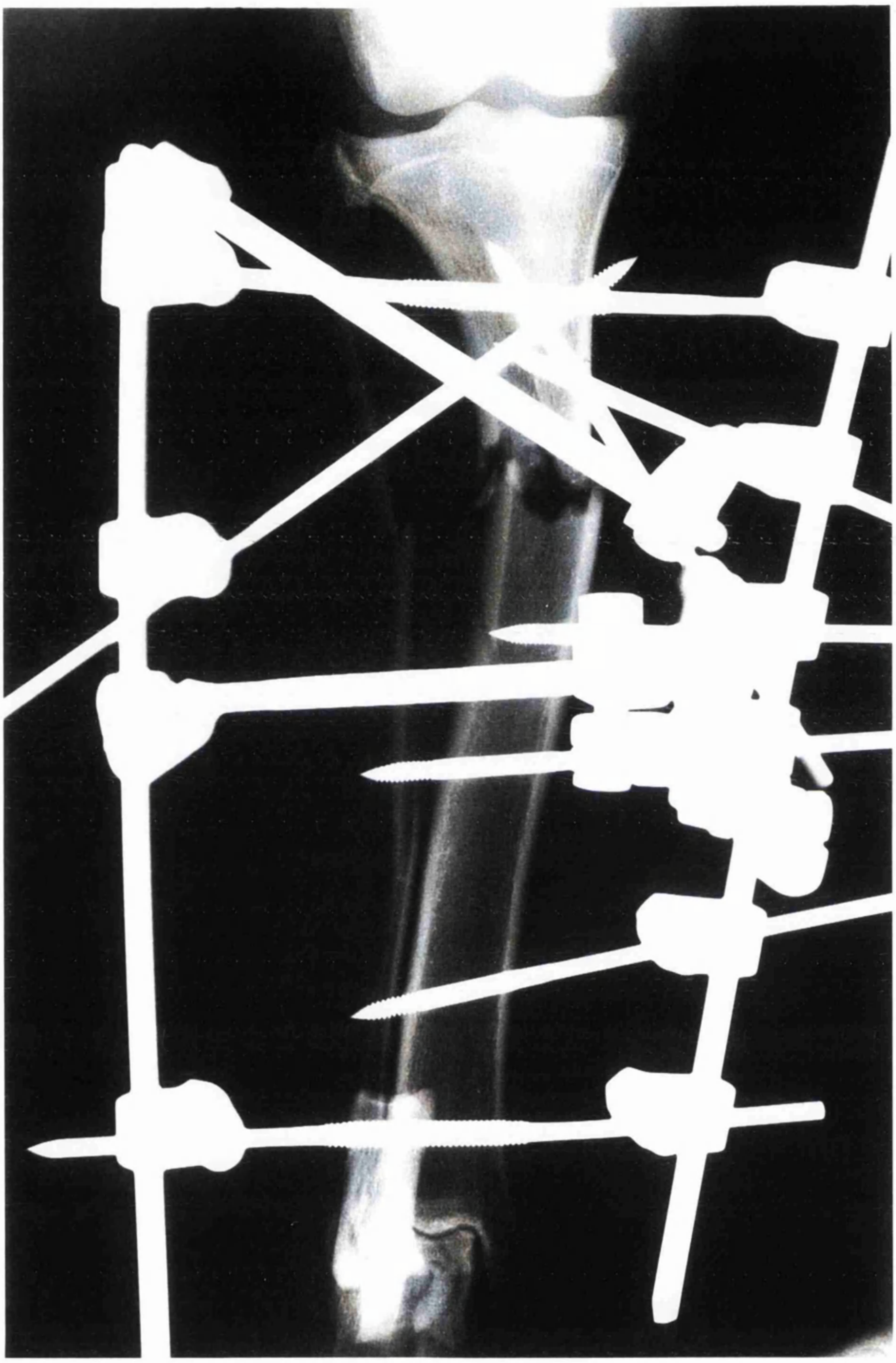

Figure 6.22.1 Radiograph obtained immediately after fracture repair shows the fracture has been repaired and stabilised with modified type II / type III external skeletal fixator. The repair process is resulting in satisfy reduction but with slight angulation.

Figure 6.22.2 Radiographs obtained on day 28 after fracture repair show the healing progress is very good. **a**, lateral view, **b**, cranial view. There is one small fragment of bone that looks denser than the rest suggestive of sequestrum in **b**. The external skeletal fixator (ESF) has been scaled down to a modified type one frame.

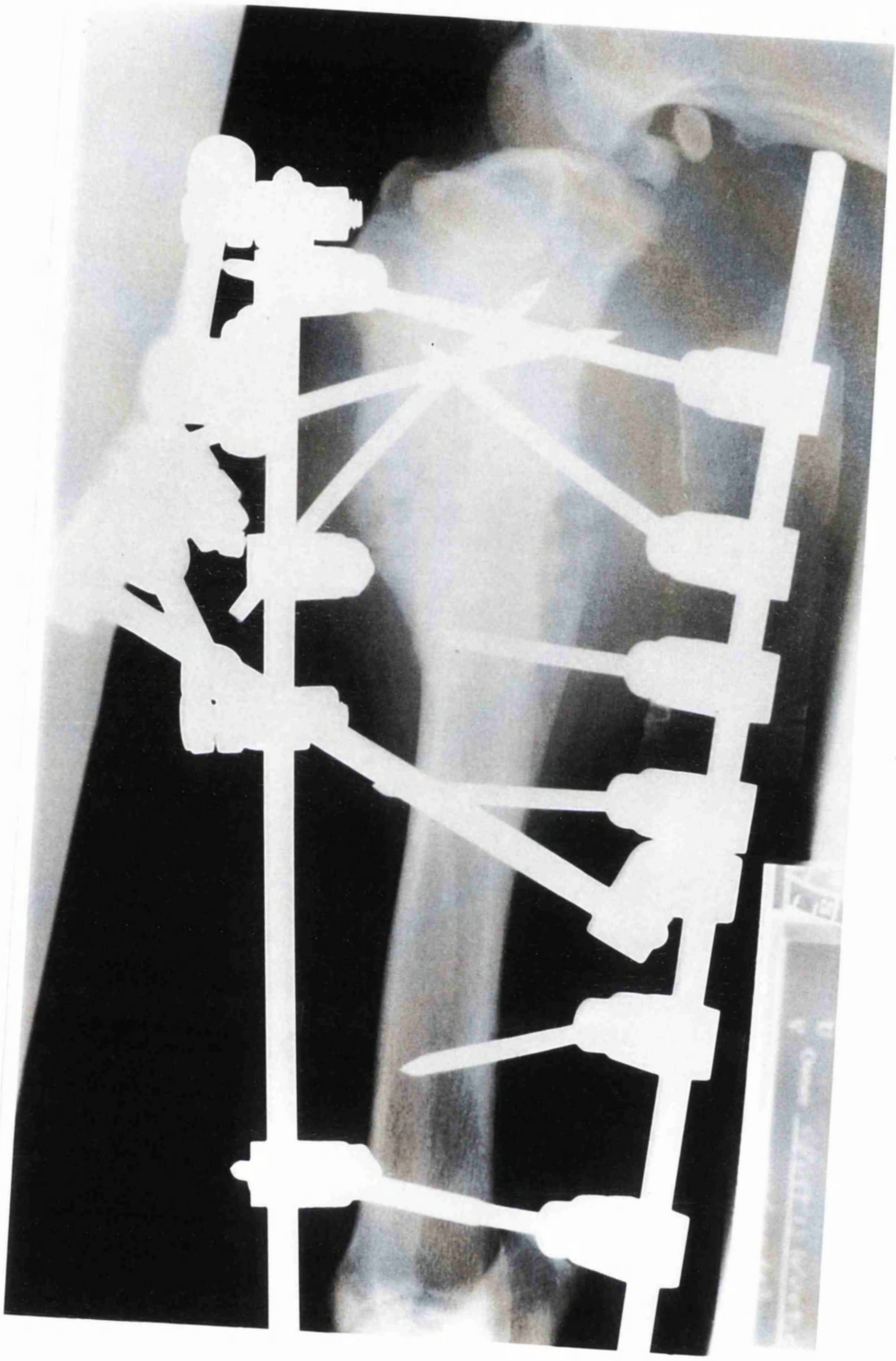

a

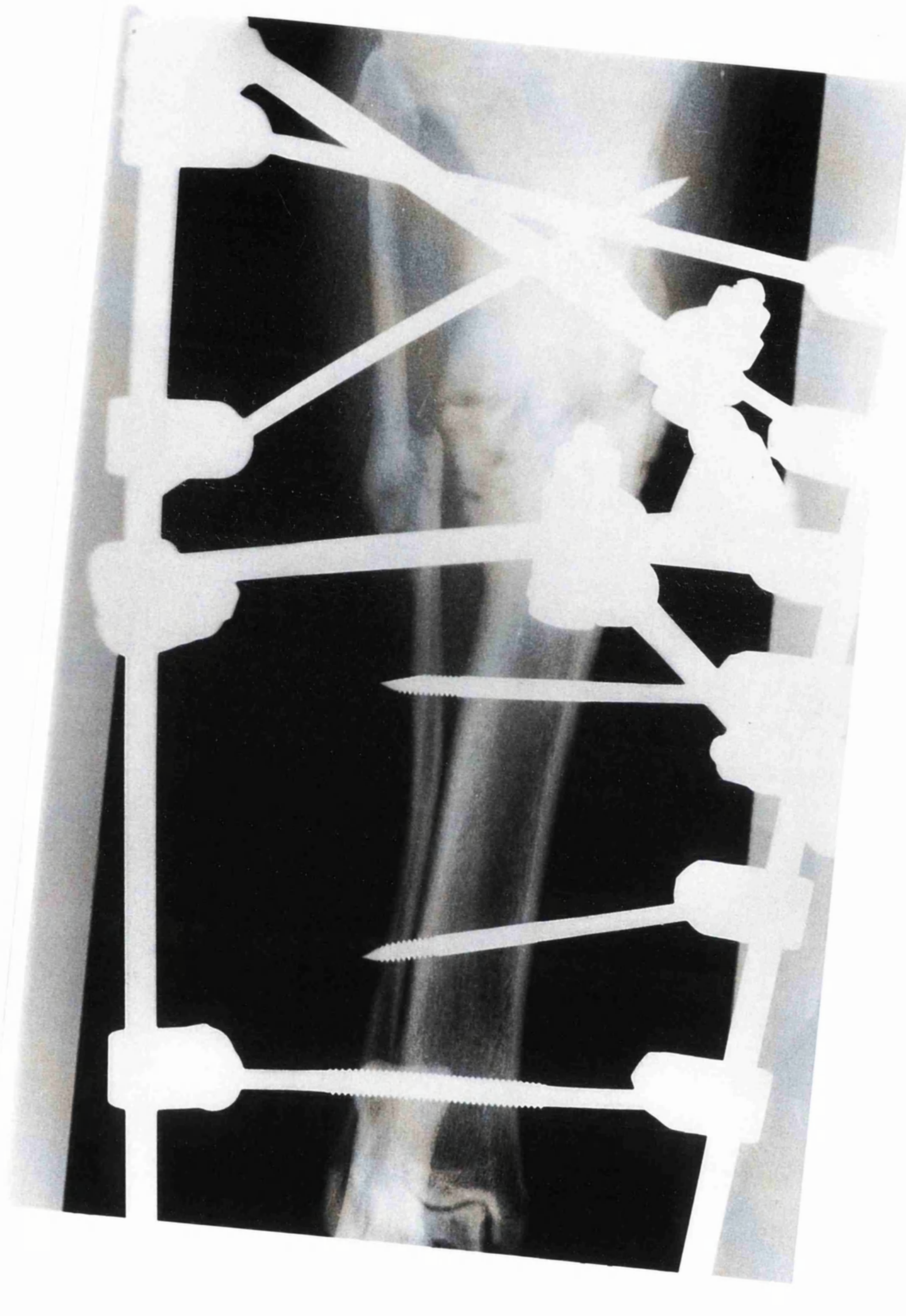

b

Figure 6.22.3 Ultrasonographic examination on day 28 after fracture repair demonstrates the fracture site (arrow) area with the presence of callus formation and appears as a rough and uneven bone surface. The fracture site is being bridged by the callus. The muscle tissue appears to have a normal ultrasonographic appearance.

Figure 6.22.4 Longitudinal scan of the tibia from lateral aspect on day 28 after fracture repair shows the fracture site (arrow) which appears as a small shallow gap on the bulging and rough bone surface.

Figure 6.22.3

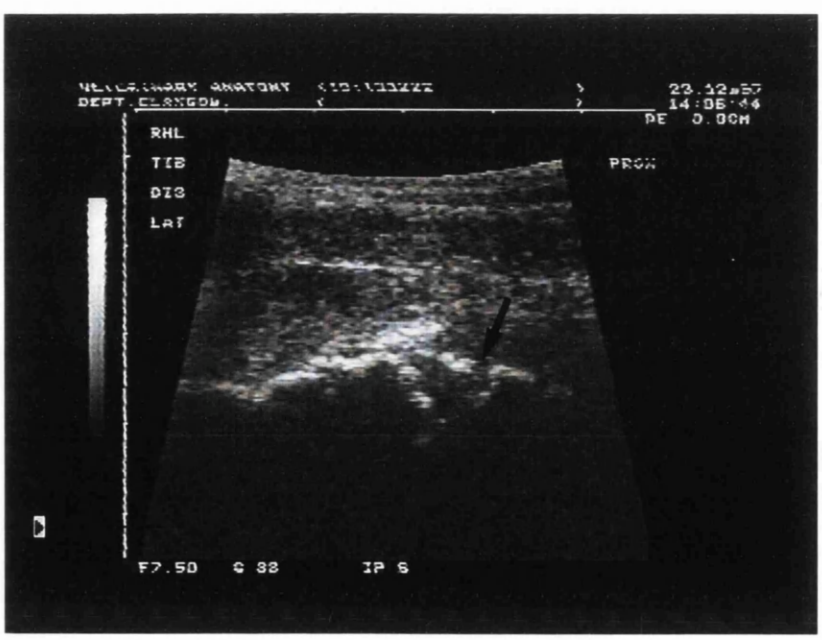

Figure 6.22.4

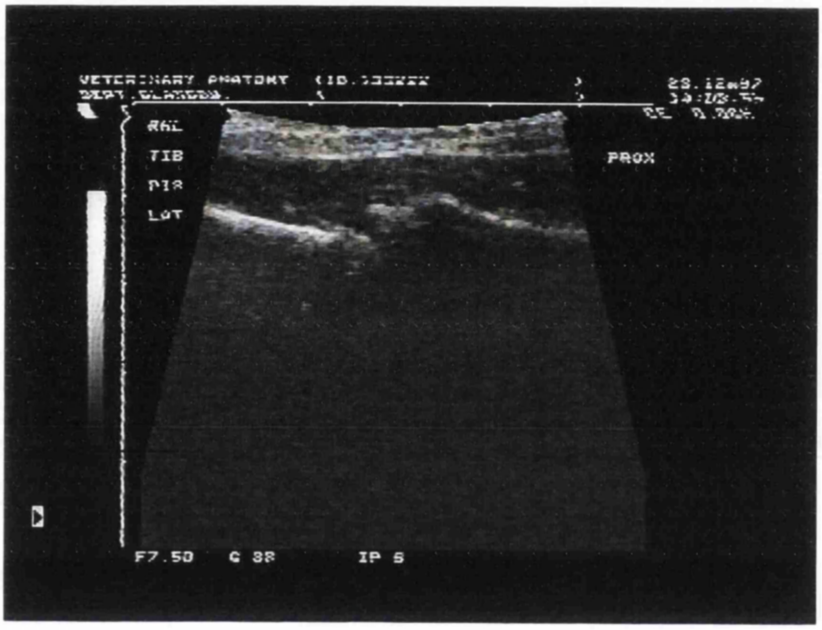

Figure 6.22.5 Longitudinal scan of the fibula on day 28 after fracture repair shows the fracture site which appears as a bulging bone surface. The fracture site has been bridged completely by the callus but the fragments are poorly align.

Figure 6.22.6 Radiographs taken at day 50 after fracture repair show satisfying bony callus formation, good reduction but suboptimal alignment. There is slight valgus angulation. The remaining part of the external fixator apparatus has now been removed. **a**, lateral view, **b**, cranial view.

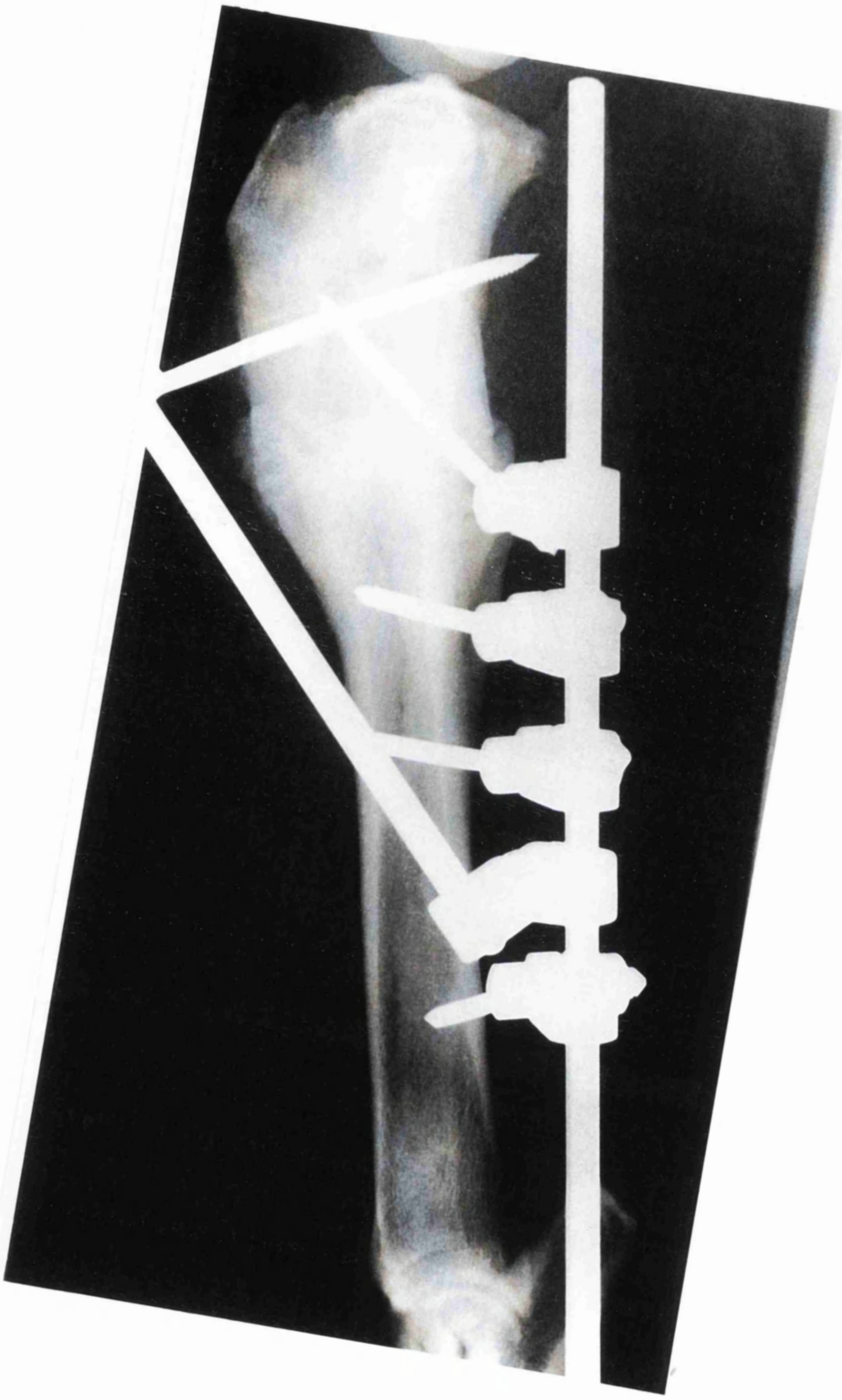

a

b

Figure 6.22.7 Longitudinal scan of the tibia on day 50 after fracture repair shows the fracture site area which appears as an uneven but less rough surface. This is suggestive of a remodelling process.

Figure 6.22.8 One hole where the pin was placed before being removed is detected on the tibia distally on longitudinal scan and appears hyperechoic (arrow). There is soft tissue reaction present around the hole which appears disorganised and hyperechoic with blood accumulation above the hole which appears anechoic.

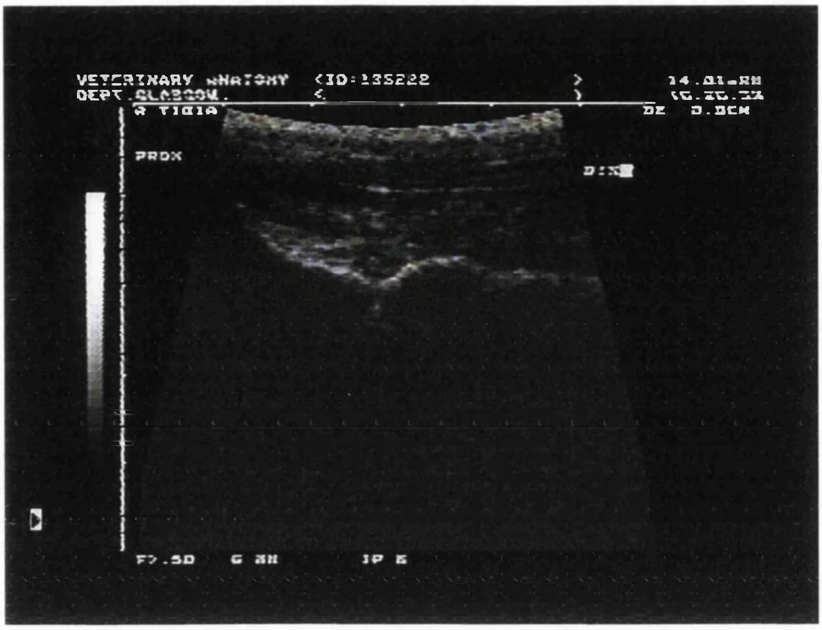

Figure 6.22.7

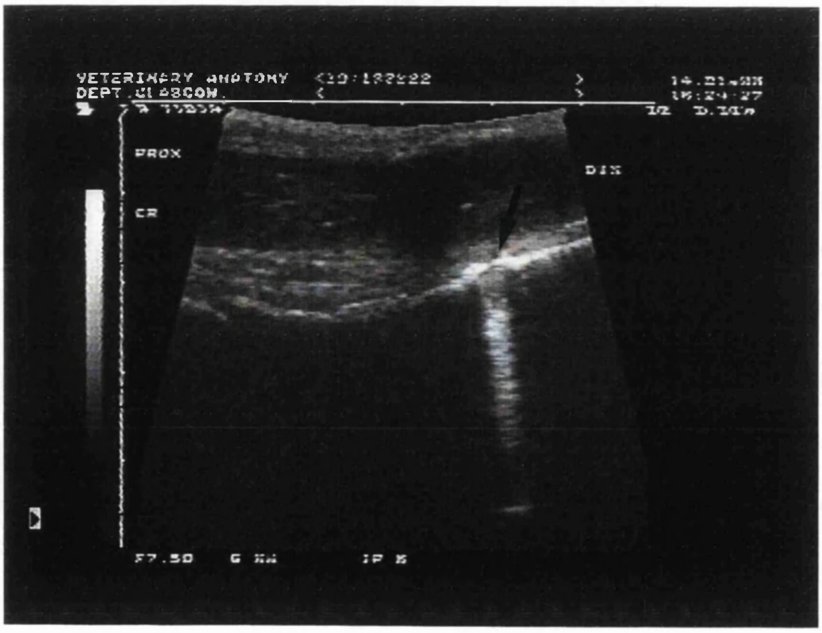

Figure 6.22.8

Figure 6.22.9 The fracture site of the fibula bone (blank arrow) imaged on day 50 after fracture repair appears less bulging and the surface has become smooth suggestive of a remodelling process.

Figure 6.22.10 Transverse scan on lateral aspect at the fracture site area on day 50 after fracture repair demonstrates the enlarged, abnormal fibula above the tibia. Half of the tibia is not seen due to shadowing artefact form the fibula. **T**, tibia. **Fi**, fibula.

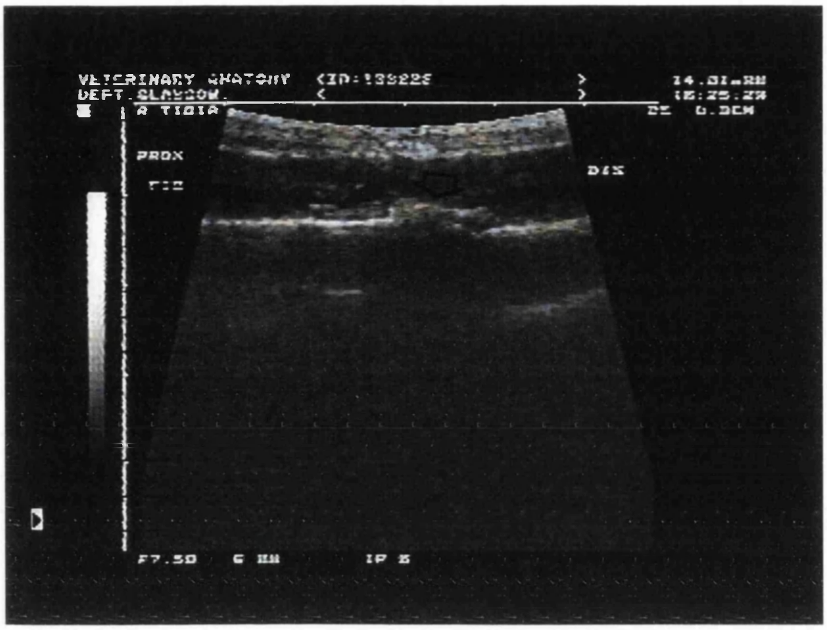

Figure 6.22.9

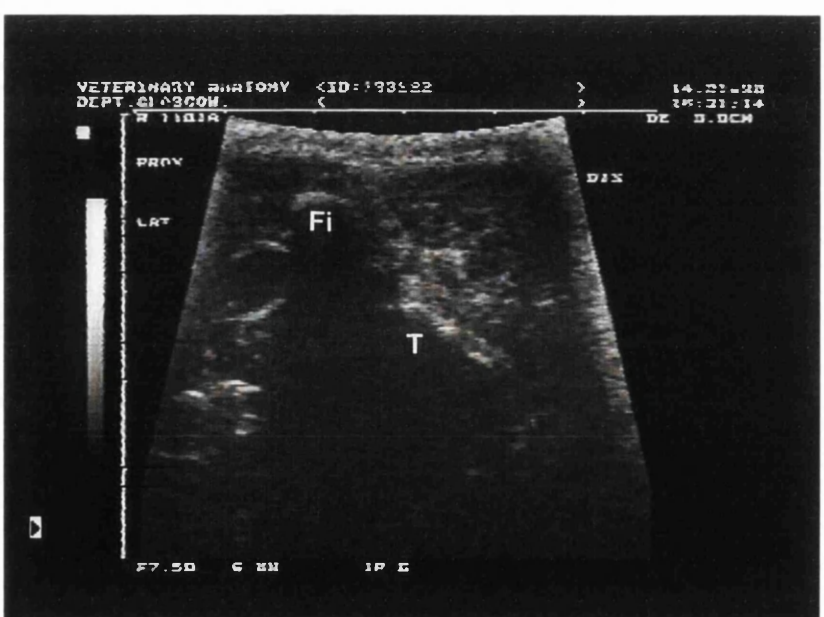

Figure 6.22.10

Case 23

A ten year old male Lakeland Terrier, weight 7.34 kg, was presented to the Glasgow University Veterinary Hospital following trauma of unknown origin three day previously. The animal was hospitalised for the first few days to correct the pre-renal azotemia. The animal was experiencing some abdominal pain which may have been due to bruising of the body wall. Radiographic examination of the humerus revealed that an oblique fracture of the left humerus had been sustained (figure 6.23.1). The fracture was reduced via a limited exposure and stabilised with an intramedullary pin and a simple type one external skeletal fixator. Radiographs obtained immediately after the fracture repair showed the fracture process resulted in satisfactory reduction and alignment (figure 6.23.2). The intramedullary pin had not been placed sufficiently distally.

Ultrasonographic examination

Ultrasonographic examination on day three post-operation demonstrated the fracture site with the presence of a fracture gap (figure 6.23.3). There was a well defined border of the bone fragment and no evidence of callus formation was detected. However, there was an hyperechoic appearance at the fracture site suggestive of soft tissue reaction and periosteal tissue reaction. One small bone fragment lying superficial to the humerus was detected on cranial aspect scan and appeared hyperechoic. The fracture site imaged from caudal aspect scan appeared hyperechoic with a small gap present (figure 6.23.4). The bone ends appeared well aligned on the caudal scan but there was also no evidence of callus formation caudally. The fracture site on a transverse scan appeared with an abnormal shape of the humerus as compared to the normal part (figure 6.23.5a and 6.23.5b). The small bone fragment cranial to the humerus appeared hyperechoic with acoustic shadowing artefact. There was no area of muscle damage detected in this case. This was because no incision has been made on the muscle in the reduction procedure. The animal failed to return for reassessment and the follow up ultrasonographic examination was not carried out.

Figure 6.23.1 A ten year old male Lakeland Terrier with an oblique fracture of the left humerus which had been sustained following trauma of unknown origin three day previously.

Figure 6.23.2 Radiographs obtained immediately after fracture repair show the fracture reduced via a limited exposure and stabilised with an intramedullary pin and a simple type one external skeletal fixator. The fracture repair process is resulting in satisfactory reduction, and alignment. A small bone fragment is remaining, lying cranial to the humerus. The intramedullary pin does not lie sufficiently distally. **a**, lateral view, **b**, cranial view.

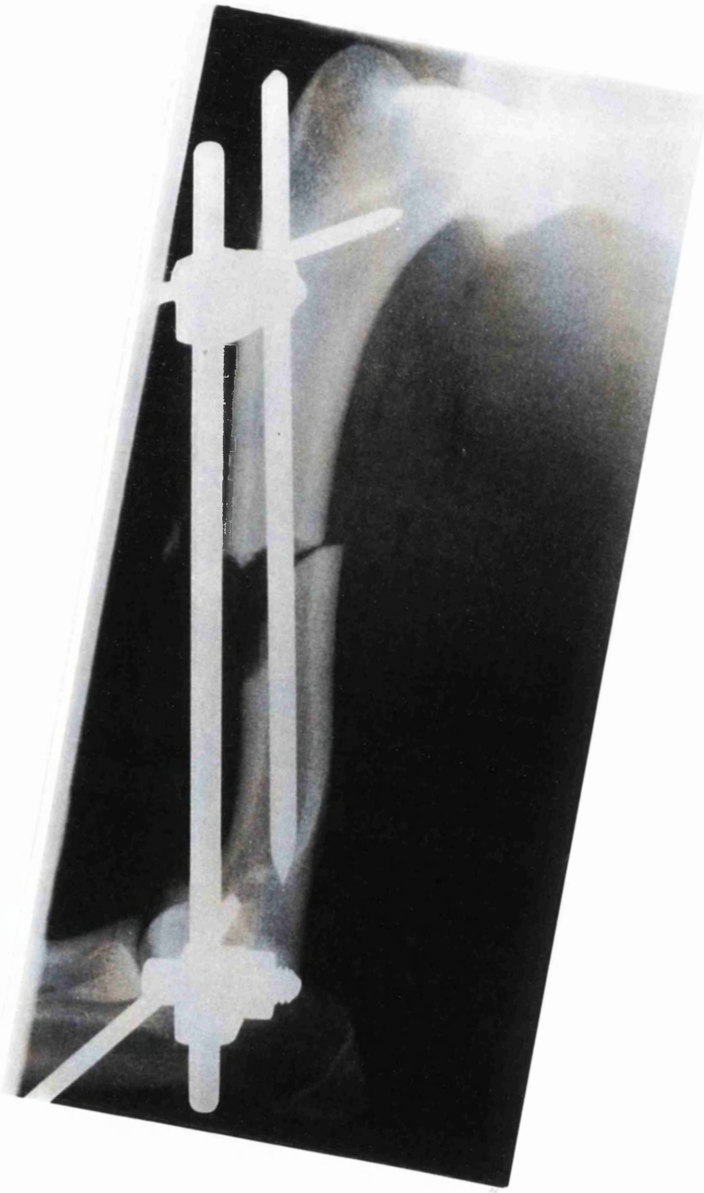

a

b

Figure 6.23.3 Longitudinal scan of the humerus from the cranial aspect on day three after fracture repair demonstrates the fracture site with the presence of a fracture gap. There is a well defined border of the bone fragment and no evidence of callus formation is detected. The hyperechoic appearance at the fracture site suggests soft tissue reaction and periosteal tissue reaction. Note also the small fragment above the humerus (arrow head) which appears hyperechoic.

Figure 6.23.4 Longitudinal scan of the humerus from caudal aspect on day three after fracture repair demonstrates the fracture site which appears hyperechoic with a small gap (arrow). Note that the bone fragments appear well aligned and there is no evidence of callus formation.

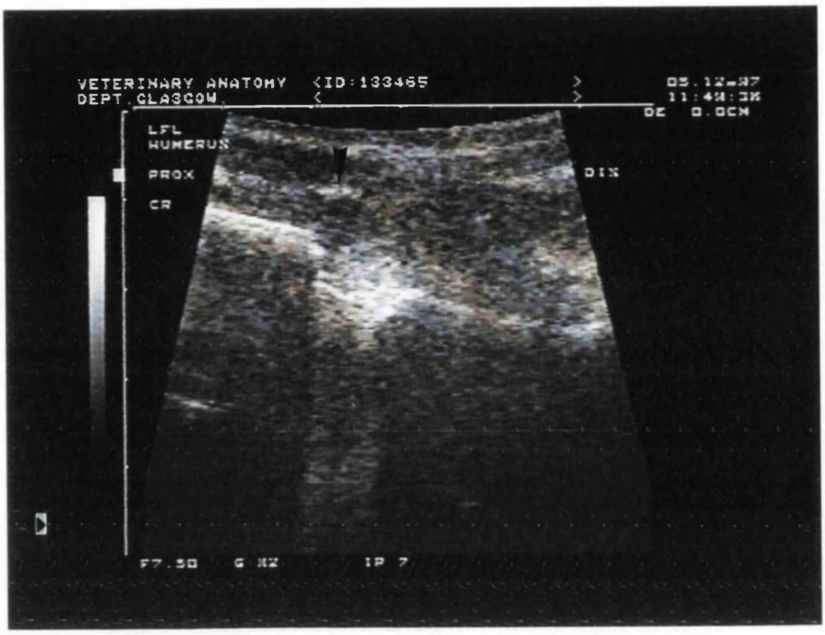

Figure 6.23.3

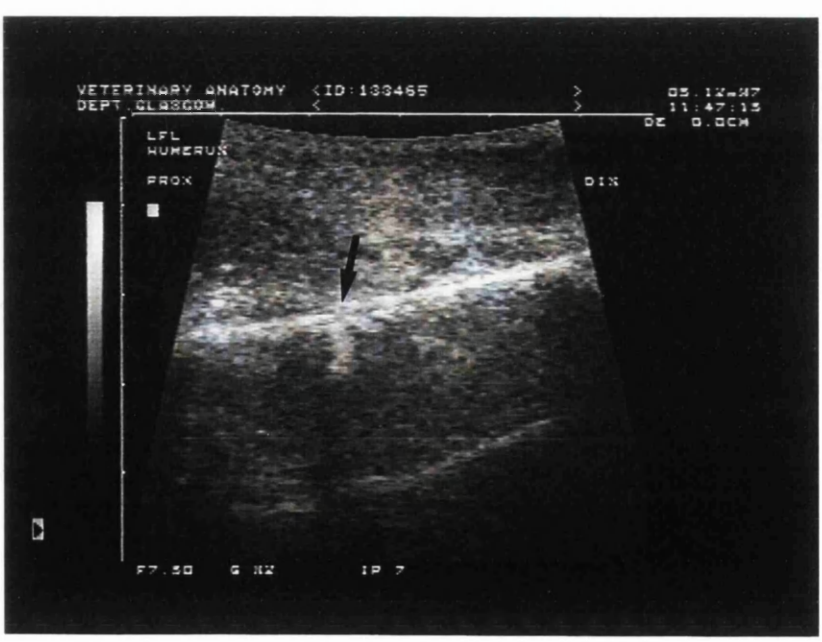

Figure 6.23.4

Figure 6.23.5 Transverse scans of the humerus at the fracture site area from cranial aspect on day three after fracture repair show the abnormal appearance of the humerus (**a**) as compared to the normal part (**b**). Note also that the small bone fragment lying cranial to the humerus (arrow head) appears hyperechoic with acoustic shadowing artefact (**a**). **H**, humerus.

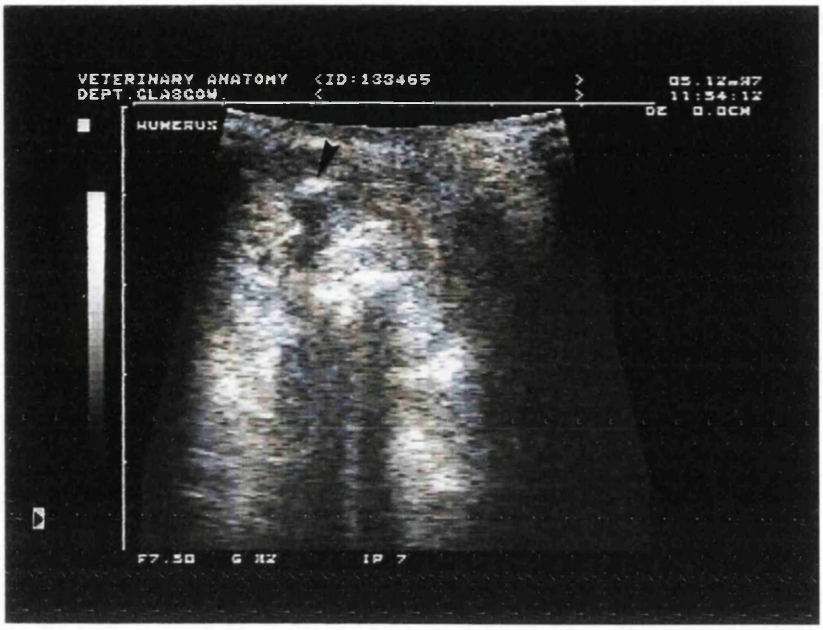

Figure 6.23.5a

Figure 6.23.5b

6.4 **Discussion**

The skeletal system has two primary functions: the first of which is to give support to the soft tissue which in turn maintains form and allows ambulation, the second is to act as a storehouse assisting in the maintenance of calcium homeostasis (Hermanson and Evans, 1993). From anthropology studies we know that bone will heal with little or no assistance, or at most just with rest and nonuse of the fractured part. This, however is not the approach that best serves the purpose of the individual with the fracture because it does not predicate that function will accompany the healing. Therefore, the basic thrust should be that the bone heal in such a way that function is not lost. Hence, the main objective of fracture repair is early return of the injured limb to full function.

The best characteristic of ultrasound scanning of the fracture site is its non-invasive biologic nature that allows repetitive evaluation of periosteal apposition. Ultrasound scanning is capable of recognising initial callus formation long before any sign of activity can be displayed by conventional radiographs (Ricciardy *et al.*, 1993). Thus, it will allow the orthopaedic surgeon to make better evaluation and, if the application is correct, earlier induction of the healing process. Quite often the ultrasonographic scanning shows initial callus formation, thus, this means that the mechanical stability of the bone fixator system is correct and the prognosis is favourable.

Almost all (91.7%) of the bone fractures encountered in the present study were caused by road traffic accidents. In other words, they were due to nonphysiologic forces, where the fracture occurred when the forces exceed the ultimate strength of the bone (DeYoung and Probst, 1993). The majority of the animals (58.3%) involved were less than 2 years of age when the fracture occurred. In one survey of bone fractures in dog and cat carried out by Philips (1979), road traffic accidents were found to be the main causes of fracture. He also reported that the majority of the fractures occurred in animals less than three years old. Thus, the results are in agreement with the present study although the group in this study were not a true random sample.

The majority of the fractures in the present study (60%) were comminuted due to the nonphysiologic forces. This is in contrast with the previous ultrasonographic studies of the bone fracture healing produced artificially (Derbyshire and Simpson, 1992; Eyres *et al.*, 1993; Hamanishi *et al.*, 1994) where none of the fractures produced in those studies were comminuted. The types of fracture were also different in the clinical cases compared to those in the experimental study which were produced artificially. There was less soft tissue trauma in the artificial fractures but rarely does a natural fracture occur at right angles to the long axis of the shaft. In two cases (case 12 and 27), a closed reduction of fracture repair was applied by using an intramedullary pin and an external fixator device. Therefore, there was no area of muscle damage or haematoma found during ultrasonographic examination.

The technique of scanning without removing the hair was applied in this study. This technique was first applied by Fornage *et al.* (1987) in the ultrasonographic evaluation of an ingested sewing needle which had migrated in the peripharyngeal soft tissue in dog. They used a great amount of paraffin oil as a coupling agent. In the present study, however, a large amount of gelling agent plus tap water was used instead. The area to be scanned was first damped with the water, and then a large amount of ultrasound gel was applied. This technique resulted in good ultrasound images up to a certain extent. The technique was found to be working well especially in the early days and up to approximately one months post-operation in the animals in this study, where the hair was still not yet fully grown. When the hair was fully grown, the use of tap water sometimes failed to help produce a good image especially in long haired animals. This might be due to the oily secretion produced on the skin surface which covered the hair, thus preventing the water and gelling agent reaching the skin surface. Thus, air entrapment occurred during ultrasonographic examination. The problem was also encountered in the animals with thick and coarse hair such as a Jack Russell Terrier. This caused air entrapment and consequently caused shadow artefact on ultrasound image. However, a combination of this technique with the technique of combing the hair to expose the skin surface before positioning the transducer helped minimise the problem. The latter technique was developed during ultrasonographic examination and was successfully applied in long haired animals.

The bone is a completely reflective target and it sends back to the transducer a very high amount of energy (Ricciardy *et al.*, 1993). Thus, when the sound beam is perpendicular to the bone long axis the ultrasonographic image of the normal long bone appears as a straight smooth hyperechoic line, with a complete shadow distally. Evaluation of the bone can only reveal the bone surface with moderate resolution of contour details Because of the physical properties of the bone tissue which has high acoustic impedance, the ultrasound beam cannot penetrate the bone. When the ultrasound beam passes through the body tissue, a portion of the beam is reflected back to the transducer. This reflection occurs at tissue interfaces of difference acoustic impedance. Because of large acoustic impedance between the soft tissue (muscle) and the bone, most of the sound beam is reflected back when it strikes the bone at right angle, i.e when the sound beam is perpendicular to the bone axis (Rantanen and Ewing, 1981). Thus, the bone appears hyperechoic and tissue interfaces deeper than the bone are hidden.

Any bone abnormality or a defect on the bone surface can be detected ultrasonographically as shown in this study. This supports the previous reports by Patten *et al.* (1992) and Kramer *et al.* (1997). Ultrasonographically, the internal bone structure cannot be evaluated, however, bone irregularities and defects of the cortical surface can be readily detected with high resolution, real time transducers (Patten *et al.*, 1992). Abnormal, irregular contours may represent reactive bone or fractures. The fractures, however, must usually have some degree of displacement before they are ultrasonographically recognisable (Craychee, 1995). In the present study, the fracture sites were easy to recognise ultrasonographically and appeared as discontinuity of the hyperechoic smooth bone surface especially when there was an obvious fracture gap present. When the fracture gap was insignificant, the fracture site appeared as an abnormality or a defect on the bone surface. The fracture sites, however, could still be recognised even when the bone was well apposed and aligned as a result of the repair process such as in cases 2, 3, 10 and 11. In case 10, the two main fragments were well united and aligned, and the fracture site was hardly seen on radiographs. Ultrasonographically, the fracture site was shown as a short hyperechoic vertical line across the bone with an insignificant fracture gap. Thus, the findings are in agreement with the previous studies and prove that ultrasonography is a reliable diagnostic tool in evaluation of the fracture site.

Ultrasonographic evaluation of the fractures of long bones could reveal the fracture site in several aspects (lateral, medial, cranial and caudal) without the need to change the animal's position. Thus, this allowed a multi-dimensional evaluation of the fracture site. For instance, in case 3, the fracture site imaged on the medial aspect of the femur appeared as a discontinuity of the bone surface indicating the presence of a fracture gap, but on the lateral aspect the fracture site appeared as a short vertical hyperechoic line with no significant gap present. The bone segments were well aligned and in good apposition on the lateral side. The short vertical hyperechoic line across the femur indicated the fracture site with the presence of some periosteal reaction. In another case (case 12), the fracture site was imaged on the cranial aspect as a discontinuity of the hyperechoic bone surface showing the presence of a fracture gap, while on the medial aspect no obvious fracture gap was seen. This could have been due to the comminuted fracture which resulted not in a straight border of the fractured bone segments as in simple fracture, and the presence of bone fragments at the fracture site. Therefore, the fracture site appeared to have good apposition on one side, but not for the other side. Thus, this enabled the ultrasonographers to evaluate the fracture site from several aspects and allowed them to have a clear idea about the nature of the fracture site.

Soft tissue damage such as haematoma, muscle tear, and muscle separation could be detected by real-time ultrasonographic imaging. Haematoma, however, was a common post-operative complication and was detected within the first few days after fracture repair. In the early stage, the haematoma appeared as an anechoic to hypoechoic structure and was relatively well circumscribed. With time, the haematoma gradually became more echogenic and textured. After several weeks, most of the haematoma had disappeared and the muscle had returned to its normal ultrasonographic appearance. Some areas of the haematomas became hyperechoic as occurred in case 15. This might have been due to the presence of residual fibrous tissue in the muscle. Although the ultrasonographic progression of haematomas is predictable, the rate at which these changes occur varies widely, and it may be difficult to determine the age of the haematoma accurately (Farrow, 1996). Haematomas have been found to have variable ultrasonographic appearances depending on the age, stage of development, location, and the frequency of the transducer (Wicks *et al*, 1978; Wisner *et al.*, 1995; Farrow, 1996). It may sometimes resemble an abscess or solid mass depending on the stage of the haematoma (Wicks, *et al.*, 1978), and may be well defined or have an irregular margin with or without internal septa (Craychee, 1995). Anderson, *et al.* (1984) have shown that the ultrasonographic appearance of a psoas haematoma varied from echopoor in non-organised haematoma to a more echogenic, complex appearance in an organised haematoma. Acutely, haematomas may appear as cystic lesions with a hypoechoic centre, and as they mature and organise, they may develop discrete septations and echogenicity may increase centrally (Wisner *et al.*, 1995).

Rupture of a blood vessel within the haematoma area is occasionally seen. In the present study it was demonstrated in case 1 and case 3. The ruptured blood vessel in case 1 was pulsating during examination. Van Holsbeeck and Introcaso, (1990) reported that haematoma formation is a hallmark of muscle rupture and occurs due to disruption of the blood vessels. A 'bell clapper' sign was detected on the top wall of the haematoma area in case 3 which was suggestive of muscle rupture or muscle tear. Previous researchers reported that fragments of torn muscle originating from the walls of the cavity can be identified within the haematoma which fills the gap. The torn muscle fragments are demonstrated ultrasonographically as free floating when gently pressure is applied, and this is referred to as the "bell clapper" sign (Fornage *et al.*, 1983; Harcke *et al.*, 1988). Thus, the findings were in accord with the previous studies.

Ultrasound artefacts are important criteria in recognising foreign material within muscle especially metal objects and fragments of bone as occurred in the present study. The bone plates, screws, intramedullary pins, kirschner wires and suture material were all imaged and recognised ultrasonographically with typical artefacts. Ultrasonographic examination also gave the possibility to define the number of screws, the localisation to surrounding tissue, loosening of screws and eventual associated inflammatory tissue swelling. A plate adhering to the bone appeared as a straight hyperechoic line and produced a reverberation artefact. This artefact is produced when the sound beam bounces back and forth between the transducer and the strong interface (Barr, 1990a). Normally, the reverberation echoes are most noticeable at higher gain setting and become less pronounced or disappear at low gain setting (Skolnick *et al.*, 1975). Reverberation artefact differs depending on the size, location, nature and number of reflectors encountered. For instance, comet tail artefact is produced by small, highly reflective interfaces such as metal objects or discrete gas bubbles (Ziskin *et al.,* 1982). This has been demonstrated in the present study. The intramedullary pin appeared hyperechoic and produced typical reverberation artefact when the sound beam hit the intramedullary pin perpendicularly on a longitudinal axis. When the sound beam hit the pin transversely, it appeared as a small hyperechoic area and produced intense comet tail artefact. Similarly, the cerclage wires appeared hyperechoic and produced comet tail artefacts due to their small size. A comet tail artefact is actually a trail of dense continuous echoes resulting from multiple internal reverberations within a small reflector such as gas or metal (Laing, 1983; Avruch and Cooperberg, 1985; Fornage and Schernberg, 1986; Penninck, 1995). Typically, the comet tail artefact tapers as the apparent distance from the transducer increases. Similarly, the brightness of the displayed echoes decreases. Comet tail artefact occurs when there is a large acoustic impedance mismatch between the reflector and the surrounding tissue (Thickman *et al.*, 1983; Ziskin *et al.*, 1982). The greater the acoustic impedance mismatch, and the broader and more perpendicular the interface between the object and surrounding tissues, the more intense the comet tail (Ziskin *et al.*, 1982). The screws used to fix the bone plate appeared as hyperechoic small round objects and produced comet tail artefact. When the bone was imaged on the opposite side of the bone plating (in case 20) the end of screw and its threads could be seen ultrasonographically.

Suture material within muscle in the present study was found to have an hyperechoic appearance on an ultrasonographic image with comet tail artefact produced distally. In certain circumstances, reverberation artefact is produced depending on the length of suture material hit by the ultrasound beam. Suture material appeared as a short hyperechoic line with reverberation artefact distally when the ultrasound beam hits perpendicular to the long axis (ie. when the fracture site was scanned transversely), and it appeared as intermittent hyperechoic lines with comet tail artefacts when only small portions of the suture material in a line were hit perpendicularly by the ultrasound beam, (ie. when the fracture site was scanned on a longitudinal plane) as in case 2 in the present study. However, suture material was only detected within the first one to two weeks of ultrasonographic examination as with time the suture materials were resolved by the body mechanism. Most of the suture material was resolved within 10 -14 days. Bone fragments within muscle imaged ultrasonographically, appeared hyperechoic with acoustic shadowing artefact distally. In case 2, a small bone fragment was imaged on ultrasound and appeared as a small hyperechoic area with acoustic shadowing artefact, but it was not demonstrated on radiographs. The sequestrum i.e. the dead bone fragment (in case 2), could also be detected ultrasonographically. It appeared as a small hyperechoic fragment surrounding by an hypoechoic area. The hypoechoic area was suggestive of a lysis process. Thus, the result suggests that ultrasound is more superior than plain radiography in detecting small bone fragments.

In case one, the two small bone fragments placed caudally adjacent to each other were imaged as one hyperechoic object with acoustic shadowing artefact on day one post-operation. On day two post-operation, they appeared as two hyperechoic areas adjacent to each other. On day one post-operation, because the two bone fragments were too close to each other so that the distance between the two adjacent fragments was less than the sound beam width, ultrasonography could not differentiate between them. Thus, they appeared as one object. On day two post-operation, the two bone fragments appeared as two different objects. This suggested that there might have been some movement involved. Thus, the distance between them increased and became larger than the sound beam width, and they appeared as two separate objects. This is referred to lateral resolution which is the ability to distinguished between the two echoforming surfaces lying adjacent to each other at right angles to the sound beam (Rantanen and Ewing, 1981).

The detection of foreign bodies in soft tissue is a common medical problem in humans (Anderson *et al.*, 1982). Occasionally, foreign bodies may not be detected for years until they are found during exploratory surgery for chronically draining wounds (Alfred and Jacobs, 1984). Experimental studies have shown that foreign bodies implanted in muscle are detectable by their acoustic shadows, although the objects themselves are not visible radiographically (Little *et al.*, 1986; Fornage and Schernberg, 1986). As suggested by Little *et al.* (1986) that the use of an high frequency transducer (7.5 or 10 MHz) could improve the definition of small foreign bodies, the present study found that with the 7.5 MHz transducer, the small foreign bodies (metal, bone fragments and suture materials) were imaged as well defined structures. Small bone fragments which were not visualised on radiographs were demonstrated in ultrasonographic examination (case 2). Thus, this result supports the previous findings. Its also proves that ultrasound is a useful non-invasive technique for the detection of foreign bodies especially bone fragments and metal objects.

Results of the present study showed that the fracture site of a long bone is better evaluated on a longitudinal scan than on a transverse scan. This is because the bone surface imaged on a longitudinal scan appears as a straight hyperechoic line. Thus, any defect or abnormality of the shaft of the long bone can be easily recognised as it will alter the normal image of the bone surface. Even when the fracture site is hardly visible on radiographs such as in case 11 due to a good alignment and apposition of the two fragments, ultrasonographic examination can still recognise the fracture site. The fracture site, however, is more easily recognised when there is a fracture gap present. It appears as discontinuity of the hyperechoic bone surface on a longitudinal scan. Conversely, on a transverse scan, the image of the exact fracture site is difficult to show on the monitor screen. This is true especially when a fracture gap is present. As the sound beam is thin, when the fracture site is scanned transversely, the beam passes through the gap between the two bone segments even though the space is narrow. Thus, the image revealed on a transverse scan is of muscle and not bony tissue. In addition, any bone deviation or angulation at the fracture site can not be detected on a transverse scan. However, it is possible to recognise the fracture site on transverse scan by comparing it with normal areas of the bone.

Initially, when the fracture occurs the small blood vessels traversing the bone in the area of the fracture are automatically severed, and a haematoma develops. The haematoma then undergoes organisation and is gradually replaced by granulation tissue. The granulation tissue develops into loose connective tissue. The fibroblasts at this time produce numerous collagenous fibres mostly parallel to the long axis of the bone and in this manner the fibrous (temporary) callus is formed (Vaughan, 1966). The time taken for the haematoma to become organised and replaced by granulation tissue varies, depends mostly on its size. Vaughan (1966) reported that it could be completed in 7 days or take as long as 30-60 days while Williams *et al.* (1989) reported that it occupies approximately three or four weeks. A soft tissue blastoma of soft callus develops around and between the fragments of bone, reducing their mobility. The soft callus contains proliferating osteoblasts, fibroblasts and osteochondroblasts, embedded in a matrix, rich in glycoproteins and collagen, into which new blood vessels grow (Williams *et al.*, 1989). The external soft callus is derived from the proliferation of osteoblasts in the osteogenic layer of the periosteum, while the internal soft callus is from endosteal cells. The enhanced proliferative activity of the osteogenic layer of the periosteum extends beyond the immediate fracture site, elevating the overlying fibrous component of the periosteum producing a soft external callus which unites the bone fragments from the fracture site (Williams *et al.*, 1989). The blood is supplied to the fracture site initially by the periosteum, but later in the regenerative process the normal centrifugal blood flow from endosteal circulation is re-established. The external and internal surface of the soft callus are electronegative throughout this process (Williams *et al.*, 1989). The external and internal soft callus are gradually converted into hard callus formation, mainly by endochondral ossification when intramembranous ossification initially predominates (Williams *et al.*, 1989). Both cellularity and vascularity continue to increase with the oxygen gradient is maintained. The pH of the matrix of the callus gradually increases to the neutral level during this phase (Williams *et al.*, 1989). There is no specific cell responsible for the deposition of bone. Any connective tissue cells of the periosteum, endosteum or marrow reticulum may differentiate into osteoblasts and produce spongy bone. The trabeculae of the spongy bone are formed in an irregular interwoven pattern and consequently this tissue is referred to as "woven bone" (Vaughan, 1966). The trabeculae of the immature bone of the primary bony callus are next removed by osteoclastic resorption and are replaced by adult, lamellar bone in which the lamellar are formed in a closed parallel arrangement (Vaughan, 1966). This stage commences at about three or four weeks after injury and continues until attainment of firm bony union, about two or three months later for most adult long bones in humans (Williams *et al.*, 1989). In the final phase of the reparative process the bone is remodelled by the resorption of excess callus until the original contour of the bone is re-established and the medullary cavity is re-canalised. This reconstruction is slow and may take many months. (Vaughan, 1966). This phase overlaps with the formation of hard callus. As a result of changes in vascularity, the oxygen supply to the fracture site returns to normal. Remodelling can be considered to be complete when the fracture site can no longer be identified either structurally or functionally (Williams *et al.*, 1989).

The soft tissue reaction was detected within 24 hours after fracture repair and appeared as an hyperechoic area surrounding the fracture site and screws when used. The periosteal tissue reaction was detected ultrasonographically as early as on day two after fracture repair and appeared as an hyperechoic area on the bone surface and around the fracture site. The soft callus that develops around and between the fragments of bone, helps to reduce their mobility. It has been reported that ultrasonography can provide an accurate indication of new bone production in the early stages of fracture healing and be able to indicate the rate of new bone production (Young *et al.*, 1990). There is also a direct correlation between changes in the amount of reflected echo and calcification of the external callus (Ricciardy, *et al.*, 1993). The increase of reflected echo and the appearance of acoustic shadow below the external callus is synchronous with an acceleration of the calcification process and indicates a good mechanical regain of the new bone formation (Ricciardy *et al.*, 1993). The decrease of reflected echo, the disappearance of acoustic shadow below the external callus, and the reappearance of longitudinal artefacts are synchronous with the loss of volume of the periosteal callus (Ricciardy *et al.*, 1993). This is due to reorganisation of good calcified new bone that has regained mechanical stability. Periosteal callus development and organisation have a variable morphology in relation to the fracture site and location, age of patient, reduction technique, and method of osteosynthesis (Ricciardy *et al.*, 1993). In the present study, the initial bone tissue production (soft callus formation) was detected as early as on day 3 after fracture repair (cases 3, 9 and 20). The soft callus imaged ultrasonographically appeared as an inhomogenous hyperechoic structure adherent to the bone surface. No shadow (artefact) was produced by the soft callus in the early stage of soft callus formation. The bone surface underneath it could still be visualised as an hyperechoic line. This was because the ultrasound beam could penetrate the early formation of soft callus which was actually the collagenous osteogenic blastoma. When the calcification process accelerated, the soft callus become mature and appeared hyperechoic with acoustic shadowing artefact distally. The bone surface underneath was no longer visible due to shadow artefact. Thus, only the rough surface of the mature callus could be seen. Mature callus has been demonstrated as an irregular separate growth with distal acoustic shadowing (Kramer *et al.*, 1997). Physically, mature callus has the same characteristic as bony tissue, therefore, only the surface can be imaged.

Previous researchers have reported that the repair process starts some distance away from the end of the fracture fragments at a point where the circulation is intact (Vaughan, 1966; Buttler, 1975; Braden and Brinker, 1976; Buttler, 1985; Harris, 1990). Similarly, in this study the callus formation was found to develop at some distance away from the fracture site. Beside the poor circulation at the fracture site, the end of the broken bone fragments are in fact a dead bone tissue. This has been shown previously by the evidence of empty osteocyte lacunae which extend for a variable distance away from the fracture site (McKibbin, 1978). Therefore, it was not participating in the proliferative activity of the bone.

The extent of callus formation in bone fracture healing is however, dependent on the rigidity of the fracture fixation. The callus formation is inversely proportional to the fracture rigidity. The increase of callus formation, however, stops when the tissue is capable of resisting motion. Fracture healing needs an adequate blood supply, and if the blood supply has been compromised as a result of injury, fracture healing will be delayed (Ackerman and Silverman, 1978). The rate at which a fracture heals depends upon the animal's age, general health and nutrition, the blood supply to the bone, and the stability of the fragments (Burk and Ackerman, 1996). Therefore, fractures in young, growing animals, in areas with a rich blood supply, and those that are rigidly immobilised heal more rapidly (Burk and Ackerman, 1996). In aged animals healing is slower and clinical union may take longer (8-16 weeks) (Vaughan, 1966). In a condition where the fragments are impacted, union is more rapid compared to the one with a gap between them. However, the healing rate is also subject to individual variation since fractures identical in position and type do not necessarily heal in the same time (Vaughan, 1966).

All of the fractures in the present series of study healed via a secondary healing process where callus formation was predominant. On follow up examination the amount of callus formation was found to be variable depending largely on rigidity of the fracture site. In many cases, the amount of callus formation was abundant either at the fracture site or at a distance from the fracture site. This suggested that some movement may have been involved. This was true especially when the fractures were comminuted where rigid fracture stability was difficult to maintain even when bone plating was applied. The presence of more than two bone fragments and gaps between the bone segments in comminuted fractures enhanced the possibility of fracture movement. Hence, it increased the amount of callus formation. Other possibilities might also occur including rotational instability for the fracture treated with intramedullary pinning and periosteal trauma at the time of injury or surgery. This is in accord with the previous studies who demonstrated that the amount of callus is indirectly proportional to stability (Braden and Brinker, 1976; Aro and Chao, 1993).

In a recent experimental study of fracture healing produced artificially in sheep, the typical course of secondary fracture healing was seen (Claes *et al.*, 1997). They reported that the gap size had a significant influence on the amount of periosteal callus formation. A 2 mm gap produced large callus formation even when interfragmentary movement was involved, but a gap as large as 6 mm produced the small callus formation and the fracture healing was delayed. Thus, they conclude that interfragmentary movement did not show a significant influence on new bone formation. In contrast, Braden and Brinker, (1976) have shown that movement at the fracture site has an important role in the amount of callus formation. In another study, Aro and Chao, (1993) stated that the two most significant factors in promoting periosteal callus formation were the amount of physiologic loading as dictated by the body weight and the presence of a significant fracture gap. In the present study, it is believed that the amount of callus formation was directly proportional to the interfragmentary movement. The evidence of pins and screws loosening detected radiographically, in the cases where the callus was abundant also strongly suggests some movement had been involved. However, the size of the fracture gaps were small in cases where there was excessive callus formation. In case 18 where the fracture gap was large, the ultrasonographic examination found no excessive callus formation and the healing process was delayed. Thus, it is in agreement with previous studies.

In case 17, despite the large fracture gap which was not bridged by the bony callus, clinically the animal was already bearing weight on the fractured limb by day 66 post-operation. Radiographically, there was a piece of bone fragment on the medial aspect of the fracture site in the femur which was not yet fully bridged by mature callus. The line between the bone fragment and the femur was still visible. Ultrasonographically, the fracture gap was clearly shown. However, the bone fragment on the medial aspect had already coalesced with the main bone segment. Thus, it is believed that the union had occurred through the bone fragment and with the addition of the intramedullary pin the fractured limb could support the body weight.

Bone plates have been reported as the most stable fixation devices available to the orthopaedic surgeon (Braden and Brinker, 1976). Bone plating provides an environment which is considered to be ideal as a pre-requisite for primary bone healing (Chawla *et al.*, 1983). When the fracture gap is decreased, the healing process is facilitated (Aro and Chao, 1993; Noordeen *et al.,* 1995). Therefore, when fixation is performed correctly with bone plates, the fracture site does not need any further stabilising, e.g., via abundant external callus. Almost immediately endothelial buds start crossing the fracture gap minimising the callus developing. This has been shown in the present study (case 10), where the fracture had been reduced with a bone plate and screws and resulted in a good alignment and fragment apposition. The healing process resulted in minimal callus formation. However, this might only happen in a simple fracture.

In a comminuted fracture, stable rigidity of the fracture site is difficult to achieve, thus, resulting in an excessive callus formation.

If the alignment of the bone fragments is anatomically accurate and is maintained by good fixation, the remodelling process will eventually change the bone at the fracture site so that it becomes difficult to recognise where the fracture occurred (Buttler, 1975). On the other hand if mal-alignment of the fracture fragments during the fixation process occurs, the remodelling process will eventually contour the bone at the fracture site in such a way as to produce a smooth contour best adapted to unite the mal-aligned fragments. Even after a longer period of time, the bone will eventually shape to the best conformation to support the load that it is carrying (Buttler, 1975). Ultrasonographically, mature callus appears as bone. There are no irregular borders and uneven surfaces.

The level of blood supply at the fracture site during the healing process is a vital factor. In a dog with a displaced fracture, the medulla is the site of the first osseous union (Rhinelander *et al.*, 1968). In the displaced fracture, the main medullary artery had been ruptured at the time of injury. Here the periosteal circulation appears to have the principle role in the earliest stage of healing. The enhanced periosteal circulation appears to be the chief early source of blood to the healing area in that it supplies the external callus, which starts at once to bridge the gap. The disrupted medullary circulation proliferates in both bone fragments but it is at first blocked by the central haematoma. Within three weeks medullary vessels have bridged the fracture gap in the presence of stable reduction of the fragments. The medullary circulation provides all the additional blood to the cortex which increases in porosity with penetration by more larger arterioles. This same circulation consistently supplies blood to the areas of earliest osseous union while periosteal callus remains interrupted by fibrocartilage. After six weeks arterioles derived from the medulla supply most of the blood even to the external callus. At twenty weeks, the periosteal circulation reverts to its normal resting functions of vascularizing the external cortical layer and forms anastomoses with medullary vessels which are still mildly increased in size and number presumably to support the residual bone remodelling. It is apparent, therefore, that over the full course of bone repair, the endosteal blood supply overshadows the periosteal (Rhinelander *et al.*, 1968).

Observations made by Eyres *et al.* (1993) in recent years revealed that with ultrasonography, the changes in the medullary region of the bone after cortication had occurred were unable to be detected even when using a frequency probe of 5 MHz. This contrasts with the experience of Maffuli *et al.* (1992), who used a 5 MHz longitudinal ultrasound transducer. They reported that cortication of the new segment occurred within seven weeks and that a medullary canal could be detected shortly thereafter. Their finding suggested that ultrasonography could determine the time of fixator removal, but Eyres *et al.* (1993) found that the presence of an hyper-reflecting solid line did not indicate full mineralization of the regenerated callus and was not associated with 'cortication' or medullary differentiation. Both the above studies had been done on experimental studies of fracture healing produced artificially. There was no comminuted fracture being produced in these studies, therefore, the observation of the medulla region was not impossible with high frequency transducer as reported by Maffuli *et al.* (1992). However, in the present clinical case study, where the fractures were comminuted with irregular borders and the fracture gaps varied widely as well as with different types of fracture reduction devices, the observation of the medullary region was almost impossible. Even with the transducer of 7.5 MHz, the medullary region was not able to be observed in this study.

A well defined hypoechoic area with acoustic enhancement artefact distally was detected at the fracture site in case 2 at 48 hours after fracture repair. This hypoechoic area was found to be enlarged on the next day of ultrasonographic examination. This well defined hypoechoic area which had developed at the fracture site was suggestive of a cystic structure. Areas of decreased echogenicity in the fracture gap have been demonstrated in previous studies (Young *et al.*, 1990; Derbyshire and Simpson, 1992) in the Ilizarov lengthening of the limb in humans. The technique pioneered in Russia by Ilizarov involves stabilising the limb with an external fixation frame and dividing the bone. After a post-operative period of 5-14 days, controlled distraction of the bone is produced by the external frame usually at a rate of 1 mm per day (Derbyshire and Simpson, 1992). The distraction is continued until the required length is achieved, and then a period of consolidation allows the new bone to strengthen (Derbyshire and Simpsom, 1992). Young *et al.* (1989) aspirated these hypoechoic areas and found them to be fluid-filled cysts, the aspiration of which they felt improved osteogenesis. In the study of Derbyshire and Simpson (1992), they found that the smaller cysts disappeared by stopping or reversing distraction for one week. However, in the present study, the hypoechoic area had disappeared when scanned on day 42 after fracture repair. Thus, fluid accumulation at the fracture site is believed to resolve itself with time.

Radiography is still regarded as an important diagnostic tool in the evaluation of bone fracture healing especially to evaluate the axial deviation or angulation of the fractured bone. However, it has a limited value in providing evidence of union in the early stage of fracture healing. The reason for this is that primary bony callus is composed of immature bone and its mineral content is so low that it is radiolucent (Vaughan, 1966). At the time when the dog is beginning to regain use of the limb, radiographically there is little or no evidence of an anchoring callus and the fracture line is wide and distinct (Vaughan, 1966). It is not until the formation of secondary bony callus begins that the callus is visible radiographically and from this time the healing process can be followed on x-ray to its completion. Radiographic evidence of union is only acceptable on x-rays taken in two planes when there is a complete external callus bridging the fragments or when callus between the fragments is calcified to a density equal to that of normal bone (Vaughan, 1966).

The main disadvantage of the ultrasonographic method was the fact that the extent of bone fracture or injury could not be assessed from the ultrasonographic picture. This has been shown earlier by Hendrich and co-workers (1995) who reported that the extent of the dislocation in a series of sternal fractures with a displacement of more than one anterior posterior thickness in the human could not be assessed from the ultrasonographic picture. Similarly, in the present study the angulation of the fragments and the deviation such as in the bone plate breakdown in case one could not be evaluated from the ultrasonographic picture. This was mainly due to the small field of view of the ultrasonographic image.

The soft tissue reaction around the screws could be detected by ultrasound within 24 to 48 hours after fracture repair as shown in case 3 and case 11, but not with the plain radiographs. Ultrasonographically, it appeared as a disorganised hyperechoic area surrounding the screws. It has been reported that movement around screws, used for internal fixation of fracture either alone or in combination with plates can occur as long as union of the fragments has not taken place (Uhthoff and Germain, 1977). The loosening and bending of plates were also common post-operative complications in fractures stabilised with bone plates and screws, which might be due to strain and stress imposed on the plate because of struggling of the animals (Chawla *et al.*, 1983). Thus, fractures treated with bone plates should not be subjected to excessive stresses, before union of the fracture has occurred. It has also been reported that the threads of freshly inserted screws are not in intimate contact with the surrounding compact bone (Uhthoff, 1973). In fact, only the load bearing surface of the screw thread was closely apposed to the bone whereas all of its other surfaces were separated from the bone by a gap measuring up to 150μm in width. This gap was invaded by undifferentiated migrating cells. In the absence of movement, the undifferentiated cells developed osteogenic potencies, ultimately leading to a solid incorporation of the screw by bone. On the other hand, movement led to their differentiation into osteoclasts and fibroblasts resulting in the formation of a fibrous collar around the screw and, with time, terminating in a loss of holding power (Uhthoff and Germain, 1977). The holding power of the screws is not finally determined at the moment of their insertion nor after cellular differentiation has occurred around the screws. Local mechanical conditions throughout the period of fracture consolidation are of equal importance. Removal of screws and pins penetrating the cortex leaves defects in the bone such as in case 12 when the external fixator pin was removed, and in case 6 when the screws were removed. Ultrasonographically, there was a defect on the bone surface which appeared as a hole with the presence of periosteal and soft tissue reaction around it.

The ultrasonographic appearance of muscle damage after surgery either due to trauma during accident or during the surgery was characteristically the same. Both types produced disorganised hypoechoic areas relative to the surrounding normal appearance of muscle. These areas gradually became smaller and eventually disappeared as the muscle healing progressed. In most cases the muscle healing progressed so that it had restored the normal ultrasonographic appearance indicating that the muscle had returned to its normal anatomical structure. This is in agreement with Carlson and Faulkner, (1983) who have reported that the muscle structure has a capability to regenerate new fibres. However, in case 16 , the area of muscle damage had become hyperechoic in appearance on day 17 after the surgery. This suggests that the damaged muscle tissue had been replaced by fibrous tissue which appeared hyperechoic on ultrasonography. Histologically, when muscle tissue is extensively damaged, it will be replaced by fibrous tissue.

Repair of injured skeletal muscle comprises of regeneration of disrupted muscle fibres and simultaneous production of connective tissue with capillaries sprouting from the borders of the injured area (Albrook *et al.*, 1966). According to the result of a previous study by Lehto and Alanen (1987), it seems clear that in the early phases of healing of a muscle rupture, ultrasonography is of considerable help in the evaluation of the severity of the injury. It can also be considered highly reliable, as it exhibits an outcome analogous to the histological examination of the injured area of muscle rupture especially during the first week following injury. Later on, as healing progresses and the amount of scar tissue decreases together with improving orientation of regenerating muscle fibres, it becomes more difficult to differentiate between normal and healing muscular tissue.

In one cat with a femoral fracture (case 10) extensive muscle damage caudo-lateral to the femur was detected by ultrasonography within 24 hours after the surgery. The area of muscle damage was not visualised on radiographs. The extensive muscle damage was believed to be due to the accident rather than the surgery. A follow up examination on day two post-operation showed that the area of muscle damage had became slightly smaller than on day one and appeared more echogenic. On day 44 post-operation, the area of muscle damage appeared hyperechoic relative to the surrounding tissue which was suggestive of the deposition of fibrous tissue. Clinically the thigh muscle was atrophied as it became smaller in size. Ultrasonographically, the distance between the femur and the skin surface was reduced. However, the muscle had a relatively normal ultrasonographic appearance.

Muscle atrophy was a common post-operation complication in the present study. Muscle atrophy has been defined as reduction in muscle fibre diameter or cross sectional area (Hulland, 1993). Within the first few days after surgery the muscle mass of the affected leg becomes enlarged which is most commonly due to swelling in the inflammatory stage. This can be determined by measuring the distance from the skin surface to the bone surface. After a few weeks of a resting period, ultrasonographic examination found the muscle mass measured from the skin surface to the bone surface had became smaller. Clinically, muscle atrophy was readily detected because the muscle mass had become smaller. This might be due to lack of use of the leg for quite some time. The ultrasonographic appearance of atrophic muscle was similar in echogenicity to normal muscle. This is an accord with Farrow (1996) who reported that although the atrophic muscle has reduced in volume, the affected muscle is otherwise indistinguishable ultrasonographically from the normal one.

Time required for healing of muscle rupture was proportional to the extent of injury and related to the location of the lesion. Muscle has a tremendous capacity for regeneration (Bullough and Vigorita, 1984). If the sarcolemmal sheaths are intact, complete regeneration of normal muscle structure will occur by regeneration of myocytes. In gross muscle ruptures, regeneration occurs by growth of undamaged muscle fibres at the wound margin and formation of new fibres. These new fibres are formed by recruiting reserve cells found in the endomysium (Bullough and Vigorita, 1984). Formation of scar tissue will inhibit the process of regeneration.

The results of this study show that the healing progress of the bone fracture and muscle injury after orthopaedic surgery could be evaluated ultrasonographically. Ultrasonography can easily recognise and detect the fracture sites of long bones as well as pelvic bones and usually this is demonstrated by the discontinuity of the bone surface. Quite often there is a gap present at the fracture site in between the two bone fragments. Soft tissue injury around the bone nearby the fracture site whether due to the trauma at the time of fracture or due to surgery can also be ascertained.

CHAPTER 7

GENERAL DISCUSSION

The current study was planned and carried out with the main objective of evaluating the potential use of the high resolution B-mode real-time ultrasound connected with a high frequency (7.5 MHz) transducer in the assessment of musculoskeletal injuries concentrating on muscle damage due to surgical operation and bone fracture repair. The ultrasonographic study of mammary gland tissue was also carried out to evaluated the use of B-mode real- time ultrasonographic imaging using a 7.5 MHz frequency transducer in detecting mammary tumour tissue and its spread into the regional lymph nodes in a small population of bitches (n=28). The present study also emphasised the importance of a high frequency (7.5 MHz) ultrasound transducer in evaluating the progression of bone repair in small animals. The high resolving power of the 7.5 MHz transducer helped to image the soft tissues and bone with considerable detail of the structures.

It was apparent from the literature that a considerable amount of information regarding muscle and bone damage had been reported in humans and large animals. However, only a limited amount of information has been published with regard to ultrasonographic imaging of this area in small animals. Real time ultrasound is very easy to use because the transducer is hand held and ultrasonographic sections can be readily obtained in all directions. High frame rates made the interpretation of the real-time images easier. It takes only a few minutes to examine and evaluate individual lesions. Detected masses can be better appreciated in three dimensions by real-time imaging, because changes can be observed between successive imaging planes. Furthermore, ultrasound equipment is relatively inexpensive and widely available, technically easy to service, and examinations may be readily performed without the need for specialised accommodation.

A comparison was made between 3.5 MHz convex linear and 7.5 MHz linear array transducers in the early study in evaluation of the thigh muscle in normal greyhound cadavers. It was obvious that the linear array transducer of 7.5 MHz frequency produced better images with higher resolution and finer detail of structures compared to the 3.5 MHz convex linear transducer.

Ultrasound would appear to be an excellent modality in imaging of normal muscle structure and muscle damage in small animals. Normal muscle appeared to have similar ultrasonographic characteristics in all healthy animals. Good detail of muscle could be visualised with an high frequency transducer and the detail of the muscle structure could be highlighted including the connective tissue fascia surrounding the muscle fibre, the endomysium. The muscle fibre orientation could be shown in transverse and longitudinal scans along the fibres' axis. Normal skeletal muscle imaged on ultrasound appeared as an homogenously hypoechoic structure with fine echoes scattered throughout the muscle parenchyma. Each muscle group could be well defined, separated by a thin hyperechoic structure which was actually the connective tissue fascia. In longitudinal image, the muscle appeared as homogenously fine parallel echoes scattered throughout the hypoechoic muscle parenchyma. In damaged muscle, the muscle structure had lost its normal ultrasonographic characteristics and appeared on ultrasound as a disorganised hypoechoic structure relative to the normal tissue.

In evaluation of old surgical sites in female cadavers ultrasound successfully determined whether the animals had had an earlier operation on the ventral abdominal midline (VAM). Ultrasound could also differentiate between the normal VAM, the VAM with a new incision site and the VAM with an old incision site. However, it could not determine the age of the surgical site exactly. The normal ventral abdominal midline (VAM) imaged ultrasonographically appeared isoechoic relative to the muscle tissue and there was no altered echogenicity along the VAM. The ventral abdominal midline with a new incision site appeared as a disorganised area with ill-defined margins which was hypoechoic relative to the surrounding tissues and this corresponded to the area of high inflammatory cells on histological section. The old surgical site at the VAM was found to have variable appearances from hypoechoic to hyperechoic and this was found to depend on the presence of fat lobules around the scar tissue and on how extensive the scar tissue was. The scar tissue with the presence of high fat lobules appeared hypoechoic on ultrasound, while the incision site with virtually no fat lobules and with extensive scar tissue appeared hyperechoic on ultrasound. This is in agreement with Laine *et al.* (1985) who reported that the scar tissue in older injuries had an echogenic appearance on ultrasound. The subcutaneous tissue imaged ultrasonographically varied in appearance from hypoechoic to hyperechoic relative to the surrounding muscle tissue. Thus, it was apparent that ultrasound could be used to determine whether the animals had had an earlier operation or were intact.

The progress of wound healing could be successfully monitored ultrasonographically using a 7.5 MHz frequency transducer as shown in this study. Early complications in the wound healing process could be detected within 24 hours after operation. Fluid accumulation within the subcutaneous tissue could be detected within 24 hours post-operation appearing anechoic to hypoechoic with acoustic shadowing artefact depending on the content of the fluid. Fluid collections in the subcutaneous tissue or muscle have similar ultrasonograpic characteristic as those elsewhere in the body. Ultrasound could show that the wound (surgical site) was successfully closed and the edges of the linea alba were well apposed. The formation of fibrous tissue at the surgical site could be seen ultrasonographically and appeared as an hypoechoic structure with acoustic shadowing artefact at the early stage, and later with time it appeared as an ill-defined hypoechoic area with an echogenic centre and casting an acoustic shadowing artefact. When the fibrous tissue matured the surgical site appeared as a disorganised hyperechoic area with acoustic shadowing artefact.

The development of a haematoma and fibrous scar tissue could be followed by ultrasonography, but it was not possible to determine the point of time after injury with complete accuracy. Nevertheless, ultrasonography could be a method of great value in the diagnosis of muscle injuries and, within certain limits, in the follow-up of the healing process.

Ultrasonography could detect muscle tissue damage after surgery and appeared to have successfully monitored the healing process. Ultrasonographic appearance of muscle damage was almost consistent in all cases. The area of muscle damage lost its normal ultrasonographic pattern and appeared as a disorganised hypoechoic structure. In certain circumstances, small anechoic areas representing fluid, and hyperechoic structures suggestive of fasciae rupture were also seen in extensive muscle damage. Muscle tissue has a capability of regenerating itself and returning to its normal ultrasonographic characteristics. However, in extensive muscle damage, muscle tissue is incapable of regenerating itself totally, resulting in formation of fibrous tissue appearing hyperechoic on ultrasound. Thus, ultrasound would appear to have a bright future in the detection of muscle damage and its healing process in small animals.

A major problem in the diagnosis of muscle injuries is the accurate determination of the extent and stage of the healing process. Apart from the difficulty of determining the size of the injuries, another problem is the interpretation of the ultrasonographical results during the process of healing after muscle injury. This is an accord with Kullmer *et al.*, (1997). Ultrasonography of muscle injuries provides much additional information. The determination of the size of the injury is possible but not very precise. However, interpretation of the ultrasonography should be made carefully.

The most exciting part in this study which is also the major portion is the ability of ultrasound with a 7.5 MHz transducer in monitoring the fracture repair process. With ultrasound, the repair process of the bone fracture could be successfully monitored without any risk of exposure to radiation of the animal. Furthermore, complication of the fracture repair could be detected at an early stage with ultrasound and the result was immediate. Haematoma formation at the fracture site could be detected within 24 hours after operation and its resolution could be successfully monitored. Suture material within the muscle appeared as hyperechoic material with comet tail artefact as shown in figures 6.2.5 and 6.4.5. However, the suture material located near to the skin surface (within the subcutaneous tissue) appeared hyperechoic with acoustic shadowing artefact as shown in figures 4.10 and 6.1.5. To understand this, the principle of ultrasound needs to be reviewed. The ultrasound transducer has a focal zone which is the part of the ultrasound beam where it is focusing, and consequently image resolution is optimal (Barr, 1990a). In the near field of the sound beam, the Fresnel zone, complex diffraction patterns may occur. Beyond the focal zone, the Fraunhefer zone, the beam begins to diverge rapidly and resolution diminishes (Barr, 1990a). Thus, when the suture material is located within the focal zone it appears hyperechoic with comet tail artefact. But when the suture material is located near to the skin (within the Fresnel zone) it appears hyperechoic with acoustic shadowing artefact. However, in both situations they appear hyperechoic. In a study by Trout *et al.* (1994) suture material within muscle has been found to have an hyperechoic appearance with reverberation artefact (comet tail artefact) and in another study by Wilson *et al.* (1989) suture material used to closed the linea alba was found to have an hyperechoic appearance with acoustic shadowing artefact. Thus, the suture material within the body appeared hyperechoic with acoustic shadowing artefact or with reverberation (comet tail) artefact depending how deep it was located in the muscle. This is an accord with the findings in this study.

The fracture site imaged longitudinally with ultrasound appeared as a discontinuity of the smooth bone surface especially when there was a fracture gap present. Any fragments of bone placed in the muscle could be detected ultrasonographically and appeared as hyperechoic structures with acoustic shadowing artefact, even when some of them were so small as to be invisible on radiographs. The ultrasonographic finding of bone chips in muscle was consistent. The fixator devices used in bone repair to fix the fracture site, bone plates with screws, intramedullary pins, lag screws and Kirschner wires were all visible ultrasonographically. All the metal objects appeared hyperechoic on ultrasound, casting reverberation artefact when large portions of the objects were struck by the sound beam. Conversely, when a small portion of a metal object was struck by the sound beam a comet tail artefact was produced.

The early formation of callus (soft callus) could be detected ultrasonographically and appeared as a disorganised hyperechoic structure with no artefact produced. However, it was invisible radiographically. Hence the progression of fracture repair could be monitored more efficiently with ultrasound than with radiography at the early stage of the healing process. The periosteal reaction can be seen as an hyperechoic structure on the bone surface at the fracture site and the surrounding area. Any obliquity of the bone at the fracture site could be detected by ultrasound. Ultrasound could also tell whether the fragments were well apposed without any gap present or conversely, image fragments with the presence of a fracture gap. Furthermore, it could also tell whether the bone fragments were well aligned or exhibited some obliquity. Ultrasound has the possibility to predict whether the repair process is proceeding well and the healing could be expected to be quick or conversely whether the repair process could be delayed. It could also tell whether there was some movement involved at the fracture site. In certain circumstances where the fragments were not well aligned and/or with the presence of a significant fracture gap, there was a tendency for movement to occur at the fracture site. In these cases, initial haemorrhage followed by excessive callus formation could be detected at the fracture site and in the surrounding area and the healing process would be expected to take longer. Thus, the presence of excessive callus formation with a longer period of healing process was suggestive that there was some movement involved during the repair process. In one case (case 20), the first fracture repair with an external fixator device alone failed. In this case ultrasound could predict from the early stage that movement was involved when the fragments were not aligned and the presence of large gap between them was evident on ultrasound. Also no well defined callus formation at the fracture site could be detected up to day 25 post-operation. It was later confirmed by radiography on day 33 post-operation, and the second repair was carried out using a bone plate. The fracture site then satisfactorily healed. In cases where the fracture site was well aligned and rigid, the healing process was rapid with minimal callus formation detected at the fracture site. With ultrasound, a three dimensional image of the fracture site could also be developed, thus the fracture site could be better evaluated. With radiography, imaging is usually only carried out in two planes and the area deep to the metal device cannot be investigated.

Ultrasound was successfully used in detecting mammary tumour tissue and its spread to the regional lymph nodes in a group of bitches. Ultrasound also proved to be more accurate than manual palpation in detection of mammary tumour tissue. The ultrasonographic appearance of mammary tumour tissue was variable depending on its size and its severity. Small areas of mammary tumour tissue appeared as ill-defined hypoechoic structures with acoustic enhancement artefact, and the larger areas of mammary tumour tissue appeared hyperechoic, sometimes with the presence of cysts. They always cast acoustic enhancement artefact. The spread of tumour tissue among the mammary glands was successfully detected by ultrasound, and ultrasound did not miss any tumour lesion of the mammary gland. The involvement of the regional lymph nodes (axillary and superficial inguinal lymph nodes) was also successfully detected by ultrasound. The enlarged lymph nodes was easily detected by ultrasound as they increased in size and their echogenicity altered. However, ultrasound could not truly determine whether the enlarged abnormal lymph nodes were due to metastatic spread of tumour tissue or due to the inflammatory process. A biopsy needed to be done for this type of confirmation. However, there was a suggestive pattern where the enlarged lymph nodes had an echogenic appearance on the first scan and on the rescan the echogenicity had not changed but the size had increased. This was suggestive of metastatic spread of tumour tissue into the lymph nodes. Ultrasonography would appear to offer potential to become a routine procedure in mammary tumour tissue detection in small animals in the future.

Because ultrasonographic examinations are rapid noninvasive, and without known-risk to the patient, they are fast becoming a common diagnostic tool. Further experience with high resolution ultrasound scanners will surely identify areas where ultrasonography can be considered to be a primary imaging technique for diagnostic purposes.

Bibliography

Ackerman, N. and **Silverman, S.** (1978). Fracture healing. *Modern Veterinary Practice* **59**:381-385

Adams, R.D. (1975). Diseases of muscle: a study in pathology. 3rd ed. Hagerstown London: Harper and Row, Medical Department.

Adams, D.R. (1986). Canine anatomy: A systemic study. The Iowa State University Press.

Akahoshi, K., Misawa, T., Fujishima, H., Chijiiwa, Y. and **Nawata, H.** (1992). Regional lymph node metastasis in gastric cancer: Evaluation with endoscopic ultrasound. *Radiology* **182**:559-5640

Alcantara, P.J. and **Stead, A.C.** (1975). Fractures of the distal femur in the dog and cat. *Journal of Small Animal Practice* **16**:649-659

Alexander, J.W. (1985). Leonard's Orthopaedic Surgery of the Dog and Cat. 3rd Ed. W.B. Saunder, Philadelphia London.

Alfred, R.H. and **Jacobs, R.** (1984). Occult foreign bodies of the foot. *Foot and Ankle* **4**:209-234

Albrook, D., Baker, W. and **Kirkaldy-Willis, W.** (1966). Muscle regeneration in experimental animals and in man. *Journal of Bone and Joint Surgery [Br]* **48**:153-169

Anderson, L.J. and **Jarrett, W.F.H.** (1966). Mammary neoplasia in the dog and cat - II. Clinico-pathological aspects of mammary tumours in the dog and cat. *Journal of Small Animal Practice* **7**:697-701

Anderson, M.A., Newmeyer, W.L. and **Kilgore, E.S.** (1982). Diagnosis and treatment of retained foreign bodies in the hand. *American Journal of Surgery* **144**:63-67

Anderson, A.M., Wilson, S.R. and **Mckee, J.P.** (1984). Psoas disease causing a characteristic change in the ultrasonographic appearance of the psoas compartment. *Journal of Canadian Medical Association* **35**:276-278

Aro, H.T. and **Chao E.Y.S.** (1993). Bone healing patterns affected by loading, fracture fragment stability, fracture types, and fracture site compression. *Clinical Orthopaedics and Related Research* **293**:8-17

Aron, D.N. (1983). Delayed union and non-union of fractures. In Bojrab, M.J. (ed). Current Techniques in Small Animal Surgery. 2nd ed. Lea and Ferbiger, Philadelphia. pp775-789

Avruch, L. and **Cooperberg, P.** (1985). The ring down artifact. *Journal of Ultrasound in Medicine* **4**:21-28

Barr, F (1990a). Principle of diagnostic ultrasound. In: Diagnostic Ultrasound in Dog and Cat. Blackwell Scientific publication, London. pp 1-19

Barr, F. (1990b). Imaging of other superficial soft tissues. In: Diagnostic Ultrasound in Dog and Cat. Blackwell Scientific publication, London. Pp 169-177

Bartrum, B.J. and **Craw, C.C.** (1983). Real-time Ultrasound: A manual for Physician and Technical Personnel. W.B. Saunders , Philadelphia.

Bassett, L.W., Ysrael, M., Gold, R.H. and **Ysrael, C.** (1991). Usefulness of mammography and sonography in women less than 35 years old. *Radiology* **180**:831-835

Becker, E.L. and **Landau, S.I.** (1986). International Dictionary of Medicine and Biology. New York, Chichester, Wiley.

Beckmann, C.R.B., Thomason, J.L., Sampson, M.B. and **Sheets, E.E.** (1985). Ultrasonographic confirmation of a thigh abscess. *Illinois Medical Journal* **167**:126-127

Bennett, D. (1975). Orthopaedic disease affecting the pelvic region of the cat. *Journal of Small Animal Practice* **16**:723-738

Berstein, I.T. and **Hansen, B.J.** (1991). Iatrogenic psoas abscess. *Scandinavian Journal of Urology and Nephrology* **25**: 85-86

Bezuidenhout, A.J. (1993). The lymphatic system. In: Miller's Anatomy of the dog, 3rd Ed. By Evans, H.E (ed.). W.B. Saunders. pp 717-757

Bloomberg, M.S. (1985). Muscle and tendon. In: Textbook of small animal surgery. Vol. II by Slatter, D.H. (ed.). W.B.Saunders, Philadelphia. pp2331-2358

Bostock, D.E. (1977). Neoplasia of the skin and mammary glands in dogs and cats. In: Current Veterinary Therapy VI. By Kirk, R.W. (ed.) Philadelphia: W.B. Saunders. pp 493-496

Bostock, D.E. (1986). Canine and feline mammary neoplasms. *British Veterinary Journal* **142**:506-515

Boyd, J.S. and **Omran, S.N.** (1991). Diagnostic ultrasonography of the bovine female reproductive tract. *In Practice* **13**:109-118

Braden, T.D. and **Brinker, W.O**. (1976). Radiologic and gross anatomy evaluation of bone healing in the dog. *Journal of American Veterinary Medical Association* **169**:1318-1323

Braden, T.D. (1991). Post traumatic osteomyelitis. *Veterinary Clinics of North America: Small Animal Practice* **21**:781-811

Braunstein, E.M., Silver, T.M., Martel, W. and **Jaffe, M.** (1981). Ultrasonographic diagnosis of extremity masses. *Skeletal Radiology* **6**:157-163

Brodey, R.S., Goldschmidt, M.H. and **Roszel, J.R.** (1983). Canine mammary gland neoplasms. *Journal of the American Animal Hospital Association* **19**:61-

Bruneton, J.N., Roux, P., Caramella, E., Demard, F., Vallicioni, J. and **Chauvel, P**. (1984). Ear, nose and throat cancer: ultrasound diagnosis of metastasis to the cervical lymph nodes. *Radiology* **152**:771-773

Bullough, P.G. and **Vigorita, V.J.** (1984). Atlas of Orthopaedic Pathology. New York, Gower Medical Publishing.

Burk, R.L. and **Ackerman, N**. (1996). Small Animal Radiology and Ultrasonography. A diagnostic atlas and text. and. Ed. W.B. Saunders. Philadelphia London.

Buttler, H.C. (1975). Resume of fracture healing. *Veterinary Clinics of North America* **5**:147-156

Buttler, H.C. (1985). Surgery of tendinous injuries and muscle injuries. In: Textbook of small animal orthopaedics. By Newton, C.D., Nunamaker, D.M. (eds.) Philadelphia: J.B. Lippincott. pp 835-842

Cady, E.B., Gardener, J.E. and **Edwards, H.T**. (1983). Ultrasonic tissue characterization of skeletal muscle. *European Journal of Clinical Investigation* **13**:469-473

Carlson, B.M. and **Faulkner, J.A**. (1983). The regeneration of skeletal muscle fibres following injury: a review. *Medicine Science Sport and Exercise* **15**:187-198

Cartee, R.E. and **Mahaffey, M.B.** (1995). The glands and lymph nodes. In: Practical veterinary ultrasonography. Cartee, et al (Eds.) Lea and Febiger book.

Cartee, R.E. and **Rumph, P.F.** (1984). Ultrasonic detection of fistulous tracts and foreign objects in muscles of horses. *Journal of American Veterinary Medical Association* **184**:1127-1132

Caywood, D.D. (1983). Osteomyelitis. *Veterinary Clinics of North America: Small Animal Practice* **13**:43-53

Chawla, S.K., Chandra, I.S, Sing, A.P. and **Nigam, J.M.** (1983). Radiographic evaluation of tibial fracture healing in sheep. *Indian Journal of Animal Science* **53**:852-857

Chretien, P.B., Behar, R.J., Kohn, Z., Moldovanu, G., Miller, D.G. and **Lawrence, W.** (1967). The canine lymphoid system: a study of the effect of surgical excision. *The Anatomical Record* **159**:5-16

Christensen, R.A., Sonnenberg, E.V., Casola, G. and **Wittish, G.R.** (1988). Interventional ultrasound in the musculoskeletal system. *Radiology Clinics North America* **26**:145-156

Claes, L., Augat, P., Suger, G. and **Wilke, H.S.** (1997). Influence of size and stability of the osteotomy gap on the success of fracture healing. *Journal of Orthopaedic Research* **15**:577-584

Cocke, W.M. and **Norton, C.** (1974). Regeneration of tibial segment from periosteum (case report). *Plastic and Reconstructive Surgery* **53**:675-676

Colby, J. (1985). Artifacts and image quality in ultrasound. *Journal of Equine Veterinary Science* **5**:295-297

Cole-Beuglet C, Soriano RZ, Kurtz AB. and **Goldberg BB**. (1983). Ultrasound analysis of 104 primary breast carcinoma classified according to histopathologic type. *Radiology* **147**:191-196

Cormack, D.H. (1987). Ham's Histology. 9th ed. J.B. Lippincott, Philadelphia, London.

Cotchin, E. (1954). Further observations on neoplasms in dogs with particular reference to site of origin and malignancy. I. Cutaneous, female genital and alimentary system. *British Veterinary Journal* **110**:218-230

Cotchin, E. (1958). Mammary neoplasms of the bitch. *Journal of Comparative Pathology* **68**:1-22

Craigmyle, M.B.L. (1986). A colour Atlas of Histology (2nd ed.). Wolfe Medical Publication, London.

Craychee, T.J. (1995). Ultrasonographic evaluation of equine musculoskeletal injury. In: Veterinary Diagnostic Ultrasound. by Nyland T.G. and Mattoon J.S. (eds.). W.B Saunders. p265-304

Culling, C.L.A. (1974). Handbook of histopathology and histochemical techniques. 3rd ed.

Curry, T.S. III, Dowdey, J.E. and **Murry, R.C. Jr**. (1990). Christensen's Physics of Diagnostic Radiology, 4th ed. Philadelphia: Lea & Febiger.

Denny, H.R. (1978). Pelvic fracture in the dog: A review of 123 cases. *Journal of Small Animal Practice* **19**:151-166

Derbyshire, N.J.D. and **Simpson, A.H.R.W.** (1992). A role for ultrasound in limb lengthening. *The British Journal of Radiology* **65**:576-580

De Young D.J. and **Probst, C.W.** (1993). Method of internal fracture fixation. In Textbook of small Animal Surgery by Slatter, D. (ed). W.B. Saunders. pp1610-1640

Dik, K.J. (1990). Ultrasonography in the diagnosis of equine lameness. *Veterinary Annual* **30:**162-171

Dik, K.J., Boroffka, S. and **Stolk, P**. (1994). Ultrasonographic assessment of the proximal digital annular ligament in the equine forelimb. *Equine Veterinary journal* **26**:59-64

Drost, W.T. (1992). Cleaning ultrasound transducers. *Veterinary Radiology and Ultrasound* **33**:367

Else, R.W. and **Hannant, D.** (1979). Some epidemiological aspects of mammary neoplasia in the bitch. *Veterinary Record* **104:**296-304

Evans, H.E. (1993). The skeleton. In: Miller's Anatomy of the Dog. 3rd ed. By Evans H.E. (ed.), W.B. Saunders, Philadelphia. pp 122-218

Eyres, K.S., Bell, M.J. and **Kanis, J.A**. (1993). Methods of assessing new bone formation during limb lengthening: ultrasonography, dual energy x-ray absorptiometry and radiography compared. *Journal of Bone and Joint Surgery [Br]* **75**:358-364

Evans, H.E. and **Christensen, G.C.** (1993). The urogenital system. In: Miller's Anatomy of the Dog, 3rd ed. By Evans, H.E. (ed.). W. B. Saunders, Philadelphia. pp 494-558

Falkenberg, J. (1961). An experimental study of the rate of fracture healing. *Acta Orthopaedica Scandinavica Supplement* No. 50.

Farrow, C.S. (1996). Musculoskeletal system. In: Small Animal ultrasound by Green, R.W. (ed.) Lippincott-Raven, Philadelphia. New York. pp 335-351

Feeney, D.A., Fletcher, T.F. and **Hardy, R.M.** (1991). Basic of diagnostic ultrasonography. In: Atlas of correlative imaging anatomy of the normal dog (Ultrasound and Compute Tomography). W.B. Saunders. pp354-366

Feu, J. Tresserra, F, Fabregas, R., Navarro, B., Grases, P.J., Suris, J.C., Fernandez, C.A. and **Alegret, X.** (1997). Metastatic breast carcinoma in axillary lymph nodes: in vitro ultrasonographic detection. *Radiology* **205**:831-835

Fidler, I.J. and **Brodey, R.S.** (1967). A necropsy study of canine malignant mammary neoplasms. *Journal of American Veterinary Medical Association* **15**:710-715

Fleischer AC, Muhletaler CA, Reynolds VH, Machin JE, Thieme GA, Bundy AL, Winfield AC. and **James AE** (1983). Palpable breast masses: Evaluation by high frequency, hand-held real-time sonography and xeromammography. *Radiology* **148**:813-817

Fornage, B.D., Touche, D.H., Segal, P. and **Rifkin, M.D.** (1983). Ultrasonography in the evaluation of muscular trauma. *Journal of Ultrasound in Medicine* **2**:549-554

Fornage, B.D., Schernberg, F.L. and **Rifkin, M.D.** (1985). Ultrasound examination of the hand. *Radiology* **155**:785-788

Fornage, B.D. and **Schernberg, F.L.** (1986). Sonographic diagnosis of foreign bodies of the distal extremities. *American Journal of Roentgenology* **147**:567-569

Fornage, B.D., Nasca, S. and **Durville, A.** (1987). Sonographic detection and three-dimensional localization of a metallic foreign body in soft tissue in a dog. *British Veterinary Journal* **143**:278-282

Fornage, B.D. and **Rifkin, M.D.** (1988). Ultrasound examination of the hand and foot. *Radiologic Clinics North America* **26**:109-129

Fornage, B.D. (1989). Ultrasonography of muscle and tendons. Examination Technique and Atlas of Normal Anatomy of the Extremities. Springer-verlag, New York.

Fornage, B.D., Sneige, N., Faroux, M.J. and **Andry, E.** (1990). Sonographic appearance and ultrasound quided fine-needle aspiration biopsy of breast carcinomas smaller than 1 cm. *Journal of Ultrasound in Medicine* **9**:559-560

Fowler, E.H., Wilson, G.P. and **Koestner, A.** (1974). Biologic behaviour of canine mammary neoplasms based on a histogenetic classification. *Veterinary Pathology* **11**:212-229

Genovese, R.L., Rantanen, N.W., Hauser, M.L. and **Simpson, B.S.** (1986). Diagnostic ultrasonography of Equine limbs. *Veterinary Clinics North America Equine Practice* **2**:145-226

Genovese, R.L., Rantanen, N.W. and **Simpson, B.S.** (1987). The use of ultrasonography in the diagnosis and management of injuries to the equine limb. *Continuing Education* **9**:945-955

Gerwing, M. and **Kramer, M.** (1995). Sonographical findings of muscle diseases in dogs and cats. *Veterinary Radiology & Ultrasound.* (Oral Abstracts) **36**: 437

Ginther, O.J (1986). Ultrasonographic imaging and reproductive events in the mare. Cross Plains: Equiservices.

Glaser, F., Knopp, W. and **Muhr, G.** (1988). Early recognition of post-operative hematoma formation. *Arch Orthopaedic Trauma Surgery* **107**:253-255

Goddard, P.J. (1995). General principles. In: Veterinary Ultrasound. by Goddard, P.J. (ed.) Cab. International University Press, Cambridge. pp1-19

Gooding, G.A.W., Hardiman, T., Sumers, M., Stess, R.,Graf, P. and **Grunfeld, C.** (1987). Sonography of the hand and foot in foreign body detection. *Journal of Ultrasound in Medicine* **6**:441-447

Graif, M., Stahl-Kent, V., Ben Ami, T., Strauss, S., Amit, Y. and **Itzchak, Y.** (1988). Sonographic detection of occult bone fractures. *Pediatric Radiology* **18**:383-385

Gunreben, G. and **Bogdahn, U.** (1991). Real-time sonography of acute and chronic muscle denervation. *Muscle and Nerve* **14**:654-664

Habel, R.E. (1978). Mammary gland. In: Applied Anatomy. Ithaca, N.Y. Robert and Habel, E. (eds.). pp:271-276

Hager, D.A. (1986). The diagnosis of deep muscle abscess using two-dimensional real time ultrasound. *American Association of Equine Practice* **32**:523-529

Hajeck, P.C., Salomonowitz, E., Turk, R., Tscholakoff, D., Kumpan, W. and **Czembirek, H**. (1986). Lymph nodes of the neck: evaluation with ultrasound. *Radiology* **158**:739-742

Hamanishi, C., Yosii, T. and **Tanaka, S.** (1994). Maturation of the distracted callus: sonographic observations in rabbits applied to patients. *Acta Orthopaedic Scandinavica* **65**:335-338

Harcke, H.T., Grissom, L.E. and **Finkelstein, M.S**. (1988). Evaluation of musculoskeletal system with sonography. *American Journal of Roentgenology* **150**:1253-1261

Hargis, A.M. (1995). Integumentary system. In: Thompson's Special Veterinary Pathology. Second ed. by Carlton, W.M. and McGavin, M.D. (eds.) Mosby Year Book. pp 461-511

Harper, A.P., Kelly-Fry. E., Noe, J.S., Bies, J. and **Jackson, V.P.** (1983). Ultrasound in the evaluation of solid breast masses. *Radiology* **146**:731-736

Harris, W.R. (1990). Fracture healing. In: Canine Orthopaedics. 2nd ed. by Whittick, W.G. (ed.) Lea and Febiger pub. Philadelphia London. Pp 158-165

Hayashi, N., Tamaki, N. Ypnekura, Y., Senda, M., Yamamoto, K. and **Torizuka, K.** (1985). Real-time sonography of palpable breast masses. *The British Journal of Radiology* **58**:611-615

Heckmatt, J.Z., Dubowitz, V. and **Leeman, S**. (1980). Detection of pathological change in dystrophic muscle with B-scan ultrasound imaging. *The Lancet* **28**:1389-1390

Heckmatt, J.Z., Leeman, S. and **Dubowitz, V**. (1982). Ultrasound imaging in the diagnosis of muscle disease. *Journal of Paediatrics* **101**:656-660

Heckmatt, J.Z., Pier, N. and **Dubowitz, V**. (1988a). Measurement of quadriceps muscle thickness and subcutaneous tissue thickness in normal children by real-time ultrasonographic imaging. *Journal of Clinical Ultrasound* **16**:171-176

Heckmatt, J.Z., Pier, N. and **Dubowitz, V**. (1988b). Real-time ultrasound imaging of muscles. *Muscle and Nerve* 11:56-65

Hendrich, C., Finkewitz, U. and **Berner, W.** (1995). Diagnostic value of ultrasonography and conventional radiography for the assessment of sternal fractures. *Injury* **26**:601-604

Henry, G.A., Patton, C.S. and **Goble, D.O**. (1986). Ultrasonographic evaluation of iatrogenic injuries of the equine accessory (carpal check) ligament and superficial digital flexor tendon. *Veterinary Radiology* **27**:132-140

Hermanson, J.W. and **Evans, H.E**. (1993), The muscular system. In: Miller's Anatomy of the Dog, third ed. By Evans H.E (ed.). W.B Saunders. Philadelphia London. pp 258-384

Herring, D.S. and **Bjornton, G**. (1985). Physics, facts, and artifacts of diagnostic ultrasound. *Veterinary Clinical North American Small Animal Practice* **15**:1107-1122

Hickman, J. (1966). Limb fractures in the dog and cat - V: fractures of the hind limb. *Journal of Small Animal Practice* **7**:163-168

Hickman, J. (1975). Greyhound injuries. *Journal of Small Animal Practice* **16**: 455-460

Homco, L.D. (1996). Lymph nodes. In Green, R.W. (ed.) Small Animal Ultrasonography. Lippincott-Raven Publisher, Philadelphia. pp305-322

Howard, C.B. and **Einhorum, M.S.** (1991). Ultrasound in the detection of subperiosteal abscess. *Journal of Bone and Joint Surgery [Br]* **73**:175-176

Hulland, J.J. (1993). Muscles and tendons.In: Pathology of Domestic Animals, 4th ed. by Jubb, J.V.S., Kennedy, P.C. and Palmer, N. (eds.) San Diego London: Academic Press. pp 183-265

Jabara, A.G. (1960). Canine mammary carcinomata. *The Australian Veterinary Journal* **36**:389-398

Jackson VP (1995). Management of solid breast nodules: what is the role of sonography? *Radiology* **196**:14-15

Jacobson, J.A., Powell, A., Craig, J.G., Bouffard, J.A. and **van Holsbeeck, M.T.** (1998). Wooden foreign bodies in soft tissue: detection at ultrasound. *Radiology* **206**:45-48

Jaffe, C.C., Rosenfield, A.T., Somer G. and **Taylor, K.J.W**. (1980). Technical factors influencing the imaging of small anechoic cysts by B-scan ultrasound. *Radiology* **135**:429-433

Jain, A.K., Kumar, S., Shiv, V., Singh, H. and **Tuli, S.M.** (1992). Retrofascial pyogenic iliac fossa abscess 20 cases studied by ultrasonography. *Acta Orthopaedic Scandinavica* **63**: 53-56

Johnson, J.A., Austin, C. and **Breur, G.J.** (1994). Incidence of canine appendicular musculoskeletal disorders in 16 veterinary teaching hospitals from 1980 through 1989. *Veterinary Comparative Orthopaedics and Traumatology* **7**:56-69

Kaplan, P.A., Anderson, J.C., Norris, M.A. and **Matamoros, A**. (1989). Ultrasonography of post traumatic soft tissue lesions. *Radiologic Clinics of North America* **27**:973-982

Kaplan, P.A., Matamoros, A. and **Anderson, C**. (1990). Sonography of the musculoskeletal system. *American Journal of Roentgenology* **155**:237-245

Kirberger, R.M. (1995). Imaging artifact in diagnostic ultrasound - A review. *Veterinary Radiology & Ultrasound* **36**:297-306

Kofler, J. and **Edinger, H.K.** (1995). Diagnostic ultrasound imaging of soft tissues in the bovine distal limb. *Veterinary Radiology & Ultrasound* **36**:246-252

Kolb, T.M., Lichy, J. and **Newhouse, J.H.** (1998). Occult cancer in women with dense breast: detection with screening ultrasound - diagnostic yield and tumour characteristics. *Radiology* **207**:191-199

Kramer, M., Gerwing, M., Hach, V. and **Schimke, E.** (1997). Sonography of the musculoskeletal system in dogs and cats. *Veterinary Radiology & Ultrasound* **38**:139-149

Kremkau, F.W. and **Taylor, K.J.W**. (1986). Artifacts in ultrasound imaging. *Journal of Ultrasound Medicine* **5**:227-237

Kullmer, K., Sievers, K.W., Rompe, J.D., Nagele, M. and **Harland, U.** (1997). Sonography and MRI of experimental muscle injuries. *Arch Orthopaedic and Traumatic Surgery* **116**:357-361

Laine, H., Harjula, A., and **Peltokallio, P**. (1985). Experience with real time sonography in muscle injuries. *Scandinavian Journal of Sports Science* **7**: 45-49

Laing, F.C. (1983). Commonly encountered artifacts in clinical ultrasound. *Seminar in Ultrasound* **4**:27-43

Lamminen, A., Jaaskelainen, J., Rapola, J. and **Suramo, I.** (1988). High frequency ultrasonography of skeletal muscle in children with neuromuscular disease. *Journal of Ultrasound in Medicine* **7**:505-509

Lang, D.C. (1980). Ultrasonic treatment of musculoskeletal conditions in the horses, dogs and cat. *Veterinary Record* **106**:427-431

Lee, R. (1976). Proximal femoral epiphyseal separation in the dog. *Journal of Small Animal Practice* **17**:669-679

Lehto, M. and **Alanen, A.** (1987). Healing of a muscle trauma: correlation of sonographical and histological findings in an experimental study in rats. *Journal of Ultrasound Medicine* **6**:425-429

Lendrum, A.C., Fraser, D.S., Sliddes, W. and **Henderson, R.C.** (1962). Histological and histochemical techniques. Journal of Clinical pathology 15:401-409

Lewallen, D.G., Caao, E.Y.S., Kasman, R.A., and **Kelly, P.J.** (1984). Comparison of the effects of compression plates and external fixators on early bone healing. *The Journal of Bone and Joint Surgery [Am]* **66**:1084-1091

Lindahl (1966). Detection of pregnancy in sheep by means of ultrasound. *Nature* **212:**642-643

Little, C.M., Parker, M.G., Callowich, M.C. and **Sartori, J.C.** (1986). The ultrasonic detection of soft tissue foreign bodies. *Investigative Radiol*ogy **21**:275-277

Maffuli, N., Hughes, T. and **Fixsen, J.A.** (1992). Ultrasonographic monitoring of limb lengthening. *Journal of Bone and Joint Surgery [Br]* **74**:130-132

Maffulli, N. and **Thornton, A.** (1995). Ultrasonographic appearance of external callus in long bone fractures. *Injury* **26**:5-12

Mahaisavariya, B., Suibnugarn, C., Mairiang, E., Saengnipanthkul, S., Laupattarakaem, W. and **Kosnwon, W.** (1991). Ultrasound for closed femoral nailing. *Journal of Clinical Ultrasound* **19**:393-397

Mahaisavariya, B. and **Laupattarakasem, W.** (1993). Ultrasound or image intensifier for closed femoral nailing. *Journal of Bone and Joint Surgery [Br]* **75**:66-68

Manthey, D.E., Storrow, A.B., Milbourn, J.M. and **Wagner, B.J.** (1996). Ultrasound versus radiography in the detection of soft tissue foreign bodies. *Annals of Emergency Medicine* **28**:7-9

Marchal, G., Oyen, R., Verschakelen, J. Gelin, J., Baert, A.L. and **Stessens, R.C.** (1985). Sonographic appearance of normal lymph nodes. *Journal of Ultrasound in Medicine* **4**:417-419

Marr, C.M., McMillan, I., Boyd, J.S., Wright, N.G. and **Murray, M.** (1993). Ultrasonographic and histological findings in equine superficial digital flexor tendon injury. *Equine Veterinary Journal* **25**:23-29

McClellan, P. (1995). Visualizing a fracture with ultrasonography. *Journal of Equine Veterinary Science* **15**:20-21

McKibbin, B. (1978). The biology of fracture healing in long bones. *Journal of Bone and Joint Surgery* **60-B**:150-162

Miller, M.E., Evans, H.E. and **Christensen, G.C.** (1979). The mammae. In: Anatomy of the Dog. Philadelphia, W.B. Saunders. pp 101-106

Milton, J.L. and **Henderson, R.A.** (1983). Surgery of muscles and tendons. In: Current techniques in small animal surgery. 2nd by Bojrab, M.J. (ed), Lea and Febiger, Philadelphia. pp 495-516

Misdorp, W., Cotchin, E., Hampe, J.F., Jabara, A.G. and **von Sandersleben, J.** (1972). Canine malignant mammary tumours. *Veterinary Pathology* **9**:447-470

Misdorp, W. and **Hart, A.A.M.** (1979a). Canine mammary cancer I. Prognosis. *Journal of Small Animal Practice* **20**:385-394

Misdorp, W. and **Hart, A.A.M.** (1979b). Canine mammary cancer II. Therapy and causes of death. *Journal of Small Animal Practice* **20**:395-404

Mittelstaedt, C.A. (1992). General Ultrasound. New York. Churchill Livingstone.

Moed, B.R., Watson, J.I., Goldsmith, P. and **van-Holsbeeck, M**. (1995). Ultrasound for the early diagnosis of fracture healing after interlocking nailing of the tibia without reaming. *Clinical Orthopedics* **310**:137-144

Morris, J.S., Dobson, J.M., Bostock, D.E. and **O'Farrell, E.** (1998). Effect of ovariohysterectomy in bitches with mammary neoplasms. *Veterinary Record* **142**:656-658

Moulton, J.E., Rosenblatt, L.S. and **Goldman, M**. (1986). Mammary tumors in a colony of beagle dogs. *Veterinary Pathology* **23**:741-749

Moulton, J.E. (1990). Tumours of the mammary gland. In: Tumours in Domestic Animals, 3rd ed. University of California Press, London. pp 518-552

Nagano, T., Nakai, Y., Taniguchi, F., Suzuki, N., Wakutani, K., Ohnishi, T., Nakayama, T., Shibamoto, T., Umaoka, Y., Ohara, A., Shimizu, T., Tamura, H. and **Ozawa, M.** (1991). Diagnostic of paraaortic and pelvic lymph node metastasis of gynecology malignant tumours by ultrasound-guided percutaneous fine-needle aspiration biopsy. *Cancer* **68**:2571-2574

Newton, C.D. and **Hohn, R.B.** (1974). Fracture nonunion resulting from cerclage appliances. *Journal of American Veterinary Medical Association* **164**:503-508

Noordeen, M.H.H., Lavy, C.B.D., Shergill, N.S., Tuite, J.D. and **Jackson, A.M.** (1995). Cyclical micromovement and fracture healing. *Journal of Bone and Joint Surgery [Br]* **77**:645-648

Nyland, T.G., Mattoon, J.S. and **Wisner, E.R.** (1995). Physical principles, instrumentation, and safety of diagnostic ultrasound. In: Veterinary Diagnostic Ultrasound. W.B. Saunders. pp 3-18

Ormrod, A.N. (1966). Limb fractures in the dog and cat - IV: fractures of the fore limb. *Journal of Small Animal Practice* **7**:155-162

Owen, L.N. (1966). Mammary neoplasia in the dog and cat - III. Prognosis and treatment of mammary tumours in the bitch. *Journal of Small Animal Practice* **7**:703-710

Park, R.D., Nyland, T.G., Lattimer, J.C., Miller, C.W. and **Lebel, J.L.** (1981). B-mode gray-scale ultrasound: Imaging artifacts and interpretation principles. *Veterinary Radiology* **22** :204-210

Parrini, L., Baratelli, M. and **Parrini M.** (1988). Ultrasound examination of hematomas after total hip replacement. *International Orthopaedics* **12**:79-82

Patsikas, M.N. and **Dessiris, A.** (1996a). The lymph drainage of the mammary glands in the bitch: a lymphographic study. Part I: the first, second, fourth and fifth mammary glands. *Anatomia Histological Embryological* **25**:132-138

Patsikas, M.N. and **Dessiris, A.** (1996b). The lymph drainage of the mammary glands in the bitch: a lymphographic study. Part II: the third mammary gland. *Anatomia Histological Embryological* **25**:139-143

Patten, R.M., Mack, L.A., Wang, K.Y. and **Lingel, J.** (1992). Nondisplaced fractures of the greater tuberosity of the humerus: sonographic detection. *Radiology* **182**:201-204

Peacock, E.E. and **Van Winkle, W.V.** (1970). Surgery and biology of wound repair. 2nd ed. W.B.Saunders, Philadelphia.

Peacock, E.E. and **Van Winkle, W.V.** (1976). Wound repair, 2nd ed. W.B. Saunders, Philadelphia.

Penninck, D.G. (1995). Imaging artifacts in ultrasound. In: Veterinary Diagnostic Ultrasound. Nyland, T.G. and Mattoon, J. (eds.). W.B. Saunders. pp 19-29

Peretti, G., Memeo, A., Peronzini, A. and **Marinoni, E.C.** (1988). Methods for the study of bone regeneration in lengthening of the limbs. *Italian Journal of Orthopaedic Traumatology* **15**:217-221

Pettine, K.A., Chao, E.Y.S. and **Kelly, P.J.** (1993). Analysis of the external fixator pin - bone interface. *Clinical Orthopaedics and Related Research* **293**:18-27

Philips, I.R. (1979). A survey of bone fracture in the dog and cat. *Journal of Small Animal Practice* **20**:661-674

Power, J.W. (1981). Muscular, tendinous, and ligamental injuries. In: Management of Trauma in Dogs and Cats. by Archibald, J., Holt, J.C., Sokolovsky, V. (Eds.). American Veterinary Pubisher 1981. pp 369-394

Priester, W.A. (1979). Occurrence of mammary neoplasms in bitches in relation to breed, age, tumour type, and geographical region from which reported. *Journal of Small Animal Practice* **20**:1-11

Pugh, C.R. (1994). Ultrasonographic examination of abdominal lymph nodes in the dog. *Veterinary Radiology & Ultrasound* **35**:110-115

Pugh, C.R., Johnson, P.J., Crawley, G. and **Finn, S.T**. (1994). Ultrasound of the equine bicipital tendon region: a case history report and review of anatomy. *Veterinary Radiology and Ultrasound* **35**:183-188

Rafailson, S.R., **Kronborg, O.** and **Fenger, C.** (1992). Echo pattern of lymph nodes in colorectal cancer: An in vitro study. *British Journal of Radiology* **65**:218-220

Rahn B.A., **Gallinaro, P.**, **Baltensperger, A.** and **Perren, S.M.** (1971). Primary bone healing (brief note). *Journal of Bone and Joint Surgery [Am]* **53**:783-786

Rantanen, N.W. and **Ewing, R.L.** (1981). Principles of ultrasound application in animals. *Veterinary Radiology* **22**:196-203

Rantanen, N.W. (1995). Physical principles of ultrasonographic diagnosis. *Journal of Equine Veterinary Science* **15**:107-110

Reef, V.B. (1992). Diagnosis of pelvic fractures in horses using ultrasonography. *Veterinary Radiology (abstr.)***33**:33

Rhinelander, F.W., **Philips, R.S.**, **Steel, W.M.** and **Beer, J.C.** (1968). Microangiography in bone healing. *Journal of Bone and Joint Surgery [Am]* **50**:643-662

Ricciardy, L., **Perissinotto, A.** and **Dabala, M.** (1992). External callus development on ultrasound and its mechanical correlation. *Italian Journal of Orthopedics and Traumatology* **18**:223-229

Ricciardy, L., **Perissinotto, A.** and **Dabala, M.** (1993). Mechanical monitoring of fracture healing using ultrasound imaging. *Clinical Orthopaedics* **293**:71-76

Richardson, E.F. and **Thacher, C.W.** (1993). Tibial fractures in cats. *Continuing Education* **15**:383-394

Richter K., **Heywang-Kobrunner S.H.**, **Winzer K.J.**, **Schmitt K.J.**, **Prihoda H.**, **Frohberg H.D.**, **Guski H.**, **Gregor P.**, **Blohmer J.U.**, **Fobbe F.**, **Doinghaus, K.**, **Lohr, G.** and **Hamm, B.** (1997). Detection of malignant and benign breast lesions with an automated ultrasound system: results in 120 cases. *Radiology* **205**:823-830

Robinson, D.E., Wilson, L.S. and **Kosoff, G.** (1981). Shadowing and enhancement in ultrasonic echograms by reflection and refraction. *Journal of Clinical Ultrasound* **9**:181-188

Rubatelli, L., Proto, E., Salmaso, R., Bortoletto, P., Candiani, F. and **Cagol, P.** (1990). Sonography of abnormal lymph nodes in vitro. *American Journal of Roentgenology* **155**:1241-1244

Saar, L.I. and **Getty, R.** (1975). Carnivore lymphatic system. In: Sisson and Grossman's Anatomy of Domestic Animals. 5th Ed. by Getty, R. (ed.). W.B.Saunders, Philadelphia. pp 1652-1670

Sarazin, L., Bonaldi, V.M., Papadatos, D. and **Chhem, K.R.** (1996). Correlative imaging and pattern approach in ultrasonography of bone lesion: a pectoral essay. *Canadian Association of Radiologists Journal* **47**:423-430

Saunders, H.M., Pugh, C.R., and **Rhodes, W.H.** (1992). Expanding application of abdominal ultrasonography. *Journal of American Animal Hospital Association* **28**:369-374

Sautet, J.Y., Ruberte, J., Lopez, C., Gine, J.M., Ordonez, G. and **Cingia, A.** (1992). Lymphatic system of the mammary glands in the dog: an approach to the surgical treatment of malignant mammary tumours. *Canine Practice* **17**:30-33

Schneider, R., Dorn, C.R. and **Taylor, D.O.N.** (1969). Factor in influencing canine mammary cancer development and postsurgical survival. *Journal National Cancer Inst.* **43**:1249-1262

Schneider, R.(1970). Comparison of age, sex, and incidence rates in human and canine breast cancer. *Cancer* **26**:419-426

Schummer, A., Wilkens, H., Vollmerhaus, B. and **Habermehl, K.H.** (1981). The anatomy of the domestic animals: the circulatory system, the skin and the cutaneous organs of the domestic mammals. vol. III. By R. Nikel, A. Schummer, E. Seiferle (eds.) Berlin: Verlag Paul Parey.

Shah, Z.R., Crass, J.R., Oravec, D.C. and **Bellon, E.M.** (1992). Ultrasonographic detection of foreign bodies in soft tissues using turkey muscle as a model. *Veterinary Radiology and Ultrasound* **33**:94-100

Shirley, I.M., Blackwell, R.J., Cusick, G., Freman, D.J., and **Vicary, F.R.** (1978). A user's guide to diagnostic ultrasound. Baltimore: University Park Press.

Silver, I.A. (1966). Symposium on mammary neoplasia in the dog and cat-I. The anatomy of the mammary gland of the dog and cat. *Journal of Small Animal Practice* **7**:689-696

Singleton W.B. (1966). Limb fractures in the dog and cat - V: fractures of the hind limb. *Journal of Small Animal Practice* **7**:163-168

Skolnick, M.L., Meire, H.B. and **Lecky, J.W.** (1975). Common artefacts in ultrasound scanning. *Journal of Clinical Ultrasound* **3**:273-280

Smeets, A.J., Zanderland, H.M., van der Voorde, F. and **Lameris, J.S.** (1990). Evaluation of abdominal lymph nodes by ultrasound. *Journal of Ultrasound in Medicine* **9**:325-330

Smith, R.K.W. and **Webbon, P.M.** (1994). Diagnostic Imaging in the Athletic Horse: Musculoskeletal ultrasonography. In: The Athletic Horse. Principle and practice of equine sport medicine. W.B.Saunders. pp297-325

Smith, R.K.W., Dyson, S.J., Head, M.J. and **Butson, R.J.** (1996). Ultrasonography of the equine triceps muscle before and after anaesthesia and in post anaesthetic myopathy. *Equine Veterinary Journal* **28**:311-319

Solbiati, L., Cioffi, V. and **Ballarati, E.** (1992). Ultrasonography of the neck. *Radiologic Clinics of North America* **30**:941-954

Sommer, F.G., Filly, R.A. and **Minton, M.J.** (1979). Acoustic shadowing due to refractive and reflective effects. *American Journal of Roentgenology* **132**:973-977

Spaulding, K.A. and **Richey, J.** (1993). Determination of the sonographic appearance of normal medial iliac lymph nodes in the dog. *Proceedings of the American College of Veterinary Radiology Annual Meeting*, scientific program. Chicago, IL.

Stavros A.T, Thickman D, Rapp CL, Dennis MA, Parker SH. and **Sisney GA**. (1995). Solid breast nodules: use of sonography to distinguish between benign and malignant lesions. *Radiology* **196**:123-134

Steiner, G.M. and **Sprigg, A**. (1992). The value of ultrasound in the assessment of bone. *The British Journal of Radiology* **65**:589-593

Takebayashi, S., Takasawa, H., Bansai, Y., Miki, H., Sasaki, R., Itoh, Y. and **Matsubara, S.** (1995). Sonographic findings in muscle strain injury: clinical and MR imaging correlation. *Journal of Ultrasound in Medicine* **14**:899-905

Tamura, M. (1992). Ultrasonography of mass lesions in dogs and cats. *Japanese Journal of Veterinary Research* **40**:63

Taylor, K.J.W., Jacobson, P., Talmont, C.A. and **Winters, R.** (1980). Manual of Ultrasonography, New York. Churchill Livingstone. pp 34-35

Thickman, D.I., Ziskin, M.C., Goldenberg, N.C. and **Linder, B.E.** (1983). Clinical manifestations of the comet tail artefact. *Journal of Ultrasound in Medicine* **2**:225-230

Trout, N.J., Penninck, D.G., Boudrieau, R.J. and **Kudisch, M.** (1994). Early postoperative ultrasonographic evaluation of incisitional sites in dogs: 15 cases (1990-1992). *Journal of American Veterinary Medical Association* **205**:1565-1568

Tsunoda-Shimizu, H. and **Saida, Y.** (1997). Ultrasonographic visibility of supraclavicular lymph nodes in normal subjects. *Journal of Ultrasound in Medicine* **16**:481-483

Uhthoff, H.K. (1973). Mechanical factors influencing the holding power of screws in compact bone. *Journal of Bone and Joint Surgery [Br]* **55**:633-639

Uhthoff, H. K and **Germain. J.P.** (1977). The reversal of tissue differentiation around screws. *Clinical orthopaedics and Related Research* **123**:248-252

van Holsbeeck, M. and **Introcaso, J.H.** (1990). Sonography of muscle. In: Musculoskeletal ultrasonography. Chicago, Mosby-year Book. pp 245-256

van Holsbeeck, M. and **Introcaso, J.H.** (1992). Musculoskeletal ultrasonography. *Radiologic Clinics of North America* **30**:907-925

Vasallo P, Wernecke K, Roos N. and **Peters PE** (1992). Differentiation of benign from malignant superficial lymphadenopathy: the role of high-resolution US. *Radiology* **183**:215-220

Vasseur, P.B. (1985). Principle of operative surgery. In: General Small Animal Surgery, by Gourley, I.M. and Vasseur, P.B. (eds.). Philadelphia: J.B. Lippincott, pp 75-104

Vaughan, L.C. (1966). Limb fractures in the dog and cat II. Histological, clinical and radiographical aspects of fracture healing. *Journal of Small Animal Practice* **7**:141-146

Vaughan, L.C. (1969). Gracilis muscle injury in greyhound. *Journal of Small Animal Practice* **10**:363-375

Vaughan, L.C. (1975). Complications associated with the internal fixation of fractures in dogs. *Journal of Small Animal Practice*, **16**:415-426

Vaughan, L.C. (1979). Muscle and tendon injuries in dogs. *Journal of Small Animal Practice* **20**:711-736

Vincent, L.M. (1988). Ultrasound of soft tissue abnormalities of the extremities. *Radiologic Clinics of North America* **26**:131-144

Wendell, B.A. and **Athey, P.A**. (1981). Ultrasonic appearance of metallic foreign bodies in parenchymal organs. *Journal of Clinical Ultrasound* **9**:133-135

Wicks, J.D., Silver, T.M. and **Bree, R.L**. (1978). Grey-scale features of hematomas: an ultrasonic spectrum. *American Journal of Roentogenology* **131**:977-980

Williams P.L., Warwick, R., Dyson, M. and **Bannister, L.H.** (1989). Grays Anatomy, Thirty-seventh edition. Churchill Livingstone. London New York. pp 545-635

Wilson, D.J. (1988). Diagnostic ultrasound in the musculoskeletal system. *Current Orthopaedics* **2**:41-50

Wilson, D.A., Badertscher, R.R., Boero, M.J., Baker, G.J. and **Foreman, J.H.** (1989). Ultrasonographic evaluation of the healing of ventral midline abdominal incisions in the horse. *Equine Veterinary Journal* **Suppl 7**:107-110

Wisner, E.R. Mattoon, J.S., Nyland, T.G. and **Baker, T.W.** (1991). Normal ultrasonographic anatomy of the canine neck. *Veterinary Radiology* **32**:185-190

Wisner, E.R., Nyland T.G. and **Mattoon, J.S.** (1994). Ultrasonographic examination of cervical masses in the dog and cat. *Veterinary Radiology and Ultrasound* **35**:310-315

Wisner, E.R., Mattoon, J.S. and **Nyland, T.G.** (1995). Ultrasonography of the neck. In: Veterinary Diagnostic Ultrasound. by Nyland T.G. and Mattoon, J.S (eds.) W.B. Saunders Philadelphia. Pp 165-177

Wu, J-J., Shyr, H.S., Chao, E.Y.S. and **Kelly, P.J.** (1984). Comparison of osteotomy healing under external fixation devices with different stiffness characteristics. *Journal of Bone and Joint Surgery [Am]* **66**:1258-1264

Yager, J.A. and **Scott, D.W.** (1993). The skin and appendages. In: Pathology of Domestic Animals. 4th ed. by Jubb, K.V.F., Kennedy, P.C. and Palmer, N (eds.) New York: Academic. pp 531-738

Yang, W.T., Mok, C.O., King, W., Tang, A. and **Metreweli, C**. (1996). Role of high frequency ultrasonography in the evaluation of palpable breast masses in chinese women: Alternative to mammography. *Journal of Ultrasound in Medicine* **15**:637-644

Yeh, H.C. and **Rabinowitz, J.G**. (1982). Ultrasonography of the extremities and pelvic girdle and correlation with computed tomography. *Radiology* **143**:519-525

Yeh, H.S. (1985). Ultrasonography of orthopedics and soft tissues extremities. In: Sanders R.C., Hill M.C. (eds.) *Ultrasound annual* 1985. New York: Raven.

Ying, M., **Ahuja, A.**, **Brook, F.**, **Brown, B.** and **Metreweli, C.** (1996). Sonographic appearance and distribution of normal cervical lymphnodes in a Chinese population. *Journal of Ultrasound in Medicine* **15**:431-436

Young, J.W.R., **Kostrubiak, I.S.**, **Resnik, C.S.** and **Paley, D.** (1989). Sonographic evaluation of bone production at the distraction site in Ilizaroz limb lengthening procedures. *American Journal of Roentgenology*, 154:125-128

Young, J.W., **Kostrubiak, I.S.**, **Resnik, C.S.** and **Paley, D.** (1990). Sonographic evaluation of bone production at the distraction site in Ilizarov limb-lengthening procedures. *American Journal of Roentgenology* **154**:125-128

Yousefzadeh, D.K., **Schumann, E.M.**, **Mulligan, G.M.**, **Bosworth, D.E.**, **Young, C.S.** and **Pringle, K.C.** (1982). The role of imaging modalities in diagnosis and management of pyomyositis. *Skeletal Radiology* **8**:285-289

Zaninovic, P. and **Simcic, V**. (1994). Epidemiology of mammary tumours in dogs. *The European Journal of Companion Animal Practice* **4**:67-76

Ziskin, M.C., **Thickman, D.I.**, **Goldenberg, N.J.**, **Lapayowker, M.S.** and **Becker, J.M.** (1982). The comet tail artifact. *Journal of Ultrasound in Medicine* **1**:1-7